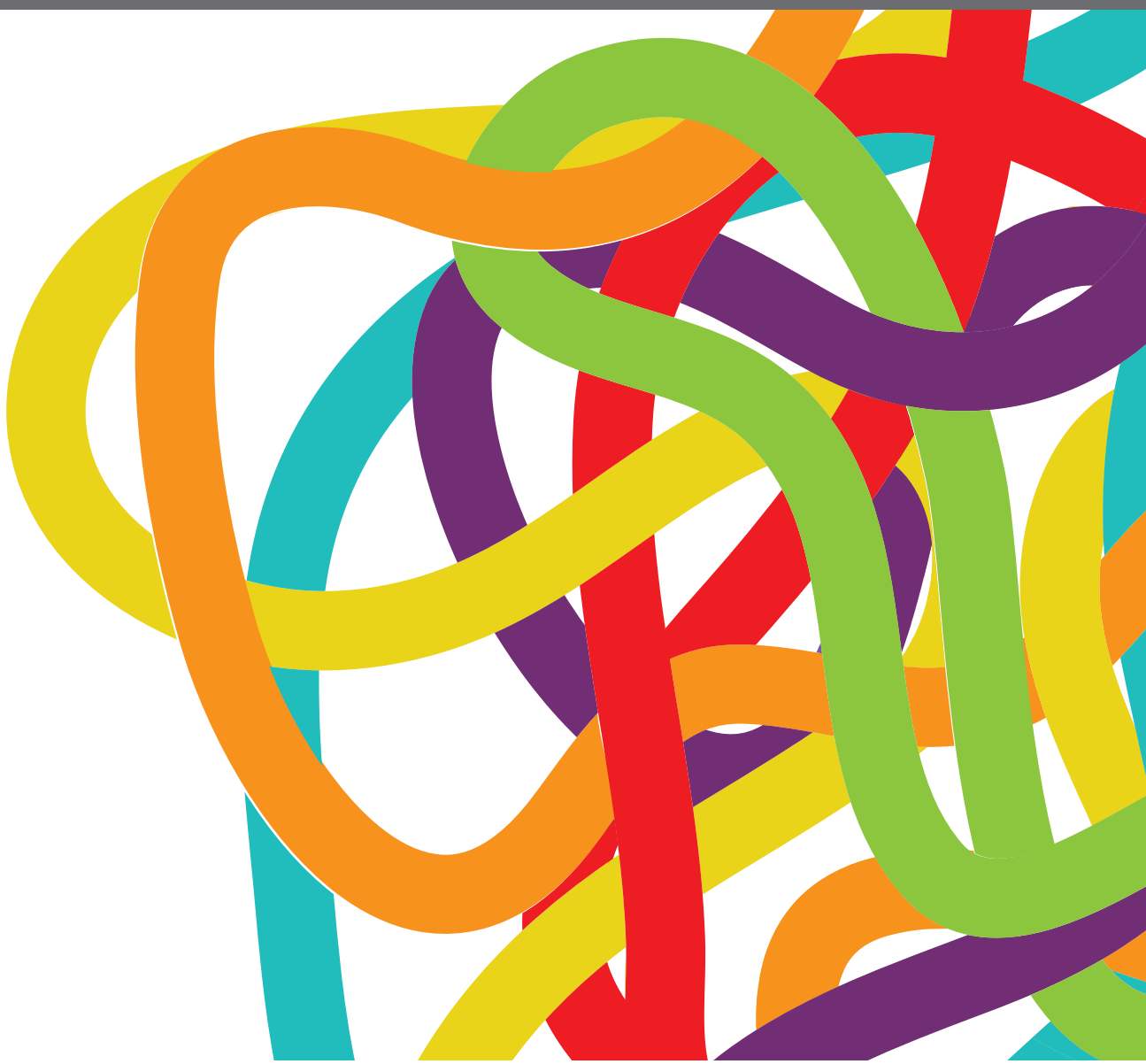
BIOMARKERS IN GENITOURINARY CANCERS, VOLUME II

EDITED BY: Riccardo Tellini, Alfredo Berruti, Michele Marchioni and Takeshi Yuasa

PUBLISHED IN: Frontiers in Oncology



frontiers Research Topics



frontiers

Frontiers eBook Copyright Statement

The copyright in the text of individual articles in this eBook is the property of their respective authors or their respective institutions or funders. The copyright in graphics and images within each article may be subject to copyright of other parties. In both cases this is subject to a license granted to Frontiers.

The compilation of articles constituting this eBook is the property of Frontiers.

Each article within this eBook, and the eBook itself, are published under the most recent version of the Creative Commons CC-BY licence. The version current at the date of publication of this eBook is CC-BY 4.0. If the CC-BY licence is updated, the licence granted by Frontiers is automatically updated to the new version.

When exercising any right under the CC-BY licence, Frontiers must be attributed as the original publisher of the article or eBook, as applicable.

Authors have the responsibility of ensuring that any graphics or other materials which are the property of others may be included in the CC-BY licence, but this should be checked before relying on the CC-BY licence to reproduce those materials. Any copyright notices relating to those materials must be complied with.

Copyright and source acknowledgement notices may not be removed and must be displayed in any copy, derivative work or partial copy which includes the elements in question.

All copyright, and all rights therein, are protected by national and international copyright laws. The above represents a summary only. For further information please read Frontiers' Conditions for Website Use and Copyright Statement, and the applicable CC-BY licence.

ISSN 1664-8714
ISBN 978-2-83250-537-3
DOI 10.3389/978-2-83250-537-3

About Frontiers

Frontiers is more than just an open-access publisher of scholarly articles: it is a pioneering approach to the world of academia, radically improving the way scholarly research is managed. The grand vision of Frontiers is a world where all people have an equal opportunity to seek, share and generate knowledge. Frontiers provides immediate and permanent online open access to all its publications, but this alone is not enough to realize our grand goals.

Frontiers Journal Series

The Frontiers Journal Series is a multi-tier and interdisciplinary set of open-access, online journals, promising a paradigm shift from the current review, selection and dissemination processes in academic publishing. All Frontiers journals are driven by researchers for researchers; therefore, they constitute a service to the scholarly community. At the same time, the Frontiers Journal Series operates on a revolutionary invention, the tiered publishing system, initially addressing specific communities of scholars, and gradually climbing up to broader public understanding, thus serving the interests of the lay society, too.

Dedication to Quality

Each Frontiers article is a landmark of the highest quality, thanks to genuinely collaborative interactions between authors and review editors, who include some of the world's best academicians. Research must be certified by peers before entering a stream of knowledge that may eventually reach the public - and shape society; therefore, Frontiers only applies the most rigorous and unbiased reviews.
Frontiers revolutionizes research publishing by freely delivering the most outstanding research, evaluated with no bias from both the academic and social point of view. By applying the most advanced information technologies, Frontiers is catapulting scholarly publishing into a new generation.

What are Frontiers Research Topics?

Frontiers Research Topics are very popular trademarks of the Frontiers Journals Series: they are collections of at least ten articles, all centered on a particular subject. With their unique mix of varied contributions from Original Research to Review Articles, Frontiers Research Topics unify the most influential researchers, the latest key findings and historical advances in a hot research area! Find out more on how to host your own Frontiers Research Topic or contribute to one as an author by contacting the Frontiers Editorial Office: frontiersin.org/about/contact

BIOMARKERS IN GENITOURINARY CANCERS, VOLUME II

Topic Editors:
Riccardo Tellini, Careggi University, Italy
Alfredo Berruti, University of Brescia, Italy
Michele Marchioni, University of Studies G. d'Annunzio Chieti and Pescara, Italy
Takeshi Yuasa, Japanese Foundation For Cancer Research, Japan

Citation: Tellini, R., Berruti, A., Marchioni, M., Yuasa, T., eds. (2022). Biomarkers in Genitourinary Cancers, Volume II. Lausanne: Frontiers Media SA. doi: 10.3389/978-2-83250-537-3

Table of Contents

06 ***Editorial: Biomarkers in Genitourinary Cancers: Volume II***
Takeshi Yuasa

08 ***Decreased Expression of ACADSB Predicts Poor Prognosis in Clear Cell Renal Cell Carcinoma***
Xianhui Liu, Weiyu Zhang, Huanrui Wang, Lin Zhu and Kexin Xu

19 ***MED10 Drives the Oncogenicity and Refractory Phenotype of Bladder Urothelial Carcinoma Through the Upregulation of hsa-miR-590***
Chia-Chang Wu, Yuan-Hung Wang, Su-Wei Hu, Wen-Ling Wu, Chi-Tai Yeh and Oluwaseun Adebayo Bamodu

35 ***Anti-Tumor Role of CAMK2B in Remodeling the Stromal Microenvironment and Inhibiting Proliferation in Papillary Renal Cell Carcinoma***
Qingan Jia, Xia Liao, Yaoyao Zhang, Binghui Xu, Yuna Song, Ganlan Bian and Xiaoliang Fu

47 ***Xpert Bladder Cancer Monitor May Avoid Cystoscopies in Patients Under "Active Surveillance" for Recurrent Bladder Cancer (BIAS Project): Longitudinal Cohort Study***
Vittorio Fasulo, Marco Paciotti, Massimo Lazzeri, Roberto Contieri, Paolo Casale, Alberto Saita, Giovanni Lughezzani, Pietro Diana, Nicola Frego, Pier Paolo Avolio, Piergiuseppe Colombo, Grazia Maria Elefante, Giorgio Guazzoni, Nicolò Maria Buffi, Michael Bates and Rodolfo Hurle

55 ***Investigating Urinary Circular RNA Biomarkers for Improved Detection of Renal Cell Carcinoma***
Madonna R. Peter, Fang Zhao, Renu Jeyapala, Shivani Kamdar, Wei Xu, Cynthia Hawkins, Andrew J. Evans, Neil E. Fleshner, Antonio Finelli and Bharati Bapat

62 ***Clinical Application of Circulating Tumor Cells and Circulating Endothelial Cells in Predicting Bladder Cancer Prognosis and Neoadjuvant Chemosensitivity***
Xiao Yang, Jiancheng Lv, Zijian Zhou, Dexiang Feng, Rui Zhou, Baorui Yuan, Qikai Wu, Hao Yu, Jie Han, Qiang Cao, Min Gu, Pengchao Li, Haiwei Yang and Qiang Lu

73 ***Identification and Validation of N6-Methyladenosine-Related Biomarkers for Bladder Cancer: Implications for Immunotherapy***
Hongyu Deng, Faqing Tang, Ming Zhou, Dongyong Shan, Xingyu Chen and Ke Cao

94 ***APOBEC Mutational Signature and Tumor Mutational Burden as Predictors of Clinical Outcomes and Treatment Response in Patients With Advanced Urothelial Cancer***
Divya Natesan, Li Zhang, Henry J. Martell, Tanya Jindal, Patrick Devine, Bradley Stohr, Carlos Espinosa-Mendez, James Grenert, Jessica Van Ziffle, Nancy Joseph, Sarah Umetsu, Courtney Onodera, Michelle Turski, Emily Chan, Arpita Desai, Rahul Aggarwal, Anthony Wong, Sima Porten, Jonathan Chou, Terence Friedlander, Lawrence Fong, Eric J. Small, Alejandro Sweet-Cordero and Vadim S. Koshkin

105 ***Tumor-Educated Platelets as a Promising Biomarker for Blood-Based Detection of Renal Cell Carcinoma***
Ruotao Xiao, Cheng Liu, Bo Zhang and Lulin Ma

115 ***Prognostic and Predictive Value of Liquid Biopsy-Derived Androgen Receptor Variant 7 (AR-V7) in Prostate Cancer: A Systematic Review and Meta-Analysis***
Tanzila Khan, Therese M. Becker, Kieran F. Scott, Joseph Descallar, Paul de Souza, Wei Chua and Yafeng Ma

128 ***Proteomic-Based Machine Learning Analysis Reveals PYGB as a Novel Immunohistochemical Biomarker to Distinguish Inverted Urothelial Papilloma From Low-Grade Papillary Urothelial Carcinoma With Inverted Growth***
Minsun Jung, Cheol Lee, Dohyun Han, Kwangsoo Kim, Sunah Yang, Ilias P. Nikas, Kyung Chul Moon, Hyeyoon Kim, Min Ji Song, Bohyun Kim, Hyebin Lee and Han Suk Ryu

140 ***Prognostic Role of Pretreatment C-Reactive Protein to Albumin Ratio in Urological Cancers: A Systematic Review and Meta-Analysis***
Minhong Wu, Yan Zhou, Qingsheng Chen, Zhiling Yu, Hongyong Gu, Pengxiu Lin, Yanling Li and Cailing Liu

149 ***Comprehensive Genomic Characterization of Tumor Microenvironment and Relevant Signature in Clear Cell Renal Cell Carcinoma***
Chuanjie Zhang, Feng Qi, Yuxiao Zheng, Xin Xia, Xiao Li and Xinwei Wang

163 ***Prognostic Significance of Pretreatment Neutrophil-to-Lymphocyte Ratio, Platelet–to–Lymphocyte Ratio, or Monocyte-to-Lymphocyte Ratio in Endometrial Neoplasms: A Systematic Review and Meta–analysis***
Jiali Leng, Fei Wu and Lihui Zhang

179 ***Liquid Biopsy Based Circulating Biomarkers in Metastatic Prostate Cancer***
Eshwari Dathathri, Khrystany T. Isebia, Fikri Abali, Martijn P. Lolkema, John W. M. Martens, Leon W. M. M. Terstappen and Ruchi Bansal

192 ***The Values of Systemic Immune-Inflammation Index and Neutrophil–Lymphocyte Ratio in Predicting Biochemical Recurrence in Patients With Localized Prostate Cancer After Radical Prostatectomy***
Shuo Wang, Xiao Yang, Ziyi Yu, Peng Du, Xinan Sheng, Yudong Cao, Xieqiao Yan, Jinchao Ma and Yong Yang

201 ***Preoperative Platelet Count Correlates With Postoperative Perineural Invasion on Specimen in Patients Treated With Radical Prostatectomy***
Fangming Wang, Fei Liu, Jing Liang, Feiya Yang and Nianzeng Xing

211 ***Urine Exosomal AMACR Is a Novel Biomarker for Prostate Cancer Detection at Initial Biopsy***
Xin Jin, Jin Ji, Decao Niu, Yuchen Yang, Shuchun Tao, Lilin Wan, Bin Xu, Shuqiu Chen, Fubo Wang and Ming Chen

220 ***Deep Learning-Based Multi-Omics Integration Robustly Predicts Relapse in Prostate Cancer***
Ziwei Wei, Dunsheng Han, Cong Zhang, Shiyu Wang, Jinke Liu, Fan Chao, Zhenyu Song and Gang Chen

236 ***New Diagnostic Model for Clinically Significant Prostate Cancer in Biopsy-Naïve Men With PIRADS 3***
Chen Huang, Feng Qiu, Di Jin, Xuedong Wei, Zongxin Chen, Ximing Wang, Xiaojun Zhao, Linchuan Guo, Jinxian Pu, Jianquan Hou and Yuhua Huang

244 ***Integrative Transcriptional Characterization of Cell Cycle Checkpoint Genes Promotes Clinical Management and Precision Medicine in Bladder Carcinoma***
Wei-Wei Shi, Jing-Zhi Guan, Ya-Ping Long, Qi Song, Qi Xiong, Bo-Yu Qin, Zhi-Qiang Ma, Yi Hu and Bo Yang

263 ***Integrated Molecular and Pharmacological Characterization of Patient-Derived Xenografts From Bladder and Ureteral Cancers Identifies New Potential Therapies***
Hervé Lang, Claire Béraud, Luc Cabel, Jacqueline Fontugne, Myriam Lassalle, Clémentine Krucker, Florent Dufour, Clarice S. Groeneveld, Victoria Dixon, Xiangyu Meng, Aurélie Kamoun, Elodie Chapeaublanc, Aurélien De Reynies, Xavier Gamé, Pascal Rischmann, Ivan Bieche, Julien Masliah-Planchon, Romane Beaurepere, Yves Allory, Véronique Lindner, Yolande Misseri, François Radvanyi, Philippe Lluel, Isabelle Bernard-Pierrot and Thierry Massfelder

279 **ASNS *Can Predict the Poor Prognosis of Clear Cell Renal Cell Carcinoma***
Xinqiang Gan, Ruiji Liu, Hong Cheng, Weipu Mao, Ninghan Feng and Ming Chen

293 ***Establishing a Prognostic Model of Ferroptosis- and Immune-Related Signatures in Kidney Cancer: A Study Based on TCGA and ICGC Databases***
Zhijun Han, Hao Wang, Jing Long, Yanning Qiu and Xiao-Liang Xing

frontiers | Frontiers in Oncology

TYPE Editorial
PUBLISHED 04 October 2022
DOI 10.3389/fonc.2022.1048736

Check for updates

OPEN ACCESS

EDITED AND REVIEWED BY
Ronald M Bukowski,
Cleveland Clinic, United States

*CORRESPONDENCE
Takeshi Yuasa
takeshi.yuasa@jfcr.or.jp

SPECIALTY SECTION
This article was submitted to Genitourinary Oncology, a section of the journal Frontiers in Oncology

RECEIVED 19 September 2022
ACCEPTED 20 September 2022
PUBLISHED 04 October 2022

CITATION
Yuasa T (2022) Editorial: Biomarkers in genitourinary cancers: Volume II. *Front. Oncol.* 12:1048736. doi: 10.3389/fonc.2022.1048736

COPYRIGHT
© 2022 Yuasa. This is an open-access article distributed under the terms of the Creative Commons Attribution License (CC BY). The use, distribution or reproduction in other forums is permitted, provided the original author(s) and the copyright owner(s) are credited and that the original publication in this journal is cited, in accordance with accepted academic practice. No use, distribution or reproduction is permitted which does not comply with these terms.

Editorial: Biomarkers in genitourinary cancers: Volume II

Takeshi Yuasa*

Department of Urology, Cancer Institute Hospital, Japanese Foundation for Cancer Research, Tokyo, Japan

KEYWORDS

biomarker, immune checkpoint inhibitor, prostate cancer, urothelial cancer, renal cell cancer

Editorial on the Research Topic
Biomarkers in genitourinary cancers: volume II

Genitourinary cancers, which consist of prostate, renal, urothelial, and testicular cancers, are some of the leading causes of global mortality (Yuasa et al.). Recently, various new technologies have been implemented in clinical practice, including robot-assisted surgery, intensity-modulated radiation therapy (IMRT), and radionuclide therapy. In addition, various anti-cancerous agents, such as antibody drug conjugates (ADCs), poly ADP-ribose polymerase (PARP) inhibitors, and immune checkpoint inhibitors, have been adopted in clinical practice (Yuasa et al.). Based on their promising anti-tumor efficacy and manageable safety profile, the paradigm of medical treatment for patients with urological malignancies is changing dramatically (Yuasa et al.). Biomarkers have grown increasingly essential in the consideration of treatment strategies.

In *Biomarkers in Genitourinary Cancers: Volume II*, various candidate biomarkers are reported. (Yang et al., Wang et al., Shi et al. Jin et al., Gan et al., Lang et al., van Laar et al.). Yang et al., Wang et al., and Shi et al. stressed the importance of circulating tumor cells (CTCs) and circulating endothelial cells (CECs), systemic inflammation markers, and the cell cycle checkpoint–related genes signature as biomarkers for bladder cancer, respectively. Jin et al. reported urine exosomal AMACR as a candidate biomarker for prostate cancer detection at biopsy. Gan et al. demonstrated that ASNS may play a significant role in the development and immune cell infiltration of clear cell renal cell cancer. In contrast, in order to explore effective therapeutic agents for individual cases, Lang et al. developed preclinical patient-derived xenograft (PDX) models that recapitulate the molecular heterogeneity of urothelial cancer, including actionable mutations. It is unknown whether these factors will advance in clinical practice or remain candidates forever.

Various factors contribute to the survival outcome of patients with malignant disease. Tumor biology and aggressiveness, which include Gleason score for prostate cancer, Fuhrman nuclear grade for renal cell cancer, and tumor grade for urothelial cancer, have been major prognostic factors in clinical practice. Another important factor related to outcome is treatment efficacy and resistance. Indeed, van Laar et al. reported the

alteration of treatment patterns and outcomes of metastatic RCC patients in the Netherlands (van Laar et al.). This factor depends on the treatment agent and may vary from day to day. In metastatic renal cell cancer, the sarcomatoid variant and high expression of PD-L1 were associated with poor outcome (1, 2). The introduction of immune checkpoint inhibitors may change this scenario (3–5). The biomarkers in this category may change as a result of revised therapeutic strategy. As such, the continued exploration of treatment-related biomarkers is important.

Author contributions

TY contributed to conception and design of the study, wrote the first draft of the manuscript, and read, and approved the submitted version.

Conflict of interest

The author declares that the research was conducted in the absence of any commercial or financial relationships that could be construed as a potential conflict of interest.

Publisher's note

All claims expressed in this article are solely those of the authors and do not necessarily represent those of their affiliated organizations, or those of the publisher, the editors and the reviewers. Any product that may be evaluated in this article, or claim that may be made by its manufacturer, is not guaranteed or endorsed by the publisher.

References

1. Fujiwara R, Kageyama S, Yuasa T. Developments in personalized therapy for metastatic renal cell carcinoma. *Expert Rev Anticancer Ther* (2022) 11:1–9. doi: 10.1080/14737140.2022.2075347

2. Thompson RH, Dong H, Kwon ED. Implications of B7-H1 expression in clear cell carcinoma of the kidney for prognostication and therapy. *Clin Cancer Res* (2007) 13:709s–15s. doi: 10.1158/1078-0432.CCR-06-1868

3. Tannir NM, Signoretti S, Choueiri TK, McDermott DF, Motzer RJ, Flaifel A, et al. Efficacy and safety of nivolumab plus ipilimumab versus sunitinib in first-line treatment of patients with advanced sarcomatoid renal cell carcinoma. *Clin Cancer Res* (2021) 27(1):78–86. doi: 10.1158/1078-0432.CCR-20-2063

4. Quhal F, Mori K, Bruchbacher A, Resch I, Mostafaei H, Pradere B, et al. First-line immunotherapy-based combinations for metastatic renal cell carcinoma: A systematic review and network meta-analysis. *Eur Urol Oncol* (2021) 4(5):755–65. doi: 10.1016/j.euo.2021.03.001

5. Taube JM, Klein A, Brahmer JR, Xu H, Pan X, Kim JH, et al. Association of PD-1, PD-1 ligands, and other features of the tumor immune microenvironment with response to anti-PD-1 therapy. *Clin Cancer Res* (2014) 20:5064–74. doi: 10.1158/1078-0432.CCR-13-3271

frontiers in Oncology

ORIGINAL RESEARCH
published: 13 January 2022
doi: 10.3389/fonc.2021.762629

Decreased Expression of ACADSB Predicts Poor Prognosis in Clear Cell Renal Cell Carcinoma

Xianhui Liu[1], *Weiyu Zhang*[1], *Huanrui Wang*[2], *Lin Zhu*[1] *and Kexin Xu*[1]*

[1] *Department of Urology, Peking University People's Hospital, Beijing, China,* [2] *Peking University Applied Lithotripsy Institute, Peking University People's Hospital, Beijing, China*

OPEN ACCESS

Edited by:
Michele Marchioni, University of Studies G. d'Annunzio Chieti and Pescara, Italy

Reviewed by:
Hailong Ruan, Huazhong University of Science and Technology, China
Jiawu Wang, First Affiliated Hospital of Chongqing Medical University, China

***Correspondence:**
Kexin Xu
cavinx@yeah.net

Specialty section:
This article was submitted to Genitourinary Oncology, a section of the journal Frontiers in Oncology

Received: *22 August 2021*
Accepted: *20 December 2021*
Published: *13 January 2022*

Citation:
Liu X, Zhang W, Wang H, Zhu L and Xu K (2022) Decreased Expression of ACADSB Predicts Poor Prognosis in Clear Cell Renal Cell Carcinoma. Front. Oncol. 11:762629. doi: 10.3389/fonc.2021.762629

Background: Previous reports have shown that short/branched chain acyl-CoA dehydrogenase (ACADSB) plays an important role in glioma, but its role in clear cell renal carcinoma (ccRCC) has not been reported.

Methods: The TIMER and UALCAN databases were used for pan-cancer analysis. RNA sequencing and microarray data of patients with ccRCC were downloaded from the Cancer Genome Atlas and Gene Expression Omnibus database. The differential expression of ACADSB in ccRCC and normal kidney tissues was tested. Correlations between ACADSB expression and clinicopathological parameters were assessed using the Wilcoxon test. The influences of ACADSB expression and clinicopathological parameters on overall survival were assessed using Cox proportional hazards models. Gene set enrichment analysis (GSEA) was performed to explore the associated gene sets enriched in different ACADSB expression phenotypes. Gene ontology (GO) and Kyoto Encyclopedia of Genes and Genomes (KEGG) pathway enrichment analyses were performed on genes with similar expression patterns to ACADSB. Correlations between ACADSB and ferroptosis-related genes were assessed using Spearman's correlation analysis.

Results: Pan-cancer analysis revealed that ACADSB is down-regulated in multiple cancers, and decreased expression of ACADSB correlates with poor prognosis in certain types of cancer. Differential expression analyses revealed that ACADSB was down-regulated in ccRCC, indicating that ACADSB expression could be a single significant parameter to discriminate between normal and tumor tissues. Clinical association analysis indicated that decreased ACADSB expression was associated with high tumor stage and grade. The Cox regression model indicated that low ACADSB expression was an independent risk factor for the overall survival of patients with ccRCC. GSEA showed that 10 gene sets, including fatty acid (FA) metabolism, were differentially enriched in the ACADSB high expression phenotype. GO and KEGG pathway enrichment

analysis revealed that ACADSB-related genes were significantly enriched in categories related to FA metabolism, branched-chain amino acid (BCAA) metabolism, and iron regulation. Spearman's correlation analysis suggested that the expression of ACADSB was positively correlated with the expression of ferroptosis driver genes.

Conclusions: ACADSB showed good diagnostic and prognostic abilities for ccRCC. The downregulation of ACADSB might promote tumorigenesis and tumor progression by inhibiting FA catabolism, BCAA catabolism, and ferroptosis in ccRCC.

Keywords: renal cancer, ACADSB, prognosis, biomarker, TCGA

INTRODUCTION

Short/branched chain acyl-CoA dehydrogenase (ACADSB) is a member of the acyl-CoA dehydrogenase family of enzymes, which is involved in the metabolism of fatty acids (FAs) and branch-chained amino acids (BCAAs) (1). Previous studies have revealed that ACADSB plays an important role in glioma, colorectal cancer (CRC), and hepatocellular carcinoma (HCC) (2–5). However, the role of ACADSB in clear cell renal cell carcinoma (ccRCC) has not yet been reported.

CcRCC is the most common and aggressive type of renal cell carcinoma (RCC), which accounts for approximately 3% of all cancers and is the third most common malignancy of the urinary system (6, 7). Worldwide, there were an estimated 403,000 new cases of RCC and 175,000 deaths due to kidney cancer in 2020 (8). Among solid tumors, ccRCC is one of the most resistant to conventional chemotherapy and radiotherapy. Targeted therapy and immune checkpoint inhibitor-based immunotherapy have substantially improved the outcomes of patients with advanced ccRCC over the past decade. However, the identification of novel diagnostic markers and therapeutic targets remains a high priority. The aim of this study was to explore the potential diagnostic and prognostic roles of ACADSB in ccRCC.

MATERIALS AND METHODS

Pan-Cancer Analysis

The tumor immune estimation resource database (TIMER; https://cistrome.shinyapps.io/timer/) (9) and the UALCAN database (http://ualcan.path.uab.edu/index.html) (10) were used for the differential expression analysis of ACADSB between tumor tissues and corresponding normal tissues. TIMER was also applied to explore the association between ACADSB expression and overall survival (OS) in different types of cancers.

Collection of ccRCC Datasets

The RNA sequencing (RNA-seq) data and clinical information of patients with ccRCC (TCGA-KIRC) were downloaded from The Cancer Genome Atlas (TCGA) using the "TCGAbiolinks" R package (11). Only patients with both RNA-seq data and valid clinical information were included in this study, and duplicated samples were excluded. The expression profiling microarray data of GSE36895 (with 29 ccRCC samples and 23 adjacent normal samples) and GSE53757 (with 72 paired ccRCC and adjacent normal samples) were downloaded from Gene Expression Omnibus (GEO) using the "GEOquery" R package (12).

Immunohistochemistry (IHC)

A tissue chip with 90 pairs of ccRCC and corresponding normal tissues was purchased from Outdo Biotech Co., Ltd. (HKidE180Su03, Shanghai, China). The experiment received ethical approval for sample use from Shanghai Outdo Biotech Co., Ltd. (Barcode: YB M-05-02). IHC was performed on tissues fixed with formaldehyde and embedded in paraffin wax. After deparaffinization and rehydration, the endogenous peroxidase activity was blocked and antigen retrieval was performed. The ACADSB antibody (13122-1-AP, 1:12000; Proteintech, CA) was incubated overnight at 4°C. After careful washing and incubation with the specified horseradish peroxidase (HRP)-conjugated secondary antibody, ACADSB expression was detected using 3,3N- diaminobenzidine tetrahydrochloride (DAB).

The intensity and extent of ACADSB staining were evaluated by two experienced pathologists. The method for calculating the score of ACADSB staining was as follows: the extent of staining in an ×200 field was scored as 0, 0%; 1, 1–25%; 2, 26–50%; and 3, 51–100%. The intensity of staining was scored as 0, no signal; 1, light brown; 2, brown; and 3, dark brown. The final score of each field was the average obtained from the two pathologists by multiplying the extent score by the intent score. The scores of ACADSB staining were categorized as follows: low expression (−/+) for scores 0–1 (−) and 2–3 (+) and high expression (++/+++) for scores 4–6 (++) and 7–9 (+++). All evaluations were performed using a Leica DM4000 M microscope.

Gene Set Enrichment Analysis

Gene-set enrichment analysis (GSEA) (13) was performed with the GSEA software (version 4.0.3). Samples from TCGA were divided into two groups based on the expression of ACADSB. The Broad Molecular Signatures Database (MSigDB v6.0) (14) set H (hallmark gene sets, 50 gene sets) were used, which summarize and represent specific well-defined biological states and pathway processes. Enrichment analysis was performed by default weighted enrichment statistics, with the random combinatorial count set as 1,000. Gene sets were judged as

significantly enriched by P<0.05 as well as false discovery rates (FDR) < 0.25.

Correlation, GO and KEGG Pathway Analysis

The genes which had greater than 0.4 Spearman correlation coefficient with ACADSB in expression level were defined as ACADSB-related genes. To explore the functional annotation and involved pathways of ACADSB-related genes, the gene ontology (GO) and Kyoto Encyclopedia of Genes and Genomes (KEGG) pathway enrichment analyses were executed *via* the "clusterprofiler" package (15).

Statistical Analysis

All statistical analyses were performed in R version 4.1.0. For RNA-seq data, raw counts data were used for differential expression analysis *via* the "DESeq2" package (16). Fragments per kilobase million (FPKM) values were converted to Transcripts per million (TPM) and log2 transformed for further analysis. For microarray data, differential expression analysis was performed using the "limma" package (17). Genes with an adjusted p value of less than 0.05 and fold change (FC) greater than 2 were regarded as differentially expressed genes (DEGs). The receiver operating characteristic (ROC) curves were plotted and areas under the curve (AUC) were calculated to investigate the diagnostic performance of ACADSB. Patients were stratified into low or high groups based on ACADSB expression, using the median expression as the cut-off value. The relationships between clinical pathologic characteristics and ACADSB expression were analyzed with Chi-squared test or Wilcoxon test. Univariate and multivariate Cox proportional hazards models were used to compare the influence of ACADSB expression on OS along with other clinicopathological parameters. P< 0.05 was considered to indicate a statistically significant difference.

RESULTS

ACADSB Is Down-Regulated in Multiple Cancers and Decreased Expression of ACADSB Correlates With Poor Prognosis in Certain Types of Cancers

Differential expression analysis using TIMER showed that ACADSB is down-regulated in multiple types of cancer, including bladder cancer (BLCA), breast cancer (BRCA), cholangiocarcinoma (CHOL), colon adenocarcinoma (COAD), esophageal carcinoma (ESCA), head and neck squamous cell carcinoma (HNSC), kidney chromophobe (KICH), kidney renal clear cell carcinoma (KIRC), kidney renal papillary cell carcinoma (KIRP), liver hepatocellular carcinoma (LIHC), lung adenocarcinoma (LUAD), lung squamous cell carcinoma (LUSC), rectum adenocarcinoma (READ), stomach adenocarcinoma (STAD), thyroid carcinoma (THCA), and uterine corpus endometrial carcinoma (UCEC; **Figure 1A**). Proteome data derived from the UALCAN database also suggest that ACADSB is down-regulated in breast cancer, colon cancer, ccRCC, and UCEC (**Figure 1B**). In addition, Kaplan–Meier analysis indicated that low expression of ACADSB is associated with poor prognosis in BRCA luminal subtype, COAD, KIRC, brain lower grade glioma (LGG), and mesothelioma (MESO) (**Figures 1C–E** and **Supplementary Figures 1A, B**).

ACADSB Is Down-Regulated in Different ccRCC Datasets

Transcript differential expression analysis using DESeq2 revealed that ACADSB was significantly down-regulated in ccRCC tissues compared with normal kidney tissues in TCGA-KIRC (log2FC = -2.0, FDR < 0.001; **Figure 2A**), GSE36895 (log2FC = -1.7, FDR < 0.001; **Figure 2B**), and GSE53757 (log2FC = -2.2, FDR < 0.001; **Figure 2C**). Further, ROC analyses showed that ACADSB expression could be a single significant parameter for discriminating between normal and tumor tissues in TCGA-KIRC (AUC = 0.952, 95% CI = 0.926–0.977, **Figure 2D**), GSE36895 (AUC = 0.931, 95% CI = 0.862–1.0, **Figure 2E**), and GSE53757 (AUC = 0.966, 95% CI = 0.935–0.998, **Figure 2F**). A total of 84 paired tumor–normal samples were included in the IHC analysis, with six pairs of samples excluded due to slices escaping from the glass slide. For normal kidney tissues, most samples (75/84, 89.3%) showed high ACADSB expression, while all ccRCC samples (84/84, 100%) showed low ACADSB expression (**Figure 2G**). Typical pictures of staining in paired tumor and normal samples are shown in **Figures 2H, I**.

Clinical Characteristics of Patients With ccRCC in the TCGA-KIRC Cohort

In the TCGA-KIRC cohort, there're 530 cases with both RNA-seq data and clinical information. Four duplicated cases and 4 cases whose overall survival time was 0 days were excluded. Therefore, a total of 522 patients with both RNA-seq data and valid survival information were included in this study. The detailed clinical characteristics are listed in **Table 1**. Patients were divided into a high expression group and a low expression group based on ACADSB expression. Among the 522 participants, 341 (65.3%) were men and 181 (34.7%) were women, with a median age of 61 years at the time of initial diagnosis; 315 (60.7%) patients had stage I or stage II disease pathology, and 204 (39.3%) patients had stage III or stage IV disease pathology. Regarding histological grade, 236 (45.9%) patients were categorized into grade 1 or grade 2, and 278 (54.1%) patients were categorized into grade 3 or grade 4. Follow-up duration was 40 months on average (range, 0.1–151.2 months). At the time of the last follow-up, 344 (68.9%) patients were tumor-free, while 155 (31.1%) patients still had tumors.

Association Between ACADSB Expression and Clinicopathological Characteristics

The relationship between ACADSB expression and clinicopathological characteristics is shown in **Figure 3**. ACADSB expression was significantly associated with pathological T stage (T1-2 vs. T3-4, P< 0.001; **Figure 3A**), pathological N stage (N0 vs. N1, P< 0.01; **Figure 3B**), pathological M stage (M0 vs. M1, P< 0.001;

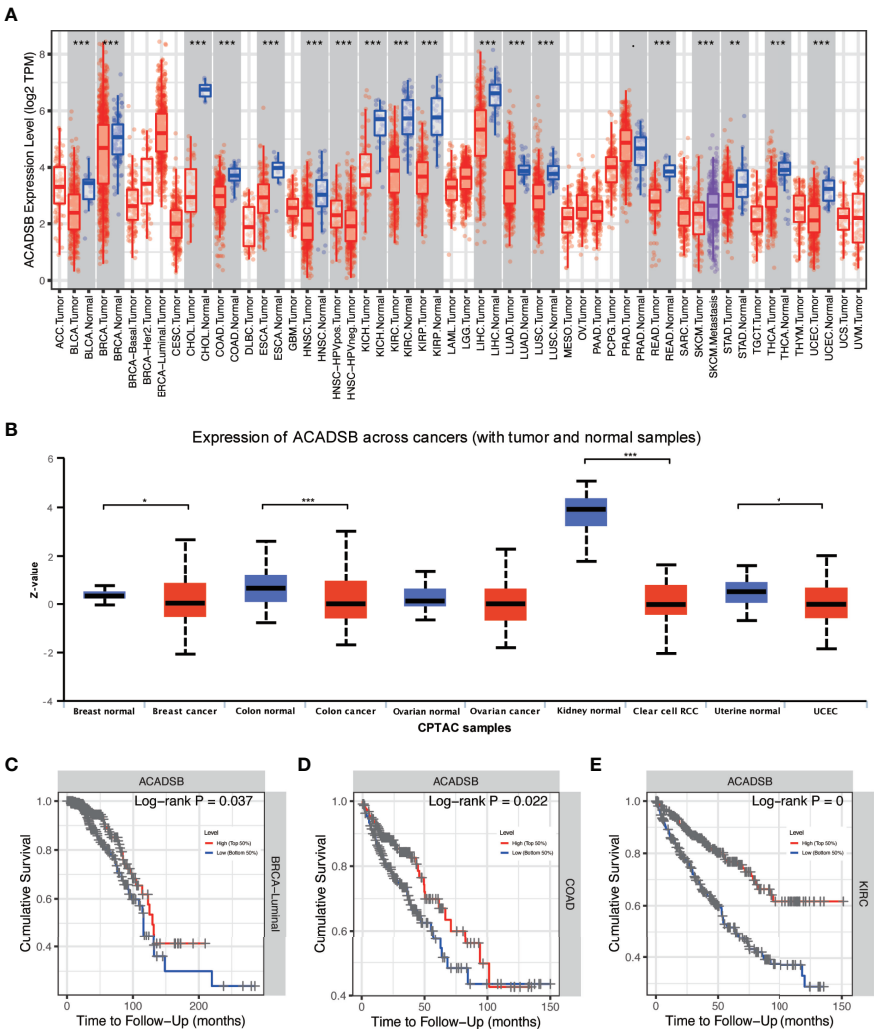


FIGURE 1 | Pan-cancer analysis of ACADSB. **(A)** Differential expressions of ACADSB in TCGA. **(B)** Differential expressions of ACADSB in UALCAN. Overall survivals comparison between high and low ACADSB groups in **(C)** BRCA-luminal subtype, **(D)** COAD, and **(E)** KIRC *p< 0.05; **p<0.01; ***p<0.001.

Figure 3C), pathological stage (stage I-II vs. stage III-IV, P< 0.001; **Figure 3D**), tumor grade (grades 1–2 vs. grades 3–4, P< 0.001; **Figure 3E**), tumor status (tumor free vs. with tumor, P< 0.001; **Figure 3F**), and sex (P< 0.01; **Figure 3G**). The differences between groups stratified by age (<65 years vs. ≥65 years; **Figure 3H**) and race (white vs. black or African American vs. Asian; **Figure 3I**) did not attain statistical significance.

Survival Outcomes and Cox Regression Analysis

Kaplan–Meier survival analysis showed that lower ACADSB expression was associated with a worse prognosis (P< 0.001; **Figure 1E**). The univariate Cox regression model revealed that age at diagnosis (HR = 1.03, 95% CI = 1.017–1.044, P< 0.001), pathological stage (HR = 3.927, 95% CI = 2.847–5.417, P< 0.001), histological grade (HR = 2.679, 95% CI = 1.895–3.787, P< 0.001), and ACADSB expression (HR = 0.421, 95% CI = 0.331–0.535, P< 0.001) were associated with the OS of patients with ccRCC. Multivariate Cox regression after adjustment indicated that age at diagnosis (HR = 1.027, 95% CI = 1.013–1.042, P< 0.001), pathological stage (HR = 2.695, 95% CI = 1.877–3.765, P< 0.001), histological grade (HR = 1.639, 95% CI = 1.137–2.364, P< 0.01), and ACADSB expression (HR = 0.577, 95% CI = 0.446–0.746, P< 0.001) were independent prognostic factors for OS in patients with ccRCC (**Figure 4** and **Supplementary Table 1**).

Gene Sets Enriched in the ACADSB High Expression Phenotype

In the hallmark dataset, 10 gene sets were significantly enriched in the ACADSB high expression phenotype, including TGF-β signaling, androgen response, UV response down, heme metabolism, bile acid metabolism, protein secretion, adipogenesis, FA metabolism, PI3K-AKT-mTOR signaling, and mitotic spindle (**Figure 5** and **Supplementary Figure 1C**).

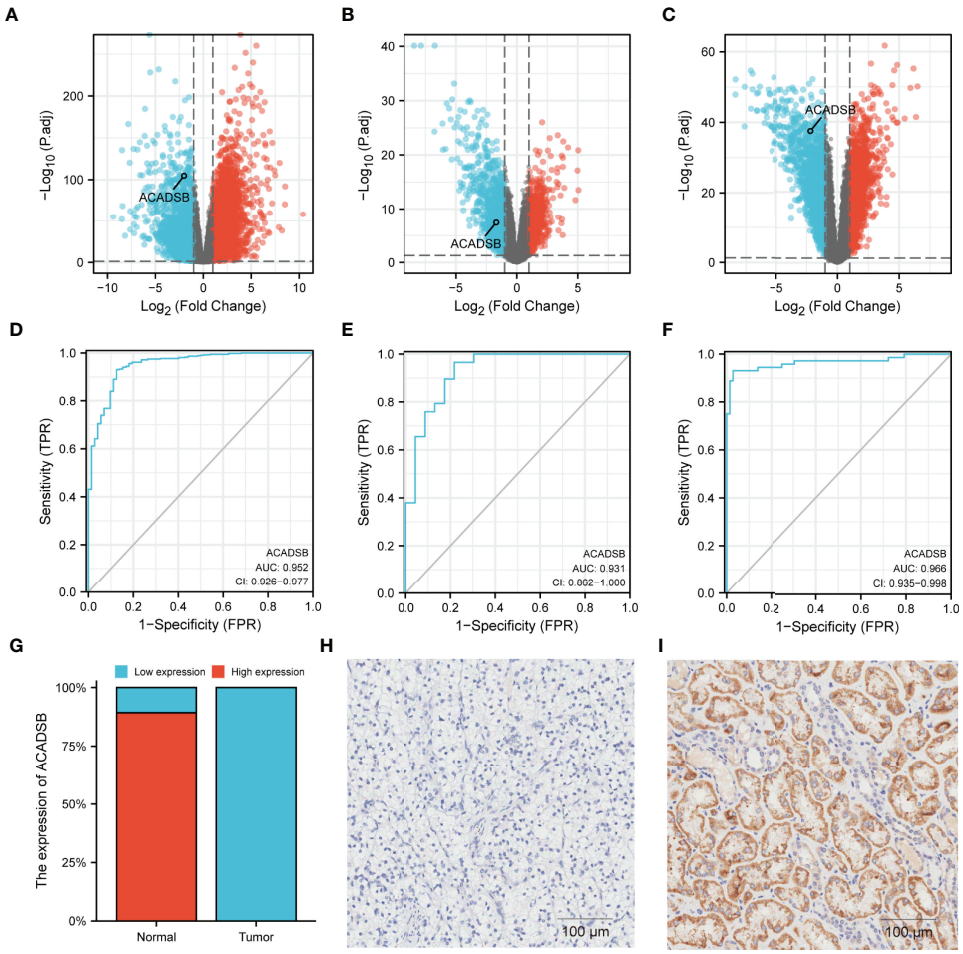


FIGURE 2 | Differential expressions of ACADSB in ccRCC datasets. Volcano plots showing the results of differential analyses in **(A)** TCGA-KIRC, **(B)** GSE36895, and **(C)** GSE53757. ROC curves showing the ability of ACADSB expression to discriminate between normal and tumor tissues in **(D)** TCGA-KIRC, **(E)** GSE36895, and **(F)** GSE53757. **(G)** The IHC result of ccRCC tissue microarray. Typical pictures of paired **(H)** tumor and **(I)** normal tissue.

GO and KEGG Analysis of ACADSB-Related Genes

In TCGA-KIRC, GSE36895, and GSE53757, 3093, 2111, and 594 respective genes had ACADSB expression with a Spearman correlation coefficient of >0.4. Two hundred and fourteen genes representing the intersection between all three datasets were defined as ACADSB-related genes (**Figure 6A**). At a false discovery rate (FDR) of 0.05, 47 GO biological processes, 13 GO cellular components, 14 GO molecular functions, and 15 KEGG pathways were significantly enriched for these genes (**Figure 6B** and **Supplementary Table 2**).

ACADSB Expression Was Associated With the Expression of Ferroptosis-Related Genes

Ferroptosis-related genes were derived from the FerrDb database (18). A total of 108 genes were identified as ferroptosis driver genes. Correlation analysis revealed that the expression of ACADSB was significantly positively correlated with the expression of 62 ferroptosis diver genes in the TCGA-KIRC dataset (**Figure 6C**). Similar results were found in GSE36895 and GSE53757 (**Supplementary Figure 1D, E**).

DISCUSSION

ACADSB is a member of the acyl-CoA dehydrogenase family of enzymes that catalyze the dehydrogenation of acyl-CoA derivatives in the metabolism of FAs and BCAAs (1). ACADSB is widely known to be associated with ACADSB deficiency (SBCADD), an autosomal recessive disorder characterized by seizures and psychomotor delay due to a defect in the catabolism of L-isoleucine (19, 20).

Recent studies have found that ACADSB plays an important role in the development and progression of malignant diseases, such as glioma (2), colorectal cancer (3), and hepatocellular carcinoma (HCC) (4, 5). Yu et al. (2) reported that ACADSB is

TABLE 1 | Clinical characteristics of patients with ccRCC in TCGA.

Characteristic	Low expression	High expression	p
N	261	261	
Sex, n (%)			0.066
Female	80 (15.3%)	101 (19.3%)	
Male	181 (34.7%)	160 (30.7%)	
Pathological T stage, n (%)			< 0.001
T1-2	138 (26.4%)	195 (37.4%)	
T3-4	123 (23.6%)	66 (12.6%)	
Pathological N stage, n (%)			0.057
N0	112 (44.1%)	126 (49.6%)	
N1	12 (4.7%)	4 (1.6%)	
Pathological M stage, n (%)			< 0.001
M0	188 (38.2%)	226 (45.9%)	
M1	53 (10.8%)	25 (5.1%)	
Pathological stage, n (%)			< 0.001
Stage I-II	125 (24.1%)	190 (36.6%)	
Stage III-IV	133 (25.6%)	71 (13.7%)	
Histological grade, n (%)			< 0.001
G1-2	91 (17.7%)	145 (28.2%)	
G3-4	169 (32.9%)	109 (21.2%)	
Tumor status, n (%)			< 0.001
Tumor free	138 (27.7%)	206 (41.3%)	
With tumor	112 (22.4%)	43 (8.6%)	
Age, median (IQR)	61 (53, 70)	60 (51, 69)	0.423

ccRCC, clear cell renal cell carcinoma; TCGA, The Cancer Genome Atlas; IQR, interquartile range.

lowly expressed in high-grade gliomas, and the lower expression of ACADSB may lead to the accumulation of short-chain acylcarnitines, which further facilitates the growth and progression of gliomas. Di et al. (3) reported that ACADSB is down-regulated in CRC, and its expression is positively correlated with the OS of patients with CRC. Their study also indicated that overexpression of ACADSB inhibits CRC cell proliferation, migration, and invasion, while knockdown of ACADSB has the opposite effect. Similar results were also found in HCC, in which the restoration of ACADSB expression caused mTORC1 activity and cell proliferation to significantly decrease (4). In this study, we first explored the expression levels of ACADSB in different types of cancer using independent datasets from TCGA and UALCAN. The downregulation of ACADSB was observed in almost all types of common cancer. Moreover, low expression levels of ACADSB also correlate with a poorer prognosis in many types of cancers, such as COAD, LGG, and ccRCC. Previous studies have reported the important role of ACADSB in COAD and LGG; however, it has not been reported in ccRCC. Thus, we focused on the role of ACADSB in ccRCC.

The differential expression analyses were performed in three independent datasets, and consistent results were obtained, indicating that ACADSB is down-regulated in ccRCC, and that ACADSB expression can be a single significant parameter to discriminate between normal and tumor tissues. The IHC results further validated the downregulation of ACADSB in ccRCC. We next investigated the correlation between ACADSB expression and the clinicopathological characteristics of patients with ccRCC using TCGA-KIRC data. Results showed that the level of ACADSB expression was negatively correlated with tumor stage and tumor grade; results also showed that ACADSB expression was an independent prognostic factor for OS independent of conventional prognostic factors, such as age at diagnosis, tumor stage, and tumor grade. These findings indicate an integral role of ACADSB in the underlying biological mechanisms of tumor development and progression of ccRCC.

To further investigate the potential functions of ACADSB in ccRCC, we conducted GSEA, GO, and KEGG analyses. The results of GSEA showed that 10 gene sets in the hallmark dataset, including FA metabolism, bile acid metabolism, heme metabolism, and adipogenesis, were differentially enriched in the ACADSB high expression phenotype. GO and KEGG enrichment analysis indicated that ACADSB-related genes were enriched in the regulation of FA degeneration and BCAA degeneration. Lip metabolism plays a critical role in the development and progression of renal cancer, and ccRCC is histologically defined by its lipid-and glycogen-rich cytoplasmic deposits (21). The tumorigenic role of lipid accumulation has been observed in many types of cancer (22, 23). ACADSB is known to regulate FA catabolism by catalyzing the dehydrogenation of acyl-CoA derivatives (1). Thus, the downregulation of ACADSB may contribute to tumor development by suppressing FA catabolism, resulting in lipid accumulation in ccRCC.

In addition to regulating FA catabolism, ACADSB also catalyzes the dehydrogenation of acyl-CoA derivatives in the metabolism of BCAAs. BCAA metabolism can influence multiple cancer phenotypes and serve as a marker of disease pathology (24). Previous studies have demonstrated that BCAA catabolism is reduced in many types of cancers, such as HCC (4), ccRCC (22), and breast cancer (25). Ericksen et al. (4) found that suppression of BCAA catabolic enzyme expression led to BCAA accumulation in liver tumors and that progressive loss of BCAA catabolism promoted tumor development and growth. Qu et al.

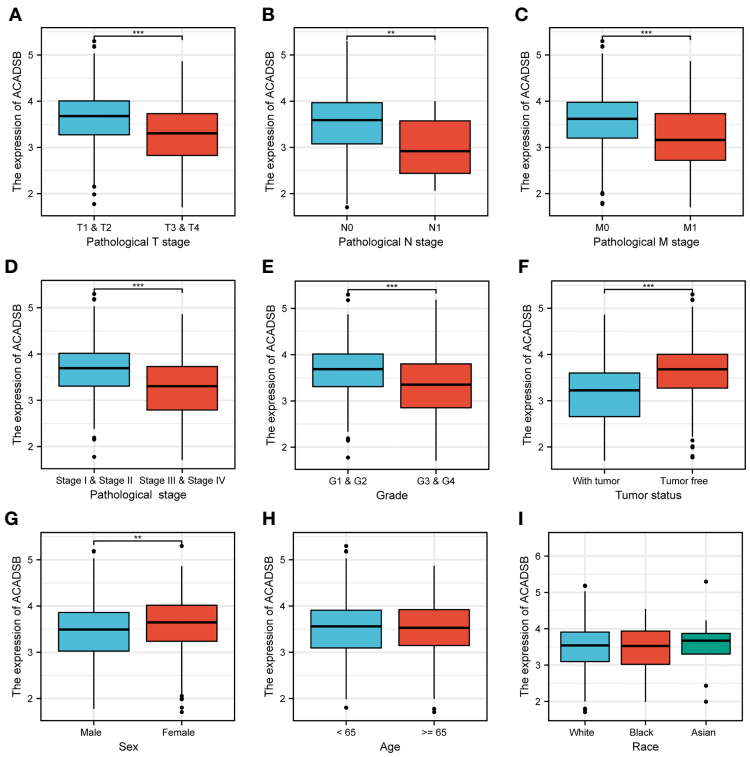


FIGURE 3 | The correlation between ACADSB expression and clinicopathological characteristics. **(A)** Pathological T stage. **(B)** Pathological N stage. **(C)** Pathological M stage. **(D)** Pathological stage. **(E)** Tumor grade. **(F)** Tumor status. **(G)** Sex. **(H)** Age. **(I)** Race *p< 0.05; **p<0.01; ***p<0.001.

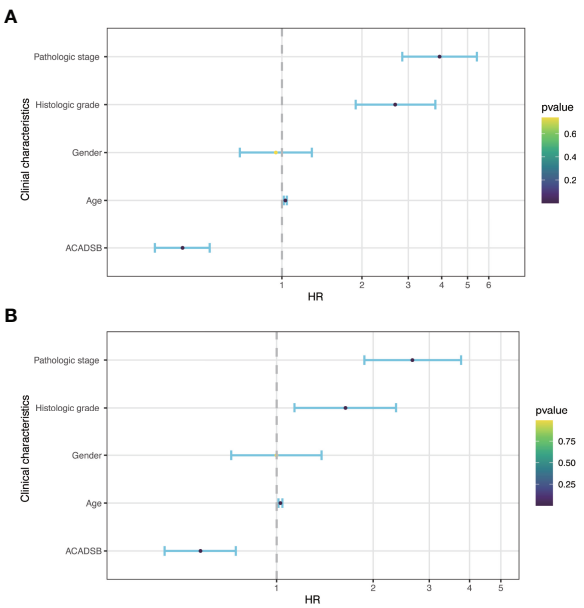


FIGURE 4 | Forest plot of hazard ratios derived from Cox model. **(A)** Univariate analysis. **(B)** Multivariate analysis.

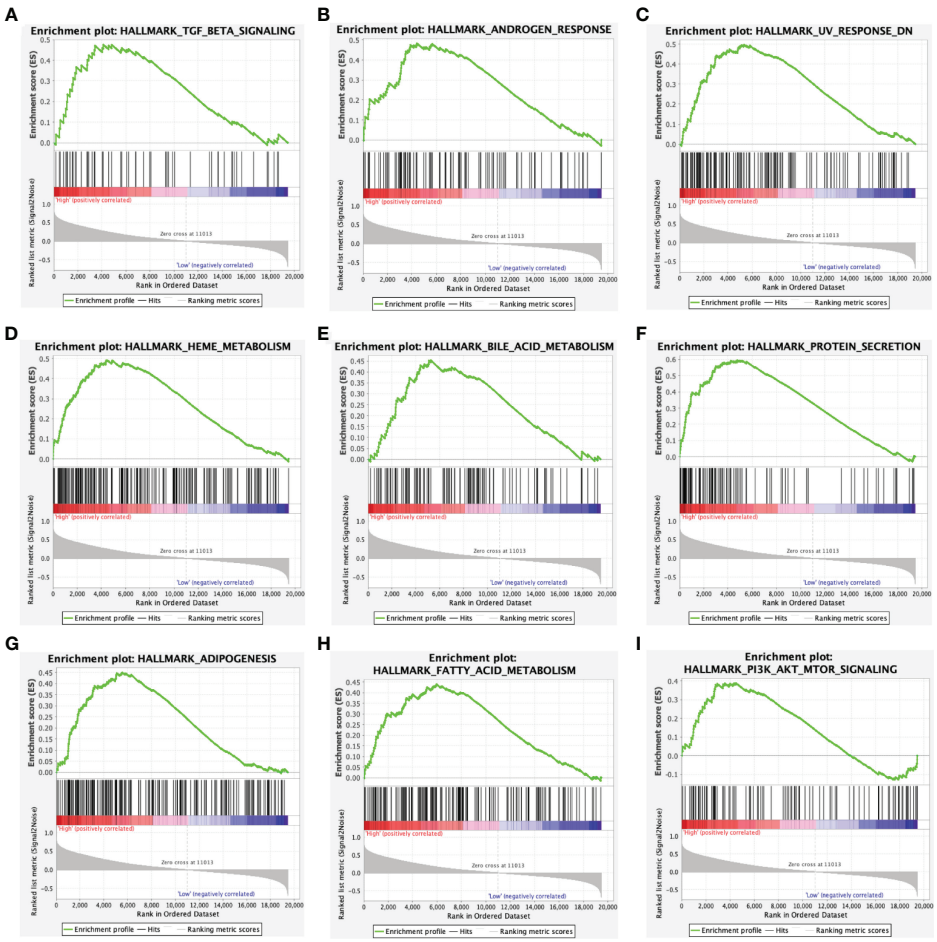


FIGURE 5 | Enrichment plots from gene set enrichment analysis. Gene sets enriched in ACADSB high phenotype: **(A)** TGF-β signaling. **(B)** Androgen response. **(C)** UV response down. **(D)** Heme metabolism. **(E)** Bile acid metabolism. **(F)** Protein secretion. **(G)** Adipogenesis. **(H)** Fatty acid metabolism. **(I)** PI3K-AKT-mTOR signaling.

(22) reported that BCAA accumulation in ccRCC induced the activation of mTORC1 and *de novo* FA synthesis and promoted cell proliferation. Therefore, the downregulation of ACADSB may also promote tumor development and growth by inhibiting BCAA catabolism.

Lipid metabolism is important for ferroptosis, an iron-dependent form of regulated cell death (RCD) that is driven by the lethal accumulation of lipid peroxidation (26, 27) and plays a key role in tumor suppression (28). In contrast, the glutathione peroxidase 4 (GPX4)/glutathione (GSH) antioxidation system acts as an endogenous antioxidant pathway to suppress ferroptosis (29, 30). Reduced FA metabolism due to inhibition of β-oxidation renders renal cancer cells highly dependent on the GPX4/GSH pathway to prevent lipid peroxidation and ferroptosis (31). Lu et al. (3) found that overexpression of ACADSB enhanced the concentrations of Fe+ and lipid peroxidation but reduced the concentration of GSH and the expression of GPX4 in CRC cell lines, suggesting a potential regulatory effect of ACADSB on CRC cell ferroptosis. In this study, GSEA indicated that FA metabolism and heme metabolism were enriched in the high-ACADSB phenotype, GO analysis revealed that ACADSB-related genes are enriched in the molecular function of metal cluster binding and iron-sulfur cluster binding, and KEGG analysis revealed that ACADSB-related genes are enriched in the peroxisome pathway. Taken together, these findings indicate the potential regulatory effect of ACADSB on ferroptosis in ccRCC.

Ferroptosis-related genes can be classified as either ferroptosis driver genes that promote ferroptosis or ferroptosis suppressor genes that prevent ferroptosis (18). Correlation analysis revealed that the expression of ACADSB was significantly positively correlated with the expression of ferroptosis driver genes, including PRKAA1, PRKAA2, and NCOA4. Song et al. (32) demonstrated that the inhibition of PRKAA1/AMPKα1 or PRKAA2/AMPKα2 by siRNA diminished erastin-induced BECN1 phosphorylation at S93/96, BECN1-SLC7A11 complex formation, and subsequent ferroptosis. Hou et al. (33) revealed that

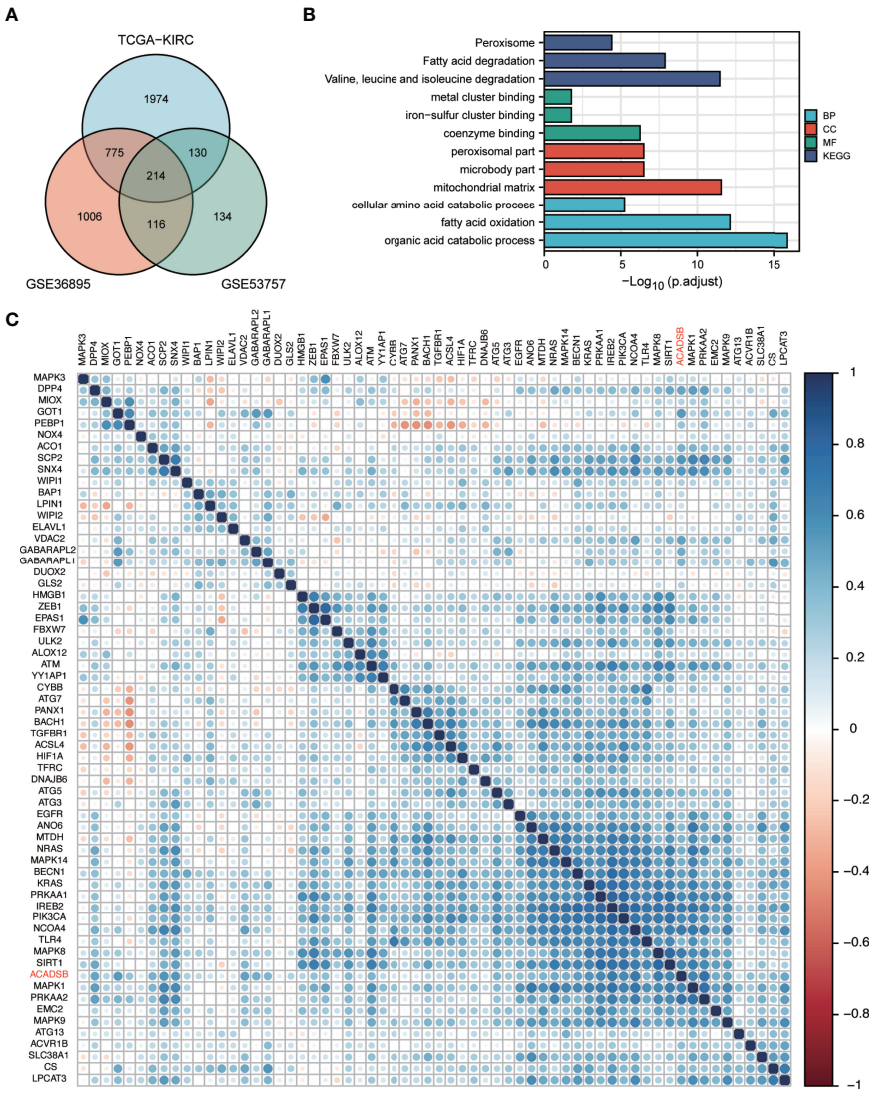


FIGURE 6 | GO and KEGG enrichment analyses of ACADSB-related genes and correlation between ACADSB with ferroptosis-related genes. **(A)** Identification of ACADSB-related genes. **(B)** GO and KEGG enrichment analyses of ACADSB-related genes. **(C)** Heatmap shows the correlation between ACADSB and ferroptosis driver gens.

the genetic inhibition of NCOA4 inhibited ferritin degradation and suppressed ferroptosis. Taken together, ACADSB might also be a potential ferroptosis driver gene, and the downregulation of ACADSB in ccRCC may promote tumor progression by suppressing ferroptosis.

In conclusion, ACADSB is down-regulated in multiple types of cancers and shows good diagnostic and prognostic abilities in ccRCC. Bioinformatic analyses revealed that ACADSB might affect the development and progression of ccRCC by regulating FA catabolism, BCAA catabolism, and ferroptosis. These findings may offer new therapeutic approaches for the clinical treatment and prognostic assessment of ccRCC. However, there were some limitations to this study. This study was mainly conducted using data from the public databases, and the potential regulations between ACADSB and ferroptosis in ccRCC were analyzed by correlation analysis, which needs to be further elucidated by molecular experiments.

DATA AVAILABILITY STATEMENT

Publicly available datasets were analyzed in this study. This data can be found here: https://portal.gdc.cancer.gov/, https://www.ncbi.nlm.nih.gov/geo/query/acc.cgi?acc=GSE36895, https://www.ncbi.nlm.nih.gov/geo/query/acc.cgi?acc=GSE53757.

ETHICS STATEMENT

The studies involving human participants were reviewed and approved by Ethics Committee of Shanghai Outdo Biotech

Company Limited. Written informed consent for participation was not required for this study in accordance with the national legislation and the institutional requirements.

AUTHOR CONTRIBUTIONS

KX and XL conceived the manuscript. XL and WZ designed and wrote the manuscript. HW and LZ helped with the bioinformatic analyses. All authors contributed to the article and approved the submitted version.

FUNDING

The present study was supported by the National Natural Science Foundation of China (NO. 81970660) from KX.

SUPPLEMENTARY MATERIAL

The Supplementary Material for this article can be found online at: https://www.frontiersin.org/articles/10.3389/fonc.2021.762629/full#supplementary-material

REFERENCES

1. Rozen R, Vockley J, Zhou L, Milos R, Willard J, Fu K, et al. Isolation and Expression of a cDNA Encoding the Precursor for a Novel Member (ACADSB) of the Acyl-CoA Dehydrogenase Gene Family. *Genomics* (1994) 24(2):280–7. doi: 10.1006/geno.1994.1617
2. Yu D, Xuan Q, Zhang C, Hu C, Li Y, Zhao X, et al. Metabolic Alterations Related to Glioma Grading Based on Metabolomics and Lipidomics Analyses. *Metabolites* (2020) 10(12):478. doi: 10.3390/metabo10120478
3. Lu D, Yang Z, Xia Q, Gao S, Sun S, Luo X, et al. ACADSB Regulates Ferroptosis and Affects the Migration, Invasion, and Proliferation of Colorectal Cancer Cells. *Cell Biol Int* (2020) 44(11):2334–43. doi: 10.1002/cbin.11443
4. Ericksen RE, Lim SL, McDonnell E, Shuen WH, Vadiveloo M, White PJ, et al. Loss of BCAA Catabolism During Carcinogenesis Enhances Mtorc1 Activity and Promotes Tumor Development and Progression. *Cell Metab* (2019) 29 (5):1151–65.e6. doi: 10.1016/j.cmet.2018.12.020
5. Sun R, Xu Y, Zhang H, Yang Q, Wang K, Shi Y, et al. Mechanistic Modeling of Gene Regulation and Metabolism Identifies Potential Targets for Hepatocellular Carcinoma. *Front Genet* (2020) 11:595242. doi: 10.3389/fgene.2020.595242
6. Capitanio U, Bensalah K, Bex A, Boorjian SA, Bray F, Coleman J, et al. Epidemiology of Renal Cell Carcinoma. *Eur Urol* (2019) 75(1):74–84. doi: 10.1016/j.eururo.2018.08.036
7. Moch H, Cubilla AL, Humphrey PA, Reuter VE, Ulbright TM. The 2016 WHO Classification of Tumours of the Urinary System and Male Genital Organs-Part A: Renal, Penile, and Testicular Tumours. *Eur Urol* (2016) 70 (1):93–105. doi: 10.1016/j.eururo.2016.02.029
8. Siegel RL, Miller KD, Jemal A. Cancer Statistics, 2020. *CA Cancer J Clin* (2020) 70(1):7–30. doi: 10.3322/caac.21590
9. Li T, Fan J, Wang B, Traugh N, Chen Q, Liu JS, et al. TIMER: A Web Server for Comprehensive Analysis of Tumor-Infiltrating Immune Cells. *Cancer Res* (2017) 77(21):e108–e10. doi: 10.1158/0008-5472.CAN-17-0307
10. Chandrashekar DS, Bashel B, Balasubramanya SAH, Creighton CJ, Ponce-Rodriguez I, Chakravarthi BVSK, et al. UALCAN: A Portal for Facilitating Tumor Subgroup Gene Expression and Survival Analyses. *Neoplasia* (2017) 19 (8):649–58. doi: 10.1016/j.neo.2017.05.002
11. Colaprico A, Silva TC, Olsen C, Garofano L, Cava C, Garolini D, et al. TCGAbiolinks: An R/Bioconductor Package for Integrative Analysis of TCGA Data. *Nucleic Acids Res* (2016) 44(8):e71. doi: 10.1093/nar/gkv1507
12. Davis S, Meltzer PS. GEOquery: A Bridge Between the Gene Expression Omnibus (GEO) and BioConductor. *Bioinformatics* (2007) 23(14):1846–7. doi: 10.1093/bioinformatics/btm254
13. Subramanian A, Tamayo P, Mootha VK, Mukherjee S, Ebert BL, Gillette MA, et al. Gene Set Enrichment Analysis: A Knowledge-Based Approach for Interpreting Genome-Wide Expression Profiles. *Proc Natl Acad Sci USA* (2005) 102(43):15545–50. doi: 10.1073/pnas.0506580102
14. Liberzon A, Birger C, Thorvaldsdottir H, Ghandi M, Mesirov JP, Tamayo P. The Molecular Signatures Database (MSigDB) Hallmark Gene Set Collection. *Cell Syst* (2015) 1(6):417–25. doi: 10.1016/j.cels.2015.12.004
15. Yu G, Wang L-G, Han Y, He Q-Y. Clusterprofiler: An R Package for Comparing Biological Themes Among Gene Clusters. *OMICS* (2012) 16 (5):284–7. doi: 10.1089/omi.2011.0118
16. Love MI, Huber W, Anders S. Moderated Estimation of Fold Change and Dispersion for RNA-Seq Data With Deseq2. *Genome Biol* (2014) 15(12):550. doi: 10.1186/s13059-014-0550-8
17. Ritchie ME, Phipson B, Wu D, Hu Y, Law CW, Shi W, et al. Limma Powers Differential Expression Analyses for RNA-Sequencing and Microarray Studies. *Nucleic Acids Res* (2015) 43(7):e47. doi: 10.1093/nar/gkv007
18. Zhou N, Bao J. FerrDb: A Manually Curated Resource for Regulators and Markers of Ferroptosis and Ferroptosis-Disease Associations. *Database (Oxf)* (2020) 2020:baaa021. doi: 10.1093/database/baaa021
19. Gibson KM, Burlingame TG, Hogema B, Jakobs C, Schutgens RB, Millington D, et al. 2-Methylbutyryl-Coenzyme A Dehydrogenase Deficiency: A New Inborn Error of L-Isoleucine Metabolism. *Pediatr Res* (2000) 47(6):830–3. doi: 10.1203/00006450-200006000-00025
20. Andresen BS, Christensen E, Corydon TJ, Bross P, Pilgaard B, Wanders RJ, et al. Isolated 2-Methylbutyrylglycinuria Caused by Short/Branched-Chain Acyl-CoA Dehydrogenase Deficiency: Identification of a New Enzyme Defect, Resolution of Its Molecular Basis, and Evidence for Distinct Acyl-CoA Dehydrogenases in Isoleucine and Valine Metabolism. *Am J Hum Genet* (2000) 67(5):1095–103. doi: 10.1086/303105
21. Du W, Zhang L, Brett-Morris A, Aguila B, Kerner J, Hoppel CL, et al. HIF Drives Lipid Deposition and Cancer in ccRCC *via* Repression of Fatty Acid Metabolism. *Nat Commun* (2017) 8(1):1769. doi: 10.1038/s41467-017-01965-8
22. Qu Y-Y, Zhao R, Zhang H-L, Zhou Q, Xu F-J, Zhang X, et al. Inactivation of the AMPK-GATA3-ECHS1 Pathway Induces Fatty Acid Synthesis That Promotes Clear Cell Renal Cell Carcinoma Growth. *Cancer Res* (2020) 80 (2):319–33. doi: 10.1158/0008-5472.CAN-19-1023
23. Carracedo A, Cantley LC, Pandolfi PP. Cancer Metabolism: Fatty Acid Oxidation in the Limelight. *Nat Rev Cancer* (2013) 13(4):227–32. doi: 10.1038/nrc3483
24. Sivanand S, Vander Heiden MG. Emerging Roles for Branched-Chain Amino Acid Metabolism in Cancer. *Cancer Cell* (2020) 37(2):147–56. doi: 10.1016/j.ccell.2019.12.011
25. Zhang L, Han J. Branched-Chain Amino Acid Transaminase 1 (BCAT1) Promotes the Growth of Breast Cancer Cells Through Improving mTOR-Mediated Mitochondrial Biogenesis and Function. *Biochem Biophys Res Commun* (2017) 486(2):224–31. doi: 10.1016/j.bbrc.2017.02.101
26. Dixon SJ, Lemberg KM, Lamprecht MR, Skouta R, Zaitsev EM, Gleason CE, et al. Ferroptosis: An Iron-Dependent Form of Nonapoptotic Cell Death. *Cell* (2012) 149(5):1060–72. doi: 10.1016/j.cell.2012.03.042
27. Stockwell BR, Friedmann Angeli JP, Bayir H, Bush AI, Conrad M, Dixon SJ, et al. Ferroptosis: A Regulated Cell Death Nexus Linking Metabolism, Redox Biology, and Disease. *Cell* (2017) 171(2):273–85. doi: 10.1016/j.cell.2017.09.021
28. Stockwell BR, Jiang X, Gu W. Emerging Mechanisms and Disease Relevance of Ferroptosis. *Trends Cell Biol* (2020) 30(6):478–90. doi: 10.1016/j.tcb.2020.02.009
29. Chen X, Kang R, Kroemer G, Tang D. Broadening Horizons: The Role of Ferroptosis in Cancer. *Nat Rev Clin Oncol* (2021) 18(5):280–96. doi: 10.1038/s41571-020-00462-0
30. Forcina GC, Dixon SJ. GPX4 at the Crossroads of Lipid Homeostasis and Ferroptosis. *Proteomics* (2019) 19(18):e1800311. doi: 10.1002/pmic.201800311
31. Miess H, Dankworth B, Gouw AM, Rosenfeldt M, Schmitz W, Jiang M, et al. The Glutathione Redox System Is Essential to Prevent Ferroptosis Caused by

Impaired Lipid Metabolism in Clear Cell Renal Cell Carcinoma. *Oncogene* (2018) 37(40):5435–50. doi: 10.1038/s41388-018-0315-z
32. Song X, Zhu S, Chen P, Hou W, Wen Q, Liu J, et al. AMPK-Mediated BECN1 Phosphorylation Promotes Ferroptosis by Directly Blocking System X Activity. *Curr Biol* (2018) 28(15):2388–99.e5. doi: 10.1016/j.cub.2018.05.094
33. Hou W, Xie Y, Song X, Sun X, Lotze MT, Zeh HJ, et al. Autophagy Promotes Ferroptosis by Degradation of Ferritin. *Autophagy* (2016) 12(8):1425–8. doi: 10.1080/15548627.2016.1187366

Conflict of Interest: The authors declare that the research was conducted in the absence of any commercial or financial relationships that could be construed as a potential conflict of interest.

Publisher's Note: All claims expressed in this article are solely those of the authors and do not necessarily represent those of their affiliated organizations, or those of the publisher, the editors and the reviewers. Any product that may be evaluated in this article, or claim that may be made by its manufacturer, is not guaranteed or endorsed by the publisher.

Copyright © 2022 Liu, Zhang, Wang, Zhu and Xu. This is an open-access article distributed under the terms of the Creative Commons Attribution License (CC BY). The use, distribution or reproduction in other forums is permitted, provided the original author(s) and the copyright owner(s) are credited and that the original publication in this journal is cited, in accordance with accepted academic practice. No use, distribution or reproduction is permitted which does not comply with these terms.

frontiers in Oncology

ORIGINAL RESEARCH
published: 13 January 2022
doi: 10.3389/fonc.2021.744937

MED10 Drives the Oncogenicity and Refractory Phenotype of Bladder Urothelial Carcinoma Through the Upregulation of hsa-miR-590

Chia-Chang Wu[1,2,3], *Yuan-Hung Wang*[4,5], *Su-Wei Hu*[1,2,4], *Wen-Ling Wu*[1,2], *Chi-Tai Yeh*[5,6*] *and Oluwaseun Adebayo Bamodu*[1,5,7*]

[1] Department of Urology, Shuang Ho Hospital, Taipei Medical University, New Taipei City, Taiwan, [2] Taipei Medical University (TMU) Research Center of Urology and Kidney, Taipei Medical University, Taipei City, Taiwan, [3] Department of Urology, School of Medicine, College of Medicine, Taipei Medical University, Taipei City, Taiwan, [4] Graduate Institute of Clinical Medicine, College of Medicine, Taipei Medical University, Taipei, Taiwan, [5] Department of Medical Research, Shuang Ho Hospital, Taipei Medical University, New Taipei City, Taiwan, [6] Department of Medical Laboratory Science and Biotechnology, Yuanpei University of Medical Technology, Hsinchu City, Taiwan, [7] Department of Hematology and Oncology, Cancer Center, Shuang Ho Hospital, Taipei Medical University, New Taipei City, Taiwan

OPEN ACCESS

Edited by:
Alfredo Berruti, University of Brescia, Italy

Reviewed by:
Felice Crocetto, Federico II University Hospital, Italy
Joseph R. Podojil, Northwestern University, United States

***Correspondence:**
Oluwaseun Adebayo Bamodu
dr_bamodu@yahoo.com; 16625@s.tmu.edu.tw
Chi-Tai Yeh
ctyeh@s.tmu.edu.tw

Specialty section:
This article was submitted to Genitourinary Oncology, a section of the journal Frontiers in Oncology

Received: *21 July 2021*
Accepted: *15 December 2021*
Published: *13 January 2022*

Citation:
Wu C-C, Wang Y-H, Hu S-W, Wu W-L, Yeh C-T and Bamodu OA (2022) MED10 Drives the Oncogenicity and Refractory Phenotype of Bladder Urothelial Carcinoma Through the Upregulation of hsa-miR-590. Front. Oncol. 11:744937. doi: 10.3389/fonc.2021.744937

Background: Dysfunctional transcription machinery with associated dysregulated transcription characterizes many malignancies. Components of the mediator complex, a principal modulator of transcription, are increasingly implicated in cancer. The mediator complex subunit 10 (MED10), a vital kinase module of the mediator, plays a critical role in bladder physiology and pathology. However, its role in the oncogenicity, metastasis, and disease recurrence in bladder cancer (BLCA) remains unclear.

Objective: Thus, we investigated the role of dysregulated or aberrantly expressed MED10 in the enhanced onco-aggression, disease progression, and recurrence of bladder urothelial carcinoma (UC), as well as the underlying molecular mechanism.

Methods: Using an array of multi-omics big data analyses of clinicopathological data, *in vitro* expression profiling and functional assays, and immunocytochemical staining, we assessed the probable roles of MED10 in the progression and prognosis of BLCA/UC.

Results: Our bioinformatics-aided gene expression profiling showed that MED10 is aberrantly expressed in patients with BLCA, is associated with high-grade disease, is positively correlated with tumor stage, and confers significant survival disadvantage. Reanalyzing the TCGA BLCA cohort (n = 454), we showed that aberrantly expressed MED10 expression is associated with metastatic and recurrent disease, disease progression, immune suppression, and therapy failure. Interestingly, we demonstrated that MED10 interacts with and is co-expressed with the microRNA, hsa-miR-590, and that CRISPR-mediated knockout of MED10 elicits the downregulation of miR-590 preferentially in metastatic UC cells, compared to their primary tumor peers. More so, silencing MED10 in SW1738 and JMSU1 UC cell lines significantly attenuates their cell proliferation, migration, invasion, clonogenicity, and tumorsphere formation (primary and secondary), with the associated downregulation of BCL-xL, MKI67, VIM, SNAI1, OCT4,

and LIN28A but upregulated BAX protein expression. In addition, we showed that high MED10 expression is a non-inferior biomarker of urothelial recurrence compared with markers of cancer stemness; however, MED10 is a better biomarker of local recurrence than any of the stemness markers.

Conclusion: These data provide preclinical evidence that dysregulated MED10/MIR590 signaling drives onco-aggression, disease progression, and recurrence of bladder UC and that this oncogenic signal is therapeutically actionable for repressing the metastatic/recurrent phenotypes, enhancing therapy response, and shutting down stemness-driven disease progression and relapse in patients with BLCA/UC.

Keywords: bladder urothelial carcinoma, MED10, hsa-miR-590, metastasis, cancer stemness, disease progression, recurrence, therapy failure

INTRODUCTION

Bladder cancer (BLCA), with 573,278 new cases in 2020 and a projected 72.9% increase in incidence by 2040, ranks as one of the most diagnosed malignancies and a leading cause of cancer-associated mortality for both sexes and all ages, globally (1). Cigarette smoking, male sex, and advanced age contribute to the development of BLCA (1, 2). BLCA is characterized by high inter- and intra-tumor heterogeneity; more than 90% of BLCA cases are in some form transitional cell or urothelial, histologically, and localized bladder urothelial carcinoma (UC), occurring anywhere from the renal pelvis to the urethra, may either be non-muscle invasive (NMIBC, T1 stage) or muscle-invasive bladder cancer (MIBC, T2–T4), with ~3 in every 4 BLCA presenting as NMIBC (3–5). More so, up to 70% of all NMIBCs recurs and an estimated 20% progresses to MIBC, regardless of local therapy, with a persisting dismal prognosis for MIBC, which continues to be characterized by less than a 50% 5-year survival rate (4). Currently, treatment modality for BLCA includes cystoscopic surveillance, intravesical therapy, chemotherapy and/or radiation therapy, and immunotherapy; however, radical cystectomy remains the treatment of choice despite the risk of enhanced morbidity or probable overtreatment of low-risk patients (2, 6, 7). Diagnosis-wise, over the last decade, liquid biopsy including various urine-associated biomarkers, such as DNA methylation and mutations, protein-based assays, mRNA, and non-coding RNA signatures, has been touted as a clinically effective modality for patient selection, and a bio-tool for precision medicine, informing therapy choice and real-time monitoring of therapeutic effects (8). Moreover, there is accruing evidence of the exploitable role of circulating tumor cells (CTCs) as biomarkers of diagnosis and prognosticators of disease recurrence, progression, and poor survival in patients with BLCA/UC (9). Howbeit, the high incidence of recurrent NMIBC and poor survival rate of MIBC, despite these advances in diagnostic (8, 9) and therapeutic strategies (6, 7), necessitate the discovery and characterization of novel actionable molecular targets and development of new therapeutic approaches.

Transcription constitutes a vital part of the bio-cellular processes essential for protein production in eukaryotic cells, as such transcription is usually (not always) enhanced in cancerous cells, to facilitate their increased metabolic activity and proliferation (10). This highlights the exploitability of the transcriptional activity in malignant cells as a probable anticancer therapeutic strategy. The mediator of RNA polymerase II transcription subunit 10 (MED10) is a middle component of the highly conserved tetramodular (head, middle, tail, and cyclin-dependent kinase) Mediator complex in humans, and reports indicate that the Mediator complex serves as "a bridge between regulatory proteins and RNA polymerase II (Pol II), thereby regulating the Pol II-dependent transcription" (11). There is accruing evidence that altered expressions of components of the Mediator complex play important roles in tumor initiation and disease progression; however, these reports are largely divergent. Zhao et al. reported a high expression of MED15 in breast cancer tissues with enhanced TGFβ/Smad3 signaling, while inhibiting MED15 suppressed the metastatic potential of a highly aggressive breast cancer cell line (12). Conversely, the decreased expression of MED15 protein is implicated in uterine leiomyosarcomas regardless of mutational status (13) and MED15 is considered a tumor suppressor in oral/oropharyngeal cancers (14). In contrast, while MED1 expression is downregulated and inversely correlated with the expression of metastasis-related genes in melanoma (15), lung cancer (16, 17), and bladder cancer (18), enhanced MED1 activity has been reported in prostate and breast cancer, likely due to its function as a hub for nuclear hormone receptors (18, 19). Moreover, in spite of reports indicating that cyclin-dependent kinase (CDK)8-Mediator module is an oncogene, several studies support the tumor-suppressor role of CDK8, under certain conditions (20). This functional diversity of the Mediator and their divergent roles in different cancer types pique research interest and, howbeit controversial, may be exploited for the discovery of a surrogate biomarker of disease progression or development of inhibitors targeting candidate Mediator. Against the background of these contradictory reports, and the yet unknown role of MED10 in BLCA, the present study investigated the probable role of dysregulated or aberrantly expressed MED10 in the enhanced onco-aggression, disease progression, and recurrence of bladder UC, as well as the underlying molecular mechanism.

MATERIAL AND METHODS

Cell Culture and Chemicals

The normal human primary bladder epithelial BdEC (ATCC® PCS-420-010™) cell line was obtained from the ATCC (American Type Culture Collection, Manassas, VA, USA), and the human bladder transition cell carcinoma cell lines SW1738 and JMSU1 were kind gifts from CTY (Taipei Medical University - Shuang Ho Hospital, New Taipei City, Taiwan) and cultured in RPMI 1640 (Thermo Fisher Scientific Inc., Bartlesville, OK, USA). Culture medium was supplemented with 10% fetal bovine serum (FBS, #26140079, Thermo Fisher Scientific Inc., Bartlesville, OK, USA) and 100 U/ml of penicillin–streptomycin (Thermo Fisher Scientific Inc., Bartlesville, OK, USA). All cells used in the study were not greater than passage number 3 (≤P.3). Cells were subcultured at ≥98% confluence or culture media changed every 48 h. Stock solutions of 100 mM in 0.01% DMSO were stored at -20°C, until use.

Antibodies

Monoclonal antibodies against MED10 (C-2: #sc-393450), BAX (B-9: #sc-7480), BCL-xL (H-5: #sc-8392), Ki67 (#sc-23900), Vimentin (V9: #sc-6260), and SNAI1 (G-7: #sc-271977) were obtained from Santa Cruz Biotechnology (Dallas, TX, USA); OCT4A (#2840) and LIN28A (#8706) were purchased from Cell Signaling Technology, Inc. (CST, Beverly, MA, USA); and GAPDH (#sc-32233) was from Santa Cruz Biotechnology (Santa Cruz, CA, USA).

Colorimetric Cell Proliferation Assay

For cell proliferation, Invitrogen alamarBlue™ high-sensitivity cell viability reagent (#A50100, Thermo Fisher Scientific Inc., Bartlesville, OK, USA) was used strictly following the manufacturer's instruction. Briefly, after 1×10^3 wild-type (WT) or MED10-silenced (shMED10) SW1738 or JMSU1 cell lines were seeded per well in triplicates with three biological replica for each assay in 96-well microtiter plates containing supplemented growth media and incubated at 37°C in humidified 5% CO_2. After 24 h, the cells were incubated with alamarBlue™ for 2 h at 37°C. The number of dye-stained viable proliferating cells was read at 570-nm absorbance wavelength in the Molecular Devices SpectraMax M3 multimode microplate reader (Molecular Devices LLC., San Jose, CA, USA).

Silencing MED10 by RNA Interference

MED10-Human, 4 unique 29mer shRNA constructs in lentiviral GFP vector containing pGFP-C-shLenti (#TL303299; MED10 Human shRNA Plasmid Kit (Locus ID 84246; OriGene Technologies Inc., Rockville, MD, USA) were packaged and transfected into SW1738 or JMSU1 cells to silence MED10. Non-effective 29-mer scrambled shRNA cassette in pGFP-C-shLenti Vector, TR30021, served as negative control. Stably transfected monoclonal SW1738 or JMSU1 cells were selected using 2 μg/ml puromycin, as recommended by the manufacturer. The effect of the lentiviral infection was enhanced by adding Sigma-Aldrich® polybrene (#TR-1003, Merck KGaA, Darmstadt, Germany). MED10 knockdown in the cells was verified by Western blotting and quantitative real-time PCR. The shRNA sequences for MED10 are as follows: shMED10#1 5′-GACAGCAGCTTCATGATATTA-3′, and shMED101#2 5′-ATCGACACCATGAAGAAATTT-3′.

MED10 Ectopic Expression

We overexpressed MED10 in BdEC cells by transfecting the human MED10 (NM_032286.2) cDNA sequence cloned into pCMV6-Entry vector (pCMV-MED10; #V0529, GeneCopoeia, Inc., Rockville, MD, USA) using Lipofectamine™ LTX with PLUS™ reagent (#15338100, Life Technologies, Thermo Fisher Scientific Inc., NY, USA). BdEC cells were seeded and cultured in 35-mm-diameter dishes till they attained 60% confluence. On transfection day, 1 mg of DNA diluted in 100 μl of serum-free medium and 6 μl of Lipofectamine™ LTX with PLUS™ reagents were then added. The DNA-PLUS mix was incubated at room temperature for 20 min, and 4 μl of Lipofectamine reagent was added, followed by an additional 20-min incubation. After incubation, the BdEC cells were carefully washed twice with serum-free media and 800 μl of serum-free transfection medium. The cells were then incubated with DNA-PLUS–Lipofectamine reagent mix in 5% humidified CO_2 incubator at 37°C for 3 h. Thereafter, recovery medium with 10% FBS was added to a final volume of 2 ml and incubated overnight. After this, the recovery medium was suctioned and fresh RPMI 1640 medium containing serum and antibiotics was added.

Bladder Cancer Tissue Damples

Bladder UC tissue samples (n = 79) were obtained from the Taipei Medical University - Shuang Ho Hospital tissue bank. The study was approved by the Institutional Review Board of the Taipei Medical University (approval number: N202102034) and compliant with recommendations from the Declaration of Helsinki for biomedical research involving human subjects. The requirement for patients' signed informed consent was waived because of the retrospective nature of the study.

Immunohistochemical and Immunofluorescence Staining Assays

Immunohistochemical (IHC) staining was performed on formalin-fixed paraffin-embedded (FFPE) samples from our BLCA/UC cohort (n = 79) consisting benign (n = 21), T1 (n = 11), T2 (n = 17), T3 (n = 9), T4 (n = 5), and metastatic (M1, n = 16) bladder UC cases. Samples were probed with primary antibodies against MED10, MKI67/Ki67, OCT4, and LIN28A at 1:200 dilution following standard IHC protocol. Protein expression was scored by two independent pathologists using the quick-score (Q-score) formula Q = I × P, where I is staining intensity [0 (no staining), 1+ (weak), 2+ (moderate), and 3+ (strong)] and P represents percentage of stained cells. Maximum Q-score = 300. For immunofluorescence (IFC) staining, WT or shMED10 tumorspheres derived from corresponding SW1738 and JMSU1 cells were fixed with 4% paraformaldehyde after they were plated onto poly-*L*-lysine-coated glass coverslips, then they were washed carefully with cold PBS thrice, permeabilized with 0.1% Triton X-100/PBS solution for 10 min, and then incubated with primary antibodies against OCT4 and LIN28A at 1:400

dilution, followed by Cy5-labeled goat anti-mouse Alexa Fluor 488 secondary antibodies (#R37120, Thermo Fisher Scientific Inc.) for 1 h. DAPI (4′,6-diamidino-2-phenylindole; #D1306, Molecular Probes, Thermo Fisher Scientific Inc.) was used for nuclear staining. Cell visualization and imaging were performed using the Nikon E800 fluorescent microscope (Nikon Instruments Inc., Melville, NY, USA).

Western Blotting Assay

Protein blots derived from 20 μg of WT or shMED10 UC cell protein samples and separated by 10% sodium dodecyl sulfate polyacrylamide gel electrophoresis (SDS-PAGE) were transferred onto polyvinylidene fluoride (PVDF) membranes using the Bio-Rad Mini-Protein electro-transfer system (Bio-Rad Laboratories, Inc., Hercules, CA, USA). The PVDF membranes were blocked for 1 h with 5% non-fat milk in Tris-buffered saline with Tween 20 (TBST) and then probed overnight at 4°C with primary monoclonal antibodies against MED10 (1:1,000, Santa Cruz), BAX (1:1,000, Santa Cruz), BCL-xL (1:1,000, Santa Cruz), MKI67/Ki67 (1:1,000, Santa Cruz), Vimentin (1:1,000, Santa Cruz), SNAI1 (1:1,000, Santa Cruz), OCT4 (1:1,000, Cell Signaling Technology), LIN28A (1:1,000, Cell Signaling Technology), and GAPDH (1:1,000, Santa Cruz). Thereafter, the membranes were incubated with secondary antibodies conjugated with horseradish peroxidase (HRP) at room temperature for 1 h and carefully washed thrice with cold 1× PBS. The protein bands were detected with the enhanced chemiluminescence detection system (Thermo Fisher Scientific Inc., Waltham, MA, USA), and protein band densitometry was done using ImageJ software version 1.49 (https://imagej.nih.gov/ij/).

Tumorsphere Formation and Self-Renewal Assay

5×10^4 WT or shMED10 SW1738 and JMSU1 cells were seeded per well in ultra-low attachment 6-well plates (Corning, Corning, NY, USA) containing RPMI 1640 supplemented with Gibco™ B-27TM supplement (#17504044, Invitrogen, Carlsbad, CA, USA), 20 ng/ml basic fibroblast growth factor (bFGF; #13256029, Invitrogen), and 20 ng/ml epidermal growth factor (EGF; #PHG0311, Invitrogen). Cells were cultured at 37°C in a humidified 5% CO_2 incubator for 6 days. Cultivated primary tumorspheres ≥ 100 μm were counted under inverted phase-contrast microscope, and then secondary tumorspheres were generated from the primary tumorspheres by dissociating them and reseeding the dissociated cells as per the primary tumorspheres, from single-cell suspension acquired using a sterile 22-G needle.

Scratch-Wound Healing Migration Assay

We used the scratch wound-healing assay to assess cell migration. Briefly, WT or shMED10 bladder UC cells were seeded and allowed to grow in 6-well plates (Corning, Corning, NY, USA) containing complete growth media with 10% FBS. Media in wells were changed to low-serum (1% FBS) growth media when cells attained >98% confluence. The median axes of the monolayered adherent cells were scratched using sterile yellow pipette tips and carefully washed with low-serum media to rid detached cells. Cell migration based on scratch-wound healing was monitored over time, and images were captured at 0 and 12 h after denudation under a light microscope using a ×10 objective lens. Thereafter, the images were analyzed using the National Institutes of Health ImageJ software version 1.49 (https://imagej.nih.gov/ij/).

Invasion Assay

Invasion assay was performed using the Corning® BioCoat™ Matrigel® invasion chambers with a 8.0–μm PET membrane in a two-24-well plate system (#354480, Corning, Corning, NY, USA). 1×10^5 WT or shMED10 JMSU1 cells were seeded per well in plates and incubated at 4°C overnight. The upper chambers contained low-serum (2% FBS) media while the lower chamber contained 600 ;μl high-serum (20% FCS) media. After 48-h incubation, the non-invaded cells in the upper chamber were carefully wiped off with sterile cotton swabs, while the invaded cells that penetrated through the membrane were fixed with ethanol, stained with crystal violet solution, and counted under light microscope from six random fields of vision.

Colony Formation Assay

2×10^4 WT or shMED10 SW1738 and JMSU1 cells were seeded into 6-well culture plates (Corning Inc., Corning, NY, USA) and incubated for 13–15 days at 37°C. Cells were then washed three times with cold 1× PBS, fixed with ice-cold methanol, stained with 0.005% crystal violet, washed with 1× PBS, and dried at room temperature. The colonies formed were assessed and counted under microscope, as well as digitally using the National Institutes of Health ImageJ software version 1.49 (https://imagej.nih.gov/ij/). In each well, the colonies with diameter ≥ 100 μm were counted over six randomly selected fields in triplicate assays.

Statistical Analysis

All data represent the mean ± standard deviation (SD) of assays performed at least 3 times in triplicates. The 2-sided Student's *t* test was used for comparison between 2 groups, whereas one-way ANOVA with Tukey's *post-hoc* test was used for comparison between 3 or more groups. Kaplan–Meier survival analyses aided comparison of survival rates between the control and test groups. All statistical analyses were performed using MS Excel (Microsoft Corporation. Microsoft Excel [Internet]. 2018. Available from: https://office.microsoft.com/excel) and GraphPad Prism version 8.0.0 for Windows (GraphPad Software, La Jolla, CA, USA). p-value < 0.05 was considered statistically significant.

RESULTS

MED10 Is Aberrantly Expressed in Patients With BLCA, and This Has an Adverse Prognostic Implication

Bioinformatics-aided analyses of the GPL570 platform [HG-U133_Plus_2] Affymetrix Human Genome U133 Plus 2.0 Array (n = 162,085) (https://www.ncbi.nlm.nih.gov/geo/query/acc.cgi?

acc=GPL570) revealed that the expression of *MED10* transcripts was significantly higher in the BLCA patients than in their normal peers (1.66-fold, $p = 0.002$) (**Figure 1A**). This was corroborated by Cox PH modeling-based volcano plot visualization of differentially expressed genes in the TCGA BLCA cohort (n = 412), showing that the overexpression of the *med10* gene was associated with increased hazard ratio (3.53-fold, $p < 0.001$) (**Figure 1B**). Survival analyses of the TCGA BLCA cohort showed that compared with their high *MED10* counterparts (n = 333), patients with low *MED10* expression (n = 56) enjoyed an 18% to 27% survival advantage from days 1,000 to 5,000 (concordance index = 48.67; hazard ratio HR = 1.78 (95% CI: 1.06–2.97), $p = 0.028$) (**Figure 1C**). Using the GPL570 platform [HG-U133_Plus_2], we also demonstrated that increased *MED10* expression positively correlated with increased pathological tumor (pT) stage (**Figure 1D**). Our hazard ratio forest plot of BLCA/UC-relevant series in the GPL570 platform showed that high *MED10* expression favors increased likelihood of disease-specific death (HR = 1.16 (95% CI: 0.85–1.58) and recurrence (HR = 1.07 (95% CI: 0.82–1.39) (**Figure 1E**). More so, *MED10* expression was elevated in patients with high-grade BLCA compared to the low-grade peers, albeit statistically insignificant (**Figure 1F**). These data indicate that MED10 is aberrantly expressed in patients with BLCA and that this has an adverse prognostic implication.

MED10 Expression Is Positively Correlated With Disease Progression, Immune Suppression, and Therapy Failure

Having demonstrated the aberrant expression of MED10 in patients with BLCA and its association with poor prognosis, we sort to gain further insight into the probable role of MED10 in disease progression and therapy response. Reanalyzing the TCGA BLCA cohort data, we demonstrated that compared to patients without metastasis (M0), *MED10* expression is upregulated in metastatic disease (M1) (**Figure 2A**). Similarly, *MED10* expression is higher in patients with recurred or progressed disease, compared with their disease-free counterparts (**Figure 2B**). Also, *MED10* transcript expression is positively correlated with increased American Joint Committee on Cancer (AJCC) tumor stage (T1 < T2 < T3 < T4) (**Figure 2C**). Interestingly, we also observed a higher median expression of MED10 in patients with progressive (PD) and stable (SD) disease, compared with their peers who had complete response/remission (CR), while the partial responders had the lowest *MED10* expression (PD > SD > CR > PR) (**Figure 2D**). More so, our systematical analysis of immune infiltrates in BLCA across diverse platforms using the TIMER 2.0 algorithm (19) showed that CD8+ cytotoxic T cells were largely inversely correlated with MED10 protein expression (Spearman's $rho_{TIMER} = 0.23$, $p < 0.05$; Spearman's $rho_{EPIC} = -0.09$, Spearman's $rho_{CIBERSORT} = -0.04$, Spearman's $rho_{XCELL} = -0.15$, $p < 0.05$), and infiltration of CD8+ effector memory T cells showed a mild positive correlation with MED10 expression (Spearman's $rho_{XCELL} = \sim 0.11$, $p < 0.05$); however, MED10 expression was positively correlated with suppressors of immune response, namely, regulatory T cells, Treg (Spearman's $rho_{CIBERSORT} = 0.03$; Spearman's $rho_{QUANTISEQ} = 0.13$, $p < 0.05$) and myeloid-derived suppressor cells, and MDSC (Spearman's $rho_{TIDE} = 0.34$, $p < 0.05$) (**Figure 2E**). Our correlative somatic copy number alteration (sCNA) analyses showed that compared to its ambivalent association with CD8+ T cells with Spearman's rho ranging from -0.78 to 0.18, high amplification of *med10* gene is positively correlated with Treg infiltration (**Figure 2F**). Of clinical relevance, we also showed that patients with concurrent high *MED10* expression and low CD8+ T cell levels in the EPIC cohort (n = 1575) exhibited the worst cumulative survival rate ($R^2 = 0.15$, $p = 4.21e\text{-}08$) (**Figure 2G**). Using the TCGA BLCA cohort (n = 408), we observed that patients bearing high *MED10* expression with or without high MDSC levels exhibited worse survival rates relative to those with concurrent low *MED10* and low MDSC levels ($R^2 = 0.13$, $p = 3.67e\text{-}07$) (**Figure 2H**). Moreover, patients with concurrent high *MED10* and low Treg levels in the TCGA BLCA cohort (n = 408) exhibited the worst cumulative survival rate, compared to those with concomitantly high *MED10* and Treg levels or those with low *MED10* expression regardless of Treg level ($R^2 = 0.13$, $p = 7.86e\text{-}07$) (**Figure 2I**). These data do indicate, at least in part, that MED10 expression is positively correlated with disease progression, immune suppression, and therapy failure.

MED10 Is Functionally Co-Expressed With hsa-miR-590 but Is Inversely Associated With Tumor-Suppressor MicroRNAs

Against the background that microRNAs (miRs) are critical regulators of gene expression, transcription, and translation (21, 22), seeking to gain some mechanistic insight into the oncogenic and immune-suppressing function of MED10 in BLCA/UC, we performed a MED10–miR association probe. Our MED10–miR association plot showed that MED10 was strongly associated with several miRs including a relatively unknown hsa-miR-590-5p (F-stat = 2.11, $p = 1.93e\text{-}05$) (**Figure 3A**). More so, using the TCGA BLCA cohort (n = 412), we demonstrated that upregulated expression of the *med10* gene is positively correlated with several oncogenic miRs (oncomiRs) including hsa-miR-590 (**Figure 3B**) but is inversely correlated with expression levels of tumor-suppressor miRs, including hsa-miR-483, hsa-miR-29c, hsa-miR-100, and hsa-miR-143 (**Figure 3C**). We also demonstrated a significant positive correlation between *MED10* and hsa-miR-590-5p transcript expression (r = 0.24, $p = 6.29e\text{-}07$) (**Figure 3D**). Consistent with this, using the GISTIC module (https://www.genepattern.org/modules/docs/GISTIC_2.0), we found that unlike in patients with diploid hsa-miR-590-5p, hsa-miR-590-5p copy number gain or amplification was associated with upregulated *MED10* transcript expression in patients with BLCA/UC (**Figure 3E**). These data indicate that MED10 is functionally co-expressed with hsa-miR-590 but is inversely associated with tumor-suppressor microRNAs.

MED10 Interacts Directly With hsa-miR-590, a Modulator of Immune Infiltration and Survival

Since co-expression does not necessarily translate into molecular interaction, having shown that MED10 is functionally co-expressed with hsa-miR-590, we probed for a probable interaction between

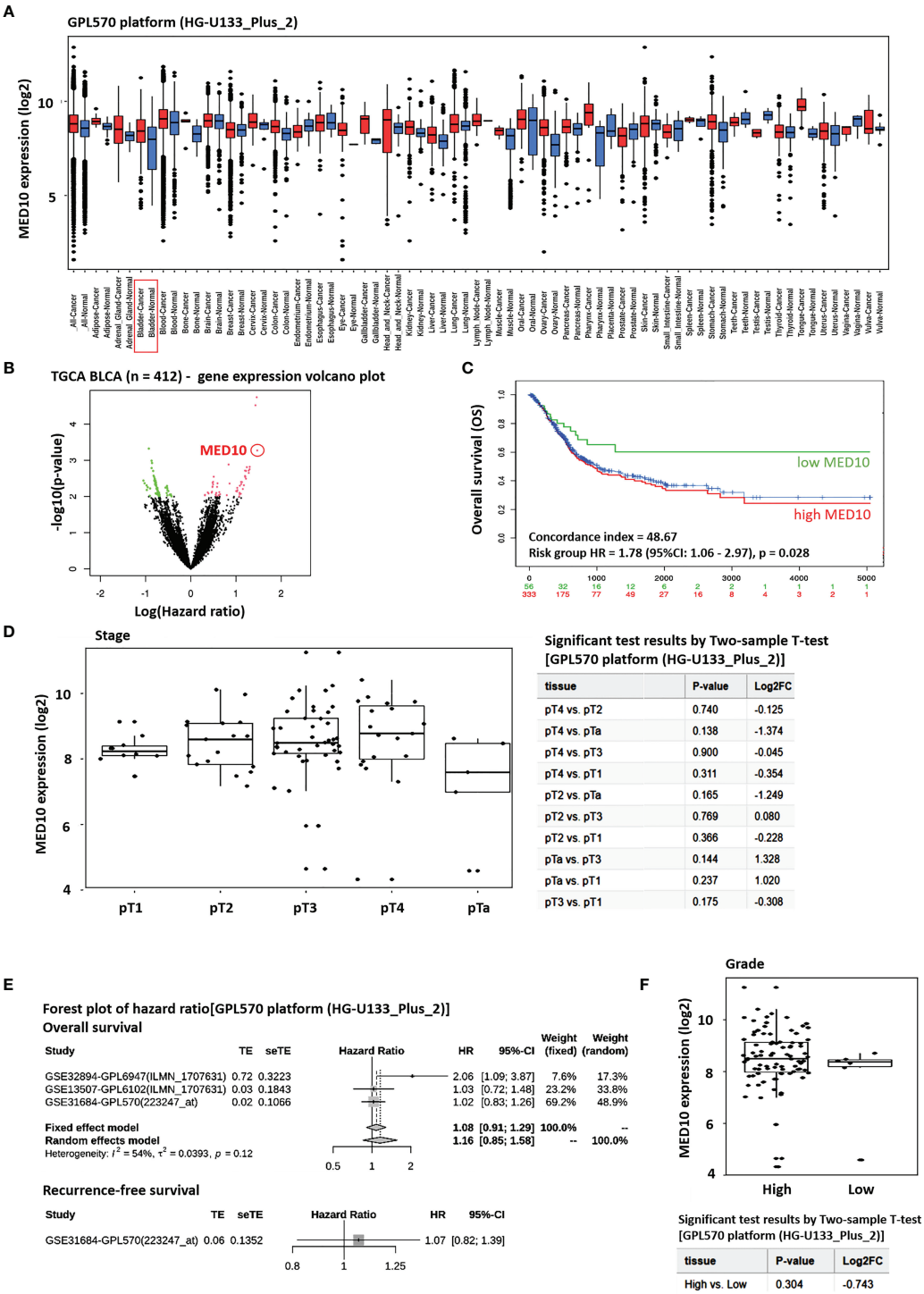


FIGURE 1 | MED10 is aberrantly expressed in patients with BLCA, and this has an adverse prognostic implication. **(A)** Box plot of the tissue-wide differential gene expression profile across cancer experiments using the GPL570 platform (HG-U133_Plus_2)]. **(B)** Volcano plot of the hazard ratios of differentially expressed genes in the TGCA BLCA cohort. MED10 is indicated by the red circle. Volcano plot was plotted with log hazard ratio (HR) on the x-axis and p-value on the y-axis, using the Cox PH model. **(C)** Kaplan–Meier plot showing the effect of altered MED10 expression on the overall survival of patients in the BLCA cohort of the GPL570 platform. **(D)** Box and dot plots showing the association between MED10 expression and tumor stage in the GPL570 platform BLCA cohort *(left)*. Chart showing the 2-sample t-test results for **(D)** *(right)*. **(E)** Forest plot of hazard ratios showing the effect of MED10 on overall and recurrence-free survival on the GPL570 platform BLCA cohort. **(F)** Box and dot plots of the MED10 expression profile based on tumor grade in the GPL570 platform BLCA cohort.

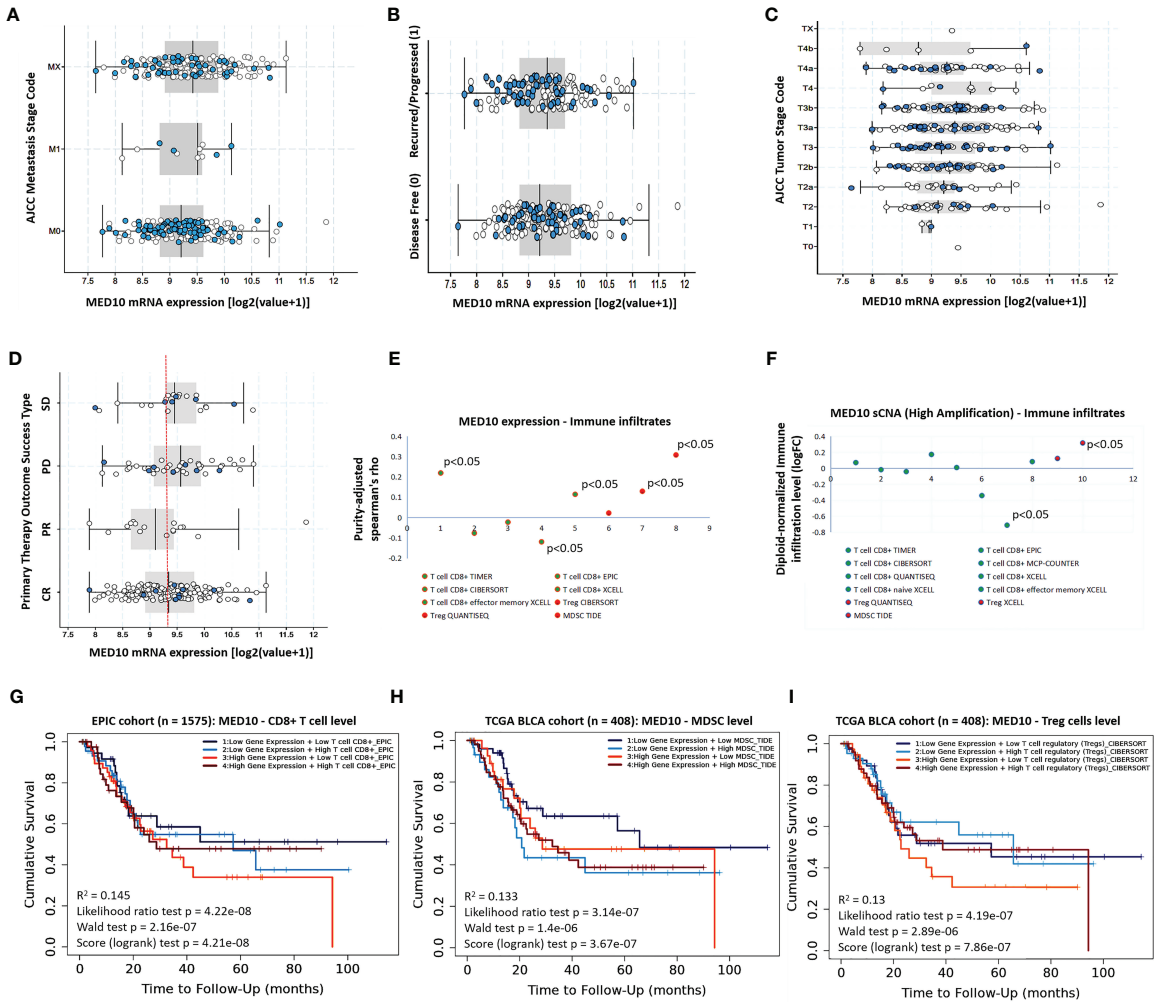
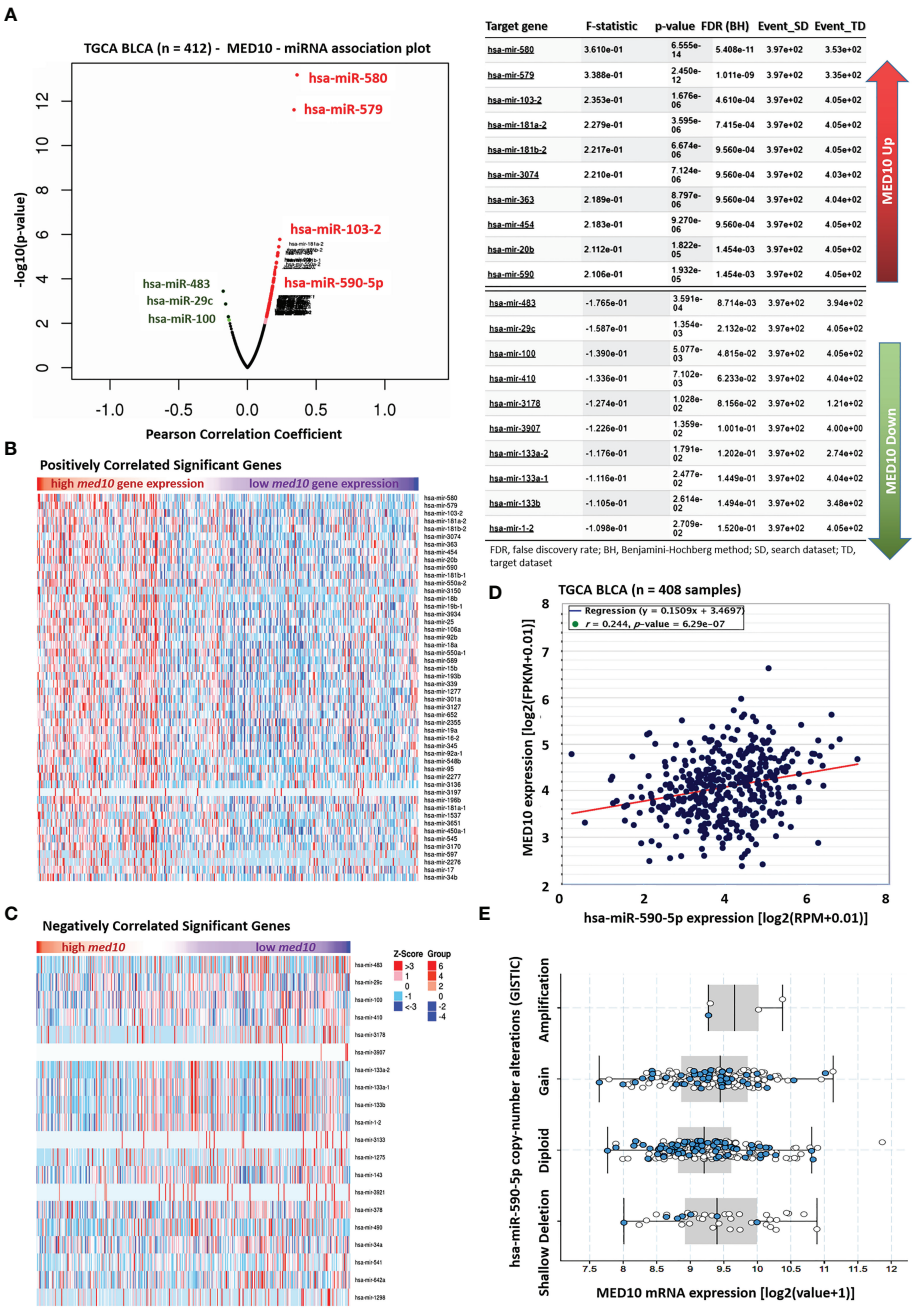


FIGURE 2 | MED10 expression is positively correlated with disease progression, immune suppression, and therapy failure. Box plots showing the association between MED10 mRNA expression and **(A)** AJCC metastasis stage, **(B)** recurrence/progression or disease-free status of patients, **(C)** AJCC tumor stage, or **(D)** primary therapy outcome success type, in the TCGA BLCA cohort. **(E)** Dot plot of the tumor purity-adjust correlation between MED10 expression and level of tumor immune infiltrates. **(F)** Dot plot of the effect of high amplification of MED10 on the diploid-normalized immune cell infiltration level. Kaplan–Meier plot showing the effect of altered MED10 expression with or without altered **(G)** CD8+ T, **(H)** MDSC, or **(I)** Treg cell level on the cumulative survival.

MED10 and hsa-miR-590. Using the mutual exclusivity test for MED10 and hsa-miR-590 in a pooled BLCA cohort (n = 786 patients, 806 samples) consisting of bladder cancer (MSK/TCGA, 2020 n = 476), bladder cancer (MSKCC, Eur Urol 2014 n = 109), bladder urothelial carcinoma (BGI, Nat Genet 2013 n = 99), bladder urothelial carcinoma (DFCI.MSKCC, Cancer Discov 2014 n = 50), and urothelial carcinoma (Cornell/Trento, Nat Gen 2016 n = 72), we confirmed the spatiotemporal association between the dyad (co-occurrence: log2 odds ratio >3, p = 0.02) (**Figure 4A**). To better understand the MED10/hsa-miR-590-5p relationship and for visualization of our hypothesized molecular interaction between MED10 and hsa-miR-590-5p in BLCA/UC cells, we employed a bioinformatics approach to generate the tertiary (3D) structure of MED10 based on sequence homology modeling (NCBI Reference Sequence: NP_115662.2) (https://www.ncbi.nlm.nih.gov/protein/NP_115662.2; **Figure 4B**). We also generated the 3D structure of hsa-miR-590 from its sequence (NCBI Reference Sequence: NR_030321.1)-derived "brackets and dots" linear structure and the minimum free energy (MFE) secondary (2D) structure (**Figure 4C**). Using the Schrödinger PyMOL 2.5 molecular interaction and visualization software (https://pymol.org/2/), we observed a high interaction propensity, broad conservation, and good complementarity between the 5′ end of hsa-miR-590 and the C-terminal RNA-binding motif of MED10, demonstrated by a shape complementarity/docking score of 14,146, atomic contact energy (ACE) of −802.59 kcal/mol, approximate MED10/hsa-miR-590-5p complex interface area of 1,990.70 Å^2, root-mean-square deviation (RMSD) of atomic positions of 4.0 Å, and a p-value of 3.11e−04, with the 3D transformation data, consisting of three rotational angles (2.42°, 0.38°, 120.70°) and three translational



Target gene	F-statistic	p-value	FDR (BH)	Event_SD	Event_TD
hsa-mir-580	3.610e-01	6.555e-14	5.408e-11	3.97e+02	3.53e+02
hsa-mir-579	3.388e-01	2.450e-12	1.011e-09	3.97e+02	3.35e+02
hsa-mir-103-2	2.353e-01	1.676e-06	4.610e-04	3.97e+02	4.05e+02
hsa-mir-181a-2	2.279e-01	3.595e-06	7.415e-04	3.97e+02	4.05e+02
hsa-mir-181b-2	2.217e-01	6.674e-06	9.560e-04	3.97e+02	4.05e+02
hsa-mir-3074	2.210e-01	7.124e-06	9.560e-04	3.97e+02	4.03e+02
hsa-mir-363	2.189e-01	8.797e-06	9.560e-04	3.97e+02	4.04e+02
hsa-mir-454	2.183e-01	9.270e-06	9.560e-04	3.97e+02	4.05e+02
hsa-mir-20b	2.112e-01	1.822e-05	1.454e-03	3.97e+02	4.05e+02
hsa-mir-590	2.106e-01	1.932e-05	1.454e-03	3.97e+02	4.05e+02
hsa-mir-483	-1.765e-01	3.591e-04	8.714e-03	3.97e+02	3.94e+02
hsa-mir-29c	-1.587e-01	1.354e-03	2.132e-02	3.97e+02	4.05e+02
hsa-mir-100	-1.390e-01	5.077e-03	4.815e-02	3.97e+02	4.05e+02
hsa-mir-410	-1.336e-01	7.102e-03	6.233e-02	3.97e+02	4.04e+02
hsa-mir-3178	-1.274e-01	1.028e-02	8.156e-02	3.97e+02	1.21e+02
hsa-mir-3907	-1.226e-01	1.359e-02	1.001e-01	3.97e+02	4.00e+00
hsa-mir-133a-2	-1.176e-01	1.791e-02	1.202e-01	3.97e+02	2.74e+02
hsa-mir-133a-1	-1.116e-01	2.477e-02	1.449e-01	3.97e+02	4.04e+02
hsa-mir-133b	-1.105e-01	2.614e-02	1.494e-01	3.97e+02	3.48e+02
hsa-mir-1-2	-1.098e-01	2.709e-02	1.520e-01	3.97e+02	4.05e+02

FDR, false discovery rate; BH, Benjamini-Hochberg method; SD, search dataset; TD, target dataset

FIGURE 3 | MED10 is functionally co-expressed with hsa-miR-590 but is inversely associated with tumor-suppressor microRNAs. **(A)** Association plot of the relationship between the expression of MED10 and miRs in the TCGA BLCA cohort *(left)*. Chart showing the 10 topmost miRs associated with upregulated or downregulated MED10 expression *(right)*. Heatmaps showing **(B)** positively and **(C)** negatively correlated significant miRs in the TCGA BLCA cohort. **(D)** Line and dot plots showing the correlation between MED10 and hsa-miR-590-5p expression levels in the TCGA BLCA cohort. FPKM, fragmented per kilobase of transcript per million; RPM, reads per million total/mapped reads. **(E)** Box and whiskers plot showing the association between MED10 mRNA expression and hsa-miR-590-5p copy number alterations.

parameters (−1.18, −53.27, −102.28) applied on the ligand molecule, hsa-miR-590 (**Figure 4D**). Furthermore, to confirm the functional and/or modulatory nature of the demonstrated MED10/hsa-miR-590-5p interaction, using agarose gel electrophoresis, we showed that the ectopic expression of MED10 in normal human primary bladder epithelial BdEC cells significantly upregulated the expression of hsa-miR-590, compared to the WT cells; more so, upon silencing MED10 (shMED10) in metastatic human bladder transition cell carcinoma SW1738 cells, hsa-miR-590 expression was markedly suppressed (**Figure 4E**). These findings indicate that

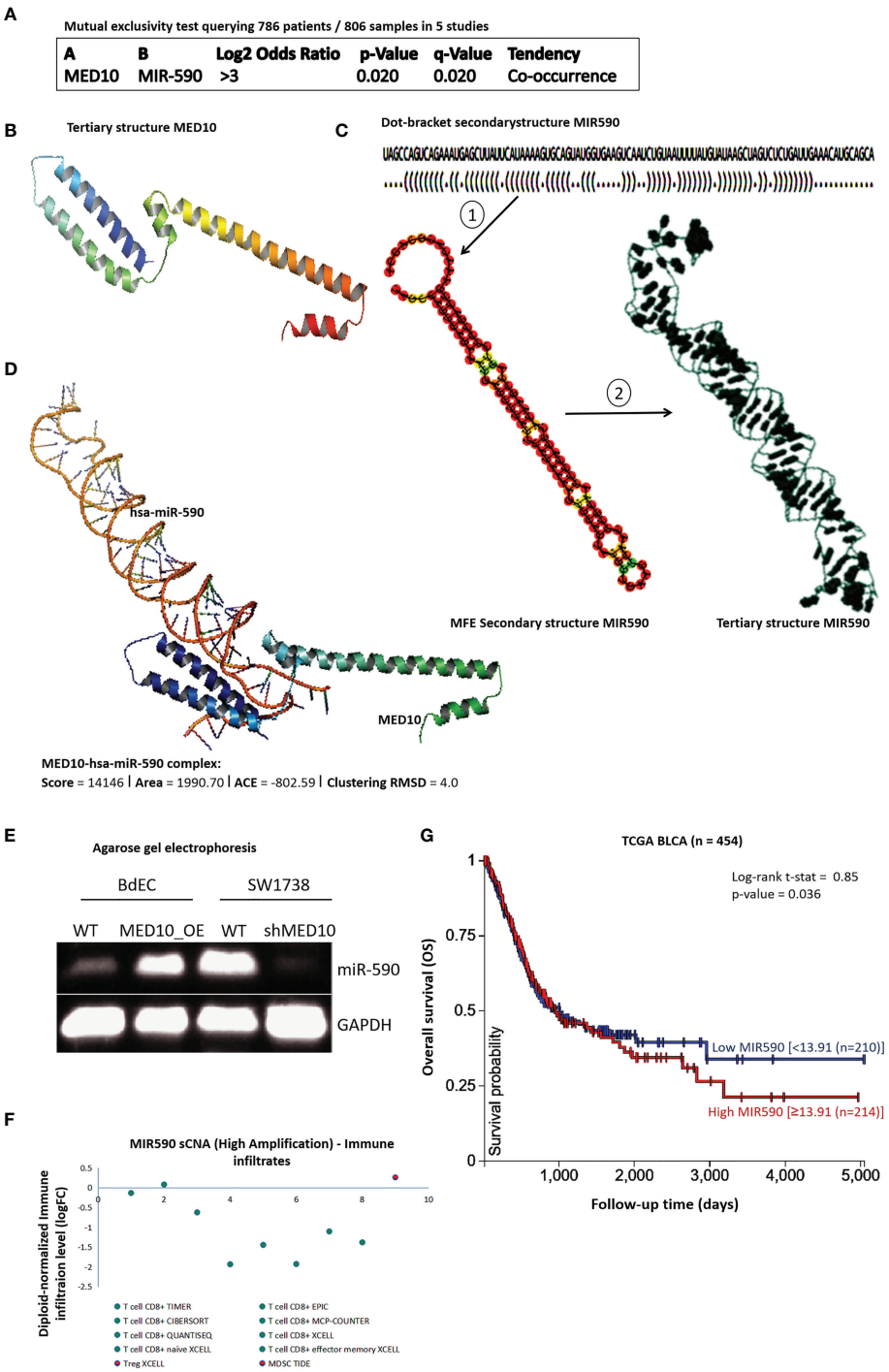


FIGURE 4 | MED10 interacts directly with hsa-miR-590, a modulator of immune infiltration and survival. **(A)** Depiction of mutual exclusivity test data showing tendency and likelihood of MED10 and hsa-miR-590 to co-occur in pool of 5 BLCA/UC studies. **(B)** Sequence-derived 3D structure of MED10. **(C)** The optimal secondary structure in dot-bracket notation with a minimum free energy (MFE) of –31.20 kcal/mol *(upper)*. The RNAfold-generated MFE secondary folding structure pattern of hsa-miR-590 *(lower left)*. The hsa-miR-590 3D structure generated based on the secondary structure in dot-bracket notation *(lower right)*. **(D)** Molecular docking showing the direct interaction between MED10 and hsa-miR-590. The 3D transformation data, consisting of three rotational angles (2.42°, 0.38°, 120.70°) and three translational parameters (–1.18, –53.27, –102.28) applied on the ligand molecule, hsa-miR-590. **(E)** Representative agarose gel electrophoresis image of the effect of altered MED10 protein expression on the expression level of hsa-miR-590 in BdEC and SW1738 cells. GAPDH served as loading control. WT, wild type. **(F)** Dot plot showing the effect of high amplification of hsa-miR-590 on the immune cell infiltration levels. **(G)** Kaplan–Meier plot of the effect of altered hsa-miR-590 expression in the TCGA BLCA cohort.

MED10 interacts directly with and upregulates hsa-miR-590 expression in BLCA/UC cells. For functional insights, using the TIMER 2.0 algorithm (23), our correlative sCNA analyses showed that akin to MED10, high amplification of hsa-miR-590 was largely correlated with suppressed CD8+ T cell infiltration level but is positively correlated with Treg infiltration (Spearman rho_{XCELL} = 0.31) (**Figure 4F**). Moreover, survival analysis of the TCGA BLCA cohort (n = 454) showed that high hsa-miR-590 expression conferred survival disadvantage compared to low expression (t-stat = 0.85, p = 0.04) (**Figure 4G**). These data indicate, at least in part, that MED10 interacts directly with hsa-miR-590, a modulator of immune infiltration and survival.

Targeting MED10 Elicits Downregulation of hsa-miR-590-5p Expression Preferentially in Metastatic, Transitional Cell (Urothelial) Carcinoma Cells

Reaffirming previous data, we demonstrated similarity in the cancer-normal differential expression profile of *MED10* (fold change, FC = 1.76, p = 5.7e-06) and hsa-miR-590-5p (FC = 5.78, p = 1.4e-30) in the TCGA BLCA cohort (**Figures 5A, B**). To rule out multifactorial inter-sample inconsistencies/variation and establish replicability of the observed expression profile, our gene detectability power analysis of the GSE81157 aggressive BLCA cohort (n = 9) showed that variation in the true abundance of *MED10* (biological coefficient of variation, BCOV = 0.17, power = 0.99) or hsa-miR-590 (BCOV = 0.45, power = 0.02) between replicate RNA samples was apparently insignificant (**Figure 5C**). Bioinformatics-aided evaluation of CRISPR-induced loss of MED10 function (criMED10) in 29 BLCA cell lines showed that increased suppression of *med10* elicited increased downregulation of hsa-miR-590 copy number in metastatic cell lines 253J, UMUC1, UMUC13, UMUC14, and JMSU1 (Spearman r = 0.30) compared with the apparent non-effect in primary tumor cell lines (Spearman r = -0.003) (**Figure 5D**). Furthermore, in a non-stratified CCLE–Broad–MIT pool of BLCA cells, criMED10 had no apparent effect (Pearson r = 0.03); however, upon extraction and probe of only transitional cell carcinoma/UC cells, we found that criMED10 elicits suppressed expression of hsa-miR-590-5p in the BC3C, UMUC1, RT112, TCCSUP, BFTC905, UMUC3, VMCUB1, KU1919, 639V, and CAL29 UC cell lines (**Figure 5E**). These data indicate that targeting MED10

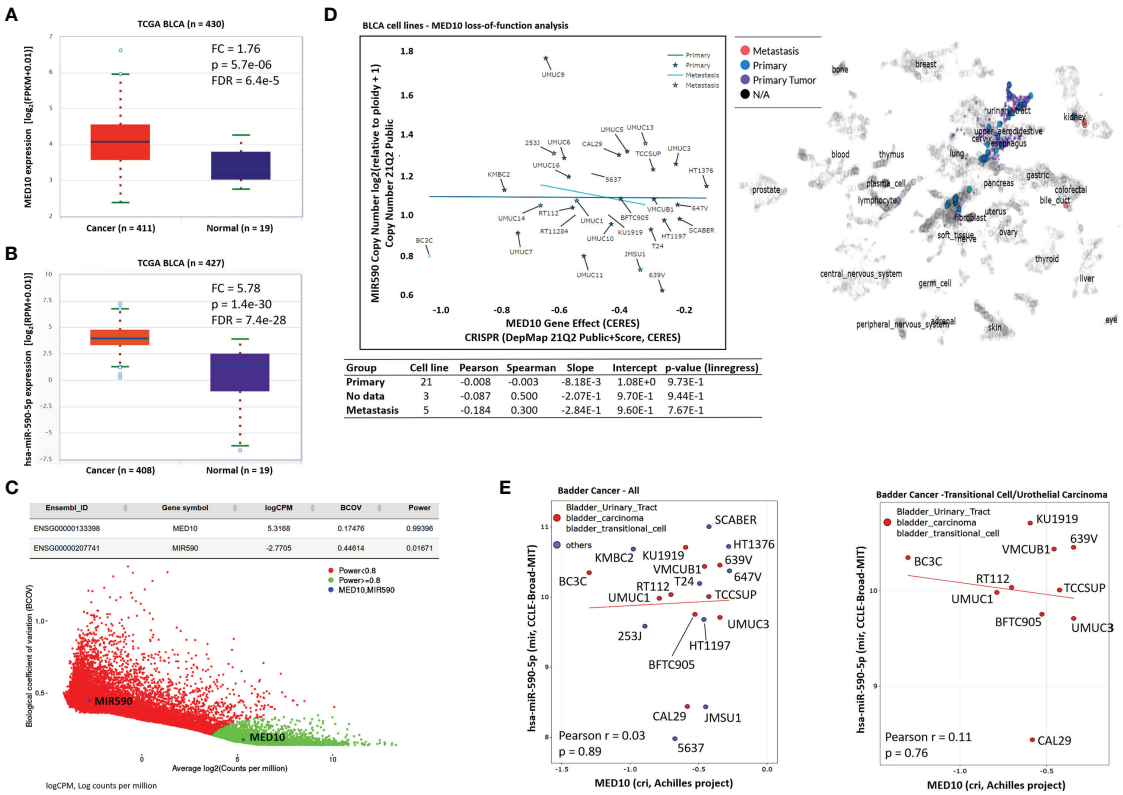


FIGURE 5 | Targeting MED10 elicits downregulation of hsa-miR-590-5p expression preferentially in metastatic, transitional cell (urothelial) carcinoma cells. Box and whisker plots of the differential expression of **(A)** MED10 or **(B)** hsa-miR-590-5p in cancer and normal samples from the TCGA BLCA cohort. **(C)** Scatter-plot of the biological coefficient of variation (BCOV) against the average abundance of MED10 and MIR590 in the GSE81157 aggressive bladder cancer cohort. **(D)** Graphical representation of the effect of MED10 loss of function on hsa-miR-590 copy number in 29 metastatic or primary BLCA cell lines from the 21Q2 Public cohort *(left)*. Chart showing the spatial distribution of the BLCA cell lines according to metastasis status *(right)*. Visualization of the effect of MED10 knockout on hsa-miR-590-5p expression in **(E)** mixed pool of BLCA cell lines *(left)*, or purely bladder transitional/UC cell lines *(right)*.

elicits downregulation of hsa-miR-590-5p expression preferentially in metastatic, transitional cell (urothelial) carcinoma cells.

shRNA-Mediated Targeting of MED10 in Bladder Urothelial Carcinoma Cells Significantly Attenuates Their Oncogenicity and Metastatic and Cancer Stemness Phenotypes

Having shown that targeting MED10 elicits downregulation of hsa-miR-590-5p expression preferentially in metastatic, transitional cell (urothelial) carcinoma cells, for functional characterization of the effect of altered MED10/hsa-miR-590-5p signaling in UC cells, we performed several functional assays. We observed that shMED10 significantly suppressed the proliferation of SW1738 (4.47-fold, $p < 0.001$) and JMSU1 (4.88-fold, $p < 0.01$) cells (**Figure 6A**). Results of our migration assays demonstrate that shMED10 markedly attenuated the migration of JMSU1 cells (2.11-fold, $p < 0.01$) (**Figure 6B**). shMED10 also significantly inhibited the invasive capability of JMSU1 cells (4.35-fold, $p < 0.01$) (**Figure 6C**). Similarly, we demonstrated that shMED10 profoundly suppressed the ability of the SW1738 (9.58-fold, $p < 0.001$) and JMSU1 (3.28-fold, $p < 0.01$) cells to form colonies (**Figure 6D**). In parallel assays, we found that shMED10 significantly downregulated the expression levels of MED10, anti-apoptosis BCL-xL, proliferation marker MKI67/Ki67, biomarkers of metastasis VIM and SNAI1, and stemness/pluripotency markers OCT4 and LIN28A, while concomitantly upregulating pro-apoptosis BAX protein in both the SW1738 and JMSU1 cells (**Figure 6E**). Because of the association of onco-aggression and disease recurrence with cancer stemness (21), we assessed for probable effects of altered MED10/hsa-miR-590 signaling on cancer stem cell activities in UC cells. Reanalysis of the AFFY_HG_U133_PLUS_2, GSE31684 UC cohort (n = 93) showed that MED10 is co-overexpressed with stemness markers CD44, SOX2, PROM1/CD133, KLF4, NANOG, and LIN28A in patients with urothelial recurrence and is concomitantly upregulated with NANOG and CD44 in patients with local recurrence, but profoundly suppressed, akin to the other stemness/pluripotency markers, in patients with non-recurrent disease (**Figure 7A**). Interestingly, using our in-house bladder UC tissue samples (n = 79), we showed that compared with the benign tissue samples, MED10 expression, alongside Ki67, OCT4, and LIN28A, is disease progression from non-muscle invasive bladder cancer (NMIBC: pT1) to muscle-invasive bladder cancer (MIBC: pT2–pT4) and more so in patients with distant metastatic disease (M1) (benign < T1 < T2 < T3/4 < M1) (**Figure 7B**). Reminiscent of the loss of self-renewal capability, we demonstrated that shMED10 significantly suppressed the ability of the SW1738 and JMSU1 cells to form primary and subsequently secondary tumorspheres, quantitatively and qualitatively (**Figure 7C**), with concomitant inhibition of the nuclear translocation and co-localization of the pluripotency/stemness markers OCT4 and LIN28A (**Figure 7D**). This is further corroborated by our biological function gene ontology (GO) enrichment analysis showing that MED10 networks with hsa-miR-590, KLF4, SOX2, OCT4/POU5F1, LIN28A, and NANOG and is implicated in "stem cell population maintenance" (GO:0019827: FDR-adjusted p = 5.0e-10), "somatic stem cell population maintenance" (GO:0035019: FDR-adjusted p = 7.2e-09), "maintenance of cell number" (GO:0098727: FDR-adjusted p = 5.0e-10), and "cell fate commitment" (GO:0045165: FDR-adjusted p = 3.3e-04) (**Supplementary Figure 1**). These data demonstrate that targeting MED10 in bladder UC cells significantly attenuates their oncogenicity and metastatic and cancer stemness phenotypes.

DISCUSSION

Bladder UC, one of the most frequently diagnosed cancers globally, is increasingly characterized by early metastasization, unabated disease recurrence after initial response, and dismal prognosis in spite of diagnostic and therapeutic advances. This necessitates the identification and characterization of probable molecular mechanisms underlying its progression as a prelude for discovery of novel actionable diagnostic and prognostic biomarkers, and development of new efficacious therapeutic strategies for patients with UC.

The Mediator complex plays an essential role in the transduction of signals from enhancer region-bond activators of transcription to promoter site-associated RNA Pol II basal transcription machinery, to activate or repress transcription factors at distant genomic regions (10, 11, 24). This alteration of transcription factor activity with associated alterations in gene expression is characteristic of human health and diseases, including BLCA (25–27). In the present study, we provide preclinical evidence that MED10, a regulator of transcription, is aberrantly expressed in patients with BLCA and this has an adverse prognostic implication. This is consistent with accruing evidence of the tumor-promoting roles of components of the multi-protein Mediator complex, including reports that Mediator subunit CDK19 is specifically expressed in prostate cancer, with upregulated expression being associated with disease progression, as observed in patients with metastatic and castration-resistant disease (28). More so, several reports indicate that other subunits of the Mediator complex, which are actively involved in regulating estrogen and androgen receptor gene expression, are altered in some endocrine malignancies, such as prostate and breast cancer (19, 20, 29). We also show, for the first time to the best of our knowledge, that MED10 expression is positively correlated with disease progression, immune suppression, and therapy failure. This is in part corroborated by reports that the upregulation of MED28 expression by FOXD3-AS1, with concomitant suppression of miR-127-3p, promoted non-small cell lung cancer (NSCLC) cell proliferation and invasion, *in vitro*, and enhanced xenograft tumor growth (30). Considering the systemic nature of cancer, and the significant alteration observed in the global immune landscape of patients with refractory, metastatic, and/or recurrent cancer, our data showing that elevated *MED10* expression is associated with low levels of tumor-infiltrating CD8+ T cells and high MDSC and Treg levels is of therapeutic

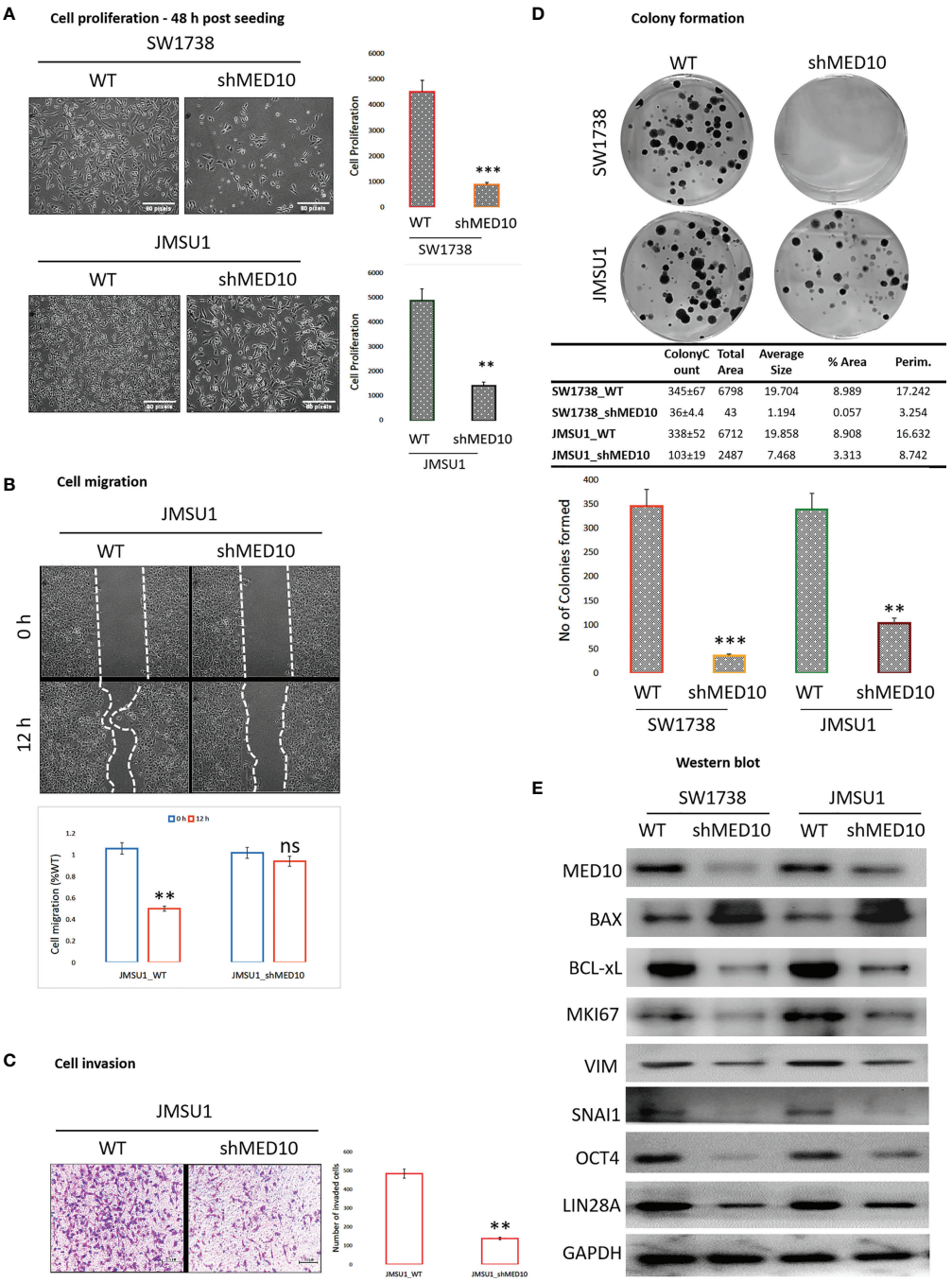


FIGURE 6 | shRNA-mediated targeting of MED10 in bladder urothelial carcinoma cells significantly attenuate their oncogenicity and metastatic phenotype. Photomicrographs and histograms showing the effect of knocking down MED10 on the **(A)** proliferation, ***(B)*** migration, **(C)** invasion, and **(D)** colony formation of SW1738 and JMSU1 cells. **(E)** Representative Western blot images showing the effect of shMED10 on the expression of MED10, BAX, BCL-xL, VIM, SNAI1, OCT4, or LIN28A protein expression level in SW1738 and JMSU1 cells. GAPDH serve as loading control. ns, not significant; **p < 0.01; ***p < 0.001.

relevance, especially as the peripheral immune system is an essential driver of effective innate and treatment-induced anticancer immune responses (31). Tregs are required to maintain host immune tolerance and often cross talk with conventional T cell signaling, including those from the principal mediator of anticancer immunity, CD8+ T cells; however, Foxp3+ Tregs suppress anticancer immunity, facilitate evasion of immunosurveillance, hamper efficient anticancer immune response, and confer resistance to therapy (31, 32). Consistent with accruing evidence that sensitivity to

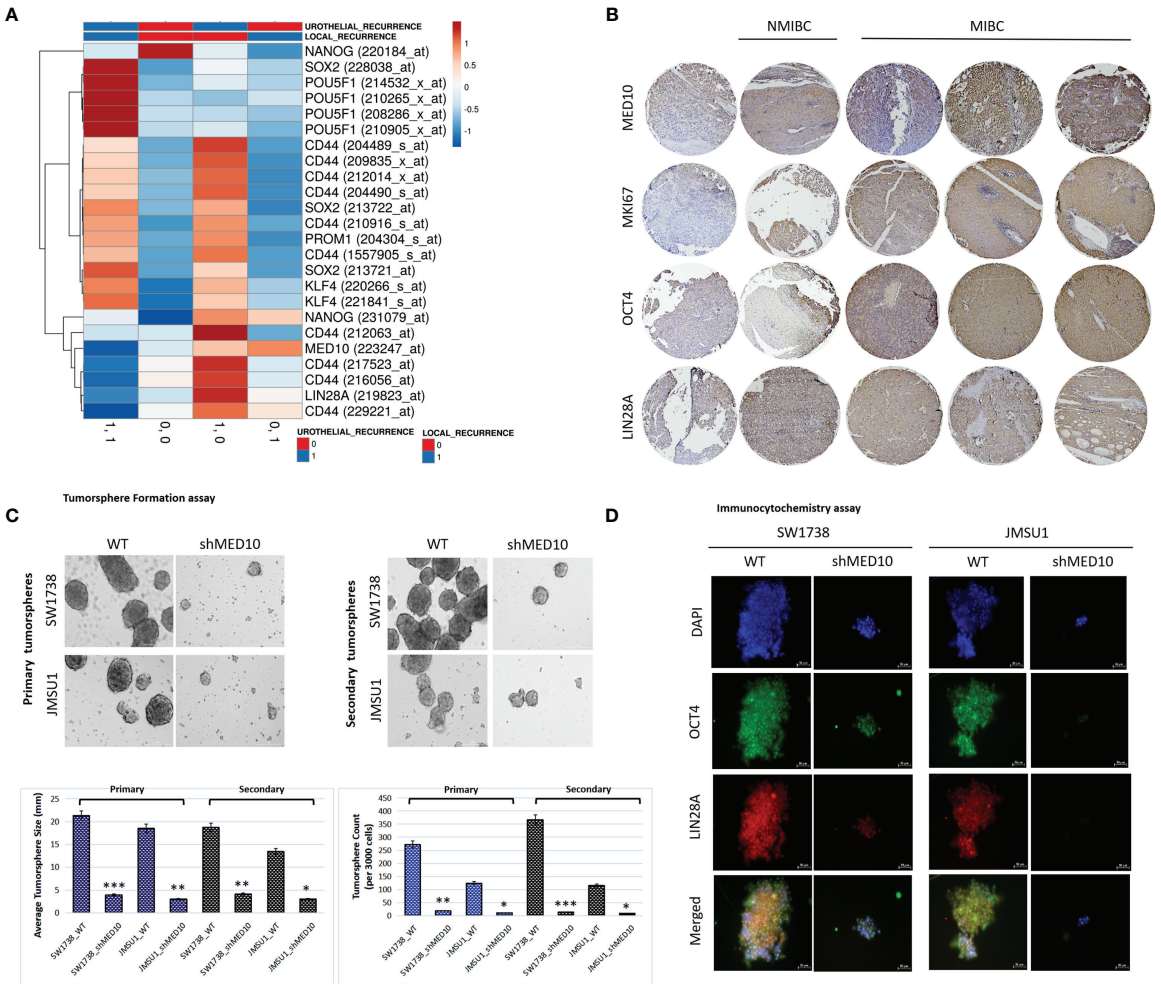


FIGURE 7 | shRNA-mediated targeting of MED10 in bladder urothelial carcinoma cells significantly attenuate their cancer stemness phenotype. **(A)** Heatmap showing the correlation between the expression of MED10, and stemness markers NANOG, SOX2, POU5F1/OCT4, CD44, PROM1/CD133, KLF4, and LIN28A in patients with urothelial recurrence or local recurrence from the AFFY_HG_U133_PLUS_2, GSE31684 cohort. Columns with similar annotations are collapsed by taking mean inside each group. Rows are centered; unit variance scaling is applied to rows. Both rows and columns are clustered using correlation distance and average linkage. 24 rows, 4 columns. **(B)** Immunohistochemistry photomicrographs of the differential expression of MED10, MKI67, OCT4, and LIN28A in benign, T1, T2, T3/4, or M1 tissue samples from the TMU-SHH UC cohort. Scale bar 200 μm. **(C)** Photomicrographs and histograms showing the effect of shMED10 on the formation of primary or secondary tumorspheres from SW1738 and JMSU1 cells. **(D)** Representative immunofluorescence images showing the effect of knocking down MED10 on the nuclear translocation and co-localization of OCT4A and LIN28A. DAPI served as nuclear marker. Scale bar 50 μm. *$p < 0.05$; **$p < 0.01$; ***$p < 0.001$.

anticancer therapy is favored by the pooling and activity of activated CD8+ T cells within the tumor microenvironment, with associated enhanced CD8+ T cell-based immune response, we posit that MED10 induces an immunosuppressive tumor microenvironment, by upregulating Treg and/or MDSC activity, dysregulating associated immune regulatory molecules, hampering lymphocyte homing, and depleting metabolites required for CD8+ T cell differentiation and function, all of which are implicated in reduced sensitivity or resistance to anticancer therapy (32 – 33). Thus, targeting MED10 may represent an alternative approach to inducing effective immune responses and/or re-invigorating preexisting anticancer immune responses.

Furthermore, against the background of the just emerging role of the Mediator complex in the regulation of non-coding RNAs, we demonstrated that MED10 is co-expressed with hsa-miR-590 and interacts directly with hsa-miR-590 but is inversely associated with tumor-suppressor microRNAs and that this interaction modulates immune infiltration and survival. The broadly documented differential expression of miRs in malignancies is increasingly considered a tenet of cancer initiation, progression, and therapy response (34). Corollary to our finding, it was recently reported that increased expression of Mediator subunit MED1 induces upregulation of the miR-191/425 cluster (namely, miR-100-5p, miR-191-5p, miR-193b-3p, miR-205-5p, miR-326, miR-422a and miR-425-5p), in breast

cancer, and that this promotes cell proliferation and migration (35). More so, concordant with our finding that high hsa-miR-590 expression conferred survival disadvantage compared to low expression, a recent study based on single-sample gene-set enrichment analysis (ssGSEA) and least absolute shrinkage and selection operator (LASSO) Cox regression modeling suggested that certain miRs are significantly associated with immune-related response and pathways that are critical for initiation and progression of head and neck squamous cell carcinoma (HNSCC) (36). In addition, the expression of these immune-related miRs was shown to be strongly correlated with immune cell infiltration and expression of immune checkpoints, thus implicating probable immunosuppressive microenvironment in patients' poor prognoses (36).

Despite common knowledge that nearly all bladder UC-specific deaths follow from metastatic disease, the genomic bio-drivers of disease progression and metastatic recurrence remain poorly understood. Interestingly, and of clinical relevance especially in the context of patient stratification for precision medicine, we demonstrated that targeting MED10 elicits downregulation of hsa-miR-590-5p expression preferentially in metastatic, transitional cell (urothelial) carcinoma cells and significantly attenuates their oncogenicity and metastatic and cancer stemness phenotypes. We posit that this preferential downregulation of the hsa-miR-590-5p sequel to MED10 inhibition is suggestive of a putative role for altered MED10/hsa-miR-590-5p signaling in the management of patients with metastatic or recurrent bladder UC, and in the light of other data present herein, we speculate that MED10 is a promising molecular candidate for urothelial cancer immunotherapy. Howbeit thematically different, the team of Lewis Chodosh in a contextually analogous study (37) demonstrated that certain genes, namely, MYLK, PEAK1, SLC2A4RG, EVC2, XIRP2, PALB2, and ESR1, and pathways such as WNT/β-catenin, PI3K/mTOR, CDK/RB, and cAMP/PKA are mutated or exhibit sCNA preferentially in metastases, compared with paired primary tumors. Pooled together with ours, these findings provide some genomic bases for developing efficacious targeted or immune-based therapy for metastatic disease. Our finding is also reminiscent of the oncogene addiction concept (38); inferring from our data, it is rationally conceivable that metastatic/recurrent bladder UC are addicted to MED10/hsa-miR-590-5p signaling, thus representing a therapeutic Achilles' heel that makes these metastatic UC cells particularly susceptible or sensitive to inhibition of MED10 singly.

Moreover, concurring that "cancer stem cells are the leading power behind tumor growth, with the ability of self-renewal, metastasis, and resistance to conventional chemotherapy" (39), our data showing that MED10 is co-overexpressed with stemness markers CD44, SOX2, PROM1/CD133, KLF4, NANOG, and LIN28A in patients with urothelial recurrence and concomitantly upregulated with NANOG and CD44 in patients with local recurrence, but profoundly suppressed, akin to the other stemness/pluripotency markers, in patients with non-recurrent disease, are also clinically relevant. This finding is also corroborated, in part, by studies showing that the master pluripotency transcription factors Oct4, Sox2, and Nanog bind to cis-acting enhancers and recruit Mediator to activate most of the pluripotent embryonic stem cell (ESC) gene expression program (40). It thus may be inferred that the reduced expression of MED10 (and by inference, pluripotency factors) "cause preferential loss of expression of super-enhancer-associated genes" which are essential for maintaining "cancer cell identity" and promoting oncogene transcription (40, 41). Once again, this bio-event is suggestive of how MED10-induced or -mediated alteration in gene (stemness, oncogenic) expression may be exploited for development of an efficacious anti-metastasis, anti-recurrence therapeutic strategy in bladder UC clinics.

CONCLUSIONS

These data provide preclinical evidence that dysregulated MED10/MIR590 signaling drives onco-aggression, disease progression, and recurrence of bladder UC and that this oncogenic signal is therapeutically actionable for repressing the metastatic/recurrent phenotypes, enhancing therapy response, and shutting down stemness-driven disease progression and relapse in patients with BLCA/UC.

DATA AVAILABILITY STATEMENT

The original contributions presented in the study are included in the article/**Supplementary Material**. Further inquiries can be directed to the corresponding authors.

ETHICS STATEMENT

The studies involving human participants were reviewed and approved by the Joint Institutional Review Board (JIRB) of Taipei Medical University. The procurement of the samples was strictly adherent to the approved IRB (No. N202102034) issued by the JIRB. Informed consent was waived because of the retrospective nature of the study. Written informed consent for participation was not required for this study in accordance with the national legislation and the institutional requirements.

AUTHOR CONTRIBUTIONS

OAB, C-CW—study conception and design, collection and assembly of data, data analysis and interpretation, and manuscript writing. Y-HW, S-WH, W-LW, C-TY, C-CW—data analysis and interpretation. OAB, C-CW—provision of resources and administrative oversight. All authors contributed to the article and approved the submitted version.

FUNDING

This study was also supported by grants from the Teh-Tzer Study Group for Human Medical Research Foundation (TMRF) [A1091044] to OAB and grants from the Ministry of Science and Technology (MOST) to C-CW [MOST-110-2314-B-038-038] and OAB [MOST-110-2314-B-038-035].

ACKNOWLEDGMENTS

The authors thank all research assistants of the Department of Medical Research & Education and Core Facility Center, Taipei Medical University - Shuang Ho Hospital, for their assistance with the molecular and cell-based assays.

SUPPLEMENTARY MATERIAL

The Supplementary Material for this article can be found online at: https://www.frontiersin.org/articles/10.3389/fonc.2021.744937/full#supplementary-material

Supplementary Figure 1 | The MED10/MIR590 signaling plays a critical role in stem cell population maintenance and cell fate determination. GO term enrichment was based on biological function. GO, gene ontology.

REFERENCES

1. Ferlay J, Ervik M, Lam F, Colombet M, Mery L, Piñeros M, et al. *Global Cancer Observatory: Cancer Today* (2020). Lyon, France: International Agency for Research on Cancer. Available at: https://gco.iarc.fr/today (Accessed [12 March 2021).
2. Lenis AT, Lec PM, Chamie K, Mshs MD. Bladder Cancer: A Review. *JAMA* (2020) 324(19):1980–91. doi: 10.1001/jama.2020.17598
3. Woldu SL, Bagrodia A, Lotan Y. Guideline of Guidelines: non-Muscle-Invasive Bladder Cancer. *BJU Int* (2017) 119(3):371–80. doi: 10.1111/bju.13760
4. Crabb SJ, Douglas J. The Latest Treatment Options for Bladder Cancer. *Br Med Bull* (2018) 128(1):85–95. doi: 10.1093/bmb/ldy034
5. Burger M, Catto JW, Dalbagni G, Grossman HB, Herr H, Karakiewicz P, et al. Epidemiology and Risk Factors of Urothelial Bladder Cancer. *Eur Urol* (2013) 63(2):234–41. doi: 10.1016/j.eururo.2012.07.033
6. Babjuk M, Burger M, Compérat EM, Gontero P, Mostafid AH, Palou J, et al. European Association of Urology Guidelines on Non-Muscle-Invasive Bladder Cancer (TaT1 and Carcinoma *In Situ*) - 2019 Update. *Eur Urol* (2019) 76(5):639–57. doi: 10.1016/j.eururo.2019.08.016
7. Alfred Witjes J, Lebret T, Compérat EM, Cowan NC, De Santis M, Bruins HM, et al. Updated 2016 EAU Guidelines on Muscle-Invasive and Metastatic Bladder Cancer. *Eur Urol* (2017) 71(3):462–75. doi: 10.1016/j.eururo.2016.06.020
8. Ferro M, La Civita E, Liotti A, Cennamo M, Tortora F, Buonerba C, et al. Liquid Biopsy Biomarkers in Urine: A Route Towards Molecular Diagnosis and Personalized Medicine of Bladder Cancer. *J Pers Med* (2021) 11(3):237. doi: 10.3390/jpm11030237
9. Crocetto F, Cimmino A, Ferro M, Terracciano D. Circulating Tumor Cells in Bladder Cancer: A New Horizon of Liquid Biopsy for Precision Medicine. *J Basic Clin Physiol Pharmacol* (2021). doi: 10.1515/jbcpp-2021-0233
10. Laham-Karam N, Pinto GP, Poso A, Kokkonen P. Transcription and Translation Inhibitors in Cancer Treatment. *Front Chem* (2020) 8:276. doi: 10.3389/fchem.2020.00276
11. Petrenko N, Jin Y, Wong KH, Struhl K. Mediator Undergoes a Compositional Change During Transcriptional Activation. *Mol Cell* (2016) 64(3):443–54. doi: 10.1016/j.molcel.2016.09.015
12. Zhao M, Yang X, Fu Y, Wang H, Ning Y, Yan J, et al. Mediator MED15 Modulates Transforming Growth Factor Beta (TGFβ)/Smad Signaling and Breast Cancer Cell Metastasis. *J Mol Cell Biol* (2013) 5(1):57–60. doi: 10.1093/jmcb/mjs054
13. Pérot G, Croce S, Ribeiro A, Lagarde P, Velasco V, Neuville A, et al. MED12 Alterations in Both Human Benign and Malignant Uterine Soft Tissue Tumors. *PloS One* (2012) 7(6):e40015. doi: 10.1371/journal.pone.0040015
14. Liyanage C, Wathupola A, Muraleetharan S, Perera K, Punyadeera C, Udagama P. Promoter Hypermethylation of Tumor-Suppressor Genes P16ink4a,RASSF1A,TIMP3, and PCQAP/MED15 in Salivary DNA as a Quadruple Biomarker Panel for Early Detection of Oral and Oropharyngeal Cancers. *Biomolecules* (2019) 9(4):148. doi: 10.3390/biom9040148
15. Ndong Jde L, Jean D, Rousselet N, Frade R. Down-Regulation of the Expression of RB18A/MED1, A Cofactor of Transcription, Triggers Strong Tumorigenic Phenotype of Human Melanoma Cells. *Int J Cancer* (2009) 124(11):2597–606. doi: 10.1002/ijc.24253
16. Kim HJ, Roh MS, Son CH, Kim AJ, Jee HJ, Song N, et al. Loss of Med1/TRAP220 Promotes the Invasion and Metastasis of Human non-Small-Cell Lung Cancer Cells by Modulating the Expression of Metastasis-Related Genes. *Cancer Lett* (2012) 321(2):195–202. doi: 10.1016/j.canlet.2012.02.009
17. Yun J, Son CH, Um SJ, Kwon HC, Lee KE, Choi PJ, et al. A Different TRAP220 Expression in Distinct Histologic Subtypes of Lung Adenocarcinoma and the Prognostic Significance. *Lung Cancer* (2011) 71(3):312–8. doi: 10.1016/j.lungcan.2010.06.012
18. Klümper N, Syring I, Vogel W, Schmidt D, Müller SC, Ellinger J, et al. Mediator Complex Subunit MED1 Protein Expression Is Decreased During Bladder Cancer Progression. *Front Med (Lausanne)* (2017) 4:30. doi: 10.3389/fmed.2017.00030
19. Cui J, Germer K, Wu T, Wang J, Luo J, Wang SC, et al. Cross-Talk Between HER2 and MED1 Regulates Tamoxifen Resistance of Human Breast Cancer Cells. *Cancer Res* (2012) 72:5625–34. doi: 10.1158/0008-5472.CAN-12-1305
20. Wu D, Zhang Z, Chen X, Yan Y, Liu X. Angel or Devil ? - CDK8 as the New Drug Target. *Eur J Med Chem* (2021) 213:113043. doi: 10.1016/j.ejmech.2020.113043
21. Stavast CJ, Erkeland SJ. The Non-Canonical Aspects of MicroRNAs: Many Roads to Gene Regulation. *Cells* (2019) 8(11):1465. doi: 10.3390/cells8111465
22. Di Leva G, Garofalo M, Croce CM. MicroRNAs in Cancer. *Annu Rev Pathol* (2014) 9:287–314. doi: 10.1146/annurev-pathol-012513-104715
23. Li T, Fu J, Zeng Z, Cohen D, Li J, Chen Q, et al. TIMER2.0 for Analysis of Tumor-Infiltrating Immune Cells. *Nucleic Acids Res* (2020) 48(W1):W509–14. doi: 10.1093/nar/gkaa407
24. Soutourina J. Transcription Regulation by the Mediator Complex. *Nat Rev Mol Cell Biol* (2018) 19(4):262–74. doi: 10.1038/nrm.2017.115
25. Guo Y, Yuan X, Li K, Dai M, Zhang L, Wu Y, et al. GABPA is a Master Regulator of Luminal Identity and Restrains Aggressive Diseases in Bladder Cancer. *Cell Death Differ* (2020) 27(6):1862–77. doi: 10.1038/s41418-019-0466-7
26. Wang KJ, Wang C, Dai LH, Yang J, Huang H, Ma XJ, et al. Targeting an Autocrine Regulatory Loop in Cancer Stem-Like Cells Impairs the Progression and Chemotherapy Resistance of Bladder Cancer. *Clin Cancer Res* (2019) 25(3):1070–86. doi: 10.1158/1078-0432.CCR-18-0586
27. Audenet F, Attalla K, Sfakianos JP. The Evolution of Bladder Cancer Genomics: What Have We Learned and How can We Use it? *Urol Oncol* (2018) 36(7):313–20. doi: 10.1016/j.urolonc.2018.02.017
28. Becker F, Joerg V, Hupe MC, Roth D, Krupar R, Lubczyk V, et al. Increased Mediator Complex Subunit CDK19 Expression Associates With Aggressive Prostate Cancer. *Int J Cancer* (2020) 146(2):577–88. doi: 10.1002/ijc.32551
29. Weber H, Garabedian MJ. The Mediator Complex in Genomic and non-Genomic Signaling in Cancer. *Steroids* (2018) 133:8–14. doi: 10.1016/j.steroids.2017.11.007
30. Zeng ZL, Zhu HK, He LF, Xu X, Xie A, Zheng EK, et al. Highly Expressed lncRNA FOXD3-AS1 Promotes Non-Small Cell Lung Cancer Progression *via* Regulating miR-127-3p/Mediator Complex Subunit 28 Axis. *Eur Rev Med Pharmacol Sci* (2020) 24(5):2525–38. doi: 10.26355/eurrev_202003_20520
31. Hiam-Galvez KJ, Allen BM, Spitzer MH. Systemic Immunity in Cancer. *Nat Rev Cancer* (2021) 21(6):345–59. doi: 10.1038/s41568-021-00347-z

32. Li C, Jiang P, Wei S, Xu X, Wang J. Regulatory T Cells in Tumor Microenvironment: New Mechanisms, Potential Therapeutic Strategies and Future Prospects. *Mol Cancer* (2020) 19(1):116. doi: 10.1186/s12943-020-01234-1
33. Groth C, Hu X, Weber R, Fleming V, Altevogt P, Utikal J, et al. Immunosuppression Mediated by Myeloid-Derived Suppressor Cells (MDSCs) During Tumour Progression. *Br J Cancer* (2019) 120(1):16–25. doi: 10.1038/s41416-018-0333-1
34. Paliouras AR, Monteverde T, Garofalo M. Oncogene-Induced Regulation of microRNA Expression: Implications for Cancer Initiation, Progression and Therapy. *Cancer Lett* (2018) 421:152–60. doi: 10.1016/j.canlet.2018.02.029
35. Nagpal N, Sharma S, Maji S, Durante G, Ferracin M, Thakur JK, et al. Essential Role of MED1 in the Transcriptional Regulation of ER-Dependent Oncogenic miRNAs in Breast Cancer. *Sci Rep* (2018) 8(1):11805. doi: 10.1038/s41598-018-29546-9
36. Ma B, Li H, Qiao J, Meng T, Yu R. Immune-Related miRNA Signature Identifies Prognosis and Immune Landscape in Head and Neck Squamous Cell Carcinomas. *Biosci Rep* (2020) 40(11):BSR20201820. doi: 10.1042/BSR20201820
37. Paul MR, Pan TC, Pant DK, Shih NN, Chen Y, Harvey KL, et al. Genomic Landscape of Metastatic Breast Cancer Identifies Preferentially Dysregulated Pathways and Targets. *J Clin Invest* (2020) 130(8):4252–65. doi: 10.1172/JCI129941
38. Pagliarini R, Shao W, Sellers WR. Oncogene Addiction: Pathways of Therapeutic Response, Resistance, and Road Maps Toward a Cure. *EMBO Rep* (2015) 16(3):280–96. doi: 10.15252/embr.201439949
39. Abugomaa A, Elbadawy M, Yamawaki H, Usui T, Sasaki K. Emerging Roles of Cancer Stem Cells in Bladder Cancer Progression, Tumorigenesis, and Resistance to Chemotherapy: A Potential Therapeutic Target for Bladder Cancer. *Cells* (2020) 9(1):235. doi: 10.3390/cells9010235
40. Whyte WA, Orlando DA, Hnisz D, Abraham BJ, Lin CY, Kagey MH, et al. Master Transcription Factors and Mediator Establish Super-Enhancers at Key Cell Identity Genes. *Cell* (2013) 153(2):307–19. doi: 10.1016/j.cell.2013.03.035
41. Clara JA, Monge C, Yang Y, Takebe N. Targeting Signalling Pathways and the Immune Microenvironment of Cancer Stem Cells - a Clinical Update. *Nat Rev Clin Oncol* (2020) 17(4):204–32. doi: 10.1038/s41571-019-0293-2

Conflict of Interest: The authors declare that the research was conducted in the absence of any commercial or financial relationships that could be construed as a potential conflict of interest.

Publisher's Note: All claims expressed in this article are solely those of the authors and do not necessarily represent those of their affiliated organizations, or those of the publisher, the editors and the reviewers. Any product that may be evaluated in this article, or claim that may be made by its manufacturer, is not guaranteed or endorsed by the publisher.

Copyright © 2022 Wu, Wang, Hu, Wu, Yeh and Bamodu. This is an open-access article distributed under the terms of the Creative Commons Attribution License (CC BY). The use, distribution or reproduction in other forums is permitted, provided the original author(s) and the copyright owner(s) are credited and that the original publication in this journal is cited, in accordance with accepted academic practice. No use, distribution or reproduction is permitted which does not comply with these terms.

frontiers in Oncology

ORIGINAL RESEARCH
published: 21 January 2022
doi: 10.3389/fonc.2022.740051

Anti-Tumor Role of CAMK2B in Remodeling the Stromal Microenvironment and Inhibiting Proliferation in Papillary Renal Cell Carcinoma

*Qingan Jia[1], Xia Liao[2], Yaoyao Zhang[1], Binghui Xu[1], Yuna Song[1], Ganlan Bian[1] and Xiaoliang Fu[3]**

[1] Xi'an Key Laboratory of Stem Cell and Regenerative Medicine, Institute of Medical Research, Northwestern Polytechnical University, Xi'an, China, [2] Department of Nutrition, First Affiliated Hospital of Xi'an Jiaotong University, Xi'an, China, [3] Department of Urology, The Second Affiliated Hospital of Air Force Medical University, Xi'an, China

OPEN ACCESS

Edited by:
Sanja Štifter,
Skejby Sygehus, Denmark

Reviewed by:
Julia Heinzelbecker,
Saarland University Hospital, Germany
Simin Li,
Southern Medical University, China

***Correspondence:**
Xiaoliang Fu
fuxiaoliang7515@163.com

Specialty section:
This article was submitted to Genitourinary Oncology, a section of the journal Frontiers in Oncology

Received: 12 July 2021
Accepted: 03 January 2022
Published: 21 January 2022

Citation:
Jia Q, Liao X, Zhang Y, Xu B, Song Y, Bian G and Fu X (2022) Anti-Tumor Role of CAMK2B in Remodeling the Stromal Microenvironment and Inhibiting Proliferation in Papillary Renal Cell Carcinoma. Front. Oncol. 12:740051. doi: 10.3389/fonc.2022.740051

The tumor microenvironment (TME) is variable across tumor types and has diverse effects on malignant progression, based on the type and number of infiltrating stromal cells. In particular, TME effector genes and their competitive endogenous RNA (ceRNA) networks play a critical role in regulating malignant tumor progression. However, the core effector molecules involved in TME modulation of kidney renal papillary cell carcinoma (KIRP) are poorly understood. To address this question, a cohort containing 233 KIRP patients was derived from The Cancer Genome Atlas (TCGA) database, and the data were processed using the ESTIMATE algorithm. We further evaluated the relationship between immune scores (ISs) and stromal scores (SSs) and disease progression and found that high SSs were associated with a poor prognosis in KIRP. Differentially expressed genes (DEGs) were therefore screened based on SS scores, resulting in 2509 DEGs, including 1668 mRNAs, 783 long noncoding (lnc)RNAs, and 58 micro (mi)RNAs. DEGs were then filtered using the random variance and subjected to hierarchical clustering using EPCLUST. Weighted gene co-expression network analysis (WGCNA) was used to assess the prognostic capacity of these DEGs and identify target ceRNA networks, and lncRNA GUSBP11/miR-432-5p/CAMK2B in the turquoise module was selected as a promising ceRNA network. From this analysis CAMK2B was selected as the core gene predicted to be involved in stromal TMA regulation. We therefore explored the expression and function of CAMK2B *in vitro* and *in vivo* and provide evidence that this protein promotes stromal TME remodulation and inhibits proliferation in KIRP. Lastly, we show that vascular endothelial growth factor (VEGF), transforming growth factor (TGF)β, and close homolog of L1 (CHL1) act as downstream effectors of CAMK2B in KIRP. Thus, in this study, we show that the TME determines prognosis of KIRP patients *via* the core effector molecule CAMK2B, which mediates both microenvironmental remodeling and tumor

progression. Based on these findings, we propose that remodeling of the stromal microenvironment could represent an improved therapeutic approach relative to immunotherapy for KIRP.

Keywords: kidney renal papillary cell carcinoma (KIRP), tumor microenvironment, CAMK2B, lncRNA GUSBP11, miR-432-5p

INTRODUCTION

According to estimates from the World Health Organization (WHO) and Chinese National Cancer Center, cancer is the leading cause of death and consequently, represents a major public health problem in a majority of countries, showing increasing incidence and mortality rates (1, 2). Kidney renal papillary cell carcinoma (KIRP) accounts for 10–20% of Renal Cell Carcinoma (RCC). However, efficacy data for drugs available in clinical practice remain largely unsatisfactory for KIRP, as patients with KIRP are often excluded from common RCC histological subtypes in clinical trials. Furthermore, the regulatory factors that mediate KIRP progression remain largely unidentified (3, 4). In recent years, the emergence of immune checkpoint inhibitors and combination treatment strategies has brought hope to patients with advanced RCC. However, additional insight into the driver and passenger alterations in KIRP-associated genes will be key to improving both management of this disease and patient prognosis.

The tumor microenvironment (TME) strongly influences clinical outcome of patients with malignant tumors, and the TME landscape varies considerably in different tumor types (5). Critically, characteristic features of the TME and the precise effect of key TME-associated genes in KIRP remain unclear. Emerging studies suggest that noncoding competing endogenous RNAs (ceRNAs), including microRNAs (miRNAs) (6) and long noncoding RNAs (lncRNAs) (7), play a critical role in the efficiency of messenger RNA (mRNA) translation in tumors (8). These noncoding RNAs modulate gene expression at both the transcriptional and post-transcriptional levels and act as master regulators for key mRNAs. However, the target genes and related effector proteins involved in TME-mediated modulation of KIRP are poorly understood.

In the present study, we aimed to explore the role of TME subtype in malignant progression of KIRP and to identify the core effectors involved in KIRP progression. Unexpectedly, we found that overall survival was associated with stromal scores (SSs), but not immune scores (ISs), derived using the ESTIMATE algorithm. We then identified and screened differentially expressed genes (DEGs) in patients with high *vs.* low SSs using weighted gene co-expression network analysis (WGCNA), leading to identification of the lncRNA GUSBP11/MiR-432-5p/CAMK2B network, based on the results of correlation strength and survival analysis. Lastly, we investigated the role of CAMK2B, a core network gene, and found that it inhibits proliferation and modulates the TME *via* downstream effector genes, including vascular endothelial growth factor (VEGF), transforming growth factor (TGF)β, and close homolog of L1 (CHL1), which mediate in stromal microenvironment regulation. Thus our findings suggest that TME remodeling may represent a possible therapeutic approach for KIRP.

MATERIALS AND METHODS

Data Acquisition and Estimation of Stromal Scores and Immune Scores

The Cancer Genome Atlas (TCGA) database contains multi-omics datasets, including gene transcript, miRNA, and lncRNA expression data from numerous cancer types. We downloaded all KIRP datasets from TCGA (https://portal.gdc.cancer.gov/) using the TCGAbiolinks package in R software (version 3.5.1), including lncRNA, mRNA, and miRNA expression profiles from KIRP samples and the corresponding clinical follow-up data. Next, we used the ESTIMATE algorithm to output stromal scores (SSs) and immune scores (ISs) and compared the differentially expressed lncRNAs, mRNAs, and miRNAs in samples with high and low SSs and ISs (high >0 and low <0) (9).

Weighted Gene Co-Expression Network Analysis

We utilized the weighted gene co-expression network analysis (WGCNA) package in R to analyze the co-expression network of selected lncRNAs and mRNAs (10). The gene expression profile matrix was first transformed into a similarity matrix based on the Pearson test between pairwise genes. Next, the similarity matrix was converted into an adjacency matrix, and scale-free gene co-expression networks were constructed by the WGCNA package. The topological overlap matrix (TOM) and dissimilarity TOM (dissTOM) were then obtained by TOM similarity and dissimilarity on the basis of the adjacency matrix. Lastly, after hierarchical clustering analysis based on dissTOM, modules were generated from the Dynamic Tree Cut method for Branch Cutting.

Tissue Samples and Clinical Data Collection

Two independent cohorts of KIRP samples were acquired for this study from patients that underwent surgery at the Air Force Military Medical University Tangdu Hospital (Xi'an, China). From cohort A, 30 paired KIRP tissues and adjacent non-tumor tissues were gathered and used for reverse transcription (RT)-PCR and immunoblotting. From cohort B, 80 KIRP specimens were collected and used for constructing tissue microarrays and performing immunohistochemistry (IHC). This study was approved by the Ethics Committee on Human Research of

Tangdu Hospital, and written informed consent was obtained from all patients.

Vector Construction, Transfection, and Lentivirus Transduction

Human full-length CAMK2B cDNA (NM_001220.5) was obtained from VectorBuilder (Guangzhou, China). This fragment was cloned into the pCDH lentiviral expression vector (System Biosciences, Palo Alto, CA, USA) and inserted between the *Xba*I and *Eco*RI sites, using the In-Fusion HD Cloning Kit (Takara, Tokyo, Japan). Plasmid constructs expressing *CAMK2B* shRNA and scramble shRNA were generated using the lentiviral expression plasmid PLKO.1 and obtained from Vectorbuilder. Lentiviral shRNA target sequences were as follows: CCGGAAGCAGGAGATCATTAA (sh1), GACCAGATGTGATTTGTTAAA (sh2), and ATAGAGGATG AAGACGCTAAA (sh3). Stable cell lines were created by antibiotic selection with puromycin for one week, beginning 72 h after transduction.

Quantitative RT-PCR Analysis

Total RNA was isolated from KIRP tissues and adjacent non-tumor tissues using TRIzol Reagent (Invitrogen, Thermo Fisher Scientific, Waltham, MA, USA). Isolated RNA was reverse transcribed using the PrimeScript RT Reagent Kit (TaKaRa, Shiga, Japan), and mRNA expression was determined by quantitative (q) qRT-PCR using SYBR Premix Ex Taq II (TaKaRa). Primers used for amplification of human genes were as follows: lncRNA GUSBP11 forward primer 5'-TCCCCTGT CCCGAAGGATTAC-3' and reverse primer 5' -TAAGGGAC TAACGGCTTCGCT-3'; miR-432-5p forward primer 5'-ACTCAAACACTTCGGACATGG-3' and reverse primer 5'-CAAAGAGCAACAGAGAGTAGCA-3'; *CAMK2B* forward primer 5'-CAGTGTACTTCAGTTGGTG-3' and reverse primer 5'-TCAGGTTTTGCTCTTC TC-3'; *GAPDH* forward primer 5'-AGGTCGGAGTCAACGGATTTG-3' and reverse primer 5'-TGTAAACCATGTAGTTGAGGTCA-3'.

Immunohistochemistry and Immunoblotting

Tumor tissue was fixed, embedded in paraffin, and sliced into 5-μm thick sections. IHC staining and immunoblotting were performed using primary antibodies to CAMK2B (1:100 dilution, Proteintech, Chicago, IL, USA), according to standard protocols, as previously described (11). Relevant bioinformatics methods, Culture conditions for cell lines, and the various functional assays for CAMK2B *in vivo* (animal models with subcutaneous xenografts) and *in vitro* (migration, proliferation, and antibodies and cell lines information) are described in the **Supplementary Materials and Methods (Doc. S1)**.

Statistical Analysis

Statistical analyses were performed using SPSS 15.0 for Windows (SPSS, Inc., Chicago, IL, USA). IHC and qRT-PCR experiments were performed at least three times, and statistical quantitative data were evaluated by Student's *t*-tests, with $P < 0.05$ considered statistically significant.

RESULTS

High SSs Are Associated With Poor Prognosis in KIRP

We analyzed a patient cohort containing 233 KIRP patients for whom expression data were available in TCGA database. These data were analyzed using the ESTIMATE algorithm, as described in the flowchart in **Figure 1A**. Infiltrating cells in the tumor tissue were assessed by incorporating two gene signatures within the ESTIMATE algorithm. SSs were designed to capture the presence of stromal cells in tumor tissue, and ISs were calculated to determine the infiltration of immune cells in tumor tissue. Based on ISs, 233 samples were divided into an IS-high (178 samples) group and an IS-low (22 samples) group. We detected no difference in overall survival (OS) between patients in the IS-high and IS-low group (**Figure 1B,** a). We then divided patients into SS-high (27 samples) and SS-low (206 samples) groups, and found a significant difference in survival between patients in these groups, with SS-high patients showing decreased survival relative to SS-low patients ($P = 1\times10^{-4}$, **Figure 1B,** b). Based on these findings, we compared gene expression profiles in the SS-high and SS-low groups.

Analysis of DEGs in SS-High vs. SS-Low Patients and WGCNA

Identification of DEGs in KIRP samples with high *vs.* low SSs using the methods described above and in **Figure 1A** revealed 1668 differentially expressed mRNAs, 783 differentially expressed lncRNAs, and 58 differentially expressed miRNAs. All DEGs in each independent dataset were analyzed using unsupervised hierarchical clustering analysis. The cluster analysis heat map shows the correlation between expression maps and group conditions (**Figure 2A**). We further performed gene ontology (GO) and Kyoto Encyclopedia of Genes and Genomes (KEGG) pathway enrichment analyses of 1189 upregulated mRNAs in SS-high subjects and identified immune response and cytokine-cytokine receptor interactions among the top pathways. Analysis of 479 downregulated mRNAs yielded oxidation-reduction process and metabolic pathways as top hits (**Supplementary Figure 1**).

We next performed sample clustering detection of lncRNAs and mRNAs and found no outlier samples, indicating it was not necessary to remove any samples in our co-expression analyses (**Figure 2B**). The most important step in this process is selection of the value for soft-threshold power (β). To determine the relative equilibrium between scale independence and mean connectivity, we analyzed the network topology with soft-threshold power from 1 to 20, eventually confirming a β value of 8 for lncRNAs and mRNAs (**Figure 2C**). Next, we identified co-expression modules by hierarchical clustering and Dynamic Branch Cutting and assigned a unique color as an identifier in each module using WGCNA (**Figure 2D**).

To identify interactions among these co-expression modules, we analyzed the connectivity of eigengenes in a cluster analysis. Seven modules (turquoise, blue, grey, brown, yellow, green, red) were generated, with the grey module representing a gene set that was not assigned to any of the modules. We then generated a heatmap plot of the adjacencies in the hub gene network, wherein red represents positive correlation with high adjacency, and blue represents negative correlation with low adjacency (**Figure 2E**).

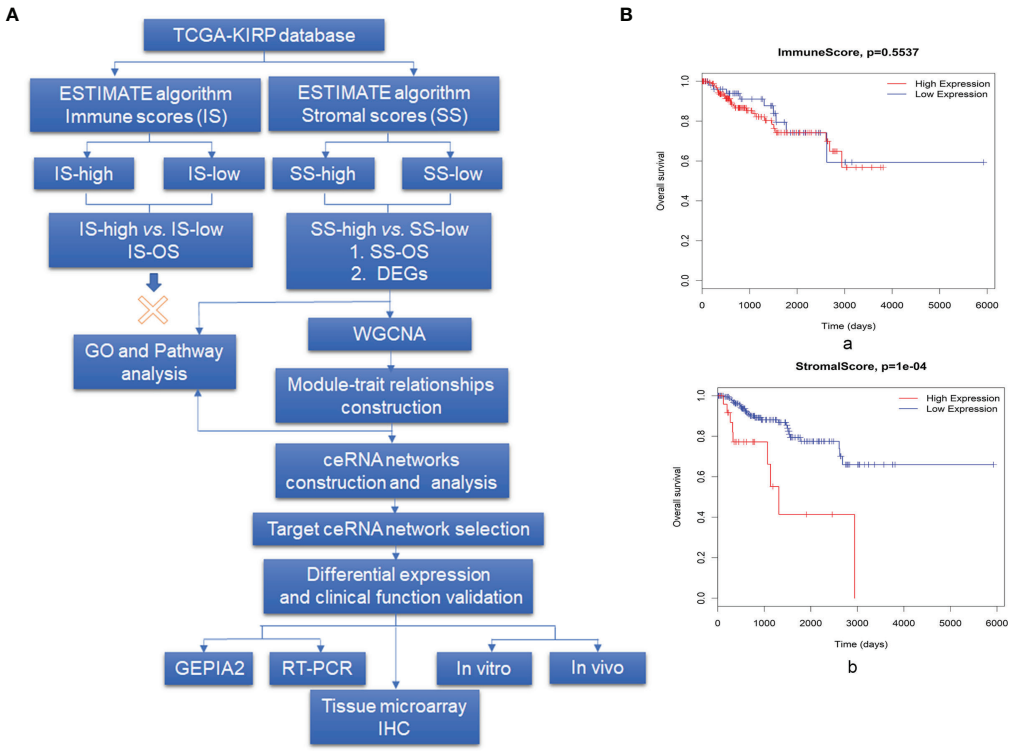


FIGURE 1 | Overview of the data preparation, processing, analysis, and validation pipeline for this study and association between prognosis and both stromal scores (SCs) and immune scores (ISs). **(A)** Flowchart describing the bioinformatics analysis pipeline and experimental validation strategy in this study. (**B**, a) Survival analysis for patients in the IS-high and IS-low groups and (b) for patients in the SS-high and SS-low groups, using the R package Survival Analysis. High SSs are associated with a poor prognosis, whereas no survival difference was observed for those with high *vs.* low ISs.

The eigengene dendrogram and heatmap were used to identify groups of correlated eigengenes, and the dendrogram revealed a significant association between these modules and KIRP clinical traits. Notably, the turquoise module was found to be negatively correlated with pathological stage of the tumor and was chosen as the focus of research for this study (**Figure 2F**). This module contained a total of 1004 differentially expressed RNAs, including 364 mRNAs, 600 lncRNAs, and 40 other noncoding RNAs. GO enrichment analyses of the 364 mRNAs in the turquoise module identified negative regulation of apoptotic process as a top function, with the largest number of enriched genes (**Figure 2G,** a), and KEGG-pathway enrichment analyses found metabolic pathway as a key mechanism (**Figure 2G,** b).

Selection of *CAMK2B* as a Key Gene Based on Correlation Strength and Survival Analyses With the Selected ceRNA Network

Through our predefined strategy based on SSs, DEGs in the turquoise module were found to be mainly associated with favorable survival outcomes in KIRP patients. We then analyzed co-expression of ceRNA networks in the turquoise module by WGCNA and built multiple groups, including RP3-416H24.1/hsa-miR-127-5p/*ITGB8*, SNHG11/hsa-miR-214-3p/*ARVCF*, SNHG11/hsa-miR-214-3p/*HDAC11*, SNHG11/hsa-miR-214-3p/*KAZN*, SNHG11/hsa-miR-214-3p/*MRPS25*, SNHG11/hsa-miR-214-3p/*PRR15L*, and GUSBP11/miR-432-5p/*CAMK2B* (**Figure 3A**).

The prognostic effects of these DEGs were analyzed and presented in a forest plot, and eight lncRNAs, including GUSBP11, IQCH-AS1, MTHFD2P1, RP11-12A2.3, RP3-416H24.1, SNHG11, TMEM51-AS1, and RP11-567M16.6, were found to exhibit pro-survival functions with longer overall survival (OS) (**Figure 3B,** a). A total of seven miRNAs, including mir-432-5p, mir-145-5p, mir-143-5p, mir-127-5p, mir-214-3p, and mir-134-5p, were correlated with a poor prognosis and shorter OS (**Figure 3B,** b). In addition, 15 mRNAs were correlated with better prognosis, including *CAMK2B*, *MACC1*, *PKHD1*, *PTPRD*, *RAB36*, *ZNF320*, *FLRT3*, *ITGB8*, *ARVCF*, *HDAC11*, *KAZN*, *MRPS25*, *P4HTM*, *PAX8*, and *DACT2* (**Figure 3B,** c). We then plotted Kaplan–Meier curves using the Cox proportional hazard regression model for SS-related lncRNAs, miRNAs, and mRNAs in KIRP and confirmed that all these genes are associated with survival (**Supplementary Figure 2**). Based on results of correlation strength and survival analyses, *CAMK2B* was selected as one of the most promising target genes.

We then assessed the prognostic impact of *CAMK2B* in 33 types of human tumors using GEPIA2 (12), and found that high expression of *CAMK2B* is associated with improved prognosis in KIRP, liver hepatocellular carcinoma (LIHC), and ovarian cancer (OV, **Figure 3C,** a). To further confirm this finding, we used

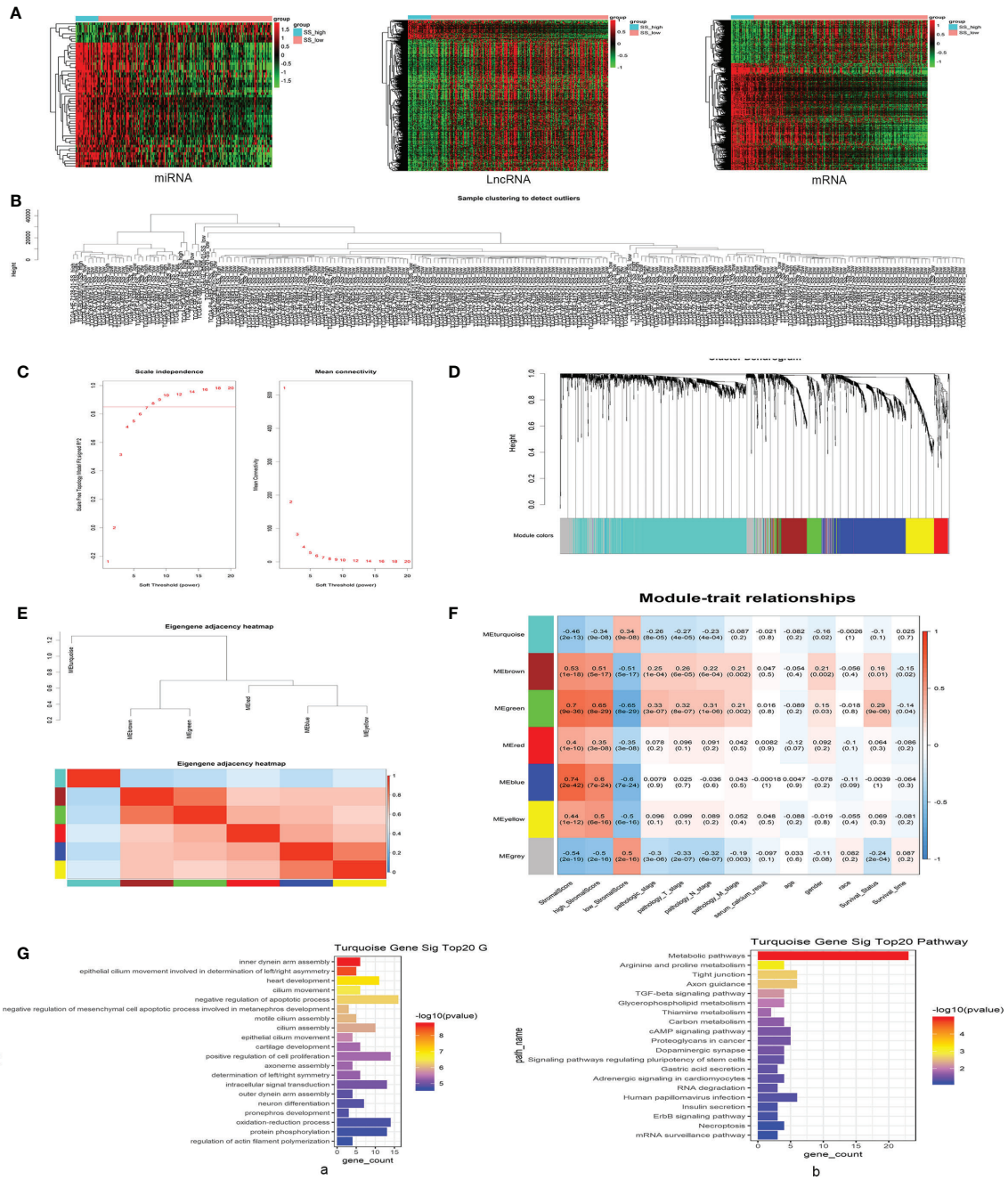


FIGURE 2 | Differentially expressed genes (DEGs) in patients with high *vs.* low SSs were evaluated using weighted gene co-expression network analysis (WGCNA), and the turquoise module was selected based on positive pathological roles in KIRP. **(A)** Unsupervised hierarchical clustering analyses for DEGs, including differentially expressed messenger (m)RNAs, long noncoding (lnc)RNAs, and micro (mi)RNAs, in SS-high and SS-low KIRP tissue samples. The cluster analysis heat map shows the correlation between expression maps and group conditions. The rows represent differentially expressed miRNAs, lncRNAs, and mRNAs, and the columns represent the samples. **(B)** Sample clustering detection revealed no outlier samples. **(C)** Soft-threshold power (β) for co-expression of lncRNAs/mRNAs was determined by analyzing the network topology with a soft-threshold power ranging from 1 to 20. **(D)** Different modules were identified by the Dynamic Tree Cutting method, and each module was assigned a color as an identifier. Six modules were generated after merging based on the correlation of modules with WGCNA. **(E)** Heatmap plot of the adjacencies in the hub gene network; red represents positive correlation with high adjacency, and blue represents negative correlation with low adjacency. Squares of red color along the diagonal represent the meta-module. **(F)** Matrix of module–trait relationships and *P*-values for selected traits. Each column corresponds to a module eigengene, and each row corresponds to a histopathological trait. Each cell contains a corresponding correlation and *P*-value. The table is color-coded by correlation according to the color legend. **(G**, a**)** Gene ontology (GO) enrichment analyses of turquoise mRNAs; significant top 20 GO terms are shown. (**G**, b) Kyoto Encyclopedia of Genes and genomes (KEGG)-pathway enrichment analyses of turquoise mRNAs; significant top 20 signaling pathways are shown.

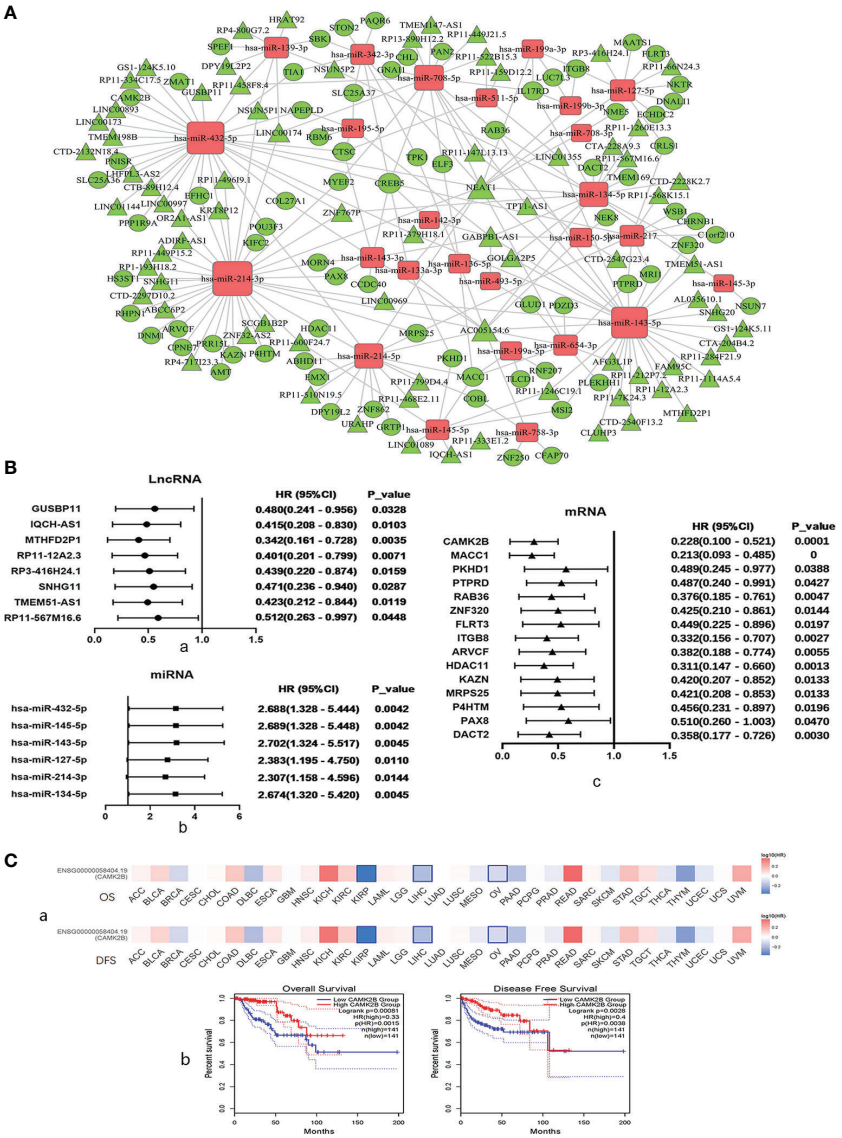


FIGURE 3 | Regulation and co-expression of competing endogenous (ce)RNA networks in the turquoise module by WGCNA and selection of *CAMK2B* as a key gene based on results of correlation strength and survival analyses. **(A)** Co-expression of ceRNA networks in the turquoise module, including lncRNA GUSBP11/miR-432-5p/*CAMK2B*, was analyzed by WGCNA. Diamonds represent miRNAs, circles represent mRNAs, and cones represent lncRNAs. Upregulated genes are shown in red, and downregulated genes are shown in green. **(B)** Hazard ratios and corresponding 95% confidence intervals were estimated using the Cox proportional hazard regression model, and the prognostic effects of these (a) lncRNAs, (b) miRNAs, and (c) mRNAsare presented in a forest plot. (**C**, a) The prognostic impact of *CAMK2B* in 33 types of human tumors was analyzed using GEPIA2, revealing that high expression of CAMK2B is associated with poor prognosis in KIRP, liver hepatocellular carcinoma (LIHC), and ovarian cancer (OV). (b) Kaplan–Meier plotter was used to analyze survival, and high expression of CAMK2B was found to be associated with longer overall survival (OS) and recurrence-free survival (RFS).

Kaplan–Meier plotter and found that that high expression of *CAMK2B* is associated with longer OS and recurrence-free survival (RFS) in KIRP (**Figure 3C,** b).

Expression and Clinical Role of CAMK2B in KIRP Samples

We next measured expression of the selected ceRNA network in KIRP tissue by qRT-PCR. We detected lower levels of lncRNA GUSBP11 (P=0.0618) and *CAMK2B* (p=0.0447) in tumor tissue samples than in the normal tissue adjacent to the carcinoma, whereas levels of miR-432-5p were found to be higher in tumor tissue (P=0.0097; **Figure 4A**). Upon further exploration, we found that high expression of lncRNA GUSBP11 is associated with no metastasis (P=0.0023; **Figure 4B,** a), early-stage disease (P=0.0023; **Figure 4B,** b), and small tumor size (P=0.0249; **Figure 4B,** c). Similarly, high expression of *CAMK2B* mRNA is associated with no metastasis (P = 0.002; **Figure 4D,** a), early-stage disease (P=0.0299; **Figure 4D,** b), and small tumor size

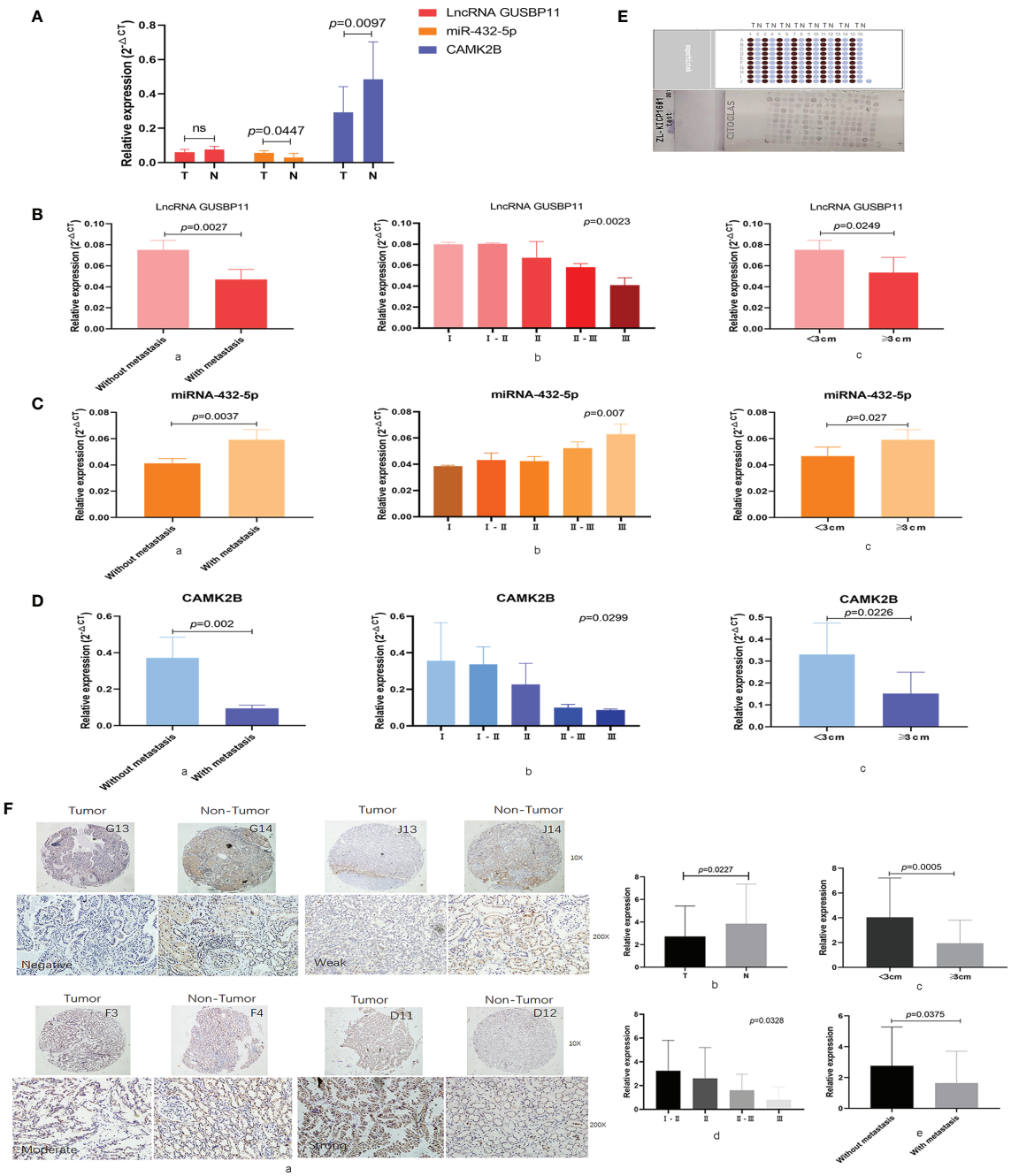


FIGURE 4 | Expression and clinical role of CAMK2B and its associated ceRNA network in KIRP samples. **(A)** Expression of the selected ceRNA network, including *CAMK2B*, mir-432-5p, and lncRNA GUSBP11, was measured using quantitative reverse transcription (qRT)-PCR in KIRP tissue and normal tissue adjacent to the carcinoma. Ns, no significance. (**B**, a) In cancer patients, high expression of lncRNA GUSBP11 is associated with no metastasis, (b) early-stage disease, and (c) small tumor size. (**C**, a) High expression of mir-432-5p was associated with tumor metastasis, (b) late-stage disease, and (c) large tumor size. (**D**, a) High expression of *CAMK2B* is associated with no metastasis, (b) early-stage disease, and (c) small tumor size. **(E)** Protein levels of CAMK2B were measured by immunohistochemistry (IHC) using tissue microarrays. (**F** a, b) Protein levels of CAMK2B are lower in tumor tissue than in paired tumor-adjacent tissue. (c) Expression of CAMK2B is higher in tumors <3 cm in size than in tumors >3 cm in size. (d) High expression of CAMK2B is positively correlated lower tumor grade. (e) High expression of CAMK2B is negatively correlated with tumor metastasis.

(*P*=0.0226; **Figure 4D,** c). In contrast, high expression of mir-432-5p is associated with tumor metastasis (*P*=0.0037; **Figure 4C,** a), late-stage disease (*P*=0.007; **Figure 4C,** b), and large tumor size (*P*=0.027; **Figure 4C,** c).

We further confirmed these findings by analyzing KIRP tumor samples and adjacent non-tumor tissues by IHC using tissue microarray (**Figure 4E, F**). Indeed, we found that protein levels of CAMK2B are lower in tumor tissue than in paired

tumor-adjacent tissue (P=0.0227, **Figure 4F,** a, b). Further, expression of CAMK2B in tumors <3 cm in size is significantly higher than in tumors >3 cm in size (P=0.0005, **Figure 4F,** c, Confirm whether the insertion of the Ethics Statement section is fine. Note that we have used the statement provided at Submission. If this is not the latest version, please let us know.). High expression of CAMK2B was also found to be associated with lower tumor grade (P=0.0328, **Figure 4F,** d) and low metastasis (P=0.0375, **Figure 4F,** e). Thus, these data confirm the expected pattern of CAMK2B expression and suggest it acts as a protective factor in KIRP.

Upregulation of *CAMK2B* Is Associated With Decreased Proliferation and Inhibition of the Tumor Stromal Microenvironment in KIRP

To evaluate the function of CAMK2B, we stably overexpressed and silenced *CAMK2B* expression in the KIRP SK-RC-39 cell line (**Figure 5A**). We found that upregulation of *CAMK2B* significantly inhibits cell proliferation (**Figure 5B,** a), whereas the reverse occurs in response to *CAMK2B* silencing (**Figure 5B,** b). Moreover, we confirmed the inhibition of proliferation in response to CAMK2B overexpression using sphere formation assays, and showed that *CAMK2B* silencing has the opposite effect (**Figure 5C**). Migration assays further showed that a lower number of *CAMK2B* overexpressing cells cross the basement membrane relative to SK-RC-39 control cells, whereas migration is enhanced after *CAMK2B* silencing (**Figure 5D**).

In nude mouse models, diminished subcutaneous tumor growth was observed in mice injected with SK-RC-39 cells stably overexpressing *CAMK2B* (P=0.0351, **Figure 5E**) as compared to mice injected with SK-RC-39 control cells. Immunohistochemical staining further revealed that SK-RC-39-CAMK2B subcutaneous tumors from these animals show significantly decreased expression of CD34 (P=0.0363), α-SMA (P=0.0451), and PCNA (P=0.0177, **Figure 5F**) relative to SK-RC-39 tumors. We also confirmed this negative correlation between expression of CAMK2B and both α-SMA (R=-0.26, **Figure 5G,** a) and CD34 (R=-0.35, **Figure 5G,** b) in human KIRP tissue using the GEPIA2 database (12), indicating that elevated CAMK2B levels are associated with decreased infiltrating fibroblasts and vascular endothelial cells. Additionally, the negative correlation between expression of CAMK2B and endothelial cells (R=-0.455) and cancer-associated fibroblast (R=-0.384) was confirmed using Xcell and EPIC. In contrast, only a weak correlation is observed between CAMK2B and immune cells (**Figure 5H**). Thus, the above findings suggest that upregulation of CAMK2B decreases proliferation and inhibits tumor stromal cell infiltration in KIRP.

CHL1, VEGF, and TGFβ Act as Downstream Effectors of CAMK2B in KIRP

In order to identify potential target genes downstream of CAMK2B, we screened for CAMK2B co-expressed genes in KIRP from TCGA database using LinkedOmics (13) and Metascape (14). We then constructed a volcano plot to visualize genes that are positively and negatively correlated with CAMK2B and identified CHL1 as the most positively correlated gene and VEGFA as the most negatively correlated gene (**Figure 6A**). Using Metascape, we found that the top 100 genes correlated with CAMK2B are significantly enriched in cellular component organization and biogenesis (**Supplementary Figure 3**). To confirm the relationship between CAMK2B, VEGFA, and CHL1 in KIRP, we measured the levels of these proteins in frozen tissue samples from KIRP patients by immunoblotting, revealing a positive correlation between CAMK2B and CHL1 and a negative correlation between CAMK2B and VEGF (**Figure 6B**). Further evaluating their expression in KIRP tissue using GEPIA2 confirmed a significant positive correlation between expression levels of *CAMK2B* and *CHL1* (R=0.7433), as well as a negative correlation between expression of *CAMK2B* and both *VEGF* (R=-0.3) and *TGFβ1* (R=-0.23, **Figure 6C**). Finally, we examined expression of several effector molecules in SK-RC-39 cells stably overexpressing *CAMK2B* or subjected to shRNA-mediated *CAMK2B* silencing. Notably, we found that expression of CHL1 and E-cadherin are significantly increased, whereas TGFβ1, VEGF, vimentin, and PCNA are significantly downregulated, in SK-RC-39 cells overexpressing CAMK2B. Conversely, when CAMK2B expression in SK-RC-39 cells is silenced using specific shRNA, the opposite expression pattern is observed (**Figure 6D**). Thus, we identify CHL1, VEGF, and TGFβ1 as downstream effectors of CAMK2B, and provide further evidence that enhanced CAMK2B expression inhibits proliferation and stromal cell infiltration.

DISCUSSION

Renal papillary cell carcinoma is insensitive to conventional radio- and chemotherapies, and consequently, surgical excision is the only useful clinical intervention that demonstrably prolongs patient survival in early-stage disease. For unresectable KIRP at an advanced stage, targeted therapy [e.g., tyrosine kinase inhibitors [TKIs)] is recommended (15). However, resistance to targeted therapy, including adaptive resistance, intrinsic resistance, and acquired resistance, remain major obstacles to treatment success (16, 17). The emergence of immune checkpoint inhibitors has further provided hope to advanced-stage KIRP patients, and studies aimed exploring strategies for immunotherapy, either alone or in combination with TKI inhibitors, in KIRP patients are urgently needed. In parallel, much remains unknown about the tumor microenvironment and molecular characteristics in KIRP, and this is therefore an important area of investigation.

During cancer progression, a series of genetic and phenotypic changes occur that, in addition to tumor-cell derived cytokines, chemokines, and metabolites, have been reported to significantly impact the TME (18). The TME is mainly composed of various immune cells, vascular endothelial cells, and fibroblasts, which generate permissive niches for tumor progression (19). Heterogeneous features of the TME determine both the diverse fates and drug responses of tumors, and the TME also has strong predictive value for tumor prognosis (20). In particular,

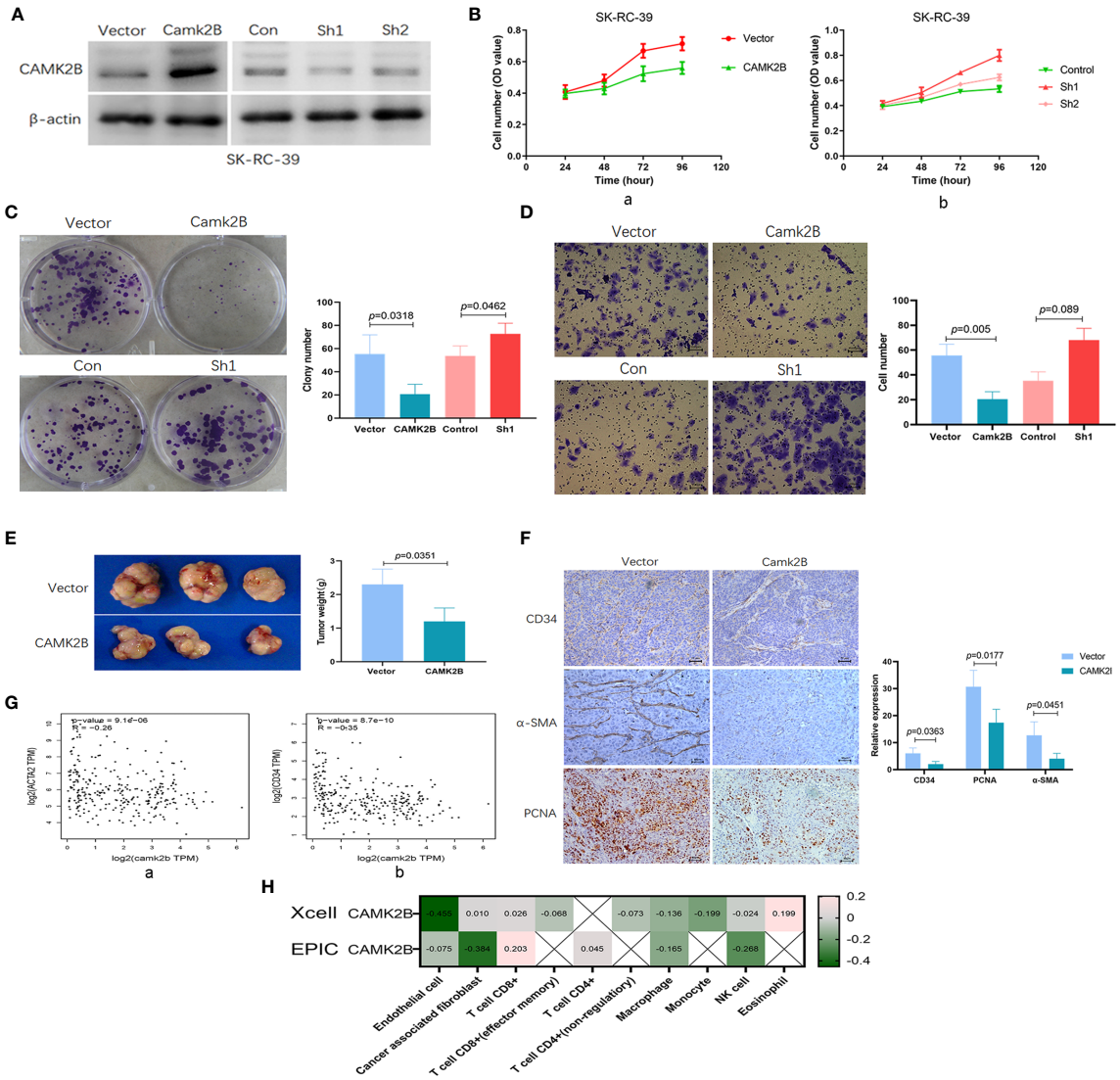


FIGURE 5 | Upregulation of CAMK2B is associated with decreases in proliferation and fibroblast infiltration, as well as inhibition of angiogenesis. **(A)** CAMK2B was overexpressed or subjected to by short-hairpin (sh) RNA-mediated silencing in SK-RC-39 cells using lentiviral transfection. **(B)** CAMK2B inhibits cell proliferation (a), and this is reversed by CAMK2B silencing, as determined using the CCK8 assay (b). **(C)** Upregulation of CAMK2B inhibits cell proliferation ability in a sphere formation assay (a), and this is reversed by CAMK2B silencing (b). **(D)** CAMK2B inhibits cell migration ability (a), whereas migration is enhanced after CAMK2B silencing (b), as measured using the Boyden Chamber migration assay. **(E)** Diminished subcutaneous tumor growth is observed in mice injected with SK-RC-39-CAMK2B cells relative to those injected with SK-RC-39 cells. **(F)** Immunohistochemical staining confirms significantly decreased expression of CD34, α-SMA, and PCNA in subcutaneous tumor tissues derived from SK-RC-39-CAMK2B cells *vs.* tissue from control cells. **(G)** Negative correlation is observed between expression of *CAMK2B* and both α-SMA and CD34 in human KIRP tissue from TCGA database using GEPIA2. **(H)** Significant negative correlations are observed between expression of CAMK2B and both endothelial cells (R=-0.455) and cancer-associated fibroblasts (R=-0.384) using Xcell and EPIC, whereas the correlation with immune cells is weak.

the importance of immune cell populations, reflecting the capacity of the immune system to sense tumor cells, has been recognized for prognosis (21). The field of cancer immunotherapy is evolving rapidly. Notably, response to immunotherapy has been shown to be dynamically regulated by the TME *via* cell-cell interactions and paracrine signals emanating from the tumor. Ipilimumab, a monoclonal antibody against CTLA-4, demonstrates response rates between 5–12.5%, but no complete responses or durable regressions were seen in renal cell carcinoma (22). Nivolumab, a monoclonal antibody that blocks the PD-1 pathway demonstrated complete responses in only 1% of renal cell carcinoma patients (23). Zhou *et al.* found increased number of tumor-infiltrating lymphocytes in high-risk KIRP patients based on expression 14 immune-related genes, but detailed materials revealed that total levels of immune cells in tumor tissues were not high (24). In this study,

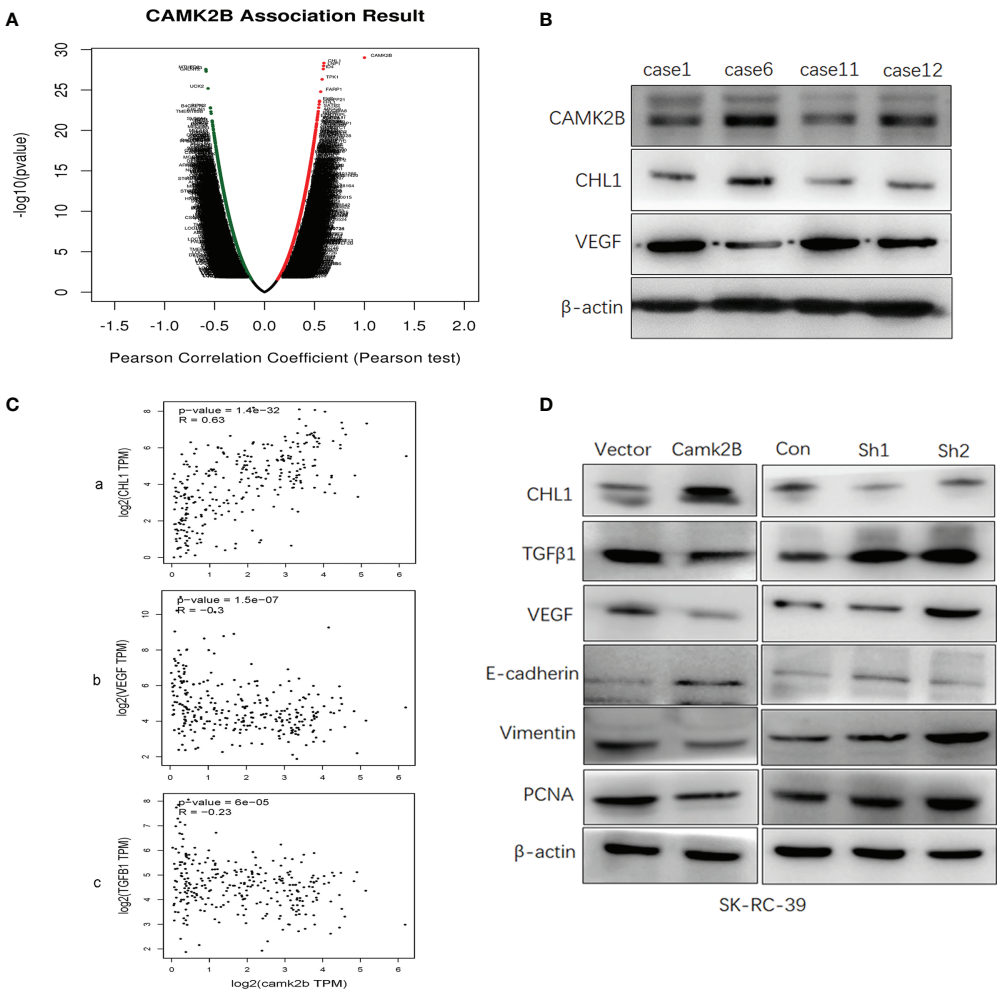


FIGURE 6 | CHL1, VEGF, and TGFβ act as downstream effectors of CAMK2B. **(A)** Genes co-expressed genes with CAMK2B in KIRP tissue were screened in TCGA database using LinkedOmics and Metascape and visualized in a volcano plot. **(B)** The protein levels of CAMK2B, CHL1, and VEGF in tissue from KIRP patients were evaluated by immunoblotting. **(C)** The correlation between the expression levels of *CAMK2B* and *CHL1* (a), *CAMK2B* and *CHL1* (b), and *CAMK2B* and *TGFβ1* (c) were evaluated in TCGA database using GEPIA2. **(D)** Expressed of several predicted effector molecules, including TGFβ1, VEGF, vimentin, PCNA, CHL1, and E-cadherin were measured in KIRP cells overexpressing or silenced for *CAMK2B*.

we surprisingly found no difference in survival for patients with high *vs.* low IS, suggesting a rationale for why immunotherapy is not effective in KIRP patients.

Tumors are supported by a complex microenvironment that is characterized by the presence of many stromal cell populations. For example, fibroblasts and endothelial cells create a desmoplastic tumor niche that plays an essential role in malignant tumor progression (25, 26). Therefore, we further explored the factors that influence KIRP progression from this perspective. To this end, we divided patients into SS-high and SS-low groups and found a significant difference in survival between patients with high *vs.* low SS, suggesting that non-immune stromal cells may play important roles in tumor progression. We further identified 1668 mRNAs, 783 lncRNAs, and 58 miRNAs that are differentially expressed in SS-high compared to SS-low tumors and analyzed these three independent datasets by WGCNA. Using these data, we then constructed co-expression networks of ceRNAs. Previous studies have demonstrated that ceRNAs affect the proliferation, growth, differentiation, apoptosis and other biological behaviors of cancer cells (27). In this study, we focused on co-expression ceRNA networks in the turquoise module, as this was found to be negatively correlated with pathological stage of the tumor.

We evaluated the expression and clinical roles for the members of the selected ceRNA network lncRNA GUSBP11/miR-432-5p/*CAMK2B* and identified a close correlation with KIRP patient survival, suggesting that the effector gene *CAMK2B* may be leveraged for prognostic and therapeutic purposes. CAMK2B belongs to the serine/threonine protein kinase family and to the Ca(2+)/calmodulin-dependent protein kinase subfamily. This protein was shown to promote neuronal survival (28), although a role in cancer has not been demonstrated. Here, to evaluate the

precise function of CAMK2B, we stably overexpressed and silenced *CAMK2B* expression in a KIRP cell line and found that upregulation of CAMK2B inhibits both proliferation and tumor stromal cell infiltration *in vivo* and *in vitro*. We then screened for genes co-expressed with CAMK2B in KIRP tissues using Metascape and identified *CHL1* as a putative CAMK2B target gene with the highest correlation. CHL1 is a member of the L1 gene family of neural cell adhesion molecules, which may also play negative role in the growth of certain cancers (29, 30). In this study, we found that expression of CAMK2B and CHL1 is positively correlated with resisting cell death, and negatively correlated with induction of angiogenesis and fibrogenesis. We therefore propose that CHL1 acts downstream of CAMK2B, and this mechanism may represent one of the targetable nodes in KIRP patients. VEGF and TGFβ1 have shown positive correlation with cancer (31), and the expression of both are negative correlated with CAMK2B, suggesting they also act as downstream effectors of CAMK2B in KIRP.

In summary, here we show that the SS-related network lncRNA GUSBP11/miR-432-5p/*CAMK2B* exhibits prognostic potential in KIRP, and CAMK2B may represent an effective therapeutic target. The cellular mechanism of action for CAMK2B mainly relates to inhibiting proliferation and remodeling angiogenesis and fibrogenesis. Thus, we further speculate that anti-fibrosis or anti-angiogenic therapy could be a better therapeutic approach than immunotherapy for KIRP, with CAMK2B as one possible target. However, several fundamental questions remain to be answered concerning the ability of CAMK2B to remodel stromal TMA. Therefore, cirrhosis mouse models with a blood vessel-rich background should be established to further elucidate the relationship among CAMK2B, fibroblasts, and vascular endothelial cells. In future studies, we will also determine if anti-angiogenesis therapy shows efficacy for clinical treatment of KIRP.

DATA AVAILABILITY STATEMENT

The original contributions presented in the study are included in the article/**Supplementary Material**. Further inquiries can be directed to the corresponding author.

ETHICS STATEMENT

The studies involving human participants were reviewed and approved by the ethics committee on Human Research of Tangdu Hospital. The patients/participants provided their written informed consent to participate in this study. The animal study was reviewed and approved by the Medical Experimental Animal Care Commission of Northwest Polytechnical University. Written informed consent was obtained from the individual(s) for the publication of any potentially identifiable images or data included in this article.

AUTHOR CONTRIBUTIONS

All authors searched the literature, designed the study, interpreted the findings, and revised the manuscript. XF and QJ conceived the study. BX, YS and GB performed the bioinformatics analyses. YZ and XL performed the majority of experiments. QJ and XL participated in data analysis and visualization. QJ drafted and prepared the manuscript. All authors contributed to the article and approved the submitted version.

FUNDING

This research project was partly supported by the Natural Science Basic Research Program of Shaanxi (2021JM-080 and 2020JQ-230), Fundamental Research Funds for the Central Universities (31020200QD032). The funders did not play any role in manuscript design, data collection, data analysis, data interpretation, or writing of the manuscript.

SUPPLEMENTARY MATERIAL

The Supplementary Material for this article can be found online at: https://www.frontiersin.org/articles/10.3389/fonc.2022.740051/full#supplementary-material

REFERENCES

1. Chen W, Zheng R, Baade PD, Zhang S, Zeng H, Bray F, et al. Cancer Statistics in China, 2015. *CA Cancer J Clin* (2016) 66:115–32. doi: 10.3322/caac.21338
2. Bray F, Ferlay J, Soerjomataram I, Siegel RL, Torre LA, Jemal A. Global Cancer Statistics 2018: GLOBOCAN Estimates of Incidence and Mortality Worldwide for 36 Cancers in 185 Countries. *CA Cancer J Clin* (2018) 68:394–424. doi: 10.3322/caac.21492
3. Courthod G, Tucci M, Di Maio M, Scagliotti GV. Papillary Renal Cell Carcinoma: A Review of the Current Therapeutic Landscape. *Crit Rev Oncol Hematol* (2015) 96:100–12. doi: 10.1016/j.critrevonc.2015.05.008
4. Powles T, Albiges L, Bex A, Grunwald V, Porta C, Procopio G, et al. ESMO Clinical Practice Guideline Update on the Use of Immunotherapy in Early Stage and Advanced Renal Cell Carcinoma. *Ann Oncol* (2021) 32:1511–9. doi: 10.1016/j.annonc.2021.09.014
5. Valkenburg KC, de Groot AE, Pienta KJ. Targeting the Tumour Stroma to Improve Cancer Therapy. *Nat Rev Clin Oncol* (2018) 15:366–81. doi: 10.1038/s41571-018-0007-1
6. Zeng Y. Principles of Micro-RNA Production and Maturation. *Oncogene* (2006) 25:6156–62. doi: 10.1038/sj.onc.1209908
7. Peng WX, Koirala P, Mo YY. LncRNA-Mediated Regulation of Cell Signaling in Cancer. *Oncogene* (2017) 36:5661–7. doi: 10.1038/onc.2017.184
8. Botti G, Scognamiglio G, Aquino G, Liguori G, Cantile M. LncRNA HOTAIR in Tumor Microenvironment: What Role? *Int J Mol Sci* (2019) 20:2279. doi: 10.3390/ijms20092279
9. Yoshihara K, Shahmoradgoli M, Martinez E, Vegesna R, Kim H, Torres-Garcia W, et al. Inferring Tumour Purity and Stromal and Immune Cell Admixture From Expression Data. *Nat Commun* (2013) 4:2612. doi: 10.1038/ncomms3612
10. Langfelder P, Horvath S. WGCNA: An R Package for Weighted Correlation Network Analysis. *BMC Bioinf* (2008) 9:559. doi: 10.1186/1471-2105-9-559
11. Jia QA, Ren ZG, Bu Y, Wang ZM, Zhang QB, Liang L, et al. Herbal Compound "Songyou Yin" Renders Hepatocellular Carcinoma Sensitive to Oxaliplatin Through Inhibition of Stemness. *Evid Based Complement Alternat Med* (2012) 2012:908601. doi: 10.1155/2012/908601
12. Tang Z, Kang B, Li C, Chen T, Zhang Z. GEPIA2: An Enhanced Web Server for Large-Scale Expression Profiling and Interactive Analysis. *Nucleic Acids Res* (2019) 47:W556–60. doi: 10.1093/nar/gkz430

13. Vasaikar SV, Straub P, Wang J, Zhang B. LinkedOmics: Analyzing Multi-Omics Data Within and Across 32 Cancer Types. *Nucleic Acids Res* (2017) 46: D956–63. doi: 10.1093/nar/gkx1090
14. Zhou Y, Zhou B, Pache L, Chang M, Khodabakhshi AH, Tanaseichuk O, et al. Metascape Provides a Biologist-Oriented Resource for the Analysis of Systems-Level Datasets. *Nat Commun* (2019) 10:1523. doi: 10.1038/s41467-019-09234-6
15. Fernandez-Pello S, Hofmann F, Tahbaz R, Marconi L, Lam TB, Albiges L, et al. And Meta-Analysis Comparing the Effectiveness and Adverse Effects of Different Systemic Treatments for Non-Clear Cell Renal Cell Carcinoma. *Eur Urol* (2017) 71:426–36. doi: 10.1016/j.eururo.2016.11.020
16. Rotow J, Bivona TG. Understanding and Targeting Resistance Mechanisms in NSCLC. *Nat Rev Cancer* (2017) 17:637–58. doi: 10.1038/nrc.2017.84
17. Santoni M, Pantano F, Amantini C, Nabissi M, Conti A, Burattini L, et al. Emerging Strategies to Overcome the Resistance to Current mTOR Inhibitors in Renal Cell Carcinoma. *Biochim Biophys Acta* (2014) 1845:221–31. doi: 10.1016/j.bbcan.2014.01.007
18. Pelizzo G, Veschi V, Mantelli M, Croce S, Di Benedetto V, D'Angelo P, et al. Microenvironment in Neuroblastoma: Isolation and Characterization of Tumor-Derived Mesenchymal Stromal Cells. *BMC Cancer* (2018) 18:1176. doi: 10.1186/s12885-018-5082-2
19. Sullivan MR, Danai LV, Lewis CA, Chan SH, Gui DY, Kunchok T, et al. Quantification of Microenvironmental Metabolites in Murine Cancers Reveals Determinants of Tumor Nutrient Availability. *Elife* (2019) 8:e44235. doi: 10.7554/eLife.44235
20. Rauner G, Kuperwasser C. Microenvironmental Control of Cell Fate Decisions in Mammary Gland Development and Cancer. *Dev Cell* (2021) 56:1875–83. doi: 10.1016/j.devcel.2021.06.016
21. Kourea H, Kotoula V. Towards Tumor Immunodiagnostics. *Ann Transl Med* (2016) 4:263. doi: 10.21037/atm.2016.07.07
22. Yang JC, Hughes H, Kammula U, Royal R, Sherry RM, Topalian SL, et al. Ipilimumab (Anti-CTLA4 Antibody) Causes Regression of Metastatic Renal Cell Cancer Associated With Enteritis and Hypophysitis. *J Immunother* (2007) 30:825–30. doi: 10.1097/CJI.0b013e318156e47e
23. Motzer RJ, Escudier B, McDermott DF, George S, Hammers HJ, Srinivas S, et al. Nivolumab Versus Everolimus in Advanced Renal-Cell Carcinoma. *New Engl J Med* (2015) 373:1803–13. doi: 10.1056/NEJMoa1510665
24. Zhou X, Qiu S, Jin D, Jin K, Zheng X, Yang L, et al. Development and Validation of an Individualized Immune-Related Gene Pairs Prognostic Signature in Papillary Renal Cell Carcinoma. *Front Genet* (2020) 11:569884. doi: 10.3389/fgene.2020.569884
25. Liao X, Bu Y, Chang F, Jia FA, Song G, Xiao XL, et al. Remodeling of Hepatic Stellate Cells Orchestrated the Stroma-Derived Oxaliplatin-Resistance Through CCN3 Paracrine in Hepatocellular Carcinoma. *BMC Cancer* (2019) 19:1192. doi: 10.1186/s12885-019-6362-1
26. Tavora B, Reynolds LE, Batista S, Demircioglu F, Fernandez I, Lechertier T, et al. Endothelial-Cell FAK Targeting Sensitizes Tumours to DNA-Damaging Therapy. *Nature* (2014) 514:112–+. doi: 10.1038/nature13541
27. Chan JJ, Tay Y. Noncoding RNA:RNA Regulatory Networks in Cancer. *Int J Mol Sci* (2018) 19:1310. doi: 10.3390/ijms19051310
28. Kool MJ, Onori MP, Borgesius NZ, van de Bree JE, Elgersma-Hooisma M, Nio E, et al. CAMK2-Dependent Signaling in Neurons Is Essential for Survival. *J Neurosci* (2019) 39:5424–39. doi: 10.1523/JNEUROSCI.1341-18.2019
29. Hotzel J, Melling N, Muller J, Polonski A, Wolters-Eisfeld G, Izbicki JR, et al. Protein Expression of Close Homologue of L1 (CHL1) is a Marker for Overall Survival in non-Small Cell Lung Cancer (NSCLC). *J Cancer Res Clin* (2019) 145:2285–92. doi: 10.1007/s00432-019-02989-x
30. Tang H, Jiang L, Zhu C, Liu R, Wu Y, Yan Q, et al. Loss of Cell Adhesion Molecule L1 Like Promotes Tumor Growth and Metastasis in Esophageal Squamous Cell Carcinoma. *Oncogene* (2019) 38:3119–33. doi: 10.1038/s41388-018-0648-7
31. Li S, Liu M, Do MH, Chou C, Stamatiades EG, Nixon BG, et al. Cancer Immunotherapy *via* Targeted TGF-Beta Signalling Blockade in TH Cells. *Nature* (2020) 587:121–5. doi: 10.1038/s41586-020-2850-3

Conflict of Interest: The authors declare that the research was conducted in the absence of any commercial or financial relationships that could be construed as a potential conflict of interest.

Publisher's Note: All claims expressed in this article are solely those of the authors and do not necessarily represent those of their affiliated organizations, or those of the publisher, the editors and the reviewers. Any product that may be evaluated in this article, or claim that may be made by its manufacturer, is not guaranteed or endorsed by the publisher.

Copyright © 2022 Jia, Liao, Zhang, Xu, Song, Bian and Fu. This is an open-access article distributed under the terms of the Creative Commons Attribution License (CC BY). The use, distribution or reproduction in other forums is permitted, provided the original author(s) and the copyright owner(s) are credited and that the original publication in this journal is cited, in accordance with accepted academic practice. No use, distribution or reproduction is permitted which does not comply with these terms.

frontiers in Oncology

ORIGINAL RESEARCH
published: 27 January 2022
doi: 10.3389/fonc.2022.832835

Xpert Bladder Cancer Monitor May Avoid Cystoscopies in Patients Under "Active Surveillance" for Recurrent Bladder Cancer (BIAS Project): Longitudinal Cohort Study

Vittorio Fasulo[1,2], Marco Paciotti[1,2], Massimo Lazzeri[2], Roberto Contieri[1,2], Paolo Casale[2], Alberto Saita[2], Giovanni Lughezzani[1,2], Pietro Diana[1,2], Nicola Frego[1,2], Pier Paolo Avolio[1,2], Piergiuseppe Colombo[1,3], Grazia Maria Elefante[3], Giorgio Guazzoni[1,2], Nicolò Maria Buffi[1,2], Michael Bates[4] and Rodolfo Hurle[2]*

[1] Department of Biomedical Sciences, Humanitas University, Milan, Italy, [2] Department of Urology, Istituto di Ricovero e Cura a Carattere Scientifico (IRCCS) Humanitas Research Hospital, Milan, Italy, [3] Department of Pathology, Istituto di Ricovero e Cura a Carattere Scientifico (IRCCS) Humanitas Research Hospital, Milan, Italy, [4] Medical and Scientific Affairs and Strategy, Oncology, Cepheid, Sunnyvale, CA, United States

Objectives: To test the hypothesis that patients under active surveillance (AS) for Non-muscle Invasive Bladder Cancer (NMIBC) who were negative on longitudinal re-testing by the Xpert® Bladder Cancer Monitor (Xpert BC Monitor) assay may avoid unnecessary cystoscopies and urine cytology (UC).

Subjects/Patients (or Materials) and Methods: This is a prospective cohort study of patients enrolled in the AS protocol for recurrent NMIBC (Bladder Cancer Italian Active Surveillance, BIAS project), whose urine samples were analyzed by Xpert BC Monitor upon entry in the study (T0). Patients who had a negative Xpert test and did not fail AS, underwent additional Xpert tests after 4 (T1), 8 (T2), and 12 (T3) months. The clinical utility of Xpert was assessed by determining the number of cystoscopies and UC that could be avoided within 1 year.

Results: Overall, 139 patients were tested with Xpert at T0. Median follow-up was 23 (IQR 17–27) months. Sixty-eight (48.9%) patients failed AS, 65 (46.7%) are currently on AS, and 6 (4.3%) were lost at follow-up. At T0 57 (41.0%) patients had a negative test and 36 (63.2%) are still in AS. In patients with 2 consecutives negative Xpert tests, we could have avoided 73.9% of unnecessary cystoscopies, missing 26.4% failure, up to avoid all cystoscopies with 4 negative tests missing only 12% of failure. All the patients with negative Xpert had negative UC. Failure-free-survival at median follow-up (23 month) stratified for having 0, 1, or ≥2 negative tests was 67.0, 55.1. and 84.1, respectively.

OPEN ACCESS

Edited by:
Michele Marchioni,
University of Studies G. d'Annunzio Chieti and Pescara, Italy

Reviewed by:
Matteo Ferro,
European Institute of Oncology (IEO), Italy
Laura Marandino,
San Raffaele Scientific Institute (IRCCS), Italy

***Correspondence:**
Massimo Lazzeri
massimo.lazzeri@humanitas.it

Specialty section:
This article was submitted to Genitourinary Oncology, a section of the journal Frontiers in Oncology

Received: 10 December 2021
Accepted: 03 January 2022
Published: 27 January 2022

Citation:
Fasulo V, Paciotti M, Lazzeri M, Contieri R, Casale P, Saita A, Lughezzani G, Diana P, Frego N, Avolio PP, Colombo P, Elefante GM, Guazzoni G, Buffi NM, Bates M and Hurle R (2022) Xpert Bladder Cancer Monitor May Avoid Cystoscopies in Patients Under "Active Surveillance" for Recurrent Bladder Cancer (BIAS Project): Longitudinal Cohort Study. Front. Oncol. 12:832835. doi: 10.3389/fonc.2022.832835

Conclusion: Our findings suggest that Xpert BC Monitor assay, when it is longitudinally repeated, could significantly reduce the number of unnecessary cystoscopies and UC during their follow-up.

Keywords: BIAS, active surveillance, Xpert BC, NMIBC, biomarker, cystoscopies, urine cytology

INTRODUCTION

Bladder cancer (BC) is one of the most common cancers, with non-muscle invasive bladder cancer (NMIBC) accounting for about 75% of new diagnoses (1). Progression to muscle-invasive, metastatic lethal disease occurs in approximately 15% of patients (2).

Due to the high relapse rate after treatment, patients with NMIBC typically undergo intensive follow-up based on urine cytology (UC) and in-office cystoscopy, which make BC one of the most expensive cancers per patient. In addition, UC is poorly sensitive for BC detection.

Some cancers are considered indolent, as they are either stagnant or "grow too slowly to be life threatening in even the longest of lifetimes" (2, 3). For this reason, active surveillance (AS) has been suggested as a safe "treatment" strategy for prostate and thyroid cancers that are both examples of cancers that are sometimes indolent and can be detected early through increased use of screening (4). For the same reason, the increasing detection of renal masses as an incidental finding has led to the adoption of this strategy for selected patients with small renal tumors (5, 6)

Following the same idea, in 2003 Soloway et al. suggested AS for selected recurrent LG NMIBC as a safe alternative to transurethral resection of bladder tumor (TURBT) treatment and this strategy has been successively widely adopted (7–9). Although TURBT is still the gold standard treatment, having both a diagnostic and therapeutic role, it is not devoid of complications. At the same time, AS protocols include frequent in-office cystoscopies, which are invasive procedures leading to discomfort of patients and risk of infections. For these reasons, new biomarkers for a less invasive, more sensitive, and more cost-effective diagnosis of BC are urgently needed in order to replace the low sensitivity of urinary cytology (UC) and the invasiveness of cystoscopy (10).

Xpert BC Monitor is a new mRNA-marker assay for BC follow-up after primary diagnosis and measures the levels of five target mRNAs from a cleared urine sample by real-time RT-PCR. Xpert BC Monitor automates and integrates sample processing, nucleic acid amplification, and the detection of target sequences outperforming cytology with a sensitivity and specificity of 73 and 90%, respectively (11, 12). The Xpert BC Monitor test is a CE-IVD test available in some but not all European countries and is not available in the United States.

In addition to biomarkers, imaging tools such as ultrasound and magnetic resonance imaging have been developed for the diagnosis of BC (NMIBC vs MIBC) and for recurrence (13). The use of a MRI-based standardized reporting system, the Vesical Imaging Reporting and Data System (VI-RADS) has been suggested to further improve the characterization of the tumor and peer-to-peer communication (14–17). MRI contraindications, cost, and availability is limiting the diffusion of this technique (18–21). An integration of imaging and biomarkers could improve test accuracy to select who could potentially avoid cystoscopy screening (22–24). Recently, the possibility of deferring cystoscopies and even TURBT using genetic panels has been investigated by Shkolyar et al. and Hurle et al. reported the preliminary data of the application of the Xpert BC monitor in patients enrolled in the Bladder Cancer Italian Active Surveillance (BIAS) project showing promising results (25–27).

In this study, we tested the hypothesis if a persistently negative Xpert BC Monitor test, may avoid unnecessary cystoscopies and replace UC in patients enrolled in the BIAS project for NMIBC.

MATERIALS AND METHODS

Study Design and Population

This is a monocentric, prospective cohort study, conducted within our Institutional AS protocol for recurrent NMIBC (BIAS project-BIAS_V1.2_27.01.2018). We included patients who met the BIAS inclusion criteria and performed at least one Xpert® BC Monitor test (Cepheid, Sunnyvale, CA, USA) (8). The BIAS inclusion criteria are recurrence of 1–5 tumors, tumors size <1 cm, absence of gross hematuria and negative UC for high-grade (HG) carcinoma). Exclusion criteria of this study were: previous history of a HG carcinoma, carcinoma *in situ* (CIS), positive UC or invalid test. All patients signed written informed consent and were able to withdraw from the protocol at any time and be offered the standard treatment.

The AS follow-up protocol consisted of UC and an in-office flexible cystoscopy every 3–4 months in the first year, and then every 6 months annually (28).

Urine samples were collected and analyzed with Xpert BC Monitor upon BIAS entry or in patients who meet the inclusion criteria during the follow-up cystoscopies. This study period was defined starting time (T0), then, if the test was negative and the patient did not fail AS, urinalyses were performed after 4 (T1), 8 (T2), and 12 (T3) months. To be tested consecutively, patients must have a negative test and still be enrolled on AS.

Cystoscopies were performed or supervised by two senior urologists and all images were stored in a digital repository archive. At each cystoscopy, new images were compared with the previous ones.

"Xpert Bladder Monitor Test" Characteristics

Urinalysis was performed with Xpert BC Monitor at each surveillance set point if they met the criteria mentioned above.

The urine biomarker tests measured the gene expression levels of five targets (ABL1, CRH, IGF2, UPK1B, and ANXA10) by RT-PCR according to the manufacturer's protocol. Xpert BC Monitor results (called LDA—linear discriminant analysis) depend on a regression algorithm that utilizes the cycle threshold results of the five mRNA targets (11, 12). Each test cartridge contains internal controls to assess the quality of starting material and PCR reaction. The time to result is about 90 min. For the analyses the cut point of the manufacturer (positive test if LDA ≥0.5) or a stricter alternative (≥0.4) was used (26).

Pathology Characteristics

All surveillance UC were performed according to the Paris classification system by experienced pathologists of our institution (29).

In cases of failure, patients underwent TURBT and all pathological specimens were reviewed by two experienced genitourinary pathologists according to the WHO and Classification of Tumors and staging according to the TNM (International Union against Cancer, 2009) (30).

The primary endpoint was to test clinical performance of the Xpert BC Monitor test, performed longitudinally, to predict AS failure free, according to the previously described criteria. Clinical utility was assessed by determining the number of in-office cystoscopies and UC that could be safely avoided within 1 year.

Statistical Analysis

Categorical variables were represented as frequencies, while continuously coded as median and interquartile range (IQR). Patient groups were compared with chi-squared tests for categorical variables. Failure was defined as achieving one of the following criteria: increased number and/or size of lesions, occurrence of hematuria, positive/suspected UC, voluntary withdrawal from the protocol, any reason to undergo TURBT even if it resulted in negative histology. Death from other causes or loss to follow-up was not considered a failure. A sub-analysis was performed considering patients who voluntarily withdrew or had a negative TURBT result as non-fail to show a more accurate test performance.

The frequency of avoided cystoscopies was determined as the number of negative Xpert calls at one time point divided by the total number of patients with 2, 3, and 4 negatives tests, respectively. The frequency of missed failure was determined as number of failures associated with a negative test divided by the total number of negative tests.

Failure-free-survival (FFS) was estimated with life-table product limit estimates. Kaplan–Meier curves were used to describe failure free survival. Log-rank test was used to compare the distribution among patients grouped based on the number of negative tests. Univariate and multivariate logistic regression model (LRM) were used to test factors associated with failure. All p-values were two sided, and statistical significance was assumed at $p < 0.05$. All analyses were performed using STATA® (version Stata/IC 16.1; StataCorp LLC, TX, USA).

RESULTS

Patients Baseline Characteristics

Overall, 139 patients performed Xpert test at T0, and were therefore enrolled in the current analysis. The median age was 73.0 years (IQR 66.0–78.0) and median follow-up from the enrolment in the study to last follow-up was 23 months (IQR 17–27). Overall, 135 (97.1%) were pTa and 4 (2.9%) pT1 at first diagnosis, and all were LG. Forty-eight patients (34.5%) had a history of bladder instillations. No patient underwent instillation in the 6 months prior to the test. Regarding last tumor recurrence, 49 (35.3%) patients were enrolled in the BIAS protocol at their first recurrence, 25 (18.0%) recurred within one year and 48 (34.5%) recurred after more than one year (**Table 1**).

AS Outcome Characteristics

Sixty-one (43.9%) were already part of the BIAS project at study enrollment, while 78 (56.1%) were newly enrolled in the protocol at beginning of this study.

A total of 68 (48.9%) patients failed AS, while 65 (46.8%) did not fail AS and 6 (4.30%) were lost at follow-up or died from other causes. There was no difference in the failure rate between those already in BIAS or just enrolled in the AS protocol ($p = 0.494$). Causes of failure are summarized in **Table 2**. Of those who did not fail on AS, 55 (84.6%) had a stable lesion, 6 (9.23%) had no lesions found at cystoscopy, and 4 (6.15%) died from other causes (**Table 2**).

Of patients who failed, 64 (94.1%) out of 68 underwent surgery in our institution. Forty-six (67.7%) were confirmed to have pTa LG, 6 (8.8%) had pTa HG, 3 (4.4%) had pT1 HG, and 9 (13.2%) patients had a negative finding (**Table 2**). No patient experienced a progression to pT2 stage BC.

TABLE 1 | Baseline characteristics of the whole population.

		Total N = 139
Age, median (IQR)		73 (66–78)
Gender, N (%)	Female	27 (19.4)
	Male	112 (80.6)
Hematuria, N (%)	No	136 (97.8)
	Yes	3 (2.20)
Smoking habit, N (%)	Non-smoker	46 (33.1)
	Current smoker	33 (23.7)
	Former smoker	35 (25.2)
	Unknown	25 (18.0)
Stage, N (%)	pTa	135 (97.1)
	pT1	4 (2.90)
Grade, N (%)	Low grade	139 (100)
Last Tumor Diagnosis before starting BIAS, N (%)	Primary tumor	54 (39.1)
	Recurrence within 1 year	26 (18.8)
	Recurrence after 1year	58 (42.0)
Adjuvant treatment? N (%)	No	81 (62.8)
	Yes	48 (37.2)
Type of adjuvant treatment, N (%)	Mitomycin C	34 (72.0)
	BCG	7 (15.0)
	Gemcitabine	2 (4.00)
	Other/Unknown	4 (9.00)

BCG, Bacillus Calmette–Guerin; BIAS, Bladder Cancer Italian Active Surveillance; IQR, interquartile range.

TABLE 2 | BIAS outcome details, pathological features and Xpert test results by active surveillance outcome.

		Total N = 139	Failure N = 68	Not Failure N = 65	Other N = 6	p-value
BIAS history, N (%)	Already enrolled	61 (100)	30 (49.2)	27 (44.3)	4 (6.56)	0.494
	Newly enrolled	78 (100)	38 (48.7)	38 (48.7)	2 (2.60)	
AS outcome details, N (%)	No more lesion	6 (100)	n.r.	6 (100)	n.r.	<0.001
	On AS	55 (100)	n.r.	55 (100)	n.r.	
	Death for other cause	6 (100)	n.r.	4 (66.6)	2 (33.3)	
	Lost at follow-up	4 (100)	n.r.	n.r.	4 (100)	
	Increase in size	32 (100)	32 (100)	n.r.	n.r.	
	Increased number	14 (100)	14 (100)	n.r.	n.r.	
	Hematuria	6 (100)	6 (100)	n.r.	n.r.	
	UC: positive\suspected	5 (100)	5 (100)	n.r.	n.r.	
	Increased N° and size	3 (100)	3 (100)	n.r.	n.r.	
	Increased size and Hematuria	5 (100)	5 (100)	n.r.	n.r.	
	UC and Increase N°	1 (100)	1 (100)	n.r.	n.r.	
	Increased size, hematuria & UC	1 (100)	1 (100)	n.r.	n.r.	
	Voluntary withdrew	1 (100)	1 (100)	n.r.	n.r.	
TURBT stage, N (%)	Negative	9 (100)	9 (100)		0 (0.00)	0.89
	pTa	52 (100)	51 (98.0)		1 (2.00)	
	pT1	3 (100)	3 (100)		0 (0.00)	
TURBT grade, N (%)	Low grade	46 (100)	45 (97.8)		1 (2.20)	0.66
	High grade	9 (100)	9 (100)		0 (0.00)	
Xpert Xpert 1st point, N (%)	Negative	57 (100)	20 (35.1)	36 (63.2)	1 (1.70)	0.005
	Positive	82 (100)	48 (58.5)	29 (35.4)	5 (6.10)	
Xpert Xpert 2nd point, N (%)	Negative	34 (100)	9 (26.5)	25 (73.5)		0.13
	Positive	12 (100)	6 (50.0)	6 (50.0)		
Xpert Xpert 3rd point, N (%)	Negative	25 (100)	4 (16.0)	21 (84.0)		0.39
	Positive	4 (100)	0 (0.00)	4 (100)		
Xpert Xpert 4th point, N (%)	Negative	25 (100)	3 (12.0)	22 (88.0)		

AS, active surveillance; BIAS, Bladder Cancer Italian Active Surveillance; n.r., not reported; TUBRT, transurethral resection of bladder tumor; UC, urinary cytology.

Xpert Test Characteristics

At the study enrolment (T0) 57 (41.0%) patients had a negative test (manufactured LDA) and of these 36 (63.2%) are still on AS. At second surveillance (T1) 34/46 (73.9%) were still negative and of those 25 (73.5%) still on AS. At third follow up (T2) 25/29 (86.2%) remained negative and of those 21 (84.0%) still on AS. At final urine detection (T3) 25/25 were negative and 21 (84.0%) currently under AS (**Figure 1**).

Avoiding Cystoscopies at Different LDA Cut Point and Sub-Analysis

Using the manufacturer's LDA (>0.5), in patients with 2 consecutive negative tests, we could have avoided 73.9% of unnecessary cystoscopies, missing 26.4% of patients who failed, while after 3 negative tests can avoid 86.2% cystoscopies, missing only 16.0% of patients who failed AS. Finally, after 4 negatives tests, all of follow-up cystoscopies could have been safely avoided, missing only 12.0% of patient who failed.

Using a stricter LDA (>0.4), in patients with 2 consecutive negative tests, we could have avoided 52.2% of unnecessary cystoscopies, missing 16.7% of patients who failed, while after 3 negative tests can avoid 55.2% cystoscopies, missing only 12.5% of patients who failed AS. Finally, after 4 negative tests, 68.0% of follow-up cystoscopies could have been avoided, missing only 11.8% of patients who failed. A sub-analysis of the stratified group is shown in **Table 3**. No correlation between lesion size and LDA was found (p >0.05).

All the patients with negative Xpert had negative UC, supporting the clinical utility of the test versus UC.

Considering the kinetics of LDA between time periods T0–1, T1–2, and T2–3: 69.6, 65.5, and 72.0% of patients, respectively, had a higher value.

FFS at 23 months (median FU) stratified for having 0, 1, or ≥2 negative test was 67.0% (95%CI 57.7–77.2), 55.1% (95%CI 31.2–73.7), and 84.1 (95%CI 65.9–93.1) respectively, (Log-rank p = 0.003, **Figure 2**). Median time to failure was 13 (IQR 5–23) months.

Basic characteristics such as age, biological-sex, smoking habits, and the number of negatives were tested at univariate and multivariate LRM for AS failure prediction. Having ≥2 negative Xpert tests was protective against failure and the only variable associated with failure in both models OR 0.25 (95%CI 0.105–0.614, p = 0.002), OR 0.25 (95%CI 0.103–0.643, p = 0.004), respectively.

DISCUSSION

In this study, the hypothesis was that having a persistently negative test could predict AS non-failure and that Xpert BC Monitor could replace UC and even avoid cystoscopy or at least extend cystoscopy follow-up interval.

In fact, our major finding is that for patients with two negative tests, cystoscopies could have been avoided in 74% of cases, missing only 26% of the tumors, and for patients with three

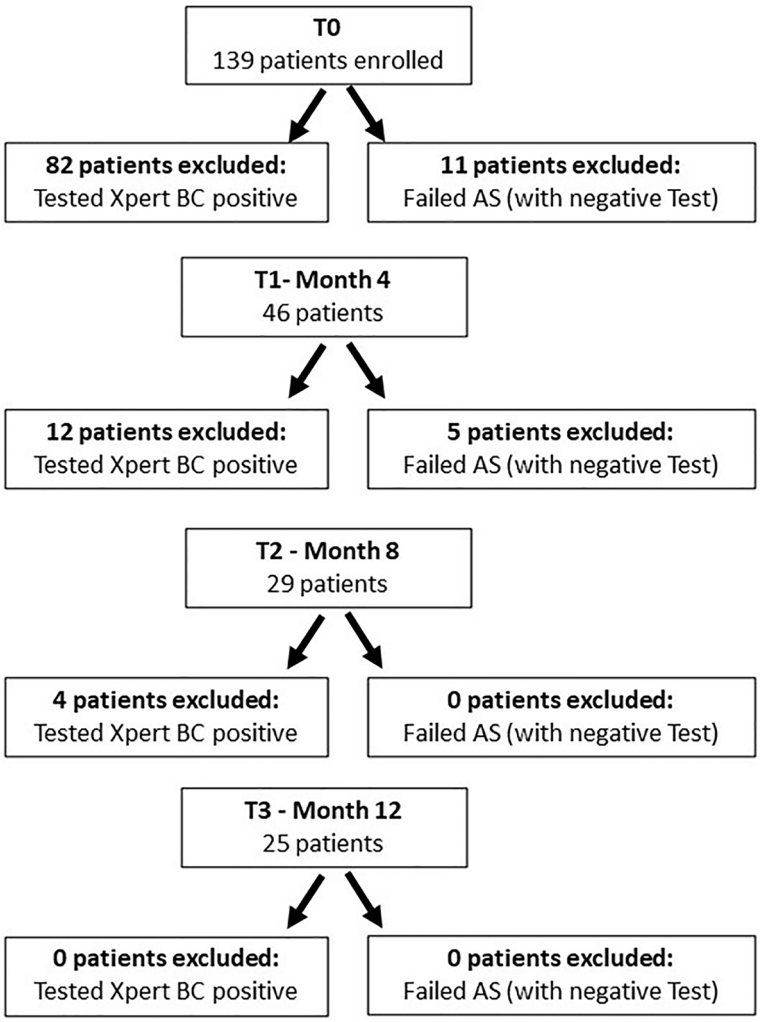


FIGURE 1 | Flow chart of enrolled and who dropped out of the study. To access the next "time point", each patient had to have tested negative on the Xpert Bladder Cancer Monitor test and had none of the active surveillance failure criteria.

TABLE 3A–B | The data are displayed with two different LDA cut points.

(A)

	Analysis LDA ≥0.5		Sub-analysis LDA ≥0.5	
	AVD. CYSTOSCOPIES (%)	**MISSED Failure (%)**	**AVD. CYSTOSCOPIES (%)**	**MISSED "real" Failure (%)**
2 NEG tests	73.9	26.4	73.9	23.5
3 NEG tests	86.2	16.0	86.2	12.0
4 NEG tests	100	12.0	100	8.00

(B)

	Analysis LDA ≥0.4		Sub-analysis LDA ≥0.4	
	AVD. CYSTOSCOPIES (%)	**MISSED Failure (%)**	**AVD. CYSTOSCOPIES (%)**	**MISSED "real" Failure (%)**
2 NEG tests	52.2	16.7	52.2	16.6
3 NEG tests	55.2	12.5	55.2	6.25
4 NEG tests	68.0	11.8	68.0	5.89

The number of avoided cystoscopies and missed failure are referred to by two different definitions of failure. Failure according to the definition of the BIAS protocol and failure according to the histological findings; (A) LDA ≥0.5, (B) LDA ≥0.4.

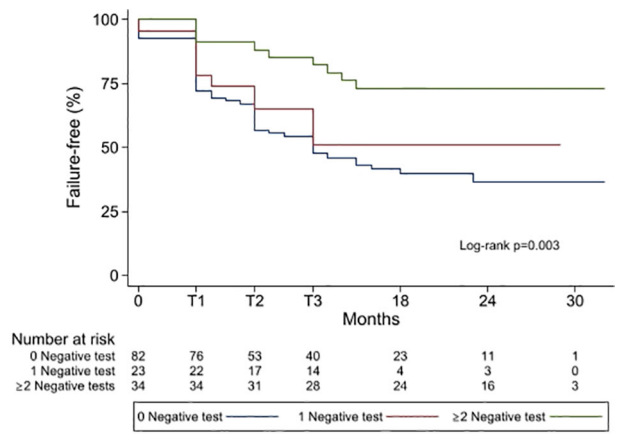


FIGURE 2 | Kaplan–Meier showing failure-free frequencies by group of patient having 0 negative test, 1 negative test or ≥2 negative tests. T1 = 4 months, T2 = 8 months, T3 = 12 months.

negative tests, even up to 84% of cases, missing only 16% of cancers. Furthermore, we did not find a single patient with negative tests and positive UC.

UC is a diagnostic test whose accuracy remains limited. The introduction of the new Paris classification improved both UC sensitivity (SE), which is ranging from 34 to 95%, and negative predictive value (NPV), ranging from 46 to 86%. However, specificity (SP) remains lower than 70% (31, 32). Accuracy varies with the experience of pathologists in interpreting the findings of urinary cytology (33). For these reasons, a lot of effort has been made in developing new tools with high precision and, at the same time, a low cost, such as UC (34).

Xpert BC Monitor has an added value because it does not require an interpretation, especially in those low-volume laboratories where the experience of the cytopathologist can influence the result of UC.

As a new low-cost test, Xpert BC Monitor has been developed with the intent of increasing accuracy of BC diagnosis (35). It is proven that Xpert BC Monitor has high SE for HG NMIBC, as reported by a study by Elsawy et al., involving 181 patients. That study shows a 73.7% SE, 79.6% SP, 29.8% positive predictive value (PPV), and 96.3% NPV, demonstrating superior diagnostic performance in detecting relapses for NMIBC patients compared to UC (36). Similarly, the study of D'Elia et al. on a cohort of 230 patients demonstrates that Xpert BC Monitor SE for HG NMIBC is significantly higher than UC (57.1% vs 85.5%) (37). Additionally, a study by van Valenberg et al. shows that Xpert BC has a higher NPV for bladder cancer patients during follow-up than both UC and another molecular test, Urovysion, with a NPV of 93, 86, and 88%, respectively (38).

Thus, our study is concordant with previous literature findings and extends the results to a specific population of patients under active surveillance. In fact, we demonstrated the superiority of Xpert BC Monitor in detecting low-grade tumors over UC.

In the era of the SARS-CoV-2 pandemic, a urinary biomarker that reduces the discomfort of patients and risk becomes essential, especially for frail elderly patients with BC (39).

Furthermore, in-office flexible cystoscopy is costly, invasive, unpleasant, and carries the risk of severe urinary tract infections and urethral strictures (40, 41). It also has low SE and SP for small and/or flat lesions, such as CIS, depending on the experience of the operator (42).

Besides Xpert BC Monitor, other mRNA-based biomarkers have been validated, like Cxbladder monitor, that Koya et al. show can reduce follow-up cystoscopies by 77.8%, confirming the utility of urinary molecular biomarkers (43). In our study, by replacing the UC with Xpert BC Monitor performed over time, we could have avoided up to 73%, 86.2%, or even up to all unnecessary cystoscopies, depending on whether the patient had two, three, or four consecutive negative tests. The panorama of emerging urinary biomarkers in the diagnosis and surveillance of NMIBC is wide, but none are currently included in daily clinical practice probably due to the availability, the cost that limits their use (44–47).

In the study of Shkolyar et al., the utility of Xpert BC Monitor is evaluated for risk stratification in cystoscopy triaging for patients presenting with hematuria, allowing for early identification of patients with intermediate and high-risk BC (25). Differently, in our study, we used it in a longitudinal follow-up setting for patients with AS, demonstrating its clear superiority over UC, and to the best of our knowledge, our study has the longest AS cohort follow-up, and is the only one using the bladder-biomarker in a repeated setting (46, 48).

The use of MRI including functional sequences has been suggested to be able to discriminate between NMIBC and MIBC (14, 15, 49–51). This imaging technique could potentially result in overstaging as tumor-associated fibrosis or inflammation can mimic the low signal intensity of the muscularis propria (52). To overcome these limitations, the VI-RADS score has been developed to help defining and standardizing the grade of BC invasion (14, 15, 51). However, potential drawbacks MRI have to be considered, such as costs and causes of artifacts (53). Recent studies also showed concordance between experienced and inexperienced readers (50), and a prospective analysis has also been published confirming the previous results (51).

Additionally, we found a fairly high failure-free survival at median time of follow up for patients with 2 or more negative tests (84.1%), which further supports the real possibility of a safe referral to cystoscopy when a patient has at least two persistently negative tests.

There are some limitations to acknowledge. First, the sample size is relatively small. Second, the population is a low-risk BC sub-cohort, so the results cannot be extended to all BC patients. However, our cohort represents patients with AS quite appropriately, including both newly enrolled patients for the BIAS project and long-time enrolled patients. In addition sub-analyses at different LDAs may be biased by the fact that only patients with a negative manufacturer's cut point have repeated the test.

DATA AVAILABILITY STATEMENT

The raw data supporting the conclusions of this article will be made available by the authors, without undue reservation upon request.

ETHICS STATEMENT

The studies involving human participants were reviewed and approved by the Humanitas Research Hospital ethics committee: BIAS project-BIAS_V1.2_27.01.2018. The patients/participants provided their written informed consent to participate in this study.

AUTHOR CONTRIBUTIONS

ML and RH contributed to the conception and design of the study. VF, ML, and RH organized the database. VF, MP, PD, NF, and PA collected the data. VF and MP performed the statistical analysis. VF wrote the first draft of the manuscript. All authors contributed to the article and approved the submitted version.

ACKNOWLEDGMENTS

The authors would like to thank Nadia Lo Iacono as study coordinator.

REFERENCES

1. Siegel RL, Miller KD, Fuchs HE, Jemal A. Cancer Statistics, 2021. *CA Cancer J Clin* (2021) 71:7–33. doi: 10.3322/caac.21654
2. Carter SM, Rogers W, Heath I, Degeling C, Doust J, Barratt A. The Challenge of Overdiagnosis Begins With Its Definition. *BMJ* (2015) 350:h869–9. doi: 10.1136/bmj.h869
3. Lowenstein LM, Basourakos SP, Williams MD, Troncoso P, Gregg JR, Thompson TC, et al. Active Surveillance for Prostate and Thyroid Cancers: Evolution in Clinical Paradigms and Lessons Learned. *Nat Rev Clin Oncol* (2019) 16:168–84. doi: 10.1038/s41571-018-0116-x
4. Maggi M, Cowan JE, Fasulo V, Washington SL, Lonergan PE, Sciarra A, et al. The Long-Term Risks of Metastases in Men on Active Surveillance for Early Stage Prostate Cancer. *J Urol* (2020) 204:1222–8. doi: 10.1097/JU.0000000000001313
5. Herrera-Caceres JO, Jewett MAS. Roles for Active Surveillance in Renal Cancer. *Curr Opin Urol* (2018) 28:375–82. doi: 10.1097/MOU.0000000000000506
6. Lazzeri M, Guazzoni G. Early 21st Century Renal Cell Carcinoma. *Cancer* (2010) 116:3080–3. doi: 10.1002/cncr.25021
7. Soloway MS, Bruck DS, Kim SS. Expectant Management of Small, Recurrent, Noninvasive Papillary Bladder Tumors. *J Urol* (2003) 170:438–41. doi: 10.1097/01.ju.0000076621.71247.6c
8. Hurle R, Pasini L, Lazzeri M, Colombo P, Buffi N, Lughezzani G, et al. Active Surveillance for Low-Risk Non-Muscle-Invasive Bladder Cancer: Mid-Term Results From the Bladder Cancer Italian Active Surveillance (BIAS) Project. *BJU Int* (2016) 118:935–9. doi: 10.1111/bju.13536
9. Petrelli F, Giannatempo P, Maccagnano C, Contieri R, Hurle R. Active Surveillance for Non-Muscle Invasive Bladder Cancer: A Systematic Review and Pooled-Analysis. *Cancer Treat Res Commun* (2021) 27:100369. doi: 10.1016/j.ctarc.2021.100369
10. Liu Y-L, Wang X-L, Yang X-H, Wu X-H, He G-X, Xie L-M, et al. Pooled Analysis of Xpert Bladder Cancer Based on the 5 mRNAs for Rapid Diagnosis of Bladder Carcinoma. *World J Surg Oncol* (2021) 19:42. doi: 10.1186/s12957-021-02154-0
11. Wallace E, Higuchi R, Satya M, McCann L, Sin MLY, Bridge JA, et al. Development of a 90-Minute Integrated Noninvasive Urinary Assay for Bladder Cancer Detection. *J Urol* (2018) 199:655–62. doi: 10.1016/j.juro.2017.09.141
12. Pichler R, Fritz J, Tulchiner G, Klinglmair G, Soleiman A, Horninger W, et al. Increased Accuracy of a Novel mRNA-Based Urine Test for Bladder Cancer Surveillance. *BJU Int* (2018) 121:29–37. doi: 10.1111/bju.14019
13. Saita A, Lughezzani G, Buffi NM, Hurle R, Nava L, Colombo P, et al. Assessing the Feasibility and Accuracy of High-Resolution Microultrasound Imaging for Bladder Cancer Detection and Staging. *Eur Urol* (2020) 77:727–32. doi: 10.1016/j.eururo.2019.03.044
14. Gandhi N, Krishna S, Booth CM, Breau RH, Flood TA, Morgan SC, et al. Diagnostic Accuracy of Magnetic Resonance Imaging for Tumour Staging of Bladder Cancer: Systematic Review and Meta-Analysis. *BJU Int* (2018) 122:744–53. doi: 10.1111/bju.14366
15. Panebianco V, Narumi Y, Altun E, Bochner BH, Efstathiou JA, Hafeez S, et al. Multiparametric Magnetic Resonance Imaging for Bladder Cancer: Development of VI-RADS (Vesical Imaging-Reporting And Data System). *Eur Urol* (2018) 74:294–306. doi: 10.1016/j.eururo.2018.04.029
16. Panebianco V, Narumi Y, Altun E, Bochner BH, Efstathiou JA, Hafeez S, et al. Multiparametric Magnetic Resonance Imaging for Bladder Cancer: Development of VI-RADS (Vesical Imaging-Reporting And Data System). *Eur Urol* (2018) 74:294–306. doi: 10.1016/j.eururo.2018.04.029
17. Woo S, Panebianco V, Narumi Y, Del Giudice F, Muglia VF, Takeuchi M, et al *Diagnostic Performance of Vesical Imaging Reporting and Data System for the Prediction of Muscle-Invasive Bladder Cancer: A Systematic Review and Meta-Analysis. Eur Urol Oncol* (2020) 3:306–15. doi: 10.1016/j.euo.2020.02.007
18. Thoeny HC, Forstner R, De Keyzer F. Genitourinary Applications of Diffusion-Weighted MR Imaging in the Pelvis. *Radiology* (2012) 263:326–42. doi: 10.1148/radiol.12110446
19. Del Giudice F, Leonardo C, Simone G, Pecoraro M, De Berardinis E, Cipollari S, et al. Preoperative Detection of Vesical Imaging-Reporting and Data System (VI-RADS) Score 5 Reliably Identifies Extravesical Extension of Urothelial Carcinoma of the Urinary Bladder and Predicts Significant Delayed Time to Cystectomy: Time to Reconsider the Nee. *BJU Int* (2020) 126:610–9. doi: 10.1111/bju.15188
20. Panebianco V, Del Giudice F, Leonardo C, Sciarra A, Catalano C, Catto JWF. VI-RADS Scoring Criteria for Alternative Risk-Adapted Strategies in the Management of Bladder Cancer During the COVID-19 Pandemic. *Eur Urol* (2020) 78:e18–20. doi: 10.1016/j.eururo.2020.04.043
21. Del Giudice F, Pecoraro M, Vargas HA, Cipollari S, De Berardinis E, Bicchetti M, et al. Systematic Review and Meta-Analysis of Vesical Imaging-Reporting and Data System (VI-RADS) Inter-Observer Reliability: An Added Value for Muscle Invasive Bladder Cancer Detection. *Cancers (Basel)* (2020) 12:2994. doi: 10.3390/cancers12102994
22. Ferro M, Katalin MO, Buonerba C, Marian R, Cantiello F, Musi G, et al. Type 2 Diabetes Mellitus Predicts Worse Outcomes in Patients With High-Grade T1 Bladder Cancer Receiving Bacillus Calmette-Guérin After Transurethral Resection of the Bladder Tumor. *Urol Oncol Semin Orig Investig* (2020) 38:459–64. doi: 10.1016/j.urolonc.2020.02.016
23. Ferro M, La Civita E, Liotti A, Cennamo M, Tortora F, Buonerba C, et al. Liquid Biopsy Biomarkers in Urine: A Route Towards Molecular Diagnosis and Personalized Medicine of Bladder Cancer. *J Pers Med* (2021) 11:237. doi: 10.3390/jpm11030237
24. Nicolazzo C, Busetto GM, Del Giudice F, Sperduti I, Giannarelli D, Gradilone A, et al. The Long-Term Prognostic Value of Survivin Expressing Circulating Tumor Cells in Patients With High-Risk Non-Muscle Invasive Bladder Cancer (NMIBC). *J Cancer Res Clin Oncol* (2017) 143:1971–6. doi: 10.1007/s00432-017-2449-8
25. Shkolyar E, Zhao Q, Mach KE, Teslovich NC, Lee TJ, Cox S, et al. Bladder Cancer Risk Stratification Using a Urinary mRNA Biomarker Panel – A Path Towards Cystoscopy Triaging. *Urol Oncol Semin Orig Investig* (2021) 39:497.e9–15. doi: 10.1016/j.urolonc.2021.02.011
26. Hurle R, Casale P, Saita A, Colombo P, Elefante GM, Lughezzani G, et al. Clinical Performance of Xpert Bladder Cancer (BC) Monitor, a mRNA-Based

Urine Test, in Active Surveillance (AS) Patients With Recurrent Non-Muscle-Invasive Bladder Cancer (NMIBC): Results From the Bladder Cancer Italian Active Surveillance (BIAS) Project. *World J Urol* (2020) 38:2215–20. doi: 10.1007/s00345-019-03002-3
27. Contieri R, Paciotti M, Lughezzani G, Buffi NM, Frego N, Diana P, et al. Long-Term Follow-Up and Factors Associated With Active Surveillance Failure for Patients With Non–Muscle-Invasive Bladder Cancer: The Bladder Cancer Italian Active Surveillance (BIAS) Experience. *Eur Urol Oncol* (2021) 28:in press. doi: 10.1016/j.euo.2021.05.002
28. Hurle R, Lazzeri M, Vanni E, Lughezzani G, Buffi N, Casale P, et al. Active Surveillance for Low Risk Nonmuscle Invasive Bladder Cancer: A Confirmatory and Resource Consumption Study From the BIAS Project. *J Urol* (2018) 199:401–6. doi: 10.1016/j.juro.2017.08.091
29. Barkan GA, Wojcik EM, Nayar R, Savic-Prince S, Quek ML, Kurtycz DFI, et al. The Paris System for Reporting Urinary Cytology: The Quest to Develop a Standardized Terminology. *Adv Anat Pathol* (2016) 23:193–201. doi: 10.1097/PAP.0000000000000118
30. Edge SB, Compton CC. The American Joint Committee on Cancer: The 7th Edition of the AJCC Cancer Staging Manual and the Future of TNM. *Ann Surg Oncol* (2010) 17:1471–4. doi: 10.1245/s10434-010-0985-4
31. Anbardar MH, Monjazeb R. Reclassification of Urinary Cytology Regarding The Paris System for Reporting Urinary Cytology With Cytohistological Correlation Demonstrates High Sensitivity for High-Grade Urothelial Carcinoma. *Diagn Cytopathol* (2020) 48:446–52. doi: 10.1002/dc.24387
32. Das S. Evaluation of Urine Cytology in Urothelial Carcinoma With Respect to the Paris System for Reporting Urinary Cytology. *J Med Sci Clin Res* (2017) 5:30461–70. doi: 10.18535/jmscr/v5i11.111
33. Malviya K, Fernandes G, Naik L, Kothari K, Agnihotri M. Utility of the Paris System in Reporting Urine Cytology. *Acta Cytol* (2017) 61:145–52. doi: 10.1159/000464270
34. Soria F, D'Andrea D, Pohar K, Shariat SF, Lotan Y. Diagnostic, Prognostic and Surveillance Urinary Markers in Nonmuscle Invasive Bladder Cancer. *Curr Opin Urol* (2018) 28:577–83. doi: 10.1097/MOU.0000000000000545
35. Cancel-Tassin G, Roupret M, Pinar U, Gaffory C, Vanie F, Ondet V, et al. Assessment of Xpert Bladder Cancer Monitor Test Performance for the Detection of Recurrence During Non-Muscle Invasive Bladder Cancer Follow-Up. *World J Urol* (2021). doi: 10.1007/s00345-021-03629-1
36. Elsawy AA, Awadalla A, Elsayed A, Abdullateef M, Abol-Enein H. Prospective Validation of Clinical Usefulness of a Novel mRNA-Based Urine Test (Xpert® Bladder Cancer Monitor) for Surveillance in Non Muscle Invasive Bladder Cancer. *Urol Oncol Semin Orig Investig* (2021) 39:77.e9–77.e16. doi: 10.1016/j.urolonc.2020.07.013
37. D´Elia C, Pycha A, Folchini DM, Mian C, Hanspeter E, Schwienbacher C, et al. Diagnostic Predictive Value of Xpert Bladder Cancer Monitor in the Follow-Up of Patients Affected by Non-Muscle Invasive Bladder Cancer. *J Clin Pathol* (2019) 72:140–4. doi: 10.1136/jclinpath-2018-205393
38. van Valenberg FJP, Hiar AM, Wallace E, Bridge JA, Mayne DJ, Beqaj S, et al. Prospective Validation of an mRNA-Based Urine Test for Surveillance of Patients With Bladder Cancer. *Eur Urol* (2019) 75:853–60. doi: 10.1016/j.eururo.2018.11.055
39. Busetto GM, Porreca A, Del Giudice F, Maggi M, D'Agostino D, Romagnoli D, et al. SARS-CoV-2 Infection and High-Risk Non-Muscle-Invasive Bladder Cancer: Are There Any Common Features? *Urol Int* (2020) 104:510–22. doi: 10.1159/000509065
40. Svatek RS, Hollenbeck BK, Holmäng S, Lee R, Kim SP, Stenzl A, et al. The Economics of Bladder Cancer: Costs and Considerations of Caring for This Disease. *Eur Urol* (2014) 66:253–62. doi: 10.1016/j.eururo.2014.01.006
41. Yeo JK, Cho DY, Oh MM, Park SS, Park MG. Listening to Music During Cystoscopy Decreases Anxiety, Pain, and Dissatisfaction in Patients: A Pilot Randomized Controlled Trial. *J Endourol* (2013) 27:459–62. doi: 10.1089/end.2012.0222
42. Burger M, Grossman HB, Droller M, Schmidbauer J, Hermann G, Drăgoescu O, et al. Photodynamic Diagnosis of Non–Muscle-Invasive Bladder Cancer With Hexaminolevulinate Cystoscopy: A Meta-Analysis of Detection and Recurrence Based on Raw Data. *Eur Urol* (2013) 64:846–54. doi: 10.1016/j.eururo.2013.03.059
43. Koya M, Osborne S, Chemaslé C, Porten S, Schuckman A, Kennedy-Smith A. An Evaluation of the Real World Use and Clinical Utility of the Cxbladder Monitor Assay in the Follow-Up of Patients Previously Treated for Bladder Cancer. *BMC Urol* (2020) 20:12. doi: 10.1186/s12894-020-0583-0
44. de Oliveira MC, Caires HR, Oliveira MJ, Fraga A, Vasconcelos MH, Ribeiro R. Urinary Biomarkers in Bladder Cancer: Where Do We Stand and Potential Role of Extracellular Vesicles. *Cancers (Basel)* (2020) 12:1400. doi: 10.3390/cancers12061400
45. Ng K, Stenzl A, Sharma A, Vasdev N. Urinary Biomarkers in Bladder Cancer: A Review of the Current Landscape and Future Directions. *Urol Oncol Semin Orig Investig* (2021) 39:41–51. doi: 10.1016/j.urolonc.2020.08.016
46. Sciarra A, Di Lascio G, Del Giudice F, Leoncini PP, Salciccia S, Gentilucci A, et al. Comparison of the Clinical Usefulness of Different Urinary Tests for the Initial Detection of Bladder Cancer: A Systematic Review. *Curr Urol* (2021) 15:22–32. doi: 10.1097/CU9.0000000000000012
47. Anastasi E, Maggi M, Tartaglione S, Angeloni A, Gennarini G, Leoncini PP, et al. Predictive Value of MCM5 (ADXBLADDER) Analysis in Urine of Men Evaluated for the Initial Diagnosis of Bladder Cancer: A Comparative Prospective Study. *Diagn Cytopathol* (2020) 48:1034–40. doi: 10.1002/dc.24530
48. Cowan B, Klein E, Jansz K, Westenfelder K, Bradford T, Peterson C, et al. Longitudinal Follow-Up and Performance Validation of an mRNA-Based Urine Test (Xpert ® Bladder Cancer Monitor) for Surveillance in Patients With Non-Muscle-Invasive Bladder Cancer. *BJU Int* (2021) 128:713–21. doi: 10.1111/bju.15418
49. Wang HJ, Pui MH, Guan J, Li SR, Lin JH, Pan B, et al. Comparison of Early Submucosal Enhancement and Tumor Stalk in Staging Bladder Urothelial Carcinoma. *Am J Roentgenol* (2016) 207:797–803. doi: 10.2214/AJR.16.16283
50. Barchetti G, Simone G, Ceravolo I, Salvo V, Campa R, Del Giudice F, et al. Multiparametric MRI of the Bladder: Inter-Observer Agreement and Accuracy With the Vesical Imaging-Reporting and Data System (VI-RADS) at a Single Reference Center. *Eur Radiol* (2019) 29:5498–506. doi: 10.1007/s00330-019-06117-8
51. Del Giudice F, Barchetti G, De Berardinis E, Pecoraro M, Salvo V, Simone G, et al. Prospective Assessment of Vesical Imaging Reporting and Data System (VI-RADS) and Its Clinical Impact on the Management of High-Risk Non–Muscle-Invasive Bladder Cancer Patients Candidate for Repeated Transurethral Resection. *Eur Urol* (2020) 77:101–9. doi: 10.1016/j.eururo.2019.09.029
52. Huang L, Kong Q, Liu Z, Wang J, Kang Z, Zhu Y. The Diagnostic Value of MR Imaging in Differentiating T Staging of Bladder Cancer: A Meta-Analysis. *Radiology* (2018) 286(2). doi: 10.1148/radiol.2017171028
53. Thoeny HC, Bellin MF, Comperat EM, Thalmann GN. Vesical Imaging-Reporting and Data System (VI-RADS): Added Value for Management of Bladder Cancer Patients? *Eur Urol* (2018) 74(3):307–8. doi: 10.1016/j.eururo.2018.06.017

Conflict of Interest: The authors declare that the research was conducted in the absence of any commercial or financial relationships that could be construed as a potential conflict of interest.

Publisher's Note: All claims expressed in this article are solely those of the authors and do not necessarily represent those of their affiliated organizations, or those of the publisher, the editors and the reviewers. Any product that may be evaluated in this article, or claim that may be made by its manufacturer, is not guaranteed or endorsed by the publisher.

Copyright © 2022 Fasulo, Paciotti, Lazzeri, Contieri, Casale, Saita, Lughezzani, Diana, Frego, Avolio, Colombo, Elefante, Guazzoni, Buffi, Bates and Hurle. This is an open-access article distributed under the terms of the Creative Commons Attribution License (CC BY). The use, distribution or reproduction in other forums is permitted, provided the original author(s) and the copyright owner(s) are credited and that the original publication in this journal is cited, in accordance with accepted academic practice. No use, distribution or reproduction is permitted which does not comply with these terms.

frontiers in Oncology

ORIGINAL RESEARCH
published: 31 January 2022
doi: 10.3389/fonc.2021.814228

Investigating Urinary Circular RNA Biomarkers for Improved Detection of Renal Cell Carcinoma

Madonna R. Peter[1,2], *Fang Zhao*[1,2], *Renu Jeyapala*[1,3], *Shivani Kamdar*[1,2], *Wei Xu*[4], *Cynthia Hawkins*[2,5], *Andrew J. Evans*[6], *Neil E. Fleshner*[7], *Antonio Finelli*[7] *and Bharati Bapat*[1,2*]

[1] Lunenfeld-Tanenbaum Research Institute, Sinai Health System, Toronto, ON, Canada, [2] Department of Laboratory Medicine & Pathobiology, University of Toronto, Toronto, ON, Canada, [3] Institute of Medical Science, University of Toronto, Toronto, ON, Canada, [4] Department of Biostatistics, Princess Margaret Cancer Centre, University Health Network, Toronto, ON, Canada, [5] Arthur and Sonia Labatt Brain Tumor Research Centre, Hospital for Sick Children, Toronto, ON, Canada, [6] Department of Laboratory Medicine, Mackenzie Health, Richmond Hill, ON, Canada, [7] Division of Urology, Department of Surgery, Princess Margaret Cancer Centre, University Health Network, Toronto, ON, Canada

OPEN ACCESS

Edited by:
Michele Marchioni,
University of Studies G. d'Annunzio Chieti and Pescara, Italy

Reviewed by:
Di Gu,
First Affiliated Hospital of Guangzhou Medical University, China
Felice Crocetto,
Federico II University Hospital, Italy

***Correspondence:**
Bharati Bapat
bapat@lunenfeld.ca

Specialty section:
This article was submitted to Genitourinary Oncology, a section of the journal Frontiers in Oncology

Received: 12 November 2021
Accepted: 27 December 2021
Published: 31 January 2022

Citation:
Peter MR, Zhao F, Jeyapala R, Kamdar S, Xu W, Hawkins C, Evans AJ, Fleshner NE, Finelli A and Bapat B (2022) Investigating Urinary Circular RNA Biomarkers for Improved Detection of Renal Cell Carcinoma. Front. Oncol. 11:814228. doi: 10.3389/fonc.2021.814228

Renal cell carcinomas (RCC) are usually asymptomatic until late stages, posing several challenges for early detection of malignant disease. Non-invasive liquid biopsy biomarkers are emerging as an important diagnostic tool which could aid with routine screening of RCCs. Circular RNAs (circRNAs) are novel non-coding RNAs that play diverse roles in carcinogenesis. They are promising biomarkers due to their stability and ease of detection in small quantities from non-invasive sources such as urine. In this study, we analyzed the expression of various circRNAs that were previously identified in RCC tumors (circEGLN3, circABCB10, circSOD2 and circACAD11) in urinary sediment samples from non-neoplastic controls, patients with benign renal tumors, and clear cell RCC (ccRCC) patients. We observed significantly reduced levels of circEGLN3 and circSOD2 in urine from ccRCC patients compared to healthy controls. We also assessed the linear variant of EGLN3 and found differential expression between patients with benign tumors compared to ccRCC patients. These findings highlight the potential of circRNA markers as non-invasive diagnostic tools to detect malignant RCC.

Keywords: renal cell carcinoma, ccRCC, circular RNA, biomarkers, liquid biopsy

INTRODUCTION

Renal cell carcinoma (RCC) is the most common malignancy of the kidney, accounting for approximately 2% of global cancer diagnoses and deaths in 2020 (1, 2). Survival with RCC is dependent on clinical stage at first diagnosis, with 5-year survival rate around 90% for localized disease and 12% for metastatic disease (3). RCC tumor subtypes range from less aggressive chromophobe, papillary type I (pRCC type I) to more aggressive pRCC Type II and clear cell RCC (ccRCC) (4). Among these, ccRCC constitute the major tumor subtype (~70%) with high metastatic potential (5).

Early detection of ccRCC is challenging as more than 50% of RCC tumors are asymptomatic and frequently detected as an incidental finding during abdominal imaging for other conditions (6). Approximately 30% of ccRCC patients are first diagnosed with metastatic disease with poor overall prognosis and survival (7). RCC is often treated with surgery based on imaging and/or needle biopsy diagnosis; however, current imaging techniques cannot accurately predict tumor histopathology (6). Furthermore, tissue-based immunohistochemical markers are insufficient for differential diagnosis (8). Several tissue-based miRNA and protein markers have been identified, but none have impacted patient management to date (9). Identifying molecular markers in liquid biopsies (i.e. serum, urine) is a promising approach, which can potentially circumvent issues of tumor tissue heterogeneity and overcome limitations in tissue availability (10). In this regard, non-invasive biomarkers that could be routinely used to screen for RCC at an early stage would be important for the clinical management of RCC.

Circular RNAs (circRNAs) are a class of endogenous noncoding RNAs associated with wide-ranging functions including regulation of key cancer driver genes (11). They are distinct from linear RNA and are produced by covalent linking of 5' and 3' ends of an RNA molecule (12). CircRNAs are abundant, stable and associated with tissue-specific and cell-specific expression patterns (13). Differential expression of these circRNAs has been demonstrated in multiple cancer types and can be detected in a variety of sources, including tumor tissue and biofluids (14–17). Several circRNAs have already been identified as differentially expressed in ccRCC tumors compared to matched benign tissue (18–21). These altered circRNAs could potentially serve as diagnostic markers to facilitate early detection of malignant disease. In this study, we selected circRNAs that were previously shown to be upregulated in ccRCC tumors and assessed whether these markers could be detected in urine samples from patients with confirmed diagnosis of ccRCC.

MATERIALS AND METHODS

Patient Cohort and Urine Sample Collection

All patients were previously recruited by the University Health Network (UHN) McCain genitourinary biobank (MGB). Informed written consent was obtained in accordance with approved research ethics board protocols by UHN and Sinai Health System (SHS). Urine samples were collected from 19 healthy non-neoplastic/normal patients, 8 patients with benign renal tumors and 76 patients with confirmed diagnosis of ccRCC. For ccRCC patients, all samples were collected prior to any surgical intervention. Each patient provided approximately 20-90mL of urine, which was then spun at 400 x *g* for 10 minutes at 4°C. The urinary sediment was stored with 2mL of supernatant in cryovials and snap frozen in liquid nitrogen. Patients' clinical data at diagnosis (sex, clinical and pathological stage, Fuhrman grade) and follow-up metastasis status were also collected (summarized in **Table 1**).

TABLE 1 | Summary of cohort clinical characteristics.

Clinical characteristic	Normal	Benign	ccRCC
Sex			
Male	9	2	53
Female	10	6	23
Fuhrman Grade			
G1	n/a	n/a	10
G2	n/a	n/a	40
G3	n/a	n/a	23
G4	n/a	n/a	3
Clinical Stage (TNM) at diagnosis			
T1	n/a	n/a	51
T2	n/a	n/a	3
T3	n/a	n/a	18
T4	n/a	n/a	3
Unknown T	n/a	n/a	1
Nx	n/a	n/a	65
N0	n/a	n/a	9
N1	n/a	n/a	1
Unknown N	n/a	n/a	1
Mx	n/a	n/a	20
M0	n/a	n/a	51
M1	n/a	n/a	5
Metastasis status post-diagnosis			
Yes	n/a	n/a	16
No	n/a	n/a	60

n/a, not applicable.

Purification of Total RNA and cDNA Conversion

Frozen urinary sediment samples were thawed, and total RNA was extracted using the QIAamp Circulating Nucleic Acid Kit (Qiagen, Hilden, Germany), specifically using the protocol for urine miRNA extraction. Contaminating DNA was digested using the Qiagen RNase-Free DNase Set followed by clean-up with the RNeasy mini kit according to manufacturer's protocol. All samples were eluted with 15µL of elution buffer and reverse transcribed using the Superscript VILO cDNA synthesis kit (ThermoFisher Scientific, Waltham, MA, USA).

qPCR Assays and Data Analysis

Using previously published datasets, we selected circRNA candidates and a linear RNA candidate that were shown to be upregulated in ccRCC tumor tissue compared to matched benign tissue (18–21). These included: circEGLN3, linear EGLN3, circABCB10, circSOD2, and circACAD11. We also selected circHIPK3, which is dysregulated in multiple cancer types, including colorectal cancer and gastric cancer (22–24). We used GAPDH mRNA as an internal control to normalize expression for each candidate RNA marker (25). Primer sequences for circRNA or linear RNA targets were either previously published or designed specifically for this study (**Supplementary Table 1**) and qPCR assays were optimized with RNA from HEK 293 cell lines. For circRNA candidates, all primers were divergent, with some specifically located on the circRNA junctional sites.

For qPCR assays, 1µL of converted cDNA sample was used for each assay, with two replicates per sample. The Power SYBR green master mix (ThermoFisher Scientific) was used, with 300nM of primers per reaction. All qPCR assays were

performed on the ThermoFisher Scientific QuantStudio6Flex real-time PCR system (95°C for 10 min, 40 cycles of 95°C for 15 sec and 60°C for 1 min, followed by melt-curve analysis). GAPDH was used as a normalizing control, with HEK 293 derived cDNA as the positive control. Non-template controls were utilized for all assays. Detection of circRNA junctional sequences were confirmed by Sanger sequencing (service provided by The Centre for Applied Genomics, Hospital for Sick Children).

The delta Ct for each candidate circRNA/linear RNA was calculated using GAPDH to assess relative expression between normal, benign and ccRCC samples. If there was no amplification of a candidate marker in a sample, the marker was considered as non-detectable and Ct value was set to the maximum (Ct 40). The Kruskal-Wallis test was used to compare delta Ct values between the three groups, followed by pairwise comparisons with Benjamini-Hochberg FDR correction. For each candidate RNA marker, the delta-delta Ct method was next used to assess differences between benign and ccRCC patients, with normal patients serving as the control group. Significantly altered markers between benign and ccRCC patients were identified by the Mann-Whitney test. Receiver operating characteristic (ROC) curve analysis was performed using the ROCR package. All statistical tests were two-sided and conducted using R v4.1.1.

RESULTS

Optimization of Candidate circRNA Detection Assays in Urinary Sediment Samples

We first assessed whether the candidate markers could be detected in HEK 293 cells and urine samples from 8 ccRCC patients. We confirmed detection of the unique junction sites of all circRNA candidates using Sanger sequencing (**Supplementary Figure 1**). Additional variants of circEGLN3 and circABCB10, as well as another candidate circRNA (circAGAP1) were also tested but not detectable in urinary sediment samples (20, 21, 26). Interestingly, two circRNA candidates, circABCB10 and circACAD11, were detectable in genomic DNA (gDNA) from HEK 293 cell lines. We assessed urine-derived gDNA samples from RCC patients and saw similar melt curve profiles for circABCB10 and circACAD11 as the equivalent RNA/cDNA samples (**Supplementary Figure 2**). The circRNA junction sequences for circABCB10 and circACAD11 were also confirmed in gDNA samples by Sanger sequencing. To eliminate the possibility of RNA contamination, gDNA samples were treated with RNase A, which would digest linear RNA and circRNA. However, these junctional sequences were still detectable in DNA samples post RNase A treatment (data not shown). Although these results are interesting and potentially indicative of circular DNA, we performed DNase digestion of all RNA samples from patients to mitigate any potential DNA contamination.

Assessment of circRNA Expression in Urinary Sediments From Normal, Benign and ccRCC Patients

We next performed qPCR analysis of all urinary sediment samples from 19 healthy control/normal patients, 8 patients with benign tumors, and 76 patients with ccRCC. While certain candidates (linear EGLN3, circHIPK3, and circSOD2) demonstrated detectable levels in all urinary sediment samples analyzed, circABCB10 was detected in 97% of samples, circEGLN3 in 69% of samples, and circACAD11 in 60% of samples.

The expression levels of each candidate marker relative to GAPDH (delta Ct) is summarized in **Figure 1**. When comparing all three patient groups, circEGLN3 levels were significantly different between the normal (non-neoplastic) group versus ccRCC patients (Kruskal-Wallis test, $p < 0.05$) (**Figure 1A**). Interestingly, the median delta Ct value of circEGLN3 (normalized by GAPDH) was higher in ccRCC patient urine samples compared to normal samples. That is, there were lower detectable levels of circEGLN3 in ccRCC urine samples compared to normal controls. This was a surprising finding since increased expression of circEGLN3 has been observed in tumor tissue from ccRCC patients compared to matched benign tissue (18, 21). Similarly, there were lower levels of circSOD2 in urine samples from benign and ccRCC patients compared to healthy controls (**Figure 1E**).

Using normal samples as a control group, we calculated the relative fold-change for each candidate and compared expression levels between the benign and ccRCC groups (**Figure 2**). We observed increased linear EGLN3 expression in urine from patients with benign tumors (relative to healthy controls) compared to ccRCC patients (**Figure 2B**). In addition, we performed ROC analysis to assess the diagnostic potential of these candidate markers. We found that detected circEGLN3 and circSOD2 levels had an AUC of 0.71 and 0.68, respectively, for separating cancer patients versus non-neoplastic patients (**Supplementary Figure 3**). These markers would need to be validated in additional cohorts to confirm their utility as diagnostic tools.

We further examined expression levels among ccRCC patients using additional clinical parameters, including Fuhrman grade, TNM staging at diagnosis, and current metastasis status. For Fuhrman grade, there was no significant difference in detection levels of any candidate circRNAs (**Supplementary Figure 4**). Similar findings were observed when analyzing clinical T stage at first diagnosis of ccRCC (**Supplementary Figure 5**). We also obtained metastasis status at first diagnosis of ccRCC for 56 patients (**Table 1**). We found significantly less circACAD11 in urine from patients with metastasis at the time of diagnosis compared to those without metastasis ($p<0.05$, Mann-Whitney Test) (**Supplementary Figure 6**). We next examined post-diagnosis metastasis status and found no significant differences in circRNA or linear RNA levels (**Supplementary Figure 7**).

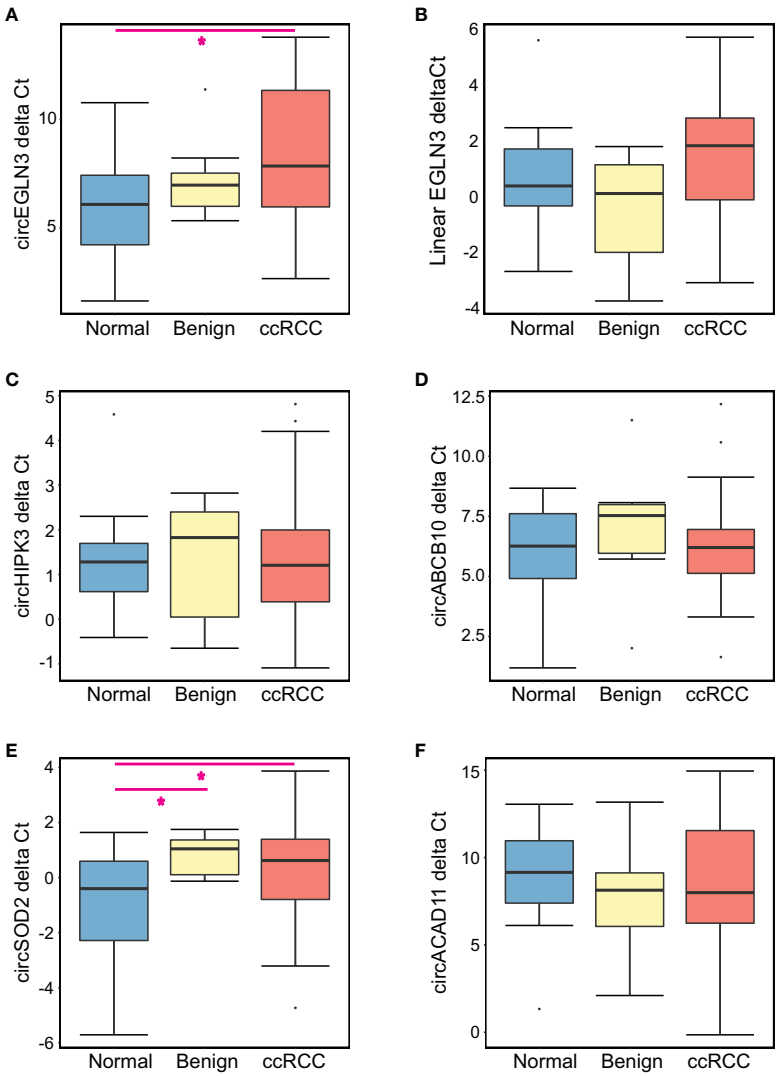


FIGURE 1 | Summary of expression levels of all candidate markers for each patient group. The delta Ct for each candidate RNA marker was calculated using GAPDH Ct values for all urine samples analyzed. Boxplots show the median delta Cts as well as the first and third quartile for **(A)** circEGLN3, **(B)** linear EGLN3, **(C)** circHIPK3, **(D)** circABCB10, **(E)** circSOD2, and **(F)** circACAD11. Kruskal-Wallis analysis was performed to compare all patient groups, with pairwise comparisons for significantly altered RNA markers (*$p < 0.05$).

DISCUSSION

Liquid biopsies offer promising minimally invasive strategies to detect malignancies, track molecular alterations associated with disease progression, and potentially predict therapeutic response (27–32). In particular, detection of circulating DNA and RNA markers in blood and urine samples are an area of active study in ccRCC (10, 33, 34). Our study has demonstrated that select RCC-related circRNAs can be detected in urine samples from ccRCC patients, and their differential expression is associated with ccRCC status. We have also demonstrated that these markers can be successfully analyzed in patients' urine samples thereby providing a non-invasive strategy for future studies. This work highlights the diagnostic potential of circSOD2, circEGLN3 and linear EGLN3 for early detection of ccRCC.

In this study, we focused on urinary samples collected around first diagnosis of ccRCC and prior to surgical intervention. We found decreased levels of circELGN3 and circSOD2 in urine from ccRCC patients compared to healthy controls. These candidates were previously shown to be upregulated in ccRCC tissue compared to matched control tissue, especially circEGLN3, which has demonstrated dysregulated expression in a few studies (18, 21, 26). The reason for these divergent expression profiles between urine and tumor tissue is unclear. Furthermore, the relative abundance of these circRNAs in non-neoplastic tissues from ccRCC patients compared to normal renal tissue from non-cancer patients is not known. Such a

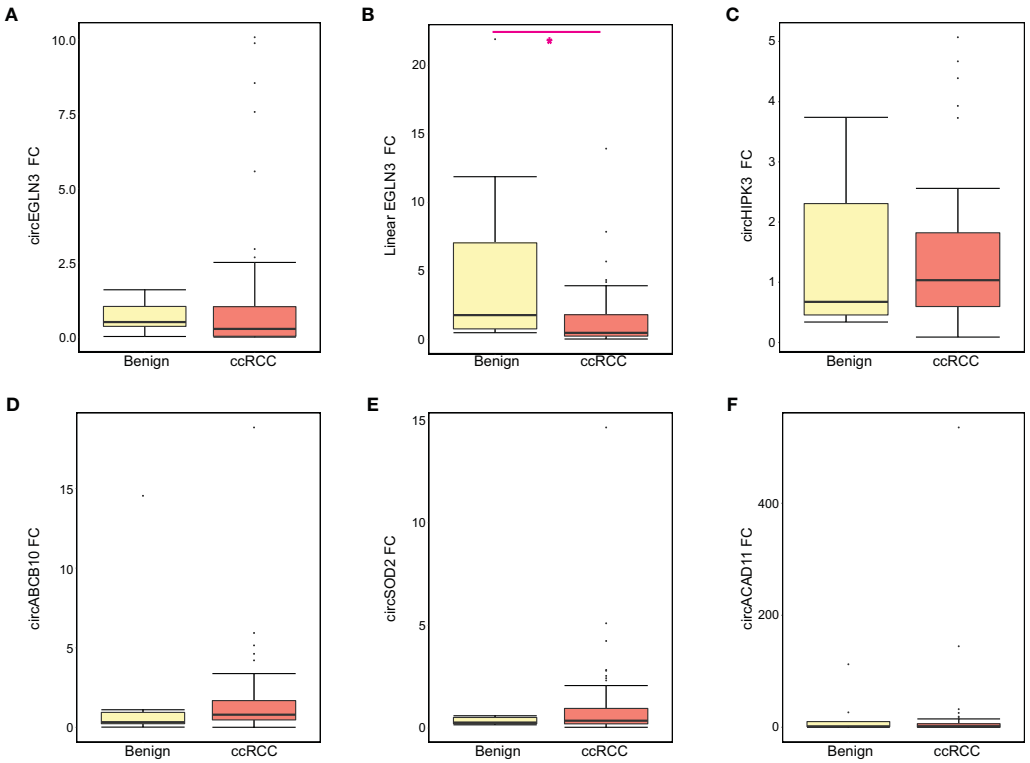


FIGURE 2 | Relative expression of all RNA candidates between benign and ccRCC groups. The relative fold-change (FC) for each RNA candidate was calculated for benign and ccRCC samples using normal samples as the control group. Boxplots show the median FC, first and third quartile for **(A)** circEGLN3, **(B)** linear EGLN3, **(C)** circHIPK3, **(D)** circABCB10, **(E)** circSOD2, and **(F)** circACAD11. Mann-Whitney test results are shown (*p < 0.05).

comparison may shed light on variations observed in circRNA expression levels in tumor tissue versus urine samples from ccRCC patients. Further separation of exosomes in urine may also help to improve detection of these markers and the ability to distinguish ccRCC from benign tumors (35).

The precise functional role(s) of these circRNAs in the development of malignant disease remain to be characterized. However, recent evidence suggests that silencing of circEGLN3 could reduce RCC cell proliferation and invasion (36). Another interesting observation was the presence of circRNA junctions in DNA from HEK 293 cells and urine samples. This could be an example of extrachromosomal circular DNA (37), but additional studies are required to further explore any connection between circRNA and circDNA. Overall, our exploratory study has found that circRNAs may serve as diagnostic markers and their detection in urine samples offer a non-invasive strategy to identify ccRCC. Additional validation in a larger series of patients is needed to confirm the utility of these circRNAs in the clinical management of aggressive disease.

DATA AVAILABILITY STATEMENT

The original contributions presented in the study are included in the article/**Supplementary Material**, further inquiries can be directed to the corresponding author.

ETHICS STATEMENT

The studies involving human participants were reviewed and approved by University Health Network and Sinai Health System. The patients/participants provided their written informed consent to participate in this study.

AUTHOR CONTRIBUTIONS

BB designed the overall study. WX and CH contributed to statistical and circRNA analysis aspects of study. MP performed qPCR assays for all samples and data analysis. FZ and RJ contributed to the optimization of qPCR assays. FZ and SK assisted with data analysis of the cohort. NF, AE, and AF performed patient recruitment and follow-up. MP and BB composed the manuscript with feedback from all co-authors involved. All authors contributed to the article and approved the submitted version.

FUNDING

This study was funded by a Give for a Cure Grant #24205 from the Cancer Research Society and a KCRNC-KCC-CUASF award.

ACKNOWLEDGMENTS

We acknowledge the UHN McCain GU Biobank for recruiting patients, collecting samples and for patient follow-up/data collection.

SUPPLEMENTARY MATERIAL

The Supplementary Material for this article can be found online at: https://www.frontiersin.org/articles/10.3389/fonc.2021.814228/full#supplementary-material

REFERENCES

1. Motzer RJ, Jonasch E, Boyle S, Carlo MI, Manley B, Agarwal N, et al. NCCN Guidelines Insights: Kidney Cancer, Version 1.2021. *J Natl Compr Canc Netw* (2020) 18(9):1160–70. doi: 10.6004/jnccn.2020.0043
2. Sung H, Ferlay J, Siegel RL, Laversanne M, Soerjomataram I, Jemal A, et al. Global Cancer Statistics 2020: GLOBOCAN Estimates of Incidence and Mortality Worldwide for 36 Cancers in 185 Countries. *CA Cancer J Clin* (2021) 71(3):209–49. doi: 10.3322/caac.21660
3. Padala SA, Barsouk A, Thandra KC, Saginala K, Mohammed A, Vakiti A, et al. Epidemiology of Renal Cell Carcinoma. *World J Oncol* (2020) 11(3):79–87. doi: 10.14740/wjon1279
4. Muglia VF, Prando A. Renal Cell Carcinoma: Histological Classification and Correlation With Imaging Findings. *Radiol Bras* (2015) 48(3):166–74. doi: 10.1590/0100-3984.2013.1927
5. Hsieh JJ, Purdue MP, Signoretti S, Swanton C, Albiges L, Schmidinger M, et al. Renal Cell Carcinoma. *Nat Rev Dis Primers* (2017) 3:17009. doi: 10.1038/nrdp.2017.9
6. Escudier B, Porta C, Schmidinger M, Rioux-Leclercq N, Bex A, Khoo V, et al. Renal Cell Carcinoma: ESMO Clinical Practice Guidelines for Diagnosis, Treatment and Follow-Up†. *Ann Oncol* (2019) 30(5):706–20. doi: 10.1093/annonc/mdz056
7. Assi HI, Patenaude F, Toumishey E, Ross L, Abdelsalam M, Reiman T. A Simple Prognostic Model for Overall Survival in Metastatic Renal Cell Carcinoma. *Can Urol Assoc J* (2016) 10(3-4):113–9. doi: 10.5489/cuaj.3351
8. Farber NJ, Kim CJ, Modi PK, Hon JD, Sadimin ET, Singer EA. Renal Cell Carcinoma: The Search for a Reliable Biomarker. *Transl Cancer Res* (2017) 6 (3):620–32. doi: 10.21037/tcr.2017.05.19
9. Marchioni M, Rivas JG, Autran A, Socarras M, Albisinni S, Ferro M, et al. Biomarkers for Renal Cell Carcinoma Recurrence: State of the Art. *Curr Urol Rep* (2021) 22(6):31. doi: 10.1007/s11934-021-01050-0
10. Lakshminarayanan H, Rutishauser D, Schraml P, Moch H, Bolck HA. Liquid Biopsies in Renal Cell Carcinoma-Recent Advances and Promising New Technologies for the Early Detection of Metastatic Disease. *Front Oncol* (2020) 10:582843. doi: 10.3389/fonc.2020.582843
11. Liu J, Zhang X, Yan M, Li H. Emerging Role of Circular RNAs in Cancer. *Front Oncol* (2020) 10:663. doi: 10.3389/fonc.2020.00663
12. Kristensen LS, Andersen MS, Stagsted LVW, Ebbesen KK, Hansen TB, Kjems J. The Biogenesis, Biology and Characterization of Circular RNAs. *Nat Rev Genet* (2019) 20(11):675–91. doi: 10.1038/s41576-019-0158-7
13. Patop IL, Wust S, Kadener S. Past, Present, and Future of circRNAs. *EMBO J* (2019) 38(16):e100836. doi: 10.15252/embj.2018100836
14. Kristensen LS, Hansen TB, Veno MT, Kjems J. Circular RNAs in Cancer: Opportunities and Challenges in the Field. *Oncogene* (2018) 37(5):555–65. doi: 10.1038/onc.2017.361
15. Wang Y, Zhang Y, Wang P, Fu X, Lin W. Circular RNAs in Renal Cell Carcinoma: Implications for Tumorigenesis, Diagnosis, and Therapy. *Mol Cancer* (2020) 19(1):149. doi: 10.1186/s12943-020-01266-7
16. Wang S, Zhang K, Tan S, Xin J, Yuan Q, Xu H, et al. Circular RNAs in Body Fluids as Cancer Biomarkers: The New Frontier of Liquid Biopsies. *Mol Cancer* (2021) 20(1):13. doi: 10.1186/s12943-020-01298-z
17. Wen G, Zhou T, Gu W. The Potential of Using Blood Circular RNA as Liquid Biopsy Biomarker for Human Diseases. *Protein Cell* (2020) 12(12):911–46. doi: 10.1007/s13238-020-00799-3
18. Franz A, Ralla B, Weickmann S, Jung M, Rochow H, Stephan C, et al. Circular RNAs in Clear Cell Renal Cell Carcinoma: Their Microarray-Based Identification, Analytical Validation, and Potential Use in a Clinico-Genomic Model to Improve Prognostic Accuracy. *Cancers (Basel)* (2019) 11 (10):1473. doi: 10.3390/cancers11101473
19. Huang Y, Zhang Y, Jia L, Liu C, Xu F. Circular RNA ABCB10 Promotes Tumor Progression and Correlates With Pejorative Prognosis in Clear Cell Renal Cell Carcinoma. *Int J Biol Markers* (2019) 34(2):176–83. doi: 10.1177/1724600819842279
20. Ma C, Qin J, Zhang J, Wang X, Wu D, Li X. Construction and Analysis of Circular RNA Molecular Regulatory Networks in Clear Cell Renal Cell Carcinoma. *Mol Med Rep* (2020) 21(1):141–50. doi: 10.3892/mmr.2019.10811
21. Lv Q, Ma C, Li H, Tan X, Wang G, Zhang Y, et al. Circular RNA Microarray Expression Profile and Potential Function of Circ0005875 in Clear Cell Renal Cell Carcinoma. *J Cancer* (2020) 11(24):7146–56. doi: 10.7150/jca.48770
22. Zheng Q, Bao C, Guo W, Li S, Chen J, Chen B, et al. Circular RNA Profiling Reveals an Abundant Circhipk3 That Regulates Cell Growth by Sponging Multiple miRNAs. *Nat Commun* (2016) 7:11215. doi: 10.1038/ncomms11215
23. Zeng K, Chen X, Xu M, Liu X, Hu X, Xu T, et al. CircHIPK3 Promotes Colorectal Cancer Growth and Metastasis by Sponging miR-7. *Cell Death Dis* (2018) 9(4):417. doi: 10.1038/s41419-018-0454-8
24. Zhou J, Wang B, Bin X, Xie C, Li B, Liu O, et al. CircHIPK3: Key Player in Pathophysiology and Potential Diagnostic and Therapeutic Tool. *Front Med (Lausanne)* (2021) 8:615417. doi: 10.3389/fmed.2021.615417
25. Kamdar S, Isserlin R, van der Kwast T, Zlotta AR, Bader GD, Fleshner NE, et al. Exploring Targets of TET2-Mediated Methylation Reprogramming as Potential Discriminators of Prostate Cancer Progression. *Clin Epigenet* (2019) 11(1):54. doi: 10.1186/s13148-019-0651-z
26. Lin L, Cai J. Circular RNA Circ-EGLN3 Promotes Renal Cell Carcinoma Proliferation and Aggressiveness *via* miR-1299-Mediated IRF7 Activation. *J Cell Biochem* (2020) 121(11):4377–85. doi: 10.1002/jcb.29620
27. Ignatiadis M, Sledge GW, Jeffrey SS. Liquid Biopsy Enters the Clinic - Implementation Issues and Future Challenges. *Nat Rev Clin Oncol* (2021) 18(5):297–312. doi: 10.1038/s41571-020-00457-x
28. Hermanns T, Savio AJ, Olkhov-Mitsel E, Mari A, Wettstein MS, Saba K, et al. A Noninvasive Urine-Based Methylation Biomarker Panel to Detect Bladder Cancer and Discriminate Cancer Grade. *Urol Oncol* (2020) 38(6):603.e601–603.e607. doi: 10.1016/j.urolonc.2020.01.007
29. Zhao F, Vesprini D, Liu RSC, Olkhov-Mitsel E, Klotz LH, Loblaw A, et al. Combining Urinary DNA Methylation and Cell-Free microRNA Biomarkers for Improved Monitoring of Prostate Cancer Patients on Active Surveillance. *Urol Oncol* (2019) 37(5):297.e9–17. doi: 10.1016/j.urolonc.2019.01.031
30. Zhao F, Olkhov-Mitsel E, Kamdar S, Jeyapala R, Garcia J, Hurst R, et al. A Urine-Based DNA Methylation Assay, ProCUrE, to Identify Clinically Significant Prostate Cancer. *Clin Epigenet* (2018) 10(1):147. doi: 10.1186/s13148-018-0575-z
31. Zhao F, Olkhov-Mitsel E, van der Kwast T, Sykes J, Zdravic D, Venkateswaran V, et al. Urinary DNA Methylation Biomarkers for Noninvasive Prediction of Aggressive Disease in Patients With Prostate Cancer on Active Surveillance. *J Urol* (2017) 197(2):335–41. doi: 10.1016/j.juro.2016.08.081
32. Ferro M, La Civita E, Liotti A, Cennamo M, Tortora F, Buonerba C, et al. Liquid Biopsy Biomarkers in Urine: A Route Towards Molecular Diagnosis and Personalized Medicine of Bladder Cancer. *J Pers Med* (2021) 11(3):237. doi: 10.3390/jpm11030237
33. Li G, Zhao A, Peoch M, Cottier M, Mottet N. Detection of Urinary Cell-Free miR-210 as a Potential Tool of Liquid Biopsy for Clear Cell Renal Cell Carcinoma. *Urol Oncol* (2017) 35(5):294–9. doi: 10.1016/j.urolonc.2016.12.007
34. Petrozza V, Pastore AL, Palleschi G, Tito C, Porta N, Ricci S, et al. Secreted miR-210-3p as Non-Invasive Biomarker in Clear Cell Renal Cell Carcinoma. *Oncotarget* (2017) 8(41):69551–8. doi: 10.18632/oncotarget.18449
35. Barth DA, Drula R, Ott L, Fabris L, Slaby O, Calin GA, et al. Circulating Non-Coding RNAs in Renal Cell Carcinoma-Pathogenesis and Potential Implications as Clinical Biomarkers. *Front Cell Dev Biol* (2020) 8:828. doi: 10.3389/fcell.2020.00828

36. Zhang G, Wang J, Tan W, Han X, Han B, Wang H, et al. Circular RNA EGLN3 Silencing Represses Renal Cell Carcinoma Progression Through the miR-1224-3p/HMGXB3 Axis. *Acta Histochem* (2021) 123(6):151752. doi: 10.1016/j.acthis.2021.151752
37. Yan Y, Guo G, Huang J, Gao M, Zhu Q, Zeng S, et al. Current Understanding of Extrachromosomal Circular DNA in Cancer Pathogenesis and Therapeutic Resistance. *J Hematol Oncol* (2020) 13(1):124. doi: 10.1186/s13045-020-00960-9

Conflict of Interest: The authors declare that the research was conducted in the absence of any commercial or financial relationships that could be construed as a potential conflict of interest.

Publisher's Note: All claims expressed in this article are solely those of the authors and do not necessarily represent those of their affiliated organizations, or those of the publisher, the editors and the reviewers. Any product that may be evaluated in this article, or claim that may be made by its manufacturer, is not guaranteed or endorsed by the publisher.

Copyright © 2022 Peter, Zhao, Jeyapala, Kamdar, Xu, Hawkins, Evans, Fleshner, Finelli and Bapat. This is an open-access article distributed under the terms of the Creative Commons Attribution License (CC BY). The use, distribution or reproduction in other forums is permitted, provided the original author(s) and the copyright owner(s) are credited and that the original publication in this journal is cited, in accordance with accepted academic practice. No use, distribution or reproduction is permitted which does not comply with these terms.

frontiers in Oncology

ORIGINAL RESEARCH
published: 03 February 2022
doi: 10.3389/fonc.2021.802188

Clinical Application of Circulating Tumor Cells and Circulating Endothelial Cells in Predicting Bladder Cancer Prognosis and Neoadjuvant Chemosensitivity

Xiao Yang[1†], Jiancheng Lv[1†], Zijian Zhou[1†], Dexiang Feng[1†], Rui Zhou[1,2], Baorui Yuan[1], Qikai Wu[1], Hao Yu[1], Jie Han[1], Qiang Cao[1], Min Gu[1], Pengchao Li[1], Haiwei Yang[1*] and Qiang Lu[1*]*

[1] Department of Urology, The First Affiliated Hospital of Nanjing Medical University, Nanjing, China, [2] Department of Pediatric Urology, Guangzhou Women and Children's Medical Center, Guangzhou Medical University, Guangzhou, China

Purpose: To investigate the role of circulating rare cells (CRCs), namely, circulating tumor cells (CTCs) and circulating endothelial cells (CECs), in aiding early intervention, treatment decision, and prognostication in bladder cancer.

Methods: A total of 196 patients with pathologically confirmed bladder cancer, namely, 141 non-muscle invasive bladder cancer (NMIBC) and 55 muscle invasive bladder cancer (MIBC) patients. There were 32 patients who received cisplatin-based neoadjuvant chemotherapy (NAC) followed by radical cystectomy (RC). Subtraction enrichment combined with immunostaining-fluorescence *in situ* hybridization (SE-iFISH) strategy was used for CTC/CEC detection. Kaplan–Meier analysis and Cox regression were used to evaluate the overall survival (OS) and recurrence-free survival (RFS). Receiver operator characteristic analysis was used to discriminate NAC sensitivity.

Results: CTCs and CECs were related to clinicopathological characteristics. Triploid CTCs, tetraploid CTCs, and total CECs were found to be higher in incipient patients than in relapse patients ($P = 0.036$, $P = 0.019$, and $P = 0.025$, respectively). The number of total CECs and large cell CECs was also associated with advanced tumor stage ($P = 0.028$ and $P = 0.033$) and grade ($P = 0.028$ and $P = 0.041$). Remarkably, tumor-biomarker-positive CTCs were associated with worse OS and RFS ($P = 0.026$ and $P = 0.038$) in NMIBC patients underwent TURBT. CECs cluster was an independent predictor of recurrence in non-high-risk NMIBC patients underwent TURBT (HR = 9.21, $P = 0.040$). For NAC analysis, pre-NAC tetraploid CTCs and small cell CTCs demonstrated the capability in discriminating NAC-sensitive from insensitive patients. Additionally, tetraploid CTCs and single CTCs elevated post-NAC would indicate chemoresistance.

OPEN ACCESS

Edited by:
Takeshi Yuasa, Japanese Foundation For Cancer Research, Japan

Reviewed by:
Gian Maria Busetto, University of Foggia, Italy
Matteo Ferro, European Institute of Oncology (IEO), Italy

***Correspondence:**
Qiang Lu
doctorlvqiang@sina.com
Haiwei Yang
haiweiyang@njmu.edu.cn
Pengchao Li
superkulian@aliyun.com

[†]*These authors have contributed equally to this work*

Specialty section:
This article was submitted to Genitourinary Oncology, a section of the journal Frontiers in Oncology

Received: *26 October 2021*
Accepted: *28 December 2021*
Published: *03 February 2022*

Citation:
Yang X, Lv J, Zhou Z, Feng D, Zhou R, Yuan B, Wu Q, Yu H, Han J, Cao Q, Gu M, Li P, Yang H and Lu Q (2022) Clinical Application of Circulating Tumor Cells and Circulating Endothelial Cells in Predicting Bladder Cancer Prognosis and Neoadjuvant Chemosensitivity. Front. Oncol. 11:802188. doi: 10.3389/fonc.2021.802188

Conclusion: CTCs and CECs may putatively guide in diagnosis, prognosis prediction, and therapeutic decision-making for bladder cancer.

Keywords: circulating tumor cells, circulating endothelial cells, bladder cancer, prognosis, neoadjuvant chemosensitivity

INTRODUCTION

Bladder cancer is a heterogeneous disease associated with various clinical outcomes. Non-muscle invasive bladder cancer (NMIBC) accounts for roughly 70–80% of bladder cancer and requires routine cystoscopy or even repeated resection (1). Muscle invasive bladder cancer (MIBC) patients have poor prognosis with approximately 50% of patients ultimately suffering from the disseminated micro-metastasis (2). To prevent early dissemination, medically fit patients with clinically localized MIBC are suggested to receive cisplatin-based combination neoadjuvant chemotherapy (NAC). Nonetheless, it still lacks solid biomarkers that can be used to determine whether NAC is necessary or beneficial.

Tissue biopsy is one of the most widely used diagnostic methods for determining the molecular phenotypes of tumors. However, invasive surgical intervention might result in trauma, metastatic risk, and high financial and time cost (3, 4). Liquid biopsy, defined as the capture of tumor-related biomarkers in a liquid sample, has been extensively explored because of its minimal intrusion, low consumption, and convenience of application. When compared to tissue biopsy, the liquid biopsy had the advantage of being easier to repeat over time in order to dynamically monitor disease progression (5). While liquid biopsies have shown potential in identifying MIBC patients for NAC, prospective trials investigating their true clinical applicability for therapy decision making are urgently needed (6, 7).

Circulating tumor cells (CTCs) and circulating endothelial cells (CECs) are the most representative of liquid biopsy due to their minimally invasively detection of cells in carcinoma patients (8). CTCs are malignant epithelial cells derived from primary tumors, representing micro-metastatic disease from the primary tumor or the propensity of evolving disease dissemination (9). CTCs have shown promise for predicting recurrence in high-risk NMIBC (10), evaluating prognosis of RC, and guiding decision-making in bladder-cancer adjuvant chemotherapy (11). However, the relevance of CTCs in NAC decision making remains unclear. CECs originate from the endothelial-cell detachment of the vessel wall and reflect endothelial injury. They have also been proposed as surrogate biomarkers for malignant cancers including colorectal, breast, pancreatic and lung cancers (12). Apart from CTCs/CECs, circulating free DNA (cfDNA) and exosomes are also significant targets for liquid biopsy (13). In bladder cancer patients, cfDNA and exosomes have been implicated in indicating cancer progression or even predicting the drug sensitivity (14, 15).

The most widely used techniques for detecting CTC/CECs include reverse transcriptase-polymerase chain reaction (RT-PCR), immunocytochemistry, flow cytometry immunofluorescence, cytomorphological criteria, and second-generation sequencing (16). Compared with subtraction enrichment combined with immunostaining-fluorescence *in situ* hybridization (SE-iFISH), these traditional detection techniques have different defects like RNA degradation or contamination during RT-PCR, reduced detection sensitivity in flow cytometry and high cost of second-generation sequencing. SE-iFISH integrates all three elements of nucleic acids, proteins, and cell morphology along the cellular bio-chain, allowing for the *in situ* phenotypic identification of tumor biomarkers (TBMs), cell-size identification and karyotypic characterization of chromosomal ploidy in CTCs/CECs (17). According to SE-iFISH analysis, CTCs/CECs are classified into diverse subtypes by chromosome ploidy and their identified TBMs including EpCAM and vimentin (8).

What remains unknown is the relationship between the CTCs/CECs and clinical diagnosis and also pathoanatomical responses to NAC in bladder cancer. The purpose of this study is to explore the utility of CTCs/CECs in the diagnosis and treatment of bladder cancer.

MATERIALS AND METHODS

Study Population

Between November 2016 and October 2019, we enrolled a total of 196 patients at the First Affiliated Hospital of Nanjing Medical University. Patients have to fulfill the following criteria for inclusion: (1) pathologically confirmed bladder cancer, and (2) aged over 18. The major exclusion criteria were as follows: (1) developed other malignancies including upper tract urothelial carcinoma, and (2) refused to sign informed consent. CTC detection was performed on all patients, while CEC detection was performed simultaneously on 133 patients. Peripheral blood (6 ml) was collected prior to any treatment. Written informed consent forms were signed by all patients. The study was approved by the affiliated hospital of Nanjing Medical University (Ethical approval number: 2017-SRFA-016) and performed according to the Declaration of Helsinki principles. The pathological diagnosis was performed by the Union for International Cancer Control TNM classification system (2009), and grade was determined according to the World Health Organization (WHO) 2004 grading of urothelial papilloma (18). High-risk tumors were defined as including any of the following: ① T1 tumor, ② high-grade tumor, ③ CIS, and ④ multiple, recurrent, and large (>3 cm) TaG1G2/LG tumors (all features must be present) (19).

CTC and CEC Enrichment, Identification and Classification

SE-iFISH approach was utilized to enrich and identify CTCs and CECs. SE-iFISH is a novel approach for detection CTCs/CECs

that combines differential phase enrichment, tumor-labeled immunofluorescence staining and i-FISH techniques. It utilizes differential phase enrichment to separate and enrich CTCs/CECs. The enriched CTCs/CECs were then subjected to tumor-labeled immunofluorescence staining and chromosomal fluorescence *in situ* hybridization simultaneously.

CTCs/CECs were enumerated as non-hematopoietic that had not CD45 expressed on the cell surface ($CD45^-$) while aneuploid CECs showed positive CD31 expression on the cell surface ($CD31^+$) and aneuploid CTCs did not express CD31 ($CD31^-$) but TBMs. The identification criteria of CTCs were as follows (**Figure 1D**): aneuploid chromosome 8 with nucleus $DAPI^+$/$CD45^-$/CD31_ or diploid chromosome 8 with nucleus $DAPI^+$/CD45_/CD31_ but positively immunofluorescent with two tumor TBMs ($EpCAM^+$/$vimentin^+$ and $EpCAM^+$/$vimentin^-$). Diploid chromosome 8 cells with $EpCAM^-$/$vimentin^+$ were not defined as CTCs due to vimentin being expressed often in white blood cells. The identification criteria of CECs included the following: aneuploid chromosome 8 with nucleus $DAPI^+$/$CD45^-$/$CD31^+$. Two or more single CTCs or CECs grouped to produce a circulating tumor microembolus (CTM) or CEC cluster. CTC can be divided into large-cell and small-cell CTCs depending on their size in comparison to white blood cells and the same for the CECs. CTCs were classified as monoploid CTC, triploid CTC, tetraploid CTC, and polyploid CTC (≥5 ploidy CTC) according to the karyotypes of chromosomes 8. Depending on whether TBMs can be detected, CTCs can be divided into tumor-biomarker (TBM)-positive CTCs and TBM-negative CTCs. TBM-positive CTCs are EpCAM positive and/or vimentin positive CTCs. CTC positive was defined as CTC number ≥3 and/or CTM ≥1, whereas CEC positive was defined as CECs number ≥2 and/or CEC cluster ≥1.

Neoadjuvant Chemotherapy Regimen and Assessment

Generally, 70 mg/m^2 cisplatin-based NAC regimens consisting of cisplatin combined with 1.0 g/m^2 gemcitabine protocols were administered. NAC was recommended for patients with extravesical disease (≥cT2N0M0). At least two cycles of NAC were performed before RC. Blood was collected from patients prior to or after two cycles of NAC. To evaluate the clinical response, Response Evaluation Criteria in Solid Tumors guideline (Version 1.1) was used. Magnetic resonance imaging was conducted to determine the diameter and volume of tumors prior to and after NAC. Two radiologists were involved to assess tumor response using MRI. T2-weighted imaging, diffusion weighted imaging (DWI), and apparent diffusion coefficient (ADC) were implemented to evaluate therapeutic response to NAC.

Follow-Up Regimen

Outpatient service and phone calls were used for follow-up. For RC, patients were usually seen every 3 months during the first year following surgery, and every 6 months from the second to fifth years. Follow-up included history, serum, and urine chemistry evaluation, and also physical examination. Every 6 months, abdomen imaging including the urinary tract (CT or MRI of the abdomen/pelvis with intravenous contrast) and chest radiography were conducted. For TURBT, patients received an additional cystoscopy and urinary cytology every 3 months in the first year following surgery and every 6 months from the second to fifth years. The endpoints of the study were as follows: (1) overall survival (OS), defined as the time period between operation and death from any cause, and (2) recurrence-free survival (RFS), defined as the time period between operation and local failure or distant metastases.

Statistical Analysis

IBM SPSS package (SPSS Inc., Chicago, IL, United States) and GraphPad Prism software (GraphPad Prism Software Inc., San Diego, CA, United States) were used for all statistical analyses. Correlations between the CTC/CEC-positive rate and clinicopathological variables were analyzed by chi-square test. For continuous variables, Student's t-test was used to compare normally distributed variables or the Wilcoxon rank-sum test was used to compare not normally distributed variables. The area under the curve (AUC) of different CTC subtypes in discriminating chemosensitivity was determined using receiver operator characteristic (ROC) analysis. The change in CTCs between pre- and post-NAC was analyzed by the paired-sample t-test. Kaplan–Meier survival plots were generated based on the numbers of different subtypes of CTCs/CECs, and survival curves were compared using log-rank tests. Hazard ratios (HRs) were derived from univariate and multivariate Cox proportional-hazard regression models. $P < 0.05$ was statistically significant, and all statistical analyses were two-sided.

RESULTS

Analysis of Quantified CTC and CEC Subtypes

The quantitative distribution of CTC subtypes according to different classification criteria among the entire CTCs is depicted in **Figure 1A**. The detected rate of CTC subtypes distribution indicated that CTCs, small cell CTCs, CTM, and TBM-positive CTCs were present in 94.90, 83.67, 21.94, and 17.86% of all 196 patients, respectively (**Figure 1B**). The distribution of CECs subtypes is depicted in **Figure 1C**.

CTCs and CECs in Relation to Clinicopathological Characteristics

Positive CTCs were present in 163 patients (83.2%), while positive CECs were detected in 105 patients (78.9%). No significant association was found between CTC/CEC positive rates and clinicopathological variables (**Table 1**). However, subgroup analyses revealed that incipient patients exhibited a higher level of triploid and tetraploid CTCs than relapse patients ($P = 0.036$ and $P = 0.019$) (**Figure 2A**).

Incipient patients also had an increased CECs level compared to relapsing patients ($P = 0.025$) (**Figure 2B**). In addition, the number of total CECs and large-cell CECs were also associated

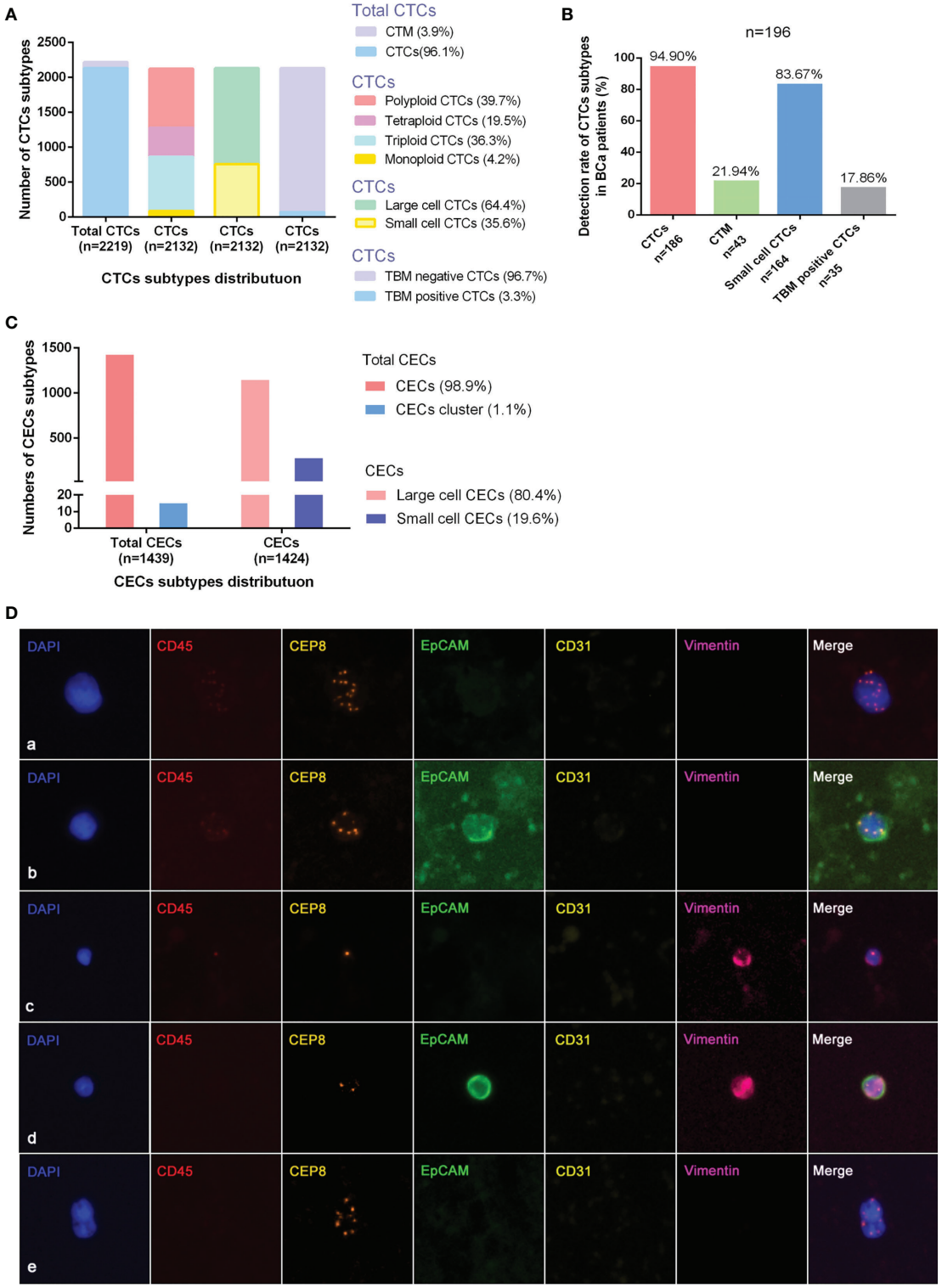


FIGURE 1 | Detection^{+} and characteristics of CTCs and CECs by SE-iFISH in bladder-cancer patients. **(A)** Quantitative composition of diverse CTC subtypes among the total number of CTCs. **(B)** Detective rate distribution of CTC subtypes among all bladder-cancer patients. **(C)** Quantitative composition of CEC subtypes among the total number of CECs. **(D)** Identification of CTCs by SE-iFISH. Line a: Polyploid, large cell, and TBM negative CTCs; Line b: Polyploid, large cell, and TBM-positive (EpCAM^{+}) CTCs; Line c: Monoploid, small cell, and TBM-positive (vimentin^{+}) CTCs; Line d: Diploid, small cell, and TBM-positive (EpCAM^{+}/vimentin^{+}) CTCs; Line e: CTM.

TABLE 1 | Relationship between CTC/CEC positive rate and clinicopathological variables.

Variables	CTCs						CECs					
	Total	Positive		Negative		*P*	Total	Positive		Negative		*P*
	n	n	%	n	%		n	n	%	n	%	
Total	196	163	83.2	33	16.8		133	105	78.9	28	21.1	
Gender												
Male	159	131	82.4	28	17.6	0.549	113	92	81.4	21	18.6	0.097
Female	37	32	86.5	5	13.5		20	13	65.0	7	35.0	
Age												
≥66	107	91	85.0	16	15.0	0.440	73	57	78.1	16	21.0	0.787
<66	89	72	80.9	17	19.1		60	48	80.0	12	20.0	
Tobacco smoking												
Yes	85	70	82.4	15	17.6	0.791	66	55	83.3	11	16.7	0.218
No	111	93	83.8	18	16.2		67	50	74.6	17	25.4	
Alcohol drinking												
Yes	67	59	88.1	8	11.9	0.187	49	43	87.8	6	12.2	0.057
No	129	104	80.6	25	19.4		84	62	73.8	22	26.3	
Stage												
NMIBC	141	117	83.0	24	17.0	0.912	90	72	80.0	18	20.0	0.667
MIBC	55	46	83.6	9	16.4		43	33	76.7	10	23.3	
Grade												
PUNLMP	8	8	100	0	0	0.376	3	3	100	0	0	0.459
Low	95	77	81.1	18	18.9		65	49	75.4	16	24.6	
High	93	78	83.9	15	16.1		65	53	81.5	12	18.5	
Lymph node metastasis												
Yes	8	8	100	0	0	0.194	6	4	66.7	2	33.3	0.450
No	188	155	82.4	33	17.6		127	101	79.5	26	20.5	
Bladder cancer history												
Incipient	43	37	86.0	6	14.0	0.567	29	22	75.9	7	24.1	0.645
Relapse	153	126	82.4	27	17.6		104	83	79.8	21	20.2	

with higher tumor stage ($P = 0.028$ and $P = 0.033$) (**Figure 2C**) and grade ($P = 0.028$ and $P = 0.041$) (**Figure 2D**).

CTCs and CECs Contributed to Predicting Oncological Outcomes

Among the 196 patients, 22 were lost to follow-up, 55 patients (31.6%) experienced recurrence and 24 patients (13.8%) died. CTCs demonstrated no significant association between NMIBC and MIBC patients, however, the number of CECs elevated significantly in MIBC patients (**Supplementary Table 1**).

TBM-Positive CTCs Predicted Poor Prognosis in NMIBC Patients Receiving TURBT

TBM-positive CTCs served as an unfavorable predictor of OS in NMIBC patients treated with TURBT (**Figure 2E**). Subsequently, we respectively evaluated the prognostic significance in high-risk NMIBC patients and non-high-risk NMIBC patients (**Supplementary Table 2**). As for high-risk NMIBC patients undergoing TURBT, RFS was significantly reduced in the TBM-positive CTC group (**Figure 2F**). While for non-high-risk NMIBC patients undergoing TURBT, there was no significant association between CTCs and prognosis (**Supplementary Table 3**).

CEC Cluster Showed a Reduced RFS in NMIBC Patients Receiving TURBT

Univariate analysis of CECs for OS and RFS prediction in all NMIBC patients receiving TURBT failed to reach statistical significance (**Supplementary Table 4**). Whereas, in non-high-risk NMIBC patients receiving TURBT, survival analysis demonstrated that positive CEC cluster did shorten RFS further (**Figure 2G**). While for MIBC patients treated with RC, CECs number ≥6 also showed a shorter RFS but without statistical difference (**Figure 2H**).

Association Between CTCs and NAC Response Rate

CTCs were quantified in a total of 32 patients prior to NAC followed by RC. A total of 18 of 32 patients were considered responsive, while the remaining 14 were considered insensitive. Pre-NAC single CTCs ($P = 0.016$), tetraploid CTCs ($P = 0.001$), and small cell CTCs ($P = 0.031$) were positively correlated with sensitivity to NAC (**Figures 3A, B**). ROC analysis was also performed to evaluate the ability of tetraploid CTCs, small cell CTCs, and CTCs in discriminating NAC-sensitive patients from resistant patients (**Figure 3C**). Results showed that the potential AUCs were 0.80 for tetraploid CTCs (95% CI = 0.62–0.92, $P < 0.001$), 0.72 for small cell CTCs (95%CI = 0.54–0.87, $P = 0.015$), and 0.77 for CTCs (95%CI = 0.59–0.90, $P = 0.002$).

Afterwards, a total of 22 patients received CTC detection after two cycles of NAC. A total of 14 of 22 were considered responsive, and the remaining 8 were considered insensitive. The proportion of polyploid CTCs elevated with the other three karyotypes CTC numbers declined (**Figure 3D**). Compared to 45 patients receiving RC without NAC, NAC group was associated with a decreased number of triploid, tetraploid and small cell CTCs ($P = 0.032$, $P = 0.004$, and $P = 0.022$) (**Supplementary Table 5**). Then we evaluated the consistency between CTC dynamics pre- and post-

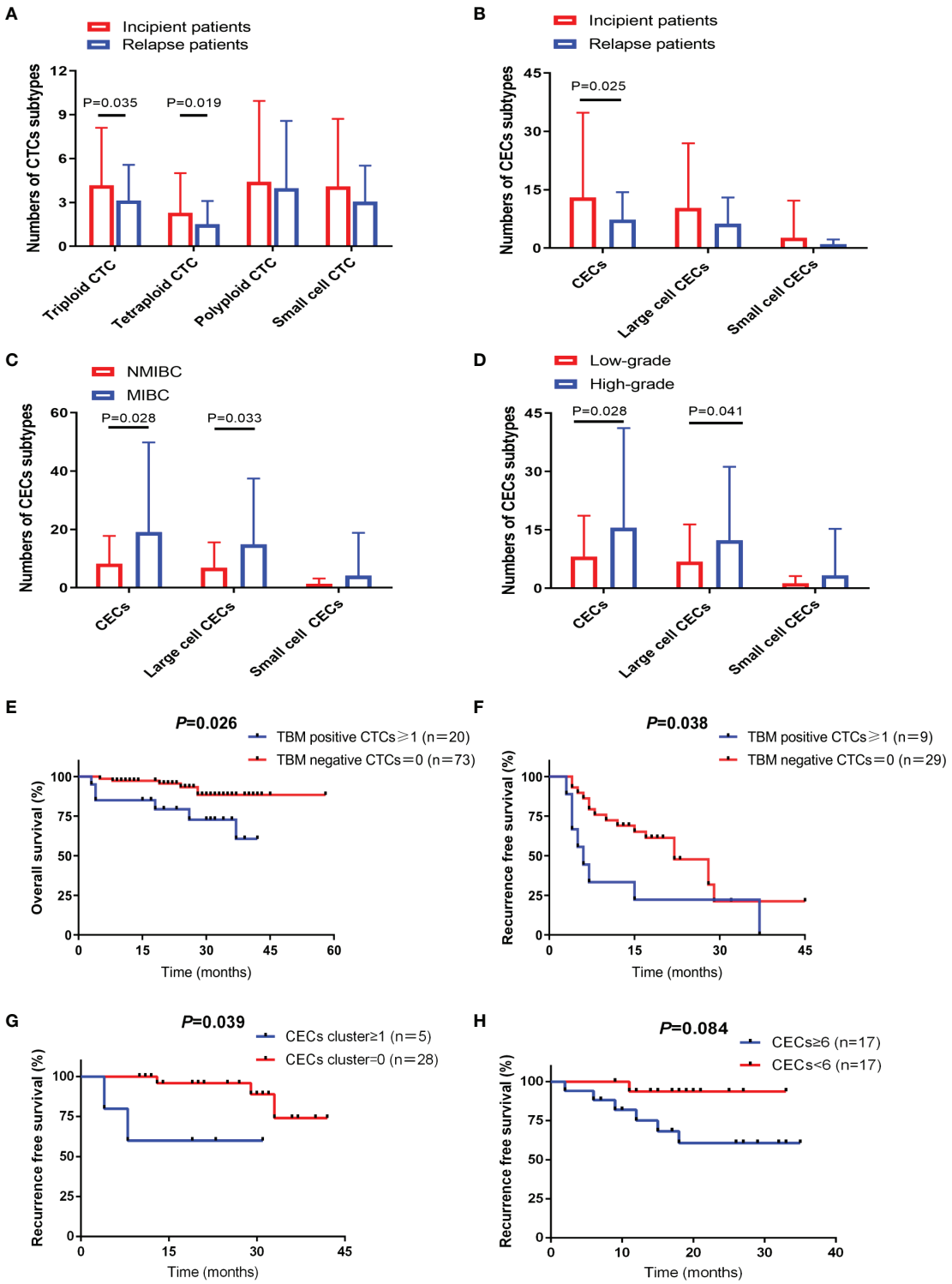


FIGURE 2 | CTC and CEC subtypes correlated with different clinical characteristics and prognosis. **(A)** Distribution of CTC subtypes in incipient and relapse bladder-cancer patients. **(B)** Distribution of CEC subtypes in incipient and relapse bladder-cancer patients. **(C)** Distribution of CEC subtypes in bladder-cancer patients according to tumor stage. **(D)** Distribution of CEC subtypes in bladder-cancer patients according to tumor grade. **(E)** TBM-positive CTC number ≥1 showed poor prognosis with shorter OS in NMIBC patients receiving TURBT. **(F)** TBM-positive CTC number ≥1 showed poor prognosis with shorter RFS in high-risk NMIBC patients receiving TURBT. **(G)** CEC cluster number ≥1 showed poor prognosis with shorter RFS in high-risk NMIBC patients receiving TURBT. **(H)** CECs number ≥6 showed poor prognosis with shorter RFS in MIBC patients receiving RC.

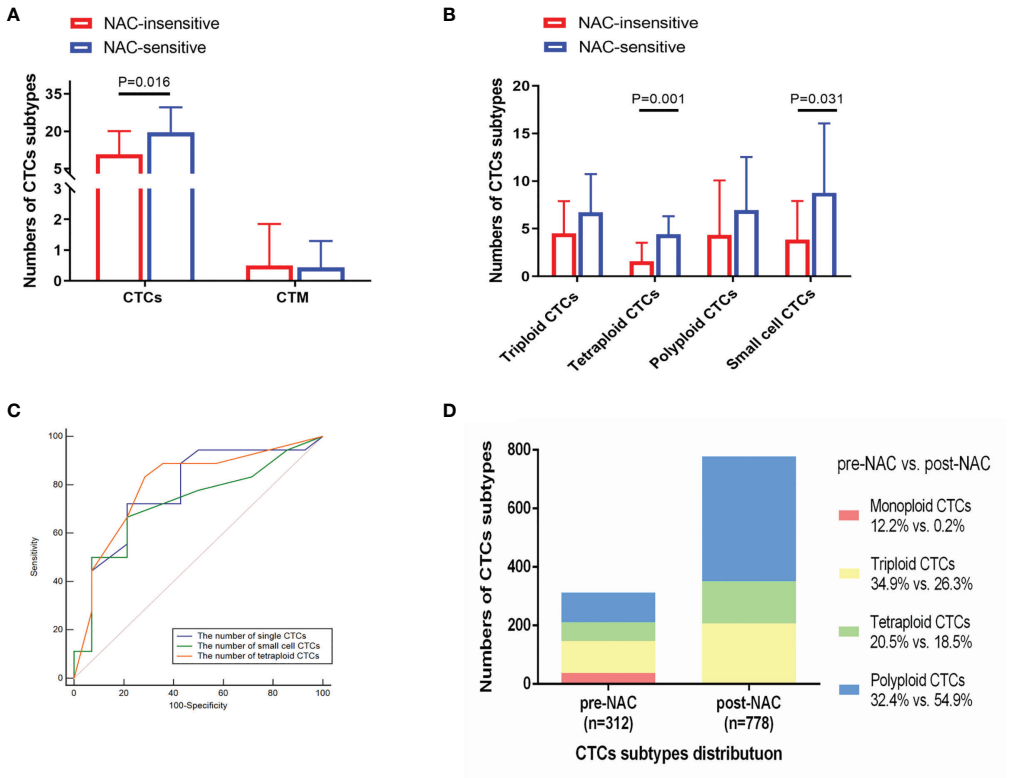


FIGURE 3 | Analysis of CTC subtypes in correlation with NAC sensitivity in 32 bladder-cancer patients. **(A, B)** NAC-sensitive patients had an increasing quantity of pre-NAC CTCs, tetraploid CTCs, and small cell CTCs compared with NAC-insensitive patients. **(C)** Receiver operator characteristic (ROC) curves analysis showed that pre-NAC CTCs, tetraploid CTCs, and small cell CTCs could differentiate NAC-sensitive patients (n = 18) from NAC-insensitive ones (n = 14). **(D)** Distribution of CTC subtypes before and after NAC.

NAC with the NAC response rate, but no significant association was observed in the 22 patients (**Supplementary Table 6**). Increased count of tetraploid CTCs and single CTCs following NAC indicated its ineffectiveness (P = 0.042 and P = 0.031) (**Table 2**).

DISCUSSION

The detection of CTCs/CECs is the most representative of liquid biopsy in carcinoma patients (20). The clinical implications of CTCs have been reported in bladder cancer; however, most of them are based on conventional strategies and provide conflicting results (21). CellSearch®, which utilized an immunomagnetic technique to detect EpCAM$^+$ CTCs, was the only FDA-approved CTC-detection platform (22), but it was always associated with a low CTC detection rate (23, 24). Additionally to this method, size-based filtration technique could considerably improve the detection efficiency (25). While all these EpCAM based techniques inevitably underestimate the quantity of CTCs due to missing EpCAM$^-$ CTCs (26).

TABLE 2 | CTC subtypes and dynamics in bladder-cancer patients with neoadjuvant chemotherapy.

CTCs Subtypes	Sensitive (n = 14)	Insensitive (n = 8)	*P*
Single	−0.29 ± 15.80	58.75 ± 75.89	**0.031**
Monoploid	−2.29 ± 6.62	−0.50 ± 1.41	0.853
Triploid	0.79 ± 7.20	10.63 ± 16.54	0.159
Tetraploid	0.00 ± 4.39	10.00 ± 15.75	**0.042**
Polyploid	1.21 ± 7.48	38.63 ± 51.29	0.074
Small cell	0.21 ± 8.45	11.00 ± 15.95	0.065
TBM positive	0.36 ± 1.45	2.75 ± 7.40	0.432
CTM	−0.21 ± 0.70	1.75 ± 4.65	0.179

Bold values provided in Table 2 means they are significant p values which were less than 0.05.

Therefore, additional molecule markers like vimentin were investigated and exploited during CTCs detection (26, 27). In present study, SE-iFISH is anticipated to facilitate elucidating how these distinct categories CTCs/CECs functionally interplay with tumor angiogenesis and therapy (8).

With regard to clinical characters analysis, we found that incipient bladder-cancer patients exhibited more triploid CTCs, tetraploid CTCs and total CECs than relapsing patients. One possible explanation is that relapsing patients might receive more routine review than incipient ones, allowing physicians to detect tumors earlier. Of note, our data highlighted the positive correlation between CECs and advanced tumor stage and grade. These data indicated that CECs were more easily detected in more advanced bladder cancer.

As reported, the epithelial to mesenchymal transition (EMT) has been proven to play a role in the tumorigenic process (28). EMT may facilitate the cancer cells to disseminate from local tumors penetrate blood vessels to become CTCs (29–31). CTCs could be classified as epithelial, mesenchymal, or epithelial–mesenchymal hybrids (32). Epithelial markers (EpCAM and E-cadherin) and mesenchymal markers (vimentin and Twist) were used frequently in CTCs detection (33, 34). In the present study, TBM-positive CTCs were defined in the study as EpCAM positive and/or vimentin-positive CTCs. Consistent with a previous study, our results also indicated a relatively low detection rate of TBM-positive CTCs (<20%) (35). To our knowledge, the present study had the largest sample size focusing exclusively on NMIBC rather than T1HG or high-risk NMIBC only. We discovered for the first time that TBM-positive CTCs might be used to predict the prognosis of NMIBC patients. The NMIBC patients receiving TURBT who harbored detectable TBM-positive CTCs were at significantly increased risk of overall mortality. Gazzaniga et al. stated similar results that the presence of CTCs is associated with a short time to the first recurrence in 44 NMIBC patients (36). Notably, NMIBC is heterogeneous cancer and most CTC-related studies on NMIBC have concentrated on T1HG or high-risk NMIBC patients (10, 37). Consistently, according to our analysis on high-risk NMIBC patients receiving TURBT, TBM-positive CTC number ≥1 showed poor prognosis with shorter RFS. Other new biomarkers like PD-L1 expression in CTCs are also in hopes of expanding the role of liquid biopsy in cancer patients (38). Interestingly, BCa patients with type 2 diabetes mellitus (T2DM) suffered a higher risk of recurrence (39). T_2DM and hyperglycemia have been shown to facilitate EMT process in various cancers (40–42). Therefore, we speculate that hyperglycemia may interfere with the production and detection of CTCs.

However, results data on the actual predictive and prognostic value of CECs in bladder cancer are scarce. Cox regression analysis in our study indicated that positive CEC cluster was an independent risk factor for non-high-risk NMIBC patients treated with TURBT. Intriguingly, although not statistically significant, CEC subtypes predicted poor prognosis of patients receiving RC. Hence, CEC subtypes would also be key players in bladder-cancer diagnosis and prognosis. And our report is also the first research to explore the utility of CECs in bladder cancer.

The cisplatin-based NAC is recommended, while it could provide a minor OS benefit of 5–6% after 10 years (43). Besides, non-responder patients with MIBC have a poor overall survival and are delayed in receiving effective treatment (44). Soave et al. found that bladder cancer patients with the presence of CTCs are more likely to receive adjuvant chemotherapy (11). Our results showed that tetraploid CTCs were the most predictive of NAC sensitivity, followed by single CTCs and small cell CTCs. We also investigated the predictive value of CTC dynamic variation before and after NAC treatment, and found that NAC-insensitive patients possessed an evident elevation of CTCs post-NAC. The number of polyploid CTCs increased most remarkably post-NAC. Thus, we postulated that polyploid CTCs could be an important factor in NAC insensitivity as it was more difficult to eliminate than other CTC subtypes. Interestingly, the most CTC subtypes were elevated post-NAC, which might be attributed to NAC induced shedding of tumor cells into the circulatory system. Several focal tumor cells will necrotize during the initial chemotherapy cycles, which could result in decreased tumor cell adhesion. Thus, the residual tumor cells might be discharged into the bloodstream. This phenomenon was also observed in breast cancer studies (45, 46). Besides, in metastatic urothelial carcinoma, Fina et al. also found that unfavorable trend of CTCs number alterations during chemotherapy may be useful to predict worse prognosis (47). From the above, CTCs may enable the evaluation of NAC response and may hold promise in screening of NAC sensitive patients, thereby allowing NAC insensitive patients to undergo RC earlier. To our knowledge, this study is the first to explore the association between CTCs and bladder cancer NAC.

The Vesical Imaging-Reporting and Data System (VI-RADS) has been demonstrated to accurately predict muscle invasion of BCa before operation (48–51). Although no correlation between CTCs/CECs and BCa stage was observed, the combination of VI-RADS and CTCs/CECs detecting may offer us a more valid judgment basis prior to surgery, particularly for patients with a VI-RADS score of 3. Apart from BCa, other prognostic factors also played a significant role in other hematuria-related genitourinary diseases, such as prostate cancer (52) and prostate surgery associated bleeding (53).

It should be noted that the results of relevant Cox analyses may be insufficiently significant due to the limited number of patients included, especially those who received NAC. While SE-iFISH is a novel CTC detection technique, its application is still limited compared to more established detection methods. As a result, the detection stability and consistency need to be further verified.

CONCLUSION

Taken together, based on SE-iFISH strategy, the amounts of single CTCs, small cell CTCs, and tetraploid CTCs could predict NAC sensitivity. Furthermore, the present study established for the first time a relationship between CECs and their subtypes with pathological stage, grade, and clinical outcome. Overall, our findings revealed that various CTCs/CECs subtypes may have

diverse potential to guide the diagnosis, prognosis prediction, and therapeutic decisions in bladder cancer, but further analytical validations are still required.

DATA AVAILABILITY STATEMENT

The original contributions presented in the study are included in the article/**Supplementary Material**. Further inquiries can be directed to the corresponding authors.

ETHICS STATEMENT

All procedures conduct in studies involving human participants comply with the ethical standards of institutions and/or national research committee, as well as with the 1964 Helsinki Declaration and its subsequent amendments or comparable ethical standards.

AUTHOR CONTRIBUTIONS

Conception: XY, PL, HYa, and QL. Interpretation or analysis of data: DF, RZ, BY, QW, QC, HYu, JH, and JCL. Preparation of the manuscript: XYu, DF, JL, and ZZ. Revision for important intellectual content: XY, DF, QL, HYa, and PCL. Supervision: QL, HYa, XY, PL, and MG. All authors contributed to the article and approved the submitted version.

FUNDING

This work was supported by the National Natural Science Foundation of China (grant nos. 82072832, 81772711, and 82073306), the "333" project of Jiangsu Province (LGY2016002 and 2018055), the Jiangsu Province's Key Provincial Talents Program (ZDRCA2016006), the Provincial Initiative Program for Excellency Disciplines of Jiangsu Province (grant No. BE2016791), the Priority Academic Program Development of Jiangsu Higher Education Institutions (grant No. JX10231801) and the Clinical Research Cultivation Program, Construction Program of Jiangsu Provincial Clinical Research Centre Support System (BL2014084).

SUPPLEMENTARY MATERIAL

The Supplementary Material for this article can be found online at: https://www.frontiersin.org/articles/10.3389/fonc.2021.802188/full#supplementary-material

REFERENCES

1. Sylvester RJ, Rodríguez O, Hernández V, Turturica D, Bauerová L, Bruins HM, et al. European Association of Urology (EAU) Prognostic Factor Risk Groups for Non-Muscle-Invasive Bladder Cancer (NMIBC) Incorporating the WHO 2004/2016 and WHO 1973 Classification Systems for Grade: An Update From the EAU NMIBC Guidelines Panel. *Eur Urol* (2021) 79(4):480–8. doi: 10.1016/j.eururo.2020.12.033
2. Yafi FA, Aprikian AG, Chin JL, Fradet Y, Izawa J, Estey E, et al. Contemporary Outcomes of 2287 Patients With Bladder Cancer Who Were Treated With Radical Cystectomy: A Canadian Multicentre Experience. *BJU Int* (2011) 108 (4):539–45. doi: 10.1111/j.1464-410X.2010.09912.x
3. Labgaa I, Villanueva A, Dormond O, Demartines N, Melloul E. The Role of Liquid Biopsy in Hepatocellular Carcinoma Prognostication. *Cancers* (2021) 13(4):659. doi: 10.3390/cancers13040659
4. Bonde A, Smith DA, Kikano E, Yoest JM, Tirumani SH, Ramaiya NH. Overview of Serum and Tissue Markers in Colorectal Cancer: A Primer for Radiologists. *Abdom Radiol* (2021) 46(12):5521–35. doi: 10.1007/s00261-021-03243-0
5. Cheung AH, Chow C, To KF. Latest Development of Liquid Biopsy. *J Thorac Dis* (2018) 10(Suppl 14):S1645–S51. doi: 10.21037/jtd.2018.04.68
6. Schardt J, Roth B, Seiler R. Forty Years of Cisplatin-Based Chemotherapy in Muscle-Invasive Bladder Cancer: Are We Understanding How, Who and When? *World J Urol* (2019) 37(9):1759–65. doi: 10.1007/s00345-018-2544-8
7. de Kruijff I, Beije N, Martens J, de Wit R, Boormans J, Sleijfer S. Liquid Biopsies to Select Patients for Perioperative Chemotherapy in Muscle-Invasive Bladder Cancer: A Systematic Review. *Eur Urol Oncol* (2021) 4 (2):204–14. doi: 10.1016/j.euo.2020.01.003
8. Lin PP. Aneuploid CTC and CEC. *Diagn (Basel Switzerland)* (2018) 8(2):26. doi: 10.3390/diagnostics8020026
9. Aoki M, Shoji H, Kashiro A, Takeuchi K, Shimizu Y, Honda K. Prospects for Comprehensive Analyses of Circulating Tumor Cells in Tumor Biology. *Cancers (Basel)* (2020) 12(5):1135. doi: 10.3390/cancers12051135
10. Nicolazzo C, Busetto GM, Gradilone A, Sperduti I, Del Giudice F, Loreni F, et al. Circulating Tumor Cells Identify Patients With Super-High-Risk Non-Muscle-Invasive Bladder Cancer: Updated Outcome Analysis of a Prospective Single-Center Trial. *Oncologist* (2019) 24(5):612–6. doi: 10.1634/theoncologist.2018-0784
11. Soave A, Riethdorf S, Dahlem R, von Amsberg G, Minner S, Weisbach L, et al. A Nonrandomized, Prospective, Clinical Study on the Impact of Circulating Tumor Cells on Outcomes of Urothelial Carcinoma of the Bladder Patients Treated With Radical Cystectomy With or Without Adjuvant Chemotherapy. *Int J Cancer* (2017) 140(2):381–9. doi: 10.1002/ijc.30445
12. Hayashi T, Fujita K, Hayashi Y, Hatano K, Kawashima A, McConkey D, et al. Mutational Landscape and Environmental Effects in Bladder Cancer. *Int J Mol Sci* (2020) 21(17):6072. doi: 10.3390/ijms21176072
13. Zhang W, Xia W, Lv Z, Ni C, Xin Y, Yang L. Liquid Biopsy for Cancer: Circulating Tumor Cells, Circulating Free DNA or Exosomes? *Cell Physiol Biochem* (2017) 41(2):755–68. doi: 10.1159/000458736
14. Herranz R, Oto J, Plana E, Fernandez-Pardo A, Cana F, Martinez-Sarmiento M, et al. Circulating Cell-Free DNA in Liquid Biopsies as Potential Biomarker for Bladder Cancer: A Systematic Review. *Cancers (Basel)* (2021) 13(6):1448. doi: 10.3390/cancers13061448
15. Liu YR, Ortiz-Bonilla CJ, Lee YF. Extracellular Vesicles in Bladder Cancer: Biomarkers and Beyond. *Int J Mol Sci* (2018) 19(9):2822. doi: 10.3390/ijms19092822
16. Palmela Leitao T, Miranda M, Polido J, Morais J, Corredeira P, Alves P, et al. Circulating Tumor Cell Detection Methods in Renal Cell Carcinoma: A Systematic Review. *Crit Rev Oncol Hematol* (2021) 161:103331. doi: 10.1016/j.critrevonc.2021.103331
17. Zhang L, Zhang X, Liu Y, Zhang T, Wang Z, Gu M, et al. PD-L1(+) Aneuploid Circulating Tumor Endothelial Cells (CTECs) Exhibit Resistance to the Checkpoint Blockade Immunotherapy in Advanced NSCLC Patients. *Cancer Lett* (2020) 469:355–66. doi: 10.1016/j.canlet.2019.10.041
18. Oosterhuis JW, Schapers RF, Janssen-Heijnen ML, Pauwels RP, Newling DW, ten Kate F. Histological Grading of Papillary Urothelial Carcinoma of the Bladder: Prognostic Value of the 1998 WHO/ISUP Classification System and Comparison With Conventional Grading Systems. *J Clin Pathol* (2002) 55 (12):900–5. doi: 10.1136/jcp.55.12.900

19. Babjuk M, Burger M, Compérat EM, Gontero P, Mostafid AH, Palou J, et al. European Association of Urology Guidelines on Non-Muscle-Invasive Bladder Cancer (TaT1 and Carcinoma *In Situ*) - 2019 Update. *Eur Urol* (2019) 76(5):639–57. doi: 10.1016/j.eururo.2019.08.016
20. Cheng J, Tang Q, Cao X, Burwinkel B. Cell-Free Circulating DNA Integrity Based on Peripheral Blood as a Biomarker for Diagnosis of Cancer: A Systematic Review. *Cancer Epidemiol Biomarkers Prev* (2017) 26(11):1595–602. doi: 10.1158/1055-9965.EPI-17-0502
21. Yan H, Dittmar F, Schagdarsurengin U, Wagenlehner F. The Clinical Application and Potential Roles of Circulating Tumor Cells in Bladder Cancer and Prostate Cancer. *Urology* (2020) 145:30–37. doi: 10.1016/j.urology.2020.06.039
22. Allard W, Matera J, Miller M, Repollet M, Connelly M, Rao C, et al. Tumor Cells Circulate in the Peripheral Blood of All Major Carcinomas But Not in Healthy Subjects or Patients With Nonmalignant Diseases. *Clin Cancer Res: Off J Am Assoc Cancer Res* (2004) 10(20):6897–904. doi: 10.1158/1078-0432.CCR-04-0378
23. Bidard F, Huguet F, Louvet C, Mineur L, Bouché O, Chibaudel B, et al. Circulating Tumor Cells in Locally Advanced Pancreatic Adenocarcinoma: The Ancillary CirCe 07 Study to the LAP 07 Trial. *Ann Oncol: Off J Eur Soc Med Oncol* (2013) 24(8):2057–61. doi: 10.1093/annonc/mdt176
24. Okubo K, Uenosono Y, Arigami T, Mataki Y, Matsushita D, Yanagita S, et al. Clinical Impact of Circulating Tumor Cells and Therapy Response in Pancreatic Cancer. *Eur J Surg Oncol: J Eur Soc Surg Oncol Br Assoc Surg Oncol* (2017) 43(6):1050–5. doi: 10.1016/j.ejso.2017.01.241
25. Khoja L, Backen A, Sloane R, Menasce L, Ryder D, Krebs M, et al. A Pilot Study to Explore Circulating Tumour Cells in Pancreatic Cancer as a Novel Biomarker. *Br J Cancer* (2012) 106(3):508–16. doi: 10.1038/bjc.2011.545
26. Handra-Luca A, Hong S, Walter K, Wolfgang C, Hruban R, Goggins M. Tumour Epithelial Vimentin Expression and Outcome of Pancreatic Ductal Adenocarcinomas. *Br J Cancer* (2011) 104(8):1296–302. doi: 10.1038/bjc.2011.93
27. Satelli A, Mitra A, Brownlee Z, Xia X, Bellister S, Overman M, et al. Epithelial-Mesenchymal Transitioned Circulating Tumor Cells Capture for Detecting Tumor Progression. *Clin Cancer Res: Off J Am Assoc Cancer Res* (2015) 21(4):899–906. doi: 10.1158/1078-0432.CCR-14-0894
28. Brabletz T, Kalluri R, Nieto M, Weinberg R. EMT in Cancer. *Nat Rev Cancer* (2018) 18(2):128–34. doi: 10.1038/nrc.2017.118
29. Guarino M. Epithelial-Mesenchymal Transition and Tumour Invasion. *Int J Biochem Cell Biol* (2007) 39(12):2153–60. doi: 10.1016/j.biocel.2007.07.011
30. Książkiewicz M, Markiewicz A, Zaczek A. Epithelial-Mesenchymal Transition: A Hallmark in Metastasis Formation Linking Circulating Tumor Cells and Cancer Stem Cells. *Pathobiology* (2012) 79(4):195–208. doi: 10.1159/000337106.
31. Pantel K, Brakenhoff R. Dissecting the Metastatic Cascade. *Nat Rev Cancer* (2004) 4(6):448–56. doi: 10.1038/nrc1370
32. Nel I, Baba H, Ertle J, Weber F, Sitek B, Eisenacher M, et al. Individual Profiling of Circulating Tumor Cell Composition and Therapeutic Outcome in Patients With Hepatocellular Carcinoma. *Transl Oncol* (2013) 6(4):420–8. doi: 10.1593/tlo.13271
33. Liu Y, Hu B, Li Z, He X, Li Y, Lu L. An Improved Strategy to Detect the Epithelial-Mesenchymal Transition Process in Circulating Tumor Cells in Hepatocellular Carcinoma Patients. *Hepatol Int* (2016) 10(4):640–6. doi: 10.1007/s12072-016-9732-7
34. Wu S, Liu S, Liu Z, Huang J, Pu X, Li J, et al. Classification of Circulating Tumor Cells by Epithelial-Mesenchymal Transition Markers. *PLoS One* (2015) 10(4):e0123976. doi: 10.1371/journal.pone.0123976
35. Ye Z, Ding Y, Chen Z, Li Z, Ma S, Xu Z, et al. Detecting and Phenotyping of Aneuploid Circulating Tumor Cells in Patients With Various Malignancies. *Cancer Biol Ther* (2019) 20(4):546–51. doi: 10.1080/15384047.2018.1538000
36. Gazzaniga P, Gradilone A, de Berardinis E, Busetto GM, Raimondi C, Gandini O, et al. Prognostic Value of Circulating Tumor Cells in Nonmuscle Invasive Bladder Cancer: A CellSearch Analysis. *Ann Oncol: Off J Eur Soc Med Oncol* (2012) 23(9):2352–6. doi: 10.1093/annonc/mdr619
37. Busetto GM, Ferro M, Del Giudice F, Antonini G, Chung BI, Sperduti I, et al. The Prognostic Role of Circulating Tumor Cells (CTC) in High-Risk Non-Muscle-Invasive Bladder Cancer. *Clin Genitourin Cancer* (2017) 15(4):e661–e6. doi: 10.1016/j.clgc.2017.01.011
38. Boffa DJ, Graf RP, Salazar MC, Hoag J, Lu D, Krupa R, et al. Cellular Expression of PD-L1 in the Peripheral Blood of Lung Cancer Patients Is Associated With Worse Survival. *Cancer Epidemiol Biomarkers Prev* (2017) 26(7):1139–45. doi: 10.1158/1055-9965.EPI-17-0120
39. Ferro M, Katalin MO, Buonerba C, Marian R, Cantiello F, Musi G, et al. Type 2 Diabetes Mellitus Predicts Worse Outcomes in Patients With High-Grade T1 Bladder Cancer Receiving Bacillus Calmette-Guerin After Transurethral Resection of the Bladder Tumor. *Urol Oncol* (2020) 38(5):459–64. doi: 10.1016/j.urolonc.2020.02.016
40. Rahn S, Zimmermann V, Viol F, Knaack H, Stemmer K, Peters L, et al. Diabetes as Risk Factor for Pancreatic Cancer: Hyperglycemia Promotes Epithelial-Mesenchymal-Transition and Stem Cell Properties in Pancreatic Ductal Epithelial Cells. *Cancer Lett* (2018) 415:129–50. doi: 10.1016/j.canlet.2017.12.004
41. Yang T, Zhou Y, Wang H, Chen S, Shen M, Hu Y, et al. Insulin Exacerbated High Glucose-Induced Epithelial-Mesenchymal Transition in Prostatic Epithelial Cells BPH-1 and Prostate Cancer Cells PC-3 *via* MEK/ERK Signaling Pathway. *Exp Cell Res* (2020) 394(1):112145. doi: 10.1016/j.yexcr.2020.112145
42. Xia B, Hou L, Kang H, Chang W, Liu Y, Zhang Y, et al. NR2F2 Plays a Major Role in Insulin-Induced Epithelial-Mesenchymal Transition in Breast Cancer Cells. *BMC Cancer* (2020) 20(1):626. doi: 10.1186/s12885-020-07107-6
43. Witjes JA, Bruins HM, Cathomas R, Compérat EM, Cowan NC, Gakis G, et al. European Association of Urology Guidelines on Muscle-Invasive and Metastatic Bladder Cancer: Summary of the 2020 Guidelines. *Eur Urol* (2021) 79(1):82–104. doi: 10.1016/j.eururo.2020.03.055
44. Vollmer T, Schlickeiser S, Amini L, Schulenberg S, Wendering DJ, Banday V, et al. The Intratumoral CXCR3 Chemokine System is Predictive of Chemotherapy Response in Human Bladder Cancer. *Sci Transl Med* (2021) 13(576):eabb3735. doi: 10.1126/scitranslmed.abb3735
45. Onstenk W, Kraan J, Mostert B, Timmermans M, Charehbili A, Smit V, et al. Improved Circulating Tumor Cell Detection by a Combined EpCAM and MCAM CellSearch Enrichment Approach in Patients With Breast Cancer Undergoing Neoadjuvant Chemotherapy. *Mol Cancer Ther* (2015) 14(3):821–7. doi: 10.1158/1535-7163.MCT-14-0653
46. Karagiannis G, Pastoriza J, Wang Y, Harney A, Entenberg D, Pignatelli J, et al. Neoadjuvant Chemotherapy Induces Breast Cancer Metastasis Through a TMEM-Mediated Mechanism. *Sci Trans Med* (2017) 9(397):eaan0026. doi: 10.1126/scitranslmed.aan0026
47. Fina E, Necchi A, Giannatempo P, Colecchia M, Raggi D, Daidone MG, et al. Clinical Significance of Early Changes in Circulating Tumor Cells From Patients Receiving First-Line Cisplatin-Based Chemotherapy for Metastatic Urothelial Carcinoma. *Bladder Cancer* (2016) 2(4):395–403. doi: 10.3233/BLC-160069
48. Del Giudice F, Leonardo C, Simone G, Pecoraro M, De Berardinis E, Cipollari S, et al. Preoperative Detection of Vesical Imaging-Reporting and Data System (VI-RADS) Score 5 Reliably Identifies Extravesical Extension of Urothelial Carcinoma of the Urinary Bladder and Predicts Significant Delayed Time to Cystectomy: Time to Reconsider the Need for Primary Deep Transurethral Resection of Bladder Tumour in Cases of Locally Advanced Disease? *BJU Int* (2020) 126(5):610–9. doi: 10.1111/bju.15188
49. Del Giudice F, Pecoraro M, Vargas HA, Cipollari S, De Berardinis E, Bicchetti M, et al. Systematic Review and Meta-Analysis of Vesical Imaging-Reporting and Data System (VI-RADS) Inter-Observer Reliability: An Added Value for Muscle Invasive Bladder Cancer Detection. *Cancers (Basel)* (2020) 12(10):2994. doi: 10.3390/cancers12102994
50. Panebianco V, Del Giudice F, Leonardo C, Sciarra A, Catalano C, Catto JWF. VI-RADS Scoring Criteria for Alternative Risk-Adapted Strategies in the Management of Bladder Cancer During the COVID-19 Pandemic. *Eur Urol* (2020) 78(1):e18–20. doi: 10.1016/j.eururo.2020.04.043
51. Yuan B, Cai L, Cao Q, Wu Q, Zhuang J, Sun X, et al. Role of Vesical Imaging-Reporting and Data System in Predicting Muscle-Invasive Bladder Cancer: A Diagnostic Meta-Analysis. *Int J Urol* (2021). doi: 10.1111/iju.14748
52. Sciarra A, Gentilucci A, Silvestri I, Salciccia S, Cattarino S, Scarpa S, et al. Androgen Receptor Variant 7 (AR-V7) in Sequencing Therapeutic Agents for Castratrion Resistant Prostate Cancer: A Critical Review. *Medicine (Baltimore)* (2019) 98(19):e15608. doi: 10.1097/MD.0000000000015608
53. Busetto GM, Giovannone R, Antonini G, Rossi A, Del Giudice F, Tricarico S, et al. Short-Term Pretreatment With a Dual 5alpha-Reductase Inhibitor Before Bipolar Transurethral Resection of the Prostate (B-TURP):

Evaluation of Prostate Vascularity and Decreased Surgical Blood Loss in Large Prostates. *BJU Int* (2015) 116(1):117–23. doi: 10.1111/bju.12917

Conflict of Interest: The authors declare that the research was conducted in the absence of any commercial or financial relationships that could be construed as a potential conflict of interest.

Publisher's Note: All claims expressed in this article are solely those of the authors and do not necessarily represent those of their affiliated organizations, or those of the publisher, the editors and the reviewers. Any product that may be evaluated in this article, or claim that may be made by its manufacturer, is not guaranteed or endorsed by the publisher.

Copyright © 2022 Yang, Lv, Zhou, Feng, Zhou, Yuan, Wu, Yu, Han, Cao, Gu, Li, Yang and Lu. This is an open-access article distributed under the terms of the Creative Commons Attribution License (CC BY). The use, distribution or reproduction in other forums is permitted, provided the original author(s) and the copyright owner(s) are credited and that the original publication in this journal is cited, in accordance with accepted academic practice. No use, distribution or reproduction is permitted which does not comply with these terms.

frontiers in Oncology

ORIGINAL RESEARCH
published: 02 March 2022
doi: 10.3389/fonc.2022.820242

Identification and Validation of N6-Methyladenosine-Related Biomarkers for Bladder Cancer: Implications for Immunotherapy

Hongyu Deng[1,2], *Faqing Tang*[1,3], *Ming Zhou*[2,3], *Dongyong Shan*[4], *Xingyu Chen*[4*] and *Ke Cao*[4*]

[1] Department of Clinical Laboratory, Hunan Cancer Hospital, The Affiliated Cancer Hospital of Xiangya School of Medicine, Central South University, Changsha, China, [2] Cancer Research Institute and School of Basic Medical Sciences, Central South University, Changsha, China, [3] NHC Key Laboratory of Carcinogenesis, Hunan Key Laboratory of Oncotarget Gene, Hunan Cancer Hospital, The Affiliated Cancer Hospital of Xiangya School of Medicine, Central South University, Changsha, China, [4] Department of Oncology, Third Xiangya Hospital, Central South University, Changsha, China

OPEN ACCESS

Edited by:
Riccardo Tellini,
Careggi University Hospital, Italy

Reviewed by:
Liuer He,
Beijing Hospital, China
Zhaoting Li,
University of Wisconsin-Madison, United States
Bin Zheng,
Shandong University, China

***Correspondence:**
Xingyu Chen
xingyuchen@csu.edu.cn
Ke Cao
csucaoke@163.com;
csucaoke@csu.edu.cn

Specialty section:
This article was submitted to Genitourinary Oncology, a section of the journal Frontiers in Oncology

Received: 22 November 2021
Accepted: 07 February 2022
Published: 02 March 2022

Citation:
Deng H, Tang F, Zhou M, Shan D, Chen X and Cao K (2022) Identification and Validation of N6-Methyladenosine-Related Biomarkers for Bladder Cancer: Implications for Immunotherapy. Front. Oncol. 12:820242. doi: 10.3389/fonc.2022.820242

N6-methyladenosine (m^6A) has emerged as one of the most important modifications of RNA. Based on the expression of 23 different modes of m^6A regulatory factors, we identified three different m^6A modification patterns in bladder cancer. The effects of the three different modes of m^6A modification on clinicopathological characteristics, immune cell infiltration levels and expression levels of immune checkpoint genes were comprehensively analyzed. In addition, the effects of different modes of m^6A modification on the therapeutic efficacy of anti-PD-L1 immunotherapy (atezolizumab) are also discussed. Our results confirm that m^6A methylation plays an important role in immune cell recruitment in the tumor microenvironment of bladder cancer, which influences the efficacy of anti-PD-L1 therapy for bladder cancer. We further confirmed the important role of FTO protein in the biological function of bladder cancer cells by performing *in vitro* experiments. FTO functions as an oncogene in bladder cancer cells, and upon FTO knockdown, the level of m^6A enzyme activity in bladder cancer cells was significantly increased, apoptosis was increased, and cell proliferation and cell invasion were reduced. In addition, our study also confirmed that K216H and K216E are probably important targets for regulating FTO. We provide new insights into the regulatory pathways of the immune microenvironment and the methylation function of m^6A in bladder cancer, which will help in designing novel diagnostic methods, prognostic tools, and therapeutic targets.

Keywords: bladder cancer, N6-methyladenosine, tumor immune microenvironment, anti-PD-L1, immune checkpoint inhibitors

Abbreviations: m^6A, N6-methyladenosine; TCGA, The Cancer Genome Atlas; GEO, Gene-Expression Omnibus; KEGG, Kyoto encyclopedia of gene and genome; GO, Gene ontology; GSEA, Gene set enrichment analysis; SsGSEA, The single-sample gene set enrichment analysis; TME, Tumor microenvironment; TMB, Tumor mutation burden; ICT, The immune checkpoint therapy; CTLA-4, Cytotoxic lymphocyte antigen-4; PD-1, Programmed cell death protein 1; PD-L1, Programmed-death ligand 1; DCs, Dendritic cells; DEGs, Differentially expressed genes; EMT, Epithelial-mesenchymal transition; ICB, Immunological checkpoint blockade; TGFb, Transforming growth factor beta

INTRODUCTION

Bladder cancer is the most common cancer of the urinary system and is characterized by a difficult early diagnosis, rapid metastasis, and resistance to treatment. Immune checkpoint therapy (ICT) targets immune pathway effectors such as cytotoxic lymphocyte antigen-4 (CTLA-4), programmed cell death protein 1 (PD-1), or programmed death-ligand 1 (PD-L1) (1). Anti PD-L1 immunotherapy has been approved by the Food and Drug Administration (FDA) for the treatment of metastatic bladder cancer (2, 3). Immunotherapeutics that target PD-1 or PD-L1 have significantly improved the survival outcomes for some patients, showing an astonishing effect in a small number of patients with sustained efficacy. The improved clinical efficacy for the detection of cancer of the urinary system including advanced-stage bladder cancer has changed the intervention measures used (4); however, some patients with bladder cancer undergoing immunotherapy show no response to ICT or display resistance to drugs, and this scenario does not meet the clinical needs of these patients (5, 6). At present, multiple studies have confirmed that the immune response resulting due to many tumors, including those found in bladder cancer, is related to the level of immune cell infiltration in the tumor microenvironment, the expression of PD-1/PD-L1, and the tumor mutation burden (TMB) (7, 8).

The microenvironment in which tumor cells grow and survive is called the tumor microenvironment (TME), which includes stromal cells such as cancer-related fibroblasts and macrophages, immune infiltrating cells (myeloid cells and lymphocytes), bone marrow-derived cells (BMDCs) such as endothelial progenitor cells and hematopoietic progenitor cells, and secretory factors such as cytokines (9). There is mounting evidence that TME plays a crucial role in tumor progression, immune escape, and has an impact on the response to immunotherapy (10, 11). A comprehensive analysis of the heterogeneity and complexity of the TME is a key step in improving the success rate of existing ICTs and the development of new immunotherapy strategies. Further exploration of the regulatory mechanisms underlying TME cell infiltration will improve the ability to guide and predict the response to immunotherapy, and may help identify new therapeutic targets.

N6-methyladenosine (m^6A) is the most common and abundant RNA modification in eukaryotes. As a reversible epigenetic modification, m^6A is found in almost all types of RNAs, including mRNAs, ribosomal RNAs (rRNAs), long noncoding RNAs (lncRNAs), microRNAs (miRNAs), small nuclear RNAs (snRNAs), and circular RNAs (circRNAs), and are dynamically regulated in many physiological processes (12, 13). The m^6A modification is a dynamic and reversible process in mammalian cells and is regulated by various methyltransferases, demethylases, and binding proteins, also known as writers, erasers, and readers, respectively. The process of m^6A methylation is catalyzed by methyltransferases such as RBM15, ZC3H13, METTL3, METTL14, WTAP, and KIAA1429, and the removal process is mediated by demethylases such as FTO and ALKBH5 (14). Further, a group of specific RNA binding proteins, such as YTHDF1/2/3, YTHDC1/2, HNRNPA2B1, and IGF2BP1/2/3 can recognize the m^6A motif, thus affecting the function of m^6A (15). Results from various studies have shown that the abnormal expression and changes to gene expression for m^6A regulatory factors are related to the dysregulation of multiple biological processes essential for the initiation, progression, metastasis, drug resistance, recurrence, and immune regulation of cancer (16).

Many studies have confirmed the special correlation between m^6A modification and changes in the TME. Li et al. (17) observed that when METTL3 was depleted, the steady-state growth of T cells was blocked and was maintained at a slow rate. Further, their research showed that METTL3 deletion resulted in a decrease in the level of m^6A, and an increase in the mRNA stability and protein levels of SOCS1, SOCS3, and CISH, thus negatively regulating the IL-7 signal production in $CD4^+$T cells. Results from another study (18) revealed the role of m^6A in dendritic cell activation, in which METTL3 mediated the m^6A modification of the transcripts for the adaptor Tirap for CD40, CD80, and TLR4. Signal adaptors enhanced the translation of METTL3 in dendritic cells, thereby enhancing TLR4/NF-κB signal transduction, producing cytokines, and stimulating T cell activation. From the perspective of immune checkpoint therapy, the m^6A binding protein YTHDF1 can be used to modulate antitumor immunity and improve immunotherapy, as it can regulate the expression of lysosomal proteinase in an m^6A dependent manner. YTHDF1 can recognize the transcription of m^6A modified transcripts and encodes a lysosomal protease to increase translation in dendritic cells. Moreover, the deletion of *YTHDF1* enhances the cross-presentation of tumor antigens and the cross initiation of $CD8^+$T cells *in vivo*. Further, Wang et al. confirmed that the deletion of *YTHDF1* enhances the therapeutic effect of the PD-L1 checkpoint blockade (19).In melanoma, elevated *FTO* expression levels promote tumor growth by reducing the methylatin of m^6A in the mRNA for PD-1 (*PDCD1*), *CXCR4*, and *SOX10* and preventing their RNA decay mediated by YTHDF2. Knockout of *FTO* in melanoma cells induces tumor cells to become sensitive to interferon-gamma (IFNγ) *in vitro* and promotes a sensitizing response of melanoma cells to anti-PD-1 antibody in mice (20). Together, these data prove that the m^6A modification plays an important role in regulating the tumor immune microenvironment, and the combined use of m^6A modulators and PD-1/PD-L1 drugs may prove to be a new strategy to enhance the clinical efficacy of tumor immunotherapy.

In this study, we examined the effect of the m^6A methylation modification on the invasion characteristics of immune microenvironment cells and the effect of anti-PD-L1 therapy on bladder cancer. Our study helps elucidate the molecular mechanism underlying the regulation of the immune microenvironment in bladder cancer and provides new predictors, potential auxiliary targets, and directions for more effective immunotherapy strategies for combating bladder cancer.

MATERIALS AND METHODS

Datasets

The gene expression profile was measured experimentally using the Illumina HiSeq 2000 RNA Sequencing platform at the University of North Carolina The Cancer Genome Atlas

(TCGA) genome characterization center. Level 3 data were downloaded from the TCGA data coordination center. This dataset shows the gene-level transcription estimates, i.e., the $\log_2$ (x+1) transformed RSEM normalized counts, and somatic mutation data was downloaded from the site https://portal.gdc.cancer.gov/. IMvigor 210 cohort is a multicenter, single-arm phase II clinical study for evaluating the safety and efficacy of Tecentriq, a PD-L1 inhibitor, in patients with advanced urothelial carcinoma (21, 22). The complete processed expression data, detailed clinical annotations, and somatic mutation data were obtained from IMvigor210CoreBiologies, which is a complete documentation software and data package for the R statistical computing environment. The software package is available free of charge under the Creative Commons 3.0 License.

Consensus Clustering for 23 m^{6}A Regulators

We identified 23 m^{6}A regulators from published literature (23, 24), including 2 erasers (*ALKBH5*, *FTO*), 13 readers (*FMR1*, *HNRNPA2B1*, *HNRNPC*, *IGF2BP1*, *IGF2BP2*, *IGF2BP3*, *YTHDC1*, *YTHDC2*, *YTHDF1*, *YTHDF2*, *YTHDF3*, *ELAVL1*, *LRPPRC*), and 8 writers (*KIAA1429*, *METTL14*, *METTL3*, *RBM15*, *RBM15B*, *WTAP*, *ZC3H13*, *CBLL1*). The consensus clustering algorithm determined the optimal number of clusters (K value) as 3. Based on the expression of the 23 m^{6}A modulators, different m^{6}A modification patterns were identified by using k-means (based on Euclidean distance), and the patients were classified into three groups for further analysis. We used the consusclusterplus R package to perform the above steps, and performed 1000 iterations (50 iterations, resampling rate of 80%) to ensure the stability of the classification (25).

Common Molecular Typing of Bladder Cancer

We used several published subtype classification systems for bladder cancer, including the Baylor subtype described by Mo et al. (26), who defined urothelial differentiation based on 18 gene markers, thus dividing the muscle-invasive bladder cancers (MIBC) and non-MIBCs (NMIBC) into basal and differentiated subgroups. Damrauer et al. (27) identified basal and luminal cancer subtypes by consensus cluster analysis and further identified 47 genes as predictors of these subtypes. The MDA subtype (28) was analyzed by using 2252 genes (2697 probes) from 73 freshly frozen primary MIBC samples, including p53 like, luminal, and basal cancer. The Lund group (29) presented a six-class system based on global mRNA expression, including the urothelial-like, genomically unstable, epithelial infiltrated, SCC-like/Mes-like, SCC-like/UroB, and Sc/NE-like cancer. TCGA genotyping (30) used 2707 genes to conduct unsupervised cluster analysis on 129 patients with MIBC. The patients were classified into four subtypes (I, II, III, and IV), using the Cartes d'Identitédes Tumeurs (CIT)-Curie subtypes (31). These classifiers were combined into an R package (BLCA subtyping) (32), which can be found at https://github.com/cit-BioInfo/BLCAsubtype. We applied these classifiers independently to the TCGA-BLCA cohort and the IMvigor210 cohort to analyze the relationship between the subtypes of different classification methods and three different m^{6}A modification patterns. Further, we interpreted the differences among the three different m^{6}A modified subtypes.

Estimation of TME Cell Infiltration

We used the single-sample gene set enrichment analysis (ssGSEA) algorithm to quantify the relative abundance of cell infiltration in TME. We obtained gene sets from the data of Qingzhu Jia et al. (33) to label the different types of TME infiltrating immune cell types. As demonstrated by Jia et al. (33), we calculated the antitumor-immunity-score as the sum of the immune cell scores of various antitumor cells. Further, the pro-tumor-immunity-score is the sum of the scores of tumor-promoting immune cells, and we define the tumor immunity score as the difference between the pro-tumor-immunity score and the antitumor-immunity-score for unified analysis. In addition, we also used the ESTIMATE algorithm (34) to estimate the ratio of the immune matrix components of each sample in the TME to further explore the differences of TME components including immune cells and stromal cells scores among different m^{6}A modification patterns. The results were presented in three forms: immune score, stromal score, and the ESTIMATE score; the higher the score from the immune score or stromal score, the more immune or matrix components in TME. The ESTIMATE score is the sum of the immune score and stromal score, which represents the level of the two components in TME.

Identification of Differentially Expressed Genes (DEGs) Among Three Types of m^{6}A Modified Patterns

DEGs were identified *via* the Bayesian method between different m^{6}A modification patterns using the limma R package (35), the absolute value of logFC > 1 as the significance criteria. We used the ssGSEA method to score the samples based on the 23 m^{6}A regulatory factors. Based on the median value of the m^{6}A score, the patients were classified into a high m^{6}A score group or a low m^{6}A score group. The difference between the two groups was analyzed by the empirical Bayes method using the limma R package, taking the corrected p-value < 0.05, and the absolute value of logFC > 1 as the significant criteria and 647 DEGs were obtained for subsequent signal pathway analysis.

Differential Signaling Pathway Enrichment Among the Three m^{6}A Modified Modes

The enrichment of signaling pathways for the DEGs expressed relative to the different phenotypes of m^{6}A were analyzed using the metascape website (36) http://metascape.org. We determined the statistically rich terms, accumulated hypergeometric p values, and enrichment factors, and used these in a filtering step. Next, according to the Kappa statistical similarity between the gene members, the remaining important terms were clustered in a hierarchical structure, and the kappa score of 0.3 was used as a threshold to convert the terms to clusters (36). We selected the

genes with the best p-value in each cluster as its representative term and displayed them in the heatmap. The databases for the KEGG pathway, GO biological processes, Reactor gene sets, Canonical pathways, and the CORE resources were used for pathway and process enrichment analysis applying a p-value < 0.01, a minimum count of 3, and an enrichment factor > 1.5 (the enrichment factor is the ratio between the observed count and the chance expected count). The GSEA analysis (37) evaluates the skewness of the two distributions for the selected gene set in the gene list sorted by a specific phenotype. The analysis gene set was obtained from the hallmark gene sets provided by the Molecular Signatures Database (https://www.gsea-msigdb.org/). In this study, we used the clusterProfiler R package to implement the GSEA analysis (38).

Construction of a Scoring System to Evaluate the Level of m^{6}A Modification in Individual Samples

To quantify the m^{6}A modification pattern in a single patient. Based on the mRNA expression level of the 23 identified m^{6}A regulatory molecules in each sample, we constructed a scoring system called m^{6}Ascore by single sample Gene Set Enrichment Analysis (ssGSEA, based on GSVA R package).

Analysis of Copy Number Variation in Different Subtypes of Somatic Cells

For copy number variation analysis, we used the GISTIC.2 to identify significantly amplified or missing parts of the genome. The burden of copy number loss or gain was calculated as the total number of genes with copy number changes at the focal and arm level.

Relationship Between Methylation of m^{6}A and the Core Biological Pathways Impacted Due to Bladder Cancer

We analyze a set of gene sets for storing genes related to certain biological processes, and further, to reveal the association between the m^{6}A gene signature and some related biological pathways, including: (1) the immune-checkpoint; (2) antigen processing machinery; (3) CD8 T-effector signature; (4) epithelial-mesenchymal transition (EMT) markers including EMT1, EMT2, and EMT3; (5) the angiogenesis signature; (7) pan-fibroblast TGF-β response signature (Pan-F-TBRS); (8) WNT targets; (9) DNA damage repair; (10) mismatch repair; (11) Nucleotide excision repair; (12) DNA replication; (13) and antigen processing and presentation.

The differential gene expression of the core biological pathway genes between the different m^{6}A phenotypes of the IMvigor210 cohort was displayed in the form of a heatmap, including: (A) FGFR3 gene signature; (B) CD8 Teff signature; (C) antigen-processing machinery; (D) immune checkpoint signature; (E) MKI67 and cell cycle genes; (F) DNA replication-dependent histones; (G) DNA damage-repair genes; (H) TGFβ receptor and ligand; (I) F-TBRS genes; (J) EMT markers; (K) angiogenesis signature.

Cell Lines and Cell Culture

The human bladder cancer cell lines were obtained from the Oncology Institute of Central South University. The cell lines were incubated at 37°C under a humidified atmosphere with 5% CO2 and cultured in DMEM (Invitrogen, CA), supplemented with 10% fetal bovine serum (FBS) (GIBCO, NY), 1 mmol/L glutamine, and 1% penicillin/streptomycin.

Cell Viability, Apoptosis, and Invasion Assays

Cell proliferation was analyzed using a commercial CCK-8 assay kit (#C0038, Beyotime). We employed fluorescence-activated Cell Sorting (FACS) to assess apoptosis with the Annexin V-FITC/PI staining kit (Mbchem). According to the manufacturer, the transwell assay was used to measure cell invasion with the 6-well insert devices (8 μm pore size; Corning Life Sciences, Bedford, MA) and Biocoat Matrigel (BD Biosciences). We counted the cells from the middle and surrounding 5 fields of view and averaged the counts.

Western Blotting

Western blotting was performed as described previously (39). Briefly, total protein was extracted with RIPA lysis buffer and estimated using the bicinchoninic acid (BCA) Protein Assay Reagent Kit. The proteins were separated using 10% SDS-PAGE and electrophoretically transferred on a polyvinylidene fluoride (PVDF) membrane. The membranes were blocked with 5% skimmed milk and incubated overnight at 4°C with primary antibodies targeting FTO (27226-1-AP) and β-actin (1:2000, Ptgcn, 66009-1-Ig) and anti-GAPDH (Abcam, ab125247), followed by incubation with the appropriate secondary antibodies for one hour. Positive bands were visualized using an enhanced chemiluminescence system.

Measurement of Total m^{6}A

Total m^{6}A content was measured in the aliquots of 200-ng of total RNA extracted from cells using an m^{6}A RNA methylation quantification kit (cat. no. P-9005; Epigentek) according to the manufacturer's instructions.

Statistical Analysis

The non-paired *t*-test was used to compare the normally distributed variables between the two groups; the Mann-Whitney U test (also known as the Wilcoxon rank-sum test) was used to estimate the statistical significance of the non-normal distribution variables. The Kruskal-Wallis test and a one-way ANOVA were used as nonparametric and parametric analysis methods (40). The correlation coefficient between TME infiltrating immune cells and the expression of m^{6}A regulatory genes was calculated using the Pearson correlation method. We used the univariate Cox regression model to calculate the risk ratio (HR) for the m^{6}A regulatory genes. The survminer R software package was used to determine the cut-off point for the correlation between the m^{6}A scores and patient survival in each data set subgroup. The "surv-cut point" function of the maximum rank statistic was used to double score the m^{6}A score

by repeatedly testing all possible cut-off points, and further, the patients were classified into "high" and "low" subgroups, according to the maximum selected log-rank statistic, to reduce the batch effect in the calculations. The Kaplan-Meier method was used to plot the survival curve for prognosis analysis, and a log-rank test was used to determine the significance of the difference. The waterfall diagram of the maftools software package was used to show the mutations in the 23 m^{6}A regulatory factors in the TCGA-BLCA cohort. The thermograms of the 23 mutations for the m^{6}A regulatory factors were plotted. All statistical P-values were bilateral, and $P < 0.05$ was considered to be statistically significant.

RESULTS

Survey of 23 m^{6}A Regulatory Factors in Bladder Cancer

In this study, we analyzed 23 m^{6}A regulatory factors related to bladder cancer, including 2 erasers (*ALKBH5*, *FTO*), 13 readers (*FMR1*, *HNRNPA2B1*, *HNRNPC*, *IGF2BP1*, *IGF2BP2*, *IGF2BP3*, *YTHDC1*, *YTHDC2*, *YTHDF1*, *YTHDF2*, *YTHDF3*, *ELAVL1*, *LRPPRC*), and 8 writers (*KIAA1429*, *METTL14*, *METTL3*, *RBM15*, *RBM15B*, *WTAP*, *ZC3H13*, *CBLL1*). We first mapped the network for the 23 m^{6}A regulatory factors in bladder cancer (**Figure 1A**), and examined the interactions and their significance for the prognosis of bladder cancer patients. We found that there were significant correlations between the expression of m^{6}A regulatory factors in writers, erasers, and readers, and most of the correlations were positive (**Supplementary Table 1**). Based on these correlations, the 23 m^{6}A regulatory factors were divided into four categories (Clusters A-D). **Figure 1B** summarizes the somatic mutation frequency of the 23 m^{6}A regulators. In 116 out of 412 patient samples, a mutation in m^{6}A regulators was observed, with a frequency of 28.16%. Most of the mutations were missense mutations, and the regulators *KIAA1429*, *METTL3*, and *ZC3H13* had the highest mutation frequency (4%), while *HNRNPC*, *YTHDF3*, and *FMR1* did not harbor any mutations. Subsequently, we found that *FMR1* and *YTHDF2*, *YTHDF1* and *KIAA1429*, *YTHDF2* and *KIAA1429*, *WTAP*, and *METTL3*, *ZC3H13* and *LRPPRC*, and *ZC3H13* and *YTHDC2* had significant symbiotic relationships (**Figure 1C**, $P < 0.05$). The differential expression analysis for the 23 m^{6}A regulatory factors

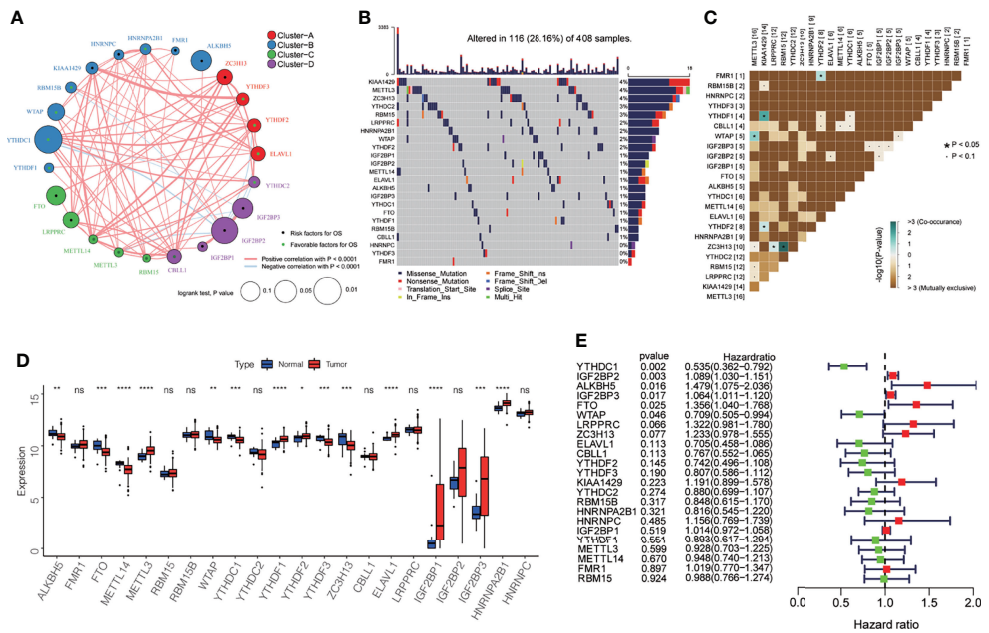


FIGURE 1 | Genetic and expression characteristics of the 23 m^{6}A regulatory genes in bladder cancer. **(A)** Depending on the correlation among the 23 m^{6}A regulatory genes, these were divided into four groups: Cluster A, red; Cluster B, blue; Cluster C, green; Cluster D, purple. The dot in the middle of each circle represents the influence of the m^{6}A regulator on OS, the favorable factors for OS are shown in green, and the risk factors are shown in black. The size of each circle represents the log-rank test p-value of the influence of the m^{6}A regulator on OS (expressed as $\log_{10}$ value). The line connecting the two m^{6}A regulatory factors represents the interaction between the factors; the red connection represents the positive correlation, and the light blue represents the negative correlation between the two factors. **(B)** Waterfall diagram showing 23 mutations of m^{6}A regulator in bladder cancer. Each column represents the patient, each color represents the mutation type, and gray indicates that there is no mutation in the gene in the sample. The bar graph above shows the TMB, and the number on the right shows the mutation frequency of each regulator. **(C)** The mutation mode of 23 m^{6}A regulatory factors; azure represents co-occurring mutations, brown represents mutually exclusive mutations, * $P < 0.05$, · $P < 0.1$. **(D)** The expression levels of 23 m^{6}A regulatory factors in cancer and normal tissues. Tumor, red; normal, blue. The top and bottom of the box indicate the quartile range of the value, the lines in the box represent the median value, and the black dot represents the abnormal value. *$P < 0.05$; **$P < 0.01$; ***$P < 0.001$; ****$P < 0.0001$; ns $P > 0.05$. **(E)** The forest map shows the univariate Cox analysis results for the impact of 23 m^{6}A regulatory factors on the OS of bladder cancer patients. Red represents risk factors, and the green represents protective factors.

in bladder cancer and its adjacent tissues is shown in **Figure 1D**. The expression of *ALKBH5*, *FTO*, *METTL14*, *WTAP*, *YTHDC1*, *YTHDF3*, and *ZC3H13* in adjacent cancer tissues was significantly higher than that in cancer tissues, while the expression of *METTL3*, *YTHDF1*, *YTHDF2*, *ELAVL1*, *IGF2BP1*, *IGF2BP3*, and *HNRNPA2B1* in cancer tissues were significantly higher than those in non-cancerous tissues. However, due to the small sample size of the paracancerous tissues, this result needs further verification. A univariate Cox regression analysis was performed to study the effect of the 23 m^{6}A regulatory factors on the overall survival (OS) of bladder cancer patients (**Figure 1E**). It was observed that six m^{6}A regulatory factors had a significant effect on the prognosis for bladder cancer patients. *YTHDC1* and *WTAP* may be protective factors (HR < 1, P < 0.05), while *IGF2BP2*, *ALKBH5*, *IGF2BP3*, and *FTO* are risk factors for bladder cancer (HR > 1, P < 0.05).

Three Different m^{6}A Modification Patterns Defined by the 23 m^{6}A Regulatory Factors

Based on the gene expression of the 23 m^{6}A regulatory factors, 407 patients with bladder cancer were classified using the R-package ConsensusClusterPlus. Our analysis showed that 3 clusters were optimal (**Figures 2A, B** and **Supplementary Figure 1A–D**) and the principal component analysis showed that all patients could be well classified into three subtypes (**Figure 2C**), and we identified three different m^{6}A modification patterns in 407 patients with bladder cancer, which we named Cluster 1-3. We plotted a heatmap (**Figure 2D**) and boxplot (**Figure 3A**) for the expression of the 23 m^{6}A regulatory factors in Cluster 1-3 and found that the expression of *IGF2 BP1, IGF2BP2, IGF2BP3, KIAA1429*, and *RBM15* in Cluster 2 was lower than in the other clusters (P < 0.01), while the expression of *METTL3*, *RBM15B*, *YTHDC1*,

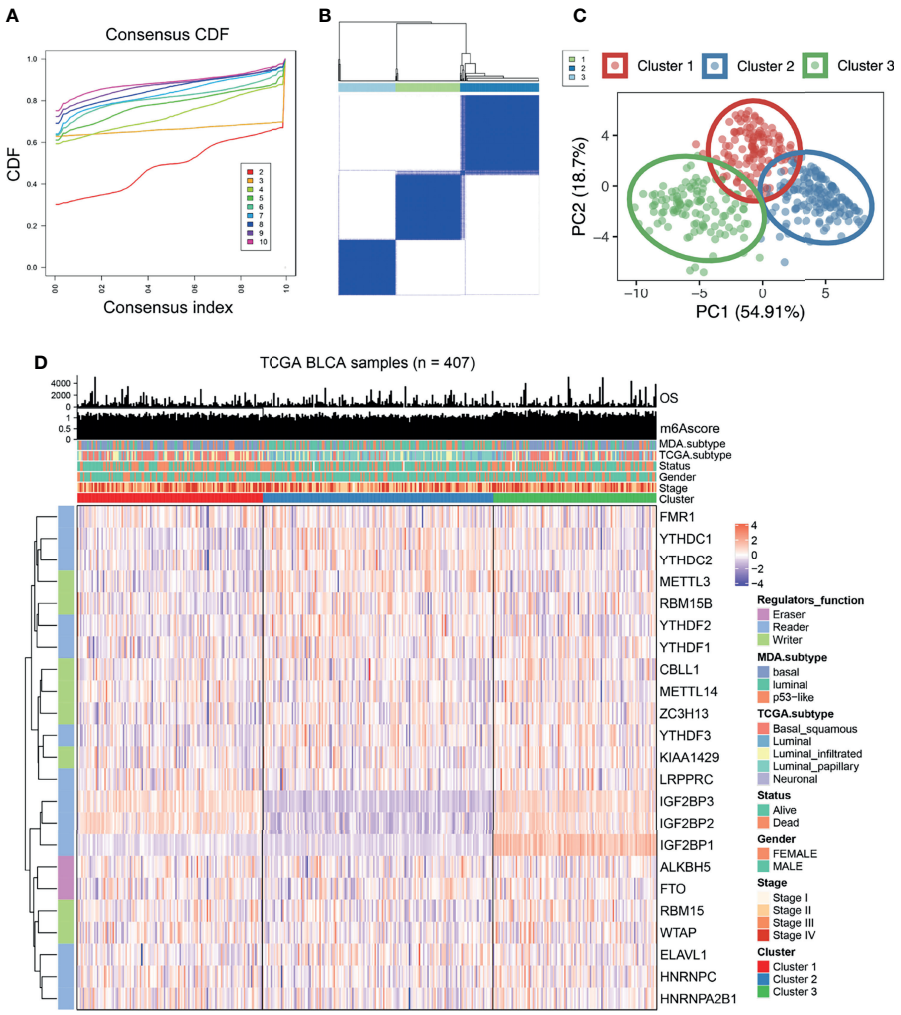


FIGURE 2 | The expression of 23 kinds of m^{6}A regulatory factors identified three different methylation patterns. **(A, B)** According to the expression of 23 m^{6}A regulatory factors, we classified 407 bladder cancer patients, and 3 was the optimal cluster number. **(C)** Principal component analysis showed that that all patients could be well classified into three subtypes. **(D)** Heatmap display showing the expression of 23 m^{6}A regulatory factors among three different m^{6}A modification patterns. The relationship between different m^{6}A modification patterns and clinical features such as OS, m^{6}Ascore, MDA typing, TCGA typing, status, gender, stage, etc.

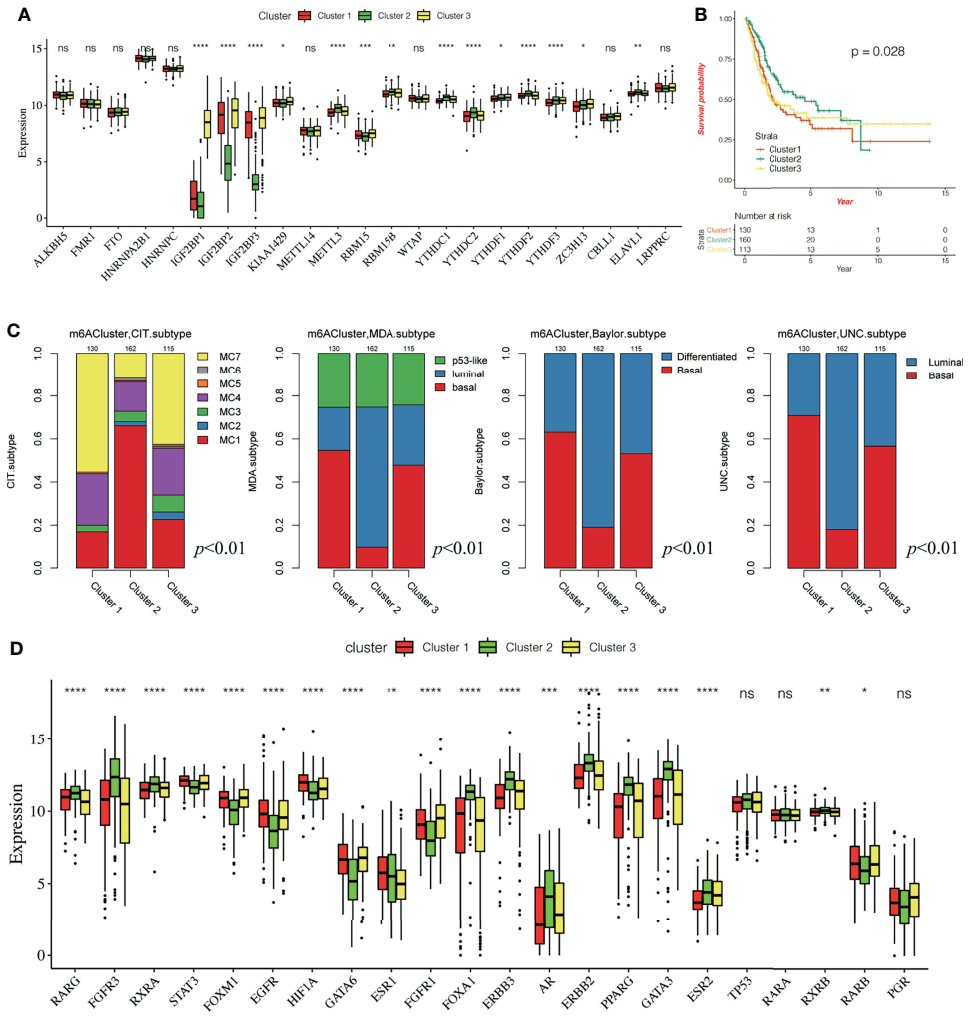


FIGURE 3 | Characteristics of three different methylation patterns of m^{6}A. **(A)** The expression of 23 m^{6}A regulatory factors varied among the three different m^{6}A modification patterns. The upper and lower end of the box indicates the quartile range of the value, the lines in the box represents the median value, the black dot represents the abnormal value, and the asterisk represents the statistical p-value, *P < 0.05; **P < 0.01; **P < 0.001, ***P < 0.0001, ****P < 0.0001. **(B)** The KM curve shows the difference in the effects of the three m^{6}A modification patterns on OS. **(C)** Comparative analysis of three different m^{6}A modification patterns and molecular typing of bladder cancer, including Bayol classification, MDA typing, CIT Curie typing, and UNC typing. **(D)** The upper and lower ends of the box represent the quartile range of values, the lines in the box represent the median value, and the black dots represent the abnormal values. The asterisk represents the statistical p-value, *P < 0.05; **P < 0.01; *P < 0.001, ***P < 0.0001, ****P < 0.0001, ns P > 0.05.

YTHDC2, *YTHDF1*, *YTHDF2*, *YTHDF3*, and *ELAVL1* was higher in Cluster 2 than the other clusters. Significantly higher overall survival was observed in the patients who had m^{6}A modifications from cluster 2 (**Figure 3B**). To better understand the potential differences between the three m^{6}A modification patterns, we compared them with the published molecular typing of bladder cancers, including Baylor, MDA, CIT-Curie, and UNC (**Figure 3C**). Using the CIT classification, Cluster 1 and Cluster 3 showed more of MC7 subtypes; whereas, more MC1 subtypes were seen in Cluster 2; Using the Baylor classification, Cluster 1 and Cluster 3 had more basal subtypes, and Cluster 2 contained more differentiated subtypes; based on the UNC classification, the basal subtype was more frequent in Cluster 1 and Cluster 3 than the luminal subtype, while Cluster 2 showed the opposite result. To further characterize the molecular differences between the RNA based subtypes, we analyzed the expression of 23 regulatory genes associated with bladder cancer (41–47), including the steroid hormone receptors ESR1/2, AR, and PGR, the nuclear receptors PPARG, three RARs (A/B/G), and three RXRs (A/B/G), the receptor tyrosine kinases ERBB2/3 and FGFR1/3, and the transcription factors FOXA1, FOXM1, GATA3/6, HIF1A, KLF4, STAT3, and TP63, We found significant differences in the expression of most regulators between Cluster 2 and the other two m^{6}A subtypes. The expression of *RARG*, *FGFR3*, *RXR3*, *FOXA1*, *ERBB3*, *AR*, *ERBB2*, *PPARG*, *GATA3*, *ESER2*, and *RXRB* in Cluster 2 was

significantly higher than that in Cluster 1 and Cluster 3, while the opposite relation was found for *STAT3*, *FOXM1*, *EGFR*, *HIF1A*, *GATA6*, *FGFR1*, and *RARB* (**Figure 3D**). Further, we identified differences in the mutation of 20 genes in the three m^{6}A modification patterns as shown in the waterfall diagram (**Supplementary Figure 1E**). and we analyzed the difference in Copy number alterations across three m^{6}A modification patterns. (**Supplementary Figures 2**, **3**).

Difference in Immune Cell Infiltration Characteristics in the Tumor Immune Microenvironment for Different m^{6}A Modification Patterns

To reveal the role of m^{6}A modification patterns in TME immunoregulation, we calculated the abundance of 28 cellular subsets in each patient sample. The heatmap shows the average difference in the infiltration level of 28 types of immune cells in the three different m^{6}A modification patterns (**Figure 4A**, **Supplementary Tables 2**, **3**), We found significant differences in the characteristics of cellular infiltration in the TME; Cluster 2 is characterized by immunosuppression, and most of the infiltrating cells are immune cells. The infiltration level was significantly lower than that of cluster1 and cluster3 (**Supplementary Figure 4A**). In addition, the anti-tumor immunity score and the pro-tumor immunity score of Cluster 2 were significantly lower than that of Cluster 1 and Cluster 3 (**Supplementary Figures 4B, C**), and the pro-tumor score of Cluster 2 is significantly higher than in Cluster 1 and Cluster 3 (**Figure 4B**). The ESTIMATE algorithm can estimate the ratio of the immune and matrix components of each sample in the TME, which is presented in the form of three scores: the immune score, stromal score, and the ESTIMATE score. We found that the three scores in Cluster 2 were significantly lower than those in

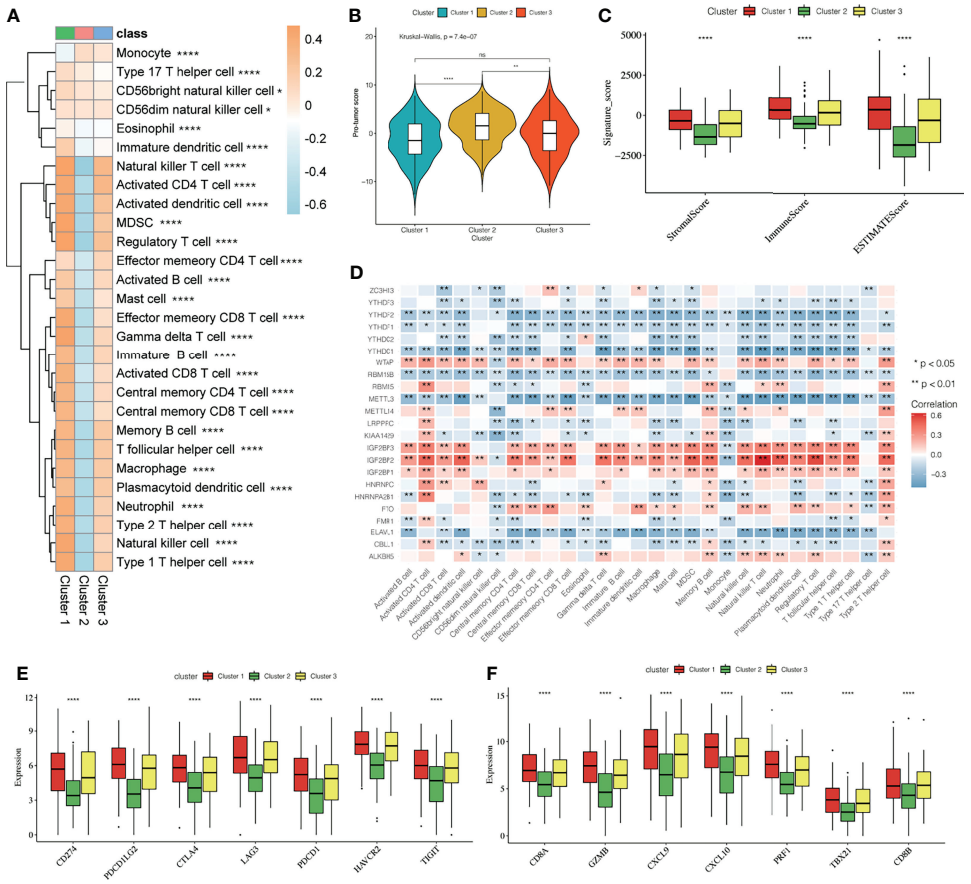


FIGURE 4 | Effect of m^{6}A modification on immune cell infiltration and immune checkpoint expression in the tumor immune microenvironment. **(A)** The thermogram shows the difference in the average level of 28 kinds of immune cell infiltration among three different m^{6}A modification patterns, the asterisk represents the statistical p-value (*P < 0.05; **P < 0.01; ***P < 0.0001). **(B)** The violin box chart shows the difference in Pro-tumor score, the asterisk represents the statistical p-value (*P < 0.05; **P < 0.01; ***P < 0.0001, ns P > 0.05). **(C)** The ESTIMATE algorithm estimates the ratio of immune and matrix components of each sample in TME. The histogram shows the difference in immune score, stromal score, and the ESTIMATE score among the three different m^{6}A modification patterns. The asterisk represents the statistical p-value (*P < 0.05; **P < 0.01; ***P < 0.0001). **(D)** Thermogram showing the 23 m^{6}A regulatory factors that were correlated with 28 kinds of immune cells. The darker color indicates a higher correlation. The asterisk represents the statistical p-value (*P < 0.05, **P < 0.01). **(E, F)** The Box plot shows the immune checkpoint-related gene **(E)** and the CD8$^+$T cell marker gene **(F)** among the three different m^{6}A modification patterns.

Cluster 1 and Cluster 3 (**Figure 4C**), suggesting that m^6A methylation may be involved in regulating the type of TME infiltrating cells and play a central role in immune regulation. However, the mechanism for how m^6A modification affects the immunophenotype is unclear. Therefore, we analyzed the correlation between the 23 m^6A regulatory factors and the 28 types of immune cells (**Figure 4D**). A heatmap of the correlation showed that the m^6A regulators were highly correlated with most of the immune cells, and *WTAP*, *IGF2BP2*, and *IGF2BP3* showed the most significant correlation with most immune cells. Further, *YTHDF2*, *YTHDC1*, *METTL3*, and *ELAVL1* showed a high negative correlation with most immune cells, indicating that these regulators may play an important role in the differentiation and recruitment of immune cells. To further explore the possible role of m^6A related phenotypes in immunotherapy, we studied the difference in the expression of the immune checkpoint related genes *CD274*, *PDCD1LG2*, *CTLA4*, *LAG3*, *PDCD1*, *HAVCR2*, *TIGIT*, and the CD8+T cell marker genes including *CD8A*, *GZMB*, *CXCL9*, *CXCL10*, *PRF1*, *TBX21*, and *CD8B* in the three different m^6A modification patterns (**Figure 4E, F**). Our results showed that the expression of these genes in Cluster 2 was significantly lower than that in Cluster 1 and Cluster 3 ($P < 0.0001$). The results suggest that m^6A methylation affects the type of TME infiltrating cells, and Cluster 2 had a significantly lower level of immune cell infiltration related to the immune checkpoint than the other two modification patterns. The gene expression in Cluster 2 is significantly low, and we speculated that the response to immunotherapy in patients showing Cluster 2 type m^6A modifications may be worse than that of Cluster 1 and Cluster 3.

Enrichment of DEGs and Signaling Pathways Involved in the Different Modes of m^6A Modification

To reveal the biological differences among the three different m^6A modification patterns, we undertook expression profiling of the patient tissue samples and identified 403 DEGs (**Figure 5A**). The Circos diagram shows the overlap of the DEGs obtained by pairwise comparison of the three different m^6A modification patterns. Cluster 2 had more DEGs than did Cluster 1, and there are more common genes in the list of DEGs obtained for Cluster 1 than that obtained for Cluster 2, and between Cluster 3 and Cluster 2 (**Figure 5B**). In **Figure 5B**, the blue lines connect genes belonging to the same ontology term showing the number of functional overlaps between different groups.

We used Metascape (36) to analyze the enrichment of signaling pathways between the different m^6A modification classes. The results are shown in the heatmap which is colored by p-values, and the white cells indicate a lack of enrichment of the term in the corresponding gene list (**Figures 5C, D**, and **Supplementary Figures 5A, B**). Additionally, a GSEA was performed for further signaling pathway enrichment analysis (**Figure 5E**), IL2/STAT5 signaling, EMT, inflammatory response, interferon-gamma response, and TNFα signaling *via* NFκB were enriched in Cluster 1. Allograft rejection, complement, EMT transition, inflammatory response, kras signaling are enriched in Cluster 3. These signaling pathways involve different core biological processes, most of which are related to the regulation of immunity, and some of them have been confirmed to have a correlation in immunotherapy (48–50), which provides a basis for further exploration of the effect of m^6A modifications on the immunophenotype.

The m^6A Score Is an Important Prognostic Biomarker and Predictor of Bladder Cancer

We constructed and evaluated a scoring system called the m^6Ascore to quantify the level of m^6A modification in each patient sample by ssGSEA, taking into account the individual differences and complexity of the m^6A modification. First, we conducted a survival analysis using the m^6Ascore and found that patients with high m^6Ascore had a poor prognosis ($p = 0.036$, **Figure 6A**). There were also significant differences in the m^6Ascore among the three different m^6A modification patterns, with the lowest and highest m^6Ascores being assigned to Cluster 3 and Cluster 2, respectively (**Figure 6B**). Next, we analyzed the differences in m^6Ascore in the MDA cancer subtype and found the highest score for the basal subtype, followed by the luminal subtype, with the lowest expression level observed in the p53-like subtype (**Figure 6C**). To explore the potential biological relevance of m^6Ascore, we classified 407 patients into a high m^6Ascore group and a low m^6Ascore group based on the expression level of the 23 m^6A regulators. We first examined the difference in the composition of immune cells between the two patient groups (**Figure 6D**). Our results showed that $CD56^{dim}$ natural killer cells, central memory CD4T cells, eosinophils, mast cells, monocytes, and type 17 T helper cells showed a significantly low enrichment in the high m^6Ascore group. Further, the activated $CD4^+$ T cells, memory B cells, natural killer T cells, neutrophils, and type 2 T helper cells showed highly significant enrichment in the low m^6Ascore group. We analyzed the DEGs, and additionally examined the signaling pathways showing enrichment *via* GO and KEGG pathway analysis between the two groups. The pathways showing enrichment for molecular function (MF), cellular component (CC), and biological process (BP) *via* GO analysis were examined. Signaling pathways enriched for BP include the xenobiotic metabolic process, hormone metabolic process, epidermis development, etc.; pathways enriched for CC included the apical part of the cell, apical plasma membrane, cornified envelope, etc.; and pathways enriched for MF include monooxygenase activity, serine-type endopeptidase activity, and other signaling pathways (**Supplementary Figures 5C–E**). A KEGG pathway analysis showed that the DEGs were mainly enriched in glutathione metabolism, ether lipid metabolism, and other signaling pathways (**Supplementary Figure 5F**). A GSEA analysis (**Figures 6E, F**) showed that pathways for the inflammatory response, interferon-gamma response, myc targets V1, TNFα signaling *via* NFκB, and other genes were concentrated in the high m^6Ascore group. These results strongly suggest a significant correlation between a high m^6Ascore and immune activation. The results also demonstrate the central role

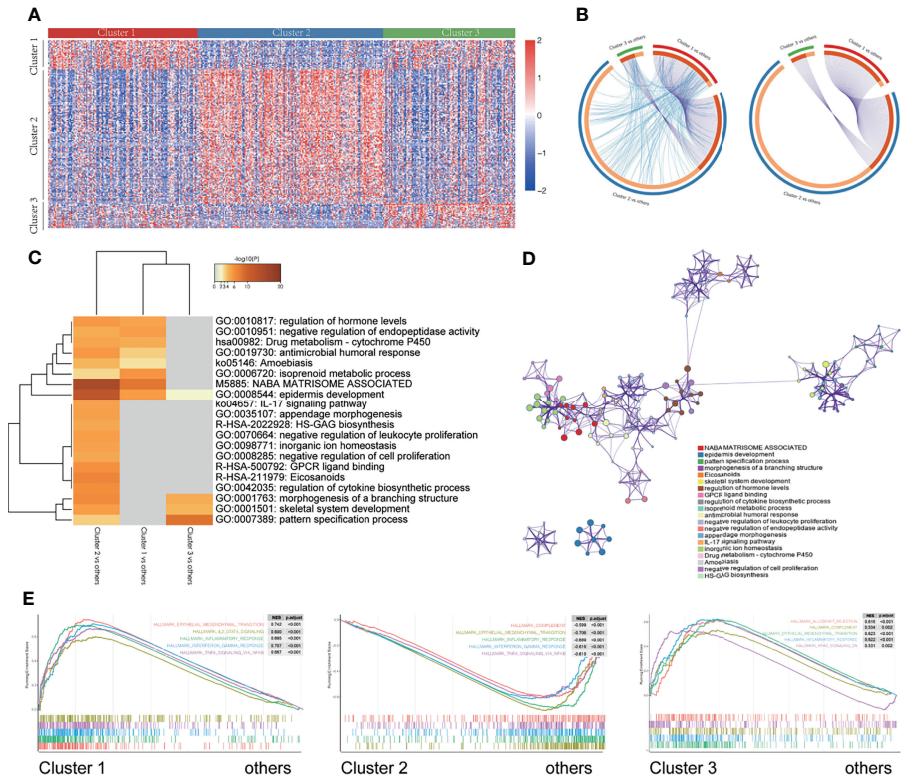


FIGURE 5 | Enrichment of different gene signaling pathways in different m^{6}A modification patterns. **(A)** Heatmap showing the expression of different genes in three different m^{6}A modification patterns. **(B)** Circos diagram showing the overlap of differentially expressed genes by pairwise comparison of three different m^{6}A modification patterns. Each arc in the outer circle represents the comparison group, and each arc in the inner circle represents a gene list. Each gene has a point on the arc. Dark orange represents the genes that appear in multiple lists, and light orange represents the only gene in the list. The purple line indicates the overlap between genes. The more purple links and the longer the dark orange arc, the higher the overlap between input gene lists, where they fall into the same ontology term (the term has to be statistically significantly enriched and with a size no larger than 100). **(C)** The thermogram shows the enrichment of gene signaling pathways with different m^{6}A modification patterns. The heat map cells are colored by their p-values, and the white cells indicate that the term lacks enrichment in the corresponding gene list. **(D)** Selected representative signal paths shown in a network layout. Each signal path is represented by a circular node, whose size is directly proportional to the number of input genes in the term. The color represents the cluster identity, i.e., nodes with the same color belong to the same cluster. Terms with similarity score > 0.3 are linked by edges (the thickness of the edge represents the similarity score). The network was visualized using Cytoscape (v3.1.2). **(E)** GSEA of the marker gene set downloaded from the MSigDB database. All transcripts were sequenced according to the multiple variations (log_2) obtained using the different analyses among three different m^{6}A modification patterns. GSEA analysis evaluated the skewness of the two distributions of the selected gene set in the sequenced gene list.

of m^{6}A methylation in different biological processes in bladder cancer, including different aspects of immune regulation. The m^{6}Ascore may be used to evaluate the characteristics of immune cell infiltration in bladder cancer tissue to predict the clinical response of patients to immunotherapy. Thus, the m^{6}Ascore may have the potential to be used as an independent prognostic biomarker to predict the OS rate of patients, guiding more effective clinical practice.

Effect of m^{6}A Methylation Modification on Anti-PD-L1 Immunotherapy for Bladder Cancer

To explore the potential effect and mechanism of m^{6}A methylation on immunotherapy for bladder cancer, we obtained data for the IMvigor210 cohort, which is an open-label, multicenter, single-arm phase II clinical study to evaluate the safety and efficacy of Tecentriq, an anti-PD-L1 agent, in patients with advanced urothelial cancer (**Supplementary Table 4**). Patients who responded in whole or in part were classified as responders and were compared with non-responders who showed the incidence of stable or progressive disease. We performed an unsupervised clustering using data for mRNA expression for the 23 m^{6}A regulatory factors from all patients. We identified three different m^{6}A modification patterns and calculate the m^{6}Ascore for subsequent analysis. Additionally, we performed a combined heatmap-based analysis (**Figure 7**) to find the correlation between the different m^{6}A methylation modes and the Lund and TCGA molecular typing for the anti-PD-L1 based immunotherapy. Further, for the three groups of m6A modification patterns, we also analyzed the differences in PD-L1 expression in immune cells (IC) and tumor cells (TC), patients' response to anti-PDL1 efficacy, TMB, m^{6}Ascore, and the important gene mutations prevalent in bladder cancer. We also analyzed the differences in the expression of genes in

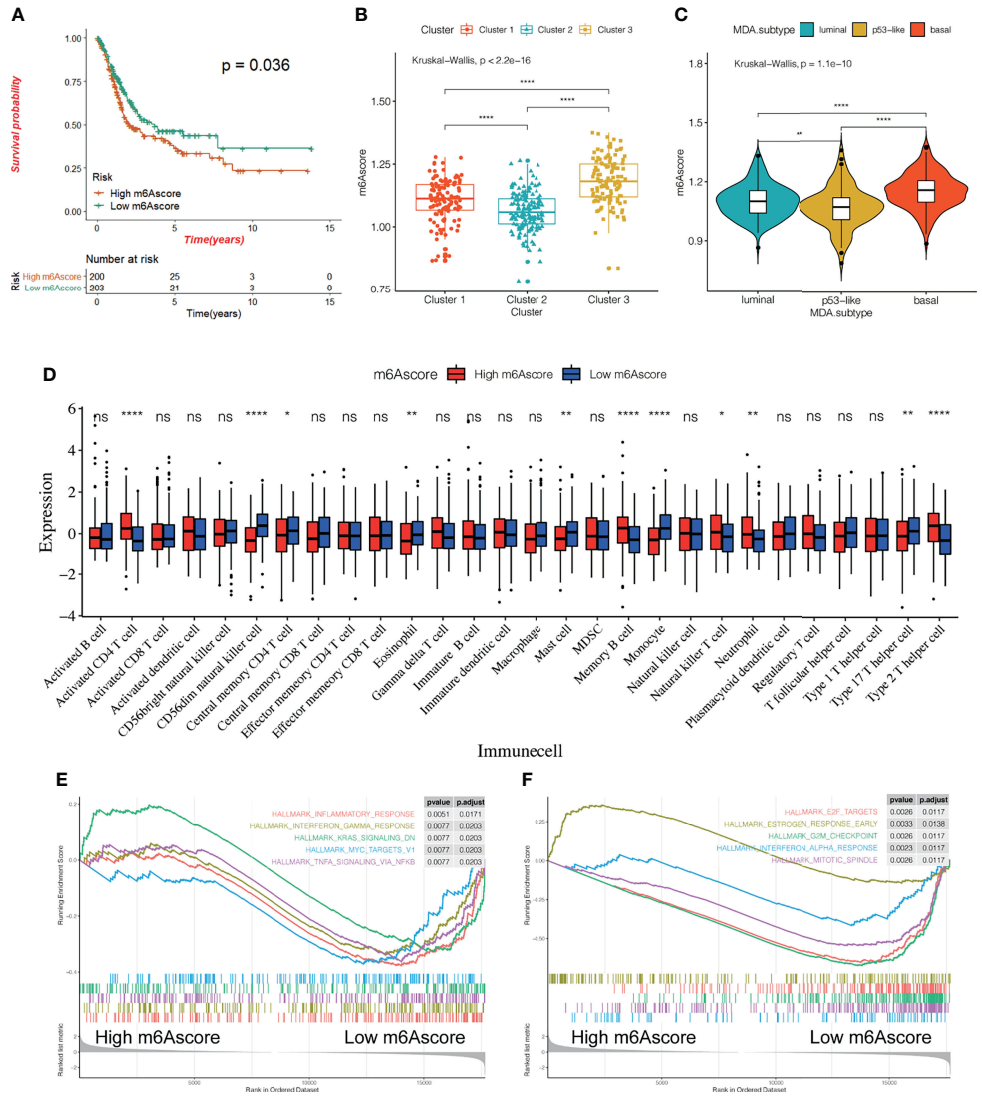


FIGURE 6 | Relationship between m^{6}Ascore and the characteristics of bladder cancer. **(A)** KM survival curve showing the effect of m^{6}Ascore on OS in the TCGA-BLCA cohort. **(B, C)** The difference of m^{6}A score among three different m^{6}A modification patterns **(B)** and MDA typing **(C)**. The asterisk represents the statistical p-value (*P < 0.05; **P < 0.01; ****P < 0.0001). **(D)** According to the expression of the m^{6}Ascore,407 patients were classified into a high m^{6}Ascore group and a low m^{6}Ascore group. The histogram shows the expression difference of 28 kinds of immune cells between the two groups. **(E, F)** All transcripts were sequenced according to the multiple variations (log_2) obtained by the two groups in the analysis. GSEA analysis evaluated the skewness of the two distributions of the selected gene set in the sequenced gene list.

important biological pathways for bladder cancer (51), including the *FGFR3* gene signature; CD8 Teff signature; antigen-processing machinery; immune checkpoint signature; MKI67 and cell cycle genes; DNA replication-dependent histones; DNA damage-repair genes; TGFβ receptor and ligand; F-TBRS genes; EMT markers; and the angiogenesis signature. In the comparison between the different m^{6}A modification patterns and the TCGA and Lund classification using a heat map-based analysis, we found that most genes in Cluster 1 were classified as subtype I and the least as subtype IV. For the Lund classification, we observed that the UroA subtype had the highest proportion in Cluster 1, the Inf type has the highest proportion in Cluster 2, and the SCCL subtype was more enriched in Cluster 1. Additionally, we found that the Cluster 3 modification mode had higher levels of PD-L1 expression in immune cells and tumor cells, a higher proportion of CR/PR (**Figure 7** and **Figure 8A**). These results suggest that m^{6}A methylation may be involved in the response to anti-PDL1 therapy. Additionally, among the three different m^{6}A methylation patterns in bladder cancer, there were differences in gene mutations (51) for *TP53*, *RB1*, *FGFR3*, *CDKN2A*, *ERBB2*, and *PIK3CA*. Patients had a greater number of *FGFR3* and *CDKN2A* mutations in Cluster 1 than in Cluster 2 or Cluster 3, while the converse was true for *TP53* mutations. There were significant differences among the

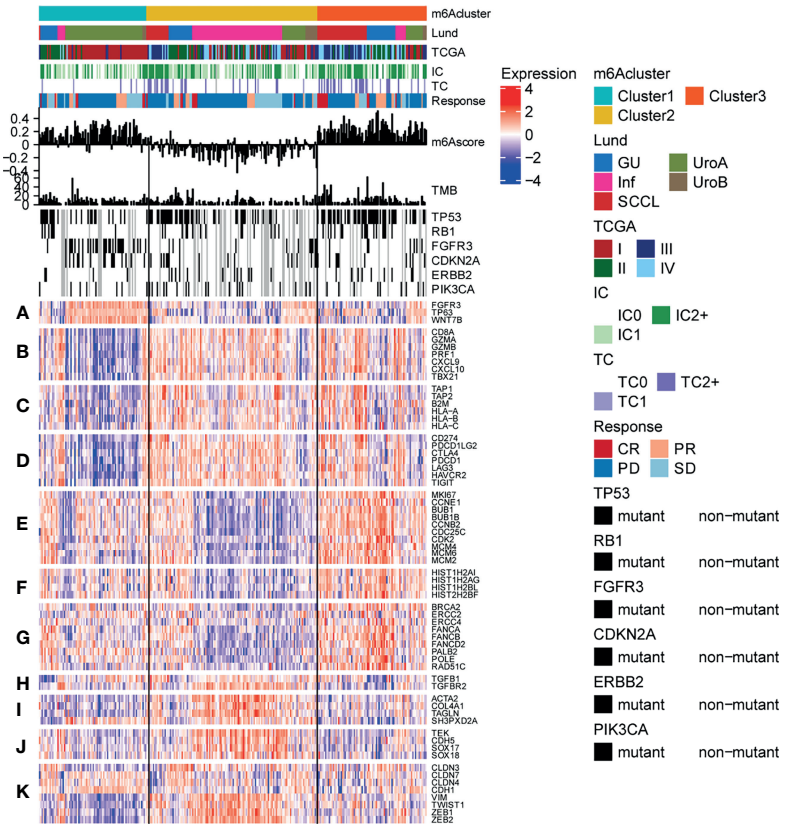


FIGURE 7 | Characteristics of m^{6}A modification in anti-PD-L1 immunotherapy cohort of bladder cancer. Heatmap representing all patients evaluated for anti-PD-L1 response, First, the sequence was based on the modified mode of m^{6}A, next by the molecular subtype, PD-L1 expression on cells (IC), PD-L1 expression on cells (TC), and the reaction to atezolizumab. The m^{6}Ascore and TMB levels of each patient are shown, and the mutation status of several genes of interest (black, mutation; gray, patients without mutation data) are shown. In addition, the lines of the heat map show the expression of the genes of interest (z-score), which are divided into the following biological classes and/or pathways: **(A)** FGFR3 gene signature; **(B)** CD8 Teff signature; **(C)** antigen-processing machinery; **(D)** immune checkpoint signature; **(E)** MKI67 and cell cycle genes; **(F)** DNA replication-dependent histones; **(G)** DNA damage-repair genes; **(H)** TGFβ receptor and ligand; **(I)** F-TBRS genes; **(J)** EMT markers; **(K)** angiogenesis signature.

three m^{6}A modification patterns in most gene sets. The expression of the *FGFR3* gene signature (*FGFR3*, *TP63*, *WNT7B*) in Cluster 1 was significantly higher than in the other two groups, while the CD8 Teff signature (*CD8A*, *GZMA*, *GZMB*, *PRF1*, *CXCL9*, *CXCL10*, *TBX21*),antigen-processing machinery (*TAP1*, *TAP2*, *B2M*, *HLA-A*, *HLA-B*, *HLA-C*), and the immune checkpoint signature (*CD274*, *PDCD1LG2*, *CTLA4*, *PDCD1*, *LAG3*, *HAVCR2*, and *TIGIT*) are less expressed in Cluster 1 than the other two modification patterns, and are highly expressed in the Cluster 3 subgroup. The CD8 Teff and the immune checkpoint signatures are often used to predict the efficacy of immunosuppression in patients with immune checkpoint suppression; a higher expression level is linked to better clinical outcomes (5, 52). Additionally, our results indicated that the expression of *MKI67* and cell cycle genes; DNA replication-dependent histones; DNA-repair genes are significantly higher in Cluster 3; TGFβ receptor and ligand; F-TBRS genes; EMT markers; angiogenesis signature show significantly increased gene expression in Cluster 2. We have observed that there are more compact types and fewer read types in Cluster 1. Compared with Lund typing, there are more SCCL types in Cluster 1, more UroA types in Cluster 1, and more infs types in Cluster 2 (**Figure 8A**). We found differences in m^{6}Ascore levels among the three m^{6}A modification patterns, with the lowest m^{6}Ascore level found in Cluster 2, while the m^{6}Ascore of Cluster 3 and Cluster 1 were the same, with no significant difference (**Figure 8B**). Differences in the m^{6}Ascore were also observed in immunophenotyping, with the excluded subtype having the highest m^{6}Ascore, and no significant difference in m^{6}Ascore found between the inflamed and desert subtypes (**Figure 8C**).

Next, we analyzed the correlation between m^{6}Ascore and biological pathway gene scores (39) in bladder cancer (**Figure 8D**). The m^{6}Ascore was positively correlated with the scores for DNA replication, mismatch repair, Fanconi, base excision repair, nucleotide excision repair, homologous recombination, cell cycle, and DDR, and negatively correlated with EMT2, EMT1, immune checkpoint, CD8 T effector, APM, etc. The effect of the m^{6}Ascore on OS was observed by plotting the KM curve, which indicated that a higher m^{6}Ascore had a

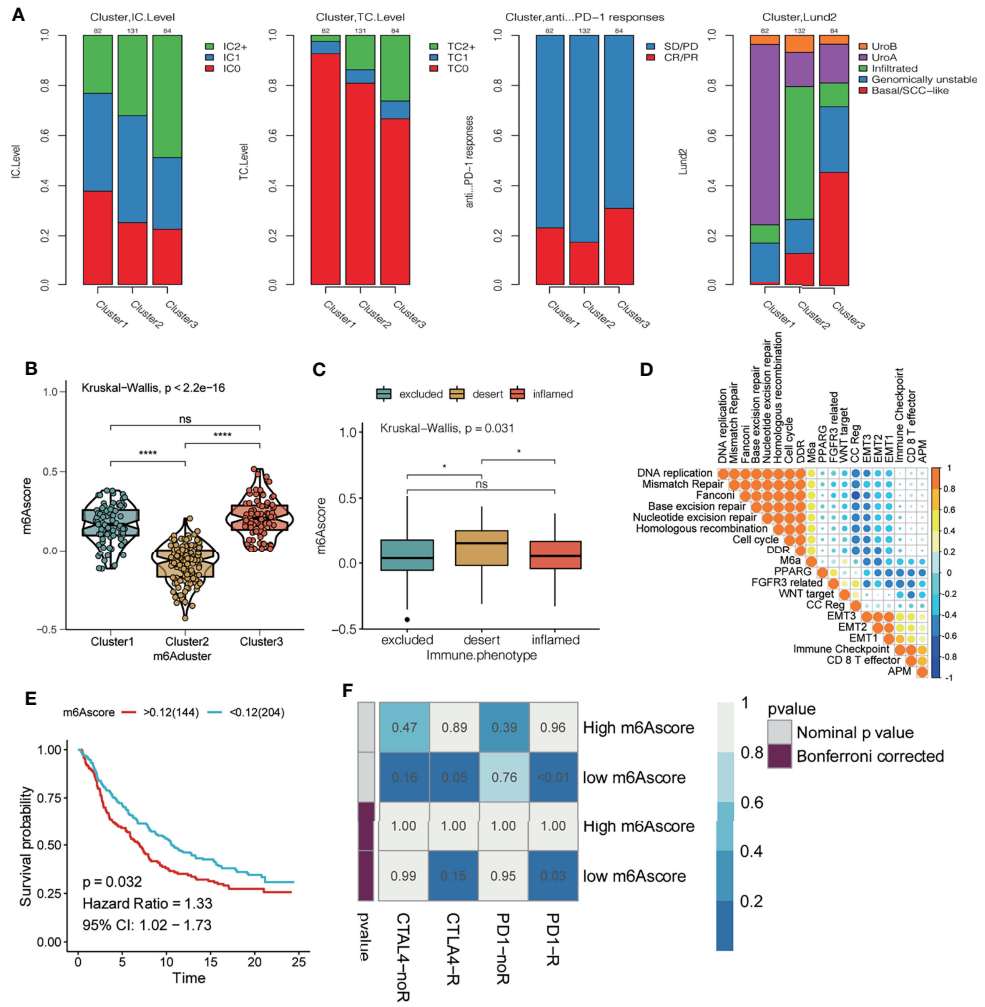


FIGURE 8 | Effect of m^{6}A modification mode on the treatment of bladder cancer with PD-L1. **(A)** From left to right, the stacking histogram shows the relationship between the three kinds of m^{6}A modification patterns and PD-L1 expression on immune cells (IC), PD-L1 expression on tumor cells (TC), response to atezolizumab, and Lund typing. **(B)** m^{6}Ascore difference between 3 different m^{6}A modification patterns. The asterisk represents the statistical p-value (*P < 0.05; ****P < 0.0001, ns P > 0.05). **(C)** The difference in m^{6}Ascore among the three immunophenotypes; the asterisk represents the statistical p-value (*P < 0.05; ****P < 0.0001). **(D)** Spearman correlation was used to analyze the relationship between the m^{6}Ascore and known gene characteristics in the IMvigor 210 cohort. The larger the circle, higher the correlation. **(E)** KM curve showing the effect of m^{6}Ascore on OS in the IMvigor210 cohort. **(F)** Using the SubMAP algorithm, we predicted response to the anti-PD1 and anti- cytotoxic T-lymphocyte-associated protein 4 (CTLA4) immunotherapy in the groups with high and low m^{6}A score. High IC score group may respond better to the PD-1 treatment (Bonferroni-corrected $P = 0.03$).

poor prognosis (P = 0.032, **Figure 8E**). Using the SubMAP algorithm, we predicted response to the anti-PD1 and anti-cytotoxic T-lymphocyte-associated protein 4 (CTLA4) immunotherapy in the groups with high and low m^{6}A score. High m^{6}Ascore group may respond better to the PD-1 treatment (Bonferroni-corrected $P = 0.03$)

FTO Might Play an Important Role in Anti-PD-L1 Immune Checkpoint Therapy

The results from our data analysis showed that patients with high expression of *FTO* had a poor prognosis in the IMvigor210 cohort (p = 0.0035; **Figure 9A**) and there were differences in *FTO* expression in the three groups (**Figure 9B**). We also queried the predictive value of *FTO* expression in the cohort for anti-PD-L1 immunotherapy and found that there was a significant difference in *FTO* expression between non-responders and objective remission groups. Non-responsive patients showed significantly higher *FTO* expression (**Figure 9C**), suggesting that *FTO* may play an important role in the anti-PD-L1 treatment of bladder cancer. Upon further examination, *FTO* expression was positively correlated with the EMT signaling pathway and negatively correlated with the DDR/cell cycle, nucleotide excision repair, Fanconi anemia pathway, and other signaling pathways (**Figure 9D**), and additionally, was negatively correlated with the protein level of PD-L1 in immune cells (**Figure 9E**). *FTO* had no significant correlation with the total PD-L1 level in tumor cells

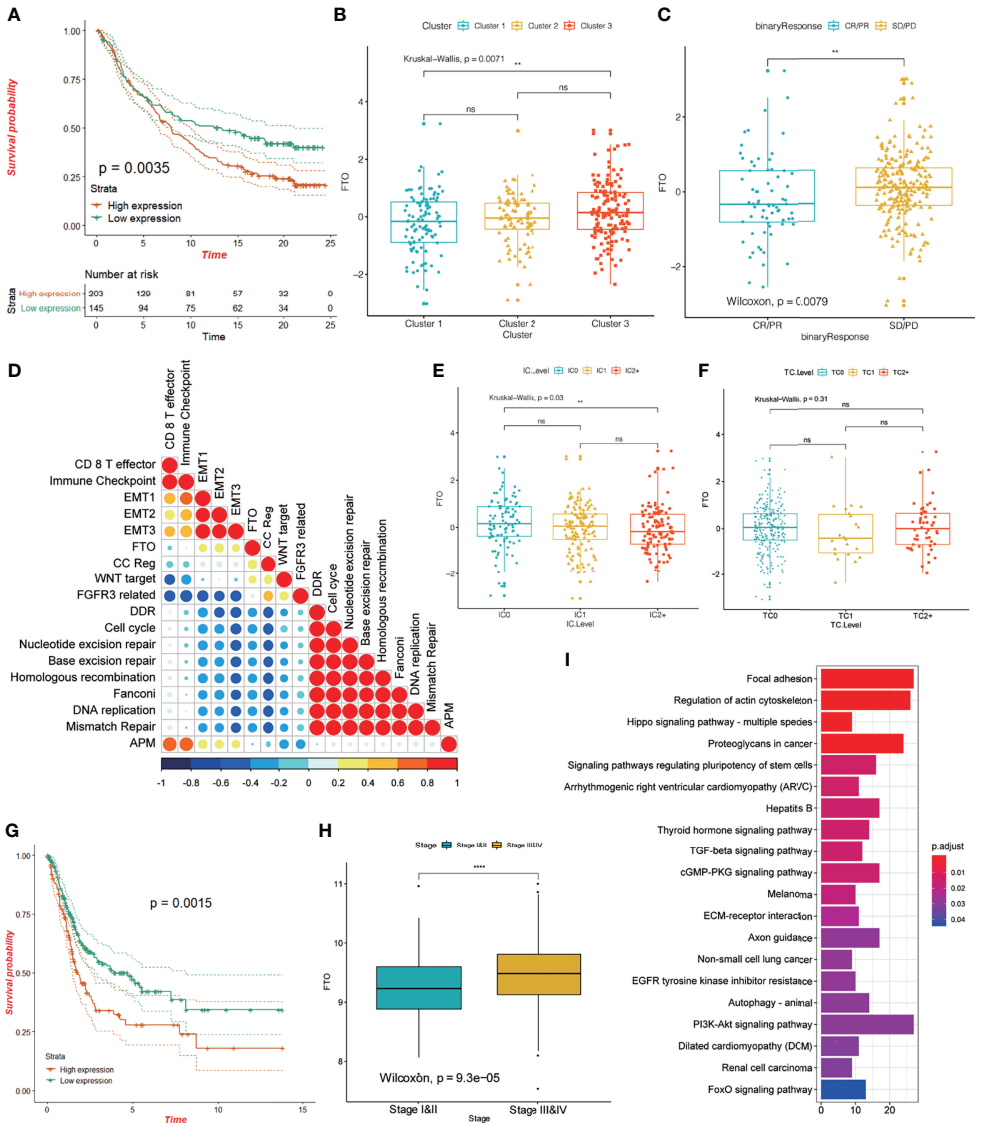


FIGURE 9 | Characteristics of *FTO* in the TCGA-BLCA cohort and anti-PD-L1 treatment cohort. **(A)** KM curve showing the effect of *FTO* on OS in the IMvigor 210 cohort. **(B)** The difference in *FTO* expression among the three different m^6A modification patterns in the IMvigor 210 cohort; the asterisk represents the statistical p-value (**P < 0.01; ****P < 0.0001, ns P > 0.05). **(C)** The difference in *FTO* expression between responders (CR/PR) and non-responders (SD/PD) in the IMvigor 210 cohort; the asterisk represents the statistical p-value (**P < 0.01; ****P < 0.0001). **(D)** Spearman's correlation was used to analyze the correlation between *FTO* expression and known gene characteristics in the IMvigor 210 cohort. Blue, negatively correlated; orange, positively correlated; and the larger circle indicates a higher correlation. **(E, F)** The relationship between *FTO* expression and PD-L1 expression in immune cells (IC), and PD-L1 expression in tumor cells (TC). The asterisk represents the statistical p-value (**P < 0.01; ****P < 0.0001, ns P > 0.05). **(G)** KM curve showing the effect of *FTO* on OS in the TCGA-BLCA cohort. **(H)** Box plot showing the difference in *FTO* expression between stage I and II and stage III and IV; the asterisk represents the statistical p-value (**P < 0.01; ****P < 0.0001). **(I)** Pearson correlation was used to calculate the correlation between *FTO* and all other protein-coding genes, and genes with a correlation coefficient R >= 0.03, and p < 0.05 were selected as *FTO*-related genes. These genes were enriched by KEGG signaling pathway analysis to study *FTO* function.

(**Figure 9F**). The analysis of data from the TCGA database showed that the prognosis of patients with a high expression of *FTO* was worse (p = 0.0015; **Figure 9G**), and *FTO* expression was higher in patients with a high stage of bladder cancer (**Figure 9H**). Additionally, the enrichment results of *FTO*-related gene pathways showed that *FTO* may be involved in the regulation of focal adhesion, the Hippo signaling pathway, the TGF-β signaling pathway, and other signal pathways (**Figure 9I**). Previous studies have confirmed that the activation of EMT and TGF-β related pathways reduces T cell migration to tumors and weakens their tumor-killing effect (5, 51). Therefore, *FTO* may play an important role in the occurrence and development of bladder cancer, the efficacy of anti-PD-L1 immune checkpoint therapy, and might be useful for predicting the prognosis.

FTO Could Be Involved in the Occurrence and Development of Bladder Cancer

We examined the nuclear, cytoplasmic, and overall expression levels of FTO in nine human bladder cancer cell lines: BIU87 cells, 5637 cells, T24 cells, EJ cells, RT4 cells, J82 cells, UM-UC-3 cells, TCCSUP cells, and human bladder epithelial immortalized SV-huv-1 cells (**Figure 10A**). Using immunofluorescence two cell lines with high FTO expression (EJ and T24 cells) and two cell lines with low FTO expression (BIU87 and RT4) were identified. We found that FTO was expressed in both cytoplasm and nucleus of these cell lines (**Figure 10B**). Subsequently, we knocked down the FTO in EJ and RT4 using siRNA. CCK-8 examination revealed that cell proliferation was reduced in the si-FTO group (**Figure 10C**), and transwell assays showed reduced cell invasion in the si-FTO group (**Figure 10D**). Flow cytometry revealed increased apoptosis after the knockdown of FTO (**Figure 10E**). The level of total cellular FTO-m^{6}A enzyme activity was significantly increased (**Figure 10F**), and total FTO protein was decreased in the si-FTO group (**Figure 10G**). These results confirm the critical role of FTO in bladder cancer.

According to our previous study (53), we confirmed the existence of important modification sites K216 for FTO protein, including K216R, K216H, K216S, and K216E. We constructed plasmids and transfected them into BIU87 and RT4 cells, as well as detected the expression of FTO protein in each group by WB (Western blot) (**Figure 11A**). The apoptosis was increased in the FTO-MT (K216H) and MT (K216E) groups (**Figure 11B**), and the cell invasion was significantly reduced in the FTO-MT (K216H) and MT (K216E) groups as observed by

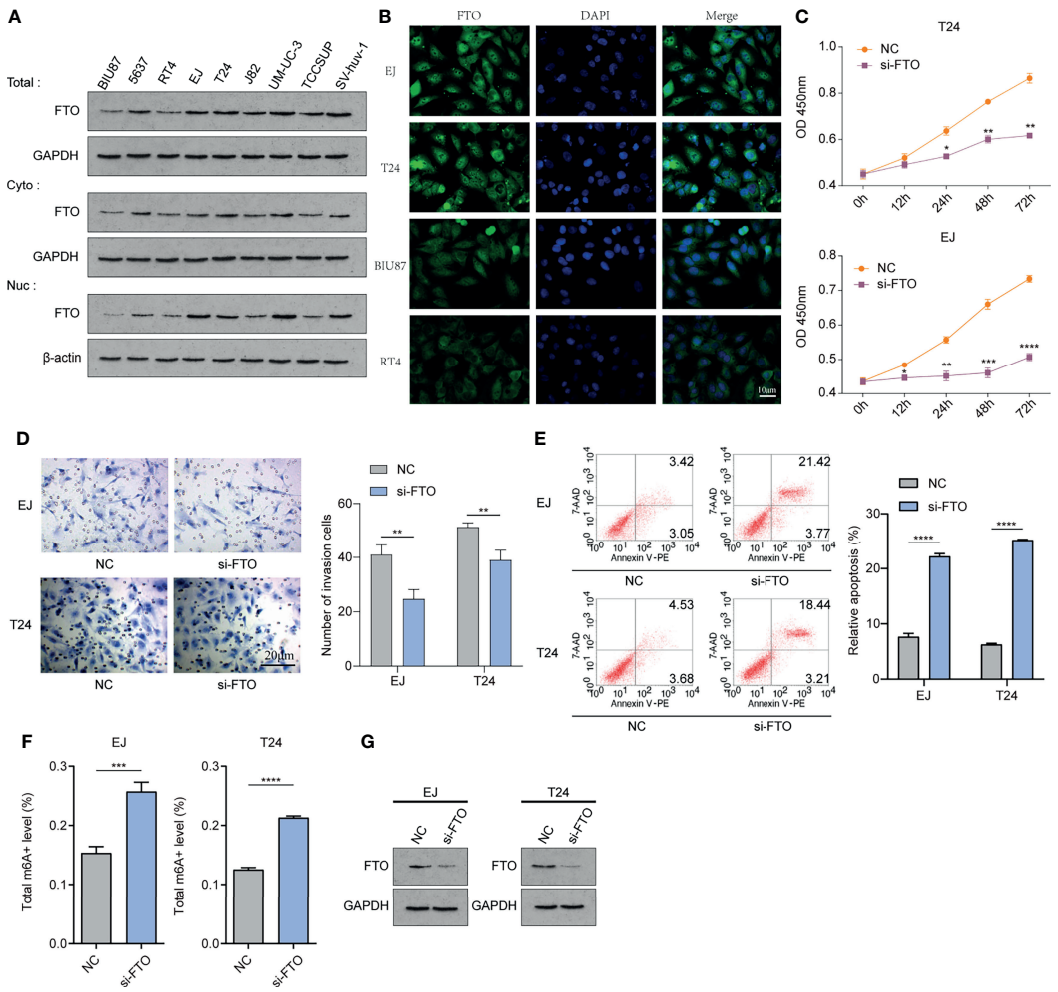


FIGURE 10 | FTO could be involved in the occurrence and development of bladder cancer *in vitro*. **(A)** Western Blot method to detect nuclear, cytoplasmic, and overall expression levels in BIU87 cells, 5637 cells, T24 cells, EJ cells, RT4 cells, J82 cells, UM-UC-3 cells, TCCSUP cells, and human bladder epithelial immortalized SV-huv-1 cells. **(B)** IF immunofluorescence method to detect the cellular localization of FTO protein. **(C)** Cell Counting Kit-8(CCK-8) to detect the proliferation level of each group of cells. **(D)** Transwell method to observe the invasion level of each group of cells. **(E)** Flow cytometry method to detect apoptosis in each group. **(F)** Detection of m^{6}A enzyme activity level in each group. **(G)** Western Blot method to detect the FTO expression level after siRNA knockdown. The histogram data for each group is the average of three independent replicates; bars represent mean ± SD; *P < 0.05, **P < 0.01, ***P < 0.001, ****P < 0.0001.

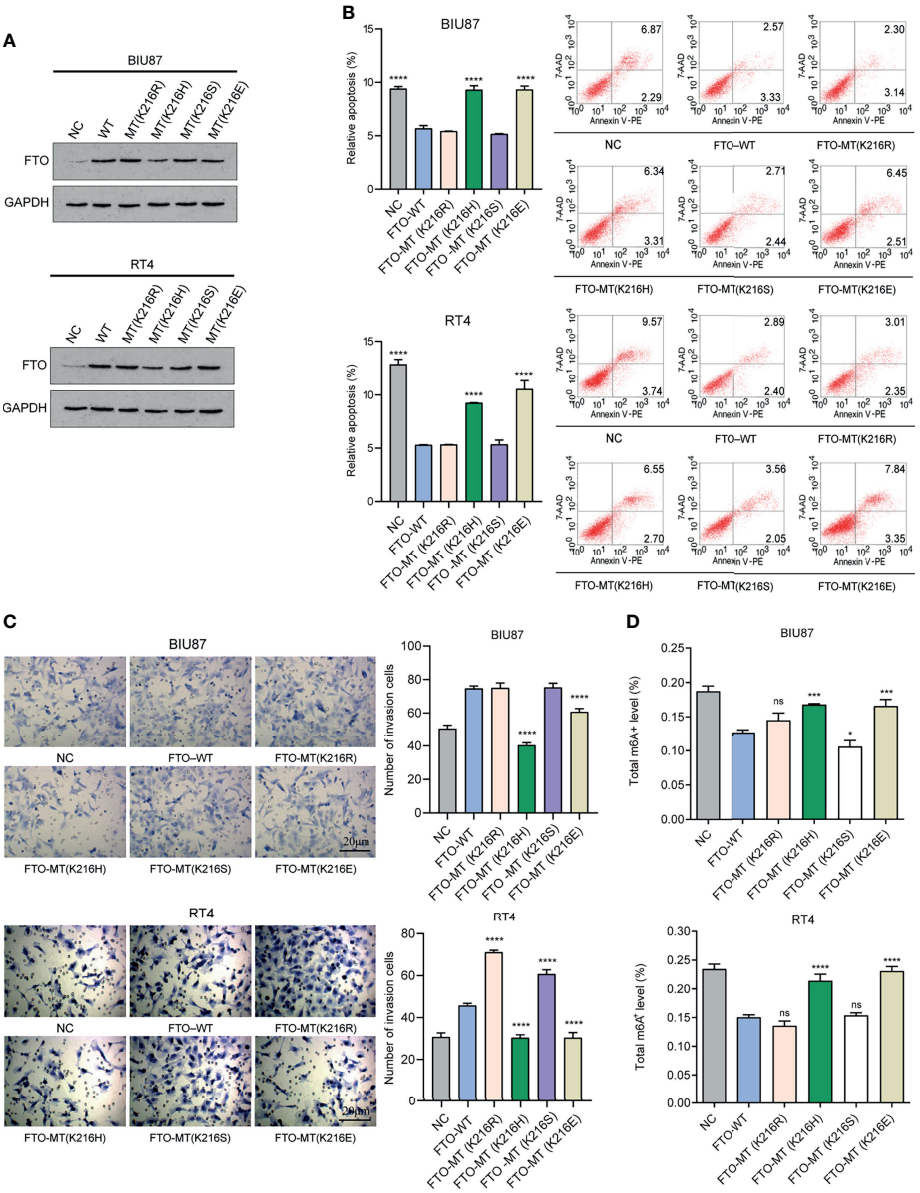


FIGURE 11 | K216H and K216E are the potential important targets for regulating FTO. **(A)** Western Blot method to detect the expression level of FTO in each group. **(B)** Flow cytometry method to detect apoptosis in each group of cells. **(C)** Transwell method to observe the level of cell invasion in each group. **(D)** Detection of m^6A enzyme activity in each group. The histogram data for each group is the average of three independent replicates; bars represent mean ± SD; *P < 0.05, ***P < 0.001, ****P < 0.0001, ns P > 0.05.

transwell assay (**Figure 11C**), and the total FTO-m^6A enzyme activity level was significantly increased in these two groups (**Figure 11D**). The above results suggest that K216H and K216E are the important targets for regulating FTO in the future.

DISCUSSION

More than 150 RNA modifications have been identified in all organisms, including 5-methylcytosine (m^5C), N6-methyladenosine (m^6A), and N1-methyladenosine (m^1A), of which the m^6A RNA methylation is considered to be the most prominent and abundant form of internal modification in eukaryotic cells (54). The study of m^6A modification in cancer is a new field of cancer research, which may reveal a new layer of epigenetic regulation in cancer, and provide new insights into the tumorigenesis, immune response, and the molecular mechanisms underlying drug resistance during therapy. Additionally, it may lead to the development of new, effective treatments (55) through the use of effective inhibitors targeting

maladjusted m^{6}A regulatory factors alone (or editing targeted mutant or dysfunctional m^{6}A sites through targeted transcriptomics), or in combination with other therapies. Targeting the m^{6}A modification may have a strong therapeutic potential for the treatment of all types of cancers, especially those that are resistant to existing treatments (56).

Due to technical and resource constraints, most studies have focused on a single TME immune cell type or a single m^{6}A. The overall infiltration characteristics of the TME mediated by the combined effects of multiple m^{6}A regulators have not been widely analyzed (57, 58). The modification of m^{6}A is a reversible process that is affected by various writers, erasers, and readers. In this study, we explored the effects of multiple m^{6}A regulators on the infiltration of immune cells in the TME of bladder cancer, the molecular mechanisms underlying m^{6}A modification in bladder carcinogenesis, the immune response, and the drug resistance of immune checkpoint inhibitors. We also provide new insights into the role of m^{6}A modification patterns in TME cell infiltration and developing more effective immunotherapy strategies.

We classified patients with bladder cancer based on the expression of 23 m^{6}A regulatory molecules and identified three different m^{6}A modification patterns. We found that Cluster 2 showed unique specificity compared with the other two types. A quantification of 28 immune cells in the immune microenvironment of bladder cancer using the ssGSEA algorithm showed that Cluster 2 had a low level of immune cell infiltration characterized by immune inhibition, which corresponds to the immune desert phenotype. Furthermore, an analysis performed using the ESTIMATE algorithm showed that the stromal and immune scores in Cluster 2 were lower than the other two subtypes, which corroborates our previous results. The expression of immune checkpoint and CD8$^+$T cell markers were lower in Cluster 2 than in the other two groups, and studies have shown that the expression of these markers is highly sensitive to immune checkpoint inhibitors (52). Thus, different m^{6}A modification patterns are significantly related to immune activation, and a comprehensive evaluation of the m^{6}A modification patterns will enable the understanding of the characteristics of TME cell infiltration. An analysis of DEGs between the different m^{6}A modification patterns uncovered m^{6}A-related signaling pathway genes. These were mainly enriched in the biological pathways related to the matrix and immune activation. In the anti-PD-L1 treatment cohort, we identified three different m^{6}A modification patterns and found significant differences in gene expression and mutations in biological pathway genes associated with the three subtypes of bladder cancer. We constructed a scoring system to quantify and evaluate the m^{6}A modification level in a single tumor and found that a high m^{6}Ascore was related to poor prognosis in the TCGA and anti-PD-L1 cohorts. Patients with a high or low m^{6}Ascore showed differences in immune cell infiltration in the tumor immune microenvironment. A GSEA signaling pathway analysis indicated that the high and low m^{6}Ascore are mainly enriched in the matrix and immune-related signaling pathways. Together, these results indicate that the m^{6}A score is a reliable tool for the comprehensive evaluation of m^{6}A modification patterns in tumors in individuals, and to determine the mode of infiltration in the TME. The expression and gene changes for m6A regulatory factors are related to a variety of biological processes, especially the matrix and immune activation. Our findings may provide new impetus for improving the clinical response of patients with bladder cancer to immunotherapy, the identification of different immunophenotypes in bladder cancer, and promoting individualized immunotherapy.

The role of *FTO* in cancer has recently garnered increasing attention. Previous studies conducted by our team have shown that *FTO*-mediated m^{6}A modification plays an important role in hepatocellular carcinoma, and the SIRT1 deacetylase can play a carcinogenic role by down-regulating *FTO*. *FTO* is an RNA demethylase that can remove the methylation of m^{6}A in mRNA both *in vitro* and *in vivo* (59, 60). *FTO* has catalytic demethylation activity for both cap-m^{6}Am and internal m^{6}A. As the abundance of m^{6}A in mRNA is much higher than that of its preferred binding target m^{6}Am, the main target of *FTO* is m^{6}A (61). Reports indicate that the *FTO*-mediated demethylation of cap-m^{6}Am leads to mRNA degradation (62), but the evidence for this is inconsistent. PCIF1 is the cap-m^{6}Am methyltransferase, which processes cap-m^{6}A alone but not internal m^{6}A. Reports indicate that the cap-m^{6}Am added by PCIF1 does not change the level of gene expression or the stability of transcripts (63–65). Additionally, studies (66) have found that the spatial distribution of *FTO* can also play a regulatory role. The N-terminus of FTO has an NLS, which can be partially distributed in the nucleus and the cytoplasm, and the distribution of FTO is different in different cell lines, its role and regulation being affected by the environment. Yang et al. (20) have shown that the induction of *FTO* can be used as an adaptive mechanism to combat metabolic stress in melanoma cells, thus increasing their proliferation, invasion, and migration, and promoting the tumorigenesis and development of melanoma in mice. Further, the authors showed that an *FTO* knockout can increase m^{6}A methylation in key oncogenic melanoma cells, including the loci for PD-1 (*PDCD1*), *CXCR4*, and *SOX10*. The inhibition of *FTO* makes melanoma cells sensitive to interferon-γ (IFN-γ) and anti-PD-1 therapy in mice, indicating that *FTO* plays an important role in promoting the occurrence of melanoma and anti-PD-1 drug resistance. The role of m^{6}A involvement with *FTO* in bladder cancer had not been reported, and we found that in the TCGA and IMvigor210 cohorts, patients with high *FTO* expression had a poor prognosis, and the expression of *FTO* was higher in patients with a higher stage of bladder cancer.

In addition, we analyzed the predictive value of *FTO* expression in the cohort subjected to anti-PD-L1 immunotherapy, and found that there was a significant difference in *FTO* expression between the non-responders and the objective remission group. The level of *FTO* expression in the patients non-responsive to anti-PD-L1 therapy was significantly higher than in patients in remission. The data showed that *FTO* expression was negatively correlated with the protein level of PD-L1 in immune cells (**Figure 9E**), was

positively correlated with the EMT signaling pathway, and negatively correlated with DDR, cell cycle, nucleoside exercise repair, Fanconi anemia pathway, and other signaling pathways. The enrichment of *FTO*-related gene pathways indicated that *FTO* might be involved in the regulation of focal adhesion/Hippo signaling pathway/TGF-β signaling, these results suggest that *FTO* plays an important role in bladder cancer. The combination of *FTO* targeted regulation and anti-PD-L1 blockers may have great therapeutic potential for reducing the resistance of bladder cancer to immunotherapy. Thus, this study furthers the understanding of the regulation of m^6A modification in the tumor immune microenvironment of the bladder cancer and contributes to the development of new predictive indicators, drug combination strategies, and new immunotherapeutic strategies for cancer immunotherapy. However, its specific role and mechanism need further experimental study.

In this study, we systematically analyzed the mutation and correlation of 23 kinds of m^6A regulatory factors in bladder cancer, and their effects on OS and immune invasion, We found three different patterns of m^6A modification and compared them with other important molecular types of bladder cancer, such as MDA, Lund, and Baylor, the effects of the three kinds of m^6A modification patterns on the mutation characteristics, clinicopathological characteristics, gene expression, immune cell infiltration level, and gene expression level of immune checkpoint regulators were comprehensively analyzed. Further, we investigated the effect of m^6A modification mode on the therapeutic efficacy of bladder cancer immune checkpoint inhibitor anti-PD-L1. Our results confirmed that m^6A methylation is involved in the process of immune cell recruitment in the TME of bladder cancer, and may affect the efficacy of anti-PD-L1 therapy. In addition, we established a method to quantify the level of m^6A modification (m6Ascore), which we found to be an important and powerful prognostic biomarker and predictor for bladder cancer. Thus, this study furthers the understanding of the regulation of m^6A modification in the tumor immune microenvironment of bladder cancer and contributes to the potential development of new predictive indicators, drug combination strategies, and new immunotherapeutic strategies for cancer immunotherapy.

CONCLUSION

This study comprehensively recognized the role of m^6A methylation modification on the invasion characteristics of bladder cancer immune microenvironment cells and the effect on the anti-PD-L1 treatment for bladder cancer. The difference in m^6A modification mode is an important factor indicating the heterogeneity and complexity of the tumor microenvironment and the immunotherapy impact. The m^6A modification mode helps decipher the molecular mechanisms underlying the immune microenvironment regulation in bladder cancer and provides new predictive indicators, possible auxiliary targets, and directions for guiding more effective immunotherapy strategies in the future.

DATA AVAILABILITY STATEMENT

The datasets presented in this study can be found in online repositories. The names of the repository/repositories and accession number(s) can be found in the article/**Supplementary Material**.

ETHICS STATEMENT

The experimental protocol was established according to the ethical guidelines of the Helsinki Declaration and was approved by the Human Ethics Committee of the Ethical Review Committee of the Third Xiangya Hospital of Central South University. Written informed consent was obtained from individuals or guardians of the participants.

AUTHOR CONTRIBUTIONS

XC and KC designed the study. XC and HD analyzed and interpreted the data. HD and XC wrote this manuscript. HD, FT, MZ, and DS conducted the experiments and edited and revised the manuscript. All authors have seen and approved the final version of the manuscript.

FUNDING

This work was supported by The Science and Technology Innovation Program of Hunan Province (2020RC2066), Hunan Provincial Natural Science Foundation of China (2020JJ5335), Science and Technology Foundation of Changsha City (kq1907127), Health Commission Science Foundation of Hunan Province (20200957), Hunan Cancer Hospital Climb Plan (QH201904), The Science and Technology Innovation Program of Hunan Province (2021RC2041), and The National Science Foundation of China (81874137).

ACKNOWLEDGMENTS

We thank our colleagues in the Department of Laboratory Medicine for helpful discussions and valuable assistance. We thank Dr. Jianming Zeng (University of Macau), and all the members of his bioinformatics team, biotrainee, for generously sharing their experience and codes. This work was carried out in part using computing resources at the High Performance Computing Center of Central South University.

SUPPLEMENTARY MATERIAL

The Supplementary Material for this article can be found online at: https://www.frontiersin.org/articles/10.3389/fonc.2022.820242/full#supplementary-material

Supplementary Figure 1 | Three m^{6}A modification patterns were identified in the TCGA-BLCA cohort through unsupervised clustering of 23 m^{6}A regulatory factors. **(A–D)** Consensus matrices of the TCGA-BLCA cohort for k = 2-5. **(E)** Waterfall diagram showing the influence of the three m^{6}A modification patterns on the mutation of the top 20 genes in the TCGA-BLCA cohort. Each column represents the patient, each color represents the mutation type, and gray indicates that there is no mutation in the gene in this sample. The bar graph above shows the TMB, and the number on the right shows the mutation frequency of each gene.

Supplementary Figure 2 | GISTIC analysis of foci of recurrent amplification and deletion. Detailed cytoband with focal amplification **(A)** and focal deletion **(B)** in Cluster 1, Cluster 2, and Cluster 3 generated with GISTIC 2.0 software. The q value of each locus is plotted horizontally.

Supplementary Figure 3 | Copy number alterations across three m6A modification patterns. Copy number Gistic score **(A)** and Copy number profiles **(B)** for Cluster 1, Cluster 2, and Cluster 3, with gains are shown in dark red and losses in midnight blue. Gene segments are placed according to their location on chromosomes, ranging from chromosome 1 to chromosome 22.

Supplementary Figure 4 | Difference of immune cell infiltration characteristics in tumor immune microenvironment for the three m^{6}A modification patterns in the TCGA-BLCA cohort. **(A)** The box plot shows the difference for 28 immune cell infiltration levels in the three m^{6}A modification patterns; the asterisk represents the statistical p-value ($^{*}P < 0.05$; $^{**}P < 0.01$; $^{***}P < 0.001$, $^{****}P < 0.0001$). **(B, C)** The differences in the antitumor immunity score and pro-tumor immunity score among three kinds of m^{6}A modification patterns; the asterisk represents the statistical p-value.

Supplementary Figure 5 | Signaling pathway enrichment analysis. **(A, B)** In the TCGA-BLCA cohort, there are three different m^{6}A modification patterns, and different gene signaling pathways are enriched; the same enrichment network has its nodes displayed as pies. Each pie sector is proportional to the number of hits that originated from a gene list. Color code for the pie sector represents a gene list and is consistent with the colors used for the table rows in the slide. The same enrichment network has its nodes colored by p-value, as shown in the legend. Darker color indicates more statistically significant nodes (see legend for p-value ranges). **(C–E)** The enrichment analysis of Gene Ontology (GO) signaling pathways in the high and low m^{6}A groups was divided into three parts: C, cellular component (CC); D, biological process (BP); E, molecular function (MF). **(F)** Enrichment analysis of KEGG signaling pathways of DEGs in high and low m^{6}A groups.

Supplementary Table 1 | Pearson correlation of 23 m^{6}A regulatory factors

Supplementary Table 2 | Immune cell marker genes

Supplementary Table 3 | Infiltration levels of 28 immune cells and anti-tumor immunity score and pro-tumor immunity scores of 407 samples in the TCGA-BLCA cohort

Supplementary Table 4 | IMvigor 210 cohort clinical information and important gene set score

REFERENCES

1. Herbst RS, Soria JC, Kowanetz M, Fine GD, Hamid O, Gordon MS, et al. Predictive Correlates of Response to the Anti-PD-L1 Antibody MPDL3280A in Cancer Patients. *Nature* (2014) 515:563–7. doi: 10.1038/nature14011
2. Inman BA, Longo TA, Ramalingam S, Harrison MR. Atezolizumab: A PD-L1-Blocking Antibody for Bladder Cancer. *Clin Cancer Res* (2017) 23:1886–90. doi: 10.1158/1078-0432.CCR-16-1417
3. Powles T, Eder JP, Fine GD, Braiteh FS, Loriot Y, Cruz C, et al. MPDL3280A (Anti-PD-L1) Treatment Leads to Clinical Activity in Metastatic Bladder Cancer. *Nature* (2014) 515:558–62. doi: 10.1038/nature13904
4. Davis AA, Patel VG. The Role of PD-L1 Expression as a Predictive Biomarker: An Analysis of All US Food and Drug Administration (FDA) Approvals of Immune Checkpoint Inhibitors. *J Immunother Cancer* (2019) 7(1):278. doi: 10.1186/s40425-019-0768-9
5. Gomez de Liano Lista A, van Dijk N, de Velasco Oria de Rueda G, Necchi A, Lavaud P, Morales-Barrera R, et al. Clinical Outcome After Progressing to Frontline and Second-Line Anti-PD-1/PD-L1 in Advanced Urothelial Cancer. *Eur Urol* (2020) 77:269–76. doi: 10.1016/j.eururo.2019.10.004
6. Wolacewicz M, Hrynkiewicz R, Grywalska E, Suchojad T, Leksowski T, Rolinski J, et al. Immunotherapy in Bladder Cancer: Current Methods and Future Perspectives. *Cancers (Basel)* (2020) 12(5):1181. doi: 10.3390/cancers12051181
7. Li Z, Zhu L, Sun H, Shen Y, Hu D, Wu W, et al. Fluorine Assembly Nanocluster Breaks the Shackles of Immunosuppression to Turn the Cold Tumor Hot. *Proc Natl Acad Sci USA* (2020) 117(52):32962–9. doi: 10.1073/pnas.2011297117
8. Schneider AK, Chevalier MF, Derre L. The Multifaceted Immune Regulation of Bladder Cancer. *Nat Rev Urol* (2019) 16:613–30. doi: 10.1038/s41585-019-0226-y
9. Chen X, Chen H, He D, Cheng Y, Zhu Y, Xiao M, et al. Analysis of Tumor Microenvironment Characteristics in Bladder Cancer: Implications for Immune Checkpoint Inhibitor Therapy. *Front Immunol* (2021) 12:672158. doi: 10.3389/fimmu.2021.672158
10. Li Z, Wang Y, Shen Y, Qian C, Oupicky D, Sun M. Targeting Pulmonary Tumor Microenvironment With CXCR4-Inhibiting Nanocomplex to Enhance Anti-PD-L1 Immunotherapy. *Sci Adv* (2020) 6(20):eaaz9240. doi: 10.1126/sciadv.aaz9240
11. Chen X, Chen H, Yao H, Zhao K, Zhang Y, He D, et al. Turning Up the Heat on non-Immunoreactive Tumors: Pyroptosis Influences the Tumor Immune Microenvironment in Bladder Cancer. *Oncogene* (2021) 40(45):6381–93. doi: 10.1038/s41388-021-02024-9
12. Dai D, Wang H, Zhu L, Jin H, Wang X. N6-Methyladenosine Links RNA Metabolism to Cancer Progression. *Cell Death Dis* (2018) 9:124. doi: 10.1038/s41419-017-0129-x
13. Tuncel G, Kalkan R. Importance of m N (6)-Methyladenosine (m (6)A) RNA Modification in Cancer. *Med Oncol* (2019) 36:36. doi: 10.1007/s12032-019-1260-6
14. Malla S, Melguizo-Sanchis D, Aguilo F. Steering Pluripotency and Differentiation With N (6)-Methyladenosine RNA Modification. *Biochim Biophys Acta Gene Regul Mech* (2019) 1862:394–402. doi: 10.1016/j.bbagrm.2018.10.013
15. Zhang Z, Luo K, Zou Z, Qiu M, Tian J, Sieh L, et al. Genetic Analyses Support the Contribution of mRNA N (6)-Methyladenosine (M (6)A) Modification to Human Disease Heritability. *Nat Genet* (2020) 52(9):939–49. doi: 10.1038/s41588-020-0644-z
16. Wang S, Sun C, Li J, Zhang E, Ma Z, Xu W, et al. Roles of RNA Methylation by Means of N (6)-Methyladenosine (m (6)A) in Human Cancers. *Cancer Lett* (2017) 408:112–20. doi: 10.1016/j.canlet.2017.08.030
17. Li HB, Tong J, Zhu S, Batista PJ, Duffy EE, Zhao J, et al. m (6)A mRNA Methylation Controls T Cell Homeostasis by Targeting the IL-7/STAT5/SOCS Pathways. *Nature* (2017) 548:338–42. doi: 10.1038/nature23450
18. Wang H, Hu X, Huang M, Liu J, Gu Y, Ma L, et al. Mettl3-Mediated mRNA m (6)A Methylation Promotes Dendritic Cell Activation. *Nat Commun* (2019) 10:1898. doi: 10.1038/s41467-019-09903-6
19. Han D, Liu J, Chen C, Dong L, Liu Y, Chang R, et al. Anti-Tumour Immunity Controlled Through mRNA m6A Methylation and YTHDF1 in Dendritic Cells. *Nature* (2019) 566(7751):270–4. doi: 10.1038/s41586-019-0916-x
20. Yang S, Wei J, Cui YH, Park G, Shah P, Deng Y, et al. m (6)A mRNA Demethylase FTO Regulates Melanoma Tumorigenicity and Response to Anti-PD-1 Blockade. *Nat Commun* (2019) 10:2782. doi: 10.1038/s41467-019-10669-0
21. Mariathasan S, Turley SJ, Nickles D, Castiglioni A, Yuen K, Wang YL, et al. TGF Beta Attenuates Tumour Response to PD-L1 Blockade by Contributing to Exclusion of T Cells. *Nature* (2018) 554(7693):544–8. doi: 10.1038/nature25501

22. Rosenberg JE, Hoffman-Censits J, Powles T, van der Heijden MS, Balar AV, Necchi A, et al. Atezolizumab in Patients With Locally Advanced and Metastatic Urothelial Carcinoma Who Have Progressed Following Treatment With Platinum-Based Chemotherapy: A Single-Arm, Multicentre, Phase 2 Trial. *Lancet* (2016) 387:1909–20. doi: 10.1016/S0140-6736(16)00561-4
23. Shi HL, Wei JB, He C. Where, When, and How: Context-Dependent Functions of RNA Methylation Writers, Readers, and Erasers. *Mol Cell* (2019) 74:640–50. doi: 10.1016/j.molcel.2019.04.025
24. Yang Y, Hsu PJ, Chen YS, Yang YG. Dynamic Transcriptomic m (6)A Decoration: Writers, Erasers, Readers and Functions in RNA Metabolism. *Cell Res* (2018) 28:616–24. doi: 10.1038/s41422-018-0040-8
25. Wilkerson MD, Hayes DN. ConsensusClusterPlus: A Class Discovery Tool With Confidence Assessments and Item Tracking. *Bioinformatics* (2010) 26:15721573. doi: 10.1093/bioinformatics/btq170
26. Mo Q, Nikolos F, Chen F, Tramel Z, Lee YC, Hayashi K, et al. Prognostic Power of a Tumor Differentiation Gene Signature for Bladder Urothelial Carcinomas. *J Natl Cancer Inst* (2018) 110:448–59. doi: 10.1093/jnci/djx243
27. Damrauer JS, Hoadley KA, Chism DD, Fan C, Tiganelli CJ, Wobker SE, et al. Intrinsic Subtypes of High-Grade Bladder Cancer Reflect the Hallmarks of Breast Cancer Biology. *Proc Natl Acad Sci USA* (2014) 111:3110–5. doi: 10.1073/pnas.1318376111
28. Choi W, Porten S, Kim S, Willis D, Plimack ER, Hoffman-Censits J, et al. Identification of Distinct Basal and Luminal Subtypes of Muscle-Invasive Bladder Cancer With Different Sensitivities to Frontline Chemotherapy. *Cancer Cell* (2014) 25:152–65. doi: 10.1016/j.ccr.2014.01.009
29. Marzouka NA, Eriksson P, Rovira C, Liedberg F, Sjodahl G, Hoglund M. A Validation and Extended Description of the Lund Taxonomy for Urothelial Carcinoma Using the TCGA Cohort. *Sci Rep* (2018) 8(1):3737. doi: 10.1038/s41598-018-22126-x
30. Robertson AG, Kim J, Al-Ahmadie H, Bellmunt J, Guo G, Cherniack AD, et al. Comprehensive Molecular Characterization of Muscle-Invasive Bladder Cancer. *Cell* (2017) 171:540–56.e525. doi: 10.1016/j.cell.2017.09.007
31. Rebouissou S, Bernard-Pierrot I, de Reynies A, Lepage ML, Krucker C, Chapeaublanc E, et al. EGFR as a Potential Therapeutic Target for a Subset of Muscle-Invasive Bladder Cancers Presenting a Basal-Like Phenotype. *Sci Trans Med* (2014) 6(244):244ra91. doi: 10.1126/scitranslmed.3008970
32. Kamoun A, de Reynies A, Allory Y, Sjodahl G, Robertson AG, Seiler R, et al. A Consensus Molecular Classification of Muscle-Invasive Bladder Cancer. *Eur Urol* (2020) 77:420–33. doi: 10.1016/j.eururo.2019.09.006
33. Jia Q, Wu W, Wang Y, Alexander PB, Sun C, Gong Z, et al. Local Mutational Diversity Drives Intratumoral Immune Heterogeneity in non-Small Cell Lung Cancer. *Nat Commun* (2018) 9:5361. doi: 10.1038/s41467-018-07767-w
34. Newman AM, Liu CL, Green MR, Gentles AJ, Feng W, Xu Y, et al. Robust Enumeration of Cell Subsets From Tissue Expression Profiles. *Nat Methods* (2015) 12:453–7. doi: 10.1038/nmeth.3337
35. Ritchie ME, Phipson B, Wu D, Hu Y, Law CW, Shi W, et al. Limma Powers Differential Expression Analyses for RNA-Sequencing and Microarray Studies. *Nucleic Acids Res* (2015) 43:e47. doi: 10.1093/nar/gkv007
36. Zhou Y, Zhou B, Pache L, Chang M, Khodabakhshi AH, Tanaseichuk O, et al. Metascape Provides a Biologist-Oriented Resource for the Analysis of Systems-Level Datasets. *Nat Commun* (2019) 10:1523. doi: 10.1038/s41467-019-09234-6
37. Castro MA, de Santiago I, Campbell TM, Vaughn C, Hickey TE, Ross E, et al. Regulators of Genetic Risk of Breast Cancer Identified by Integrative Network Analysis. *Nat Genet* (2016) 48:12–21. doi: 10.1038/ng.3458
38. Yu G, Wang LG, Han Y, He QY. clusterProfiler: An R Package for Comparing Biological Themes Among Gene Clusters. *OMICS* (2012) 16:284–7. doi: 10.1089/omi.2011.0118
39. Zeng Q, Liu J, Cao P, Li J, Liu X, Fan X, et al. Inhibition of REDD1 Sensitizes Bladder Urothelial Carcinoma to Paclitaxel by Inhibiting Autophagy. *Clin Cancer Res* (2018) 24:445–59. doi: 10.1158/1078-0432.CCR-17-0419
40. Hazra A, Gogtay N. Biostatistics Series Module 3: Comparing Groups: Numerical Variables. *Indian J Dermatol* (2016) 61:251–60. doi: 10.4103/0019-5154.182416
41. DeGraff DJ, Cates JM, Mauney JR, Clark PE, Matusik RJ, Adam RM. When Urothelial Differentiation Pathways Go Wrong: Implications for Bladder Cancer Development and Progression. *Urol Oncol Seminars Original Invest* (2013) 31:802–11. doi: 10.1016/j.urolonc.2011.07.017
42. Choi W, Czemiak B, Ochoa A, Su XP, Siefker-Radtke A, Dinney C, et al. Intrinsic Basal and Luminal Subtypes of Muscle-Invasive Bladder Cancer. *Nat Rev Urol* (2014) 11:400–10. doi: 10.1038/nrurol.2014.129
43. Eriksson P, Aine M, Veerla S, Liedberg F, Sjodahl G, Hoglund M. Molecular Subtypes of Urothelial Carcinoma are Defined by Specific Gene Regulatory Systems. *BMC Med Genomics* (2015) 8:25. doi: 10.1186/s12920-015-0101-5
44. Breyer J, Wirtz RM, Laible M, Schlombs K, Erben P, Kriegmair MC, et al. ESR1, ERBB2, and Ki67 mRNA Expression Predicts Stage and Grade of non-Muscle-Invasive Bladder Carcinoma (NMIBC). *Virchows Archiv* (2016) 469:547–52. doi: 10.1007/s00428-016-2002-1
45. Dadhania V, Zhang M, Zhang L, Bondaruk J, Majewski T, Siefker-Radtke A, et al. Meta-Analysis of the Luminal and Basal Subtypes of Bladder Cancer and the Identification of Signature Immunohistochemical Markers for Clinical Use. *Ebiomedicine* (2016) 12:105–17. doi: 10.1016/j.ebiom.2016.08.036
46. Jones RT, Felsenstein KM, Theodorescu D. Pharmacogenomics: Biomarker-Directed Therapy for Bladder Cancer. *Urol Clinics North Am* (2016) 43:77–+. doi: 10.1016/j.ucl.2015.08.007
47. Lim S, Koh MJ, Jeong HJ, Cho NH, Choi YD, Cho DY, et al. Fibroblast Growth Factor Receptor 1 Overexpression Is Associated With Poor Survival in Patients With Resected Muscle Invasive Urothelial Carcinoma. *Yonsei Med J* (2016) 57:831–9. doi: 10.3349/ymj.2016.57.4.831
48. Liu RY, Zeng YY, Lei Z, Wang LQ, Yang HP, Liu ZY, et al. JAK/STAT3 Signaling is Required for TGF-Beta-Induced Epithelial-Mesenchymal Transition in Lung Cancer Cells. *Int J Oncol* (2014) 44:1643–51. doi: 10.3892/ijo.2014.2310
49. Gu GY, Gao TH, Zhang L, Chen XY, Pang Q, Wang YN, et al. NKAP Alters Tumor Immune Microenvironment and Promotes Glioma Growth *via* Notch1 Signaling. *J Exp Clin Cancer Res* (2019) 38(1):291. doi: 10.1186/s13046-019-1281-1
50. Karn T, Denkert C, Weber KE, Holtrich U, Hanusch C, Sinn BV, et al. Tumour Mutational Burden and Immune Infiltration as Independent Predictors of Response to Neoadjuvant Immune Checkpoint Inhibition in Early TNBC in GeparNuevo. *Ann Oncol* (2020) 31:S58–8. doi: 10.1016/j.annonc.2020.03.230
51. Gouin KH 3rd, Ing N, Plummer JT, Rosser CJ, Ben B, Cheikh C, et al. An N-Cadherin 2 Expressing Epithelial Cell Subpopulation Predicts Response to Surgery, Chemotherapy and Immunotherapy in Bladder Cancer. *Nat Commun* (2021) 12(1):4906. doi: 10.1038/s41467-021-25103-7
52. Chen X, Xu R, He D, Zhang Y, Chen H, Zhu Y, et al. CD8+ T Effector and Immune Checkpoint Signatures Predict Prognosis and Responsiveness to Immunotherapy in Bladder Cancer. *Oncogene* (2021) 40(43):6223–34. doi: 10.1038/s41388-021-02019-6
53. Liu X, Liu J, Xiao W, Zeng Q, Bo H, Zhu Y, et al. SIRT1 Regulates N (6) -Methyladenosine RNA Modification in Hepatocarcinogenesis by Inducing RANBP2-Dependent FTO SUMOylation. *Hepatology* (2020) 72(6):2029–50. doi: 10.1002/hep.31222
54. Liu J, Dou X, Chen C, Chen C, Liu C, Xu MM, et al. N (6)-Methyladenosine of Chromosome-Associated Regulatory RNA Regulates Chromatin State and Transcription. *Science* (2020) 367(6477):580–6. doi: 10.1126/science.aay6018
55. Zhou Z, Lv J, Yu H, Han J, Yang X, Feng D, et al. Mechanism of RNA Modification N6-Methyladenosine in Human Cancer. *Mol Cancer* (2020) 19 (1):104. doi: 10.1186/s12943-020-01216-3
56. Huang H, Weng H, Chen J. m (6)A Modification in Coding and Non-Coding RNAs: Roles and Therapeutic Implications in Cancer. *Cancer Cell* (2020) 37:270–88. doi: 10.1016/j.ccell.2020.02.004
57. Zhang B, Wu Q, Li B, Wang D, Wang L, Zhou YL. m (6)A Regulator-Mediated Methylation Modification Patterns and Tumor Microenvironment Infiltration Characterization in Gastric Cancer. *Mol Cancer* (2020) 19:53. doi: 10.1186/s12943-020-01170-0
58. He L, Li H, Wu A, Peng Y, Shu G, Yin G. Functions of N6-Methyladenosine and its Role in Cancer. *Mol Cancer* (2019) 18:176. doi: 10.1186/s12943-019-1109-9
59. Mauer J, Luo X, Blanjoie A, Jiao X, Grozhik AV, Patil DP, et al. Reversible Methylation of m (6)Am in the 5' Cap Controls mRNA Stability. *Nature* (2017) 541:371–5. doi: 10.1038/nature21022

60. Fu Y, Jia G, Pang X, Wang RN, Wang X, Li CJ, et al. FTO-Mediated Formation of N6-Hydroxymethyladenosine and N6-Formyladenosine in Mammalian RNA. *Nat Commun* (2013) 4:1798. doi: 10.1038/ncomms2822
61. Wei J, Liu F, Lu Z, Fei Q, Ai Y, He PC, et al. Differential m (6)A, m (6)Am, and m (1)A Demethylation Mediated by FTO in the Cell Nucleus and Cytoplasm. *Mol Cell* (2018) 71(6):973–85.e975. doi: 10.1016/j.molcel.2018.08.011
62. Zhang X, Wei LH, Wang Y, Xiao Y, Liu J, Zhang W, et al. Structural Insights Into FTO's Catalytic Mechanism for the Demethylation of Multiple RNA Substrates. *Proc Natl Acad Sci USA* (2019) 116(8):2919–24. doi: 10.1073/pnas.1820574116
63. Sendinc E, Valle-Garcia D, Dhall A, Chen H, Henriques T, Navarrete-Perea J, et al. PCIF1 Catalyzes M6am mRNA Methylation to Regulate Gene Expression. *Mol Cell* (2019) 75:620–30.e629. doi: 10.1016/j.molcel.2019.05.030
64. Boulias K, Toczydlowska-Socha D, Hawley BR, Liberman N, Takashima K, Zaccara S, et al. Identification of the m (6)Am Methyltransferase PCIF1 Reveals the Location and Functions of m (6)Am in the Transcriptome. *Mol Cell* (2019) 75(3):631–43.e638. doi: 10.1016/j.molcel.2019.06.006
65. Akichika S, Hirano S, Shichino Y, Suzuki T, Nishimasu H, Ishitani R, et al. Cap-Specific Terminal N (6)-Methylation of RNA by an RNA Polymerase II-Associated Methyltransferase. *Science* (2019) 363(6423):eaav0080. doi: 10.1126/science.aav0080
66. Sanchez-Pulido L, Andrade-Navarro MA. The FTO (Fat Mass and Obesity Associated) Gene Codes for a Novel Member of the Non-Heme Dioxygenase Superfamily. *BMC Biochem* (2007) 8:23. doi: 10.1186/1471-2091-8-23

Conflict of Interest: The authors declare that the research was conducted in the absence of any commercial or financial relationships that could be construed as a potential conflict of interest.

Publisher's Note: All claims expressed in this article are solely those of the authors and do not necessarily represent those of their affiliated organizations, or those of the publisher, the editors and the reviewers. Any product that may be evaluated in this article, or claim that may be made by its manufacturer, is not guaranteed or endorsed by the publisher.

Copyright © 2022 Deng, Tang, Zhou, Shan, Chen and Cao. This is an open-access article distributed under the terms of the Creative Commons Attribution License (CC BY). The use, distribution or reproduction in other forums is permitted, provided the original author(s) and the copyright owner(s) are credited and that the original publication in this journal is cited, in accordance with accepted academic practice. No use, distribution or reproduction is permitted which does not comply with these terms.

frontiers in Oncology

ORIGINAL RESEARCH
published: 07 March 2022
doi: 10.3389/fonc.2022.816706

APOBEC Mutational Signature and Tumor Mutational Burden as Predictors of Clinical Outcomes and Treatment Response in Patients With Advanced Urothelial Cancer

*Divya Natesan[1], Li Zhang[1], Henry J. Martell[2], Tanya Jindal[1], Patrick Devine[1], Bradley Stohr[1], Carlos Espinosa-Mendez[2], James Grenert[1], Jessica Van Ziffle[1], Nancy Joseph[1], Sarah Umetsu[1], Courtney Onodera[1], Michelle Turski[1], Emily Chan[1], Arpita Desai[1], Rahul Aggarwal[1], Anthony Wong[1], Sima Porten[1], Jonathan Chou[1], Terence Friedlander[1], Lawrence Fong[1], Eric J. Small[1], Alejandro Sweet-Cordero[2] and Vadim S. Koshkin[1]**

[1] Helen Diller Family Cancer Center, University of California San Francisco, San Francisco, CA, United States, [2] Department of Pediatrics, Benioff Children's Hospital, University of California, San Francisco, San Francisco, CA, United States

OPEN ACCESS

Edited by:
Alfredo Berruti,
University of Brescia, Italy

Reviewed by:
Rohan Garje,
The University of Iowa, United States
Panagiotis J. Vlachostergios,
Cornell University, United States

***Correspondence:**
Vadim S. Koshkin
vadim.koshkin@ucsf.edu

Specialty section:
This article was submitted to Genitourinary Oncology, a section of the journal Frontiers in Oncology

Received: 17 November 2021
Accepted: 10 February 2022
Published: 07 March 2022

Citation:
Natesan D, Zhang L, Martell HJ, Jindal T, Devine P, Stohr B, Espinosa-Mendez C, Grenert J, Van Ziffle J, Joseph N, Umetsu S, Onodera C, Turski M, Chan E, Desai A, Aggarwal R, Wong A, Porten S, Chou J, Friedlander T, Fong L, Small EJ, Sweet-Cordero A and Koshkin VS (2022) APOBEC Mutational Signature and Tumor Mutational Burden as Predictors of Clinical Outcomes and Treatment Response in Patients With Advanced Urothelial Cancer. Front. Oncol. 12:816706. doi: 10.3389/fonc.2022.816706

Introduction: Tumor mutational burden (TMB) and APOBEC mutational signatures are potential prognostic markers in patients with advanced urothelial carcinoma (aUC). Their utility in predicting outcomes to specific therapies in aUC warrants additional study.

Methods: We retrospectively reviewed consecutive UC cases assessed with UCSF500, an institutional assay that uses hybrid capture enrichment of target DNA to interrogate 479 common cancer genes. Hypermutated tumors (HM), defined as having TMB ≥10 mutations/Mb, were also assessed for APOBEC mutational signatures, while non-HM (NHM) tumors were not assessed due to low TMB. The logrank test was used to determine if there were differences in overall survival (OS) and progression-free survival (PFS) among patient groups of interest.

Results: Among 75 aUC patients who had UCSF500 testing, 46 patients were evaluable for TMB, of which 19 patients (41%) had HM tumors and the rest had NHM tumors (27 patients). An additional 29 patients had unknown TMB status. Among 19 HM patients, all 16 patients who were evaluable for analysis had APOBEC signatures. HM patients (N=19) were compared with NHM patients (N=27) and had improved OS from diagnosis (125.3 months *vs* 35.7 months, p=0.06) but inferior OS for patients treated with chemotherapy (7.0 months *vs* 13.1 months, p=0.04). Patients with APOBEC (N=16) were compared with remaining 56 patients, comprised of 27 NHM patients and 29 patients with unknown TMB, showing APOBEC patients to have improved OS from diagnosis (125.3 months *vs* 44.5 months, p=0.05) but inferior OS for patients treated with chemotherapy (7.0 months *vs* 13.1 months, p=0.05). Neither APOBEC nor HM status were associated with response to immunotherapy.

Conclusions: In a large, single-institution aUC cohort assessed with UCSF500, an institutional NGS panel, HM tumors were common and all such tumors that were evaluated for mutational signature analysis had APOBEC signatures. APOBEC signatures and high TMB were prognostic of improved OS from diagnosis and both analyses also predicted inferior outcomes with chemotherapy treatment.

Keywords: bladder cancer, APOBEC mutational signature, tumor mutational burden, next-generation sequencing, urothelial cancer, hypermutated, biomarkers, immune checkpoint inhibitor (ICI)

INTRODUCTION

Urothelial carcinoma (UC) is a common malignancy with treatment options that have advanced significantly in recent years. Most patients are initially diagnosed with non-muscle-invasive bladder cancer (NMIBC) or muscle-invasive bladder cancer (MIBC) but many unfortunately progress to metastatic disease. Patients diagnosed with MIBC in the absence of distant metastases are treated with cisplatin-based neoadjuvant chemotherapy (1). Patients with metastatic or advanced urothelial cancer (aUC), who have distant metastases outside the organ where tumor originated, are generally considered to have incurable disease. However, many options to delay progression and extend survival are available including chemotherapy, immunotherapy (IO), and now increasingly targeted agents as well. The typical 1st line standard of care (SOC) treatment is platinum-based chemotherapy, followed by IO as 2nd line at the time of progression or as switch maintenance therapy. Enfortumab vedotin (EV) is now approved following progression on at least one prior line of therapy and has phase III data supporting its use following progression on platinum-based chemotherapy and IO (2). Sacituzumab govitecan also recently received accelerated approval in treatment-refractory aUC (3).

In recent years this has been a dynamic treatment landscape with a variety of agents and combination therapies being investigated in clinical trials. This rapid expansion of treatment options highlights the need for novel prognostic and predictive biomarkers in aUC since decisions need to be made among multiple available treatment options. These are frequently very consequential decisions as the rate of patient attrition with each successive therapy is high (4). Next-generation sequencing (NGS) and other biomarkers such as tumor mutational burden (TMB), tumor PD-L1 expression and microsatellite instability (MSI) are frequently utilized to make decisions about treatments (5, 6). NGS to identify specific mutations in aUC patients is especially important as one agent in particular, erdafitinib, is now approved for a biomarker selected population of patients with *FGFR3* alterations (7).

Abbreviations: UC, urothelial carcinoma; NMIBC, non-muscle-invasive bladder cancer; MIBC, muscle-invasive bladder cancer; Auc, advanced urothelial cancer; IO, immunotherapy; SOC, standard of care; EV, enfortumab vedotin; NGS, next-generation sequencing; TMB, tumor mutational burden; MSI, microsatellite instability; UCSF, University of California, San Francisco; APOBEC, apolipoprotein B mRNA editing catalytic polypeptide-like; EMR, electronic medical record; IRB, institutional review board; ORR, observed response rate; HM, hypermutated; NHM, non-hypermutated; PFS, progression-free survival; OS, overall survival; DDR, DNA damage repair.

Numerous NGS platforms are commercially available, but many institutions also have proprietary institutional panels that can detect clinically-relevant alterations. At the University of California, San Francisco (UCSF) the UCSF500 panel utilizes tumor tissue samples to detect 479 oncologic genes and select introns of 47 genes. NGS panels, including UCSF500, can also define TMB which can potentially serve as an important biomarker. Previous analyses have shown that increased TMB is prognostic of longer overall survival (OS) in UC regardless of treatment given (8). High TMB was also associated with improved responses in patients treated with IO in aUC clinical trials, including nivolumab and atezolizumab (9–11). Pembrolizumab has additionally received a tumor-agnostic approval for patients whose tumors have high TMB based on observed clinical benefit (12). On the other hand, the role of TMB as a predictive marker for chemotherapy response is still being explored and available data has not been conclusive (13). Additional prognostic and predictive information may be available from assessment of other biomarkers, including the presence of apolipoprotein B mRNA editing catalytic polypeptide-like (APOBEC) enzyme mutational signature. APOBEC family of enzymes function as cytosine deaminases with a likely role in antiretroviral defense. In bladder tumors and other malignancies they are likely responsible for hypermutation and contribute to cancer mutagenesis (14, 15). Tumors harboring APOBEC mutational signature have been shown to have a higher TMB (16). Previously reported data also suggests that presence of APOBEC signature is prognostic of improved outcomes (17), and may be associated with improved responses to immunotherapy (9, 16). The association of APOBEC mutational signature with chemotherapy responses has not been explored as extensively.

Leveraging data from UCSF500 tumor testing in patients with advanced bladder cancer, we performed a retrospective analysis assessing the prognostic and predictive value of TMB and APOBEC mutational signature in this patient population. We hypothesized that presence of both TMB and APOBEC would be associated with more favorable clinical outcomes and would be predictive of improved responses to immunotherapy while not having predictive value in assessing potential response to chemotherapy.

MATERIALS AND METHODS

Study Design

This was a single-institution, retrospective study assessing clinical and treatment outcomes in urothelial carcinoma

patients whose tumor tissue was assessed with UCSF500, an institutional NGS assay. Eligible patients had to meet the following criteria: 1) have a pathologically documented diagnosis of bladder cancer, upper tract urothelial cancer or urethral cancer, 2) have available UCSF500 results from a tumor biopsy sample, and 3) have demographic, clinical, and treatment data available for abstraction from the electronic medical record (EMR). The data for this retrospective review were collected for eligible patients under a UCSF Institutional Review Board (IRB) approved protocol. A total of 75 patients with clinical and treatment data spanning the time period from April 2016 through April 2020 were included in the analysis.

Molecular Analyses

NGS results from tumor samples included in this analysis were obtained using the institutional UCSF500 panel developed and utilized at UCSF. The UCSF500 Cancer Gene Test uses capture-based next-generation sequencing to target and analyze the coding regions of 479 cancer genes, as well as select introns of 47 genes. As part of this test, genomic DNA is extracted from paraffin embedded tumor tissue and a paired normal tissue sample (paraffin embedded or blood sample) if available. Target enrichment is performed by hybrid capture using custom oligonucleotides. Sequencing of captured libraries is performed on an Illumina HiSeq 2500 by a CLIA-certified laboratory: UCSF Genomic Sequencing Services Lab at Institute for Human Genetics (San Francisco, CA). Sequence reads are de-duplicated to allow for accurate allele frequency determination and copy number calling. The analysis uses open source or licensed software for alignment to the human reference sequence UCSC build hg19 (NCBI build 37) and variant calling. Additionally, microsatellite instability analysis is performed with MSIsensor (18).

Patients who had paired tumor and normal tissue samples available were also potentially assessed for TMB and APOBEC mutational signature analysis. Patients who only had tumor samples (no normal samples) were not considered evaluable for TMB or APOBEC as there was no normal sample to remove germline variants. Among patient samples assessed for TMB, hypermutated samples were defined as those with ≥10 mutations per megabase of DNA sequenced (19). Mutational signatures were extracted from the panel sequencing data using deconstructSigs (20). Only samples with ≥50 total somatic mutations were analyzed for mutational signatures, the recommended threshold for deconstructSigs. Trinucleotide counts were normalized for the trinucleotide composition of the UCSF500 panel footprint using the "tri.counts.method" option in deconstructSigs. Version two of the COSMIC mutational signature set was used as reference (21), in addition to a cisplatin mutational signature (22), resulting in a reference set of 31 mutational signatures.

Clinical and Response Assessment

Retrospective chart review of the EMR was undertaken for all patients included in the analysis. Collected data included patient demographics and tumor characteristics. Relevant clinical and treatment characteristics were also collected including dates of initial diagnosis and onset of metastatic disease, administered treatments and treatment responses; and final follow-up and vital status. For patients who were treated in the metastatic setting with chemotherapy or with immune checkpoint inhibitors, the dates of treatment start and finish and responses to treatment were recorded.

Response to and progression on treatment was assessed retrospectively by the chart abstractor based on available information in notes and radiographic studies. Imaging studies used to define treatment response or progression were done at the discretion of the treating provider. Radiology and pathology results were assessed based on information available in the electronic medical record; no central review was performed.

Overall survival (OS) was defined as the time from initial diagnosis until the date of death, if available. For treatment specific outcomes, observed response rate (ORR) was defined by the chart abstractor as the best response to treatment. OS was defined as the time from treatment start until the date of death, whereas progression-free survival (PFS) was defined as the time from treatment start until date of progression or date of death, whichever happened first.

Statistical Analyses

Two major analyses were undertaken as part of this study. As part of the TMB analysis, patients whose tumors were evaluable for TMB were divided into Hypermutated (HM; TMB ≥ 10 mut/Mb) *vs*. Non-hypermutated (NHM; TMB < 10 mut/Mb) groups and outcomes were compared between these groups. As part of the APOBEC analysis, patients with hypermutated tumors which were detected to have APOBEC mutational signatures were compared to Other (non-APOBEC) patients whose tumors were not known to harbor an APOBEC mutational signature due to either being NHM or having too few mutations to be evaluable for TMB. To assess prognostic outcomes in these comparison groups, we evaluated median OS from initial diagnosis regardless of treatment administered. To assess predictive value of these biomarkers for specific treatments including chemotherapy and immune checkpoint inhibitors in aUC patients, we compared ORR to the treatment for metastatic disease, as well as median PFS and median OS from treatment initiation for metastatic disease.

Continuous variables were summarized using median and range and categorical variables were described with frequency and percent of total. Continuous variables were compared between the groups by Wilcoxon rank sum test and categorical variables were compared between the groups by Chi-squared test. The logrank test was used to assess if there were differences in OS from initial diagnosis, IO initiation, and chemotherapy initiation in addition to PFS from IO initiation and chemotherapy initiation.

RESULTS

Clinical Characteristics

Among 75 eligible patients that underwent UCSF500 testing, 46 patients had tissue evaluable for tumor mutational burden (TMB). Of the 46 evaluable cases, 19 patients were hypermutated, while the remaining 27 patients had non-hypermutated tumors. Of the

evaluable hypermutated cases, 16 were positive for APOBEC mutational signatures (**Figure 1**). The remaining 3 HM patients were found to not be evaluable for APOBEC mutational signature analysis due to insufficient number of mutations. Consequently, they were excluded from further APOBEC analysis comparisons as their APOBEC mutational status was unknown.

The demographic and clinical characteristics of patients included in the TMB and APOBEC analyses are shown in **Tables 1**, **2**, respectively. Patients included in this analysis were representative of the population with aUC, with a median age in the late 60s and the majority of patients were men. Median follow-up for all patients from initial diagnosis was 15.5 months. Most patients in this study were Caucasian but a significant minority were Asian or Hispanic/Latino, reflecting the patient population served by the UCSF Helen Diller Family Comprehensive Cancer Center. Notably, in the group of patients with APOBEC mutational signatures, there was a numerically higher percentage of patients with primary bladder tumors and of patients whose tumors had a pure urothelial histology, although this did not quite meet statistical significance. More patients with either HM or APOBEC tumors had a prior smoking history relative to the comparison groups. Most commonly observed tumor alterations were also representative of what has previously been described in the bladder tumor mutational landscape (23) and overall were fairly consistent across the two comparisons. However, fewer *FGFR3* alterations were observed in the HM or APOBEC groups than in the comparison groups; these differences were not statistically significant. Testing for PD-L1 status was limited but from the collected data, the percentages of tumors with increased PD-L1 expression were comparable across subgroups.

TMB Analysis

In the comparison of outcomes for 19 patients with hypermutated tumors (TMB ≥ 10 mut/Mb) and 27 patients with non-hypermutated tumors (TMB < 10 mut/Mb), HM patients had longer median OS (125.3 months *vs* 35.7 months, p = 0.06) from initial diagnosis, suggesting HM status to be a positive prognostic marker (**Figure 2A** and **Table 3**). At the time of data cutoff, 74% of HM patients and 59% of NHM patients were alive. A total of 9 HM patients were treated with IO, and 6 HM patients were treated with chemotherapy.

In comparing outcomes with IO treatment, no significant differences were observed for the 9 HM patients relative to the 13 NHM patients who received treatment with an immune checkpoint inhibitor (**Figures 2B, C** and **Table 3**). HM patients were treated with Pembrolizumab (6/9, 33%) and Atezolizumab (3/9, 33%) and NHM patients were treated with Pembrolizumab (8/13, 62%), Atezolizumab (3/13, 23%), Nivolumab/Ipilimumab (1/13, 8%), and Durvalumab/Tremelimumab (1/13, 8%). Numerically higher ORR was observed in the HM group among evaluable patients (4/8, 50%) relative to the NHM group (4/12, 33%), although this difference was not statistically significant. Similarly, median PFS (4.1 *vs* 3.3 months, p=0.52) and OS (12.4 *vs* 14.1 months, p=0.49) from treatment start for the two groups were comparable.

On the other hand, in comparing outcomes with platinum-based chemotherapy treatment for the 6 HM patients and 8 NHM patients, response rates for evaluable HM patients (3/5, 60%) and NHM patients (5/8, 63%) were similar. Importantly, HM patients were found to have shorter PFS (4.3 *vs* 9.0 months, p<0.001) and OS (7.0 *vs* 13.1 months, p=0.04) relative to the NHM patients (**Figures 2D, E** and **Table 3**). Chemotherapy treatment received by HM patients included cisplatin-based chemotherapy (4/6, 67%), carboplatin-based chemotherapy (1/6, 17%), and FOLFOX (1/6, 17%) while NHM patients received carboplatin-based chemotherapy (4/8, 50%) and cisplatin-based chemotherapy (4/8, 50%).

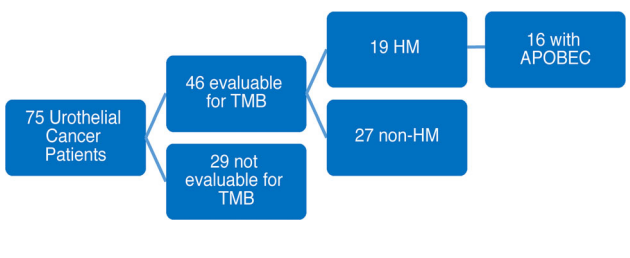


FIGURE 1 | Consort Diagram for the study.

APOBEC Analysis

There were 16 patients with APOBEC mutational signature and 56 patients in the Other category without a known APOBEC mutational signature (including 27 non-HM patients and 29 patients who were not evaluable for TMB). APOBEC patients had a longer median OS from initial diagnosis relative to Other patients (125.3 months *vs* 44.5 months, p = 0.05) (**Figure 3A** and **Table 4**). About 81% of APOBEC patients and 63% of Other patients were alive at the time of analysis. Of the APOBEC patients, 8 received IO and 5 received chemotherapy.

Comparing the 8 APOBEC patients with the 25 Other patients that were treated with immunotherapy regimens, although evaluable APOBEC patients had numerically higher ORR to IO treatment (4/7, 57%), relative to evaluable Other patients (8/25, 32%), this difference was not statistically significant. Similarly, the difference in median OS (12.4 *vs*. 14.1, p=0.27) and median PFS (4.1 *vs*. 3.3, p=0.25) were also not statistically significant between these two groups (**Figures 3B, C** and **Table 4**). APOBEC patients received Pembrolizumab (5/8, 63%) and Atezolizumab (3/8, 38%) while Other patients received Pembrolizumab (17/25, 68%), Atezolizumab (4/25, 16%), Nivolumab (2/25, 8%), Nivolumab/Ipilimumab (1/25, 4%), and Durvalumab/Tremelimumab (1/25, 4%).

In comparing chemotherapy treatment outcomes, the ORR were similar among APOBEC (3/5, 60%) and Other (9/15, 60%) patients. Importantly, despite the similarity in response rates, APOBEC patients had shorter median PFS (4.3 *vs*. 7.0, p=0.01) and OS (7.0 *vs* 13.1, p=0.05) relative to the 15 Other patients (**Figures 3D, E** and **Table 4**). APOBEC patients were treated with cisplatin-based chemotherapy (4/5, 80%) and carboplatin-based chemotherapy (1/5, 20%) while Other patients were treated with cisplatin-based chemotherapy (9/15, 60%), carboplatin-based chemotherapy (5/15, 33%), capecitabine (1/15, 7%).

TABLE 1 | Clinical characteristics of patients in the hypermutated and non-hypermutated groups.

	TMB Analysis		
	HM (N=19)	**NHM (N=27)**	**P-value**
Median Age at Diagnosis (Range)	65 (50,87)	69 (40,87)	0.13
Gender			1.00
Male	12 (63%)	17 (63%)	
Female	7 (37%)	10 (37%)	
Race/Ethnicity			0.50
Asian	1 (5%)	1 (4%)	
Black or African American	0 (0%)	4 (15%)	
Hispanic or Latino	2 (11%)	1 (4%)	
White	14 (74%)	21 (78%)	
Unknown	2 (11%)	0 (0%)	
Smoking History (Ever Smoker)	13 (68%)	13 (48%)	0.29
Primary Tumor Location			0.29
Bladder	16 (84%)	20 (74%)	
Upper Tract	1 (5%)	5 (19%)	
Urethra	0 (0%)	1 (4%)	
Multiple	1 (5%)	0 (0%)	
N/A	1 (5%)	1 (4%)	
Histology			0.33
Pure Urothelial	14 (74%)	19 (70%)	
Pure Squamous	0 (0%)	2 (7%)	
Squamous Component	3 (16%)	1 (4%)	
Small Cell / NE	1 (5%)	2 (7%)	
Adenocarcinoma	0 (0%)	1 (4%)	
Sarcomatoid	0 (0%)	2 (7%)	
Urachal	1 (5%)	0 (0%)	
Biopsy Source			0.96
Primary Tumor*	10 (53%)	14 (52%)	
Metastatic	9 (47%)	13 (48%)	
Most Common Alterations (N)	TERT (16, 84%)	TERT (20, 74%)	N/A
	TP53 (13, 68%)	KDM6A (13, 48%)	
	KMT2D (7, 37%)	TP53 (13, 48%)	
	PIK3CA (7, 37%)	CDKN2A (8, 30%)	
	ARID1A (6, 32%)	CDKN2B (8, 30%)	
	CDKN2A (6, 32%)	FGFR3 (7, 26%)	
	ERBB2 (6, 32%)	ARID1A (6, 22%)	
	KDM6A (6, 32%)	ELF3 (5, 19%)	
	CCND1 (3, 16%)	KMT2D (5, 19%)	
	CDKN2B (3, 16%)	RB1 (5, 19%)	
	RB1 (3, 16%)		
	FGFR3 (2, 11%)		
PD-L1 Available	4 (21%)	10 (37%)	0.73
Positive (CPS≥10)**	2 (50%)	4 (40%)	
Negative (CPS<10)**	2 (50%)	6 (60%)	
MSI-High Tumor	1 (5%)	0 (0%)	0.86
Metastatic Disease			
At Diagnosis	2 (11%)	4(15%)	0.28
Anytime during Follow-up	13 (68%)	19 (70%)	0.89
Definitive Surgery	11 (58%)	19 (70%)	0.53
Definitive Radiation Therapy	2 (11%)	1 (4%)	0.36

HM, hypermutated; NHM, non-hypermutated; NE, neuroendocrine; MSI, microsatellite instability.

**Includes either bladder or upper tract.*

***Percentages are out of available PD-L1 data.*

N/A, Not Applicable.

DISCUSSION

In this large cohort of patients with aUC whose tumors were all assessed with the UCSF500 test, our institutional DNA-based NGS panel, a significant proportion of evaluable tumors were found to have TMB ≥10 mutations/Mb and all of the hypermutated tumors evaluable for mutational signatures were found to have APOBEC mutational signatures. Increased tumor mutational burden and presence of APOBEC mutational signatures were both found to be prognostic of improved overall survival in this patient population. Neither of these biomarkers were predictive of outcomes with immune checkpoint inhibitor treatment. However, both hypermutated status and presence of APOBEC mutational signatures were associated with inferior outcomes with platinum-

TABLE 2 | Clinical characteristics of patients in the APOBEC and Other groups.

APOBEC Analysis			
	APOBEC (N=16)	**Other (N=56)**	**P-Value**
Median Age at Diagnosis (Range)	65 (51, 86)	68 (31, 87)	0.66
Gender			0.92
Male	10 (62%)	38 (68%)	
Female	6 (38%)	18 (32%)	
Race/Ethnicity			0.56
Asian	1 (6%)	9 (16%)	
Black or African	0 (0%)	1 (2%)	
Hispanic or Latino	1 (6%)	1 (2%)	
White	12 (75%)	44 (79%)	
Unknown	2 (13%)	1 (2%)	
Smoking History (Ever Smoker)	11 (69%)	25 (45%)	0.16
Primary Tumor Location			0.08
Bladder	13 (81%)	38 (68%)	
Upper Tract	1 (6%)	15 (27%)	
Urethra	0 (0%)	2 (4%)	
Multiple	1 (6%)	0 (0%)	
N/A	1 (6%)	1 (2%)	
Histology			0.78
Pure Urothelial	13 (81%)	35 (63%)	
Pure Squamous	0 (0%)	2 (4%)	
Squamous Component	2 (13%)	8 (14%)	
Small Cell / NE	1 (6 %)	2 (4%)	
Adenocarcinoma	0 (0%)	3 (5%)	
Plasmacytoid	0 (0%)	3 (5%)	
Micropapillary	0 (0%)	1 (2%)	
Sarcomatoid	0 (0%)	2 (4%)	
Biopsy Source			0.75
Primary Tumor*	7 (44%)	27 (48%)	
Metastatic	9 (56%)	29 (52%)	
Most Common Alterations (N)	TERT (14, 88%)	TERT (40, 71%)	N/A
	TP53 (10, 63%)	TP53 (31, 55%)	
	KMT2D (6, 38%)	CDKN2A (20, 36%)	
	ARID1A (6, 38%)	KDM6A (19, 34%)	
	ERBB2 (6, 38%)	CDKN2B (18, 66%)	
	KDM6A (6, 38%)	ARID1A (12, 21%)	
	CDKN2A (5, 31%)	FGFR3 (11, 20%)	
	PIK3CA (5, 31%)	RB1 (11, 20%)	
	CCND1 (3, 19%)	KMT2D (10, 18%)	
	CDKN2B (3, 19%)	ERBB2 (9, 16%)	
	RB1 (3, 19%)		
	FGFR3 (2, 13%)		
PD-L1 Available	4 (25%)	24 (43%)	0.63
Positive (CPS≥10)**	2 (50%)	15 (63%)	
Negative (CPS<10)**	2 (50%)	9 (37%)	
MSI-High Tumor	1 (6%)	0 (0%)	0.50
Metastatic Disease			
At Diagnosis	1 (6%)	11(20%)	0.28
Anytime During Follow-up	10 (63%)	40 (71%)	0.49
Definitive Surgery	10 (63%)	36 (64%)	1
Definitive Radiation Therapy	2 (13%)	1 (2%)	0.06

HM, hypermutated; NHM, non-hypermutated; NE, neuroendocrine; MSI, microsatellite.

**Includes either bladder or upper tract.*

***Percentages are out of available PD-L1 data.*

N/A, Not Applicable.

based chemotherapy treatment, nominating them as potential negative predictive markers for aUC patients treated with chemotherapy.

Urothelial cancers are frequently amongst the most highly mutated tumors (24). In the IMvigor211 clinical trial of patients with platinum-refractory urothelial carcinoma, the median TMB in tumors was 9.6 mutations/Mb (11). This high mutation burden in urothelial carcinoma is frequently driven by the genetic instability caused by APOBEC mutagenesis (23). As an example, in the IMvigor130 clinical trial, presence of APOBEC mutational signatures was associated with higher TMB (25). However, urothelial carcinomas have high mutational

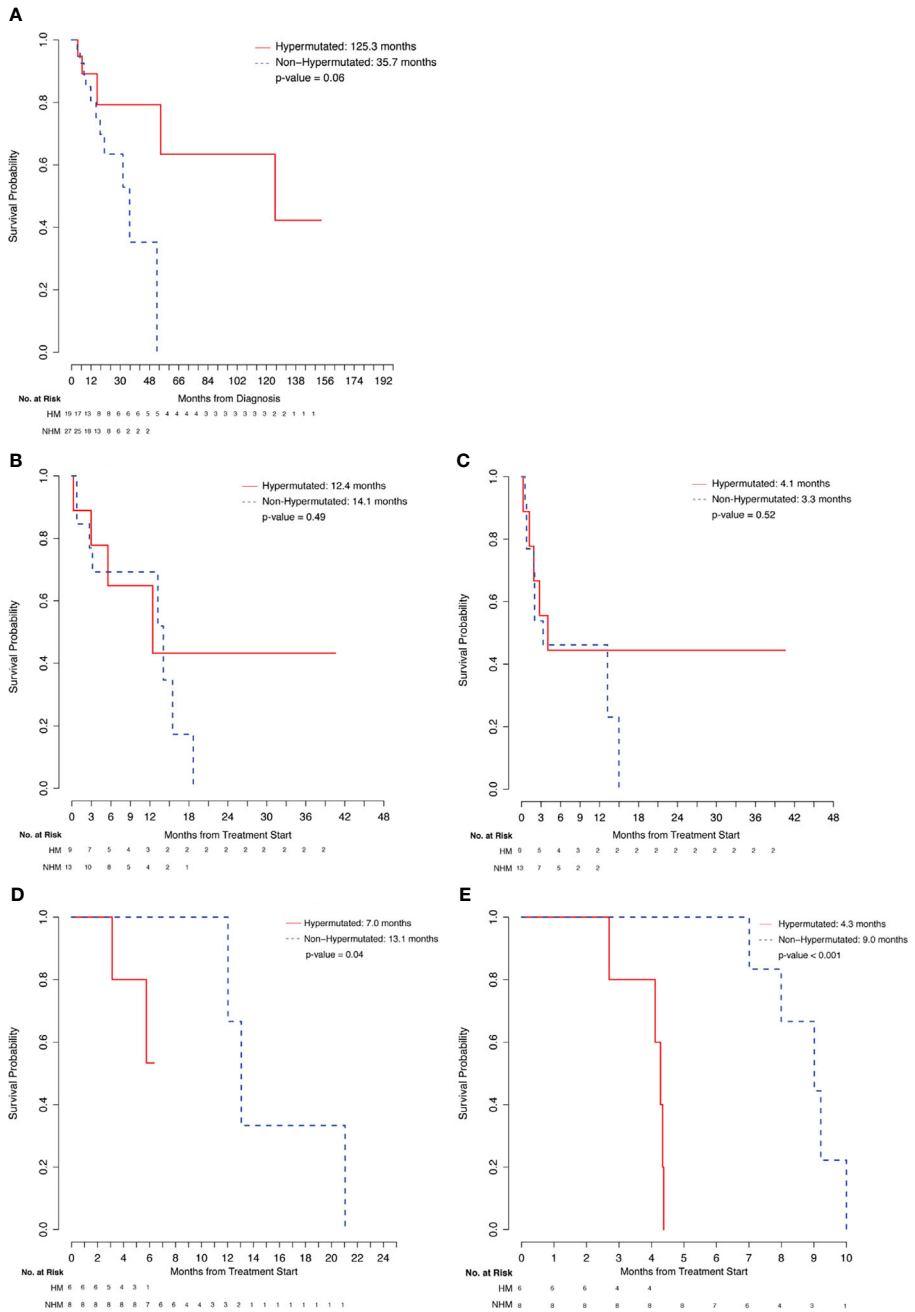


FIGURE 2 | Comparison of hypermutated patients. **(A)** Overall Survival from Diagnosis. **(B)** Overall Survival from Immunotheraphy Start. **(C)** Progression-Free Survival from Immunotherapy Start. **(D)** Overall survival from Chemotherapy Start. **(E)** Progression-Free Survival from Chemotherapy Start.

complexity and alternate mechanisms of mutagenesis that can account for a high TMB. Thus, it is not necessarily the case that urothelial tumors with a high TMB overlap completely with tumors harboring APOBEC mutational signatures and the two can be used as distinct biomarkers. In this dataset however, among 19 tumors with high TMB, all 16 tumors evaluable for mutational analysis were found to have APOBEC mutational signatures. Although the overall numbers were too small to draw definitive conclusions, the most common mutations present across the different subsets of HM and non-HM, as well as APOBEC and non-APOBEC tumors were fairly consistent. Most common mutations included *TERTp* and *TP53* in all groups. Importantly, the targetable *FGFR3* alterations were more commonly found in non-HM and non-APOBEC tumors. This is consistent with previously reported findings showing APOBEC-low tumors to have more *FGFR3* mutations, while

TABLE 3 | Comparison of outcomes in hypermutated vs non-hypermutated patients.

HM vs. NHM			
Patient Group (N)	**Comparison**	**Median Survival (months)**	**p-value**
HM (19) vs NHM (27)	OS from initial diagnosis	125.3 vs 35.7	0.06
	From IO Start		
HM (9) vs	OS	12.4 vs 14.1	0.49
NHM (13)	PFS	4.1 vs 3.3	0.52
	From Chemotherapy Start		
HM (6) vs	OS	7.0 vs 13.1	**0.04**
NHM (8)	PFS	4.3 vs 9.0	**<0.001**

HM, hypermutated; NHM, non-hypermutated; OS, overall survival; PFS, progression-free survival; IO, immunotherapy.
Bold: statistically significant.

APOBEC-high tumors are more likely to have mutations in DNA damage response genes and chromatin regulatory genes (17). All this suggests that the population included in this analysis was fairly representative of the patterns of mutational complexity found in bladder cancer.

Our initial hypothesis was that presence of TMB and APOBEC signatures would be independently associated with more favorable clinical outcomes. Prior studies have suggested that higher TMB levels are associated with improved overall survival and decreased recurrence rates in patients with muscle-invasive bladder cancer (8). Presence of APOBEC signatures was also found to be associated with improved overall survival in muscle-invasive bladder cancer (17). Our findings in this study based on samples obtained from patients with metastatic disease as well as localized disease were overall in agreement with this prior data, as we found improved OS for high TMB patients relative to low TMB patients and for APOBEC patients versus patients without APOBEC mutational signatures. The potential genomic instability reflected by high TMB and associated with APOBEC signatures may account for these improved outcomes leading to the tumor being more vulnerable to immune surveillance. Median overall survival from initial diagnosis and independent of treatment was longer in all comparison groups of this dataset than a median OS that would be expected from a purely metastatic urothelial cancer cohort timed from initial metastatic disease diagnosis. This was due to the inclusion of patients with MIBC who had curative intent treatment and never had progression to metastatic disease as well as inclusion of patients who were initially diagnosed with localized disease many years prior to eventual progression to metastatic disease.

We additionally hypothesized that increased TMB and presence of APOBEC mutational signatures would be predictive of responses to immune checkpoint inhibitors. Analyses from clinical trials in urothelial carcinoma have indicated that APOBEC mutational signatures and high TMB are both associated with improved outcomes with immunotherapy agents including both anti-PD-1 antibody nivolumab and anti-PD-L1 antibody atezolizumab (9, 11, 16, 25). The genomic instability and plethora of mutations in the tumor associated with these biomarkers are thought to be the mechanisms underlying enhanced response to immune checkpoint inhibitors. While we did not see this association in the current analysis, this may have been the consequence of relatively small numbers being compared. Other biomarkers, such as PD-L1 status, may have served as additional confounders leading to these findings not being observed in the current dataset. Most patients included in our analysis had unknown PD-L1 status. However, for patients with available PD-L1 status, there was no significant difference in PD-L1 expression across the subgroups being compared.

The potential impact of TMB and APOBEC as biomarkers of response to chemotherapy in bladder cancer was less clear from the outset based on previously available data. Prior studies have suggested that APOBEC-induced mutagenesis is clonally enriched in chemotherapy-treated urothelial cancer (26). A study in a cohort of 73 aUC patients subsequently treated with chemotherapy showed increased expression of APOBEC mRNA in tumor samples to be associated with longer OS (27). However no data regarding APOBEC mutational signatures as predictors of response to chemotherapy were previously available. TMB status was likewise not shown to be predictive of responses to second-line chemotherapy in the Keynote-045 trial with Pembrolizumab in platinum-refractory urothelial cancer (13). Due to the limitations of these data we hypothesized that neither high TMB, nor presence of APOBEC mutational signatures would be predictive of responses to chemotherapy. However, the analysis presented here revealed that high TMB and presence of APOBEC mutational signatures were both associated with inferior chemotherapy outcomes. These inferior outcomes were not readily explained by other potential prognostic or predictive genomic biomarkers in this patient population. Among all patients who received chemotherapy there were no appreciable differences, in either the HM *vs* NHM or Apobec *vs* Other analyses, between the comparison subgroups in terms of tumor alterations in TP53, RB1 or DNA damage repair (DDR) genes. Consequently, our analysis is the first to nominate high TMB and presence of APOBEC mutational signatures as negative predictive biomarkers of chemotherapy response in patients with aUC. Since these tumors are more highly mutated, they are likely more aggressive and, as a result, may not respond to traditional chemotherapy treatment. While the mechanism explaining these findings is not immediately clear, a potential explanation may be that chemotherapy treatments are causing immune cell depletion in these otherwise immunologically responsive tumors. Alternatively, a clonal selection of more aggressive variants in these genomically unstable tumors may be taking place under

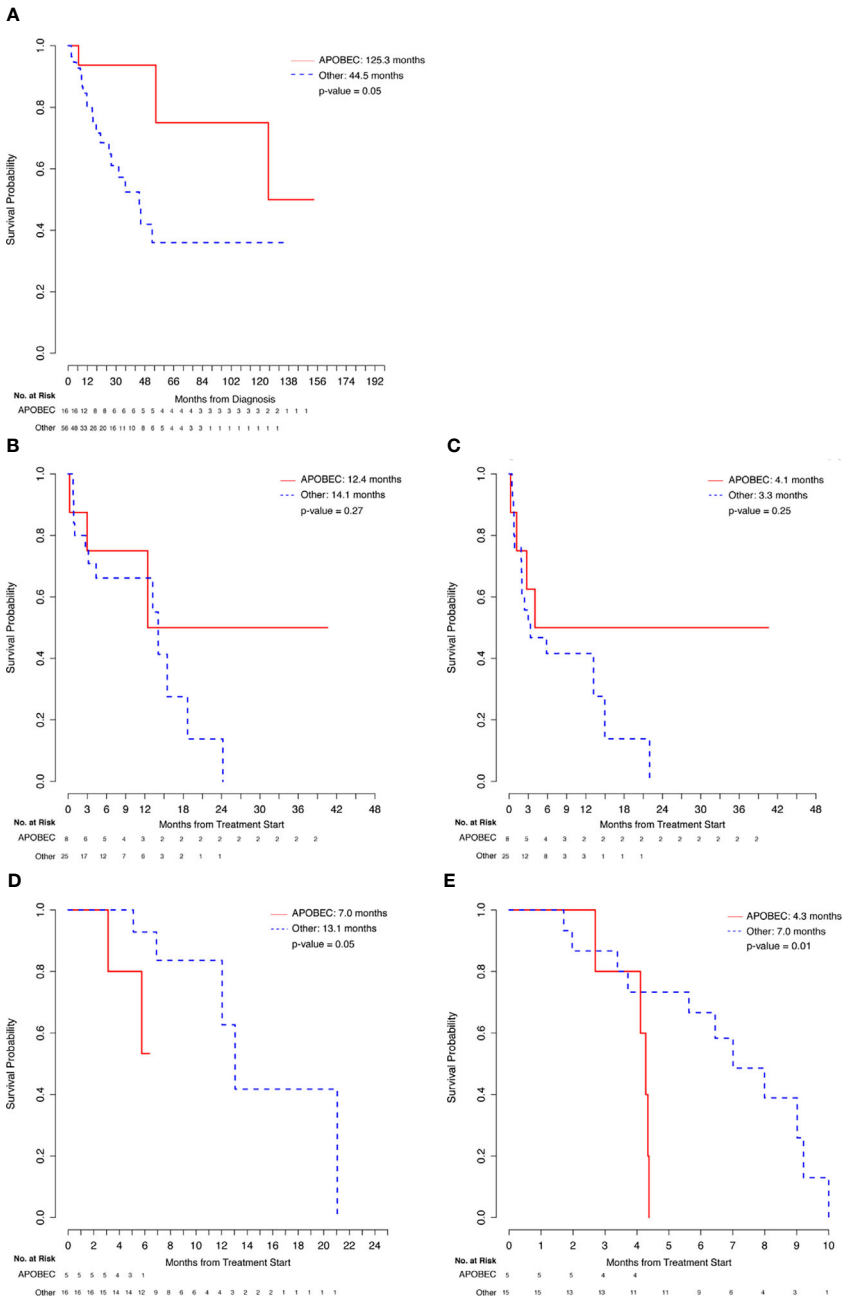


FIGURE 3 | Comparison of APOBEC and Other patients. **(A)** Overall Survival from Diagnosis. **(B)** Overall Survival from Immunotherapy Start. **(C)** Progression-Free Survival from Immunotherapy Start. **(D)** Overall Survival from Chemotherapy Start. **(E)** Progression-Free Survival from Chemotherapy Start.

selective pressure from chemotherapy treatment. These potential mechanisms should also be further assessed in future studies.

While retrospective data presented in this manuscript should be further validated, conclusions derived from these findings can help inform clinical decision making and clinical trial design for patients with aUC. Based on this data, it can be surmised that patients with high TMB and APOBEC mutational signatures may have better outcomes overall but may also not do as well with chemotherapy treatment. Although we did not observe these biomarkers to be predictive of responses to immunotherapy treatments, other studies have suggested improved responses to treatments with both anti-PD-1 and anti-PD-L1 immune checkpoint inhibitors in high TMB patients and patients with APOBEC mutational signatures. Consequently, in the appropriate clinical context, treatments with immune checkpoint inhibitors may be considered in lieu

TABLE 4 | Comparison of outcomes in APOBEC vs Other patients.

APOBEC vs. Other			
Patient Group (N)	**Comparison**	**Median Survival (months)**	**p-value**
APOBEC (16) vs Other (56)	OS from initial diagnosis	125.3 vs 44.5	**0.05**
	From IO Start		
APOBEC (8) vs	OS	12.4 vs 14.1	0.27
Other (25)	PFS	4.1 vs 3.3	0.25
	From Chemotherapy Start		
APOBEC (5) vs	OS	7.0 vs 13.1	**0.05**
Other (15)	PFS	4.3 vs 7.0	**0.01**

HM, hypermutated; NHM, non-hypermutated; OS, overall survival; PFS, progression-free survival; IO, immunotherapy.
Bold: statistically significant.

of chemotherapy in selected patients with high TMB or presence of APOBEC mutational signatures.

There were limitations to this study, including the retrospective nature of this analysis, a design which introduces numerous confounders. As an example, the presence of other putative biomarkers, such as PD-L1 status and other unknown genomic alterations, may have confounded the results in this relatively small sample size. Radiographic responses were not reviewed according to strict RECIST criteria but were assessed by a single investigator to help address potential inter-observer heterogeneity. The study was also limited to a single academic center and the findings may be difficult to generalize to other academic institutions or community sites. It is also unknown whether data obtained from UCSF500 platform can be generalized to other NGS platforms. In spite of these limitations, this study presents important hypothesis-generating data that can inform future studies and potentially impact clinical decision making.

CONCLUSIONS

This single-institution retrospective analysis in a large cohort of patients with advanced urothelial cancer, revealed findings that supported prior data nominating high TMB and APOBEC mutational signatures as positive prognostic markers in this patient population. This was additionally the first study to nominate TMB-high status and APOBEC mutational signatures as predictive biomarkers indicating inferior responses to chemotherapy treatment in patients with advanced urothelial cancer. While these findings should be further validated, they can nevertheless inform treatment decisions and clinical trial design for patients with advanced urothelial carcinoma in the appropriate clinical context.

DATA AVAILABILITY STATEMENT

The original contributions presented in the study are included in the article/supplementary material. Further inquiries can be directed to the corresponding author.

ETHICS STATEMENT

The studies involving human participants were reviewed and approved by University of California, San Francisco Institutional Review Board. Written informed consent for participation was not required for this study in accordance with the national legislation and the institutional requirements.

AUTHOR CONTRIBUTIONS

Concept: DN and VK. Data collection: DN, LZ, HM, TJ, PD, BS, JG, JZ, NJ, SU, CO, EC, and VK. Data analysis and interpretation: all authors. All authors contributed to the article and approved the submitted version.

ACKNOWLEDGMENTS

We acknowledge the generous support of EC and Edward Y. Chan in helping make this study and manuscript possible.

REFERENCES

1. Grossman HB, Natale RB, Tangen CM, Speights VO, Vogelzang NJ, Trump DL, et al. Neoadjuvant Chemotherapy Plus Cystectomy Compared With Cystectomy Alone for Locally Advanced Bladder Cancer. *N Engl J Med* (2003) 349:859–66. doi: 10.1056/NEJMoa022148
2. Powles T, Rosenberg JE, Sonpavde GP, Loriot Y, Durán I, Lee JL, et al. Enfortumab Vedotin in Previously Treated Advanced Urothelial Carcinoma. *N Engl J Med* (2021) 384:1125–35. doi: 10.1056/NEJMoa2035807
3. Petrylak DP, Tagawa ST, Jain RK, Bupathi M, Balar AV, Rezazadeh A, et al. Early Results of TROPHY-U-01 Cohort 2: Sacituzumab Govitecan (SG) in Platinum-Ineligible Patients (Pts) With Metastatic Urothelial Cancer (mUC) Who Progressed After Prior Checkpoint Inhibitor (CPI) Therapy. *J Clin Oncol* (2020) 38:5027–7. doi: 10.1200/JCO.2020.38.15_suppl.5027
4. Swami U, Grivas P, Pal SK, Agarwal N. Utilization of Systemic Therapy for Treatment of Advanced Urothelial Carcinoma: Lessons From Real World Experience. *Cancer Treat Res Commun* (2021) 27:100325. doi: 10.1016/j.ctarc.2021.100325
5. Umar A, Boland CR, Terdiman JP, Syngal S, de la Chapelle A, Rüschoff J, et al. Revised Bethesda Guidelines for Hereditary Nonpolyposis Colorectal Cancer (Lynch Syndrome) and Microsatellite Instability. *J Natl Cancer Inst* (2004) 96:261–8. doi: 10.1093/jnci/djh034

6. Powles T, Morrison L. Biomarker Challenges for Immune Checkpoint Inhibitors in Urothelial Carcinoma. *Nat Rev Urol* (2018) 15:585–7. doi: 10.1038/s41585-018-0056-3
7. Loriot Y, Necchi A, Park SH, Garcia-Donas J, Huddart R, Burgess E, et al. Erdafitinib in Locally Advanced or Metastatic Urothelial Carcinoma. *N Engl J Med* (2019) 381:338–48. doi: 10.1056/NEJMoa1817323
8. Zhang C, Shen L, Qi F, Wang J, Luo J. Multi-Omics Analysis of Tumor Mutation Burden Combined With Immune Infiltrates in Bladder Urothelial Carcinoma. *J Cell Physiol* (2020) 235:3849–63. doi: 10.1002/jcp.29279
9. Galsky MD, Saci A, Szabo PM, Han GC, Grossfeld G, Collette S, et al. Nivolumab in Patients With Advanced Platinum-Resistant Urothelial Carcinoma: Efficacy, Safety, and Biomarker Analyses With Extended Follow-Up From CheckMate 275. *Clin Cancer Res* (2020) 26:5120–8. doi: 10.1158/1078-0432.CCR-19-4162
10. Rosenberg JE, Hoffman-Censits J, Powles T, van der Heijden MS, Balar AV, Necchi A, et al. Atezolizumab in Patients With Locally Advanced and Metastatic Urothelial Carcinoma Who Have Progressed Following Treatment With Platinum-Based Chemotherapy: A Single-Arm, Multicentre, Phase 2 Trial. *Lancet* (2016) 387:1909–20. doi: 10.1016/s0140-6736(16)00561-4
11. Powles T, Durán I, van der Heijden MS, Loriot Y, Vogelzang NJ, De Giorgi U, et al. Atezolizumab Versus Chemotherapy in Patients With Platinum-Treated Locally Advanced or Metastatic Urothelial Carcinoma (IMvigor211): A Multicentre, Open-Label, Phase 3 Randomised Controlled Trial. *Lancet* (2018) 391:748–57. doi: 10.1016/S0140-6736(17)33297-X
12. Marabelle A, Fakih M, Lopez J, Shah M, Shapira-Frommer R, Nakagawa K, et al. Association of Tumour Mutational Burden With Outcomes in Patients With Advanced Solid Tumours Treated With Pembrolizumab: Prospective Biomarker Analysis of the Multicohort, Open-Label, Phase 2 KEYNOTE-158 Study. *Lancet Oncol* (2020) 21:1353–65. doi: 10.1016/S1470-2045(20)30445-9
13. Bellmunt J, de Wit R, Fradet Y, Climent MA, Petrylak DP, Lee JL, et al. 747p Association of TMB With Efficacy of Pembrolizumab (Pembro) in Patients (Pts) With Advanced Urothelial Cancer (UC): Results From KEYNOTE-045 and KEYNOTE-052. *Ann Oncol* (2020) 31:S580–1. doi: 10.1016/j.annonc.2020.08.819
14. Harris RS, Petersen-Mahrt SK, Neuberger MS. RNA Editing Enzyme APOBEC1 and Some of its Homologs can Act as DNA Mutators. *Mol Cell* (2002) 10:1247–53. doi: 10.1016/S1097-2765(02)00742-6
15. Lada AG, Dhar A, Boissy RJ, Hirano M, Rubel AA, Rogozin IB, et al. AID/APOBEC Cytosine Deaminase Induces Genome-Wide Kataegis. *Biol Direct* (2012) 7:47. doi: 10.1186/1745-6150-7-47
16. Galsky MD, Arija JÁA, Bamias A, Davis ID, De Santis M, Kikuchi E, et al. Atezolizumab With or Without Chemotherapy in Metastatic Urothelial Cancer (IMvigor130): A Multicentre, Randomised, Placebo-Controlled Phase 3 Trial. *Lancet* (2020) 395(10236):1547–57. doi: 10.1016/S0140-6736(20)30230-0
17. Glaser AP, Fantini D, Wang Y, Yu Y, Rimar KJ, Podojil JR, et al. APOBEC-Mediated Mutagenesis in Urothelial Carcinoma is Associated With Improved Survival, Mutations in DNA Damage Response Genes, and Immune Response. *Oncotarget* (2018) 9:4537–48. doi: 10.18632/oncotarget.23344
18. Niu B, Ye K, Zhang Q, Lu C, Xie M, McLellan MD, et al. MSIsensor: Microsatellite Instability Detection Using Paired Tumor-Normal Sequence Data. *Bioinformatics* (2014) 30:1015–6. doi: 10.1093/bioinformatics/btt755
19. Campbell BB, Light N, Fabrizio D, Zatzman M, Fuligni F, de Borja R, et al. Comprehensive Analysis of Hypermutation in Human Cancer. *Cell* (2017) 171:1042–56.e10. doi: 10.1016/j.cell.2017.09.048
20. Rosenthal R, McGranahan N, Herrero J, Taylor BS, Swanton C. DeconstructSigs: Delineating Mutational Processes in Single Tumors Distinguishes DNA Repair Deficiencies and Patterns of Carcinoma Evolution. *Genome Biol* (2016) 17:31. doi: 10.1186/s13059-016-0893-4
21. Tate JG, Bamford S, Jubb HC, Sondka Z, Beare DM, Bindal N, et al. COSMIC: The Catalogue Of Somatic Mutations In Cancer. *Nucleic Acids Res* (2019) 47:D941–47. doi: 10.1093/nar/gky1015
22. Boot A, Huang MN, Ng AWT, Ho SC, Lim JQ, Kawakami Y, et al. In-Depth Characterization of the Cisplatin Mutational Signature in Human Cell Lines and in Esophageal and Liver Tumors. *Genome Res* (2018) 28:654–65. doi: 10.1101/gr.230219.117
23. Robertson AG, Kim J, Al-Ahmadie H, Bellmunt J, Guo G, Cherniack AD, et al. Comprehensive Molecular Characterization of Muscle-Invasive Bladder Cancer. *Cell* (2017) 171:540–56.e25. doi: 10.1016/j.cell.2017.09.007
24. Alexandrov LB, Nik-Zainal S, Wedge DC, Aparicio SA, Behjati S, Biankin AV, et al. Signatures of Mutational Processes in Human Cancer. *Nature* (2013) 500(7463)415–21. doi: 10.1038/nature12477
25. Galsky MD. Tumor, immune, and stromal characteristics associated with clinical outcomes with atezolizumab (atezo) + platinum-based chemotherapy (PBC) or atezo monotherapy (mono) versus PBC in metastatic urothelial cancer (mUC) from the phase III IMvigor130 study2020; ASCO Virtual Scientific Program. *Am Soc Clin Oncol*.
26. Faltas BM, Prandi D, Tagawa ST, Molina AM, Nanus DM, Sternberg C, et al. Clonal Evolution of Chemotherapy-Resistant Urothelial Carcinoma. *Nat Genet* (2016) 48(12):1490–9. doi: 10.1038/ng.3692
27. Mullane SA, Werner L, Rosenberg J, Signoretti S, Callea M, Choueiri TK, et al. Correlation of Apobec Mrna Expression With Overall Survival and Pd-L1 Expression in Urothelial Carcinoma. *Sci Rep* (2016) 6:27702. doi: 10.1038/srep27702

Conflict of Interest: VK reports serving in a consulting or advisory role for AstraZeneca, Clovis, Janssen, Pfizer, EMD Serono, Seattle Genetics/Astellas, Dendreon, Guidepoint, GLG, and receiving research funding for the institution from Endocyte, Nektar, Clovis, Janssen and Taiho, all unrelated to the current submission. LF reports research support from Abbvie, Bavarian Nordic, Bristol Myer Squibb, Corvus, Dendreon, Janssen, Merck, and Roche/Genentech, and also declares serving as a scientific advisory board member to Actym, Allector, Astra Zeneca, Atreca, Bioalta, Bolt, Bristol Myer Squibb, Immunogenesis, Merck, Merck KGA, Nutcracker, RAPT, Scribe, Senti, Soteria, TeneoBio, and Roche/Genentech, all unrelated to the current submission.

The remaining authors declare that the research was conducted in the absence of any commercial or financial relationships that could be construed as a potential conflict of interest.

The reviewer RG declared a past co-authorship with one of the authors VK to the handling Editor.

Publisher's Note: All claims expressed in this article are solely those of the authors and do not necessarily represent those of their affiliated organizations, or those of the publisher, the editors and the reviewers. Any product that may be evaluated in this article, or claim that may be made by its manufacturer, is not guaranteed or endorsed by the publisher.

Copyright © 2022 Natesan, Zhang, Martell, Jindal, Devine, Stohr, Espinosa-Mendez, Grenert, Van Ziffle, Joseph, Umetsu, Onodera, Turski, Chan, Desai, Aggarwal, Wong, Porten, Chou, Friedlander, Fong, Small, Sweet-Cordero and Koshkin. This is an open-access article distributed under the terms of the Creative Commons Attribution License (CC BY). The use, distribution or reproduction in other forums is permitted, provided the original author(s) and the copyright owner(s) are credited and that the original publication in this journal is cited, in accordance with accepted academic practice. No use, distribution or reproduction is permitted which does not comply with these terms.

frontiers in Oncology

ORIGINAL RESEARCH
published: 07 March 2022
doi: 10.3389/fonc.2022.844520

Tumor-Educated Platelets as a Promising Biomarker for Blood-Based Detection of Renal Cell Carcinoma

Ruotao Xiao[1†], *Cheng Liu*[1†], *Bo Zhang*[2] *and Lulin Ma*[1*]

[1] Department of Urology, Peking University Third Hospital, Beijing, China, [2] Department of Pathology, School of Basic Medical Sciences, Peking University Health Science Center, Beijing, China

OPEN ACCESS

Edited by:
Michele Marchioni,
University of Studies G. d'Annunzio Chieti and Pescara, Italy

Reviewed by:
Myron Best,
Amsterdam University Medical Center, Netherlands
Francesco Pepe,
University of Naples Federico II, Italy

***Correspondence:**
Lulin Ma
malulinpku@163.com

[†]These authors have contributed equally to this work

Specialty section:
This article was submitted to Genitourinary Oncology, a section of the journal Frontiers in Oncology

Received: 28 December 2021
Accepted: 07 February 2022
Published: 07 March 2022

Citation:
Xiao R, Liu C, Zhang B and Ma L (2022) Tumor-Educated Platelets as a Promising Biomarker for Blood-Based Detection of Renal Cell Carcinoma. Front. Oncol. 12:844520. doi: 10.3389/fonc.2022.844520

Purpose: Tumor-educated platelets (TEPs) are a promising liquid biopsy in many cancers. However, their role in renal cell carcinoma (RCC) is unknown. Thus, this study explored the diagnostic value of TEPs in RCC patients.

Methods: Platelets were prospectively collected from 24 RCC patients and 25 controls. RNA-seq was performed to identify the differentially expressed genes (DEGs) between RCC patients and controls. Besides, RNA-seq data of pan-cancer TEPs were downloaded and randomly divided into training and validation sets. A pan-cancer TEP model was developed in the training set using the support vector machine (SVM) and validated in the validation set and our RCC dataset. Finally, an RCC-based TEP model was developed and optimized through the SVM algorithms and recursive feature elimination (RFE) method.

Result: Two hundred three DEGs, 64 (31.5%) upregulated and 139 (68.5%) downregulated, were detected in the platelets of RCC patients compared with controls. The pan-cancer TEP model had a high accuracy in detecting cancer in the internal validation (training set, accuracy 98.8%, AUC: 0.999; validation set, accuracy 95.4%, AUC: 0.972; different tumor subtypes, accuracy 86.6%–96.1%, AUC: 0.952–1.000). However, the pan-cancer TEP model in the external validation had a scarce diagnostic value in RCC patients (accuracy 48.7%, AUC: 0.615). Therefore, to develop the RCC-based TEP model, the gene biomarkers mostly contributing to the model were selected using the RFE method. The RCC-based TEP model containing 68 gene biomarkers reached a diagnostic accuracy of 100% (AUC: 1.000) in the training set, 88.9% (AUC: 0.963) in the validation set, and 95.9% (AUC: 0.988) in the overall cohort.

Conclusion: TEPs could function as a minimally invasive blood biomarker in the detection of RCC.

Keywords: renal cell carcinoma, tumor-educated platelets, biomarkers, diagnosis, liquid biopsy

INTRODUCTION

Renal cell carcinoma (RCC) is the 10th most frequently diagnosed cancer worldwide accounting for more than 90% of kidney tumors (1, 2). It is derived from the epithelial cells of the renal tubules. Localized RCC has a relatively favorable oncologic outcome after curative surgery, with a 5-year cancer-specific survival rate of 71%~88% (3). However, approximately 20% ~30% of patients already have metastasis at the time of diagnosis, with a median survival less than 2 years after cytoreductive surgery and adjuvant therapy (4, 5). Therefore, early detection of RCC is associated with a higher possibility of resecting the tumor, obtaining a better survival outcome. Blood-based tumor biomarkers have been developed in many cancers for screening and monitoring the tumor, such as alpha-fetoprotein in hepatocellular carcinoma, carcinoembryonic antigen in colorectal cancer, and prostate-specific antigen in prostate cancer (6–8). However, up to now, the diagnosis of RCC is still performed by the examination of images from the ultrasound scan, computed tomography, and magnetic resonance. Thus, blood-based biomarkers for the early diagnosis of RCC, as well as its screening and longitudinal monitoring, are still lacking.

Diagnostic tools for non-invasive tumors have rapidly developed in recent years, generating a new domain in cancer research called "liquid biopsy." Liquid biopsy allows to obtain information on the tumor through the analysis of human blood, urine, cerebrospinal fluid, and other body fluids, so as to obtain an early diagnosis and monitoring of the tumors (9). The markers analyzed in these samples, such as circulating tumor cells, circulating tumor DNA, circulating tumor RNA, and exosomes, have been widely studied in many cancers (10–13). However, the practical application of such markers for the non-invasive detection of RCC has been hampered by their low accuracy and high cost (14, 15). Therefore, the investigation of more cost-effective approaches is of paramount importance to enable urologists to diagnose RCC through a blood biopsy.

Accumulating evidence suggested the existence of a wide variety of cross-talk between platelets and tumor cells, promoting tumor progression and metastasis (16). Besides, tumor cells can modify the RNA profile of the platelets, indicating that the platelet transcriptome can be potentially used to diagnose cancer (16). Best et al. (17, 18) performed a series of studies on the platelet transcriptome, bringing a novel insight into the role of liquid biopsy. They indeed found that the platelets called tumor-educated platelets (TEPs), which are platelets modified by the tumor, can be used as a high-accuracy biomarker to distinguish patients with pan-cancer and non-small cell lung cancer (NSCLC) from healthy individuals (17, 18). The following studies further confirmed that TEPs can be used as a liquid biopsy in the diagnosis of sarcoma cancer, primary thyroid cancer (PTC), ovarian cancer, and glioblastoma (GBM) (19–22). However, there is still a lack of evidence to illustrate whether platelet RNA could also change in patients with RCC. Besides, the diagnostic value of TEPs in patients with RCC is still unknown. Therefore, the aim of this study was to characterize the transcriptome of TEPs from patients with RCC and controls to investigate whether they could be used as a blood-based biomarker in the detection of RCC.

MATERIAL AND METHODS

Sample Collection and Platelet Isolation

Patients diagnosed with RCC were prospectively recruited from the Peking University Third Hospital between October 2020 and May 2021 after the approval of the study by the Peking University Third Hospital Medical Science Research Ethics Committee (IRB:00006761-M2021003). In addition, patients with benign renal tumor (BN) and healthy donors (HD) were also recruited and used as the control group. The donors subjected to antiplatelet therapy or diagnosed with blood disease, acute infection, autoimmune disease, and severe renal and liver dysfunction were excluded from this study. Finally, 49 platelet samples from 24 patients with RCC, 12 patients with BN, and 13 HD were included in this study.

Platelets were obtained from the peripheral whole blood collected using 10 ml purple-cap vacutainers containing EDTA. Platelets were isolated within 24 h after blood collection to minimize their activation and RNA degeneration by two-step centrifugations at room temperature according to the protocol reported by Best et al. (23). The platelet pellet was harvested after centrifugation and resuspended in 1 ml TRIzol reagent. Finally, the platelet pellet was stored at −80°C for further analysis. Platelets were randomly collected and purity was assessed by morphological analysis, using the criteria of less than 1~5 leukocytes per one million platelets (23).

RNA Preparation and Sequencing

RNA was extracted from the platelets and assessed using the RNA Nano 6000 Assay Kit of the Bioanalyzer 2100 system. A total amount of RNA ≥100 ng and integrity number ≥7 were used as input material for the RNA sample preparation. Briefly, mRNA was purified from the total RNA using the poly-T oligo-attached magnetic beads. Fragmentation was carried out using divalent cations under high temperature in First-Strand Synthesis Reaction Buffer (5×). The first-strand cDNA was synthesized using random hexamer primer and M-MuLV Reverse Transcriptase (RNase H–). The second-strand cDNA synthesis was subsequently performed using DNA Polymerase I and RNase H. The remaining overhangs were converted into blunt ends *via* exonuclease/polymerase activity. After adenylation of the 3′ ends of the DNA fragments, the adaptor with hairpin loop structure was ligated to prepare the adaptor for the hybridization. The library fragments were purified using the AMPure XP system (Beckman Coulter, Beverly, USA) to select cDNA fragments of a preferential length of 370~420 bp. The PCR was performed using Phusion High-Fidelity DNA polymerase, Universal PCR primers, and Index (X) Primer. The PCR products were purified by the AMPure XP system and the library quality was assessed on the Agilent Bioanalyzer 2100 system. The clustering of the index-coded samples was performed on a cBot Cluster Generation System using TruSeq PE Cluster Kit v3-cBot-HS (Illumina) according to the manufacturer's instructions. After cluster generation, the library preparation was sequenced on an Illumina NovaSeq 6000 platform, and 150 bp paired-end reads were generated.

Transcriptome Analysis

Raw reads in the fastq format were firstly processed through in-house perl scripts. In this step, clean reads were obtained by removing from raw data the reads containing the adaptor, those containing ploy-N, and reads of low quality. Thus, downstream analysis was performed on the clean data with high quality. Reference genome and gene model annotation files were downloaded directly from the genome website. The index of the reference genome was built using Hisat2 v2.0.5, and paired-end clean reads were aligned to the reference genome using Hisat2 v2.0.5. StringTie (1.3.3b) was used to assemble and annotate new transcripts for those genes that were not successfully mapped (24). The new transcripts were called "novel. number."

The number of reads mapped to each gene was counted using Feature Counts v1.5.0-p3, and then the fragments per kilo base of transcript per million mapped fragments (FPKM) of each gene were calculated based on the length of the gene and read count mapped to this gene (25, 26). The differential expression of the genes in the two groups was evaluated using the edgeR package in R (3.22.5) (27). The *P*-values were adjusted using the Benjamini and Hochberg method (27). A false discovery rate (FDR) <0.05 and an absolute log2 fold change >1 were set as the threshold for a significant differential expression.

Gene Ontology (GO) enrichment analysis and Kyoto Encyclopedia of Genes and Genomes (KEGG) pathway analysis of the differentially expressed genes (DEGs) were performed by the cluster Profiler R package, in which the gene length bias was corrected. GO terms and KEGG pathways with FDR <0.05 were considered significantly enriched by the differentially expressed genes.

Model Development and Validation Using the Support Vector Machine

The RNA-sequence data of pan-cancer and HD samples were downloaded from the Gene Expression Omnibus with the accession number GSE68086 (https://www.ncbi.nlm.nih.gov/geo/query/acc.cgi?acc=GSE68086). A total of 228 pan-cancer samples and 55 HD samples were available in the GSE68086 database, which were randomly divided into training and internal validation sets at a 6:4 ratio using the "caret" package in R. In addition, 1,072 DEGs reported by Best et al. (17) were selected as classification features to perform an internal validation. A support vector machine (SVM) algorithm (radial basis function, RBF) was developed for binary sample classification using the "e1072" package in R and optimized by the training set using a 10-fold internal cross-validation to determine the best gamma and cost parameters. After optimization, the SVM parameters were fixed and validated in both the training set and internal validation set, as well as in different tumor subtypes. The external validation in our dataset was performed by the overlap of the DEGs of GSE68086 and RCC, including the 1,051 DEGs that were normalized by FPKM and selected as classification features. The SVM algorithm was developed, optimized, and internally validated as described above. Then, the SVM algorithm was externally validated in the RCC dataset to determine whether the pan-cancer TEP model could be applied specifically to RCC patients.

Besides, our aim was to develop an effective TEP-based classifier for patients with RCC. For this purpose, our patients and controls were randomly divided into training and validation sets at a 6:4 ratio and the DEGs were identified as mentioned above. The recursive feature elimination (RFE) method was used to narrow down the features in the training group to further optimize the DEGs to the model (28). After optimization, the DEGs were selected as classification features. The development, optimization, and validation of the SVM model were achieved as described above.

The predicted sample classes and actual sample classes were compared using the confounding matrix to measure the performance of the model by determining the sensitivity, specificity, and accuracy. The performance of the model was also evaluated by the receiver operating characteristic (ROC) curve and the area under the curve (AUC) using the "pROC" package in R. Overall, the flowchart of this study is summarized in **Figure 1**.

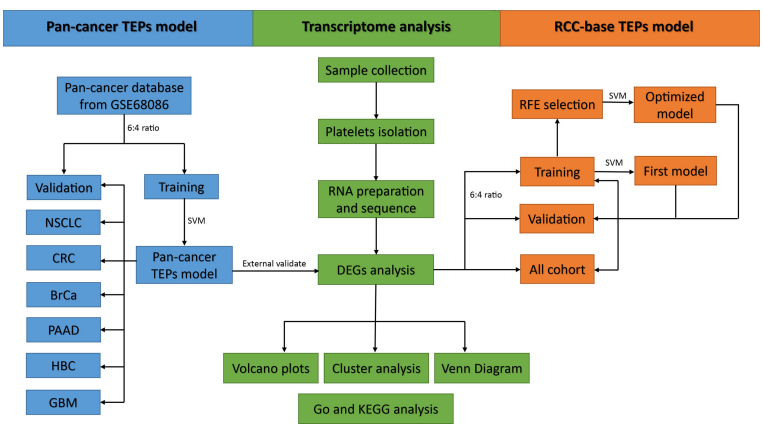


FIGURE 1 | Flowchart of the main analytic steps in our study.

RESULTS

Patients' Characteristics

A total of 49 samples consisting of 24 RCC and 25 non-RCC control (13 HD, 12 BN) were used in this study. The baseline data including age, gender, BMI, complications, and laboratory indices between the RCC and control groups were similar, as shown in **Table 1**. A total of 18 cases, 2 cases, and 4 cases in the RCC group were clear cell renal cell carcinoma (ccRCC), papillary renal cell carcinoma (pRCC), and chromophobe renal cell carcinoma (chRCC), respectively (**Table 2**). Besides, 5 cases and 4 cases were combined with the involvement of lymph nodes and distant metastasis, respectively, at the time of diagnosis. Among the BN in the control group, 11 cases and 1 case were angiomyolipoma and oncocytoma, respectively. Platelets' purity was assessed by morphological analysis, with satisfactory purity results (**Supplementary Figure 1**).

TABLE 2 | The pathological data of patients with RCC.

Variables	RCC patients (*N* = 24)
Tumor size, cm	6.61 ± 2.71
Histologic subtypes	
ccRCC	18 (75)
pRCC	2 (8.3)
chRCC	4 (16.7)
WHO/ISUP nuclear grade	
I–II	11 (45.8)
III–IV	9 (37.5)
Unknown	4 (16.7)
T stage	
T1–T2	6 (25)
T3–T4	18 (75)
N stage	
N0	19 (79.2)
N1	5 (20.8)
M stage	
M0	20 (83.3)
M1	4 (16.7)

ccRCC, clear cell renal cell carcinoma; pRCC, papillary renal cell carcinoma; chRCC, chromophobe renal cell carcinoma.

DEGs Between the RCC and non-RCC Groups

After the RNA-seq of the platelets of each sample, a mean read count of 40~50 million reads per sample was obtained. The general RNA expression patterns among individuals and among groups were similar (**Supplementary Figure 2**). Besides, the RNA profile of each sample in our dataset had a moderate to high correlation with the samples in the pan-cancer dataset (**Supplementary Table 1**). A total of 37,008 RNAs were detected in our platelet dataset. An FDR <0.05 and an absolute log2 fold change >1 were used as the statistical cutoffs to determine the DEGs between the RCC and non-RCC groups. Eventually, 203 DEGs were identified between the RCC and non-RCC groups, with 64 (31.5%) upregulated genes and 139 (68.5%) downregulated genes (**Figure 2A** and **Supplementary Table 2**). Furthermore, the non-RCC controls were randomly divided into A and B groups, but only 9 DEGs were identified between the A and B groups using the same criteria, suggesting that the DEGs between the RCC and non-RCC groups are mainly caused by cancer (**Figure 2B**). In subgroup analysis, the DEGs could also be identified in local RCC (59 DEGs) and metastatic RCC (39 DEGs) compared with controls (**Supplementary Figure 3**). Unsupervised hierarchical clustering analysis based on 203 DEGs showed that the TEP RNA could satisfactorily distinguish RCC and non-RCC individuals with only minor overlaps (**Figure 2C**). Besides, the DEGs in our dataset were also compared with the DEGs reported in NSCLC described by Best et al. (18), GBM described by Sol et al. (22), and PTC described by Shen et al. (20). The results showed that different tumor types only have a minor overlap of platelet DEGs, suggesting that the effects of the tumor on TEP RNA probably depend on the specific type of tumor (**Figure 2D**).

The GO analysis revealed that DEGs were enriched in three main categories, namely, "biological process", "cellular component", and "molecular function" (**Figure 3A** and **Supplementary Table 3**). The DEGs in the biological process were enriched in several pathways including humoral immune response, antimicrobial

TABLE 1 | The baseline data between the RCC and control groups.

Variables	Total (*N* = 49)	RCC (*N* = 24)	Control (*N* = 25)	*P*
Age, years	52.84 ± 12.05	53.82 ± 11.92	51.88 ± 12.34	0.567
Gender				
Men	25 (51)	14 (58.3)	11 (44)	0.396
Women	24 (49)	10 (41.7)	14 (56)	
BMI, kg/m^2	24.69 ± 3.32	24.72 ± 2.91	24.66 ± 3.73	0.943
Complications				
Hypertension	17 (34.7)	10 (41.7)	7 (28)	0.377
Diabetes mellitus	8 (16.3)	3 (12.5)	5 (20)	0.702
Cardiovascular disease	5 (10.2)	3 (12.5)	2 (8)	0.667
Laboratory indices				
WBC, ×10^9/L	6.58 ± 1.97	6.46 ± 2.28	6.70 ± 1.65	0.681
HGB, g/L	138.76 ± 19.17	140.67 ± 24.25	136.92 ± 12.82	0.506
PLT, ×10^9/L	244.16 ± 77.16	248.08 ± 93.03	240.40 ± 59.85	0.731
MPV, fl	10.53 ± 1.2	10.33 ± 1.36	10.72 ± 1.01	0.259
PDW, fl	12.53 ± 2.75	12.09 ± 3.15	12.95 ± 2.29	0.281

BMI, body mass index; WBC, white blood cell; HGB, hemoglobin; PLT, platelet count; MPV, mean platelet volume; PDW, platelet distribution width.

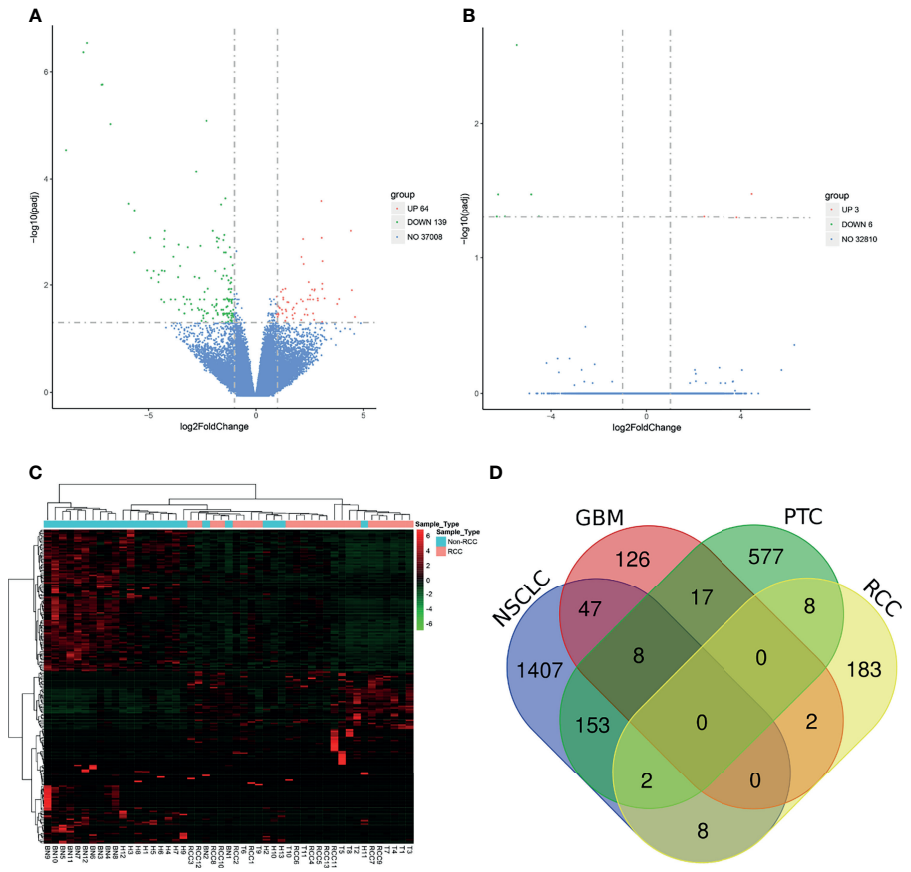


FIGURE 2 | Analysis of differentially expressed genes (DEGs) in the platelet between the renal cell carcinoma (RCC) and control groups. **(A)** Volcano plot of DEGs between the RCC group and the control group. **(B)** Volcano plot of DEGs between groups A and B in the control group. **(C)** Unsupervised cluster analysis of DEGs in those platelet samples. **(D)** Venn diagram of DEGs in four different tumor types.

humoral response, and defense response to bacterium. Besides, the cellular component category contains several GO terms such as vacuolar lumen, immunoglobulin complex, and lysosomal lumen, while the molecular function category contains the terms antigen binding, glycosaminoglycan binding, and immunoglobulin receptor binding. The KEGG pathway enrichment analysis showed that the DEGs were mainly enriched in pancreatic secretion, protein digestion and absorption, and fat digestion and absorption (**Figure 3B** and **Supplementary Table 4**).

Development and Validation of the Pan-Cancer TEP Model

The GSE68086 database contains 228 pan-cancer samples and 55 HD samples, including 139 pan-cancer samples and 39 HD in the training set and the remaining in the validation set. The SVM algorithm containing 1,072 DEG features was trained using the sample from the training set by a 10-fold internal validation to develop the pan-cancer TEP model. The best gamma and cost parameters were identified as 0.001 and 10, and then, the SVM parameter was locked. Subsequently, the pan-cancer TEP model was validated in both the training and validation sets. The AUC of the model in the training and validation sets was 0.999 and 0.972, respectively (**Figures 4A, B**). Besides, the sensitivity, specificity, and accuracy in the training set were 99.3%, 97.4%, and 98.8%, respectively, while in the validation set, these were 97.8%, 81.3%, and 95.4%, respectively (**Figures 4C, D**).

Next, the pan-cancer dataset was separated into NSCLC, colorectal cancer (CRC), pancreatic cancer (PAAD), breast cancer (BrCa), hepatobiliary cancer (HBC), GBM, and HD subgroups to internally validate the predictive value of the pan-cancer TEP model in detecting cancer in different tumor subtypes. These subgroups were validated using the pan-cancer TEP model. The results revealed that the pan-cancer TEP model could also detect the specific tumor contained in the model development. The AUC of the model for different tumor types ranged from 0.952 to 1.000 (**Figures 4A, B**), and the accuracy ranged from 86.6% to 96.1% (**Figure 4E**). The model was also used to detect RCC using our database to externally validate the performance of the pan-cancer TEP model in RCC. The accuracy and AUC of the pan-cancer TEP model for RCC were only 48.7% and 0.615, respectively, suggesting that the pan-cancer TEP model had a scarce diagnostic value in detecting RCC (**Figures 4F, G**).

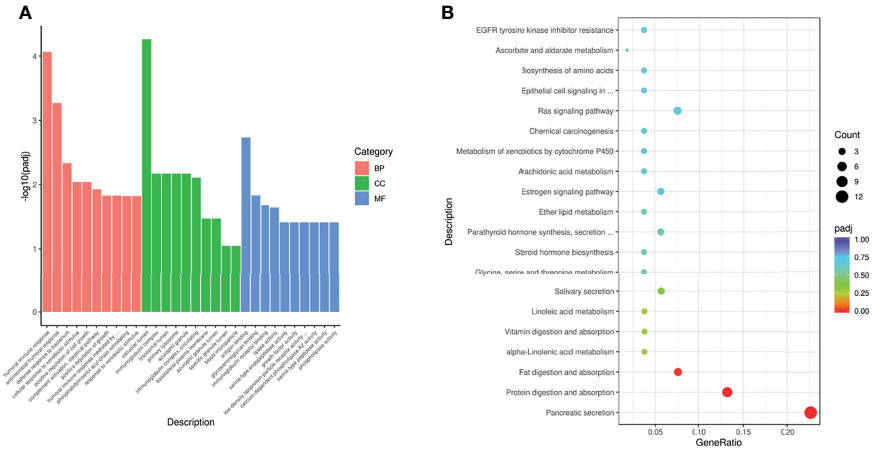


FIGURE 3 | GO **(A)** and KEGG **(B)** enrichment analysis of DEGs between the RCC and control groups.

Development and Optimization of the RCC-Based TEP Model

Our dataset including 24 RCC and 25 non-RCC was randomly divided into training and validation sets at a 6:4 ratio. The RCC-based TEP model was preliminarily developed using the 203 DEGs in the training set. The best gamma and cost identified were 0.00001 and 100 after the 10-fold internal validation. The primary RCC-based TEP model showed an excellent performance in the training set, validation set, and overall cohort, with an AUC of 0.987, 0.975, and 0.978, respectively (**Figure 5A**). Besides, the sensitivity, specificity, and accuracy in the training set (100%, 87.5%, and 93.5%), validation set (100%, 88.9%, and 94.4%), and overall cohort (100%, 88%, and 93.9%) were also favorable (**Figures 5B–D**). Next, the RFE method was used to select the optimal biomarkers to achieve a high prediction and few DEGs. After RFE selection, 68 DEGs were chosen as the optimal biomarkers in the RCC-based TEP model (**Figure E** and **Supplementary Table 5**). Then, the optimized RCC-based TEP model was developed in the training set and validated in the training set, validation set, and overall cohort (gamma and cost were 0.001 and 10). Finally, the AUC of the optimized model was 1.000, 0.963, and 0.988, respectively (**Figure 5F**). The sensitivity, specificity, and accuracy in the training set (100%, 100%, and 100%), validation set (77.8%, 100%, and 88.9%), and all cohorts (91.7%, 100%, and 95.9%) were also satisfying (**Figures 5G–I**). In the subgroup analysis, the RCC-based TEP model also showed a high accuracy in detecting both local (accuracy: 95.2%, AUC:0.991) and metastatic RCC (accuracy: 100%, AUC:1.000) (**Supplementary Figure 4**). The optimized RCC-based TEP model was comparable to the first model but with fewer biomarkers, and an external validation was easier to be performed.

DISCUSSION

Platelets are non-nucleated blood cells in the human circulation and cannot synthesize RNA on their own. The RNA repository of platelets including mRNA, miRNA, and lncRNA was mainly derived from megakaryocytes, and some of them are endocytosed from circulation. Tumor cells can directly bind to the platelets through selectin-P and glycoprotein-IIa/IIIb to directly "educate" platelets to participate in tumor progression and metastasis, or indirectly educate them by secreting extracellular molecular substances such as thrombin, tissue factor, matrix metalloproteinase, and ADP (29–31). This "education" process also causes specific changes in the RNA profile of the platelets. Preclinical studies showed that tumor cells may affect the RNA profile of the platelets through the following mechanisms (32): 1) secreting tumor-derived cytokines that affect the maturation of megakaryocytes, 2) inducing protein translation in the platelets and accelerating the degradation of RNA, 3) stimulating specific splicing events of the pre-RNA in the platelets, and 4) sequestrating the tumor-derived RNA. The above mechanisms suggest the presence of a highly dynamic RNA profile in the platelets, which makes them feasible for liquid biopsy in the detection of cancer.

Calverley et al. (33) were the first to discover that the mRNA profile of the platelets in patients with metastatic lung cancer is significantly altered compared with that in the HD, with 3 upregulated genes and 197 downregulated genes. Besides, Nilsson et al. (34) revealed a distinct RNA signature in platelets from glioma patients compared with that from healthy individuals. They also discovered that platelets isolated from glioma and prostate cancer patients contain the cancer-associated RNA biomarkers EGFRvIII and PCA3, respectively. Subsequently, they enrolled 77 patients with NSCLC and found that platelets can be used for the non-invasive detection of EML4-ALK rearrangements in these patients predicting the outcome of the therapy (35). Another study demonstrated that the RNA of the platelets can also predict the response to the therapy with abiraterone in patients with castration-resistant prostate cancer (36). These results suggest that platelet RNA partially reflects the molecular characteristics of a primary tumor and predicts the therapeutic response to a specific drug.

The development of second-generation high-throughput sequencing technology allowed Best et al. (17, 18) to bring the concept of TEPs to the forefront of "liquid biopsy" of the tumor

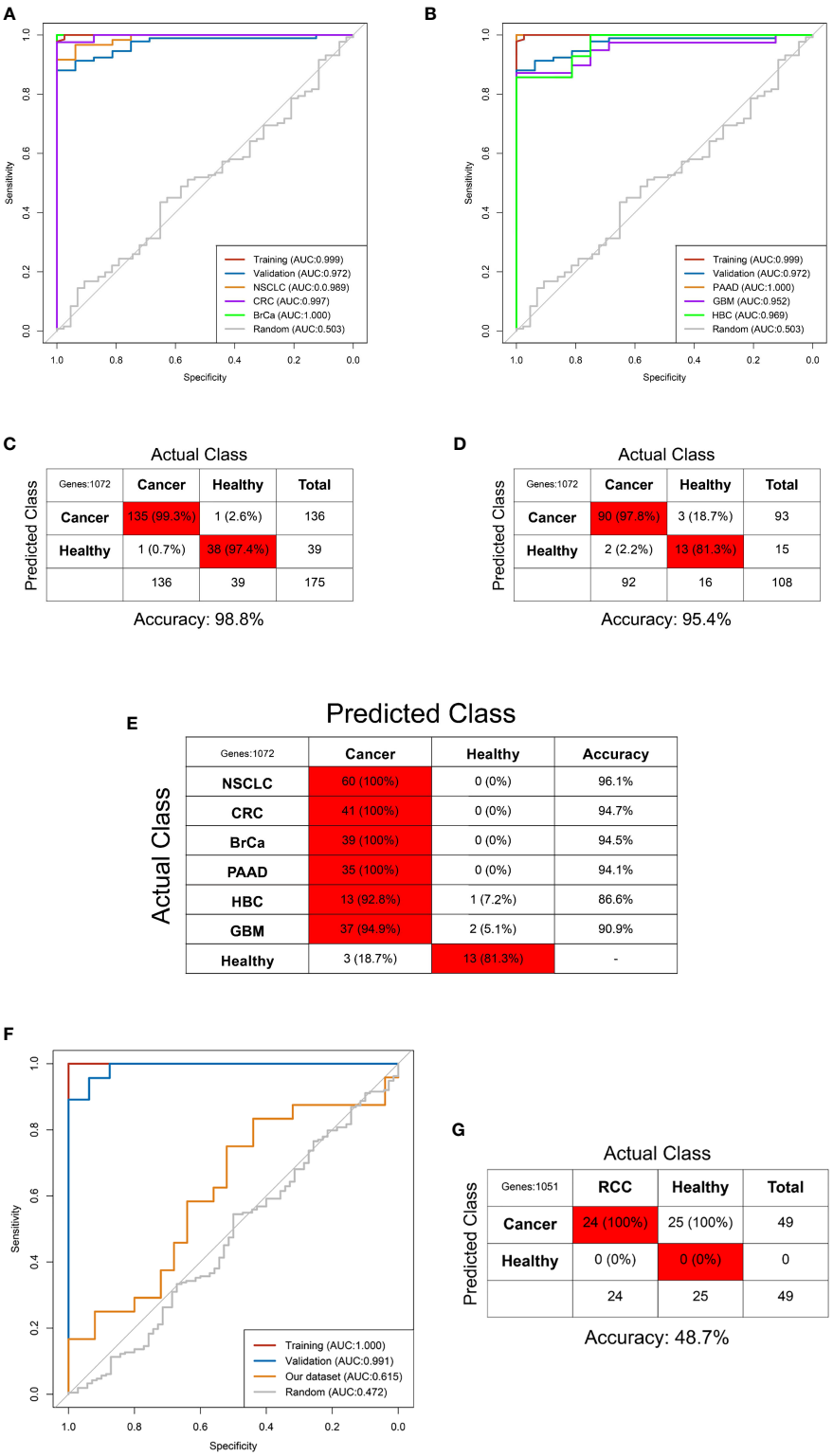


FIGURE 4 | Predictive accuracy of the pan-cancer TEP model shown by the ROC curves in the internal **(A, B)** and external validation **(F)** and the confounding matrix in the training **(C)**, validation **(D)**, and internal different tumor types **(E)** and external RCC patients **(G)**.

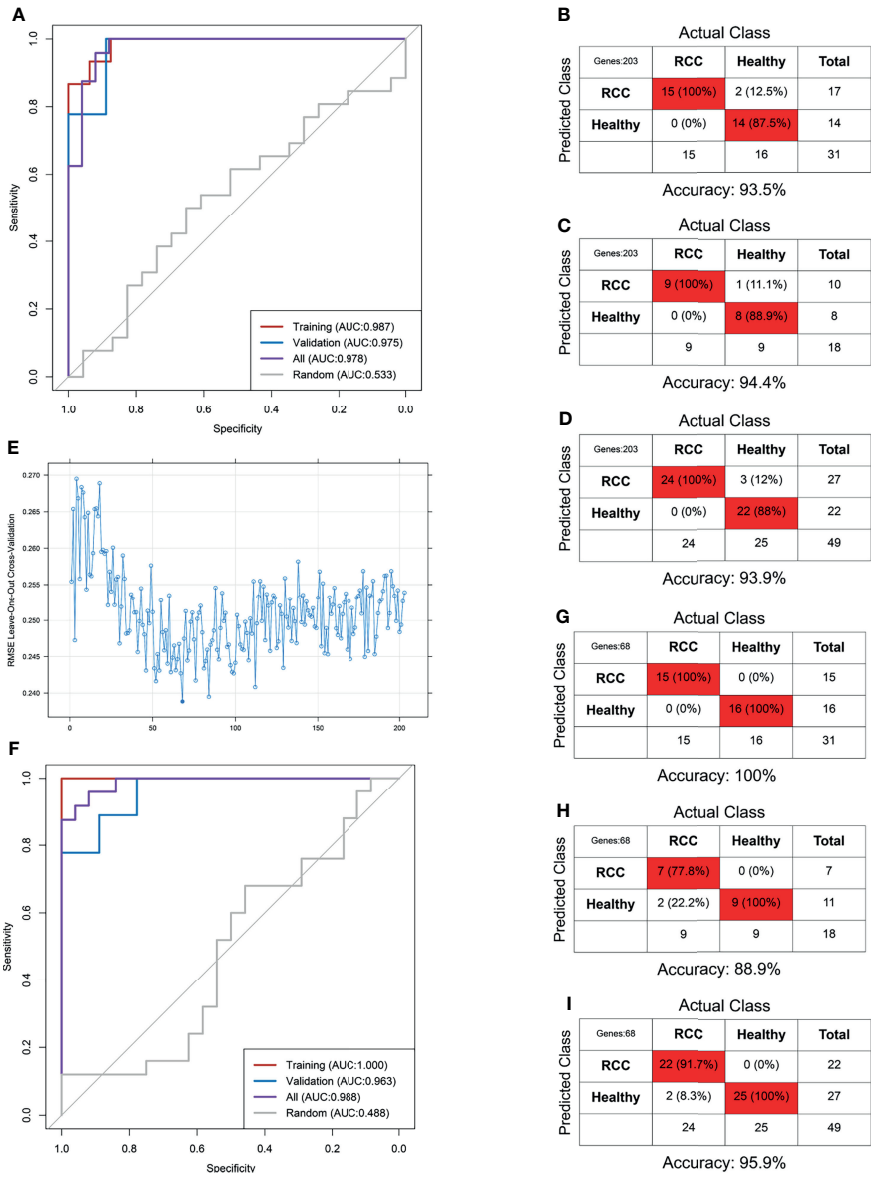


FIGURE 5 | The RCC-based TEP model for the detection of RCC. The ROC curve **(A)** and the confounding matrix in the training set **(B)**, validation set **(C)**, and overall cohort **(D)** of the primary model. The ROC curve **(F)** and the confounding matrix in the training set **(G)**, validation set **(H)**, and overall cohort **(I)** of the optimized model after REF selection **(E)**.

through a series of exploratory studies. In 2015, they prospectively enrolled 228 pan-cancer and 55 HD with RNA-seq on platelet samples, discovering that TEPs allow not only the detection of cancer when present (accuracy 96%) but also the evaluation of the type of cancer (accuracy 71%) across six different types. They also expanded the study cohorts to further explore the diagnostic value of TEPs for NSCLC, including 779 NSCLC patients and 339 controls, and they optimized the algorithm (18). Their results using the particle-swarm optimization-enhanced algorithms demonstrated that TEPs enable the detection of early (accuracy 81%) and late (accuracy 88%) NSCLC, regardless of the age of the individuals, smoking habits, whole-blood storage time, and various inflammatory conditions (18). After the protocol was reported by Best et al. (23), several studies explored the diagnostic value of TEPs in patients with sarcoma, PTC, ovarian cancer, and GBM, with an excellent predictive accuracy (19–22).

Despite that, to our knowledge, evidence that TEPs could serve as a diagnostic tool in patients with RCC is still lacking. The aim of this study was to investigate the diagnostic value of TEPs in patients with RCC, and several noteworthy findings were found and described. Firstly, the TEP transcriptome was significantly altered in patients with RCC compared with that in controls. The alteration in TEPs was different compared with other cancers and the majority of the alteration was exclusive,

which was consistent with the findings reported by Heinhuis et al. (19). Secondly, the pan-cancer TEP model had an excellent performance in detecting patients with pan-cancer and specific cancer contained in the model development, but it could not be used to distinguish those with RCC. To our knowledge, the pan-cancer TEP model contains six types of tumors but without RCC. The low diagnostic accuracy of the pan-cancer TEP model for RCC patients also explains that different tumors had heterogeneous effects on the platelet RNA, and the pan-cancer TEP model is not universal for all cancers. The TEP model should be cancer-specific. Eventually, the TEP model for RCC patients was developed and optimized with satisfactory accuracy. It is worth noting that the model only contains 68 gene signatures, but the accuracy was comparable to other TEP models reported in the above cancers. Our hypothesis is that TEPs could be used as a promising tool for liquid biopsy in RCC populations, although an external validation is still needed.

This study has some limitations. Firstly, the sample number is relatively low especially when divided into training and validation sets due to the prospective nature of the study. Thus, more samples are needed to develop a more robust prediction algorithm. Secondly, the TEP model was not externally validated in another RCC cohort, potentially leading to an overestimation of the predictive accuracy. Thirdly, although the TEP model demonstrated high predictive accuracy in our analytic cohorts, more than half of the enrolled patients had cancer at an advanced stage (T3–T4). Thus, it is necessary to include more patients with low-stage RCC to verify our findings in a prospective study. Finally, the potential role of TEPs as a universal biomarker still needs to be verified in additional different types of tumors, and the function of altered RNAs in platelets still needs to be investigated.

CONCLUSION

Our dataset provided a preliminary reference and resource for the TEP RNA profile in patients with RCC. Our results demonstrated that the pan-cancer TEP model barely detected RCC. Thus, the RCC-based TEP model was developed using our dataset with high accuracy in cancer detection.

DATA AVAILABILITY STATEMENT

The original contributions presented in the study are publicly available. These data can be found here: NCBI, PRJNA799249, https://www.ncbi.nlm.nih.gov/bioproject/PRJNA799249.

ETHICS STATEMENT

The studies involving human participants were reviewed and approved by Peking University Third Hospital Medical Science Research Ethics Committee (IRB:00006761). The patients/participants provided their written informed consent to participate in this study.

AUTHOR CONTRIBUTIONS

Study concept and design: LM and BZ. Analysis and interpretation of data: RX and CL. Drafting of the manuscript: RX and CL. Critical revision of the manuscript: LM. All authors read and approved the final manuscript.

FUNDING

This work was supported by grants from the Natural Science Foundation of China (82070778, 81972381, 82173385).

ACKNOWLEDGMENTS

We thank all the participants for their selfless contribution of their blood samples in this study.

SUPPLEMENTARY MATERIAL

The Supplementary Material for this article can be found online at: https://www.frontiersin.org/articles/10.3389/fonc.2022.844520/full#supplementary-material

Supplementary Figure 1 | The purity of platelets of 6 different samples **(A–F)** in morphological analysis after two-steps configuration (Wright-Giemsa stain, 400×).

Supplementary Figure 2 | Gene expression analysis of platelet samples. **(A)** Gene expression box plot; **(B)** Principal component analysis plot; **(C)** Sample correlation heatmap matrix.

Supplementary Figure 3 | Analysis of differentially expressed genes (DEGs) in the platelet of local **(A)** and metastatic **(B)** RCC compared to control group.

Supplementary Figure 4 | The optimized RCC-based TEP model for the detection of RCC. ROC curve **(A)** and confound matrix in local **(B)** and metastatic **(C)** RCC.

REFERENCES

1. Hsieh JJ, Purdue MP, Signoretti S, Swanton C, Albiges L, Schmidinger ML, et al. Renal Cell Carcinoma. *Nat Rev Dis Primers* (2017) 3:17009. doi: 10.1038/nrdp.2017.9
2. Chow WH, Dong LM, Devesa SS. Epidemiology and Risk Factors for Kidney Cancer. *Nat Rev Urol* (2010) 7:245–57. doi: 10.1038/nrurol.2010.46
3. Leibovich BC, Lohse CM, Crispen PL, Boorjian SA, Thompson RH, Blute ML, et al. Histological Subtype is an Independent Predictor of Outcome for Patients With Renal Cell Carcinoma. *J Urol* (2010) 183:1309–15. doi: 10.1016/j.juro.2009.12.035
4. Wiechno P, Kucharz J, Sadowska M, Michalski W, Sikora-Kupis B, Jonska-Gmyrek J, et al. Contemporary Treatment of Metastatic Renal Cell Carcinoma. *Med Oncol* (2018) 35:156. doi: 10.1007/s12032-018-1217-1
5. Méjean A, Ravaud A, Thezenas S, Colas S, Beauval JB, Bensalah K, et al. Sunitinib Alone or After Nephrectomy in Metastatic Renal-Cell Carcinoma. *N Engl J Med* (2018) 379:417–27. doi: 10.1056/NEJMoa1803675

6. Lilja H, Ulmert D, Vickers AJ. Prostate-Specific Antigen and Prostate Cancer: Prediction, Detection and Monitoring. *Nat Rev Cancer* (2008) 8:268–78. doi: 10.1038/nrc2351
7. Zheng Y, Zhu M, Li M. Effects of Alpha-Fetoprotein on the Occurrence and Progression of Hepatocellular Carcinoma. *J Cancer Res Clin Oncol* (2020) 146:2439–46. doi: 10.1007/s00432-020-03331-6
8. Nicholson BD, Shinkins B, Pathiraja I, Roberts NW, James TJ, Mallett S, et al. Blood CEA Levels for Detecting Recurrent Colorectal Cancer. *Cochrane Database Syst Rev* (2015) 2015:CD011134. doi: 10.1002/14651858.CD011134.pub2
9. Ignatiadis M, Sledge GW, Jeffrey SS. Liquid Biopsy Enters the Clinic - Implementation Issues and Future Challenges. *Nat Rev Clin Oncol* (2021) 18:297–312. doi: 10.1038/s41571-020-00457-x
10. Ye Q, Ling S, Zheng S, Xu X. Liquid Biopsy in Hepatocellular Carcinoma: Circulating Tumor Cells and Circulating Tumor DNA. *Mol Cancer* (2019) 18:114. doi: 10.1186/s12943-019-1043-x
11. Rolfo C, Mack PC, Scagliotti GV, Baas P, Barlesi F, Bivona TG, et al. Liquid Biopsy for Advanced Non-Small Cell Lung Cancer (NSCLC): A Statement Paper From the IASLC. *J Thorac Oncol* (2018) 13:1248–68. doi: 10.1016/j.jtho.2018.05.030
12. Cirillo M, Craig AFM, Borchmann S, Kurtz DM. Liquid Biopsy in Lymphoma: Molecular Methods and Clinical Applications. *Cancer Treat Rev* (2020) 91:102106. doi: 10.1016/j.ctrv.2020.102106
13. Normanno N, Cervantes A, Ciardiello F, De Luca A, Pinto C. The Liquid Biopsy in the Management of Colorectal Cancer Patients: Current Applications and Future Scenarios. *Cancer Treat Rev* (2018) 70:1–8. doi: 10.1016/j.ctrv.2018.07.007
14. Cimadamore A, Gasparrini S, Massari F, Santoni M, Cheng L, Lopez-Beltran A, et al. Emerging Molecular Technologies in Renal Cell Carcinoma: Liquid Biopsy. *Cancers (Basel)* (2019) 11:196. doi: 10.3390/cancers11020196
15. Lakshminarayanan H, Rutishauser D, Schraml P, Moch H, Bolck HA. Liquid Biopsies in Renal Cell Carcinoma-Recent Advances and Promising New Technologies for the Early Detection of Metastatic Disease. *Front Oncol* (2020) 10:582843. doi: 10.3389/fonc.2020.582843
16. Haemmerle M, Stone RL, Menter DG, Afshar-Kharghan V, Sood AK. The Platelet Lifeline to Cancer: Challenges and Opportunities. *Cancer Cell* (2018) 33:965–83. doi: 10.1016/j.ccell.2018.03.002
17. Best MG, Sol N, Kooi I, Tannous J, Westerman BA, Rustenburg F, et al. RNA-Seq of Tumor-Educated Platelets Enables Blood-Based Pan-Cancer, Multiclass, and Molecular Pathway Cancer Diagnostics. *Cancer Cell* (2015) 28:666–76. doi: 10.1016/j.ccell.2015.09.018
18. Best MG, Sol N, In 't Veld SGJG, Vancura A, Muller M, Niemeijer AN, et al. Swarm Intelligence-Enhanced Detection of Non-Small-Cell Lung Cancer Using Tumor-Educated Platelets. *Cancer Cell* (2017) 32:238–52.e9. doi: 10.1016/j.ccell.2017.07.004
19. Heinhuis KM, In 't Veld SGJG, Dwarshuis G, van den Broek D, Sol N, Best MG, et al. RNA-Sequencing of Tumor-Educated Platelets, a Novel Biomarker for Blood-Based Sarcoma Diagnostics. *Cancers (Basel)* (2020) 12:1372. doi: 10.3390/cancers12061372
20. Shen Y, Lai Y, Xu D, Xu L, Song L, Zhou J, et al. Diagnosis of Thyroid Neoplasm Using Support Vector Machine Algorithms Based on Platelet RNA-Seq. *Endocrine* (2021) 72:758–83. doi: 10.1007/s12020-020-02523-x
21. Pastuszak K, Supernat A, Best MG, In 't Veld SGJG, Łapińska-Szumczyk S, Łojkowska A, et al. Implatelet Classifier: Image-Converted RNA Biomarker Profiles Enable Blood-Based Cancer Diagnostics. *Mol Oncol* (2021) 15:2688–701. doi: 10.1002/1878-0261.13014
22. Sol N, In 't Veld SGJG, Vancura A, Tjerkstra M, Leurs C, Rustenburg F, et al. Tumor-Educated Platelet RNA for the Detection and (Pseudo)progression Monitoring of Glioblastoma. *Cell Rep Med* (2020) 1:100101. doi: 10.1016/j.xcrm.2020.100101
23. Best MG, In 't Veld SGJG, Sol N, Wurdinger T. RNA Sequencing and Swarm Intelligence-Enhanced Classification Algorithm Development for Blood-Based Disease Diagnostics Using Spliced Blood Platelet RNA. *Nat Protoc* (2019) 14:1206–34. doi: 10.1038/s41596-019-0139-5
24. Pertea M, Pertea GM, Antonescu CM, Chang TC, Mendell JT, Salzberg SL. StringTie Enables Improved Reconstruction of a Transcriptome From RNA-Seq Reads. *Nat Biotechnol* (2015) 33:290–5. doi: 10.1038/nbt.3122
25. Liao Y, Smyth GK, Shi W. Featurecounts: An Efficient General Purpose Program for Assigning Sequence Reads to Genomic Features. *Bioinformatics* (2014) 30:923–30. doi: 10.1093/bioinformatics/btt656
26. Bray NL, Pimentel H, Melsted P, Pachter L. Near-Optimal Probabilistic RNA-Seq Quantification. *Nat Biotechnol* (2016) 34:525–7. doi: 10.1038/nbt.3519
27. Robinson MD, McCarthy DJ, Smyth GK. Edger: A Bioconductor Package for Differential Expression Analysis of Digital Gene Expression Data. *Bioinformatics* (2010) 26:139–40. doi: 10.1093/bioinformatics/btp616
28. Wottschel V, Chard DT, Enzinger C, Filippi M, Frederiksen JL, Gasperini C, et al. SVM Recursive Feature Elimination Analyses of Structural Brain MRI Predicts Near-Term Relapses in Patients With Clinically Isolated Syndromes Suggestive of Multiple Sclerosis. *NeuroImage Clin* (2019) 24:102011. doi: 10.1016/j.nicl.2019.102011
29. Pang JH, Coupland LA, Freeman C, Chong BH, Parish CR. Activation of Tumour Cell ECM Degradation by Thrombin-Activated Platelet Membranes: Potentially a P-Selectin and GPIIb/IIIa-Dependent Process. *Clin Exp Metastasis* (2015) 32:495–505. doi: 10.1007/s10585-015-9722-5
30. Kessenbrock K, Plaks V, Werb Z. Matrix Metalloproteinases: Regulators of the Tumor Microenvironment. *Cell* (2010) 141:52–67. doi: 10.1016/j.cell.2010.03.015
31. Gay LJ, Felding-Habermann B. Contribution of Platelets to Tumour Metastasis. *Nat Rev Cancer* (2011) 11:123–34. doi: 10.1038/nrc3004
32. Schubert S, Weyrich AS, Rowley JW. A Tour Through the Transcriptional Landscape of Platelets. *Blood* (2014) 124:493–502. doi: 10.1182/blood-2014-04-512756
33. Calverley DC, Phang TL, Choudhury QG, Gao B, Oton AB, Weyant MJ, et al. Significant Downregulation of Platelet Gene Expression in Metastatic Lung Cancer. *Clin Transl Sci* (2010) 3:227–32. doi: 10.1111/j.1752-8062.2010.00226.x
34. Nilsson RJ, Balaj L, Hulleman E, van Rijn S, Pegtel DM, Walraven M, et al. Blood Platelets Contain Tumor-Derived RNA Biomarkers. *Blood* (2011) 118:3680–3. doi: 10.1182/blood-2011-03-344408
35. Nilsson RJ, Karachaliou N, Berenguer J, Gimenez-Capitan A, Schellen P, Teixido C, et al. Rearranged EML4-ALK Fusion Transcripts Sequester in Circulating Blood Platelets and Enable Blood-Based Crizotinib Response Monitoring in Non-Small-Cell Lung Cancer. *Oncotarget* (2016) 7:1066–75. doi: 10.18632/oncotarget.6279
36. Tjon-Kon-Fat LA, Lundholm M, Schröder M, Wurdinger T, Thellenberg-Karlsson C, Widmark A, et al. Platelets Harbor Prostate Cancer Biomarkers and the Ability to Predict Therapeutic Response to Abiraterone in Castration Resistant Patients. *Prostate* (2018) 78:48–53. doi: 10.1002/pros.23443

Conflict of Interest: The authors declare that the research was conducted in the absence of any commercial or financial relationships that could be construed as a potential conflict of interest.

Publisher's Note: All claims expressed in this article are solely those of the authors and do not necessarily represent those of their affiliated organizations, or those of the publisher, the editors and the reviewers. Any product that may be evaluated in this article, or claim that may be made by its manufacturer, is not guaranteed or endorsed by the publisher.

Copyright © 2022 Xiao, Liu, Zhang and Ma. This is an open-access article distributed under the terms of the Creative Commons Attribution License (CC BY). The use, distribution or reproduction in other forums is permitted, provided the original author(s) and the copyright owner(s) are credited and that the original publication in this journal is cited, in accordance with accepted academic practice. No use, distribution or reproduction is permitted which does not comply with these terms.

frontiers in Oncology

SYSTEMATIC REVIEW
published: 18 March 2022
doi: 10.3389/fonc.2022.868031

Prognostic and Predictive Value of Liquid Biopsy-Derived Androgen Receptor Variant 7 (AR-V7) in Prostate Cancer: A Systematic Review and Meta-Analysis

Tanzila Khan[1,2,3], *Therese M. Becker*[2,3,4], *Kieran F. Scott*[1,2], *Joseph Descallar*[4,5], *Paul de Souza*[1,2,6], *Wei Chua*[1,2,4,7] *and Yafeng Ma*[2,3,4*]

[1] School of Medicine, Western Sydney University, Campbelltown, NSW, Australia, [2] Medical Oncology, Ingham Institute of Applied Medical Research, Liverpool, NSW, Australia, [3] Centre of Circulating Tumour Cell Diagnostics & Research, Ingham Institute of Applied Medical Research, Liverpool, NSW, Australia, [4] South West Sydney Clinical School, University of New South Wales, Liverpool Hospital, Liverpool, NSW, Australia, [5] Ingham Institute of Applied Medical Research, Liverpool, NSW, Australia, [6] School of Medicine, University of New South Wales, Kensington, NSW, Australia, [7] Medical Oncology, Liverpool Hospital, Liverpool, NSW, Australia

OPEN ACCESS

Edited by:
Riccardo Tellini,
Careggi University Hospital, Italy

Reviewed by:
Hideki Maeda,
Meiji Pharmaceutical University, Japan
Aasems Jacob,
Pikeville Medical Center, United States
Haoran Liu,
Stanford University, United States
Carlo Cattrini,
Azienda Ospedaliero Universitaria Maggiore della Carità, Italy

***Correspondence:**
Yafeng Ma
yafeng.ma@unsw.edu.au

Specialty section:
This article was submitted to Genitourinary Oncology, a section of the journal Frontiers in Oncology

Received: 02 February 2022
Accepted: 21 February 2022
Published: 18 March 2022

Citation:
Khan T, Becker TM, Scott KF, Descallar J, de Souza P, Chua W and Ma Y (2022) Prognostic and Predictive Value of Liquid Biopsy-Derived Androgen Receptor Variant 7 (AR-V7) in Prostate Cancer: A Systematic Review and Meta-Analysis. Front. Oncol. 12:868031. doi: 10.3389/fonc.2022.868031

In advanced prostate cancer, access to recent diagnostic tissue samples is restricted and this affects the analysis of the association of evolving biomarkers such as AR-V7 with metastatic castrate resistance. Liquid biopsies are emerging as alternative analytes. To clarify clinical value of AR-V7 detection from liquid biopsies, here we performed a meta-analysis on the prognostic and predictive value of androgen receptor variant 7 (AR-V7) detected from liquid biopsy for patients with prostate cancer (PC), three databases, the Embase, Medline, and Scopus were searched up to September 2021. A total of 37 studies were included. The effects of liquid biopsy AR-V7 status on overall survival (OS), radiographic progression-free survival (PFS), and prostate-specific antigen (PSA)-PFS were calculated with RevMan 5.3 software. AR-V7 positivity detected in liquid biopsy significantly associates with worse OS, PFS, and PSA-PFS (P <0.00001). A subgroup analysis of patients treated with androgen receptor signaling inhibitors (ARSi such as abiraterone and enzalutamide) showed a significant association of AR-V7 positivity with poorer OS, PFS, and PSA-PFS. A statistically significant association with OS was also found in taxane-treated patients (P = 0.04), but not for PFS (P = 0.21) or PSA-PFS (P = 0.93). For AR-V7 positive patients, taxane treatment has better OS outcomes than ARSi (P = 0.01). Study quality, publication bias and sensitivity analysis were integrated in the assessment. Our data show that liquid biopsy AR-V7 is a clinically useful biomarker that is associated with poor outcomes of ARSi-treated castrate resistant PC (CRPC) patients and thus has the potential to guide patient management and also to stratify patients for clinical trials. More studies on chemotherapy-treated patients are warranted.

Systematic Review Registration: PROSPERO, CRD42021239353.

Keywords: prostate cancer, AR-V7, liquid biopsy, prognosis, meta-analysis

INTRODUCTION

Prostate cancer (PC) is one of the most common male cancers. The androgen receptor (AR) pathway is critical in maintaining normal prostate tissue homeostasis, cancer development and progression (1). Therapies for PC include surgery and radiation for localized or early-stage cancer, while for advanced or metastatic PC, androgen deprivation therapy (ADT), with or without chemotherapy is the standard of care. However, patients eventually develop castration resistant PC (CRPC). Recent incorporation of novel androgen receptor signaling inhibitors (ARSi, e.g., enzalutamide (Enz), abiraterone (Abi)) and taxane-based chemotherapy have improved outcomes of CRPC patients over the past two decades (2).

Biomarkers detected in liquid biopsy (such as circulating tumor cells and cell-free tumor DNA) demonstrate good concordance with biomarkers detected in conventional tissue biopsy, especially for metastatic CRPC (3). Liquid biopsy is emerging as a reliable source of biological data for biomarker discovery, especially in advanced PC when tissue biopsy is often not obtainable or can be used longitudinally to monitor tumor evolution and changes in biomarker characteristics. In CRPC, one of most promising prognostic markers is the constitutively active AR splice variant 7 (AR-V7). AR-V7 lacks the ligand binding domain and substitutes for functional AR even in the absence of the ligand testosterone, and differentially regulates AR-dependent gene expression (4). Thus far, current literature suggests that expression or nuclear subcellular location of AR-V7 is associated with overall survival (OS) and progression free survival (PFS) when found in tissue biopsy (5) or liquid biopsy [whole blood (6, 7), circulating tumor cells (8), and exosomes (9, 10)]. However, the study cohorts are variable in patient numbers and stages and also treatment options; the clinical relevance of AR-V7, especially liquid biopsy detectable AR-V7, is still not clear or widely accepted and need further investigation.

To clarify the clinical utility of AR-V7 detection from liquid biopsies, we undertook a comprehensive systematic review and meta-analysis to evaluate the available data from the clinical studies published up to September 2021. Prognostic and predictive value of liquid biopsy derived AR-V7 data in PC patients were evaluated from 37 studies that met the inclusion criteria.

METHODS

Study Design and Literature Searches

This study was conducted according to preferred reporting items for systematic reviews and meta-analysis (PRISMA) (11). The protocol has been registered on PROSPERO (CRD42021239353). Detailed literature searches up to September 10, 2021 in the Embase, PubMed, and Scopus databases were conducted thoroughly to check the prognostic role of AR-V7 in PC. The used search terms were (~Androgen Receptor Variant 7) OR (~ARV7) OR (~AR3) AND (~"prostate cancer"). The searched study citations were imported to EndNote (version X9) for duplicate checking and title and/or abstract screening and then uploaded to the online systematic review research tool Rayyan (https://www.rayyan.ai/) for independent systematic review according to selection criteria. Two independent, blinded observers (TK and YM) reviewed all candidate articles. Any discrepancies in the article selections were resolved by discussion.

Selection Criteria

Pre-set exclusion criteria of this study were: (1) publication type: review articles, letters, comments, questionnaires, conference papers, corrections, reply to editor, case reports, book chapters, abstracts only, research highlights, summaries; (2) non-human studies (animal or cell line study); (3) non-prostate cancer; (4) AR-V7 data are not derived from human; (5) survival data not related to AR-V7 or with insufficient data to calculate the hazard ratios (HRs) and their 95% CIs, or the Kaplan–Meier (K–M) curve unable to calculate HRs and 95% CI parameters. Finally, studies were only included when they met the following criteria: (1) AR-V7 assayed in liquid biopsies (whole blood, circulating tumor cells, PBMC, plasma, exosome); (2) A reported relationship between AR-V7 and prognostic/predictive indicators, namely, OS, PFS, and PSA-PFS; (3) patient cohorts with n >25, and (4) English language only.

Data Extraction and Quality Assessment

This study focuses on the prognostic value of AR-V7 detected from liquid biopsy and its predictive value for ARSi and chemotherapy. According to a pre-designed table, the items of data extraction included the last name of the first author, publication year, study country, number of patients included, age of patient, sample resource (processing method) and AR-V7 detection method, type of therapies, endpoints of oncological outcomes, HRs and 95% CIs (from univariate or multivariate Cox analysis), follow-up durations and definitions of OS, PFS, and PSA-PFS (**Supplementary Table 1**). When HRs and 95% CIs were not presented in the study, an Engauge Digitizer (version 12.1) was used to digitalize the K–M survival curve to re-calculate HRs and 95% CI as described previously (12). Data was extracted by two authors (TK and YM) independently and any inconsistencies were resolved by discussion. Notably, when several publications were retrieved reporting the same trial or patient cohort or from same author(s), study question and data from this publication were discussed by two authors (TK and YM) and uniqueness of the included data was ensured.

The adapted Newcastle–Ottawa Scale (NOS) scales for cohort study (13) were used to evaluate the quality of enrolled studies, which embraced three aspects, namely, patient selection, comparability, and assessment of outcome with a total score of 9. In addition, the quality of statistical evaluation was assessed to give a maximal score of 1 as described in **Supplementary Table 2**; a score of 7 or more is considered as high-quality and a score of 6 or less is considered as low quality.

Statistical Analysis

Pooled HR and 95% CI were used to evaluate the prognostic and predictive value of AR-V7 presence or high expression (in some studies, authors set a threshold to discriminate high or low expression level) on the patient survival parameters (OS, PFS,

PFA-PFS) in Review Manager 5.3 software (RevMan v.5.3, Denmark). The Cochran Q and I^2 statistical methods were applied to evaluate the heterogeneity among included studies and a random effects model was used for data consolidation. If the heterogeneity was very high, only a descriptive score was given. Further subgroup analysis based on patient treatment was also conducted. The inverted funnel plots with Egger's test were used to analyze potential publication bias with R software. A sensitivity analysis was carried out to assess the influence of each individual study on the pooled results by sequentially excluding each study. A two-tailed p-value <0.05 was regarded as statistically significant.

RESULTS

Search Results, Study and Patient Characteristics

The flowchart outlining the results of the literature search and application of the strategic inclusion and exclusion criteria is presented in **Figure 1**. A total of 1,180 relevant articles were identified in initial database searches (Embase: 321, Medline: 537, Scopus: 322). After screening research title and abstract to remove duplicates (n = 410) and excluding the non-relevant studies based on publication type (n = 353), non-human studies (n = 193), non-prostate cancer (n = 5) and foreign language (n = 3) followed by a review of full text for eligibility, 37 articles were identified based on inclusion criteria 'human data', 'AR-V7', 'liquid biopsy', and 'survival'. Although we initially only searched quite a broad terminology 'prostate cancer', all 37 studies investigated CRPC (n = 4) or metastatic CRPC (mCRPC) (n = 33) as defined in the reports (**Supplementary Table 1**). Baseline characteristics of all eligible articles are listed in **Table 1**. All articles were published from 2014 to 2021 and included studies from Europe (46%), America and Canada (46%), and Asia-Pacific (8%). Liquid biopsy AR-V7 was detected from CTC (n = 28), PBMC (n = 2), whole blood (n = 4) or exosomes (n = 3). The patient cohort size ranged from 26 to 202 and the median or mean patient age ranged from 56 to 78. CTC enrichment methods included (modified) AdnaTest ® (Qiagen) (n = 13), Oncoquick® (Greiner Bio-One GmbH) (n = 1), red blood cell (RBC) lysis (n = 3), and immunomagnetic beads-based methods (such as CellSearch® or IsoFlux®, dynabeads) (n = 9). The method of AR-V7 detection was primarily by PCR (quantitative PCR and droplet digital PCR, 92%). Endpoint of patient outcomes include OS (n = 30), PFS (n = 28) and PSA-PFS (n = 10) (**Table 1**).

Thirty studies including 976 AR-V7 positive (or high level, as defined by authors) and 2,056 AR-V7 negative (or low level) patients were used for OS comparison, while 28 studies including 697 AR-V7 positive and 1,553 AR-V7 negative patients were used for PFS analysis and 10 studies including 216 AR-V7 positive and 425 AR-V7 negative patients for PSA-PFS analysis. Most patients in the cohort of studies were treated with ARSi (either enzalutamide, abiraterone, or not specified) or taxane-based chemotherapy. Some reports included miscellaneous treatments [such as Bipolar Androgen-based therapy (32)]. Overall AR-V7 positive patients had significantly worse OS (HR 3.36, 95% CI 2.56–4.41, P <0.00001), PFS (HR 2.96, 95% CI 2.20–3.98, P <0.00001) and PSA-PFS (HR 4.34, 95% CI 2.15–8.76, P <0.00001) than AR-V7 negative patients. Due to significant study heterogeneity (I^2 ≥80%), random effects model was applied to calculate HR value and 95% CI for all survival parameters.

Predictive Value of AR-V7 for ARSi-Treatment

AR-V7 positive patients treated with ARSi (enzalutamide or abiraterone) had significant poorer OS (HR 4.34, 95% CI 3.00–6.28, P <0.00001), PFS (HR 2.89, 95% CI 2.15–3.87, P <0.00001) and PSA-PFS (HR 4.69, 95% CI 2.50–8.82, P <0.0001) compared with AR-V7 negative patients (**Figures 2**–**4**). When analyzed based on specific treatment, compared to negative patients, AR-V7 positive patients also had significant worse OS (Enz: HR 2.93, 95% CI 1.71–5.01, P <0.0001; Abi: HR 6.59, 95% CI 2.18–19.94, P = 0.0008, respectively) (**Figure 2**), PFS (Enz: HR 4.38, 95% CI 2.44–7.84, P <0.0001; Abi: HR 6.88, 95% CI 1.99–23.73, P = 0.002, respectively) (**Figure 3**) and PSA-PFS (Enz: HR 7.40, 95% CI 2.66–20.60, one study, P = 0.0008; Abi: HR 11.39, 95% CI 4.53–28.67, two studies, P <0.00001, respectively) (**Figure 4**).

Chemotherapy-Treated Patients and Outcome Association With AR-V7

In the subgroup analysis of the patients treated with taxane-based chemotherapy, the association of AR-V7 positivity with worse OS was observed (HR 1.70, 95% CI 1.03–2.81, P = 0.04) (**Figure 2**), but no conclusive association between AR-V7 positive status and worse PFS and PSA-PFS were apparent, likely due to inadequate power (PFS: HR 1.81, 95% CI 0.71–4.61, P = 0.21, **Figure 3**; PSA-PFS: HR 0.93, 95% CI 0.21–4.22, P = 0.93, **Figure 4**). It is to be emphasised that data is only derived from two studies and a total of 129 patients (**Figure 4**).

AR-V7 Effect on Non-Defined (Miscellaneous) Treatments

For the studies in which the authors did not clarify treatments and were unable to be classified as either ARSi or taxane chemotherapy, AR-V7 presence is associated with worse OS (HR 3.47, 95% CI 1.85–6.49, P = 0.0001, 5 studies) and PFS (3 studies, HR 1.68, 95% CI 1.03–2.76, P = 0.04) (**Figures 2**, **3**).

ARSi vs. Chemotherapy in AR-V7 Positive or Negative Patients

Four studies compared treatment response in AR-V7 positive or negative patients. Taxane treatment is linked to superior OS (HR 0.54, 95% CI 0.34–0.87, P = 0.01) in patients positive for AR-V7, compared to ARSi (**Figure 5A**). In contrast, for AR-V7 negative patients, OS in taxane or ARSi treated patients is not significantly different (HR 1.17, 95% CI 0.71–1.92, P = 0.54) (**Figure 5B**).

Quality Assessment, Publication Bias and Sensitivity Analysis

Thirty five articles were assessed as high-quality studies while 2 were deemed low quality studies (**Table 1** and **Supplementary Table 2**). Overall, the average quality of studies is 8.5. Publication

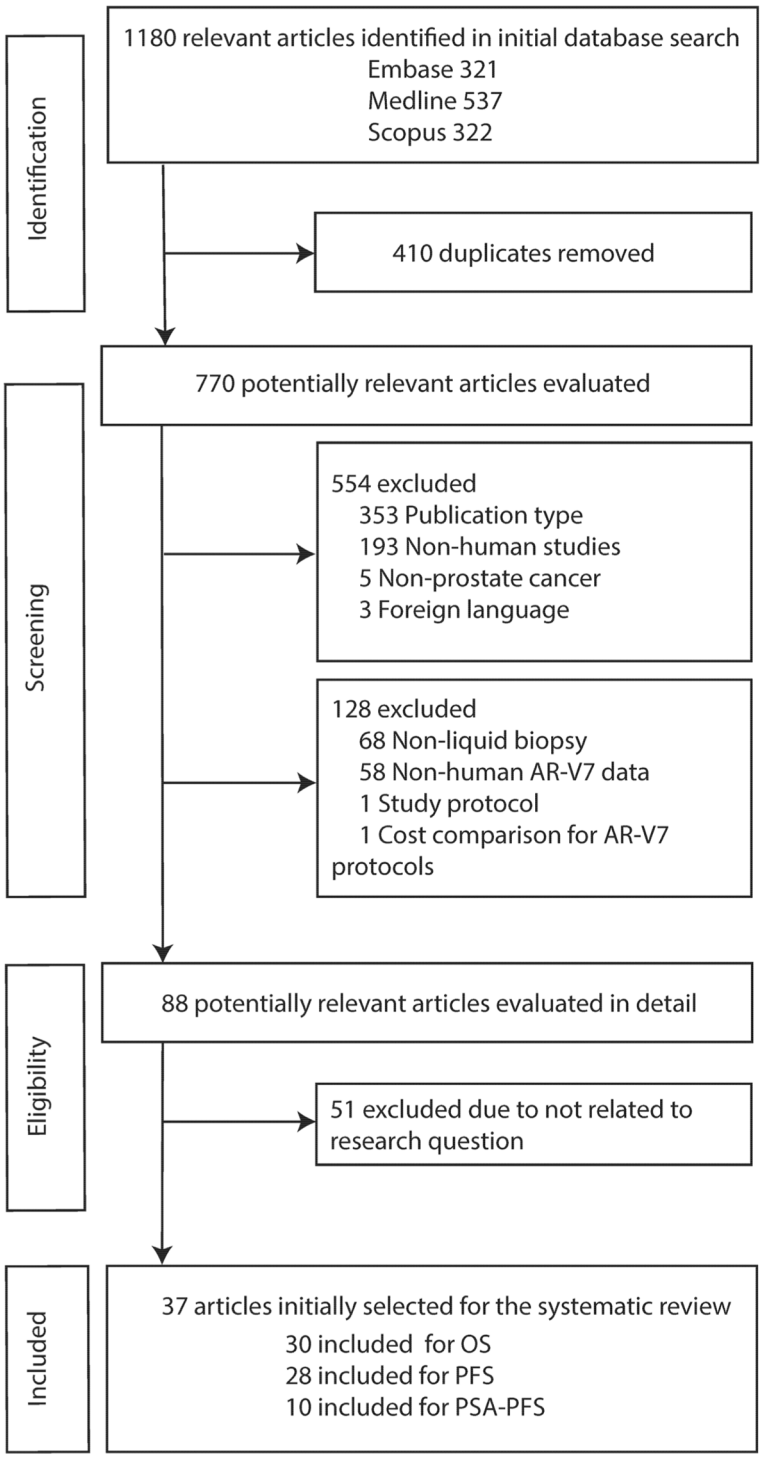


FIGURE 1 | Flow chart of literature search and study selection.

biases were evaluated for subgroups with more than 10 publications; no publication bias was observed for OS (Egger's test P = 0.9925, 15 publications, **Supplementary Figure 1A**) whereas publication bias was observed for PFS (Egger's test P = 0.0411, 17 publications, **Supplementary Figure 1B**) in ARSi-treated subgroups. Sensitivity analyses were performed on the subgroups of more than 6 studies and the results were relatively stable except for overall survival in chemotherapy-treated group,

TABLE 1 | The basic characteristics of eligible studies.

Study	Year, country	Study type	Patients	Age	Resource, method	Treatment	Endpoint outcome	Follow up (month)	NOS score
Antonarakis et al. (14)	2015 US	Pros	37 CTC+	67 (46–82)[b]	CTCs (mAdna), qRT-PCR	Taxane	OS, PFS, PSA-PFS	7.7 (0.7–19.0)[b]	10
Antonarakis et al. (15)	2017 US	Pros	53 CTC–, 113 CTC+/AR-V7-, 36 CTC+/AR-V7+	70 71 70[a]	CTCs (mAdna), qRT-PCR	Abi/Enz	OS, PFS, PSA-PFS	CTC–:15.0 CTC+/ ARV7-: 21.7 CTC+/ ARV7+: 14.6[a]	9
Antonarakis et al. (16)	2014 US	Pros	Enz:31, Abi: 31	Enz:70 (56–84), Abi:69 (48–79)[b]	CTCs (mAdna), qRT-PCR	Abi/Enz	OS, r PFS, PSA-PFS	Enz: 5.4 (1.4–9.9) Abi: 4.6 (0.9–8.2)[b]	9
Armstrong et al. (17)	2019 US	Pros, blinded, multi-center	118	73 (45–92)[b]	CTCs (Adna, CellSearch), qRT-PCR	Abi/Enz	OS, PFS	19.6[a]	10
Armstrong et al. (18)	2020 US	Pros, blinded	ARSi:118 Taxane: 51	72 (48–82) 72 (45–87)[b]	CTCs (Adna, CellSearch), qRT-PCR	ARSi, Taxane	OS, PFS	ARSi:35 Tax:23[a]	9
Belderbos et al. (19)	2019 Netherlands	Pros	94	69 (65–75)[c]	CTCs (CellSearch), qRT-PCR)	Cabazitaxel ARSi	OS	NA	9
Cattrini et al. (20)	2019 Italy	Pros	39	72 (56–84)[b]	CTCs (Adna), qRT-PCR	ARSi, Taxane	OS	NA	8
Chung et al. (21)	2019 US	Pros	37	72 (67–79)[c]	CTCs (Dynabeads), qRT-PCR	Abi/Enz	OS, rPFS, PSA-PFS	11.4 (4.7–21.3)[c]	7
De Laere et al. (22)	2019 Belgium	Pros multi-center	168	76 ± 7.7[e]	CTCs (CellSearch), RNA-seq	Abi/Enz	OS, PFS	12.4 (7–17.3)[c]	10
Del Re et al. (23)	2017 Italy	Pros	36	66 (51–81)[b]	Plasma exosomes (exoRNeasy), ddPCR	ARSi	OS, PFS	9 (2.0–31.0)[b]	8
Del Re et al. (9)	2021 Italy	Retros	84	78 (47–91)[b]	Plasma exosomes (exoRNeasy), ddPCR	ARSi	OS, PFS	NA	9
Del Re et al. (10)	2019 Italy	Retros	73	NA	Plasma exosomes (exoRNeasy), ddPCR	Abi/Enz	OS, PFS	NA	7
Erb et al. (24)	2020 Germany	Pros	26	74.3 ± 9[a]	CTCs (OncoQuick), IHC	ARSi, Taxane	PFS	NA	6
Graf et al. (25)	2020 US	Pros, cross-sectional	193	69 (62.5–75)[c]	CTCs (RBC lysis), IF	ARSi, Taxane	OS	28.4 (24.4–33.0)[c]	9
Gupta et al. (26)	2019 US	Pros	ARSi:120 Radium:20	ARSi:73 (45–92) Radium:72 (54–86)[b]	CTCs (Adna, CellSearch), qRT-PCR and Epic assay	Abi/Enz, Radium	PFS	NA	9
Joncas et al. (27)	2019 Canada	Pros	35	75 (67,79)[c]	EVs (UC, miRNeasy), ddPCR	ARSi, Taxane	OS, PFS	27 (16,33)[c]	8
Kwan et al. (28)	2019 Australia	Pros	115	72 (46–91)[b]	WB, qRT-PCR	ARSi, Taxane	OS	15.5 (1.4–29)[b]	10
Lorenzo et al. (29)	2021 Italy	Pros, multi-center	53 (45 data only)	72.1 (54–86)[b]	CTCs, (Flow cytometry)	Enz	OS, rPFS	27[a]	10
Maillet et al. (30)	2019 France	Pros	41	73[a]	CTCs (AdnaTest), qRT-PCR	ARSi	OS, rPFS, PSA-PFS	31 ARSi treated patients: 10.5[a]	8
Marín et al. (31)	2020 Spain	Pros	136	ARSi:70.2 (53.3–93.3)	PBMC and CTCs (IsoFlux) qRT-PCR	Abi/Enz, Taxane	OS, rPFS, PSA-PFS	ARSi:14.9 (1.5–57.9) Tax:13.8	10

(Continued)

TABLE 1 | Continued

Study	Year, country	Study type	Patients	Age	Resource, method	Treatment	Endpoint outcome	Follow up (month)	NOS score
				Tax: 62.8 (32.8–79.4)[b]				(1.37–82.27)[a]	
Markowski et al. (32)	2021 US	Multicohort phase II	Post-Abi: 29, Post-Enz: 30	Post-Abi: 71 (49–85) Post-Enz: 74 (50–89)[b]	CTCs (Adna), qRT-PCR	BAT, ARSi	rPFS	NA	7
Miyamoto et al. (33)	2018 US	Pros	27	67[d]	CTCs (CTC-iChip), ddPCR	Abi	OS, rPFS	13.0[a]	8
Okegawa et al. (34)	2018 Japan	Retros	49 CTC–, 23 CTC+/AR-V7–, 26 CTC+/AR-V7+	69 71 72[d]	CTCs (on-chip FC), PCR	Abi/Enz	OS, rPFS, PSA-PFS	20.7 (3.0–37.0)[b]	9
Onstenk et al. (35)	2015 Netherlands	Pros, multi-center, phase II	29	70 ± 7[e]	CTCs (CellSearch), qRT-PCR	Cabazitaxel	OS, PFS	7 (2–27)[b]	7
Qu et al. (36)	2017 US	Retros	Abi: 81, Enz: 51	Abi: 68.3 (62–74) Enz:69.0 (63–74)[c]	PBMC(Ficol), ddPCR	Abi/Enz	OS, PFS (TTF)	29.7 (3.6–47.5) 23.9 (0.9–48.3)[b]	10
Scher et al. (37)	2018 US	Pros, cross-sectional	142	69.5 ± 9.6[e]	CTCs (RBC lysis), IF	ARSi, Taxane	OS	4.3 years	8
Scher et al. (38)	2017 US	Pros, cross-sectional	161	68 (45–91)[b]	CTCs (RBC lysis), IF	ARSi, Taxane	OS	11 (1–30)[a]	9
Scher et al. (39)	2016 US	Pros, cross-sectional	161	68 (45–91)[b]	CTCs, IF	ARSi, Taxane	OS, PFS	36	10
Seitz et al. (40)	2017 Germany	Pros	85	71 (66–74)[c]	WB, ddPCR	Abi/Enz	OS, rPFS, PSA-PFS	7.6 (4.7–12.7)[c]	8
Sepe et al. (41)	2019 Italy	Pros	Abi:26, Enz: 11	75 (68–80)[b]	CTCs (Adna), qRT-PCR	Abi/Enz	OS, rPFS, PSA-PFS	25[a]	9
Sharp et al. (8)	2019 UK	Pros	181	CTC–:71.0 (66.8–75.6), CTC +/AR-V7–: 69.6 (64.9-72.3), CTC +/AR-V7–: 70.4 (65.3–74.6)[c]	CTCs (Adna, CellSearch), qRT-PCR	ARSi, Taxane	OS	19 (11–31)[c]	10
Škereňová et al. (42)	2018 Czech Republic	Retros	41	71 (54–82)[b]	CTCs (Adna), qRT-PCR	Docetaxel	OS	23.5[a]	7
Stuopelyte et al. (6)	2020 Lithuania	Pros	102	75.4 (11.4)[c]	WB, qRT-PCR	Abi	PFS, OS	30.5[a]	9
Tagawa et al. (43)	2019 US	Pros	54	71 (53–84)[b]	CTCs, ddPCR	Taxane	PFS	NA	7
Todenhöfer et al. (7)	2016, Canada	Pros	37	70 (53–87)[b]	WB, qRT-PCR	Abi	OS PSA-PFS	NA	8
Tommasi et al. (44)	2018 Italy	Pros	44	71.5 (55-87)[b]	CTCs (Adna), qRT-PCR	ARSi, Taxane	PFS	20.5[a]	7
Wang et al. (45)	2018 China	Pros	36	56.2 ± 8.6[e]	CTCs (immuno-beads), qRT-PCR	Abi/Enz	PFS	NA	6

Studies are labeled as last name of first author, et al. and presented in alphabetical order; Patient number and age are all patients included in study; Pros, prospective; Retros, retrospective. [a]median, [b]median (range), [c]median IQR, [d]mean, [e]mean ± STD. WB, whole blood; CTC, circulating tumor cells; RBC, red blood cell lysis; PBMC, peripheral blood mononuclear cell; Ficoll, density gradient medium; Adna, AdnaTest ProstateCancerPanel AR-V7; mAdna, modified Adna; IF, immunofluorescent staining; qRT-PCR, quantitative real time-polymerase chain reaction; ddPCR, droplet digital PCR; UC, ultracentrifuge; FC, flow cytometry; ARSi, androgen receptor signaling inhibitor; Abi, abiraterone; Enz, Enzalutamide; BAT, bipolar androgen therapy; NA, not available; some studies include healthy control for threshold setting or discovery cohort (the data is lack and not included in table).

where missing data in one study (31) had a significant effect on data outcome (**Supplementary Table 3**).

DISCUSSION

AR splice variants have been proposed as a cause of resistance to ARSi and taxane-based chemotherapy (46). AR-V7, the most-studied AR splice variant, is emerging as a clinically relevant biomarker in CRPC, with a detection incidence ranging between 20 and 60%, depending on biopsy source, detection methods, and disease stage. Given that tumor tissue of advanced PC is rarely available and archival tissue may not reflect the biology of the current tumor stage, liquid biopsies, mainly blood, are becoming attractive resources for AR-V7 and other biomarker evaluation. Technical advances, different detection methods for

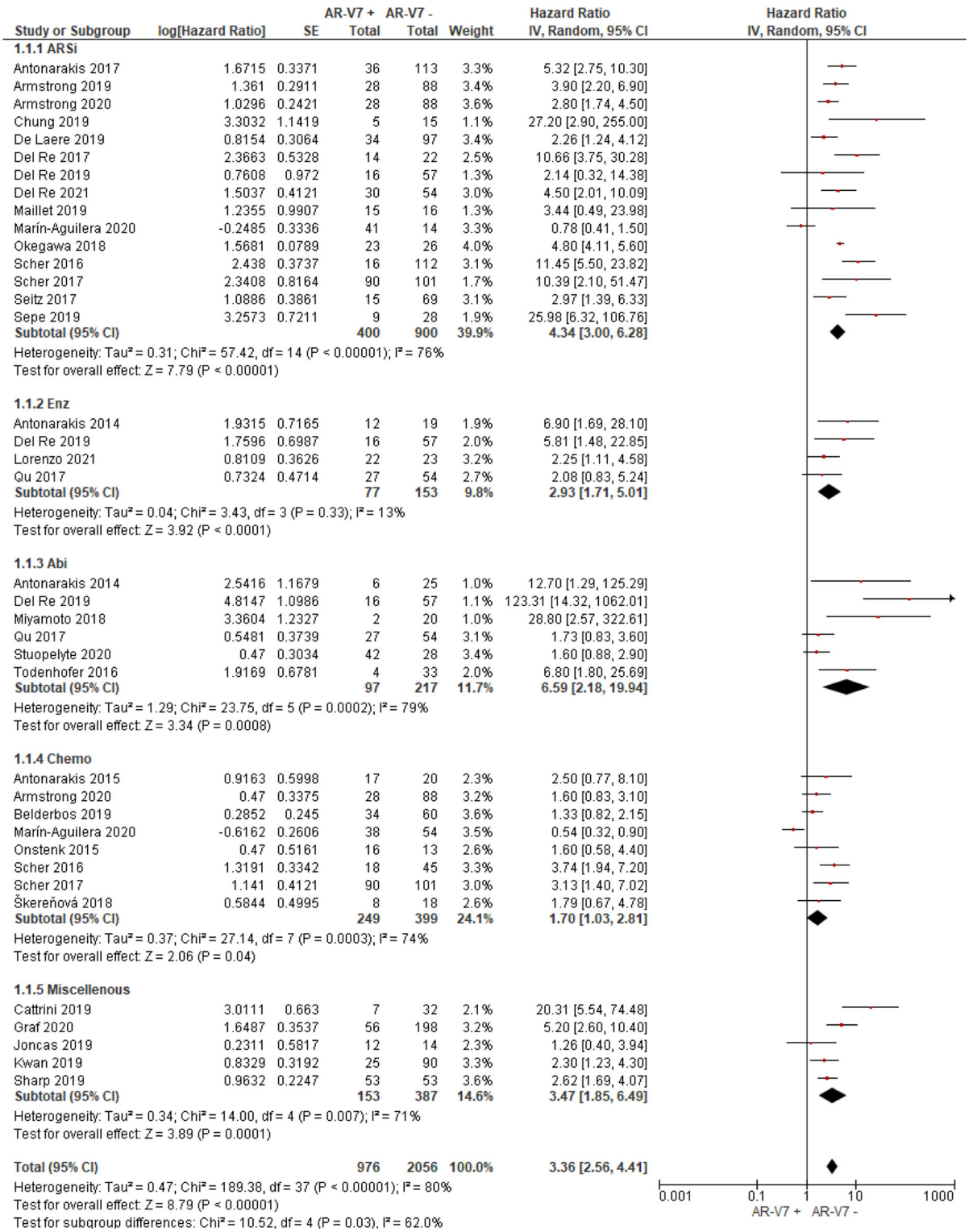


FIGURE 2 | Forest plot of hazard ratios (HRs) for association of liquid biopsy AR-V7 status with overall survival (OS) in all included studies. Pooled HRs were calculated using random effect model. AR-V7, androgen receptor splice variant 7; CI, confidence interval and bars indicate 95% CIs. Subgroup analysis (ARSi, enzalutamide or abiraterone; Enz, enzalutamide; Abi, abiraterone; Chemo, taxane based chemotherapy; Miscellaneous, treatments that do not belong to above treatments or not clearly defined) were assessed.

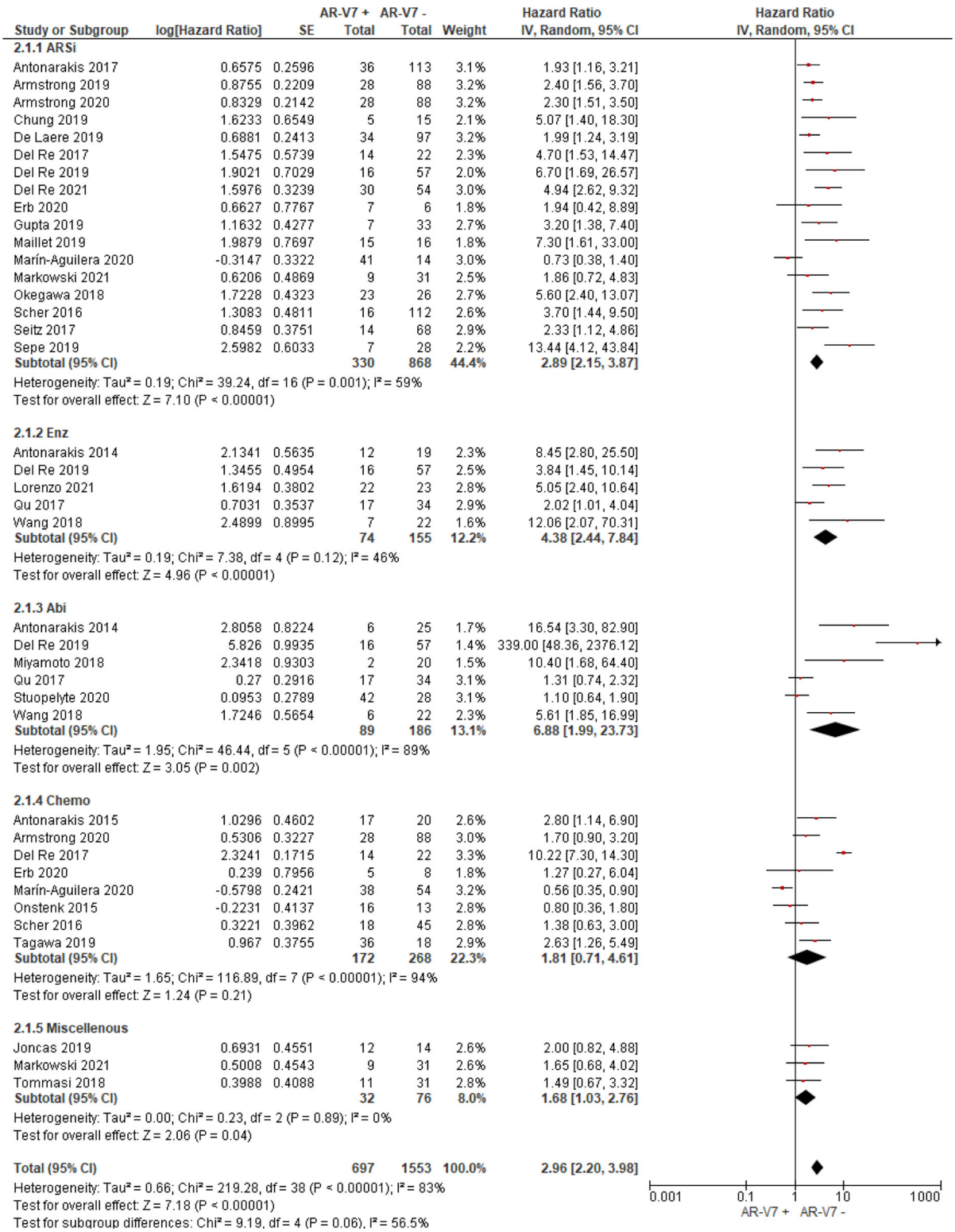


FIGURE 3 | Forest plot of hazard ratios (HRs) for association of liquid biopsy AR-V7 status with PFS in all studies. Pooled HRs were calculated using random effect model. AR-V7: androgen receptor splice variant 7. CI, confidence interval and bars indicate 95% CIs. Subgroup analysis (ARSi, enzalutamide or abiraterone; Enz, enzalutamide; Abi, abiraterone; Chemo, taxane based chemotherapy; Miscellaneous, treatments that do not belong to above treatments or not clearly defined) were assessed.

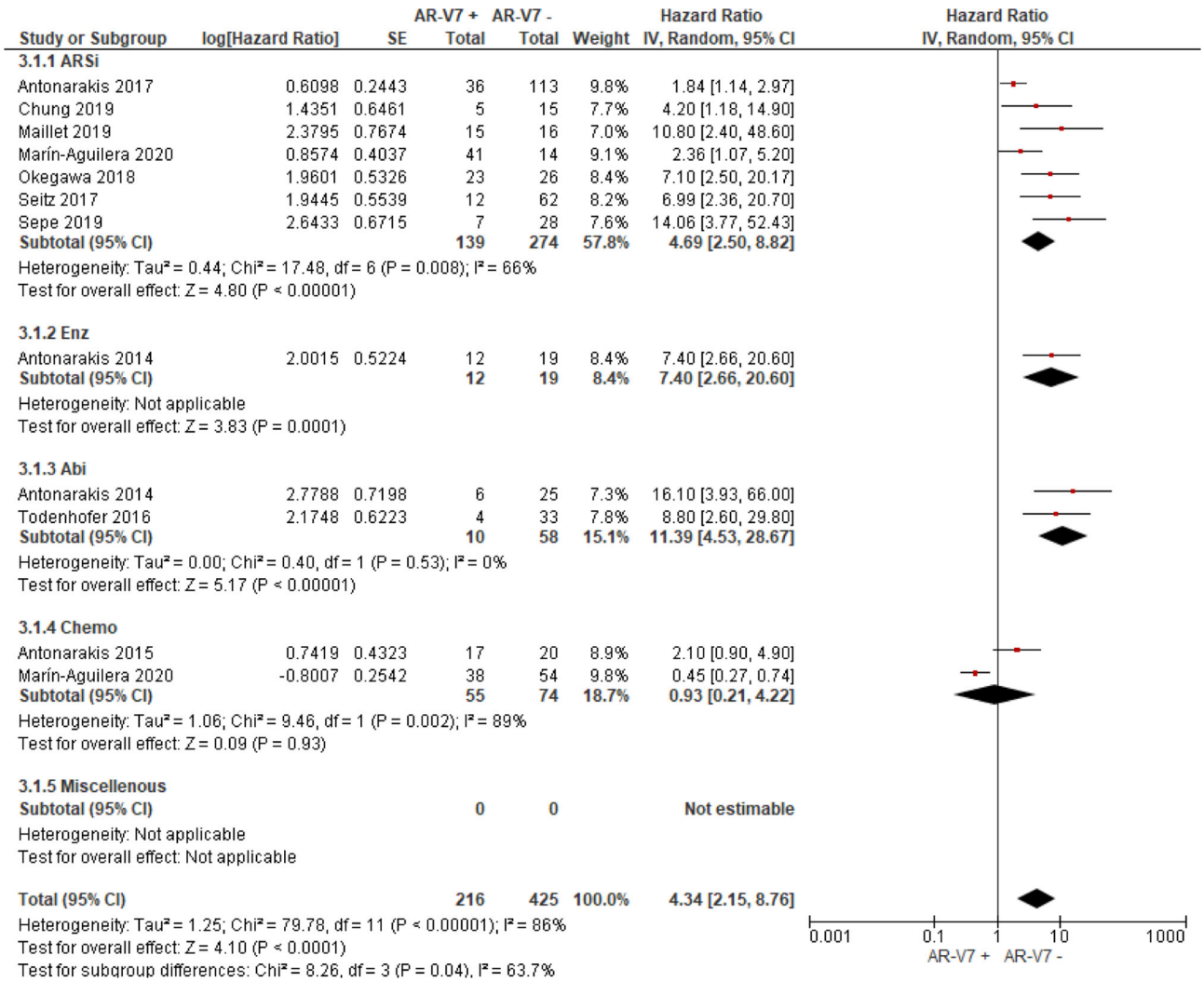


FIGURE 4 | Forest plot of hazard ratios (HRs) for association of liquid biopsy AR-V7 status with PSA-PFS in all studies. Pooled HRs were calculated using random effect model. AR-V7, androgen receptor splice variant 7; CI, confidence interval and bars indicate 95% CIs. Subgroup analysis (ARSi, enzalutamide or abiraterone; Enz, enzalutamide; Abi, abiraterone; Chemo, taxane based chemotherapy; Miscellaneous, treatments that do not belong to above treatments or not clearly defined) were assessed.

AR-V7 from liquid biopsies are now available, including modified AdnaTest ProstateCancer, and droplet digital PCR of CTCs enriched by various CTC isolation platforms (see **Table 1**). We recently confirmed CTC-based AR-V7 testing is more reliable than exosomal RNA and cell free tumor RNA in plasma (47). Accumulating reports on the association of AR-V7 detectability in liquid biopsy with therapy response and patient survival have prompted us to perform this systematic review and meta-analysis on the prognostic and predictive utility of liquid biopsy-based AR-V7 identification. Our data show that liquid biopsy detectable AR-V7 significantly associates with poor outcomes to ARSi treatment as shown for OS, PFS, PSA-PFS ($P < 0.001$). This strongly supports the notion that AR-V7 detection from CRPC patient liquid biopsies has prognostic and predictive power. This observation is highly clinically relevant and could affect how clinicians make treatment decisions for patients with (metastatic) CRPC and when to transition patients to taxane-based chemotherapy.

While on taxane-based treatment, the association of AR-V7 presence with poorer outcome is still significant ($P = 0.04$) for OS data and lack adequate power for PFS ($P = 0.21$) or PSA-PFS ($P = 0.93$). However, there are relatively fewer publications in this subgroup, so these conclusions are based on weaker datasets compared to the ARSi treated subgroup; for instance, the omitting one publication changes the P-value and AR-V7 impact on OS would no longer be significant (**Supplementary Table 3**). Our data agree with a recent report that AR-V7 may contribute to taxane resistance by circumventing taxane-induced inhibitory effects both *in vitro* (cell lines) and *in vivo* (PC tissue) (43, 48). On the other hand, we cannot exclude the possibility

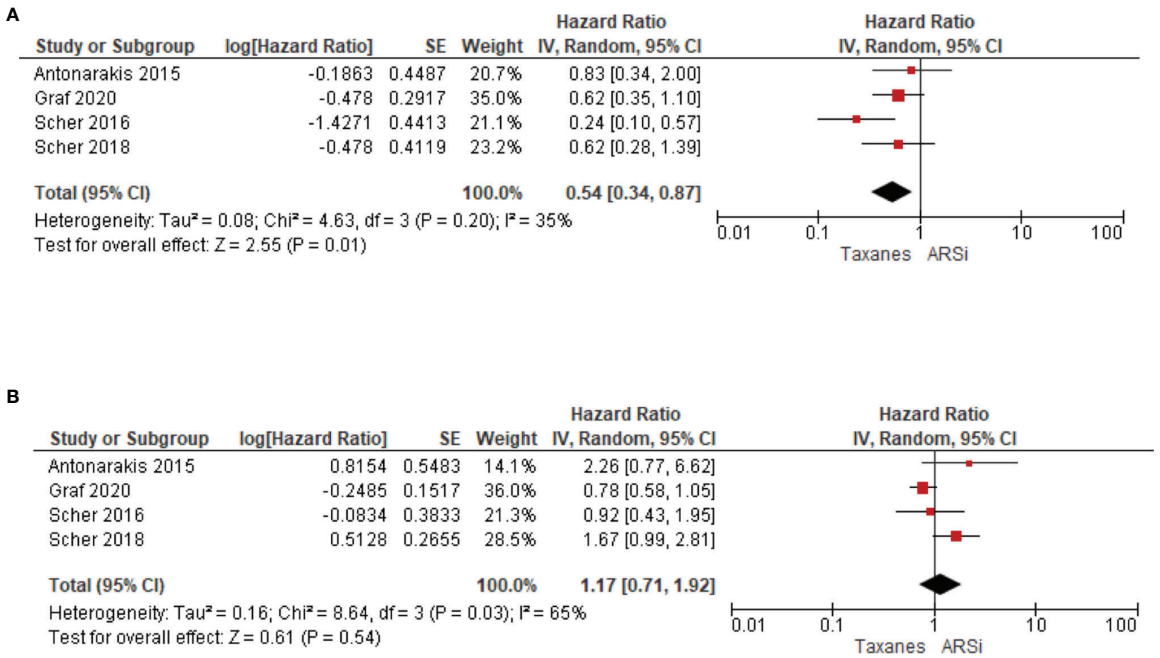


FIGURE 5 | Forest plots for association of liquid biopsy AR-V7 status with OS in **(A)** AR-V7 positive (ARSi vs. Chemotherapy) and **(B)** AR-V7 negative patients (ARSi vs. Chemotherapy). Pooled HRs were calculated using random effect model. AR-V7, androgen receptor splice variant 7; CI, confidence interval and bars indicate 95% CIs.

that AR-V7 expression was induced in CRPC patients who had received ARSi prior to chemotherapy, and that its effect on OS has not been completely washed out by taxanes. We note that four studies suggest that chemotherapy would be a better option compared to ARSi (HR 0.54, P = 0.01) in AR-V7 positive CRPC, suggesting that AR-V7 determination is important in chemotherapy-treated patients. More studies in this subgroup are warranted.

Three other meta-analyses on AR-V7 prognostication (13, 49, 50) have been published recently, but given the common inaccessibility of current tissue biopsies, our meta-analysis exclusively focuses on liquid biopsies and includes the most up-to-date studies. Further, we not only include all studies with author self-reported HR and 95% CI, but also calculate HR and 95% CI with established methods (12) for some papers with insufficient and incomplete statistical reporting. Nevertheless, our systematic review has limitations. We only examined OS, PFS, and PSA-PFS, and did not assess other treatment outcomes such as PSA response. Discrepancies in the definition of PSA response (e.g., extent of PSA fall in a specific timeframe) exist across studies and given our selection criteria, papers were excluded if they only reported PSA response without survival data. Secondly, statistical power was limited by the numbers of studies available and small sample sizes in some of the subgroups analysed. Thirdly, included study designs differed greatly in biological material investigated (type of liquid biopsy and content such as CTCs or exosomes). For some studies, patients were enrolled from a single centre, potentially leading to publication bias and selection bias. Also, no randomized study has ever directly compared the predictive value of AR-V7 in patients treated with chemotherapy vs. ARSi. Therefore, the results are indirect with potential bias. Lastly, the variability of techniques used to determine AR-V7 positivity, namely, qRT-PCR and ddPCR of mRNA derived from CTC, whole blood, exosome, could result in differing conclusions. The cut-off value is essential in defining and interpretation of AR-V7 positivity, due to the continuous nature of this variable; more work is required to answer the question of whether the degree of AR-V7 presence is important. Last but not least, other CTC AR detection methods have been adopted such as RNA-seq and immunostaining. Despite the variety of methodologies, we found that liquid biopsy detectable AR-V7 correlates with disease outcomes (**Supplementary Figure 2**).

In conclusion, ARSi and taxane-based chemotherapy are approved treatment options for CPRC patients and are used globally. Use of emerging methodologies, such as liquid biopsy-determined AR-V7, to optimize utility of a known predictive biomarker could help to guide the optimal treatment sequencing pathway for each patient in a personalised manner and is therefore of clinical importance. Standardization of liquid biopsy AR-V7 detection would underpin utility in clinical practice. Avoiding ineffective therapies or early switching to more effective approaches should ensure better outcomes for patients. However, further studies on chemotherapy-treated patient cohort and direct comparison of chemotherapy vs. ARSi are warranted.

DATA AVAILABILITY STATEMENT

The original contributions presented in the study are included in the article/**Supplementary Material**. Further inquiries can be directed to the corresponding author.

AUTHOR CONTRIBUTIONS

Project development, methodology, data collection and analysis: TK and YM. Conceptualization: YM and TK. Project development: TB, KS, PDS and WC. Statistics: JD, TK and YM. Manuscript writing, editing, and reviewing: all authors. All authors listed have made a substantial, direct, and intellectual contribution to the work and approved it for publication.

FUNDING

TK received an Ingham Institute/Narellan Rotary Club Men's health grant 2018 and a WSU School of Medicine Androgen Receptor Research scholarship.

SUPPLEMENTARY MATERIAL

The Supplementary Material for this article can be found online at: https://www.frontiersin.org/articles/10.3389/fonc.2022.868031/full#supplementary-material

Supplementary Table 2 | Quality assessment of included studies based on adapted NOS scales.

Supplementary Table 3 | Sensitivity analysis of subgroups with more than 6 studies.

Supplementary Figure 1 | Inverted funnel plot to evaluate potential publication bias in OS **(A)** and PFS **(B)** of ARSi treated patients.

Supplementary Figure 2 | Forest plot of hazard ratios (HRs) for association of liquid biopsy AR-V7 status with OS **(A)**, PFS **(B)**, PSA-PFS **(C)** in all studies. Subgroup analysis were performed based on AR-V7 detection technique type. Pooled HRs were calculated using random effect model. AR-V7: androgen receptor splice variant 7. CI: confidence interval and bars indicate 95% CIs. PCR, polymerase chain reaction; qRT-PCR, quantitative real time PCR; ddPCR, droplet digital PCR; IF, immunofluorescence; IHC, immunohistochemistry; FC, flow cytometry; RNA-seq, RNA-sequencing.

REFERENCES

1. Lonergan PE, Tindall DJ. Androgen Receptor Signaling in Prostate Cancer Development and Progression. *J Carcinog* (2011) 10:20–. doi: 10.4103/1477-3163.83937
2. Cattrini CA-O, España R, Mennitto A, Bersanelli MA-O, Castro EA-O, Olmos D, et al. Optimal Sequencing and Predictive Biomarkers in Patients With Advanced Prostate Cancer. *Cancers* (2021) 13:4522. doi: 10.3390/cancers13184522
3. Wyatt AW, Annala M, Aggarwal R, Beja K, Feng F, Youngren J, et al. Concordance of Circulating Tumor DNA and Matched Metastatic Tissue Biopsy in Prostate Cancer. *J Natl Cancer Inst* (2017) 109:djx118. doi: 10.1093/jnci/djx118
4. Shafi AA, Putluri V, Arnold JM, Tsouko E, Maity S, Roberts JM, et al. Differential Regulation of Metabolic Pathways by Androgen Receptor (AR) and its Constitutively Active Splice Variant, AR-V7, in Prostate Cancer Cells. *Oncotarget* (2015) 6:31997–2012. doi: 10.18632/oncotarget.5585
5. Sharp A, Coleman I, Yuan W, Sprenger C, Dolling D, Rodrigues DN, et al. Androgen Receptor Splice Variant-7 Expression Emerges With Castration Resistance in Prostate Cancer. *J Clin Invest* (2019) 129:192–208. doi: 10.1172/JCI122819
6. Stuopelyte K, Sabaliauskaite R, Bakavicius A, Haflidadóttir BS, Visakorpi T, Väänänen RM, et al. Analysis of AR-FL and AR-V1 in Whole Blood of Patients With Castration Resistant Prostate Cancer as a Tool for Predicting Response to Abiraterone Acetate. *J Urol* (2020) 204(1):71–8. doi: 10.1097/JU.0000000000000803
7. Todenhöfer T, Azad A, Stewart C, Gao J, Eigl BJ, Gleave ME, et al. AR-V7 Transcripts in Whole Blood RNA of Patients With Metastatic Castration Resistant Prostate Cancer Correlate With Response to Abiraterone Acetate. *J Urol* (2016) 197(1):135–42. doi: 10.1016/j.juro.2016.06.094
8. Sharp A, Welti JC, Lambros MBK, Dolling D, Rodrigues DN, Pope L, et al. Clinical Utility of Circulating Tumour Cell Androgen Receptor Splice Variant-7 Status in Metastatic Castration-Resistant Prostate Cancer. *Eur Urol* (2019) 76(5):676–85. doi: 10.1016/j.eururo.2019.04.006
9. Del Re M, Conteduca V, Crucitta S, Gurioli G, Casadei C, Restante G, et al. Androgen Receptor Gain in Circulating Free DNA and Splicing Variant 7 in Exosomes Predict Clinical Outcome in CRPC Patients Treated With Abiraterone and Enzalutamide. *Prostate Cancer Prostatic Dis* (2021) 24(2):524–31. doi: 10.1038/s41391-020-00309-w
10. Del Re M, Crucitta S, Sbrana A, Rofi E, Paolieri F, Gianfilippo G, et al. AR-V7 and AR-FL Expression Is Associated With Clinical Outcome: A Translational Study in Patients With Castrate Resistant Prostate Cancer. *BJU Int* (2019) 124:693–700. doi: 10.1111/bju.14792
11. Liberati A, Altman DG, Tetzlaff J, Mulrow C, Gøtzsche PC, Ioannidis JPA, et al. The PRISMA Statement for Reporting Systematic Reviews and Meta-Analyses of Studies That Evaluate Health Care Interventions: Explanation and Elaboration. *PloS Med* (2009) 6(7):e1000100. doi: 10.1136/bmj.b2700
12. Tierney JF, Stewart LA, Ghersi D, Burdett S, Sydes MR. Practical Methods for Incorporating Summary Time-to-Event Data Into Meta-Analysis. *Trials* (2007) 8:16–. doi: 10.1186/1745-6215-8-16
13. Wang J, Zhang Y, Wei C, Gao X, Yuan P, Gan J, et al. Prognostic Value of Androgen Receptor Splice Variant 7 in the Treatment of Metastatic Castration-Resistant Prostate Cancer: A Systematic Review and Meta-Analysis. *Front Oncol* (2020) 10:562504. doi: 10.3389/fonc.2020.562504
14. Antonarakis ES, Lu C, Luber B, Wang H, Chen Y, Nakazawa M, et al. Androgen Receptor Splice Variant 7 and Efficacy of Taxane Chemotherapy in Patients With Metastatic Castration-Resistant Prostate Cancer. *JAMA Oncol* (2015) 1(5):582–91. doi: 10.1001/jamaoncol.2015.1341
15. Antonarakis ES, Lu C, Luber B, Wang H, Chen Y, Zhu Y, et al. Clinical Significance of Androgen Receptor Splice Variant-7 Mrna Detection in Circulating Tumor Cells of Men With Metastatic Castration-Resistant Prostate Cancer Treated With First- and Second-Line Abiraterone and Enzalutamide. *J Clin Oncol* (2017) 35(19):2149–56. doi: 10.1200/JCO.2016.70.1961
16. Antonarakis ES, Lu C, Wang H, Luber B, Nakazawa M, Roeser JC, et al. AR-V7 and Resistance to Enzalutamide and Abiraterone in Prostate Cancer. *New Engl J Med* (2014) 371(11):1028–38. doi: 10.1056/NEJMoa1315815
17. Armstrong AJ, Halabi S, Luo J, Nanus DM, Giannakakou P, Szmulewitz RZ, et al. Prospective Multicenter Validation of Androgen Receptor Splice Variant 7 and Hormone Therapy Resistance in High-Risk Castration-Resistant Prostate Cancer: The PROPHECY Study. *J Clin Oncol* (2019) 37(13):1120–9. doi: 10.1200/JCO.18.01731
18. Armstrong AJ, Luo J, Nanus DM, Giannakakou P, Szmulewitz RZ, Danila DC, et al. Prospective Multicenter Study of Circulating Tumor Cell AR-V7 and Taxane Versus Hormonal Treatment Outcomes in Metastatic Castration-Resistant Prostate Cancer. *JCO Precis Oncol* (2020) 4:1285–301. doi: 10.1200/PO.20.00200
19. Belderbos BPS, Sieuwerts AM, Hoop EO, Mostert B, Kraan J, Hamberg P, et al. Associations Between AR-V7 Status in Circulating Tumour Cells, Circulating Tumour Cell Count and Survival in Men With Metastatic Castration-Resistant Prostate Cancer. *Eur J Cancer* (2019) 121:48–54. doi: 10.1016/j.ejca.2019.08.005

20. Cattrini C, Rubagotti A, Zinoli L, Cerbone L, Zanardi E, Capaia M, et al. Role of Circulating Tumor Cells (CTC), Androgen Receptor Full Length (AR-FL) and Androgen Receptor Splice Variant 7 (AR-V7) in a Prospective Cohort of Castration-Resistant Metastatic Prostate Cancer Patients. *Cancers* (2019) 11 (9):1365. doi: 10.3390/cancers11091365
21. Chung JS, Wang Y, Henderson J, Singhal U, Qiao Y, Zaslavsky AB, et al. Circulating Tumor Cell–Based Molecular Classifier for Predicting Resistance to Abiraterone and Enzalutamide in Metastatic Castration-Resistant Prostate Cancer. *Neoplasia (United States)* (2019) 21(8):802–9. doi: 10.1016/j.neo.2019.06.002
22. De Laere B, Oeyen S, Mayrhofer M, Whitington T, van Dam PJ, Van Oyen P, et al. TP53 Outperforms Other Androgen Receptor Biomarkers to Predict Abiraterone or Enzalutamide Outcome in Metastatic Castration-Resistant Prostate Cancer. *Clin Cancer Res* (2019) 25(6):1766–73. doi: 10.1158/1078-0432.CCR-18-1943
23. Del Re M, Biasco E, Crucitta S, Derosa L, Rofi E, Orlandini C, et al. The Detection of Androgen Receptor Splice Variant 7 in Plasma-Derived Exosomal RNA Strongly Predicts Resistance to Hormonal Therapy in Metastatic Prostate Cancer Patients. *Eur Urol* (2017) 71(4):680–7. doi: 10.1016/j.eururo.2016.08.012
24. Erb HHH, Sparwasser P, Diehl T, Hemmerlein-Thomas M, Tsaur I, Jüngel E, et al. AR-V7 Protein Expression in Circulating Tumour Cells is Not Predictive of Treatment Response in Mcrpc. *Urologia Internationalis* (2020) 104(3):253–62. doi: 10.1159/000504416
25. Graf RP, Hullings M, Barnett ES, Carbone E, Dittamore R, Scher HI. Clinical Utility of the Nuclear-Localized AR-V7 Biomarker in Circulating Tumor Cells in Improving Physician Treatment Choice in Castration-Resistant Prostate Cancer. *Eur Urol* (2020) 77(2):170–7. doi: 10.1016/j.eururo.2019.08.020
26. Gupta S, Hovelson DH, Kemeny G, Halabi S, Foo WC, Anand M, et al. Discordant and Heterogeneous Clinically Relevant Genomic Alterations in Circulating Tumor Cells vs Plasma DNA From Men With Metastatic Castration Resistant Prostate Cancer. *Genes Chromosomes Cancer* (2019) 59(4):225–39. doi: 10.1002/gcc.22824
27. Joncas FH, Lucien F, Rouleau M, Morin F, Leong HS, Pouliot F, et al. Plasma Extracellular Vesicles as Phenotypic Biomarkers in Prostate Cancer Patients. *Prostate* (2019) 79(15):1767–76. doi: 10.1002/pros.23901
28. Kwan EM, Fettke H, Docanto MM, To SQ, Bukczynska P, Mant A, et al. Prognostic Utility of a Whole-Blood Androgen Receptor-Based Gene Signature in Metastatic Castration-Resistant Prostate Cancer. *Eur Urol Focus* (2021) 7:63–70. doi: 10.1016/j.euf.2019.04.020
29. Di Lorenzo G, Zappavigna S, Crocetto F, Giuliano M, Ribera D, Morra R, et al. Assessment of Total, PTEN(-), and AR-V7(+) Circulating Tumor Cell Count by Flow Cytometry in Patients With Metastatic Castration-Resistant Prostate Cancer Receiving Enzalutamide. *Clin Genitourin Cancer* (2021) 19:e286–98. doi: 10.1016/j.clgc.2021.03.021
30. Maillet D, Allioli N, Peron J, Plesa A, Decaussin-Petrucci M, Tartas S, et al. Improved Androgen Receptor Splice Variant 7 Detection Using a Highly Sensitive Assay to Predict Resistance to Abiraterone or Enzalutamide in Metastatic Prostate Cancer Patients. *Eur Urol Oncol* (2021) 4:609–17. doi: 10.1016/j.euo.2019.08.010
31. Marín-Aguilera M, Jiménez N, Reig Ò, Montalbo R, Verma AK, Castellano G, et al. Androgen Receptor and its Splicing Variant 7 Expression in Peripheral Blood Mononuclear Cells and in Circulating Tumor Cells in Metastatic Castration-Resistant Prostate Cancer. *Cells* (2020) 9(1):203. doi: 10.3390/cells9010203
32. Markowski MC, Wang H, Sullivan R, Rifkind I, Sinibaldi V, Schweizer MT, et al. A Multicohort Open-Label Phase II Trial of Bipolar Androgen Therapy in Men With Metastatic Castration-Resistant Prostate Cancer (RESTORE): A Comparison of Post-Abiraterone Versus Post-Enzalutamide Cohorts. *Eur Urol* (2021) 79:692–9. doi: 10.1016/j.eururo.2020.06.042
33. Miyamoto DT, Lee RJ, Kalinich M, LiCausi JA, Zheng Y, Chen T, et al. An RNA-Based Digital Circulating Tumor Cell Signature is Predictive of Drug Response and Early Dissemination in Prostate Cancer. *Cancer Discovery* (2018) 8(3):288–303. doi: 10.1158/2159-8290.CD-16-1406
34. Okegawa T, Ninomiya N, Masuda K, Nakamura Y, Tambo M, Nutahara K. AR-V7 in Circulating Tumor Cells Cluster as a Predictive Biomarker of Abiraterone Acetate and Enzalutamide Treatment in Castration-Resistant Prostate Cancer Patients. *Prostate* (2018) 78(8):576–82. doi: 10.1002/pros.23501
35. Onstenk W, Sieuwerts AM, Kraan J, Van M, Nieuweboer AJM, Mathijssen RHJ, et al. Efficacy of Cabazitaxel in Castration-Resistant Prostate Cancer is Independent of the Presence of AR-V7 in Circulating Tumor Cells. *Eur Urol* (2015) 68(6):939–45. doi: 10.1016/j.eururo.2015.07.007
36. Qu F, Xie W, Nakabayashi M, Zhang H, Jeong SH, Wang X, et al. Association of AR-V7 and Prostate-Specific Antigen RNA Levels in Blood With Efficacy of Abiraterone Acetate and Enzalutamide Treatment in Men With Prostate Cancer. *Clin Cancer Res* (2017) 23(3):726–34. doi: 10.1158/1078-0432.CCR-16-1070
37. Scher HI, Graf RP, Schreiber NA, Jayaram A, Winquist E, McLaughlin B, et al. Assessment of the Validity of Nuclear-Localized Androgen Receptor Splice Variant 7 in Circulating Tumor Cells as a Predictive Biomarker for Castration-Resistant Prostate Cancer. *JAMA Oncol* (2018) 4(9):1179–86. doi: 10.1001/jamaoncol.2018.1621
38. Scher HI, Graf RP, Schreiber NA, McLaughlin B, Lu D, Louw J, et al. Nuclear-Specific AR-V7 Protein Localization is Necessary to Guide Treatment Selection in Metastatic Castration-Resistant Prostate Cancer. *Eur Urol* (2017) 71(6):874–82. doi: 10.1016/j.eururo.2016.11.024
39. Scher HI, Lu D, Schreiber NA, Louw J, Graf RP, Vargas HA, et al. Association of AR-V7 on Circulating Tumor Cells as a Treatment-Specific Biomarker With Outcomes and Survival in Castration-Resistant Prostate Cancer. *JAMA Oncol* (2016) 2(11):1441–9. doi: 10.1001/jamaoncol.2016.1828
40. Seitz AK, Thoene S, Bietenbeck A, Nawroth R, Tauber R, Thalgott M, et al. AR-V7 in Peripheral Whole Blood of Patients With Castration-Resistant Prostate Cancer: Association With Treatment-Specific Outcome Under Abiraterone and Enzalutamide. *Eur Urol* (2017) 72(5):828–34. doi: 10.1016/j.eururo.2017.07.024
41. Sepe P, Verzoni E, Miodini P, Claps M, Ratta R, Martinetti A, et al. Could Circulating Tumor Cells and ARV7 Detection Improve Clinical Decisions in Metastatic Castration-Resistant Prostate Cancer? The Istituto Nazionale Dei Tumori (INT) Experience. *Cancers* (2019) 11(7):980. doi: 10.3390/cancers11070980
42. Škereňová M, Mikulová V, Čapoun O, Švec D, Kološtová K, Soukup V, et al. Gene Expression Analysis of Immunomagnetically Enriched Circulating Tumor Cell Fraction in Castration-Resistant Prostate Cancer. *Mol Diagnosis Ther* (2018) 22(3):381–90. doi: 10.1007/s40291-018-0333-0
43. Tagawa ST, Antonarakis ES, Gjyrezi A, Galletti G, Kim S, Worroll D, et al. Expression of AR-V7 and Arv(567es) in Circulating Tumor Cells Correlates With Outcomes to Taxane Therapy in Men With Metastatic Prostate Cancer Treated in TAXYNERGY. *Clin Cancer Res* (2019) 25(6):1880–8. doi: 10.1158/1078-0432.CCR-18-0320
44. Tommasi S, Pilato B, Carella C, Lasorella A, Danza K, Vallini I, et al. Standardization of CTC AR-V7 PCR Assay and Evaluation of its Role in Castration Resistant Prostate Cancer Progression. *Prostate* (2018) 79(1):54–61. doi: 10.1002/pros.23710
45. Wang S, Yang S, Nan C, Wang Y, He Y, Mu H. Expression of Androgen Receptor Variant 7 (AR-V7) in Circulated Tumor Cells and Correlation With Drug Resistance of Prostate Cancer Cells. *Med Sci Monitor* (2018) 24:7051–6. doi: 10.12659/MSM.909669
46. Galletti G, Leach BI, Lam L, Tagawa ST. Mechanisms of Resistance to Systemic Therapy in Metastatic Castration-Resistant Prostate Cancer. *Cancer Treat Rev* (2017) 57:16–27. doi: 10.1016/j.ctrv.2017.04.008
47. Nimir M, Ma Y, Jeffreys SA, Opperman T, Young F, Khan T, et al. Detection of AR-V7 in Liquid Biopsies of Castrate Resistant Prostate Cancer Patients: A Comparison of AR-V7 Analysis in Circulating Tumor Cells, Circulating Tumor RNA and Exosomes. *Cells* (2019) 8(7):688. doi: 10.3390/cells8070688
48. Zhang G, Liu X, Li J, Ledet E, Alvarez X, Qi Y, et al. Androgen Receptor Splice Variants Circumvent AR Blockade by Microtubule-Targeting Agents. *Oncotarget* (2015) 6(27):23358–71. doi: 10.18632/oncotarget.4396
49. Wang Z, Shen H, Ma N, Li Q, Mao Y, Wang C, et al. The Prognostic Value of Androgen Receptor Splice Variant 7 in Castration-Resistant Prostate Cancer Treated With Novel Hormonal Therapy or Chemotherapy: A Systematic Review and Meta-Analysis. *Front Oncol* (2020) 10:572590. doi: 10.3389/fonc.2020.572590
50. Zhou J, Liu R. The Association Between Androgen Receptor Splice Variant 7 Status and Prognosis of Metastatic Castration-Resistant Prostate Cancer: A

Systematic Review and Meta-Analysis. *Andrologia* (2020) 52(7):e13642. doi: 10.1111/and.13642

Conflict of Interest: The authors declare that the research was conducted in the absence of any commercial or financial relationships that could be construed as a potential conflict of interest.

Publisher's Note: All claims expressed in this article are solely those of the authors and do not necessarily represent those of their affiliated organizations, or those of the publisher, the editors and the reviewers. Any product that may be evaluated in this article, or claim that may be made by its manufacturer, is not guaranteed or endorsed by the publisher.

Copyright © 2022 Khan, Becker, Scott, Descallar, de Souza, Chua and Ma. This is an open-access article distributed under the terms of the Creative Commons Attribution License (CC BY). The use, distribution or reproduction in other forums is permitted, provided the original author(s) and the copyright owner(s) are credited and that the original publication in this journal is cited, in accordance with accepted academic practice. No use, distribution or reproduction is permitted which does not comply with these terms.

frontiers in Oncology

ORIGINAL RESEARCH
published: 24 March 2022
doi: 10.3389/fonc.2022.841398

Proteomic-Based Machine Learning Analysis Reveals PYGB as a Novel Immunohistochemical Biomarker to Distinguish Inverted Urothelial Papilloma From Low-Grade Papillary Urothelial Carcinoma With Inverted Growth

Minsun Jung[1,2†], Cheol Lee[3†], Dohyun Han[4,5†], Kwangsoo Kim[4], Sunah Yang[4], Ilias P. Nikas[6], Kyung Chul Moon[1,3,7], Hyeyoon Kim[1,5], Min Ji Song[8], Bohyun Kim[9], Hyebin Lee[10] and Han Suk Ryu[1,3,8*]*

[1] Department of Pathology, Seoul National University College of Medicine, Seoul, South Korea, [2] Department of Pathology, Severance Hospital, Yonsei University College of Medicine, Seoul, South Korea, [3] Department of Pathology, Seoul National University Hospital, Seoul, South Korea, [4] Transdisciplinary Department of Medicine and Advanced Technology, Seoul National University Hospital, Seoul, South Korea, [5] Proteomics Core Facility, Biomedical Research Institute, Seoul National University Hospital, Seoul, South Korea, [6] School of Medicine, European University Cyprus, Nicosia, Cyprus, [7] Kidney Research Institute, Medical Research Center, Seoul National University College of Medicine, Seoul, South Korea, [8] Center for Medical Innovation, Biomedical Research Institute, Seoul National University Hospital, Seoul, South Korea, [9] Department of Pathology, Konkuk University Medical Center, Konkuk University School of Medicine, Seoul, South Korea, [10] Department of Radiation Oncology, Kangbuk Samsung Hospital, Sungkyunkwan University School of Medicine, Seoul, South Korea

Background: The molecular biology of inverted urothelial papilloma (IUP) as a precursor disease of urothelial carcinoma is poorly understood. Furthermore, the overlapping histology between IUP and papillary urothelial carcinoma (PUC) with inverted growth is a diagnostic pitfall leading to frequent misdiagnoses.

Methods: To identify the oncologic significance of IUP and discover a novel biomarker for its diagnosis, we employed mass spectrometry-based proteomic analysis of IUP, PUC, and normal urothelium (NU). Machine learning analysis shortlisted candidate proteins, while subsequent immunohistochemical validation was performed in an independent sample cohort.

Results: From the overall proteomic landscape, we found divergent 'NU-like' (low-risk) and 'PUC-like' (high-risk) signatures in IUP. The latter were characterized by altered metabolism, biosynthesis, and cell–cell interaction functions, indicating oncologic significance. Further machine learning-based analysis revealed SERPINH1, PKP2, and PYGB as potential diagnostic biomarkers discriminating IUP from PUC. The

OPEN ACCESS

Edited by:
Alfredo Berruti, University of Brescia, Italy

Reviewed by:
Jianming Lu, Guangzhou First People's Hospital, China
Di Gu, First Affiliated Hospital of Guangzhou Medical University, China

***Correspondence:**
Hyebin Lee
hyebin.lee@samsung.com
Han Suk Ryu
nash77@snu.ac.kr

†These authors have contributed equally to this work and share first authorship

Specialty section:
This article was submitted to Genitourinary Oncology, a section of the journal Frontiers in Oncology

Received: *22 December 2021*
Accepted: *24 February 2022*
Published: *24 March 2022*

Citation:
Jung M, Lee C, Han D, Kim K, Yang S, Nikas IP, Moon KC, Kim H, Song MJ, Kim B, Lee H and Ryu HS (2022) Proteomic-Based Machine Learning Analysis Reveals PYGB as a Novel Immunohistochemical Biomarker to Distinguish Inverted Urothelial Papilloma From Low-Grade Papillary Urothelial Carcinoma With Inverted Growth. Front. Oncol. 12:841398. doi: 10.3389/fonc.2022.841398

immunohistochemical validation confirmed PYGB as a specific biomarker to distinguish between IUP and PUC with inverted growth.

Conclusion: In conclusion, we suggest PYGB as a promising immunohistochemical marker for IUP diagnosis in routine practice.

Keywords: inverted urothelial papilloma, papillary urothelial carcinoma, transitional cell carcinoma (TCC), tandem mass spectrometry (MS/MS), machine learning analysis, immunohistochemistry, biomarkers, differential diagnosis

INTRODUCTION

Inverted urothelial papilloma (IUP) is an uncommon neoplasm that accounts for less than 1% of bladder tumors (1). Although IUP generally exhibits a benign behavior, it has often been reported to show a synchronous/metachronous occurrence with papillary urothelial carcinoma (PUC), raising a concern of having an indeterminate malignant potential (1–3). The malignant potential of IUP has been reinforced by recent genomic data, where a high-risk subset of IUP was shown to harbor key driver oncogenes predisposing to PUC at the genomic level, including *FGFR3* and *TERT* promoter mutations, although the frequency varied between studies (4–6). From the perspective of diagnostic accessibility, nevertheless, it remains controversial whether genomic tests should always be used to predict the oncogenic risk of IUP. Notably, previous studies also have exhibited considerable discordance between genomic mutations and their corresponding protein levels (7, 8). Therefore, assessing the oncogenic potential at the protein level with immunohistochemistry would be preferred, as the latter is a technique widely practiced in diagnostic pathology.

Along with the difficulty to identify the high-risk IUPs, the absence of reliable biomarkers to differentiate IUP from low-grade PUC with inverted growth is another unsolved issue in pathology diagnostics. IUP and PUC with inverted growth are well-known to share several microscopic features, such as slender trabeculae and mild cytomorphological atypia, which could lead to misinterpretation (3). Some ancillary tests, namely, Ki-67, p53, cytokeratin 20, and HER2 immunohistochemistry and genomics assays such as *in situ* hybridization or next-generation sequencing might be helpful in this context (6, 9–12). However, the use of these approaches is hampered by their limited accuracy and applicability (10).

Recent advances in proteomics have enabled in-depth functional analyses of several types of tumors (13–15). In contrast to genomic analysis, the proteomic layer directly reflects proteins, the final units controlling cellular functions. In addition, proteomics-based analysis is more likely to successfully discover a protein-based biomarker that can subsequently be used in immunohistochemistry, the most widely used ancillary diagnostic tool in practice. In previous studies, we presented proteome-based novel diagnostic markers of bladder urothelial carcinoma in liquid-based cytology and Formalin-fixed paraffin embedded (FFPE) specimens (16, 17). In this study, we performed a clinical proteomic analysis to identify proteome-based molecular profiles stratifying the risk in IUP and discover a reliable protein biomarker for the pathological diagnosis of IUP.

MATERIALS AND METHODS

Patient Selection and Clinicopathological Review

FFPE tissue specimens were procured from the Pathology Department of the Seoul National University Hospital. The diagnoses were reviewed by three board-certified pathologists (MJ, KM, and HR), using hematoxylin and eosin slides, according to the 2016 World Health Organization Classification (18). The IUPs included in this study showed inverted trabeculae, cords, or nests of thin urothelium with intact maturation pattern and no cytological atypia (**Supplementary Figure S1**). Any patient with a previous history of bladder tumor and/or intravesical treatment was excluded. Clinical information was obtained from the medical records. The regional Institutional Review Board (IRB) approved the experimental protocols (IRB No. H-2009-163-1160).

For proteomic analysis, 31 tissue specimens, consisting of 9 IUP, 12 PUC, and 10 normal urothelium (NU), were included (**Supplementary Table S1**). All IUP and PUC specimens were cystoscopically resected from the urinary bladder. All PUCs were non-invasive (stage Ta) and 83.3% (10/12) were high-grade. For validation, we performed immunohistochemical staining in an independent validation cohort composed of 25 IUP and 16 PUC with inverted growth (**Supplementary Table S1**). The inverted growth pattern accounted for variable portions (mean ± S.D., 52 ± 32%) of PUCs with inverted growth. The overall demographics of the specimens for validation were similar to those of the proteomic cohort, except most (81.2%) PUCs with inverted growth in the validation cohort were low-grade. All patients with IUP, except for one, were followed up for 12–52 months (median, 31 months) by urine cytology, cystoscopy, or computed tomography, and no one showed recurrence.

Liquid Chromatography With Tandem Mass Spectrometry Analysis and Data Processing

Tandem mass spectrometry (LC–MS/MS) analysis was conducted following the methods used in our previous study (17). Briefly, target areas were macro-dissected from unstained FFPE slides. After filter-aided sample preparation and desalting

procedures, a liquid chromatography-tandem mass spectrometry (LC–MS/MS)-based proteomic study was conducted, using a Q Exactive HF-X Hybrid Quadrupole-Orbitrap mass spectrometer (Thermo Fisher Scientific, Waltham, MA) and an Ultimate 3000 RSLC system (Dionex, Sunnyvale, CA), according to the instructions of the manufacturer. The MaxQuant.Live version 1.2 (Max Planck Institute of Biochemistry, Munich, Germany) was used to perform BoxCar acquisition (19). The MS1 resolution was set to 120,000 at m/z 200 for BoxCar, and the acquisition cycle comprised two BoxCar scans at 12 boxes (scaled width, 1 Th overlap) with a maximum ion injection time of 20.8 per box with the individual AGC target set to 250,000. The MaxQuant version 1.6.1.0 (RRID : SCR_014485) (20) was employed with the Andromeda engine (21) to process the MS raw files. In the global parameter, the BoxCar was set as the experimental type. All search parameters were set as the default parameter of the software. For label-free quantification, the iBAQ algorithm was used as part of the MaxQuant platform (22). Raw LC–MS/MS data were uploaded into the PRIDE database (RRID : SCR_003411; Accession ID: PXD027602).

Bioinformatic Analysis of the Proteomic Data

Proteomic data were analyzed using the Perseus software (RRID : SCR_015753, Max Planck Institute of Biochemistry). For comparisons, we performed an analysis of variance (ANOVA) and a two-sided t-test with a permutation-based false discovery rate (FDR) at significance level <0.05. Gene Ontology-biologic process (GOBP) and Gene Ontology-molecular function (GOMF) annotations were explicated using the Toppgene Suite (RRID : SCR_005726) (23). Protein–protein interaction (PPI) network models were constructed from the String database (24) and were illustrated using Cytoscape (RRID : SCR_003032) (25). The canonical pathway data were analyzed through the use of Ingenuity Pathway Analysis (Qiagen, RRID : SCR_008653, Hilden, Germany) (26).

Clinical Validation of Risk Prediction Biomarkers of Inverted Urothelial Papilloma Using the TCGA Database

The TCGA bladder cancer (BLCA) dataset was used to determine the impact of the IUP-risk biomarkers on the prognosis of bladder cancer (27), under the R environment (R Foundation for Statistical Computing, RRID : SCR_001905, Vienna, Austria; packages "survival" and "survminer"). The RNA sequencing data were chosen for clinical validation because there is no publicly available cohort that contains both high-throughput proteomics and prognostic information in bladder neoplasms. For 405 patients, the gene expression and survival data were obtained from the cBioPortal for Cancer Genomics (https://docs.cbioportal.org/; RRID : SCR_014555) (28, 29). The prognostic effects of the log2-transformed gene expression levels were assessed by calculating a hazard ratio (HR) with 95% confidence interval (CI) using univariate Cox proportional hazard models. Kaplan–Meier analysis and log-rank test were used to compare overall survival outcomes, according to the low vs. high gene expression levels, using the median as a cutoff.

Machine Learning-Based Stepwise Selection of Diagnostic Biomarkers for Inverted Urothelial Papilloma

First, we used a feature selection method for supporting vector machines with radial basis function kernel to choose the proteome with discriminative power between IUP and PUC (30). Next, the high-ranked proteins, selected from the machine learning analysis, were screened using The Human Protein Atlas (https://www.proteinatlas.org/; RRID : SCR_006710) (31, 32). Briefly, the antibody staining intensities (high, score 4; medium, score 3; low, score 2; not detected, score 1) were multiplied by the positive samples proportion showing each staining and then the scores were summed. For multiple antibodies, these scores were averaged. The finalized immunoscores in bladder urothelial carcinoma were compared against the relative fold changes derived from the t-test between IUP and PUC; when a protein was relatively overexpressed in urothelial carcinoma according to the public database but downregulated in PUC compared to IUP in the proteomic analysis, the protein was excluded. The finally selected markers were validated using immunohistochemistry.

Immunohistochemical Validation of Diagnostic Biomarker of Inverted Urothelial Papilloma

A validation cohort, consisting of IUP (n = 25) and PUC with inverted growth (n = 16), was utilized independently from those used for the proteomic analysis. Immunostaining assays for SERPINH1 (1:200, sc-5293, RRID : AB_627757, Santa Cruz Biotechnology, Dallas, TX) and PYGB (1:2,000, HPA031067, RRID : AB_2673722, Sigma-Aldrich, St. Louis, MO) were conducted in IUP and PUC with inverted growth, using an automated BenchMark ULTRA System (Roche Diagnostics, Rotkreuz, Switzerland). The immunostained glass slides were digitally scanned using an Aperio Digital Pathology Slide Scanner AT2 (Leica Biosystems, Buffalo Grove, IL). Expression of SERPINH1 and PYGB was quantified by "H-score" [1 ∗ (% cells 1+) + 2 ∗ (% cells 2+) + 3 ∗ (% cells 3+)], with an interpretation ranging from 0 to 300 (33), using the QuPath platform for bioimage analysis (RRID : SCR_018257) (34). The area under the receiver operating characteristic (AUROC) was calculated using MedCalc version 20.019 (MedCalc Software Ltd, RRID : SCR_015044, Ostend, Belgium) and the optimal level of H-score with corresponding sensitivity and specificity were estimated on the basis of the Youden index.

RESULTS

Proteomic Signatures Divide Low Risk and High Risk in Inverted Urothelial Papilloma

Overall, the LC–MS/MS proteomic assay identified 9,890 and quantified 5,057 proteins, which were present in ≥20% of all

samples, from peptides with high confidence (FDR <0.01). The normalized protein abundance is provided as **Supplementary Table S2**. Principal component analysis demonstrated that IUP was closer to PUC than NU (**Supplementary Figure S2**). Using a one-way ANOVA test among the three groups (**Supplementary Figure S3A**), 698 differentially expressed proteins (DEPs) were identified, and these proteins were used to stratify the risks in IUP compared with PUC and NU (**Figure 1A**, left). Specifically, 'NU-like' IUP signatures, namely, upregulation of SELENBP1, OGDH, and CKB (total, n = 66) and downregulation of TOP2B, NOC2L, and COA3 (total, n = 83), were similar between IUP and NU, as opposed to PUC (**Figure 1A**, left). On the other hand, 'PUC-like' IUP signatures, namely, upregulation of TSTD1, EOGT, and CIT (total, n = 120) and downregulation of DPH6, VPS13D, and SHPRH (total, n = 429), were similar between IUP and PUC, as opposed to NU (**Figure 1A**, left). We investigated the clinical significance of the 40 most significant proteins of the 'NU-like' and 'PUC-like' IUP signatures (**Figure 1A**, right) through survival analysis using the TCGA database. Univariate Cox analysis identified the significance impact of OGDH (HR = 1.469, 95% CI = 1.105–1.954, p = 0.008), SPON1 (HR = 1.092, 95% CI = 1.019–1.170, p = 0.012), PYGB (HR = 1.277, 95% CI = 1.080–1.511, p = 0.004), EPHX1 (HR = 1.159, 95% CI = 1.026–1.309, p = 0.017), SRP68 (HR = 1.643, 95% CI = 1.118–2.415, p = 0.011), and SETD3 (HR = 1.647, 95% CI = 1.180–2.299, p = 0.003) expression on poor urothelial carcinoma outcomes (**Figure 1B**). Among these proteins, low expression of SRP68 and high expression of SETD3 were concordantly observed in the 'NU-like' and 'PUC-like' IUP signatures, respectively (**Figure 1A**, right). These results are consistent with the ones derived from the BCLA survival analysis using the TCGA data; in the latter, low SRP68 expression was associated with favorable, whereas high SETD3 with poor prognosis (**Figure 1C**).

We investigated the molecular functions associated with upregulated and downregulated proteomes in each group. Overall, the GOBP analysis showed significant enrichment of metabolism in all signatures and especially in the upregulated 'NU-like' IUP signatures (**Figure 1D**). The downregulated proteins of the 'NU-like' IUP signatures were also enriched in immune response, the upregulated 'PUC-like' IUP signatures were biased towards transport/membrane, transcription, and translation, while the downregulated 'PUC-like' IUP signatures were enriched in cell–cell interaction, responses to stimuli, and transport/membrane functions (**Figure 1D**). **Figure 1E** summarizes the top 10 significant GOBP terms of each signature set that showed concordant membership. The PPI networks of the proteins included in these top 10 GOBPs consistently highlighted metabolism in the upregulated 'NU-like' IUP proteins, immune response and metabolism in the downregulated 'NU-like' IUP proteins, metabolism and biosynthesis in the upregulated 'PUC-like' IUP proteins, and cell–cell interaction in the downregulated 'PUC-like' IUP proteins (**Figure 1F**). Previous studies identified metabolism, cell proliferation, immune response, and intercellular communication as constitutively altered functions in urothelial carcinoma (35, 36). Enhanced metabolism/biosynthesis functions and decreased cell–cell interaction/adhesion, consistent with what was found in the 'PUC-like' IUP signatures, were previously shown to promote PUC by supporting cell proliferation and structural breakdown (35, 37–39). Therefore, the results suggested altered metabolism, biosynthesis, and cell–cell interaction functions were consistent with the 'PUC-like' (high-risk) IUP.

Activation of Metabolism and Inhibition of Structure-Related Processes Are Distinctive Functions of Inverted Urothelial Papilloma

To further characterize the distinct pathobiology of IUP, we identified DEPs (permutation-based t-test FDR <0.05) between IUP and PUC, namely, PKP2, PYGB, SERPINH1, and TUBB, and those between IUP and NU, namely, ALDH1L1, JUP, COL14A1, and VIM (**Figure 2A** and **Supplementary Figures S3A, B**). GOBP-based 2D annotation enrichment analysis, as previously described (40), revealed that IUP was distinctly enhanced in the metabolism of amines and carboxylic acids yet repressed in cell response, transport/membrane, adhesion, interaction, and extracellular matrix (ECM) (**Figure 2B**). Similarly, IUP-common DEPs, or the intersecting proteins derived from the comparisons of IUP with PUC or NU, jointly coded for similar GOBP themes relevant to the oncologic significance of IUP as mentioned earlier, namely, metabolism, cell–cell interaction, cytoskeleton formation, and transport/membrane (**Figures 2C, D**). The representative IUP-common DEPs selected from the top 10 most significant GOBPs, namely, PKP2, ALDH1L1, CKB, SERPINH1, and TUBB, interacted towards upregulated processes related to desmosome formation or metabolism and downregulated processes related to cell–cell interaction, cell activation, and ECM (**Figure 2E**). In line with this, IPA for these IUP-common DEPs confirmed the activation of metabolism (z-score ≥2.0) and inhibition of cytoskeleton formation/cell–cell interaction (z-score ≤−2.0) as the constitutive pathways in IUP (**Figure 2F**). **Figure 2G** illustrates the activation of the TCA cycle and inhibition of the actin-cytoskeleton signaling in the IUP-common DEPs.

Proteome-Based Machine Learning Analysis Identified Candidate Biomarkers for the Diagnosis of Inverted Urothelial Papilloma

To translate the findings from proteomics to IUP diagnosis in practice, we selected proteome features discriminating IUP from PUC and NU, using support vector machine-based machine learning. The lowest error rates, along with keeping the protein lists short, were achieved at 0.4% between IUP and PUC, corresponding to 10 proteins (**Figure 3A**), and at 0.13% between IUP and NU, corresponding to 3 proteins (**Figure 3B**). We failed to find GOBPs implicated in these proteome sets due to the small numbers. However, GOMF analysis identified aldehyde, glycogen, and redox metabolism enriched for the proteomes of IUP compared to PUC (**Figure 3C**), whereas aldehyde metabolism, cytoskeleton, and cell–cell interaction overrepresented by the proteomes of IUP

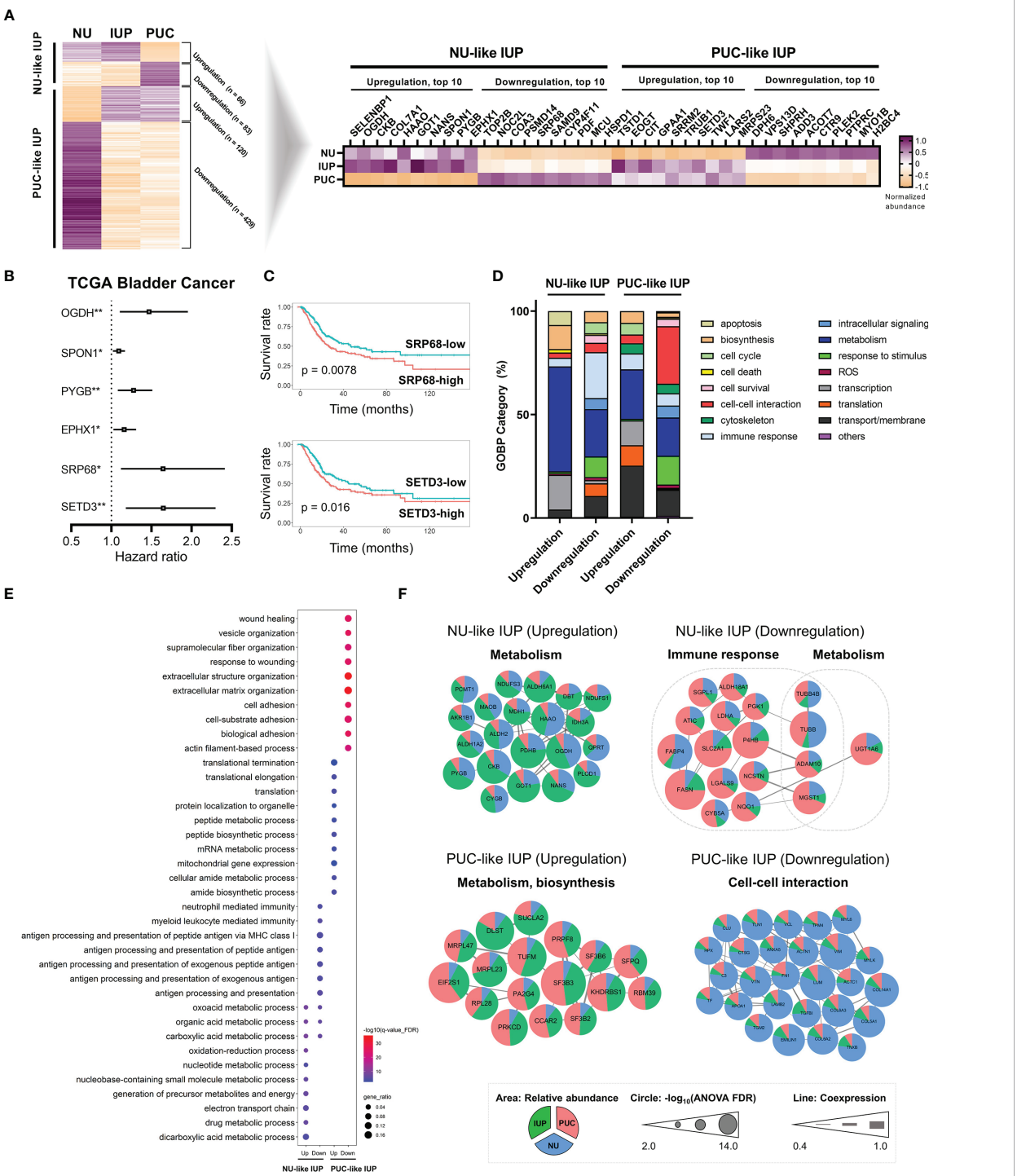


FIGURE 1 | Proteomics-based oncologic signatures of inverted urothelial papilloma (IUP). **(A)** 'Papillary urothelial carcinoma (PUC)-like' IUP and 'normal urothelium (NU)-like' IUP signatures selected from the ANOVA-based differentially expressed proteins (left). The 40 top-ranked proteins of each signature are summarized (right). **(B)** Hazard ratios with 95% confidence intervals of the significant univariate Cox analysis results of the 40 proteins in the TCGA bladder cancer (BLCA) dataset. (*p < 0.05, **p < 0.01). **(C)** Kaplan–Meier graphs of SRP68 and SETD3 in the TCGA BLCA dataset. **(D)** Distribution of Gene Ontology-Biologic Process (GOBP) categories enriched in the upregulated and downregulated proteomes of 'NU-like' IUP and 'PUC-like' IUP signatures. **(E)** The top 10 significantly associated GOBPs. **(F)** Protein–protein interaction networks of the proteomes included in the top 10 significant GOBPs and their related functions. Unconnected proteins are not presented.

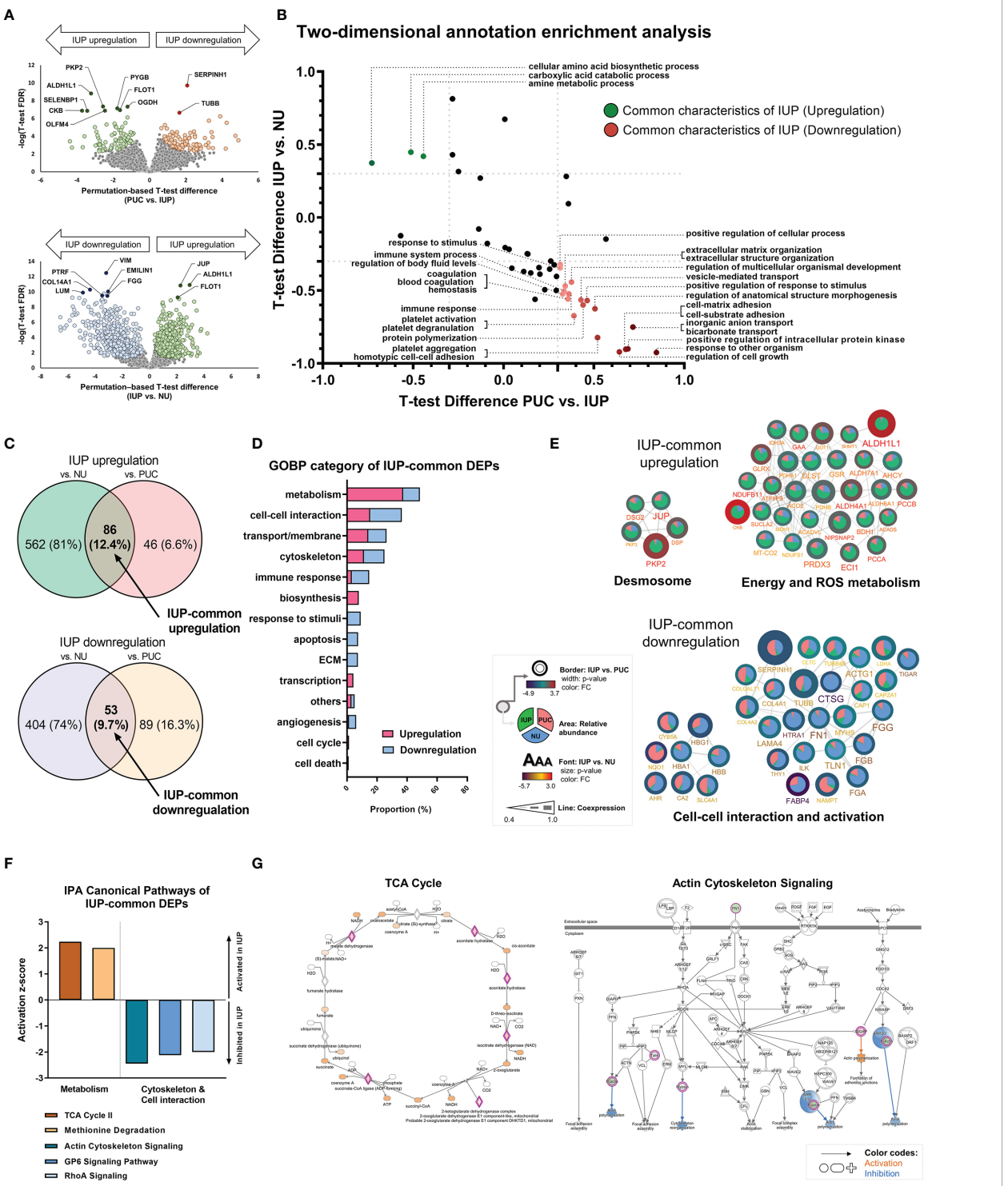


FIGURE 2 | Unique functional profiles of inverted urothelial papilloma (IUP). **(A)** Differentially expressed proteins (DEPs) identified by using t-tests between IUP and papillary urothelial carcinoma (PUC) (upper) and between IUP and normal urothelium (NU) (lower). **(B)** Matched Gene Ontology-Biologic Processes (GOBPs) commonly enriched in the DEPs from both comparisons (PUC vs. IUP and IUP vs. NU). **(C)** DEPs commonly upregulated or downregulated in IUP compared with NU and PUC (IUP-common DEPs). **(D)** GOBP categories related to the IUP-common DEPs. **(E)** Protein–protein interaction networks of the upregulated and downregulated IUP-common DEPs and their related functions. Unconnected proteins are not presented. **(F)** Ingenuity Pathway Analysis (IPA)-canonical pathways predicted to be activated (metabolism) or inhibited (cytoskeleton and cell–cell interaction) in IUP. **(G)** Detailed IPA pathways (TCA and actin-cytoskeleton signaling) showing activated (orange) or inhibited (blue) components in IUP.

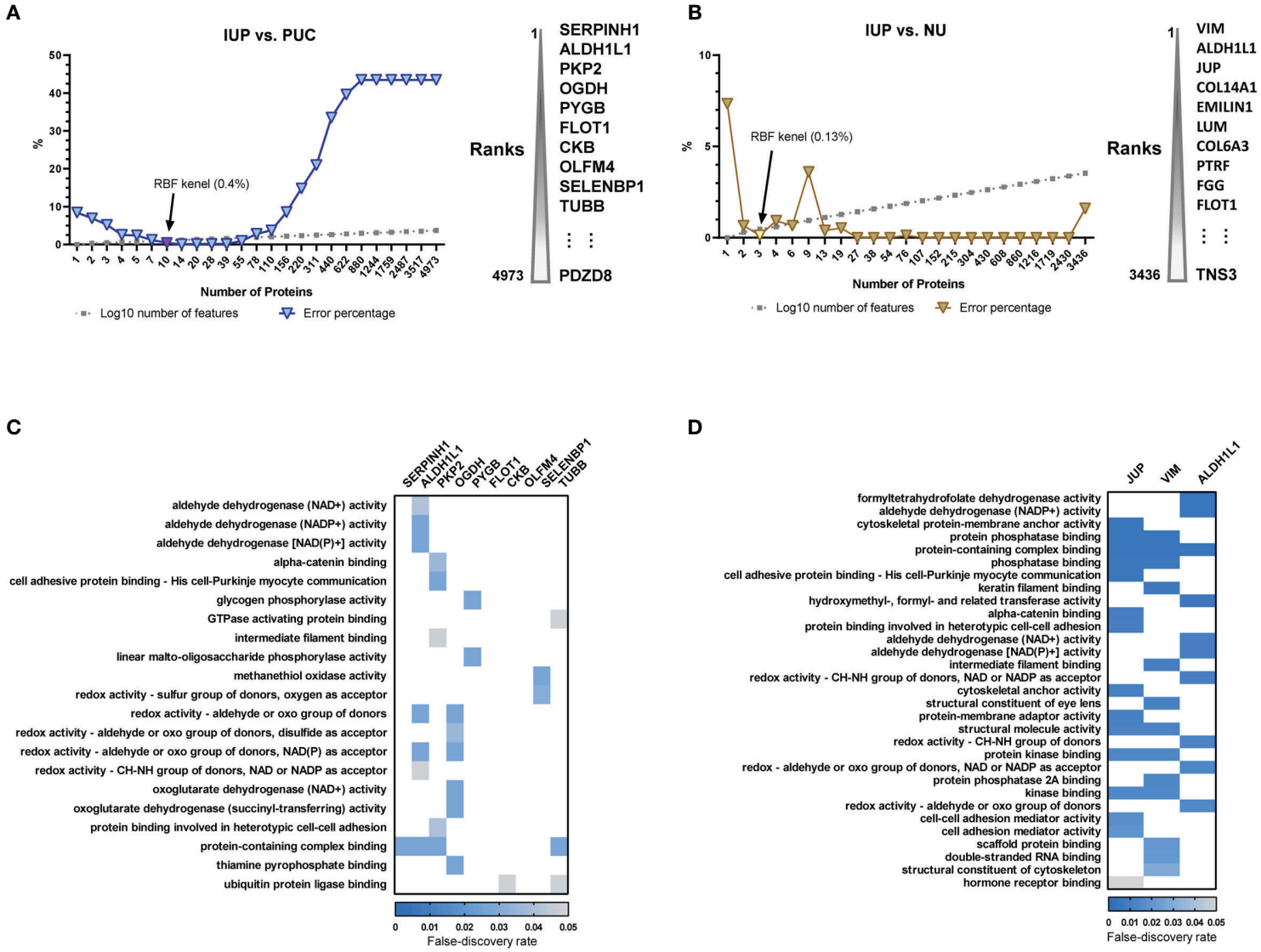


FIGURE 3 | Biomarker discovery of inverted urothelial papilloma (IUP) diagnosis. **(A)** The 10 optimal biomarkers of IUP vs. papillary urothelial carcinoma (PUC), identified by a support vector machine. **(B)** The three optimal biomarkers of IUP vs. normal urothelium (NU) identified by a support vector machine. **(C)** Gene Ontology-Molecular Functions (GOMFs) enriched in the 10 optimal biomarkers of IUP vs. PUC. **(D)** GOMFs enriched in the three optimal biomarkers of IUP vs. NU.

compared to NU (**Figure 3D**). The results corroborated the indispensable roles of metabolism and cytoskeleton/cell interaction-related functions in IUP compared to PUC and NU.

PYGB Distinguishes Inverted Papilloma From Inverted Papillary Urothelial Carcinoma

To prioritize protein biomarkers for IUP diagnosis, the top 10 candidates selected by machine learning analysis between IUP and PUC were further shortlisted, based on the t-test FDR and the machine learning rank order (**Figure 4A**), resulting in the five most robust proteins; SERPINH1, ALDH1L1, PKP2, OGDH, and PYGB (**Figure 4B**). These were additionally narrowed down, based on the similarity between the proteomic profiles and knowledge-based immuno-expression in bladder urothelial carcinoma (**Figure 4B**, green heatmap); ALDH1L1, PKP2, and OGDH were excluded due to the discordancy. Finally, SERPINH1 and PYGB were selected as candidate biomarkers for the distinction between IUP and PUC (**Figure 4B**).

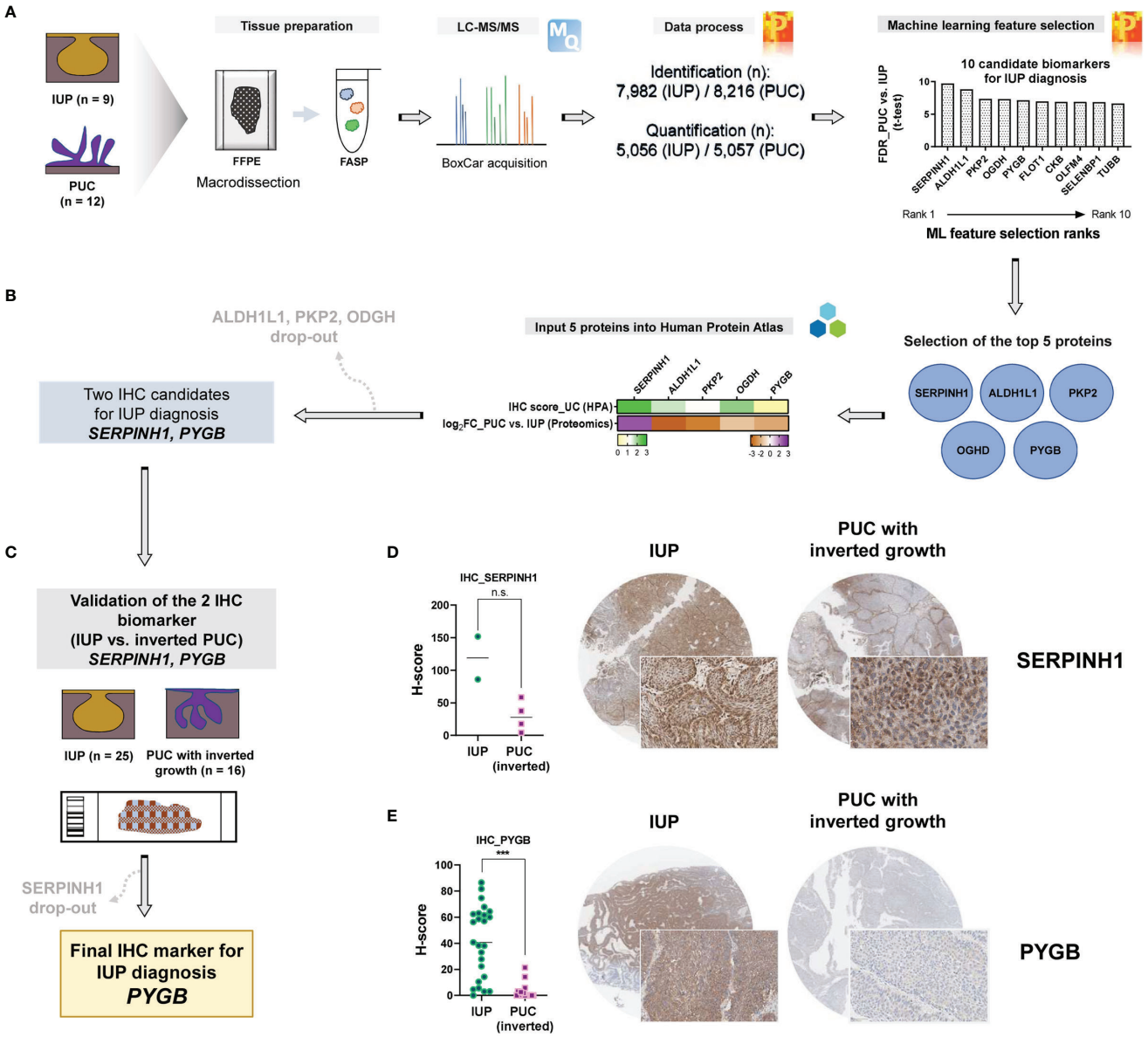


FIGURE 4 | Identification of PYGB as an accurate biomarker to differentiate inverted urothelial papilloma (IUP) from papillary urothelial carcinoma (PUC) with inverted growth. **(A)** Summary of the machine learning feature selection of 10 candidate biomarkers. **(B)** Selection of the five top-ranked proteins and further narrowing-down to the two proteins (SERPINH1 and PYGB), based on The Human Protein Atlas. **(C)** Immunohistochemical validation of SERPINH1 and PYGB in an independent cohort of IUP and PUC with inverted growth. **(D)** SERPINH1 immunostaining in IUP vs. PUC with inverted growth (Mann–Whitney $p = 0.1333$; n.s., not significant). **(E)** PYGB immunostaining in IUP vs. PUC with inverted growth (***Mann–Whitney $p < 0.0001$).

Differential diagnosis of IUP and PUC with inverted growth is one of the common pitfalls in pathological diagnosis of bladder neoplasms due to the morphologic similarity (3, 11, 12). We aimed to resolve this challenge by validating SERPINH1 and PYGB using immunohistochemistry in IUPs and PUCs with inverted growth. To achieve our goal, we additionally enrolled an independent cohort comprising IUP (n = 25) and PUC with inverted growth (n = 16) (**Figure 4C**). In a pilot test, discordantly to the proteomic analysis, SERPINH1 appeared to be diffusely expressed in IUPs compared to PUCs with inverted growth (Mann–Whitney p = 0.1333; **Figure 4D**); SERPINH1 was precluded from further study. However, PYGB was significantly upregulated in IUP compared with PUC with inverted growth (Mann–Whitney p <0.0001; **Figure 4E**), verifying the differential expression found in the proteomic data. The AUROC for the diagnosis of IUP vs. PUC with inverted growth using the PYGB H-score was 0.923 (p <0.0001) and the sensitivity and specificity were 72% (95% CI = 50.6–87.9%) and 100% (95% CI = 79.4–100%), respectively, when H-score 21.4 was set as the cutoff (**Supplementary Figure S4**). The morphology and clinical follow-up of IUPs were similar regardless of whether the immunostaining to PYGB was positive or not. Therefore, we propose that PYGB might be a useful immunohistochemical biomarker for differentiation of IUP from low-grade PUC with inverted growth.

DISCUSSION

In the current study, we applied in-depth proteomics-based machine learning analysis and presented two novel findings as follows: 1) the comprehensive proteomic landscape of IUP to stratify its oncologic risk by identifying two subgroups, a low-risk and a high-risk and 2) a novel immunohistochemical biomarker PYGB to differentiate IUP from PUC with inverted growth.

The oncologic risk of IUP has been controversial in the literature (41–44). Up to 10% of IUPs have been reported to eventually progress into urothelial carcinoma (3). Our in-depth proteomic analysis indicated the presence of a high-risk IUP subgroup, sharing similar proteomic landscapes with PUC. First, based on the similarity of the 698 DEPs found among the three groups, the proteomic profile of IUP was clearly clustered into two risk-stratifying subgroups; the 'NU-like' IUP signatures that were most likely to indicate a low-risk group and the 'PUC-like' IUP signatures that were suspected to indicate an aggressive tumor behavior. The 'NU-like' IUP signatures included upregulation of proteins related to tumor-suppressive functions, namely, SELENBP1, OGDH, CKB, and GOT1 (45–48), besides downregulation of proteins related to oncogenic property, such as TOP2B, NOC2L, PSMD14, SRP68, CYP4F11, PDF, MCU, and HSPD1 (48–54). On the contrary, the 'PUC-like' IUP signatures prioritized proteins previously implicated in cancer promotion, including enrichment of oncogenes [CIT, GPAA1, SRRM2, SETD3, TWF1, and MRPS23 (55–60)] and low expression of tumor-suppressor proteins [SHPRH and ADD3 (61, 62)]. Especially, the survival analysis of the BLCA TCGA dataset further validated SRP68 and SETD3 as potential predictive candidates for the 'NU-like' (low-risk) or 'PUC-like' (high-risk) IUP. SRP68 is a key component of SRP ribonucleoprotein complex regulating endoplasmic reticulum trafficking for protein export and tumor cell mobility (63–65). We showed that low *SRP68* mRNA expression was significantly associated with favorable BLCA prognosis in the TCGA dataset. A previous study also demonstrated that SRP68 was upregulated in bladder cancer compared with adjacent normal tissue and also suggested a key oncogenic function of SRP68 in urothelial carcinoma; this is concordant with our study, where SRP68 was highly expressed in PUC compared to the other two groups (51). High abundance of SETD3, one of the top proteins for high-risk 'PUC-like' IUP signatures, was associated with poor prognosis in the TCGA BLCA dataset. As an epigenetic regulator, SETD3 was previously suggested as a crucial oncogenic modulator in bladder cancer (56). Taken together, the application of SRP68 and SETD3 might be considered as potential biomarkers for identifying the high-risk IUPs.

In this study, a Gene Ontology analysis presented the biologic networks of the 'PUC-like' IUP signatures; these were characterized by alteration of metabolism, biosynthesis, and cell–cell interaction. Concordant findings have been reported in previous studies, showing alteration of macromolecules/metabolites and structural frameworks associated with tumorigenesis and progression of PUC (35, 37). In addition, membrane and transport functions were also enriched in the 'PUC-like' IUP signatures, also in accordance with a prior study that showed alteration in membrane transporters was associated with the malignant behavior of urothelial carcinoma (66). With the enrichment analysis, therefore, we suggest that unique cellular processes might promote an aggressive behavior of IUPs.

Moreover, using commonly expressed proteins in IUP based on the cross-comparison of the DEPs between IUP and NU or IUP and PUC, we also identified unique biological characteristics of IUP. Interestingly, the aforementioned GOBP functions related to the oncologic signatures of IUP, namely, metabolism, cell–cell interaction, and transport/membrane, were similarly enriched here. These results further support the innate significance of these functions in the tumor biology and the potential transformation of IUP. Also, the altered themes of transport/membrane, immune response, and response to stimuli in the IUP-common DEPs may reflect the hyperplastic process in reaction to inflammation, infection, and environmental stress previously suggested regulating IUP pathogenesis (3).

For the first time, along with proteome-based biologic analysis, we successfully discovered PYGB as a novel specific biomarker for the differentiation of IUP from low-grade PUC with inverted growth, using a machine learning feature selection and immunohistochemical validation. PYGB is a brain form of glycogen phosphorylase that supports survival and proliferation of various cell types (67). Glycogen comprises the major glucose storage, and glycogen metabolism balances glucose utilization and energy production (68). Glycogen phosphorylase regulates debranching of glycogen, mobilizing glucose to enter glycolysis

pathway or a pentose-phosphate shunt (67). Recent studies revealed that IUP harbors frequent *HRAS* mutation at higher rates than that observed in PUC with or without inverted growth (6, 11). While uncontrolled activation of the RAS pathway transduces cellular proliferation in IUP (69), upregulated PYGB presumably fuels energy and anabolic sources required for the growth of IUP and downregulation of PYGB in PUC might concur with the metabolic reprogramming (67). In addition, altered energy and ROS metabolism, enriched in the upregulated IUP-common proteome, might corroborate the lack of glycogen deposit in IUP associated with hypoxia (68).

There are limitations in the study. Due to the rarity, the number of IUP included in the validation of the immunostaining for PYGB is relatively small. We are planning an external validation study to confirm the usefulness of PYGB by involving multiple institutions. In addition, the functional role of PYGB in IUP was not validated because *in vitro* or *in vivo* models of IUP are not available. Further studies are needed to confirm the biofunctions of PYGB in IUP.

CONCLUSION

In conclusion, we comprehensively investigated the in-depth proteomic landscape of IUP and found proteome signatures associated with oncologic risk. For the first time, we also discovered PYGB as an accurate biomarker to differentiate IUP from low-grade PUC with inverted growth. In difficult cases, a novel immunohistochemical biomarker such as PYGB can be particularly helpful to establish an accurate diagnosis and prevent a potentially unnecessary treatment.

DATA AVAILABILITY STATEMENT

The datasets presented in this study can be found in online repositories. Proteomic data are available via ProteomeXchange (http://www.proteomexchange.org/) with identifier PXD027602.

ETHICS STATEMENT

The studies involving human participants were reviewed and approved by the Institutional Review Board, Seoul National University Hospital. Written informed consent for participation was not required for this study in accordance with the national legislation and the institutional requirements.

AUTHOR CONTRIBUTIONS

MJ and HSR designed the research, analyzed the data, and drafted the paper. CL, DH, KK, SY, KCM, HK, MJS, and BK were responsible for data collection and analysis. DH, KK, and SY were responsible for statistical analysis. MJ, IPN, HL, and HSR contributed to the study design and revised the manuscript. All authors listed have made a substantial, direct, and intellectual contribution to the work and approved it for publication.

FUNDING

This research was funded by the National Research Foundation of Korea (NRF) funded by the Ministry of Science, ICT and Future Planning (NRF-2019R1C1C1006640, 2021R1F1A1063982, 2021R1A2C4086635, and 2022R1A2C4001439).

SUPPLEMENTARY MATERIAL

The Supplementary Material for this article can be found online at: https://www.frontiersin.org/articles/10.3389/fonc.2022.841398/full#supplementary-material

REFERENCES

1. Hodges KB, Lopez-Beltran A, Maclennan GT, Montironi R, Cheng L. Urothelial Lesions With Inverted Growth Patterns: Histogenesis, Molecular Genetic Findings, Differential Diagnosis and Clinical Management. *BJU Int* (2011) 107:532–7. doi: 10.1111/j.1464-410X.2010.09853.x
2. Asano K, Miki JUN, Maeda S, Naruoka T, Takahashi H, Oishi Y. Clinical Studies on Inverted Papilloma of the Urinary Tract: Report of 48 Cases and Review of the Literature. *J Urol* (2003) 170:1209–12. doi: 10.1097/01.ju.0000085342.15918.d7
3. Sweeney MK, Rais-Bahrami S, Gordetsky J. Inverted Urothelial Papilloma: A Review of Diagnostic Pitfalls and Clinical Management. *Can Urol Assoc J* (2017) 11:66–9. doi: 10.5489/cuaj.4136
4. Lott S, Wang M, Zhang S, MacLennan GT, Lopez-Beltran A, Montironi R, et al. FGFR3 and TP53 Mutation Analysis in Inverted Urothelial Papilloma: Incidence and Etiological Considerations. *Mod Pathol* (2009) 22:627–32. doi: 10.1038/modpathol.2009.28
5. Cheng L, Davidson DD, Wang M, Lopez-Beltran A, Montironi R, Wang L, et al. Telomerase Reverse Transcriptase (TERT) Promoter Mutation Analysis of Benign, Malignant and Reactive Urothelial Lesions Reveals a Subpopulation of Inverted Papilloma With Immortalizing Genetic Change. *Histopathol* (2016) 69:107–13. doi: 10.1111/his.12920
6. Isharwal S, Hu W, Sarungbam J, Chen YB, Gopalan A, Fine SW, et al. Genomic Landscape of Inverted Urothelial Papilloma and Urothelial Papilloma of the Bladder. *J Pathol* (2019) 248:260–5. doi: 10.1002/path.5261
7. Park ES, Rabinovsky R, Carey M, Hennessy BT, Agarwal R, Liu W, et al. Integrative Analysis of Proteomic Signatures, Mutations, and Drug Responsiveness in the NCI 60 Cancer Cell Line Set. *Mol Cancer Ther* (2010) 9:257–67. doi: 10.1158/1535-7163.MCT-09-0743
8. Myhre S, Lingjaerde OC, Hennessy BT, Aure MR, Carey MS, Alsner J, et al. Influence of DNA Copy Number and mRNA Levels on the Expression of Breast Cancer Related Proteins. *Mol Oncol* (2013) 7:704–18. doi: 10.1016/j.molonc.2013.02.018
9. Jones TD, Zhang S, Lopez-Beltran A, Eble JN, Sung MT, MacLennan GT, et al. Urothelial Carcinoma With an Inverted Growth Pattern Can be Distinguished From Inverted Papilloma by Fluorescence *In Situ* Hybridization, Immunohistochemistry, and Morphologic Analysis. *Am J Surg Pathol* (2007) 31:1861–7. doi: 10.1097/PAS.0b013e318060cb9d
10. Sun JJ, Wu Y, Lu YM, Zhang HZ, Wang T, Yang XQ, et al. Immunohistochemistry and Fluorescence *In Situ* Hybridization Can

Inform the Differential Diagnosis of Low-Grade Noninvasive Urothelial Carcinoma With an Inverted Growth Pattern and Inverted Urothelial Papilloma. *PloS One* (2015) 10:e0133530. doi: 10.1371/journal.pone.0133530
11. Almassi N, Pietzak EJ, Sarungbam J, Tickoo SK, Reuter VE, Solit DB, et al. Inverted Urothelial Papilloma and Urothelial Carcinoma With Inverted Growth Are Histologically and Molecularly Distinct Entities. *J Pathol* (2020) 250:464–5. doi: 10.1002/path.5390
12. Sanguedolce F, Calo B, Chirico M, Falagario U, Busetto GM, Zanelli M, et al. Distinctive Morphological and Molecular Features of Urothelial Carcinoma With an Inverted Growth Pattern. *J Pathol Trans Med* (2021) 55:239–46. doi: 10.4132/jptm.2021.04.20
13. Harel M, Ortenberg R, Varanasi SK, Mangalhara KC, Mardamshina M, Markovits E, et al. Proteomics of Melanoma Response to Immunotherapy Reveals Mitochondrial Dependence. *Cell* (2019) 179:236–50.e18. doi: 10.1016/j.cell.2019.08.012
14. Lee KM, Lee H, Han D, Moon WK, Kim K, Oh HJ, et al. Combined the SMAC Mimetic and BCL2 Inhibitor Sensitizes Neoadjuvant Chemotherapy by Targeting Necrosome Complexes in Tyrosine aminoacyl-tRNA Synthase-Positive Breast Cancer. *Breast Cancer Res* (2020) 22:130. doi: 10.1186/s13058-020-01367-7
15. Beck L, Harel M, Yu S, Markovits E, Boursi B, Markel G, et al. Clinical Proteomics of Metastatic Melanoma Reveals Profiles of Organ Specificity and Treatment Resistance. *Clin Cancer Res* (2021) 27:2074–86. doi: 10.1158/1078-0432.CCR-20-3752
16. Lee H, Kim K, Woo J, Park J, Kim H, Lee KE, et al. Quantitative Proteomic Analysis Identifies AHNAK (Neuroblast Differentiation-Associated Protein AHNAK) as a Novel Candidate Biomarker for Bladder Urothelial Carcinoma Diagnosis by Liquid-Based Cytology. *Mol Cell Proteomics* (2018) 17:1788–802. doi: 10.1074/mcp.RA118.000562
17. Park JH, Lee C, Han D, Lee JS, Lee KM, Song MJ, et al. Moesin (MSN) as a Novel Proteome-Based Diagnostic Marker for Early Detection of Invasive Bladder Urothelial Carcinoma in Liquid-Based Cytology. *Cancers (Basel)* (2020) 12:1018. doi: 10.3390/cancers12041018
18. Humphrey PA, Moch H, Cubilla AL, Ulbright TM, Reuter VE. The 2016 WHO Classification of Tumours of the Urinary System and Male Genital Organs-Part B: Prostate and Bladder Tumours. *Eur Urol* (2016) 70:106–19. doi: 10.1016/j.eururo.2016.02.028
19. Wichmann C, Meier F, Virreira Winter S, Brunner AD, Cox J, Mann M. MaxQuant.Live Enables Global Targeting of More Than 25,000 Peptides. *Mol Cell Proteomics* (2019) 18:982–94. doi: 10.1074/mcp.TIR118.001131
20. Tyanova S, Temu T, Cox J. The Maxquant Computational Platform for Mass Spectrometry-Based Shotgun Proteomics. *Nat Protoc* (2016) 11:2301–19. doi: 10.1038/nprot.2016.136
21. Cox J, Neuhauser N, Michalski A, Scheltema RA, Olsen JV, Mann M. Andromeda: A Peptide Search Engine Integrated Into the Maxquant Environment. *J Proteome Res* (2011) 10:1794–805. doi: 10.1021/pr101065j
22. Schwanhausser B, Busse D, Li N, Dittmar G, Schuchhardt J, Wolf J, et al. Global Quantification of Mammalian Gene Expression Control. *Nat* (2011) 473:337–42. doi: 10.1038/nature10098
23. Chen J, Bardes EE, Aronow BJ, Jegga AG. Toppgene Suite for Gene List Enrichment Analysis and Candidate Gene Prioritization. *Nucleic Acids Res* (2009) 37:W305–W11. doi: 10.1093/nar/gkp427
24. Szklarczyk D, Gable AL, Lyon D, Junge A, Wyder S, Huerta-Cepas J, et al. String V11: Protein-Protein Association Networks With Increased Coverage, Supporting Functional Discovery in Genome-Wide Experimental Datasets. *Nucleic Acids Res* (2019) 47:D607–D13. doi: 10.1093/nar/gky1131
25. Shannon P, Markiel A, Ozier O, Baliga NS, Wang JT, Ramage D, et al. Cytoscape: A Software Environment for Integrated Models of Biomolecular Interaction Networks. *Genome Res* (2003) 13:2498–504. doi: 10.1101/gr.1239303
26. Kramer A, Green J, Pollard JJr., Tugendreich S. Causal Analysis Approaches in Ingenuity Pathway Analysis. *Bioinf* (2014) 30:523–30. doi: 10.1093/bioinformatics/btt703
27. Robertson AG, Kim J, Al-Ahmadie H, Bellmunt J, Guo G, Cherniack AD, et al. Comprehensive Molecular Characterization of Muscle-Invasive Bladder Cancer. *Cell* (2017) 171:540–56.e25. doi: 10.1016/j.cell.2017.09.007
28. Cerami E, Gao J, Dogrusoz U, Gross BE, Sumer SO, Aksoy BA, et al. The Cbio Cancer Genomics Portal: An Open Platform for Exploring Multidimensional Cancer Genomics Data. *Cancer Discov* (2012) 2:401–4. doi: 10.1158/2159-8290.CD-12-0095
29. Gao J, Aksoy BA, Dogrusoz U, Dresdner G, Gross B, Sumer SO, et al. Integrative Analysis of Complex Cancer Genomics and Clinical Profiles Using the Cbioportal. *Sci Signaling* (2013) 6:pl1. doi: 10.1126/scisignal.2004088
30. Tyanova S, Temu T, Sinitcyn P, Carlson A, Hein MY, Geiger T, et al. The Perseus Computational Platform for Comprehensive Analysis of (Prote) Omics Data. *Nat Methods* (2016) 13:731–40. doi: 10.1038/nmeth.3901
31. Uhlen M, Bjorling E, Agaton C, Szigyarto CA, Amini B, Andersen E, et al. A Human Protein Atlas for Normal and Cancer Tissues Based on Antibody Proteomics. *Mol Cell Proteomics* (2005) 4:1920–32. doi: 10.1074/mcp.M500279-MCP200
32. Uhlen M, Fagerberg L, Hallstrom BM, Lindskog C, Oksvold P, Mardinoglu A, et al. Proteomics. Tissue-Based Map of the Human Proteome. *Sci* (2015) 347:1260419. doi: 10.1126/science.1260419
33. Aeffner F, Wilson K, Martin NT, Black JC, Hendriks CLL, Bolon B, et al. The Gold Standard Paradox in Digital Image Analysis Manual Versus Automated Scoring as Ground Truth. *Arch Pathol Lab Med* (2017) 141:1267–75. doi: 10.5858/arpa.2016-0386-RA
34. Bankhead P, Loughrey MB, Fernandez JA, Dombrowski Y, McArt DG, Dunne PD, et al. QuPath: Open Source Software for Digital Pathology Image Analysis. *Sci Rep* (2017) 7:16878. doi: 10.1038/s41598-017-17204-5
35. Lindgren D, Liedberg F, Andersson A, Chebil G, Gudjonsson S, Borg A, et al. Molecular Characterization of Early-Stage Bladder Carcinomas by Expression Profiles, Fgfr3 Mutation Status, and Loss of 9q. *Oncogene* (2006) 25:2685–96. doi: 10.1038/sj.onc.1209249
36. Li J, Abraham S, Cheng L, Witzmann FA, Koch M, Xie J, et al. Proteomic-Based Approach for Biomarkers Discovery in Early Detection of Invasive Urothelial Carcinoma. *Proteomics Clin Applications* (2008) 2:78–89. doi: 10.1002/prca.200780027
37. Sjodahl G, Lauss M, Lovgren K, Chebil G, Gudjonsson S, Veerla S, et al. A Molecular Taxonomy for Urothelial Carcinoma. *Clin Cancer Res* (2012) 18:3377–86. doi: 10.1158/1078-0432.CCR-12-0077-T
38. Jung M, Lee JH, Kim B, Park JH, Moon KC. Transcriptional Analysis of Immunohistochemically Defined Subgroups of Non-Muscle-Invasive Papillary High-Grade Upper Tract Urothelial Carcinoma. *Int J Mol Sci* (2019) 20:570. doi: 10.3390/ijms20030570
39. Jung M, Jang I, Kim K, Moon KC. CK14 Expression Identifies a Basal/Squamous-Like Type of Papillary Non-Muscle-Invasive Upper Tract Urothelial Carcinoma. *Front Oncol* (2020) 10:623. doi: 10.3389/fonc.2020.00623
40. Tyanova S, Albrechtsen R, Kronqvist P, Cox J, Mann M, Geiger T. Proteomic Maps of Breast Cancer Subtypes. *Nat Commun* (2016) 7:10259. doi: 10.1038/ncomms10259
41. Stein BS, Rosen S, Kendall AR. The Association of Inverted Papilloma and Transitional Cell Carcinoma of the Urothelium. *J Urol* (1984) 131:751–2. doi: 10.1016/s0022-5347(17)50609-6
42. Witjes JA, van Balken MR, van de Kaa CA. The Prognostic Value of a Primary Inverted Papilloma of the Urinary Tract. *J Urol* (1997) 158:1500–5. doi: 10.1016/S0022-5347(01)64253-8
43. Broussard JN, Tan PH, Epstein JI. Atypia in Inverted Urothelial Papillomas: Pathology and Prognostic Significance. *Hum Pathol* (2004) 35:1499–504. doi: 10.1016/j.humpath.2004.09.010
44. Ho H, Chen YD, Tan PH, Wang M, Lau WK, Cheng C. Inverted Papilloma of Urinary Bladder: Is Long-Term Cystoscopic Surveillance Needed? A Single Center's Experience. *Urol* (2006) 68:333–6. doi: 10.1016/j.urology.2006.03.014
45. Reszka E. Selenoproteins in Bladder Cancer. *Clinica Chimica Acta; Int J Clin Chem* (2012) 413:847–54. doi: 10.1016/j.cca.2012.01.041
46. Mello AA, Leal MF, Rey JA, Pinto GR, Lamarao LM, Montenegro RC, et al. Deregulated Expression of SRC, LYN and CKB Kinases by DNA Methylation and its Potential Role in Gastric Cancer Invasiveness and Metastasis. *PloS One* (2015) 10:e0140492. doi: 10.1371/journal.pone.0140492
47. Loras A, Suarez-Cabrera C, Martinez-Bisbal MC, Quintas G, Paramio JM, Martinez-Manez R, et al. Integrative Metabolomic and Transcriptomic Analysis for the Study of Bladder Cancer. *Cancers (Basel)* (2019) 11:686. doi: 10.3390/cancers11050686
48. Stroggilos R, Mokou M, Latosinska A, Makridakis M, Lygirou V, Mavrogeorgis E, et al. Proteome-Based Classification of Nonmuscle

Invasive Bladder Cancer. *Int J Cancer* (2020) 146:281–94. doi: 10.1002/ijc.32556
49. Downie D, McFadyen MC, Rooney PH, Cruickshank ME, Parkin DE, Miller ID, et al. Profiling Cytochrome P450 Expression in Ovarian Cancer: Identification of Prognostic Markers. *Clin Cancer Res* (2005) 11:7369–75. doi: 10.1158/1078-0432.CCR-05-0466
50. Sheth A, Escobar-Alvarez S, Gardner J, Ran L, Heaney ML, Scheinberg DA. Inhibition of Human Mitochondrial Peptide Deformylase Causes Apoptosis in C-Myc-Overexpressing Hematopoietic Cancers. *Cell Death Dis* (2014) 5: e1152. doi: 10.1038/cddis.2014.112
51. Zekri AR, Hassan ZK, Bahnassy AA, Khaled HM, El-Rouby MN, Haggag RM, et al. Differentially Expressed Genes in Metastatic Advanced Egyptian Bladder Cancer. *Asian Pac J Cancer Prev* (2015) 16:3543–9. doi: 10.7314/apjcp.2015.16.8.3543
52. Vultur A, Gibhardt CS, Stanisz H, Bogeski I. The Role of the Mitochondrial Calcium Uniporter (MCU) Complex in Cancer. *Pflgers Archiv Eur J Physiol* (2018) 470:1149–63. doi: 10.1007/s00424-018-2162-8
53. Wang Q, Ding J, Nan G, Lyu Y, Ni G. LncRNA Noc2l-4.1 Functions as a Tumor Oncogene in Cervical Cancer Progression by Regulating the miR-630/YAP1 Pathway. *J Cell Biochem* (2019) 120:16913–20. doi: 10.1002/jcb.28949
54. Lv J, Zhang S, Wu H, Lu J, Lu Y, Wang F, et al. Deubiquitinase PSMD14 Enhances Hepatocellular Carcinoma Growth and Metastasis by Stabilizing GRB2. *Cancer Lett* (2020) 469:22–34. doi: 10.1016/j.canlet.2019.10.025
55. Lyng H, Brovig RS, Svendsrud DH, Holm R, Kaalhus O, Knutstad K, et al. Gene Expressions and Copy Numbers Associated With Metastatic Phenotypes of Uterine Cervical Cancer. *BMC Genomics* (2006) 7:268. doi: 10.1186/1471-2164-7-268
56. Ding B, Yan L, Zhang Y, Wang Z, Zhang Y, Xia D, et al. Analysis of the Role of Mutations in the KMT2D Histone Lysine Methyltransferase in Bladder Cancer. *FEBS Open Bio* (2019) 9:693–706. doi: 10.1002/2211-5463.12600
57. Jin X, Pang W, Zhang Q, Huang H. MicroRNA-486-5p Improves Nonsmall-Cell Lung Cancer Chemotherapy Sensitivity and Inhibits Epithelial-Mesenchymal Transition by Targeting Twinfilin Actin Binding Protein 1. *J Int Med Res* (2019) 47:3745–56. doi: 10.1177/0300060519850739
58. Zhang XX, Ni B, Li Q, Hu LP, Jiang SH, Li RK, et al. GPAA1 Promotes Gastric Cancer Progression *via* Upregulation of GPI-Anchored Protein and Enhancement of Erbb Signalling Pathway. *J Exp Clin Cancer Res* (2019) 38:214. doi: 10.1186/s13046-019-1218-8
59. Chen S, Lv L, Zhan Z, Wang X, You Z, Luo X, et al. Silencing of Long Noncoding RNA SRRM2-As Exerts Suppressive Effects on Angiogenesis in Nasopharyngeal Carcinoma *via* Activating MYLK-Mediated GGMP-PKG Signaling Pathway. *J Cell Physiol* (2020) 235:7757–68. doi: 10.1002/jcp.29382
60. Shou J, Yu C, Zhang D, Zhang Q. Overexpression of Citron Rho-Interacting Serine/Threonine Kinase Associated With Poor Outcome in Bladder Cancer. *J Cancer* (2020) 11:4173–80. doi: 10.7150/jca.43435
61. Zhang M, Huang N, Yang X, Luo J, Yan S, Xiao F, et al. A Novel Protein Encoded by the Circular Form of the SHPRH Gene Suppresses Glioma Tumorigenesis. *Oncogene* (2018) 37:1805–14. doi: 10.1038/s41388-017-0019-9
62. Yang JL, Wang CCN, Cai JH, Chou CY, Lin YC, Hung CC. Identification of Gsn and LAMC2 as Key Prognostic Genes of Bladder Cancer by Integrated Bioinformatics Analysis. *Cancers (Basel)* (2020) 12:1809. doi: 10.3390/cancers12071809
63. Iakhiaeva E, Bhuiyan SH, Yin J, Zwieb C. Protein SRP68 of Human Signal Recognition Particle: Identification of the RNA and SRP72 Binding Domains. *Protein Sci Publ Protein Soc* (2006) 15:1290–302. doi: 10.1110/ps.051861406
64. Krust B, El Khoury D, Nondier I, Soundaramourty C, Hovanessian AG. Targeting Surface Nucleolin With Multivalent HB-19 and Related Nucant Pseudopeptides Results in Distinct Inhibitory Mechanisms Depending on the Malignant Tumor Cell Type. *BMC Cancer* (2011) 11:333. doi: 10.1186/1471-2407-11-333
65. Gao Y, Zhang Q, Lang Y, Liu Y, Dong X, Chen Z, et al. Human Apo-SRP72 and SRP68/72 Complex Structures Reveal the Molecular Basis of Protein Translocation. *J Mol Cell Biol* (2017) 9:220–30. doi: 10.1093/jmcb/mjx010
66. Chan TC, Wu WJ, Li WM, Shiao MS, Shiue YL, Li CF. SLC14A1 Prevents Oncometabolite Accumulation and Recruits HDAC1 to Transrepress Oncometabolite Genes in Urothelial Carcinoma. *Theranostics* (2020) 10:11775–93. doi: 10.7150/thno.51655
67. Ritterson Lew C, Guin S, Theodorescu D. Targeting Glycogen Metabolism in Bladder Cancer. *Nat Rev Urol* (2015) 12:383–91. doi: 10.1038/nrurol.2015.111
68. Favaro E, Bensaad K, Chong MG, Tennant DA, Ferguson DJ, Snell C, et al. Glucose Utilization *via* Glycogen Phosphorylase Sustains Proliferation and Prevents Premature Senescence in Cancer Cells. *Cell Metab* (2012) 16:751–64. doi: 10.1016/j.cmet.2012.10.017
69. Pylayeva-Gupta Y, Grabocka E, Bar-Sagi D. RAS Oncogenes: Weaving a Tumorigenic Web. *Nat Reveiws Cancer* (2011) 11:761–74. doi: 10.1038/nrc3106

Conflict of Interest: The authors declare that the research was conducted in the absence of any commercial or financial relationships that could be construed as a potential conflict of interest.

Publisher's Note: All claims expressed in this article are solely those of the authors and do not necessarily represent those of their affiliated organizations, or those of the publisher, the editors and the reviewers. Any product that may be evaluated in this article, or claim that may be made by its manufacturer, is not guaranteed or endorsed by the publisher.

Copyright © 2022 Jung, Lee, Han, Kim, Yang, Nikas, Moon, Kim, Song, Kim, Lee and Ryu. This is an open-access article distributed under the terms of the Creative Commons Attribution License (CC BY). The use, distribution or reproduction in other forums is permitted, provided the original author(s) and the copyright owner(s) are credited and that the original publication in this journal is cited, in accordance with accepted academic practice. No use, distribution or reproduction is permitted which does not comply with these terms.

frontiers | Frontiers in Oncology

SYSTEMATIC REVIEW
published: 11 April 2022
doi: 10.3389/fonc.2022.879803

Prognostic Role of Pretreatment C-Reactive Protein to Albumin Ratio in Urological Cancers: A Systematic Review and Meta-Analysis

Minhong Wu[1†], Yan Zhou[2†], Qingsheng Chen[1], Zhiling Yu[1], Hongyong Gu[1], Pengxiu Lin[1], Yanling Li[1] and Cailing Liu[1]*

[1] Department of Urology, Yichun People's Hospital, Yichun, China, [2] Department of Nursing, Wanzai County Traditional Chinese Medicine Hospital, Yichun, China

Background: To investigate the potential prognostic role of C-reactive protein to albumin ratio (CAR) in patients with urinary cancers, including renal cell carcinoma (RCC), bladder cancer (BC), and prostate cancer (PC).

Methods: We searched and screened literatures with PubMed, Embase, Cochrane Library, and Web of Science in January 2022. We applied combined hazard ratios (HRs) and 95% confidence intervals (CIs) to assess the associations.

Results: Thirteen studies including 2,941 cases were analyzed in our study. Merged results indicated that highly pretreated CAR was associated with inferior overall survival (HR 2.21, 95% CI 1.86-2.62, $p < 0.001$) and progression-free survival (HR 1.85, 95% CI 1.36-2.52, $p < 0.001$) for urinary cancers. In a subgroup analysis of OS by tumor type, CAR can be a predictor in RCC (HR 2.10, 95% CI 1.72-2.56), BC (HR 3.35, 95% CI 1.94-5.80), and PC (HR 2.20, 95% CI 1.43-3.37). In a subgroup analysis of PFS by tumor type, CAR can be a predictor in BC (HR 1.76, 95% CI 1.03-3.02), and RCC (HR 1.90, 95% CI 1.25-2.89). The reliability and robustness of results were confirmed.

Conclusions: High pretreated CAR was effective predictor of poor survival in patients with urinary cancers and can act as prognostic factor for these cases.

Systematic Review Registration: PROSPERO (CRD42022306414).

Keywords: urological cancer, C-reactive protein, albumin, prognosis, meta-analysis

OPEN ACCESS

Edited by:
Michele Marchioni, University of Studies G. d'Annunzio Chieti and Pescara, Italy

Reviewed by:
Georges Mjaess, Free University of Brussels, Belgium
Liangyou Gu, People's Liberation Army General Hospital, China

***Correspondence:**
Minhong Wu
wuminhong301@126.com

†These authors share first authorship

Specialty section:
This article was submitted to Genitourinary Oncology, a section of the journal Frontiers in Oncology

Received: *20 February 2022*
Accepted: *14 March 2022*
Published: *11 April 2022*

Citation:
Wu M, Zhou Y, Chen Q, Yu Z, Gu H, Lin P, Li Y and Liu C (2022) Prognostic Role of Pretreatment C-Reactive Protein to Albumin Ratio in Urological Cancers: A Systematic Review and Meta-Analysis. Front. Oncol. 12:879803. doi: 10.3389/fonc.2022.879803

INTRODUCTION

Urinary neoplasms, including renal cell carcinoma (RCC), bladder cancer (BC) and prostate cancer (PC), are usual cancers with increased morbidity and mortality. These three tumors were among the 10 most common malignancies in the United States in 2019 (1). In general, most cancers of the urinary system are found at a local stage. Tumor excision is the preferred management and can achieve well-pleasing outcomes. Nevertheless, some patients may develop metastasis at initial diagnosis, and most local tumors eventually progress to relapsing or metastatic disease. With the development of molecular targeted drugs (2, 3) and immunotherapy (4), the survival of urinary

tumors has been greatly improved. However, the long-term survival of these tumors remains disappointing. Therefore, it is of interest to study the prognostic biomarkers in these cases in order to better understand their underlying mechanisms and contribute to the optimal treatment of urinary tumors.

There was increasing evidence of a link between tumor-caused inflammatory response and tumorigenesis and disease progression (5). Kinds of inflammatory and immune response factors have been reported as survival biomarkers for various cancers (6). The C-reactive protein to albumin ratio (CAR) is a measure of serum C-reactive protein (CRP) and albumin and is generated as the CRP level divided by the albumin level. The ratio was originally suggested to forecast the prognosis of acute hospitalized patients (7). Recently, various centers have explored the application of CAR as a prognostic biomarker for kinds of cancers, including gastric cancer (8), colorectal cancer (9), non-small-cell lung cancer (10), gallbladder cancer (11), etc. As for urinary neoplasms, a lot of studies have examined the prognostic value of CAR in RCC. After combining data from these studies, a meta-analysis confirmed that high pretreated CAR was effective predictor of poor survival in cases with RCC (12). Nevertheless, data with potential bias from univariable analysis was included, and the latest studies could not be included (13). Moreover, several studies focusing on the prognostic role of CAR in BC and PC have been published (14–17). This situation encouraged us to conduct the present study to present an integrated review of all related evidence exploring the value of CAR on outcomes in urological cancer patients.

METHODS

Literature Searching

Our study was performed and presented following the PRISMA guidelines. The protocol has been presented on PROSPERO (No. CRD42022306414). A comprehensive literature search was conducted with MEDLINE, Embase, Cochrane Library, and Web of Science electronic databases. We searched and screened the potential literatures up to January 2022. The key words embraced: "C-reactive protein to albumin ratio" (e.g., "CAR", "C-reactive protein to albumin ratio", "C-reactive protein-to-albumin ratio", "C-reactive protein/albumin ratio"), "urinary cancer" (e.g., "renal cell carcinoma", "bladder cancer", "prostate cancer", "urothelial carcinoma", "testicular cancer", "penile cancer") and "prognosis" (e.g., "survival", "prognosis", "outcome", "progression", "recurrence", "metastasis", "mortality"). A manual screen of study references was also conducted to obtain possibly relevant literatures. The language of included studies was restricted to English.

Study Inclusion and Exclusion

To be eligible for inclusion, studies must meet the following criteria: (1) studies focusing on the association between pretreated CAR and prognosis of urological cancers, including renal cell carcinoma (RCC), bladder cancer (BC), prostate cancer (PC); (2) studies reported the correlation of pretreated CAR with overall survival (OS), and progression-free survival (PFS); (3) studies directly offered hazard ratios (HRs) with 95% confidence intervals (CIs) in the multivariable cox analyses; (4) studies published in peer-reviewed journals. Exclusion studies according to exclusion criteria: (1) studies didn't provided HRs with 95% CIs for pretreated CAR in the multivariable cox analyses; (2) duplicated studies; (3) not original articles, such as conference abstracts, reviews, letters or case reports. Two researchers (QSC, ZLY) screened and assessed the literatures independently. The dispute was settled through discussion.

Data Extraction

In the light of a pre-designed standardized form, data were extracted by two researchers (QSC, ZLY) as following: study features (author's name, year of publication, region, study design, and number of study cases); patient and tumor characteristics (age, cancer type [renal cell carcinoma, bladder cancer, prostate cancer], cancer stage, detailed treatment strategy, follow-up duration, endpoints of outcome); characteristics of study methodology (detailed value of cut-off, determine method of cut-off, statistical methods of cox analyses, adjusted factors); the detailed HRs with 95% CIs of each study and endpoint.

Quality Evaluation

The New-castle-Ottawa Scale (NOS) was applied to assess the quality of the included studies. There were 9 items in total (18). The value of NOS higher than 6 was believed as high quality.

Statistical Analysis

HRs with related 95% CI in each qualified study were combined to assess the prognostic role of pretreated CAR in cases with urinary tumors. In each meta-analysis, Higgins I-Squared statistics and Cochran's Q test were used to evaluate heterogeneity among the enrolled literature. $I^2 > 50\%$ and/or $P<0.1$ were believed as measures of significant heterogeneity. In the case of significant heterogeneity, the random-effects model was applied to calculate the aggregate HRs and 95% CI. Otherwise, the fixed effects model was applied. Subgroup analyses of overall survival and progression-free survival were also conducted. Publication bias was evaluated by funnel plots, checked by Egger's and Begg's tests. We also conducted sensitivity analysis to examine the stability of the findings. Stata 12.0 (Stata Corporation, College Station) was applied for all statistical analyses.

RESULTS

Included Literature

Literature search identified 242 studies, and no article was discovered through reference screening. As shown in the flow chart of the literature searching (**Figure 1**), 125 records retained after excluding duplicated studies. After screening literature titles and abstracts, 16 full-text papers retained for next evaluation. Two papers were removed due to lacking data from multivariable analysis, one article was excluded due to duplicate study. Finally, 13 literatures were included for evidence synthesis (13–17, 19–26).

Study Features

Only data on RCC, BC and PC was identified, studies about the prognostic role of CAR in other urinary cancers were lacking.

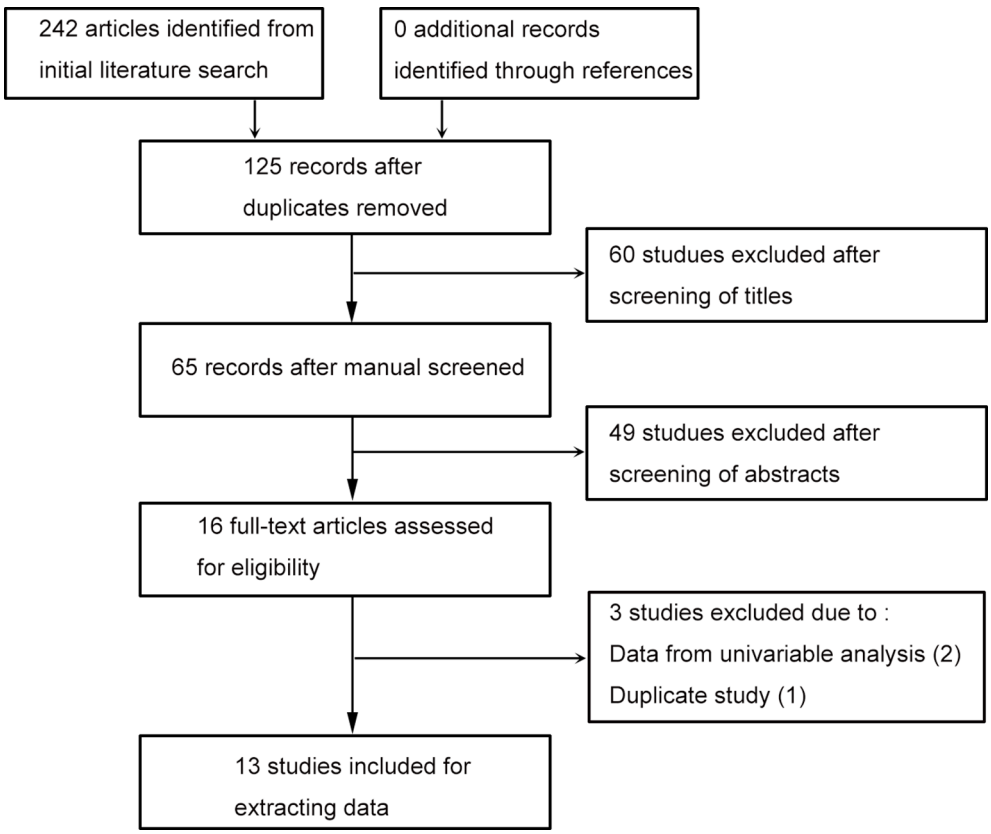


FIGURE 1 | Flowchart of study searching and screening.

Table 1 outlined the main features of all enrolled studies. All studies were published recently (2015–2021) by Asian (Chinese, Japanese and India) researchers. All studies retrospectively analyzed data, nine of them based on single-center patients, four of them based on multi-institutional patients. The median or mean age of subjects ranged from 37 to 73.5 years, and the sample size ranged from 31 to 699. Of all studies, three looked at BC (14–16), eight looked at RCC (13, 19–24, 26), and two looked at PC (17, 25). Most patients were in various stages of the disease and undergo surgery. All studies provided the results of a multivariate Cox analysis. The adjusted factors included patient and tumor characteristics, as detailed in **Table 2**. All studies had high quality, with NOS scores ranging from 6 to 8, as shown in **Table 3**.

CAR and OS in Urological Cancers

There were 11 literatures on OS of urological cancers (13, 16, 17, 19–26). Since there was no significant heterogeneity among these literatures (I^2 = 28.6%, p = 0.165), a fixed model was used for analysis. Pooled results showed that higher levels of CAR were associated with poorer OS for urological cancers (HR 2.21, 95% CI 1.86-2.62, p < 0.001). Subgroup analysis by cancer type showed that higher CAR levels were associated with poorer OS in RCC (HR 2.10, 95% CI 1.72-2.56, p < 0.001), BC (HR 3.35, 95% CI 1.94-5.80, p < 0.001), and PC (HR 2.20, 95% CI 1.43-3.37, p < 0.001) (**Figure 2A**). In addition to cancer type, a subgroup analysis of OS included many other variables, including year of publication, region, study design, sample size, cancer stage, and so on. The results for these grouping variables were still significant (**Table 4**).

CAR and PFS in Urological Cancers

There were 7 literatures on PFS of urological cancers (13–15, 19, 22–24). Pooled results showed that higher levels of CAR were associated with poorer PFS for urological cancers (HR 1.85, 95% CI 1.36-2.52, p < 0.001). Subgroup analysis by cancer type showed that higher CAR levels were associated with poorer PFS in BC (HR 1.76, 95% CI 1.03-3.02, p = 0.039), RCC (HR 1.90, 95% CI 1.25-2.89, p = 0.003) (**Figure 2B**). In addition to cancer type, a subgroup analysis of PFS included many other variables, including year of publication, region, study design, sample size, and so on. The results for these grouping variables were still significant (**Table 4**).

Publication Bias

The funnel diagram of OS and PFS was shown in **Figure 3**, and the two were visually symmetric. Begg's and Egger's quantitative tests also showed that there was a low probability of publication bias for OS (P = 0.104 and 0.182) and PFS (P = 0.368 and 0.659).

TABLE 1 | Baseline features of included studies.

Author	Year	Country	Study Design	Case Number	Age (Years)	Cancer type	Stage	Treatment	Cut-off (g/L)	Determine the cut-off value	COX
Zhang (14)	2021	China	RTP, SC	127	66 (29–87) R	BC	Non-metastatic	Surgery	0.165	ROC curve	MV
Kuroda (15)	2021	Japan	RTP, SC	102	71 (49-83) R	BC	Non-metastatic	Surgery	0.17	ROC curve	MV
Ueda (13)	2020	Japan	RTP, SC	131	67 (21-91) R	RCC	All	Targeted therapy	1	Median	MV
Zhang (16)	2019	China	RTP, SC	209	67 (29-87) R	BC	Non-metastatic	Surgery	0.2	X-tile	MV
Uchimoto (17)	2019	Japan	RTP, MI	221	73.5 ± 7.6	PC	All	Androgen-signaling inhibitors or docetaxel	0.5	ROC curve	MV
Tsujino (19)	2019	Japan	RTP, MI	699	61.9 ± 11.7	RCC	All	Surgery	0.073	ROC curve	MV
Konishi (20)	2019	Japan	RTP, MI	176	67 (59-74)	RCC	Metastatic	Targeted therapy	0.05	ROC curve	MV
Gao (21)	2019	China	RTP, SC	108	57 (23-78) R	RCC	All	Surgery	0.094	ROC curve	MV
Barua (22)	2019	India	RTP, SC	31	62 ± 3.14	RCC	Metastatic	Surgery	0.11	ROC curve	MV
Agizamhan (23)	2018	China	RTP, MI	82	37 (2-71) R	RCC	All	Surgery	0.083	ROC curve	MV
Guo (24)	2017	China	RTP, SC	570	51.43 ± 13.52	RCC	All	Surgery	0.08	ROC curve	MV
Yamashita (25)	2016	Japan	RTP, SC	79	72 (52-86) R	PC	All	Chemotherapy	0.07	NR	MV
Chen (26)	2015	China	RTP, SC	406	58 (24–80) R	RCC	All	Surgery	0.06	ROC curve	MV

RTP, retrospective; SC, single center; MI, multi-institutional; BC, bladder cancer; RCC, renal cell carcinoma; PC, prostate cancer; ROC, receiver-operating characteristic; MV, multivariate; NR, not reported; R, range.

TABLE 2 | Follow-up and oncological outcomes.

Author	Year	Follow-up duration, month	Outcome	Adjusted factors
Zhang (14)	2021	NR	PFS	Smoking, tumor size, T stage, N stage, AGR, NLR, PLR, albumin, hemoglobin
Kuroda (15)	2021	38.9 (6.1-162.2) R	PFS	Pathological T stage, tumor grade, lymph node metastasis, lymphovascular invasion, preoperative eGFR, postoperative CAR, preoperative PLR
Ueda (13)	2020	NR	OS, PFS	Performance status, prior nephrectomy, IMDC risk classification, albumin, CRP, NLR, NLR/albumin ratio
Zhang (16)	2019	NR	OS	Systemic immune inflammation index, T stage, N stage, M stage, tumor size, tumor margin, vessel invasion, NLR, PLR
Uchimoto (17)	2019	14	OS	ADT duration, visceral mets at first-line treatment, bone mets at first-line treatment, ECOG-PS at first-line treatment
Tsujino (19)	2019	73	OS, PFS	ECOG-PS, T classification, metastasis at diagnosis, UISS, BMI, tumor size, nuclear grade, NLR
Konishi (20)	2019	NR	OS	Age, ECOG PS, sex, IMDC model
Gao (21)	2019	54.5 (7.3-74.2) R	OS	Subtype, fuhrman grade, T stage, N stage, M stage, platelet level
Barua (22)	2019	16.5 ± 1.5	OS, PFS	Age, T stage, fuhrman nuclear grade, tumor necrosis, lymph node status, microscopic invasion, PLR, LMR, systemic immune inflammation index, scan to surgery time
Agizamhan (23)	2018	31 (2–108) R	OS, PFS	Age, fuhrman grade, pT status, pN status, tumor thrombus, NLR, PLR
Guo (24)	2017	NR	OS, PFS	Age, BMI, pathological type, fuhrman grade, pT status, pN status, pM status, serum globulin, NLR, PLR
Yamashita (25)	2016	15.1 (1.8-53.4) R	OS	Age, ECOG PS, significant pain, combination therapy, PSA at docetaxel initiation, androgen deprivation therapy administration period, hemoglobin, NLR, ALP, LDH
Chen (26)	2015	63 (1-151) R	OS	Age, TNM stage, tumor necrosis, lymphovascular invasion, hemoglobin, Ca, GPS, mGPS

PFS, progression-free survival; OS, overall survival; AGR, albumin/globulin ratio; NLR, neutrophil to lymphocyte ratio; PLR, platelet to lymphocyte ratio; eGFR, estimated glomerular filtration rate; CAR, C–reactive protein to albumin ratio; IMDC, International Metastatic Renal Cell Carcinoma Database Consortium; CRP, C-reactive protein; ADT, androgen deprivation therapy; UISS, UCLA integrated staging system; BMI, body mass index; ALP, alkaline phosphatase; LDH, lactate dehydrogenase; GPS, the Glasgow Prognostic Score; NR, not reported; R, range.

Sensitivity Analysis

Sensitivity analysis was further conducted to examine the effect of a single study on the overall results. There was no significant change in HRs associated with CAR and OS or PFS in patients with urinary cancers (**Figure 4**).

DISCUSSION

The present study attempted to systematically review the available literatures and to evaluate the prognostic significance of CAR in urogenital malignancies using a meta-analysis. Based on high-quality

TABLE 3 | Newcastle–Ottawa scale for risk of bias assessment.

Study	Year	Selection				Comparability	Outcome			Overall
		Representativeness of exposed cohort	Selection of nonexposed	Ascertainment of exposure	Outcome not present at start		Assessment of outcome	Adequate follow-up length	Adequacy of follow-up	
Zhang (14)	2021	1	1	1	1	1	1	1	0	7
Kuroda (15)	2021	1	1	1	1	0	1	1	1	7
Ueda (13)	2020	1	1	1	1	0	1	1	0	6
Zhang (16)	2019	1	1	1	1	1	1	1	0	7
Uchimoto (17)	2019	1	1	1	1	1	1	1	1	8
Tsujino (19)	2019	1	1	1	1	1	1	1	1	8
Konishi (20)	2019	1	1	1	1	1	1	1	0	7
Gao (21)	2019	1	1	1	1	1	1	1	1	8
Barua (22)	2019	0	1	1	1	0	1	1	1	6
Agizamhan (23)	2018	1	1	1	1	0	1	1	1	7
Guo (24)	2017	1	1	1	1	0	1	1	0	6
Yamashita (25)	2016	0	1	1	1	0	1	1	1	6
Chen (26)	2015	1	1	1	1	0	1	1	1	7

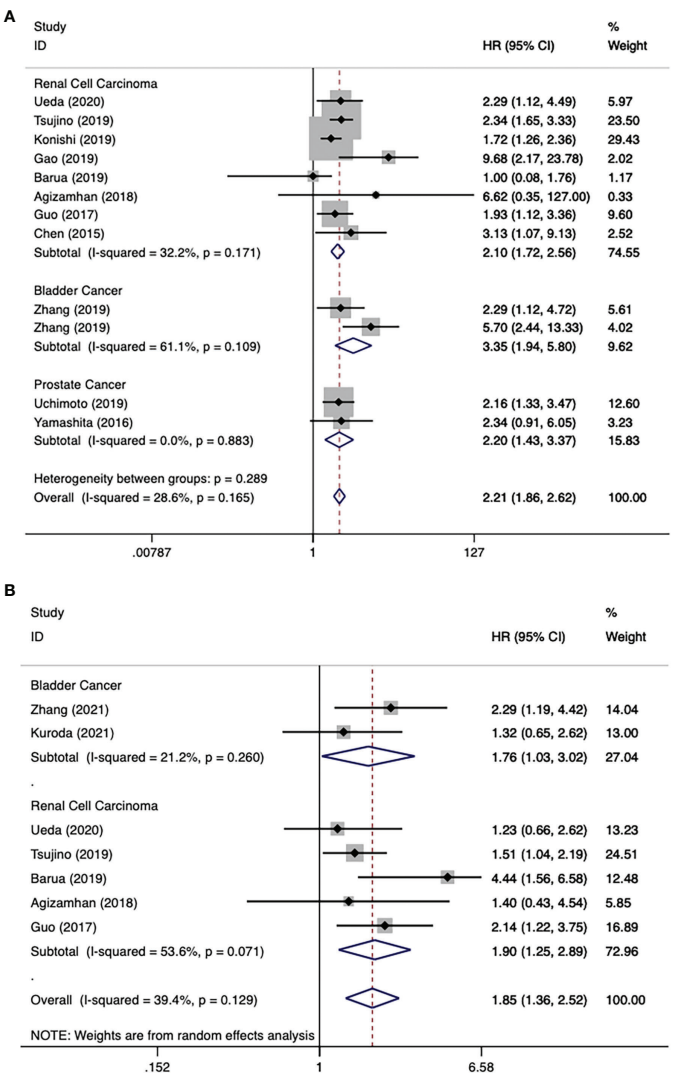


FIGURE 2 | Forest plot reflects the association between CAR and OS/PFS for urological cancers. **(A)** CAR and OS; **(B)** CAR and PFS.

TABLE 4 | Subgroup analysis of overall survival and progression-free survival.

Subgroup	Studies	HR (95% CI)	P value	Heterogeneity	
				I^2 (%)	P value
Overall survival					
Year of publication					
2019-2020	8	2.44 (1.79-3.31)	<0.001	50.8	0.047
2015-2018	4	2.23 (1.45-3.43)	<0.001	0.0	0.760
Region					
China	6	2.95 (2.09-4.17)	<0.001	45.2	0.104
Others	6	2.02 (1.66-2.45)	<0.001	0.0	0.735
Study design					
Single center	8	2.64 (1.97-3.53)	<0.001	35.4	0.146
Multi-institutional	4	2.02 (1.64-2.49)	<0.001	0.0	0.492
Sample size					
> 200	6	2.40 (1.92-3.00)	<0.001	0.50	0.413
< 200	6	1.98 (1.52-2.57)	<0.001	45.7	0.101
Site of carcinoma					
Renal Cell Carcinoma	8	2.10 (1.72-2.56)	<0.001	32.2	0.171
Bladder Cancer	2	3.51 (1.44-8.55)	0.006	61.1	0.109
Prostate Cancer	2	2.20 (1.43-3.37)	<0.001	0.0	0.883
Cancer stage					
All	8	2.38 (1.91-2.96)	<0.001	0.0	0.459
Non-metastatic	2	3.51 (1.44-8.55)	0.006	61.1	0.109
Metastatic	2	1.68 (1.24-2.29)	0.001	0.0	0.509
Cut-off value					
> 0.1	5	2.45 (1.79-3.35)	<0.001	25.6	0.251
< 0.1	7	2.12 (1.73-2.59)	<0.001	36.5	0.150
NOS score					
>= 7	8	2.62 (1.90-3.62)	<0.001	50.4	0.049
< 7	4	2.02 (1.38-2.96)	<0.001	0.0	0.798
Progression-free survival					
Year of publication					
2020-2021	3	1.57 (1.06-2.33)	0.023	0.0	0.371
2017-2019	4	2.12 (1.29-3.46)	0.003	58.7	0.064
Region					
China	3	2.09 (1.40-3.12)	<0.001	0.0	0.771
Others	4	1.77 (1.07-2.95)	0.027	65	0.035
Study design					
Single center	5	2.04 (1.33-3.11)	0.001	51.1	0.085
Multi-institutional	2	1.50 (1.05-2.14)	0.026	0.0	0.912
Sample size					
> 130	3	1.59 (1.20-2.11)	0.001	0.0	0.433
< 130	4	2.23 (1.53-3.25)	<0.001	52.2	0.099
Site of carcinoma					
Renal Cell Carcinoma	5	1.90 (1.25-2.89)	0.003	53.6	0.071
Bladder Cancer	2	1.77 (1.10-2.86)	0.019	21.2	0.260
Cut-off value					
> 0.1	4	2.01 (1.14-3.55)	0.016	63.2	0.043
< 0.1	3	1.66 (1.23-2.24)	0.001	0.0	0.572
NOS score					
>= 7	4	1.59 (1.20-2.11)	0.001	0.0	0.662
< 7	3	2.25 (1.15-4.42)	0.018	68.7	0.041

HR, hazard ratio; CI, confidence interval; NOS, Newcastle-Ottawa Scale.

studies, high level of pretreated CAR was found to be significantly correlated to poorer OS and PFS after combining the data. Subgroup analysis by cancer type remained significant for RCC, BC, and PC. Subgroup analyses of several variables of OS and PFS did not alter the direction of the findings. Publication bias checks and sensitivity analyses also confirmed the reliability and robustness of our findings. CRP and albumin are common hematologic indexes in clinic, which are easy to measure and low cost. Thus, CAR can be applied as a competent prognostic indicator for urinary tumors.

For urological tumors, a comprehensive meta-analysis initially examined CAR as a prognostic factor in cases with RCC. They identify that high pretreated CAR was correlated to poorer OS and PFS (12). The associations of CAR and clinicopathological characteristics were also explored. High level of pretreatment CAR was identified to associated with several adverse factors, such as higher Fuhrman grade, higher TNM stage, venous thrombus formation, lymph node invasion, distant metastasis. However, the data from univariable analysis

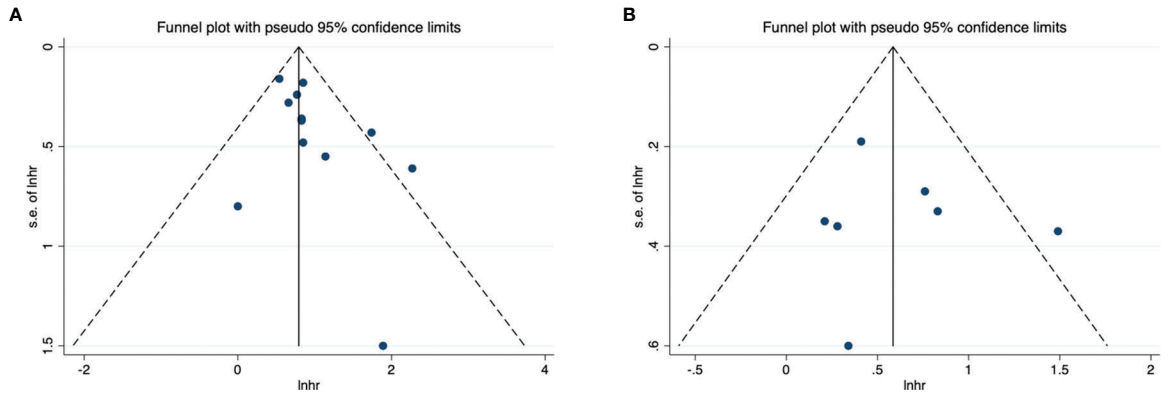


FIGURE 3 | Funnel plot for publication bias. **(A)** correlation of CAR with OS in urological cancers; **(B)** correlation of CAR with PFS in urological cancers.

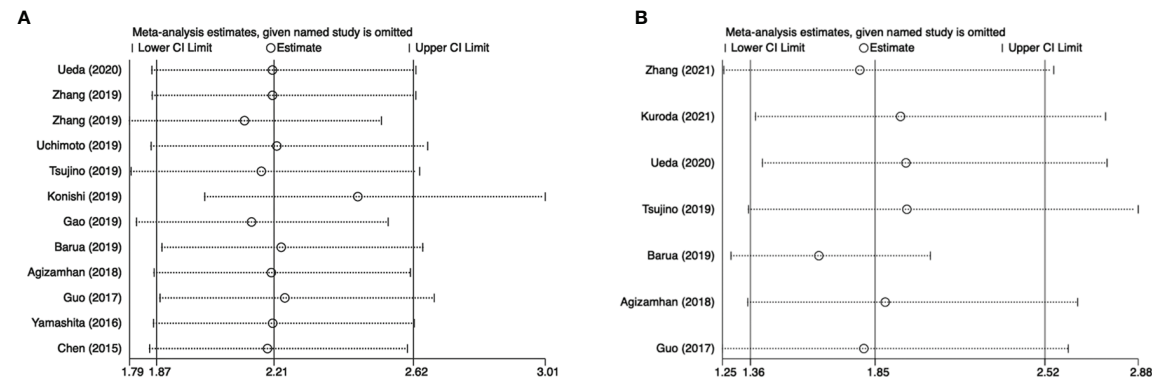


FIGURE 4 | Results of sensitivity analysis. **(A)** correlation of CAR with OS in urological cancers; **(B)** correlation of CAR with PFS in urological cancers.

was included, which may bring in potential bias (27). And newly published articles cannot be included. Moreover, several studies investigating the prognostic role of CAR in BC and PC have been published (14–17). In this case, we only included data from multivariable analyses. The present study provided the latest and most integrated evidence of the prognostic role of CAR in urinary tumors. Based on adjusted data, we have found similar results to study by Zhou et al. (12). More detailed results about BC and PC were reported in the present study. Pretreatment CAR remained to be an important prognosis predictor for patients with BC and PC.

Inflammatory reactions promote the development of tumors by influencing the microenvironment of urinary tumors. Cancer cell proliferation, necrosis, invasion, and hypoxia trigger immune responses in the tumor microenvironment, and in turn trigger the generation of various of inflammatory factors (28). Serum C-reactive protein and albumin are indexes of chronic inflammation and malnutrition in cancer patients (29, 30). C-reactive protein is an acute phase protein generated in the liver that stimulates cancer-related inflammatory factors such as IL-1, IL-6, and TNF-A, resulting in progression of malignance (31). The studies showed that high CRP level was associated with poorer survival outcomes in urological cancer cases (32). Serum albumin level reflects the nutritional status of patients. Low serum albumin levels indicate malnutrition. Hypoalbuminemia is caused by nutrient intakes and tumor overconsumption and induces stimulation of inflammatory factors such as IL-1, IL-6, and TNF-A (33). CAR was generated in the light of CRP and albumin levels. Thus, CAR provides a biological basis and is considered a promising prognostic tool for urinary tumors.

There was increasing evidence of a link between tumor-caused inflammatory response and tumorigenesis and disease progression (5). Kinds of inflammatory and immune response factors have been reported as survival biomarkers for various cancers (6). Many other inflammatory biomarkers that were also prognostic in urologic tumors, such as neutrophil-to-lymphocyte ratio (NLR) (34), platelet-to-lymphocyte ratio (PLR) (35), lymphocyte-to-monocyte ratio (LMR) (36), etc. Based on published studies, similar meta-analyses about the prognostic role of these biomarkers in urological tumors also have been performed by many researchers. They are common hematologic indexes in clinic, easily to measure and low cost, which can be

widely used. However, which marker was the best predictor, the studies comparing these markers were inadequate. We believed that combining these markers for prediction and improving prediction efficiency may be the direction of future researches.

However, some of the limitations of this systematic review should be explained. First of all, only 13 studies have been enrolled in the meta-analysis, which may lack statistical power, especially for BC and PC. Second, all enrolled studies were performed in Asia. Therefore, we should be careful to apply the results of the present study in patients from western countries. Third, all the included studies were cohort studies with retrospective design, which may result in selection bias. Fourthly, different cut-off values of CAR in different studies may lead to inconsistent outcome thresholds. Lastly, due to inadequate literatures, other urinary cancers were not analyzed in our study, and the endpoint cancer-specific survival was not studied.

Taken together, the present study identified that pretreatment CAR level could be a likely predictor for cases with urinary tumors. Nevertheless, well-designed prospective studies also are wanted to validate these results.

DATA AVAILABILITY STATEMENT

The original contributions presented in the study are included in the article/supplementary material. Further inquiries can be directed to the corresponding author.

AUTHOR CONTRIBUTIONS

Protocol/project development: MW and YZ. Data collection or management: QC, ZY, and HG. Data analysis: PL, YL, and CL. Manuscript writing/editing: MW and YZ. All authors read and approved the final manuscript.

REFERENCES

1. Siegel RL, Miller KD, Jemal A. Cancer Statistics, 2020. *CA: Cancer J Clin* (2020) 70(1):7–30. doi: 10.3322/caac.21590
2. Rini BI, Escudier B, Tomczak P, Kaprin A, Szczylik C, Hutson TE, et al. Comparative Effectiveness of Axitinib Versus Sorafenib in Advanced Renal Cell Carcinoma (AXIS): A Randomised Phase 3 Trial. *Lancet* (2011) 378 (9807):1931–9. doi: 10.1016/S0140-6736(11)61613-9
3. Escudier B, Eisen T, Stadler WM, Szczylik C, Oudard S, Siebels M, et al. Sorafenib in Advanced Clear-Cell Renal-Cell Carcinoma. *N Engl J Med* (2007) 356(2):125–34. doi: 10.1056/NEJMoa060655
4. Kantoff PW, Higano CS, Shore ND, Berger ER, Small EJ, Penson DF, et al. Sipuleucel-T Immunotherapy for Castration-Resistant Prostate Cancer. *N Engl J Med* (2010) 363(5):411–22. doi: 10.1056/NEJMoa1001294
5. Diakos CI, Charles KA, McMillan DC, Clarke SJ. Cancer-Related Inflammation and Treatment Effectiveness. *Lancet Oncol* (2014) 15(11): e493–503. doi: 10.1016/S1470-2045(14)70263-3
6. Fang Y, Zheng T, Zhang C. Prognostic Role of the C-Reactive Protein/ Albumin Ratio in Patients With Gynecological Cancers: A Meta-Analysis. *Front Oncol* (2021) 11:737155. doi: 10.3389/fonc.2021.737155
7. Fairclough E, Cairns E, Hamilton J, Kelly C. Evaluation of a Modified Early Warning System for Acute Medical Admissions and Comparison With C-Reactive Protein/Albumin Ratio as a Predictor of Patient Outcome. *Clin Med (Lond)* (2009) 9(1):30–3. doi: 10.7861/clinmedicine.9-1-30
8. Yu Q, Li KZ, Fu YJ, Tang Y, Liang XQ, Liang ZQ, et al. Clinical Significance and Prognostic Value of C-Reactive Protein/Albumin Ratio in Gastric Cancer. *Ann Surg Treat Res* (2021) 100(6):338–46. doi: 10.4174/astr.2021.100.6.338
9. Tamai K, Okamura S, Makino S, Yamamura N, Fukuchi N, Ebisui C, et al. C-Reactive Protein/Albumin Ratio Predicts Survival After Curative Surgery in Elderly Patients With Colorectal Cancer. *Updates Surg* (2021) 74(1):153–62. doi: 10.1007/s13304-021-01011-9
10. Araki T, Tateishi K, Sonehara K, Hirota S, Komatsu M, Yamamoto M, et al. Clinical Utility of the C-Reactive Protein:Albumin Ratio in non-Small Cell Lung Cancer Patients Treated With Nivolumab. *Thorac Cancer* (2021) 12 (5):603–12. doi: 10.1111/1759-7714.13788
11. Bao Y, Yang J, Duan Y, Chen Y, Chen W, Sun D. The C-Reactive Protein to Albumin Ratio is an Excellent Prognostic Predictor for Gallbladder Cancer. *Biosci Trends* (2021) 14(6):428–35. doi: 10.5582/bst.2020.03326
12. Zhou W, Zhang GL. C-Reactive Protein to Albumin Ratio Predicts the Outcome in Renal Cell Carcinoma: A Meta-Analysis. *PloS One* (2019) 14 (10):e0224266. doi: 10.1371/journal.pone.0224266
13. Ueda K, Ogasawara N, Yonekura S, Matsunaga Y, Hoshino R, Kurose H, et al. The Prognostic Value of Systemic Inflammatory Markers in Advanced Renal Cell Carcinoma Patients Treated With Molecular Targeted Therapies. *Anticancer Res* (2020) 40(3):1739–45. doi: 10.21873/anticanres.14127
14. Zhang W, Yang F, Kadier A, Chen Y, Yu Y, Zhang J, et al. Development of Nomograms Related to Inflammatory Biomarkers to Estimate the Prognosis of Bladder Cancer After Radical Cystectomy. *Ann Transl Med* (2021) 9 (18):1440. doi: 10.21037/atm-21-4097
15. Kuroda K, Tasaki S, Horiguchi A, Ito K. Postoperative C-Reactive Protein-to-Albumin Ratio Predicts Poor Prognosis in Patients With Bladder Cancer Undergoing Radial Cystectomy. *Mol Clin Oncol* (2021) 14(3):54. doi: 10.3892/mco.2021.2216
16. Zhang W, Wang R, Ma W, Wu Y, Maskey N, Guo Y, et al. Systemic Immune-Inflammation Index Predicts Prognosis of Bladder Cancer Patients After Radical Cystectomy. *Ann Transl Med* (2019) 7(18):431. doi: 10.21037/atm.2019.09.02
17. Uchimoto T, Komura K, Fujiwara Y, Saito K, Tanda N, Matsunaga T, et al. Prognostic Impact of C-Reactive Protein-Albumin Ratio for the Lethality in Castration-Resistant Prostate Cancer. *Med Oncol* (2019) 37(1):9. doi: 10.1007/s12032-019-1332-7
18. Stang A. Critical Evaluation of the Newcastle-Ottawa Scale for the Assessment of the Quality of Nonrandomized Studies in Meta-Analyses. *Eur J Epidemiol* (2010) 25(9):603–5. doi: 10.1007/s10654-010-9491-z
19. Tsujino T, Komura K, Hashimoto T, Muraoka R, Satake N, Matsunaga T, et al. C-Reactive Protein-Albumin Ratio as a Prognostic Factor in Renal Cell Carcinoma - A Data From Multi-Institutional Study in Japan. *Urol Oncol* (2019) 37(11):812.e1–8. doi: 10.1016/j.urolonc.2019.04.002
20. Konishi S, Hatakeyama S, Tanaka T, Ikehata Y, Tanaka T, Hamano I, et al. C-Reactive Protein/Albumin Ratio is a Predictive Factor for Prognosis in Patients With Metastatic Renal Cell Carcinoma. *Int J Urol* (2019) 26(10):992–8. doi: 10.1111/iju.14078
21. Gao J, Agizamhan S, Zhao X, Jiang B, Qin H, Chen M, et al. Preoperative C-Reactive Protein/Albumin Ratio Predicts Outcome of Surgical Papillary Renal Cell Carcinoma. *Future Oncol* (2019) 15(13):1459–68. doi: 10.2217/fon-2018-0611
22. Barua SK, Singh Y, Baruah SJ, PR T, PK B, Sarma D, et al. Predictors of Progression-Free Survival and Overall Survival in Metastatic Non-Clear Cell Renal Cell Carcinoma: A Single-Center Experience. *World J Oncol* (2019) 10 (2):101–11. doi: 10.14740/wjon1188
23. Agizamhan S, Qu F, Liu N, Sun J, Xu W, Zhang L, et al. Preoperative Neutrophil-to-Lymphocyte Ratio Predicts the Surgical Outcome of Xp11.2 Translocation/TFE3 Renal Cell Carcinoma Patients. *BMC Urol* (2018) 18 (1):60. doi: 10.1186/s12894-018-0374-z
24. Guo S, He X, Chen Q, Yang G, Yao K, Dong P, et al. The C-Reactive Protein/ Albumin Ratio, a Validated Prognostic Score, Predicts Outcome of Surgical

Renal Cell Carcinoma Patients. *BMC Cancer* (2017) 17(1):171. doi: 10.1186/s12885-017-3119-6
25. Yamashita S, Kohjimoto Y, Iguchi T, Koike H, Kusumoto H, Iba A, et al. Prognostic Factors and Risk Stratification in Patients With Castration-Resistant Prostate Cancer Receiving Docetaxel-Based Chemotherapy. *BMC Urol* (2016) 16:13. doi: 10.1186/s12894-016-0133-y
26. Chen Z, Shao Y, Fan M, Zhuang Q, Wang K, Cao W, et al. Prognostic Significance of Preoperative C-Reactive Protein: Albumin Ratio in Patients With Clear Cell Renal Cell Carcinoma. *Int J Clin Exp Pathol* (2015) 8 (11):14893–900.
27. Komura K, Hashimoto T, Tsujino T, Muraoka R, Tsutsumi T, Satake N, et al. The CANLPH Score, an Integrative Model of Systemic Inflammation and Nutrition Status (SINS), Predicts Clinical Outcomes After Surgery in Renal Cell Carcinoma: Data From a Multicenter Cohort in Japan. *Ann Surg Oncol* (2019) 26(9):2994–3004. doi: 10.1245/s10434-019-07530-5
28. Kinoshita A, Onoda H, Imai N, Iwaku A, Oishi M, Tanaka K, et al. The C-Reactive Protein/Albumin Ratio, a Novel Inflammation-Based Prognostic Score, Predicts Outcomes in Patients With Hepatocellular Carcinoma. *Ann Surg Oncol* (2015) 22(3):803–10. doi: 10.1245/s10434-014-4048-0
29. McMillan DC. Systemic Inflammation, Nutritional Status and Survival in Patients With Cancer. *Curr Opin Clin Nutr Metab Care* (2009) 12(3):223–6. doi: 10.1097/MCO.0b013e32832a7902
30. Coussens LM, Werb Z. Inflammation and Cancer. *Nature* (2002) 420 (6917):860–7. doi: 10.1038/nature01322
31. Asegaonkar SB, Asegaonkar BN, Takalkar UV, Advani S, Thorat AP. C-Reactive Protein and Breast Cancer: New Insights From Old Molecule. *Int J Breast Cancer* (2015) 2015:145647. doi: 10.1155/2015/145647
32. Zhou L, Cai X, Liu Q, Jian ZY, Li H, Wang KJ. Prognostic Role of C-Reactive Protein In Urological Cancers: A Meta-Analysis. *Sci Rep* (2015) 5:12733. doi: 10.1038/srep12733
33. Almasaudi AS, Dolan RD, Edwards CA, McMillan DC. Hypoalbuminemia Reflects Nutritional Risk, Body Composition and Systemic Inflammation and Is Independently Associated With Survival in Patients With Colorectal Cancer. *Cancers (Basel)* (2020) 12(7):1986. doi: 10.3390/cancers12071986
34. Mjaess G, Chebel R, Karam A, Moussa I, Pretot D, Abi Tayeh G, et al. Prognostic Role of Neutrophil-to-Lymphocyte Ratio (NLR) in Urological Tumors: An Umbrella Review of Evidence From Systematic Reviews and Meta-Analyses. *Acta Oncol* (2021) 60(6):704–13. doi: 10.1080/0284186X.2021.1886323
35. Li DY, Hao XY, Ma TM, Dai HX, Song YS. The Prognostic Value of Platelet-To-Lymphocyte Ratio in Urological Cancers: A Meta-Analysis. *Sci Rep* (2017) 7(1):15387. doi: 10.1038/s41598-017-15673-2
36. Gu L, Li H, Chen L, Ma X, Li X, Gao Y, et al. Prognostic Role of Lymphocyte to Monocyte Ratio for Patients With Cancer: Evidence From a Systematic Review and Meta-Analysis. *Oncotarget* (2016) 7(22):31926–42. doi: 10.18632/oncotarget.7876

Conflict of Interest: The authors declare that the research was conducted in the absence of any commercial or financial relationships that could be construed as a potential conflict of interest.

Publisher's Note: All claims expressed in this article are solely those of the authors and do not necessarily represent those of their affiliated organizations, or those of the publisher, the editors and the reviewers. Any product that may be evaluated in this article, or claim that may be made by its manufacturer, is not guaranteed or endorsed by the publisher.

Copyright © 2022 Wu, Zhou, Chen, Yu, Gu, Lin, Li and Liu. This is an open-access article distributed under the terms of the Creative Commons Attribution License (CC BY). The use, distribution or reproduction in other forums is permitted, provided the original author(s) and the copyright owner(s) are credited and that the original publication in this journal is cited, in accordance with accepted academic practice. No use, distribution or reproduction is permitted which does not comply with these terms.

frontiers | Frontiers in Oncology

ORIGINAL RESEARCH
published: 16 May 2022
doi: 10.3389/fonc.2022.749119

Comprehensive Genomic Characterization of Tumor Microenvironment and Relevant Signature in Clear Cell Renal Cell Carcinoma

Chuanjie Zhang[1†], *Feng Qi*[2†], *Yuxiao Zheng*[2†], *Xin Xia*[3], *Xiao Li*[2*] *and Xinwei Wang*[4*]

[1] Department of Urology, Ruijin Hospital, Shanghai Jiao Tong University School of Medicine, Shanghai, China, [2] Department of Urology, Jiangsu Cancer Hospital and Jiangsu Institute of Cancer Research and Affiliated Cancer Hospital of Nanjing Medical University, Nanjing, China, [3] Department of Anatomy, Nanjing Medical University, Nanjing, China, [4] Department of Medical Oncology, Jiangsu Cancer Hospital and Jiangsu Institute of Cancer Research and Affiliated Cancer Hospital of Nanjing Medical University, Nanjing, China

OPEN ACCESS

Edited by:
Riccardo Tellini,
Careggi University Hospital, Italy

Reviewed by:
Haowei He,
Jinling Hospital, China
Luca Lambertini,
Careggi University Hospital, Italy

***Correspondence:**
Xiao Li
leex91@163.com
Xinwei Wang
18320743@qq.com

[†]These authors have contributed equally to this work

Specialty section:
This article was submitted to Genitourinary Oncology, a section of the journal Frontiers in Oncology

Received: 29 July 2021
Accepted: 07 April 2022
Published: 16 May 2022

Citation:
Zhang C, Qi F, Zheng Y, Xia X, Li X and Wang X (2022) Comprehensive Genomic Characterization of Tumor Microenvironment and Relevant Signature in Clear Cell Renal Cell Carcinoma. Front. Oncol. 12:749119. doi: 10.3389/fonc.2022.749119

Purpose: To systematically investigate the characterization of tumor microenvironment (TME) in clear cell renal cell carcinoma (ccRCC), we performed a comprehensive analysis incorporating genomic alterations, cellular interactions, infiltrating immune cells, and risk signature.

Patients and Methods: Multi-omics data including RNA-seq, single-nucleotide variant (SNV) data, copy number variation (CNV) data, miRNA, and corresponding prognostic data were obtained from The Cancer Genome Atlas (TCGA) and the International Cancer Genome Consortium (ICGC) database. The CIBERSORT algorithm was utilized to identify prognostic TME subclusters, and TMEscore was further quantified. Moreover, the mutational landscape of TCGA-KIRC was explored. Lastly, TIDE resource was applied to assess the significance of TMEscore in predicting immunotherapeutic benefits.

Results: We analyzed the TME infiltration patterns from 621 ccRCC patients and identified 5 specific TME subclusters associated with clinical outcomes. Then, we found that TMEcluster5 was significantly related to favorable prognosis and enriched memory B-cell infiltration. Accordingly, we depicted the clustering landscape of TMEclusters, TMEscore levels, tumor mutation burden (TMB), tumor grades, purity, and ploidy in all patients. Lastly, TIDE was used to assess the efficiency of immune checkpoint blockers (ICBs) and found that the TMEscore has superior predictive significance to TMB, making it an essential independent prognostic biomarker and drug indicator for clinical use.

Conclusions: Our study depicted the clustering landscape of TMEclusters, TMEscore levels, TMB, tumor grades, purity, and ploidy in total ccRCC patients. The TMEscore was proved to have promising significance for predicting prognosis and ICB responses, in accordance with the goal of developing rationally individualized therapeutic interventions.

Keywords: ccRCC, TMEscore, TCGA, ICGC, immunotherapy

INTRODUCTION

Kidney cancer is a common urological malignancy worldwide, in which clear cell renal cell carcinoma (ccRCC) accounts for nearly 85% of all diagnosed cases, along with increasingly annual cancer-related deaths (1). Currently, surgical intervention, incorporating laparoscopic partial nephrectomy (LPN) or radical nephrectomy (RN), remains the treatment of choice (2, 3). Moreover, increasing studies have brought intensive insights into the immune-related therapeutic targets, especially the significant role of tumor microenvironment (TME) in cancer progression and drug responses (4–6). The structure of TME mainly consisted of parental tumor cells, tumor-associated macrophages (TAMs), mesenchymal stem cells (MSCs), dendritic cells (DCs), cytotoxic T cells, helper T cells, and other inflammatory-related factors, which were robustly demonstrated to be associated with prognosis across multiple malignancies, including urothelial cancer, lung cancer, gastric cancer, melanoma, and breast cancer (7–9). Meanwhile, TME heterogeneity was a pivotal determinant for therapeutic efficiency and exhibited different profiles during the process of tumor progression (10, 11).

ccRCC was significantly correlated with immune infiltration and precious intensive efforts were devoted to explore more sensitive biomarkers to improve immunotherapy precision, including immune-related signature, tumor mutation burden (TMB), and other specific immune cells (12–14). To date, we could utilize the advanced computational methods to infer the abundance of immune cells and other cell types, including ssGSEA, CIBERSORT, and ESTIMATE (15–17). Several cohorts investigated the clinical efficiency of TME, and potential mechanisms uncovering the TME and immunotherapy response have been well experimentally characterized across several malignancies (18). Job et al. explored the heterogeneity of tumor stromal composition and developed a TME-based classification of intrahepatic cholangiocarcinoma to detect potentially targetable cancer subtypes (19). Dai et al. identified extracellular $KRAS^{G12D}$ that acted as a hub mediator of cancer cell–macrophage communication and also provided a novel KRAS-targeted anticancer strategy based on TME (20). Furthermore, Wu et al. further demonstrated that gemcitabine treatment resulted in metabolic changes in residual tumor cells, leading to the resistance to T-cell-mediated killing (21). However, the comprehensive landscape of TME in ccRCC and the potential relationships of TME with genomic mutation burden or other related risk signatures have been limitedly elucidated. In addition, Programmed death ligand 1 (PD-L1, CD274), expressed on tumor and/or immune cells in the TME, interacts with PD-1 on tumor-infiltrating lymphocytes, attenuating effector T-cell responses and allowing tumors to escape immune attack (22, 23). Previous studies have indicated that aberrant expressions of TME-related genes could trigger TME remodeling, thereby impacting immune checkpoint blocker (ICB) efficacy. For instance, Siglec-15 suppresses antigen-specific T-cell responses *in vitro* and *in vivo*. Targeting Siglec-15 amplifies anti-tumor immunity in the TME, functioning as a potential target for normalization of cancer immunotherapy (24). Based on the *in vivo* epigenetic *CRISPR* screen, Li et al. identified Asf1a as a key modulator of lung adenocarcinoma sensitivity to anti-PD-1 therapy. Asf1a deficiency synergized with anti-PD-1 immunotherapy by promoting M1-like macrophage polarization and T-cell activation (25). Therefore, whether TME-related signature could predict ICB efficacy of RCC is a promising and interesting project to deal with.

In the present research, we adopted two well-characterized algorithms to infer the specific fractions of 22 immune cells based on the renal cell carcinoma cohort gene expression profiles (26, 27). The TME infiltration patterns of 683 tumors extracted from patients were well estimated and we systematically correlated the TME sub-clusters with genomic characteristics, somatic mutation profiles, clinical or pathological features of ccRCC, and drug responses. Accordingly, we further conducted a methodology to quantify the TME infiltration pattern as the TMEscore, which was assessed from multiple aspects to be a robust prognostic marker or predictive factor for response to immune-checkpoint inhibitors in ccRCC.

MATERIALS AND METHODS

Kidney Cancer Datasets and Data Preprocessing

We carefully screened the kidney cancer databases and filtered out the samples with incomplete genomic or clinical information. In total, we obtained the KIRC RNA-seq (N = 530), single-nucleotide variant (SNV) data (N = 417), copy number variation (CNV) data (N = 534), miRNA (N = 592), and corresponding prognostic data (screened only with survival information, N = 527) from The Cancer Genome Atlas (TCGA) database (https://portal.gdc.cancer.gov/projects/TCGA-KIRC). Moreover, we downloaded the RNA-seq of 91 samples with clinical data from the International Cancer Genome Consortium (ICGC) database (https://dcc.icgc.org/projects/RECA-EU). In addition, the Fragments Per Kilobase Million (FPKM) format of RNA-seq data from TCGA-KIRC was transformed into TPM (Transcripts Per Million), and the Reads Per Kilobase Million (RPKM) format of RNA-seq data from ICGC was normalized into TPM. Lastly, the patients with incomplete survival information or expression data were excluded in this study.

Estimation of Infiltrating Immune Cells in TME and Consensus Clustering

CIBERSORT (https://cibersort.stanford.edu/) is a developed algorithm utilized for deconvolving the expression matrix of immune cell subtypes based on the principle of linear support vector regression. Therefore, we pre-processed the RNA-seq (TPM normalized) data to infer the proportion of immune cells in tumor samples using the CIBERSORT algorithm and the LM22 gene signature. According to the proportion of immune cells analyzed by the CIBERSORT tool, we only selected the samples with $p < 0.05$ (N = 512 from total 618 samples). Based on the elbow (the square error of the WSSE

group, which was obtained by looking for the "elbow point") and gap statistics (the point where *Wk* falls the fastest, the value of *k* corresponding to the maximum value of Gap), we used the ConsensusClusterPlus package to find the TMEcluster with the best optimized *K* categories. Moreover, we conducted a total of 1,000 times iterations to achieve the robustness and stability of results and evaluate the potential relativity between survival outcomes and the classifications.

According to the TMEcluster results, the clustering results were mapped to RNA-seq data, and the limma package was utilized to search differentially expressed genes (DEGs) with $p <$ 1e-03 and $|\log_2 FC|>2$ as the cutoff value. We thus chose the class-specific differential genes and obtained the cluster signature genes using the random forest method to remove the redundant genes. Functional enrichment analysis was performed to observe the significant pathways that these signatures might be involved in. We referred to the algorithm introduced by Sotiriou et al. (28) and Cox regression model to calculate the TMEscore in ccRCC as the following: TMEscore = $\Sigma \log_2(X+1) - \Sigma \log_2(Y+1)$, where X is the expression value of the positive gene set of Cox coefficient and Y is the expression value of the gene set of Cox coefficient. Last, we sought the best breakpoint of TMEscore using the maxstat package and then divided the samples into TMEscore-high and TMEscore-low to further analyze the prognosis between two main types.

The Mutational Landscape of TCGA-KIRC

According to the downloaded TCGA-KIRC single-nucleotide polymorphism (SNP) data (N = 336 with TCGAbiolinks package), CNV data (N = 534), methylation data (N = 483), and survival data (N = 539 with cgdsr package), we intersected them with the RNA-seq data and finally derived 210 samples.

A variety of mutation types existed in cancers, including C > A, C > G, C > T, T > A, T > C, and T > G. Based on the six basic mutational types, we then considered one base upstream and downstream of the mutation site. Each base had four categories of A, T, C, and G; thus, a total of 96 mutation types were obtained with 4 * 6 * 4. In order to investigate different types of mutations, researchers introduced the concept of "Mutational Signature" and have already identified a total of 21 various Mutational Signatures across 30 malignancies. The frequencies of the 96 mutational types in different cancers were different. Combined analysis of the occurrence of 96 mutation types can be used as a fixed mutation pattern. Several Mutational Signatures were currently included in the COSMIC database, some of which were known, such as signature4 and signature29, and were related to exposure to the smoking environment. Accordingly, we used the maftools package (https://bioconductor.org/packages/release/bioc/html/maftools.html) and the SomaticSignatures package (https://bioconductor.org/packages/release/bioc/html/SomaticSignatures.html) to map the mutational landscape and characteristics in ccRCC.

The GISTIC algorithm was used to detect common CNV regions in all samples, including chromosome arm horizontal CNV and the smallest common region across samples. The GISTIC algorithm parameter determined the peak interval with the 0.95 as the confidence level, and the others remained default parameters. We selected the corresponding GISTIC module in GenePattern to conduct the analysis. Meanwhile, we utilized the ABSOLUTE package (https://software.broadinstitute.org/cancer/cga/absolute_download) to conduct the tumor purity and ploidy analysis based on the CNV results. The ABSOLUTE algorithm was applied to calculate scores from the pre-designed cancer karyotype and somatic mutation frequency and then integrated them, from which the highest score was the optimal model. Then, the tumor purity and ploidy were accordingly inferred.

Integrative Analysis in TME of ccRCC

Firstly, we identified the differential transcriptome of miRNA or mRNA across several clusters and conducted functional enrichment analysis to uncover the specific biological processes in different TME subgroups. Furthermore, we conducted prognostic analysis of differential genes in the TME-high- and TME-low groups. We aimed to depict the molecular and clinical characteristics across TME subgroups from comprehensive omics data. Finally, the TIDE tool (http://tide.dfci.harvard.edu/) from Harvard University was used to assess the clinical efficiency of immune checkpoint inhibition therapy, where higher TIDE predictive scores correlated with poor therapeutic effect and worse prognosis. The whole process of analysis was illustrated in **Figure 1**.

RESULTS

Landscape of Infiltrating Immune Cells in TME and Clustering Analysis

According to the integrated RNA-seq data (N = 618), we utilized the CIBERSORT package within 1,000 interactions to obtain the differential fractions of various immune cells across 512 samples, including CD4 cell, CD8 cell, B cell, and monocytes (**Figure 2A**). The clinical characteristics of all 618 ccRCC patients included in this study were shown in **Table 1**. We further depicted the potential associations among immune cells and their respective prognostic significance. We found that the Tregs cells and T follicular helper cells correlated negatively with survival outcomes, while Mast resting cells and T gamma delta cells were associated positively with prognosis in Cox regression models ($p <$ 0.0001, **Figure 2B**; **Table S1**). Moreover, we combined with ConsensusClusterPlus package and iterated 1,000 times (K = 1:10) to stabilize the classification categories, obtaining the optimized classification of the samples (**Figure S1**). We observed that the TMEcluster classifications were significantly associated with survival outcomes when k = 5, among which the TMEcluster4 (N = 35) had the worst prognosis and TMEcluster5 (N = 105) had the best prognosis (**Figure 2C**). We further compared the immune cell proportions across different TMEclusters and found the significant survival differences across these 5 clusters (**Figures 2D**, **3**; **Figure S2**).

Identification of Significant Prognostic Signature Associated With TME

We set the cutoff value with $p <$ 1e-3 and $|\log FC| > 2$ to screen the DEGs and obtained a total of 13,571 genes across different

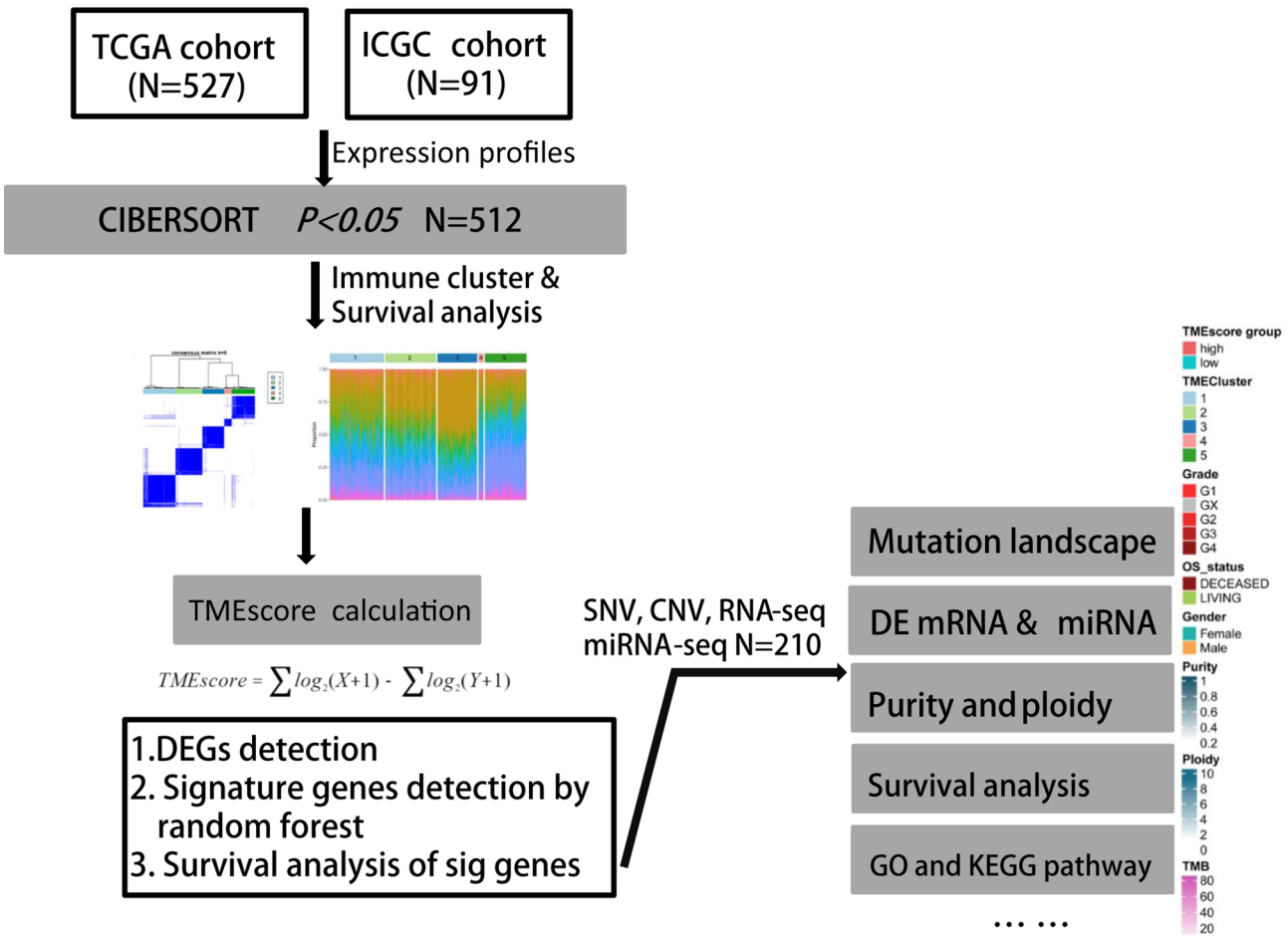


FIGURE 1 | Flowchart of analytical process of TME phenotypes and TMEscore in our study based on two independent ccRCC cohorts.

clusters (**Figure 4A**; **Table S2**). Functional analysis indicated that these genes were mainly involved in humoral immune response, immunoglobulin-mediated immune response, and B-cell-mediated immunity (**Figure 4B**). Additionally, we utilized the Cox regression model to analyze the genes with survival outcomes and divided the samples into two groups, namely, TME-high and TME-low groups. Kaplan–Meier analysis indicated that patients in the TME-low group suffered from worse prognosis than those in the TME-high group (**Figure 4C**). The Sankey diagram also revealed the potential associations among TMEcluster, groups, and vital status (**Figure 4D**; **Table S3**).

Profiles of Cancer Somatic Genome and Relationships With TME

We performed the statistical analysis of the mutation data in 210 tumor samples, including mutation annotations, proportions of base change, and the top 10 drivers (**Figure S3**). In KIRC, the missense mutations occurred the most frequently, and the main types were SNP, followed by DEL and INS (**Figure S3**). In these samples, the top 10 mutated drivers included VHL, TTN, and PBRM1 (**Figure S3**). We further divided the patients into TME-high and TME-low groups, and the differential mutated profiles are illustrated in **Figure 4E**. Accordingly, we observed that VHL harbored the most mutated sites in KIRC distributed across nearly half of the cases. Furthermore, the oncogenetic drivers of UBBP4, SPEN, and BDP1 exhibited significantly differential mutated frequencies between two groups, and we illustrated the results in boxplots (**Figure 5A**). We then classified the mutations into 96 types and calculated the distributed frequencies in 210 KIRC samples (**Figure 5B**; **Table S4**). The relationships between mutated frequencies and specific signature were estimated based on the COSMIC dataset. We performed the non-negative matrix factorization incorporating the 210 samples as the rows and the 96 mutated types as the columns. We extracted the features and compared them with included signature in COSMIC. The mutated features in the TME-high group were mainly associated with signature5 and signature12, while those in the TME-low group correlated with signature5, signature6, and signature24. Signature6 was found to be involved in DNA mismatch repair defect, and signature 24 was associated with aflatoxin exposure (**Figure 5C**).

We also used the GISTIC software to analyze the CNV in two groups and found that the amplification of 15p, 5q, and 5p and the

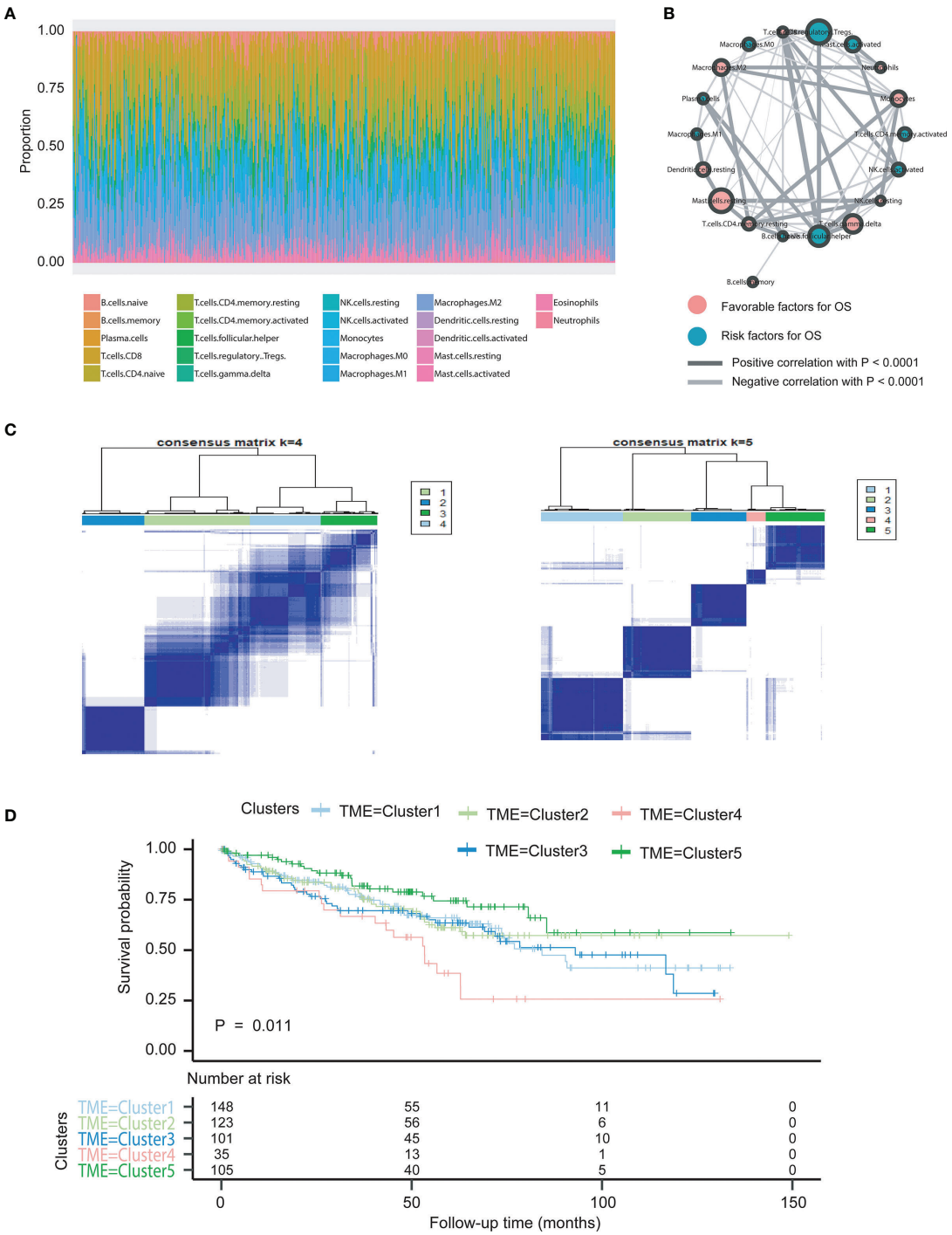


FIGURE 2 | Illustration of landscape of TME in ccRCC patients and characterization of TME subclusters. **(A)** The specific 22 immune fractions represented by different colors in each sample were shown in barplot via CIBERSORT algorithm. **(B)** Cellular interaction of cell types in tumor micro environment. Favorable factors for overall survival were indicated in pink, and hazard factors for overall survival were shown in dark green. The lines connecting TME cells represented their cellular interactions, where the thickness of the lines indicated the strength of correlation calculated by Spearman correlation analysis. Positive correlation was indicated in black and negative correlation in silver. **(C)** Clustering analysis based on ConsensusClusterPlus package was conducted and indicates the optimized categories were 5 for classifications of TME phenotypes. **(D)** Kaplan-Meier curves with log-rank test for overall survival (OS) of all cancer patients from seven two cohorts (TCGA, ICGC) with the TME infiltration classes. The number of patients in TMEcluster 1, 2, 3, 4 and 5 phenotypes were n=148, n=123, n=101, n=35, and n=105, respectively. Log-rank test showed an overall statistical result of P=0.011, where patients with TMEcluster 5 were with the most favorable outcomes.

TABLE 1 | Clinical characteristics of all 618 ccRCC patients included in this study.

Variables	TCGA (*N* = 537)	ICGC (*N* = 91)
Age (mean ± SD)	60.59 ± 12.14	60.47 ± 9.97
Follow-up (years)	3.12 ± 2.23	4.14 ± 1.73
Status		
Alive	367 (68.34)	61 (67.03)
Dead	170 (31.66)	30 (32.97)
Gender		
Male	346 (64.43)	52 (57.14)
Female	191 (35.57)	39 (42.86)
AJCC-T		
T1	275 (51.21)	54 (59.34)
T2	69 (12.85)	13 (14.28)
T3	182 (33.89)	22 (24.18)
T4	11 (2.05)	2 (2.20)
AJCC-N		
N0	240 (44.69)	79 (86.81)
N1	17 (3.17)	2 (2.20)
Unknow	280 (52.14)	10 (10.99)
AJCC-M		
M0	426 (79.33)	81 (89.01)
M1	79 (14.71)	9 (9.89)
Unknow	32 (5.96)	1 (1.10)
Pathological stage		
I	269 (50.09)	–
II	57 (10.61)	–
III	125 (23.28)	–
IV	83 (15.46)	–
Unknow	3 (0.56)	–
Grade		
G1	14 (2.61)	–
G2	230 (42.83)	–
G3	207 (38.54)	–
G4	78 (14.53)	–
Unknow	8 (1.49)	–
TMB levels		
Low	109 (20.30)	–
High	101 (18.81)	–
Unknown	327 (60.89)	

Data are shown as n (%).

TCGA, The Cancer Genome Atlas; ICGC, International Cancer Genome Consortium; AJCC, American Joint Committee on Cancer.

deletions of 9q, 15p, and 14q were the most prominent in the TME-high group. However, the amplification of 7q and 5q and the deletions of 9q, 3p, and 14q were the most significant in the TME-low group (**Figure 6A**). Moreover, we totally detected 102 amplifications and 79 copy number deletions in TME-high samples (MCRs, *q*-value < 1e-4) in **Figure 6B**. Among them, 5q11.2, 17q12, and 4q34.1 were the most significantly amplified regions and 4p16.1, 3q29, and 1q21.3 were the most significantly deleted regions. In TME-low samples, we totally detected 87 amplifications and 58 copy number deletions, among which 17q12, 20p13, and 5q11.2 were the most significantly amplified regions and 4p16.1, 1q21.3, and 12p13.31 were the most significantly deleted regions (**Figure 6C**). The tumor purity and ploidy of the samples were estimated based on the ABSOLUTE software. The range of tumor purity was 0.28–1 and the ploidy of the tumor cell genome was 1.78–9.06, indicating that the genome disorders occurred commonly during tumorigenesis (**Table S5**). Furthermore, Wilcoxon test suggested that no significant difference was observed between high and low TMEscore groups in **Figure S4**.

Comprehensive Results and Significance of TMEscore in Predicting Immunotherapeutic Benefits

Differential analysis revealed a total of 45 differentially expressed miRNAs and 163 mRNAs between TME-high and TME-low groups (**Tables S6, S7**). Functional enrichment analysis suggested that these differential genes were mainly involved in B-cell-mediated immunity, humoral immune response, and other cancer-related pathways (**Figures S5, S6**; **Table S8**). The log-rank test revealed 19 survival-related miRNAs and 23 mRNAs, including hsa-mir-21, hsa-mir-223, hsa-mir-146b, hsa-mir-139, SAA1, SLC27A2, PPP1R1A, and SAA2 (**Figure 7**; **Table S9**). We further illustrated the comprehensive genomic landscape integrating TMEcluster, TMEscores, mutation features (purity, ploidy, and TMB), and clinical characteristics (age, gender, and overall status) in **Figure 8A** and **Table S10**. The TIDE dataset was utilized to estimate the clinical efficiency of immune checkpoint blockade (ICBs) therapy between two groups (**Table S11**). We accordingly found that the TIDE scores in the low TMEscore group were calculated significantly lower than that in the high TMEscore group (Wilcoxon test, p = 6.9e−06). The higher TIDE predictive scores in tumor correlated with worse effect of ICBs and poor survival outcomes. In the current analysis, we thus speculated that KIRC patients with higher TMEscores might benefit from better ICB efficiency and optimistic prognosis (**Figure 8B**). Additionally, we also conducted the receiver operating characteristic (ROC) curves to compare the differential power in predicting efficiency of ICBs between traditional TMB and established TMEscores, in which the TIDE scores were defined as the observation value. Overall, the TMEscore was proved to be an effective indicator for tumor prognosis and ICB efficiency based on Bootstrap test with p-value = 0.0436 (**Figure 8C**).

DISCUSSION

In this study, we integrated the multi-omics data of ccRCC cohorts (TCGA-KIRC, ICGC-ccRCC) to depict the genomic features of TME and evaluate the prognostic significance of TMEscore in clinical utility, especially guiding more valuable immunotherapy strategies. Firstly, we used the CIBERSORT to infer the fractions of immune-infiltrating cells in TME and exhibit the relatively specific profiles of immune cells. Subsequent consensus clustering analysis indicated that patients in TMEcluster5 showed better prognosis, in which the memory B cell accounted for the most abundant infiltrating proportions. Accordingly, the differential genes among the 5 clusters indicated that the functional enrichment pathways were humoral immune response and immunoglobulin-mediated immune response, especially the B-cell-mediated immunity. Meanwhile, we calculated the TMEscore as a robust prognostic factor, in which patients with a lower TMEscore suffer from worse survival outcomes. Mutational analysis revealed the

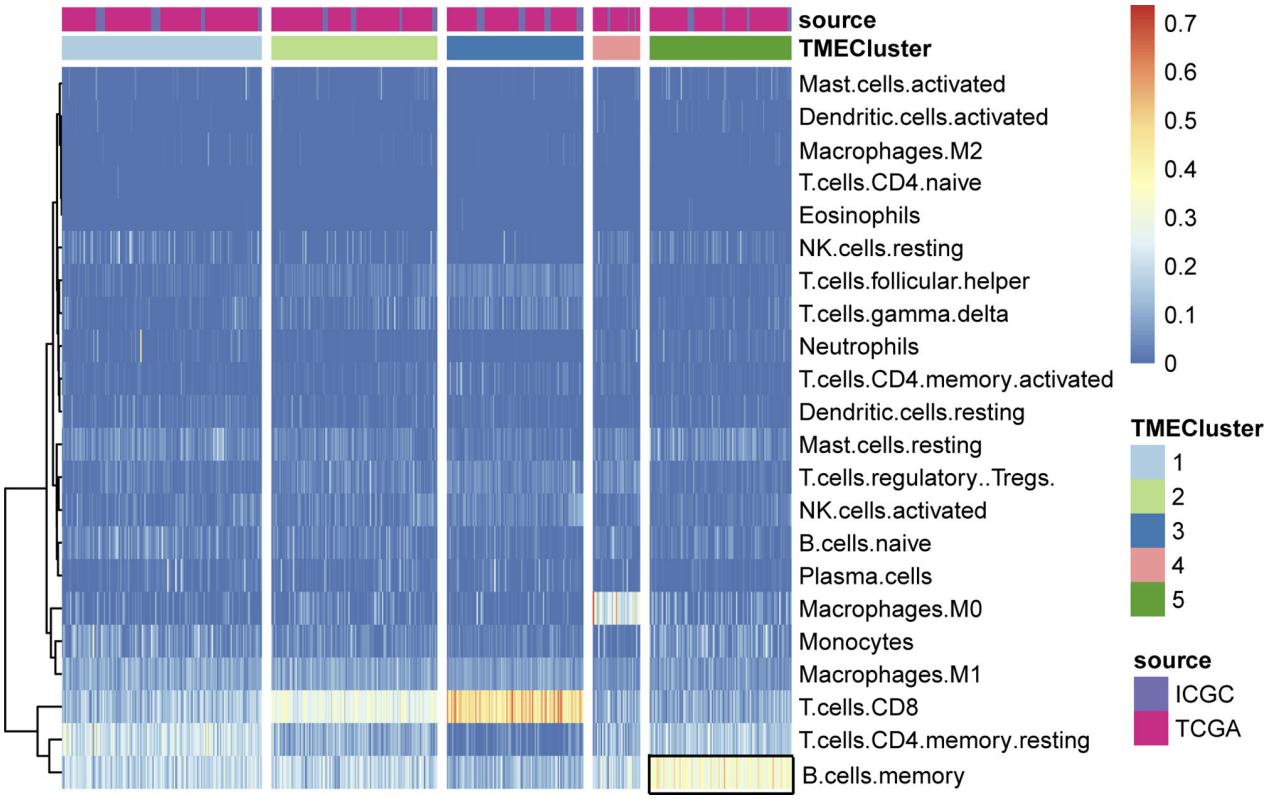


FIGURE 3 | Unsupervised clustering of TME cells for patients in the two cohorts. We assessed the differential infiltrating levels of immune cells in various clusters, where the memory B cells exhibited significantly enrichment in TME cluster5.

differential mutation burden between two TME groups, especially the gene clusters of UBBP4, SPEN, BDP1, and DNAH2, and we further uncovered the associations of the low TMEscore group with signature6, signature5, and signature24 included in the COSMIC dataset (29).

Blockade drugs targeting the PD1/PDL1 signaling pathway have brought novel insights into the treatment strategies and exhibit relatively satisfactory efficiency across multiple tumors, including breast cancer, colon cancer, bladder cancer, advanced gastric cancer, and kidney cancer (30–32). However, the powerful biomarkers are warranted for predicting the drug response of immune checkpoint inhibitors. Previous researchers found that PD-1 or PD-L1 expression levels, MSI status, and mutational load were not ideal factors for predicting the benefits of drugs with lower sensitivity (33–35). So far, whether TMB correlates with improved survival outcomes or promotion of immunotherapies remains controversial in ccRCC and large cohorts are needed to validate its significance (36). As a result, it is urgent to develop a predictive biomarker of checkpoint immunotherapy for maximizing the therapeutic benefit. Intensive research has revealed the crucial role of TME in checkpoint inhibitor immunotherapy (37, 38). In our study, we further integrated the comprehensive landscape of interactions across tumor-infiltrating immune cells and relationships with clinical characteristics of renal cancer.

Our study suggested that the quantified TMEscore was a prognostic factor for ccRCC and significantly correlated with molecular sub-clusters. Dongqiang Zeng et al. have already uncovered the strong positive associations of TMEscore with mutation burden and predicted neo-antigen burden in more than 1,000 gastric tumor patients (32, 39). So far, the predictive biomarkers in clinical utility and strategies to assess clinical response have mainly shown interest in T-cell compartment, partially ignoring the contributions to anti-tumor immunity of other immune subsets (40, 41). However, Petitprez et al. confirmed the significance of immune subtypes in patients with soft-tissue sarcoma and disclosed the potential ability of B cells in forming tertiary lymphoid structures to guide new insights into clinical treatments (42). Of note, Helmink et al. further demonstrated and supported that the memory B cells were enriched in the tumors of responders for ICB treatment, implicating the foreground of novel biomarkers (43). Furthermore, our results suggested that a higher TMEscore was positively related to the subgroup of TMEcluster5, in which memory B cells revealed higher infiltrating levels compared with other immune cells. Meanwhile, patients with a higher TMEscore were associated with better ICB therapeutic efficiency, emphasizing that memory B-cell activation was the core mechanism of sensitivity to checkpoint blockade. These findings might facilitate the precise immunotherapy strategy and

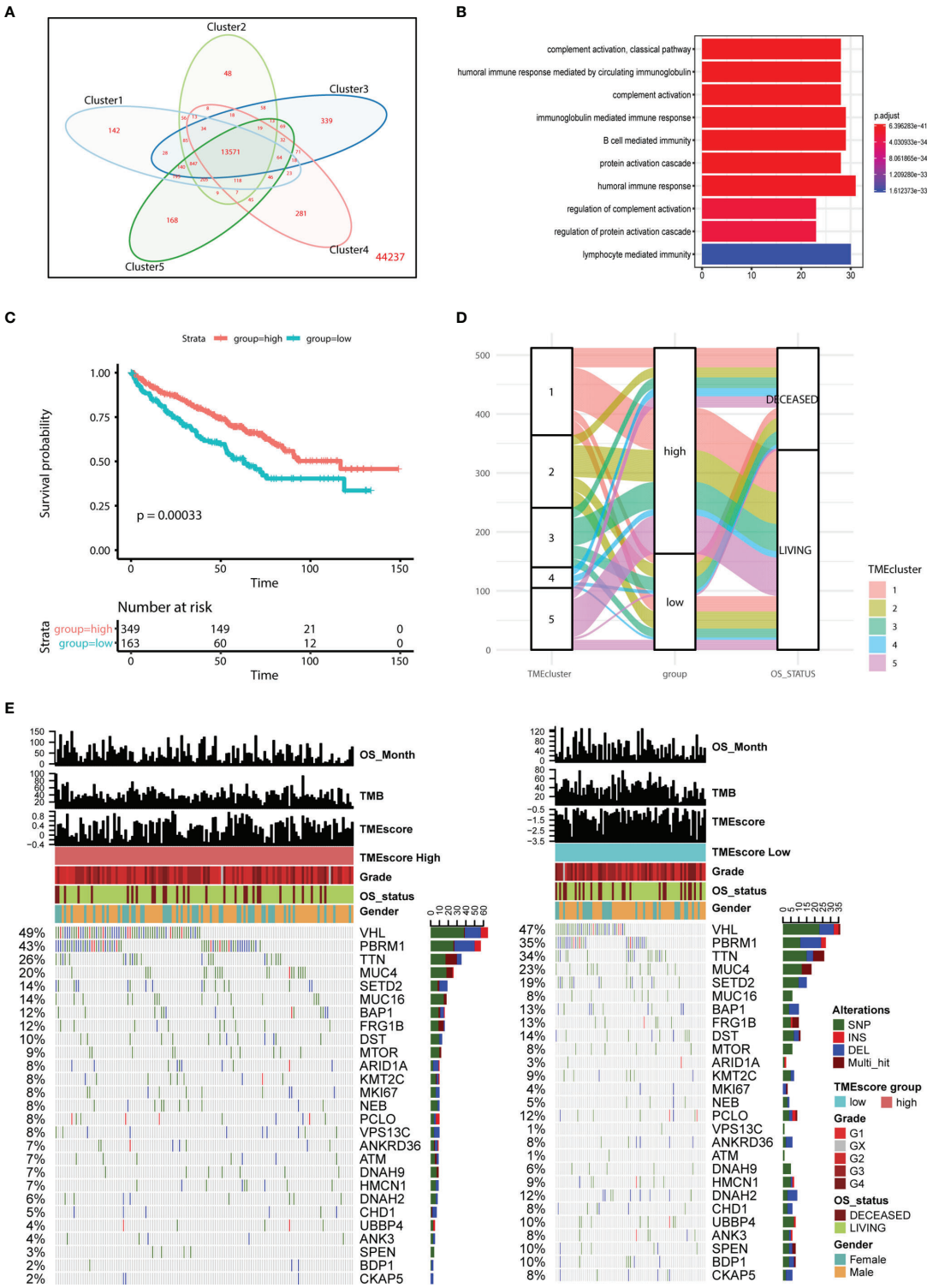


FIGURE 4 | Construction of TMEscore and integrative analysis in TME. **(A, B)** Venn diagram showed the totally 13571 intersected genes, in which functional enrichment analysis indicates the genes might be involved in B cell mediated immunity, humoral immune response, lymphocyte medicated immunity and other cancer-related immune crosstalk. **(C, D)** Kaplan-Meier analysis and mulberry map indicate the patients in low TMEscore group correlate with poor survival outcomes (log-rank test, $P < 0.001$). **(E)** Mutated profiles of top variant genes correlated with TMEscore. Single nucleotide variants: dark green, InDel (insertion or deletion): red, frameshift: blue, Multi_hit: brown. TMEscores, TCGA molecular subtypes, TMEscore, gender, and overall survival status are shown as specific annotations.

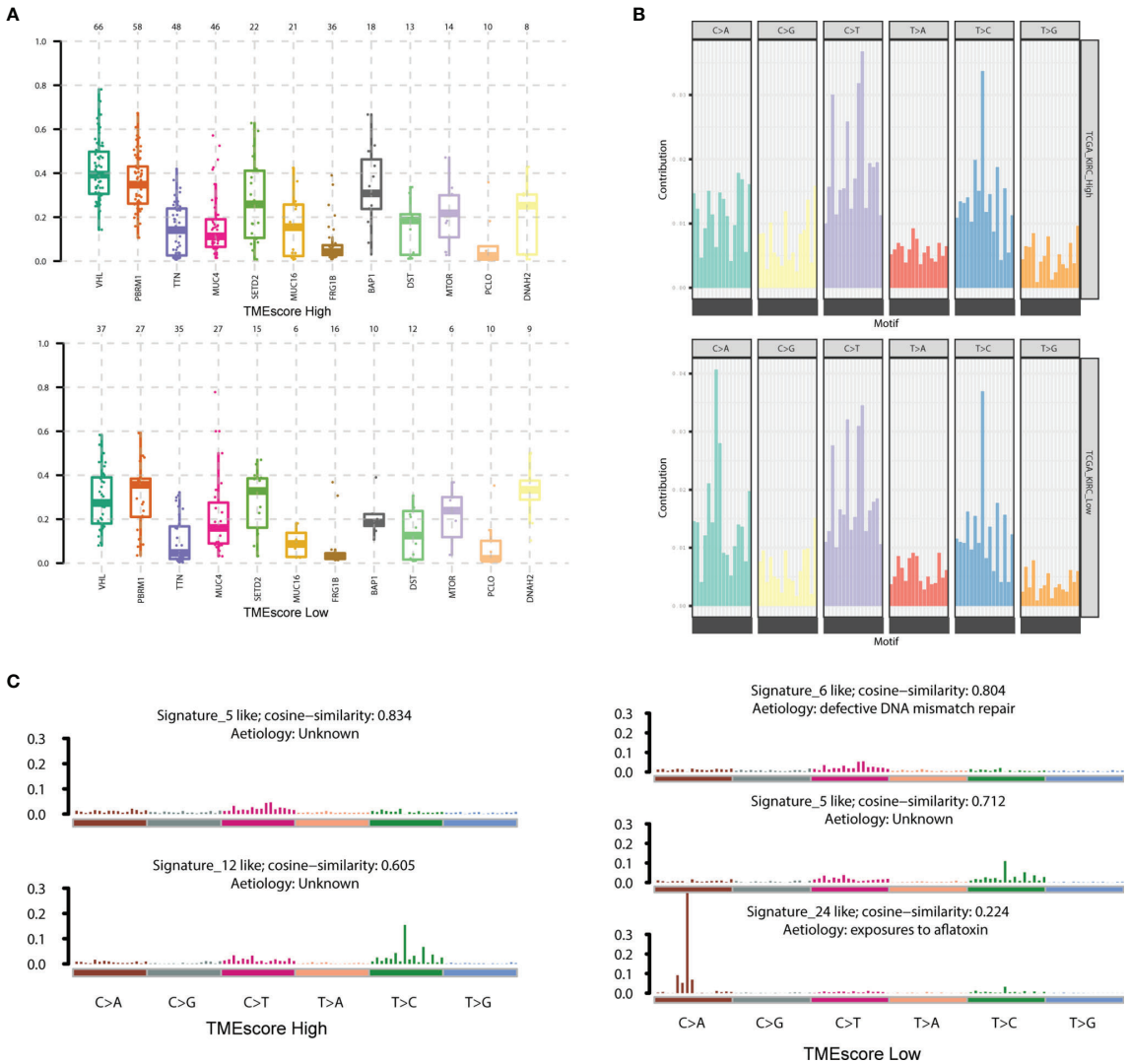


FIGURE 5 | Characterization of mutated profiles and related signature between two TMEscore groups. **(A)** The oncogenetic drivers of UBBP4, SPEN and BDP1 exhibited significantly differential mutated frequencies between two groups and we illustrated the results in boxplot. **(B)** We accordingly classified the mutations into 96 types and calculated the distributed frequencies in 210 KIRC samples. **(C)** We extracted the features and compared them with included signature in COSMIC dataset. The mutated features in TME-high group were mainly associated with signature5, signature12, while those in TME-low group correlated with signature5, signature6, signature24. The signature6 was found to be involved in DNA mismatch repair defect, and signature 24 was associated with Aflatoxin exposure.

the combined management of both activation of memory B cell and traditional ICB. In addition, Netti et al. also found that PTX3 could modulate the immunoflogosis in TME and function as a prognostic factor for patients with ccRCC (44). Analysis of complement system activation on tumor tissues showed the co-expression of PTX3 with C1q, C3aR, C5R1, and CD59. The expression of PTX3 can affect the immunoflogosis in the ccRCC microenvironment, by activating the classical pathway of CS (C1q) and releasing pro-angiogenic factors (C3a and C5a). The upregulation of CD59 also inhibits the complement-mediated cellular lysis. Although this study uncovered the tight associations between PTX3 and TME remodeling, the predictive efficiency of PTX3 in ccRCC was not well elucidated and validated. Our established signature is a model constructed by multiple genes and has strong robustness. Calculation and application of our TMEscore would be useful for clinical prediction and ICB treatment of ccRCC.

Apart from the associations with immune filtration analysis, we further discussed the TMEscore with mutation profiles in ccRCC. We completely illustrated the mutational landscape in both groups and found the differential mutated frequencies of drivers between two TMEscore levels, including UBBP4, SPEN, and BDP1. In particular, Sharma et al. (45) also reported that the deleterious mutation of SPEN p.S1078* emerges as a putative potential therapeutic target in advanced-stage urothelial carcinoma. Additionally, we first analyzed the relationships

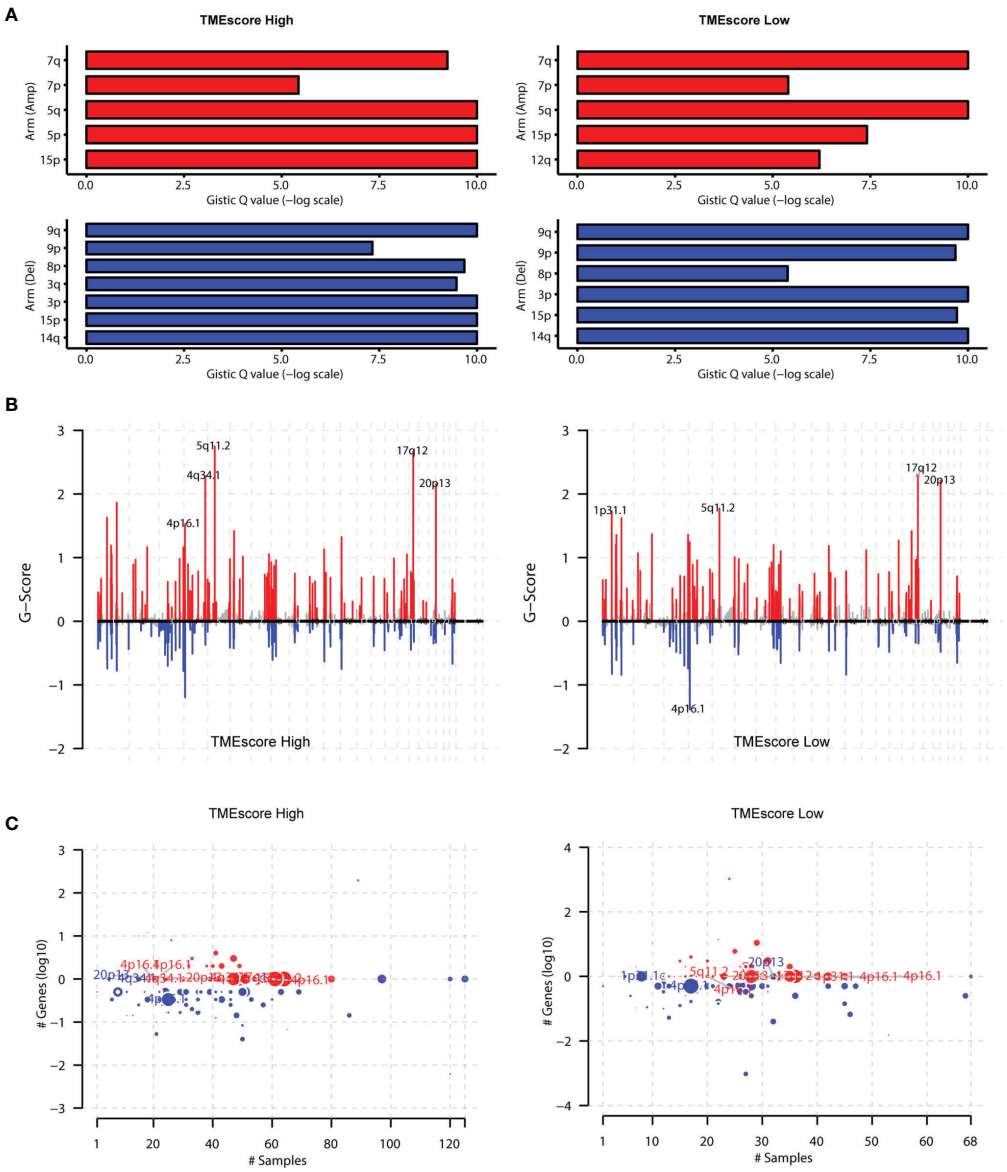


FIGURE 6 | Assessment of copy number variation (CNV) burden in two TMEscore groups. **(A)** We also conducted the GISTIC software to analyse the copy number variations in two groups and found that the amplification of 15p, 5q, 5p and deletions of 9q, 15p, 14q were the most prominent in TME-high group. However, the amplification of 7q, 5q and the deletions of 9q, 3p, 14q were the most significant in the TME-low group. **(B)** Besides, we totally detected 102 amplifications TME-high samples (MCRs, q-value<1e-4), among which 5q11.2, 17q12, and 4q34.1 were the most significantly amplified regions. In TME-low samples, we totally detected 87 amplifications and found 17q12, 20p13, 5q11.2 were the most significantly amplified regions. **(C)** The 79 copy number deletions in TME-high samples were detected, among which 4p16.1, 3q29, and 1q21.3 were the most significantly deleted regions. However, 1q21.3, 12p13.31 were the most significantly deleted regions in TMEscore low group.

between mutated distributions with a specific signature in the COSMIC dataset in two TMEscore groups. The included signature6 and signature24 were significantly associated with defective DNA mismatch repair, chromosomal instability, and exposure of aflatoxin, which might be one of the underlying explanations for the patients with poor survival outcomes in the low TMEscore group. Furthermore, we still detected the associations of mutation features in high TMEscore with signature5 and signature12 matched with unknown etiology annotations, and large cohorts with in-depth somatic mutated sequencing are warranted. Of note, CNV data were utilized to infer the tumor purity and ploidy and there was no significant difference between two TMEscore groups. We thus speculated that tumor purity might not function as a vital determinant for prognosis in two TMEscore levels. Moreover, differential analysis revealed the significant immune-related miRNAs (hsa-miR-29b-

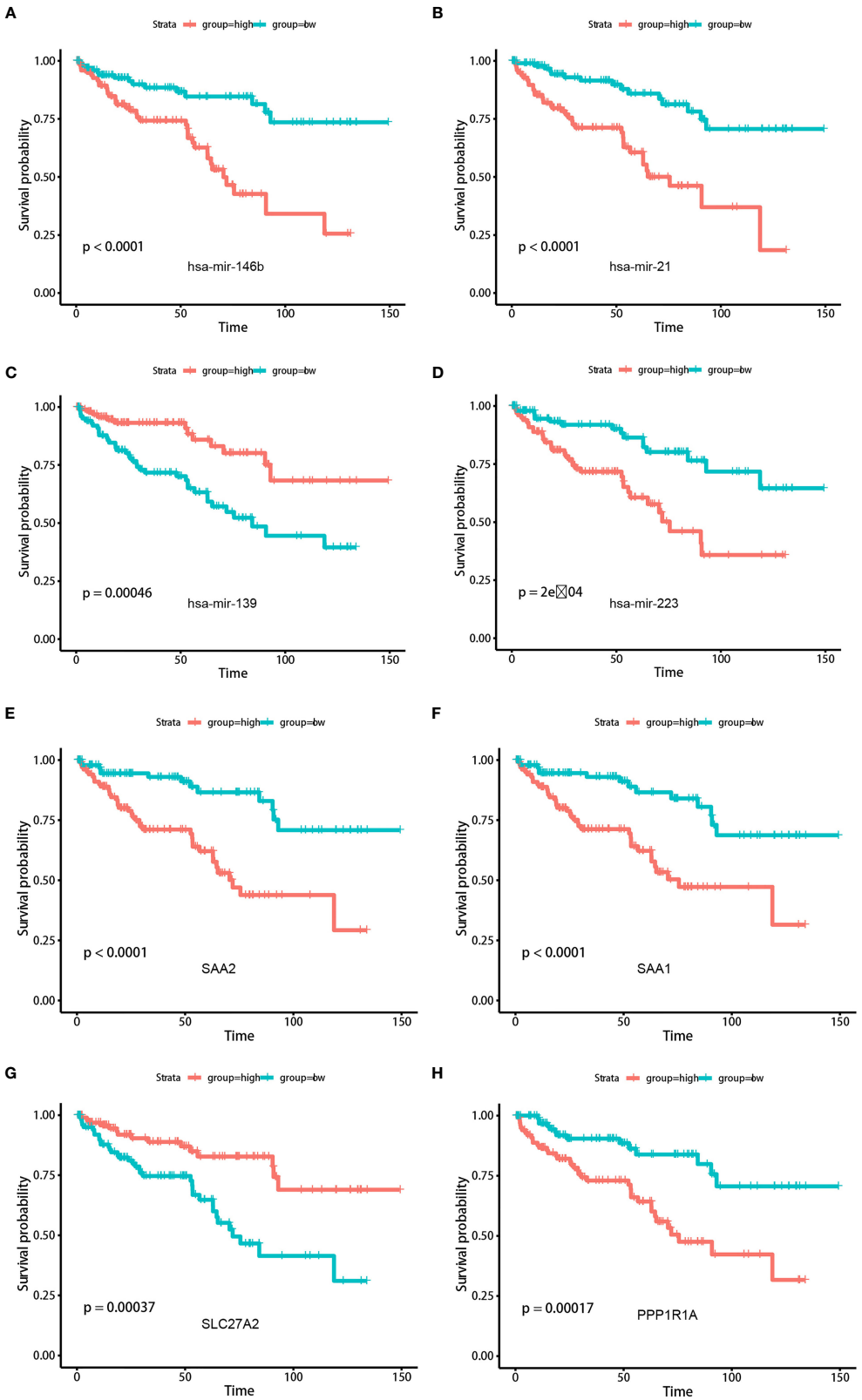


FIGURE 7 | Kaplan-Meier analysis was conducted to assess the significantly risk signature expressed differentially (top miRNAs and mRNAs) in two TMEscore groups. **(A)** hsa-mir-146b. **(B)** hsa-mir-21. **(C)** hsa-mir-139. **(D)** hsa-mir-223. **(E)** SAA2. **(F)** SAA1. **(G)** SLC27A2. **(H)** PPP1R1A.

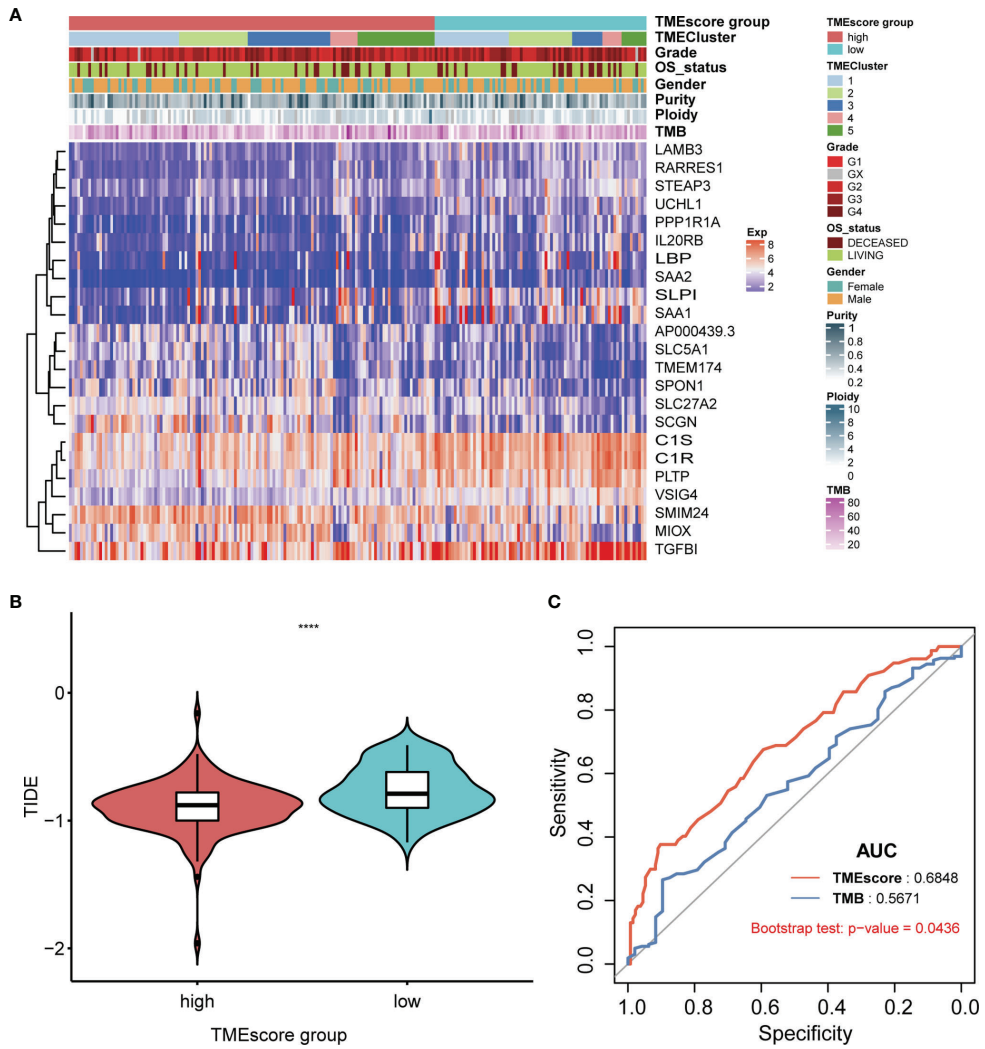


FIGURE 8 | Systematic exhibition of TMEscore with other variables and associations with ICB efficiency compared with TMB. **(A)** Illustration of comprehensive genomic landscape integrating TMEcluster, TMEscores, mutation features (purity, ploidy, TMB) and clinical characteristics (age, gender, overall status). **(B)** In the current analysis, we found that KIRC patients with higher TME-scores might benefit from better ICBs efficiency and optimistic prognosis. **(C)** Compared with traditional indicator of TMB, TMEscore possess the more predictive sensitivity based on the ROC curve with 0.684.

3p, hsa-miR-139-5p, and hsa-miR-142-5p), among which Montero-Conde et al. supported the idea that the hsa-miR-139-5p/HNRNPF axis served as a novel regulatory mechanism associated with the modulation of major thyroid cancer signaling pathways and tumor virulence (46, 47). Subsequent Kaplan–Meier analysis further identified 19 TMEscore-related prognostic miRNAs and 23 hub mRNAs (SAA1, SLC27A2, PPP1R1A, SAA2, etc.). We last drew the heatmap to exhibit the top 23 TMEscore-related hazard signatures combined with integrative analysis of TMB, purity, and subclusters between two groups, providing significantly therapeutic targets for ccRCC.

However, there were still several limitations in our work. Firstly, the fractions or prognostic value of TMEscore-related immune cells or risk signature are not validated by flow cytometry or other experimental studies. Apart from only two centers of TCGA or ICGC patients, other independent cohorts in our hospitals with more ccRCC patients were warranted to further support the clinical significance of TMEscore in predicting prognosis. Furthermore, we just utilized the TIDE dataset to estimate the ICB efficiency and we should enroll eligible patients treated with ICB drugs to compare the indicative value of TMEscore with TMB. As we observed that not all patients with high TMEscore gained better benefit of immunotherapy, more clinical factors should be incorporated to integrative models for the improvement of predictive accuracy.

Overall, our study systematically revealed unique biological insights into TMEscore in ccRCC, the major subtype of kidney cancer, combining complementary genomic, transcriptome, and mutation profiles with clinical characteristics, providing an invaluable bioinformatic resource for subsequent research

on TME in ccRCC tumorigenesis. For the first time, we characterize in detail the TME subcluster, the establishment of TMEscore, the potential associations of TMEscore with mutation profiles, CNV burden, risk signature, and ICB efficiency. The TMEscore, as we have quantified, was proved to have promising significance for predicting prognosis and ICB responses, in accordance with the goal of developing rationally individualized therapeutic interventions.

DATA AVAILABILITY STATEMENT

The original contributions presented in the study are included in the article/**Supplementary Material**. Further inquiries can be directed to the corresponding authors.

AUTHOR CONTRIBUTIONS

CZ: formal analysis, investigation, visualization, writing—original draft, and writing—review and editing. FQ: formal analysis, data curation, methodology, software, and writing—review and editing. YZ: formal analysis, data curation, methodology, supervision, validation, and writing—review and editing. XX: data curation. XL and XW: conceptualization, funding acquisition, project administration, resources, supervision, and writing—review and editing. All authors contributed to the article and approved the submitted version.

FUNDING

This work was supported by grants from the Medical Research Project of Jiangsu Provincial Health and Family Planning Commission (No. H2018052), and the Young Talents Program of Jiangsu Cancer Hospital (No. 2017YQL-04).

SUPPLEMENTARY MATERIAL

The Supplementary Material for this article can be found online at: https://www.frontiersin.org/articles/10.3389/fonc.2022.749119/full#supplementary-material

REFERENCES

1. Siegel RL, Miller KD, Jemal A. Cancer Statistics, 2020. *CA Cancer J Clin* (2020) 70:7–30. doi: 10.3322/caac.21590
2. Adamy A, Favaretto RL, Nogueira L, Savage C, Russo P, Coleman J, et al. Recovery of Renal Function After Open and Laparoscopic Partial Nephrectomy. *Eur Urol* (2010) 58:596–601. doi: 10.1016/j.eururo.2010.05.044
3. Gershman B, Thompson RH, Boorjian SA, Lohse CM, Costello BA, Cheville JC, et al. Radical Versus Partial Nephrectomy for Ct1 Renal Cell Carcinoma. *Eur Urol* (2018) 74:825–32. doi: 10.1016/j.eururo.2018.08.028
4. Barata PC, Rini BI. Treatment of Renal Cell Carcinoma: Current Status and Future Directions. *CA Cancer J Clin* (2017) 67:507–24. doi: 10.3322/caac.21411
5. Immune Atlases Created for Kidney, Lung Cancers. *Cancer Discovery* (2017) 7:658–9. doi: 10.1158/2159-8290.CD-NB2017-075
6. Rathmell WK, Rathmell JC, Linehan WM. Metabolic Pathways in Kidney Cancer: Current Therapies and Future Directions. *J Clin Oncol* (2018) JCO2018792309. doi: 10.1200/JCO.2018.79.2309
7. Bailey SR, Maus MV. Gene Editing for Immune Cell Therapies. *Nat Biotechnol* (2019) 37:1425–34. doi: 10.1038/s41587-019-0137-8
8. Seifert L, Werba G, Tiwari S, Giao Ly NN, Alothman S, Alqunaibit D, et al. The Necrosome Promotes Pancreatic Oncogenesis *via* CXCL1 and Mincle-Induced Immune Suppression. *Nat* (2016) 532:245–9. doi: 10.1038/nature17403
9. Zhong Y, Ma Z, Wang F, Wang X, Yang Y, Liu Y, et al. *In Vivo* Molecular Imaging for Immunotherapy Using Ultra-Bright Near-Infrared-IIb Rare-Earth Nanoparticles. *Nat Biotechnol* (2019) 37:1322–31. doi: 10.1038/s41587-019-0262-4
10. Englinger B, Pirker C, Heffeter P, Terenzi A, Kowol CR, Keppler BK, et al. Metal Drugs and the Anticancer Immune Response. *Chem Rev* (2019) 119:1519–624. doi: 10.1021/acs.chemrev.8b00396
11. Vitale I, Manic G, Coussens LM, Kroemer G, Galluzzi L. Macrophages and Metabolism in the Tumor Microenvironment. *Cell Metab* (2019) 30:36–50. doi: 10.1016/j.cmet.2019.06.001
12. Flippot R, Dalban C, Laguerre B, Borchiellini D, Gravis G, Negrier S, et al. Safety and Efficacy of Nivolumab in Brain Metastases From Renal Cell Carcinoma: Results of the GETUG-AFU 26 NIVOREN Multicenter Phase II Study. *J Clin Oncol* (2019) 37:2008–16. doi: 10.1200/JCO.18.02218
13. Miao D, Margolis CA, Gao W, Voss MH, Li W, Martini DJ, et al. Genomic Correlates of Response to Immune Checkpoint Therapies in Clear Cell Renal Cell Carcinoma. *Sci* (2018) 359:801–6. doi: 10.1126/science.aan5951
14. Zhang C, Li Z, Qi F, Hu X, Luo J. Exploration of the Relationships Between Tumor Mutation Burden With Immune Infiltrates in Clear Cell Renal Cell Carcinoma. *Ann Transl Med* (2019) 7:648. doi: 10.21037/atm.2019.10.84
15. Ruan H, Li S, Tong J, Cao Q, Song Z, Wang K, et al. The Screening of Pivotal Gene Expression Signatures and Biomarkers in Renal Carcinoma. *J Cancer* (2019) 10:6384–94. doi: 10.7150/jca.30656
16. Verbiest A, Couchy G, Job S, Caruana L, Lerut E, Oyen R, et al. Molecular Subtypes of Clear-Cell Renal Cell Carcinoma are Prognostic for Outcome After Complete Metastasectomy. *Eur Urol* (2018) 74:474–80. doi: 10.1016/j.eururo.2018.01.042
17. Xiong Y, Qi Y, Bai Q, Xia Y, Liu L, Guo J. Relevance of Arm Somatic Copy Number Alterations for Oncologic Outcomes and Tumor Immune Microenvironment in Clear Cell Renal Cell Carcinoma. *Ann Transl Med* (2019) 7:646. doi: 10.21037/atm.2019.10.54
18. Jafari S, Molavi O, Kahroba H, Hejazi MS, Maleki-Dizaji N, Barghi S, et al. Clinical Application of Immune Checkpoints in Targeted Immunotherapy of Prostate Cancer. *Cell Mol Life Sci* (2020) 77(19):3693–710. doi: 10.1007/s00018-020-03459-1
19. Job S, Rapoud D, Dos Santos A, Gonzalez P, Desterke C, Pascal G, et al. Identification of Four Immune Subtypes Characterized by Distinct Composition and Functions of Tumor Microenvironment in Intrahepatic Cholangiocarcinoma. *Hepatology* (2019) 72(3):965–81. doi: 10.1002/hep.31092
20. Dai E, Han L, Liu J, Xie Y, Kroemer G, Klionsky DJ, et al. Autophagy-Dependent Ferroptosis Drives Tumor-Associated Macrophage Polarization via Release and Uptake of Oncogenic KRAS Protein. *Autophagy* (2020) 16(11):1–15. doi: 10.1080/15548627.2020.1714209
21. Wu C, Tan X, Hu X, Zhou M, Yan J, Ding C. Tumor Microenvironment Following Gemcitabine Treatment Favors Differentiation of Immunosuppressive Ly6C(high) Myeloid Cells. *J Immunol* (2020) 204:212–23. doi: 10.4049/jimmunol.1900930
22. Gibney GT, Weiner LM, Atkins MB. Predictive Biomarkers for Checkpoint Inhibitor-Based Immunotherapy. *Lancet Oncol* (2016) 17:e542–51. doi: 10.1016/S1470-2045(16)30406-5
23. Sun C, Mezzadra R, Schumacher TN. Regulation and Function of the PD-L1 Checkpoint. *Immun* (2018) 48:434–52. doi: 10.1016/j.immuni.2018.03.014

24. Wang J, Sun J, Liu LN, Flies DB, Nie X, Toki M, et al. Siglec-15 as an Immune Suppressor and Potential Target for Normalization Cancer Immunotherapy. *Nat Med* (2019) 25:656–66. doi: 10.1038/s41591-019-0374-x
25. Li F, Huang Q, Luster TA, Hu H, Zhang H, Ng WL, et al. *In Vivo* Epigenetic CRISPR Screen Identifies Asf1a as an Immunotherapeutic Target in Kras-Mutant Lung Adenocarcinoma. *Cancer Discovery* (2020) 10:270–87. doi: 10.1158/2159-8290.CD-19-0780
26. Becht E, Giraldo NA, Lacroix L, Buttard B, Elarouci N, Petitprez F, et al. Estimating the Population Abundance of Tissue-Infiltrating Immune and Stromal Cell Populations Using Gene Expression. *Genome Biol* (2016) 17:218. doi: 10.1186/s13059-016-1070-5
27. Newman AM, Liu CL, Green MR, Gentles AJ, Feng W, Xu Y, et al. Robust Enumeration of Cell Subsets From Tissue Expression Profiles. *Nat Methods* (2015) 12:453–7. doi: 10.1038/nmeth.3337
28. Sotiriou C, Wirapati P, Loi S, Harris A, Fox S, Smeds J, et al. Gene Expression Profiling in Breast Cancer: Understanding the Molecular Basis of Histologic Grade to Improve Prognosis. *J Natl Cancer Inst* (2006) 98:262–72. doi: 10.1093/jnci/djj052
29. Tate JG, Bamford S, Jubb HC, Sondka Z, Beare DM, Bindal N, et al. COSMIC: The Catalogue Of Somatic Mutations In Cancer. *Nucleic Acids Res* (2019) 47: D941–7. doi: 10.1093/nar/gky1015
30. Awad MM, Hammerman PS. Durable Responses With PD-1 Inhibition in Lung and Kidney Cancer and the Ongoing Search for Predictive Biomarkers. *J Clin Oncol* (2015) 33:1993–4. doi: 10.1200/JCO.2015.61.4172
31. Gourd E. EMA Restricts Use of Anti-PD-1 Drugs for Bladder Cancer. *Lancet Oncol* (2018) 19:e341. doi: 10.1016/S1470-2045(18)30433-9
32. Tauriello DVF, Palomo-Ponce S, Stork D, Berenguer-Llergo A, Badia-Ramentol J, Iglesias M, et al. TGFbeta Drives Immune Evasion in Genetically Reconstituted Colon Cancer Metastasis. *Nat* (2018) 554:538–43. doi: 10.1038/nature25492
33. Gonzalez-Rodriguez P, Engskog-Vlachos P, Zhang H, Murgoci AN, Zerdes I, Joseph B. SETD2 Mutation in Renal Clear Cell Carcinoma Suppress Autophagy *via* Regulation of ATG12. *Cell Death Dis* (2020) 11:69. doi: 10.1038/s41419-020-2266-x
34. Vijayalakshmi K, Shankar V, Bain RM, Nolley R, Sonn GA, Kao CS, et al. Identification of Diagnostic Metabolic Signatures in Clear Cell Renal Cell Carcinoma Using Mass Spectrometry Imaging. *Int J Cancer* (2019) 147 (1):256–65. doi: 10.1002/ijc.32843
35. Yeong J, Zhao Z, Lim JCT, Li H, Thike AA, Koh VCY, et al. PD-L1 Expression Is an Unfavourable Prognostic Indicator in Asian Renal Cell Carcinomas. *J Clin Pathol* (2020) 73(8):463–9. doi: 10.1136/jclinpath-2019-206092
36. Damotte D, Warren S, Arrondeau J, Boudou-Rouquette P, Mansuet-Lupo A, Biton J, et al. The Tumor Inflammation Signature (TIS) Is Associated With Anti-PD-1 Treatment Benefit in the CERTIM Pan-Cancer Cohort. *J Transl Med* (2019) 17:357. doi: 10.1186/s12967-019-2100-3
37. Chen B, Chen W, Jin J, Wang X, Cao Y, He Y. Data Mining of Prognostic Microenvironment-Related Genes in Clear Cell Renal Cell Carcinoma: A Study With TCGA Database. *Dis Markers* (2019) 2019:8901649. doi: 10.1155/2019/8901649
38. Lee K, Hwang H, Nam KT. Immune Response and the Tumor Microenvironment: How They Communicate to Regulate Gastric Cancer. *Gut Liver* (2014) 8:131–9. doi: 10.5009/gnl.2014.8.2.131
39. Zeng D, Li M, Zhou R, Zhang J, Sun H, Shi M, et al. Tumor Microenvironment Characterization in Gastric Cancer Identifies Prognostic and Immunotherapeutically Relevant Gene Signatures. *Cancer Immunol Res* (2019) 7:737–50. doi: 10.1158/2326-6066.CIR-18-0436
40. Dumont C, Jacquier A, Verine J, Noel F, Goujon A, Wu CL, et al. CD8(+)PD-1(-)ILT2(+) T Cells Are an Intratumoral Cytotoxic Population Selectively Inhibited by the Immune-Checkpoint HLA-G. *Cancer Immunol Res* (2019) 7:1619–32. doi: 10.1158/2326-6066.CIR-18-0764
41. Fu Q, Xu L, Wang Y, Jiang Q, Liu Z, Zhang J, et al. Tumor-Associated Macrophage-Derived Interleukin-23 Interlinks Kidney Cancer Glutamine Addiction With Immune Evasion. *Eur Urol* (2019) 75:752–63. doi: 10.1016/j.eururo.2018.09.030
42. Petitprez F, de Reynies A, Keung EZ, Chen TW, Sun CM, Calderaro J, et al. B Cells are Associated With Survival and Immunotherapy Response in Sarcoma. *Nat* (2020) 577:556–60. doi: 10.1038/s41586-019-1906-8
43. Helmink BA, Reddy SM, Gao J, Zhang S, Basar R, Thakur R, et al. B Cells and Tertiary Lymphoid Structures Promote Immunotherapy Response. *Nat* (2020) 577:549–55. doi: 10.1038/s41586-019-1922-8
44. Netti GS, Lucarelli G, Spadaccino F, Castellano G, Gigante M, Divella C, et al. PTX3 Modulates the Immunoflogosis in Tumor Microenvironment and is a Prognostic Factor for Patients With Clear Cell Renal Cell Carcinoma. *Aging (Albany NY)* (2020) 12:7585–602. doi: 10.18632/aging.103169
45. Sharma J, Deb B, George IA, Kapil S, Coral K, Kakkar N, et al. Somatic Mutations Profile of a Young Patient With Metastatic Urothelial Carcinoma Reveals Mutations in Genes Involved in Ion Channels. *Front Oncol* (2019) 9:435. doi: 10.3389/fonc.2019.00435
46. Montero-Conde C, Grana-Castro O, Martin-Serrano G, Martinez-Montes AM, Zarzuela E, Munoz J, et al. Hsa-miR-139-5p is a Prognostic Thyroid Cancer Marker Involved in HNRNPF-Mediated Alternative Splicing. *Int J Cancer* (2020) 146:521–30. doi: 10.1002/ijc.32622
47. Tu J, Zhao Z, Xu M, Lu X, Chang L, Ji J. NEAT1 Upregulates TGF-Beta1 to Induce Hepatocellular Carcinoma Progression by Sponging Hsa-Mir-139-5p. *J Cell Physiol* (2018) 233:8578–87. doi: 10.1002/jcp.26524

Conflict of Interest: The authors declare that the research was conducted in the absence of any commercial or financial relationships that could be construed as a potential conflict of interest.

Publisher's Note: All claims expressed in this article are solely those of the authors and do not necessarily represent those of their affiliated organizations, or those of the publisher, the editors and the reviewers. Any product that may be evaluated in this article, or claim that may be made by its manufacturer, is not guaranteed or endorsed by the publisher.

Copyright © 2022 Zhang, Qi, Zheng, Xia, Li and Wang. This is an open-access article distributed under the terms of the Creative Commons Attribution License (CC BY). The use, distribution or reproduction in other forums is permitted, provided the original author(s) and the copyright owner(s) are credited and that the original publication in this journal is cited, in accordance with accepted academic practice. No use, distribution or reproduction is permitted which does not comply with these terms.

frontiers | Frontiers in Oncology

SYSTEMATIC REVIEW
published: 16 May 2022
doi: 10.3389/fonc.2022.734948

Prognostic Significance of Pretreatment Neutrophil-to-Lymphocyte Ratio, Platelet–to–Lymphocyte Ratio, or Monocyte-to-Lymphocyte Ratio in Endometrial Neoplasms: A Systematic Review and Meta–analysis

Jiali Leng[1†], *Fei Wu*[2] *and Lihui Zhang*[2*]

[1] Division of Obstetrics and Gynecology, The Second Hospital of Jilin University, Jilin University, Changchun, China,
[2] Division of Obstetrics and Gynecology, The Second Hospital of Jilin University, Changchun, China

OPEN ACCESS

Edited by:
Alfredo Berruti,
University of Brescia, Italy

Reviewed by:
Albert Biete,
University of Barcelona, Spain
Georges Mjaess,
Free University of Brussels, Belgium

***Correspondence:**
Lihui Zhang
lihui3572@sina.com

†ORCID:
Jiali Leng
orcid.org.0000-0002-3763-7908

Specialty section:
This article was submitted to Genitourinary Oncology, a section of the journal Frontiers in Oncology

Received: 01 July 2021
Accepted: 31 March 2022
Published: 16 May 2022

Citation:
Leng J, Wu F and Zhang L (2022) Prognostic Significance of Pretreatment Neutrophil-to-Lymphocyte Ratio, Platelet–to–Lymphocyte Ratio, or Monocyte-to-Lymphocyte Ratio in Endometrial Neoplasms: A Systematic Review and Meta–analysis. Front. Oncol. 12:734948. doi: 10.3389/fonc.2022.734948

Aim: Neutrophil–lymphocyte ratio (NLR), platelet–lymphocyte ratio (PLR), or monocyte–lymphocyte ratio (MLR) has been shown to be related to the poor prognosis of cervical cancer, ovarian cancer, breast cancer, and other malignant tumors, but their role in predicting the prognosis of endometrial cancer is still controversial. Therefore, we conducted this meta-analysis to evaluate the effectiveness of NLR more accurately, PLR, or MLR in predicting the prognosis of endometrial cancer (EC).

Methods: This review systematically searched for relevant publications in databases of the Cochrane Library, PubMed, EMBASE, CNKI, WanFang, VIP, and CBM. Pooled hazard ratios (HR) with 95% confidence intervals (95% CI) were determined and used to explore the association between inflammatory biomarkers (NLR, PLR, and MLR) and overall survival (OS), progression-free survival (PFS), and disease-free survival (DFS) in a random-effects model. We also conducted subgroup analysis and publication bias in this meta-analysis. Stata 12.0 was used for statistical analysis.

Results: This meta-analysis contained 14 eligible studies including 5,274 patients. Our results showed that NLR or PLR was associated with OS [NLR: HR, 2.51; 95% CI, 1.70–3.71; p <0.001 in univariate analysis (Ua); HR, 1.87; 95% CI, 1.34–2.60; p <0.001 in multivariate analysis (Ma); PLR: HR, 2.50; 95% CI, 1.82–3.43; p <0.001 in Ua; HR, 1.86; 95% CI, 1.22–2.83; p = 0.004 in Ma], but MLR was not associated with OS (HR, 1.44; 95% CI, 0.70–2.95; p = 0.325 in Ua; HR, 1.01; 95% CI, 0.39–2.60; p =0.987 in Ma). A further subgroup analysis found that the correlations were not affected by race, cutoff value, sample size, or treatment. Our meta-analysis showed that NLR or PLR was associated with DFS (NLR: HR, 2.50; 95% CI, 1.38–4.56; p =0.003 in Ua; HR, 2.06;

95% CI, 1.26–3.37, P =0.004 in Ma; PLR: HR, 1.91; 95% CI, 1.30–2.81; p = 0.001 in Ua), and NLR was associated with PFS only in the univariate analysis (HR, 1.71; 95% CI, 1.04–2.81; p =0.035 in Ua; HR, 1.79; 95% CI, 0.65–4.89; P =0.257 in Ma), but MLR was not associated with DFS (HR, 0.36; 95% CI, 0.03–4.13; p =0.409 in Ua).

Conclusions: Our results indicated that pretreatment NLR and PLR were biomarkers of poor prognosis in patients with endometrial cancer. The results indicated that NLR or PLR was associated with OS and disease-free survival DFS, and NLR was associated with PFS only in univariate analysis, but MLR was not associated with OS or DFS.

Keywords: endometrial cancer, neutrophil-to-lymphocyte ratio, monocyte-to-lymphocyte ratio, prognosis, platelet–to–lymphocyte ratio

INTRODUCTION

Endometrial cancer (EC) is one of the most common malignant tumors in women, mostly in postmenopausal women. Each year, more than 140,000 women worldwide suffer from endometrial cancer, and it is estimated that more than 40,000 women die from this cancer (1). In recent years, the incidence of endometrial cancer has remained high and has a trend in the younger generation (2, 3). At present, the first choice of treatment is surgery, supplemented by radiotherapy and/or chemotherapy. However, a systematic review reported an overall recurrence risk of 13% for all endometrial cancer patients and 3% for patients at low risk (4). Therefore, we urgently need effective biomarkers for an individualized prediction of the treatment outcome and prognosis of endometrial cancer.

In recent years, many studies have confirmed that the occurrence and development of malignant tumors are closely related to inflammation, and the level of inflammation indicators can affect the prognosis of patients with malignant tumors. Among the common inflammatory indicators: neutrophil–lymphocyte ratio (NLR) has played a good predictive role in the prognosis of patients with colorectal cancer, gastric cancer, liver cancer, pancreatic cancer, ovarian cancer, breast cancer and urological tumors (5–7). Pretreatment thrombocytosis is related to the decreased survival rate of lung cancer, kidney cancer, ovarian cancer, vulvar cancer, and cervical cancer. Some studies have also reported that the platelet-to-lymphocyte ratio (PLR) and the monocyte-to-lymphocyte ratio (MLR) have been shown to be associated with the poor prognosis of a series of malignant tumors (8–14). However, they are still controversial for predicting the prognosis of endometrial cancer patients. Jianpei Li (15) concluded that C-reactive protein (CRP) was identified as the independent prognostic factor, but not NLR or PLR or MLR. Furthermore, Rong Cong et al. (16) indicated that the pretreatment NLR, PLR, and MLR were independent prognostic markers for OS in EC patients, and the combination of NLR, PLR, and MLR provided better prognostic value than any single ratio. As more studies are published, the prognostic values of NLR, PLR, or MLR in EC are still unclear. Therefore, the purpose of this study is to explore the influence of preoperative NLR, PLR, and MLR on predicting the prognosis of endometrial cancer patients.

MATERIALS AND METHODS

Search Strategy

A systematic review was performed in accordance with the Preferred Reporting Items for Systematic Reviews and Meta-analyses guideline (registered name: Jiali Leng; ID number: CRD42021227644). We conducted a systematic literature search for potentially eligible studies. We searched PubMed, EMBASE, the Cochrane Library, CNKI, WanFang, VIP, and CBM databases systematically using the following key terms: ("platelet lymphocyte ratio" OR "PLR" OR "neutrophil lymphocyte ratio" OR "NLR" OR "monocyte lymphocyte ratio" OR "MLR") AND ("endometrial neoplasms" OR "endometrial cancer") (see Appendix for details). The search was updated in October 2020 without language or date restrictions.

Selection Criteria

Eligible studies must fulfill all of the following criteria (1): patients with endometrial cancer diagnosed by histopathology (2), provide pretreatment cutoff values of NLR or PLR or MLR (3), provided a hazard ratio (HR) with the corresponding 95% confidence interval (CI) (4), the measured outcome indicators include overall survival (OS) or progression-free survival (PFS) or disease-free survival (DFS), and (5) the included studies were cohort studies. The exclusion criteria were as follows (1): insufficient data for estimating HR and 95% CI values and (2) full text is not unavailable. All evaluations were independently conducted by two reviewers to ensure the comprehensiveness and accuracy of the included studies.

Data Extraction

Two investigators independently collected information from each included eligible study. The data were extracted as follows: name of the first author, country of study, year of publication, sample size, age, follow-up time, tumor FIGO staging, histological type, tumor grade, treatment method, interval between blood count measurement and surgical treatment, cutoff value of each inflammation indicators (NLR, PLR, and MLR), and the corresponding HR and 95% CI values of OS, PFS, or DFS. Two reviewers independently evaluated each study and reached a consensus after a discussion.

Quality Assessment

Two independent investigators use the Newcastle Ottawa Quality Assessment Scale (NOS) (17) to evaluate the quality of the eligible studies. An article with a NOS score of 6 or more stars was considered as a high-quality article.

Statistical Analysis

HR and 95% CI were used to assess the association between NLR/PLR/MLR and OS, DFS, and PFS. Cochran's *Q* test and Higgins I^2 statistic were used to test the heterogeneity of the combined data. Random-effects model was adopted in all of our studies. We further conducted subgroup analyses by race (Asian or non-Asian), sample (<300 or ≥300), treatment (surgery or surgery + chemistry or surgery + radiation or surgery + chemistry + radiation), NLR cutoff value (<2.20 or ≥2.20), PLR cutoff value (<175 or ≥175), and MLR cutoff value (<0.20 or ≥0.20). Egger's test was used to assess the publication bias, and P <0.05 was considered statistically significant. All statistical analyses were performed using STATA 12.0 software.

RESULTS

Search Results and Eligible Study Characteristics

A total of 716 articles from the primary literature were searched in the databases of Cochrane Library, PubMed, EMBASE, CNKI, WanFang, VIP, and CBM. A flow chart for the selection of eligible studies is presented in **Figure 1**. First of all, 208 duplicate records were found and removed. Then, 482 studies were excluded after the initial evaluation of titles and abstracts. Among the remaining 26 articles, 12 were further excluded because they were letters, meeting abstracts, or had insufficient data. Finally, 14 available studies were included in this meta-analysis (15, 16, 18–29).

The characteristics of the 14 studies are summarized in **Table 1**. Of the 14 publications, 11 assessed the relationship between NLR and OS in univariate analysis (Ua) and 10 in multivariate analysis (Ma), 4 studies evaluated the association between NLR and DFS in Ua and 2 studies in Ma, 2 assessed the relationship between NLR and PFS in Ua and 2 in multivariate analysis, 8 studies evaluated the association between PLR and OS in Ua and 6 studies in Ma, four evaluated between PLR and DFS in Ua, 5 studies evaluated the association between MLR and OS in Ua and 4 studies in Ma, and two evaluated between MLR and DFS in Ua. A total of 5,274 patients were enrolled, with sample numbers ranging from 32 to 1,111. The study quality assessment, as per the Newcastle–Ottawa Quality Assessment Scale, yielded scores ranging from 6 to 8, with a mean score of 7.1.

Association of Pre-Treatment NLR With Overall Survival

The association between NLR and OS was assessed in 11 studies in univariate analysis consisting of 4,235 patients and 10 studies in multivariate analysis consisting of 3,817 patients. Our results showed that NLR was associated with OS (HR, 2.51; 95% CI, 1.70–3.71; p <0.001 in Ua; HR, 1.87; 95% CI, 1.34–2.60, p <0.001 in Ma) (**Figure 2A**, **B**). We also performed a subgroup analysis by race, cutoff value, sample size, and treatment (**Table 2**). A further subgroup analysis found that this correlation was not affected by race (Asian: HR, 3.09; 95% CI, 1.96–4.87; p <0.001 in Ua; HR, 2.11; 95% CI, 1.54–2.91, p <0.001 in Ma) or NLR cutoff value (<2.20: HR, 2.62; 95% CI, 1.38–4.99; p =0.003 in Ua; HR, 2.31; 95% CI, 1.44–3.70; p <0.001 in Ma; ≥2.20: HR, 2.50; 95% CI, 1.36–4.58; p =0.003 in Ua; HR, 1.60; 95% CI, 1.09–2.36; p =0.016 in Ma) or sample size (<300: HR, 2.73; 95% CI, 1.59–4.68; p <0.001 in Ua; HR, 1.77; 95% CI, 1.40–2.23, p <0.001 in Ma; ≥300: HR, 2.34; 95% CI, 1.14–4.82,

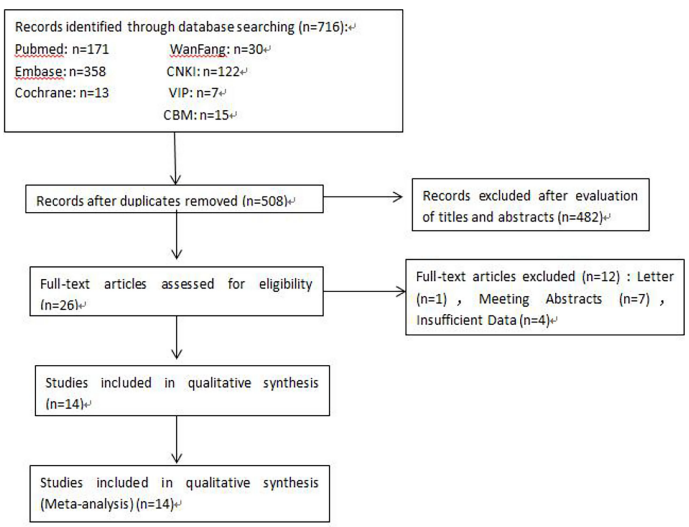


FIGURE 1 | Screening flow chart.

TABLE 1 | Characteristics of the included studies.

Study	Country	Sample size	Age (year)	Follow-up (months)	Tumor stage	Histological type	Tumor grade	Treatment	Interment	Inflammatory indicators	Outcome indicators	NOS scores
Tadashi Aoyama 2019	Japan	197	Median, 59	Unclear	I – IV	Endometrioid, other	1–3	S	Unclear	NLR, PLR	OS, PFS	7
Günsu Kimyon Cömert, 2018	Turkey	497	Median, 58	Median, 24	I – IV	Endometrioid, clear cell, serous, mucinous, mixed, undifferentiated, not reported	1–3	S, C, R	8 ± 6 days	NLR, PLR, MLR	OS, DFS	7
Rong Cong, 2020	China	1,111	Median, 56	Median, 40	I – IV	Endometrioid, stromal sarcoma, clear cell, serous, carcinosarcoma, mixed	1–3	S	Within 2 weeks	NLR, PLR, MLR	OS	7
M Cummings, (20)	UK	605	Median, 65	Median, 81.5	I – IV	Endometrioid, clear cell, serous, carcinosarcoma, mixed	1–3	S, C, R	Within 2 weeks	NLR, PLR, MLR	OS	8
Ling Ding, 2017	China	185	Mean, 59.29	Mean, 65.84 ± 24.73	I – IV	Type I, type II	1–3	S, C, R	Within 1 week	NLR, PLR	OS, DFS	8
Wan Kyu Eo,2016	Korea	255	Median, 44	Median, 51.3	I – IV	Endometrioid, clear cell, serous, mixed, undifferentiated, mucinous, squamous	1–3	S	Within 2 weeks	NLR, PLR, MLR	OS, DFS	6
Tomoko Haruma, 2015	Japan	320	Median, 57.5	1–130	I – IV	Endometrioid, clear cell, serous, mixed, undifferentiated, squamous, carcinosarcoma	1–3	S, C	Within 1 month	NLR, PLR	OS、DFS	8
Kaori Kiuchi, 2018	Japan	32	Median, 59.5	Unclear	Clinical stage IV B	Endometrioid, serous, clear cell	1–3	S, C, R	Unclear	NLR, PLR	OS	7
Jianpei Li, 2015	China	282	Median, 53	75	I – IV	Type I, type II	1–3	S, C	within 2 weeks	NLR, PLR	OS	7
Isa Temur, 2018	Turkey	763	Median, 58	60	I – IV	Type I, type II	1–3	S, C, R	Unclear	NLR	OS	7
Miaolong He, 2013	China	212	Median, 54	Median, 57.5	I – IV	Endometrioid	1–3	S, C, R	Within 2 weeks	NLR	OS	7
Katarzyna Holub, 2020	France	155	Median, 63.1	Median, 46.5	I – III	Endometrioid, others	1–3	S, C, R	Within 3 months	NLR, MLR	OS, PFS	7
Ryoko Takahashi, 2015	Japan	508	Mean, 58	60	I – IV	Endometrioid, others	1–3	S, C, R	Before surgery	NLR	OS	6
Jing Wang, 2016	China	152	Mean, 58	Unclear	I – IV	Type I, type II	1–3	S (+ R)	Before surgery	NLR	OS, PFS	7

p =0.021 in Ua; HR, 1.87; 95% CI, 1.06–3.29; p =0.030 in Ma) or treatment (surgery: HR, 3.76; 95% CI, 2.67–5.30; p <0.001 in Ua; HR, 2.71; 95% CI, 1.83–4.02; p <0.001 in Ma; surgery + chemistry: HR, 4.09; 95% CI, 1.95–8.59; p <0.001 in Ua; HR, 2.83; 95% CI, 1.28–6.30, p =0.011 in Ma; surgery + chemistry + radiation: HR, 2.03; 95% CI, 1.39–2.96, p <0.001 in Ua; HR, 1.66; 95% CI, 1.15–2.40, p =0.006 in Ma).

Association of Pre-treatment NLR With DFS

The association between NLR and DFS was assessed in 4 studies in a univariate analysis consisting of 1,257 patients and 2 studies in a multivariate analysis consisting of 505 patients. Our meta-analysis showed that NLR was associated with DFS (HR, 2.50; 95% CI, 1.38–4.56, P =0.003 in Ua; HR, 2.06; 95% CI, 1.26–3.37; P =0.004 in Ma) (**Figure 3A**, **B**). A further subgroup analysis (**Table 3**) found that this correlation was not affected by race (Asian: HR, 3.19; 95% CI, 2.16–4.73, p <0.001 in Ua; HR, 2.06; 95% CI, 1.26–3.37, p =0.004 in Ma) or NLR cutoff value (<2.20: HR, 2.71; 95% CI, 1.26–5.82; p =0.011 in Ma; ≥2.20: HR, 2.70; 95% CI, 1.68–4.34; p <0.001 in Ua) or sample size (<300: HR, 4.11; 95% CI, 2.43–6.94, p <0.001 in Ua; HR, 2.71; 95% CI, 1.26–5.82; p =0.011 in Ma) or treatment (surgery: HR, 3.68; 95% CI, 1.55–8.75; p =0.003 in Ua; surgery + chemistry: HR, 2.37; 95% CI, 1.34–4.17; p =0.003 in Ua; surgery + chemistry + radiation: HR, 2.71; 95% CI, 1.26–5.82; p =0.011 in Ma).

Association of Pre-treatment NLR With PFS

The association between NLR and PFS was assessed in 2 studies in a univariate analysis consisting of 352 patients and 2 studies in

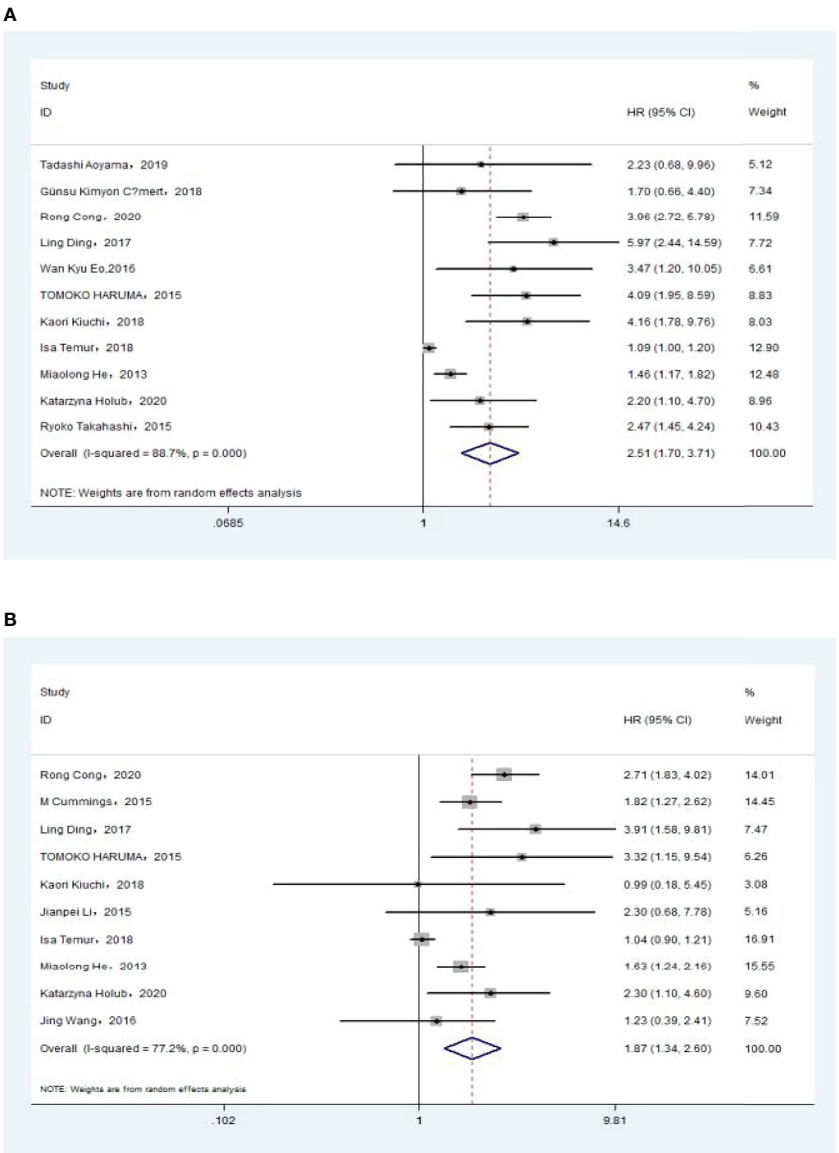


FIGURE 2 | **(A)**Relationship between *neutrophil–lymphocyte ratio (*NLR) and overall survival in univariate analysis. **(B)** Relationship between NLR and overall survival in multivariate analysis.

TABLE 2 | The results of the subgroup analysis for **neutrophil–lymphocyte ratio** (NLR) and overall survival are summarized below.

	HR	Lci	Ua				Ma	
			Hci	*P*	HR	Lci	Hci	*P*
NLR < 2.20	2.62	1.38	4.99	*P* = 0.003	2.31	1.44	3.70	*P* < 0.001
NLR ≥ 2.2	2.50	1.36	4.58	*P* = 0.003	1.60	1.09	2.36	*P* = 0.016
Asian	3.09	1.96	4.87	*P* < 0.001	2.11	1.54	2.91	*P* < 0.001
Non-Asian	1.41	0.87	2.27	*P* = 0.164	1.52	0.92	2.51	*P* = 0.101
Sample < 300	2.73	1.59	4.68	*P* < 0.001	1.77	1.40	2.23	*P* < 0.001
Sample ≥ 300	2.34	1.14	4.82	*P* = 0.021	1.87	1.06	3.29	*P* = 0.03
Surgery (S)	3.76	2.67	5.30	*P* < 0.001	2.71	1.83	4.02	*P* < 0.001
Surgery + chemistry (S+C)	4.09	1.95	8.59	*P* < 0.001	2.83	1.28	6.30	*P* = 0.011
Surgery + radiation (S+R)	–	–	–	–	1.23	0.49	3.04	*P* = 0.66
Surgery + chemistry + radiation (S+C+R)	2.03	1.39	2.96	*P* < 0.001	1.66	1.15	2.40	*P* = 0.006
Total	2.51	1.70	3.71	*P* < 0.001	1.87	1.34	2.60	*P* < 0.001

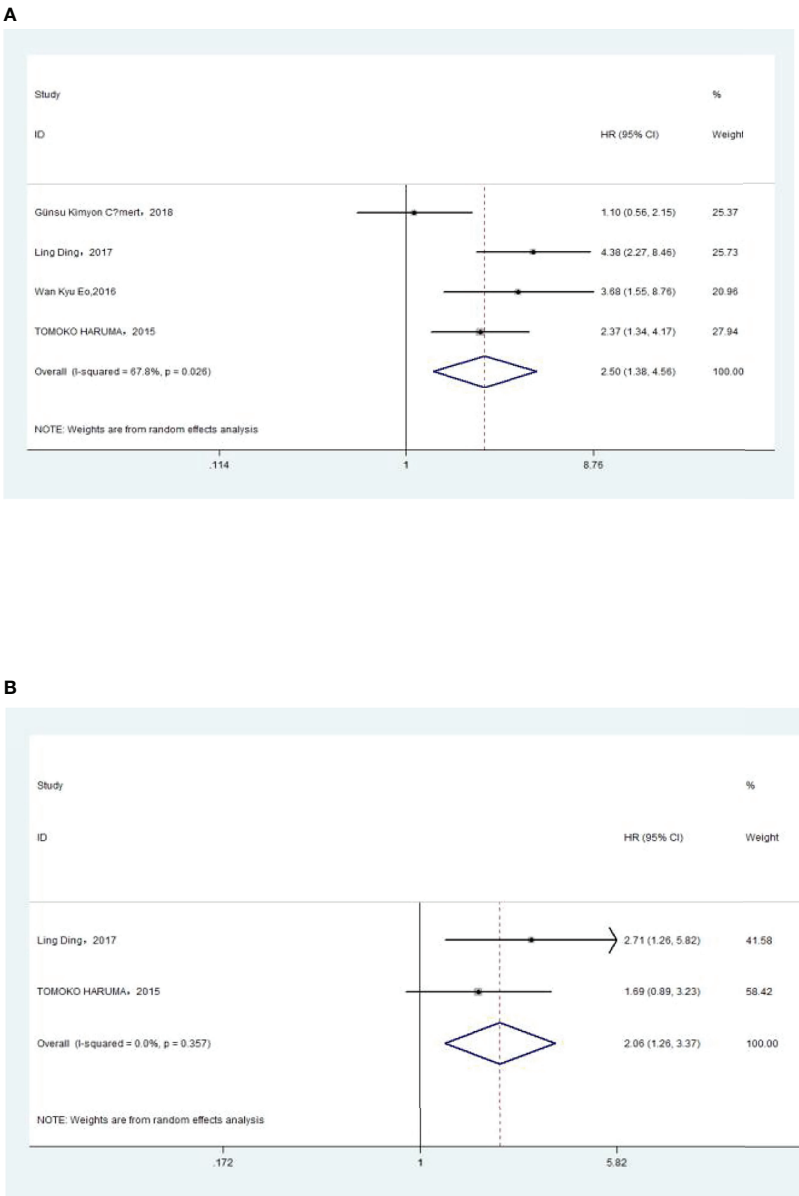


FIGURE 3 | **(A)** Relationship between neutrophil–lymphocyte ratio (NLR) and disease-free survival (DFS) in univariate analysis. **(B)** Relationship between NLR and DFS in multivariate analysis.

a multivariate analysis consisting of 349 patients. Our meta-analysis showed that NLR was associated with PFS only in the univariate analysis (HR, 1.71; 95% CI, 1.04–2.81; P =0.035 in Ua; HR, 1.79; 95% CI, 0.65–4.89; p =0.257 in Ma) (**Figure 4A**, **B**). A further subgroup analysis (**Table 4**) found that this correlation was not affected by race (Asian: HR, 2.36; 95% CI, 1.11–5.03, p =0.026 in Ua) or NLR cutoff value (<2.20: HR, 2.36; 95% CI, 1.11–5.03; p =0.026 in Ua; ≥2.20: HR, 2.79; 95% CI, 1.72–4.53; p <0.001 in Ma) or treatment (surgery: HR, 2.36; 95% CI, 1.11–5.03, p =0.026 in Ua; surgery + radiation: HR, 2.79; 95% CI, 1.72–4.53; p <0.001 in Ma).

Association of Pre-Treatment PLR With Overall Survival

The association between PLR and OS was assessed in 8 studies in a univariate analysis consisting of 3,202 patients and 6 studies in a multivariate analysis consisting of 3,012 patients. Our results showed that PLR was associated with OS (HR, 2.50; 95% CI, 1.82–3.43; p <0.001 in Ua; HR, 1.86; 95% CI, 1.22–2.83; p =0.004 in Ma) (**Figure 5A**, **B**). A further subgroup analysis (**Table 5**) found that this correlation was not affected by race (Asian: HR, 2.32; 95% CI, 1.44–3.75, p =0.001 in Ua; non-Asian: HR, 2.78; 95% CI, 2.01–3.84; p <0.001 in Ua; HR, 2.01; 95% CI, 1.42–2.84,

TABLE 3 | The results of the subgroup analysis for neutrophil–lymphocyte ratio (NLR) and disease-free survival are summarized below.

	Ua				Ma			
	HR	**Lci**	**Hci**	***P***	**HR**	**Lci**	**Hci**	***P***
NLR < 2.20	2.20	0.57	8.52	$P = 0.254$	2.71	1.26	5.82	$P = 0.011$
NLR ≥ 2.2	2.70	1.68	4.34	$P < 0.001$	1.69	0.89	3.23	$P = 0.110$
Asian	3.19	2.16	4.73	$P < 0.001$	2.06	1.26	3.37	$P = 0.004$
Non-Asian	1.10	0.56	2.16	$P = 0.781$	–	–	–	–
Sample < 300	4.11	2.43	6.94	$P < 0.001$	2.71	1.26	5.82	$P = 0.011$
Sample ≥ 300	1.65	0.78	3.49	$P = 0.191$	1.69	0.89	3.23	$P = 0.110$
S	3.68	1.55	8.75	$P = 0.003$	–	–	–	–
S+C	2.37	1.34	4.17	$P = 0.003$	1.69	0.89	3.23	$P = 0.110$
S+R	–	–	–	–	–	–	–	–
S+C+R	2.20	0.57	8.52	$P = 0.254$	2.71	1.26	5.82	$P = 0.011$
Total	2.50	1.38	4.56	$P = 0.003$	2.06	1.26	3.37	$P = 0.004$

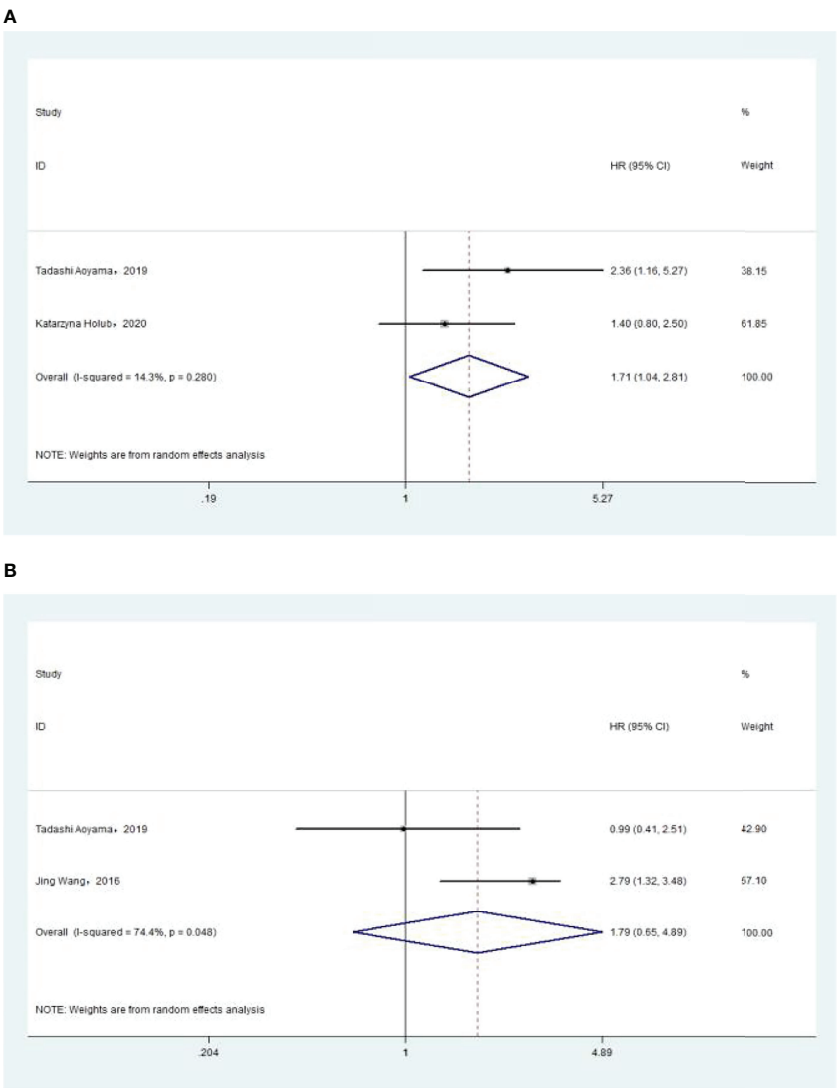


FIGURE 4 | **(A)** Relationship between neutrophil–lymphocyte ratio (NLR) and progression-free survival (PFS) in univariate analysis. **(B)** Relationship between NLR and PFS in multivariate analysis.

TABLE 4 | The results of the subgroup analysis for neutrophil–lymphocyte ratio (NLR) and progression-free survival are summarized below.

	Ua				Ma			
	HR	**Lci**	**Hci**	***P***	**HR**	**Lci**	**Hci**	***P***
NLR < 2.20	2.36	1.11	5.03	*P* = 0.026	0.99	0.40	2.45	*P* = 0.983
NLR ≥ 2.2	1.40	0.79	2.47	*P* = 0.247	2.79	1.72	4.53	*P* < 0.001
Asian	2.36	1.11	5.03	*P* = 0.026	1.79	0.65	4.89	*P* = 0.257
Non-Asian	1.40	0.79	2.47	*P* = 0.247	–	–	–	–
Sample < 300	–	–	–	–	–	–	–	–
Sample ≥ 300	–	–	–	–	–	–	–	–
S	2.36	1.11	5.03	P=0.026	0.99	0.40	2.45	*P* = 0.983
S+C	–	–	–	–	–	–	–	–
S+R	–	–	–	–	2.79	1.72	4.53	*P* < 0.001
S+C+R	1.40	0.79	2.47	P=0.247	–	–	–	–
Total	1.71	1.04	2.81	P=0.035	1.79	0.65	4.89	*P* = 0.257

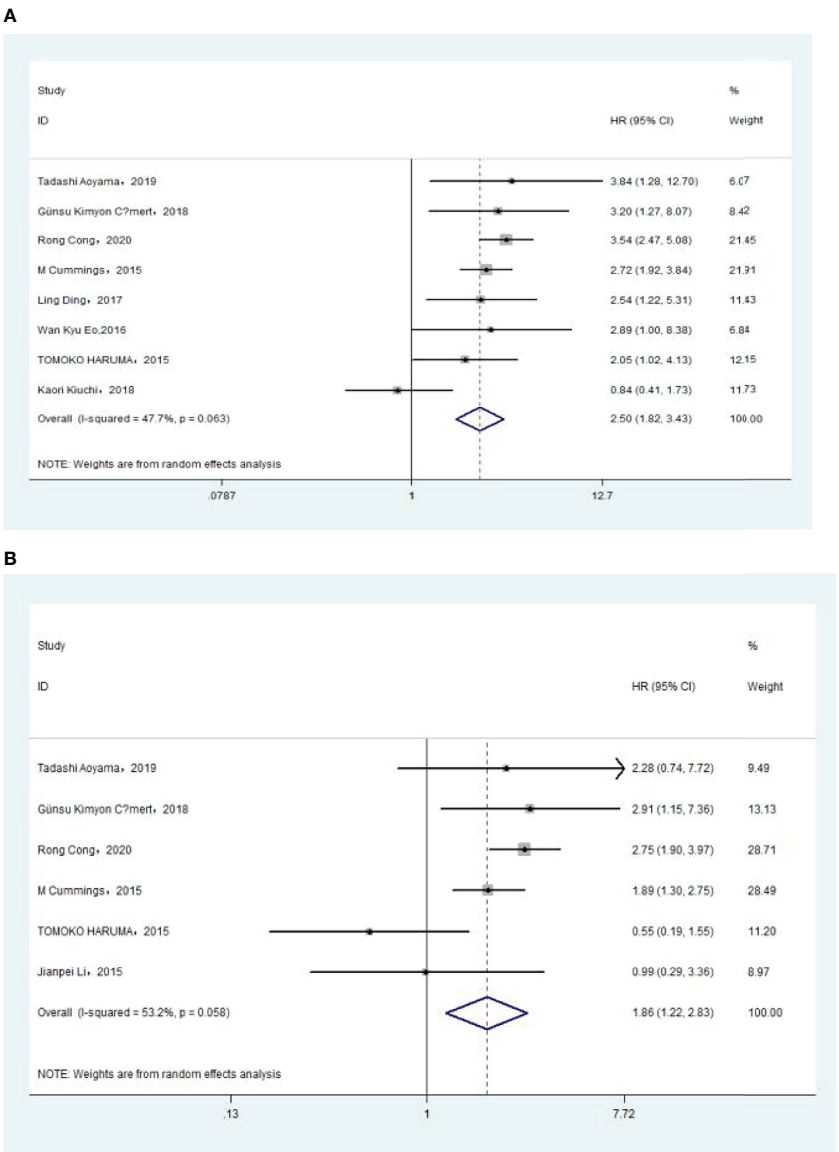


FIGURE 5 | **(A)** Relationship between platelet–lymphocyte ratio (PLR) and overall survival (OS) in univariate analysis. **(B)** Relationship between PLR and OS in multivariate analysis.

TABLE 5 | The results of the subgroup analysis for platelet–lymphocyte ratio and overall survival are summarized below.

	Ua				Ma			
	HR	**Lci**	**Hci**	***P***	**HR**	**Lci**	**Hci**	***P***
PLR < 175	3.06	2.32	4.05	*P* < 0.001	1.78	0.72	4.41	*P* = 0.214
PLR ≥ 175	2.14	1.10	4.15	*P* = 0.025	1.83	1.30	2.57	*P* = 0.001
Asian	2.32	1.44	3.75	*P* = 0.001	1.47	0.65	3.33	*P* = 0.353
Non-Asian	2.78	2.01	3.84	*P* < 0.001	2.01	1.42	2.84	*P* < 0.001
Sample < 300	2.05	1.01	4.16	*P* = 0.047	1.53	0.66	3.56	*P* = 0.325
Sample ≥ 300	2.96	2.36	3.72	*P* < 0.001	1.92	1.16	3.18	*P* = 0.011
S	3.50	2.52	4.85	*P* < 0.001	2.70	1.90	3.84	*P* < 0.001
S+C	2.05	1.02	4.13	*P* = 0.044	0.70	0.32	1.56	*P* = 0.385
S+R	–	–	–	–	–	–	–	–
S+C+R	2.09	1.19	3.66	*P* = 0.01	2.01	1.42	2.84	*P* = 0.001
Total	2.50	1.82	3.43	*P* < 0.001	1.86	1.22	2.83	*P* = 0.004

p <0.001 in Ma) or PLR cutoff value (<175: HR, 3.06; 95% CI, 2.32–4.05; *p* <0.001 in Ua; ≥175: HR, 2.14; 95% CI, 1.10–4.15; *p* =0.025 in Ua; HR, 1.83; 95% CI, 1.30–2.57; *p* =0.001 in Ma) or sample size (<300: HR, 2.05; 95% CI, 1.01–4.16; *p* =0.047 in Ua; ≥300: HR, 2.96; 95% CI, 2.36–3.72; *p* <0.001 in Ua; HR, 1.92; 95% CI, 1.16–3.18; *p* =0.011 in Ma) or treatment (surgery: HR, 3.50; 95% CI, 2.52–4.85; *p* <0.001 in Ua; HR, 2.70; 95% CI, 1.90–3.84; *p* <0.001 in Ma; surgery + chemotherapy: HR, 2.05; 95% CI, 1.02–4.13; *p* =0.044 in Ua; surgery + chemotherapy + radiation: HR, 2.09; 95% CI, 1.19–3.66; *p* =0.010 in Ua; HR, 2.01; 95% CI, 1.42–2.84; *p* <0.001 in Ma).

Association of Pre-Treatment PLR With DFS

The association between PLR and DFS was assessed in 4 studies in a univariate analysis consisting of 1,257 patients. Our meta-analysis showed that PLR was associated with DFS (HR, 1.91; 95% CI, 1.30–2.81; *p* =0.001 in Ua) (**Figure 6**). A further subgroup analysis (**Table 6**) found that this correlation was not affected by race (Asian: HR, 2.13; 95% CI, 1.47–3.08; *p* <0.001 in Ua) or PLR cutoff value (≥175: HR, 2.03; 95% CI, 1.09–3.77; *p* =0.025 in Ua) or sample size (<300: HR, 2.67; 95% CI, 1.64–4.37; *p* <0.001 in Ua) or treatment (surgery: HR, 3.08; 95% CI, 1.30–7.31; *p* =0.011 in Ua).

Association of Pre-Treatment MLR With Overall Survival

The association between MLR and OS was assessed in 5 studies in a univariate analysis consisting of 2,623 patients and 4 studies in a multivariate analysis consisting of 2,126 patients. Our results showed that MLR was not associated with OS (HR, 1.44; 95% CI, 0.70–2.95; *p* =0.325 in Ua; HR, 1.01; 95% CI, 0.39–2.60; *p* =0.987 in Ma) (**Figure 7A, B**). A further subgroup analysis (**Table 7**) found that this correlation was not affected by race (Asian: HR, 0.23; 95% CI, 0.00–22.06; *p* =0.528 in Ua; HR, 0.37; 95% CI, 0.02–8.45; *p* =0.532 in Ma; non-Asian: HR, 2.30; 95% CI, 0.51–10.36; *p* =0.278 in Ma) or MLR cutoff value (<0.20: HR, 2.30; 95% CI, 0.51–10.36; *p* =0.278 in Ma; ≥0.20: HR, 0.23; 95% CI, 0.00–22.06; *p* =0.528 in Ua; HR, 0.37; 95% CI, 0.02–8.45; *p* =0.532 in Ma) or sample size (<300: HR, 0.33; 95% CI, 0.00–73.9; *p* =0.688 in Ua; HR, 0.63; 95% CI, 0.01–48.82; *p* =0.837 in Ma) or treatment (surgery: HR, 0.23; 95% CI, 0.00–22.06; *p* =0.528 in Ua; HR, 0.37; 95% CI, 0.02–8.45; *p* =0.532 in Ma; surgery + chemotherapy + radiation: HR, 2.30; 95% CI, 0.51–10.36; *p* =0.278 in Ma).

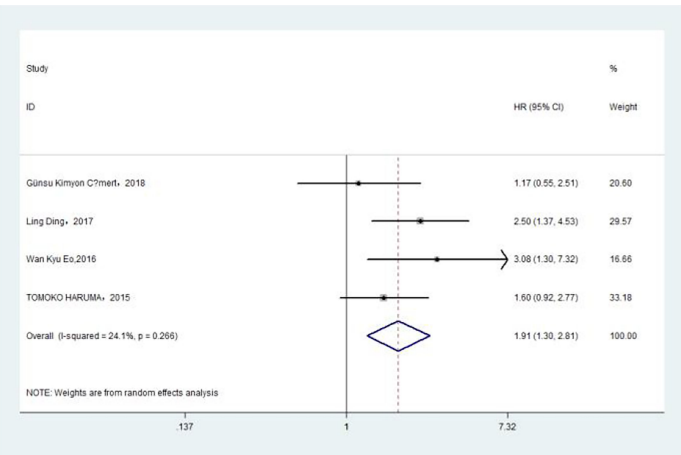


FIGURE 6 | Relationship between platelet–lymphocyte ratio and disease-free survival in univariate analysis.

TABLE 6 | The results of the subgroup analysis for platelet–lymphocyte ratio (PLR) and disease-free survival are summarized below.

			Ua	
	HR	**Lci**	**Hci**	***P***
PLR < 175	1.78	0.85	3.72	*P* = 0.129
PLR ≥ 175	2.03	1.09	3.77	*P* = 0.025
Asian	2.13	1.47	3.08	*P* < 0.001
Non-Asian	1.17	0.55	2.50	*P* = 0.685
Sample < 300	2.67	1.64	4.37	*P* < 0.001
Sample ≥ 300	1.44	0.92	2.24	*P* = 0.112
S	3.08	1.30	7.31	*P* = 0.011
S+C	1.60	0.92	2.77	*P* = 0.095
S+R	–	–	–	–
S+C+R	1.78	0.85	3.72	*P* = 0.129
Total	1.91	1.30	2.81	*P* = 0.001

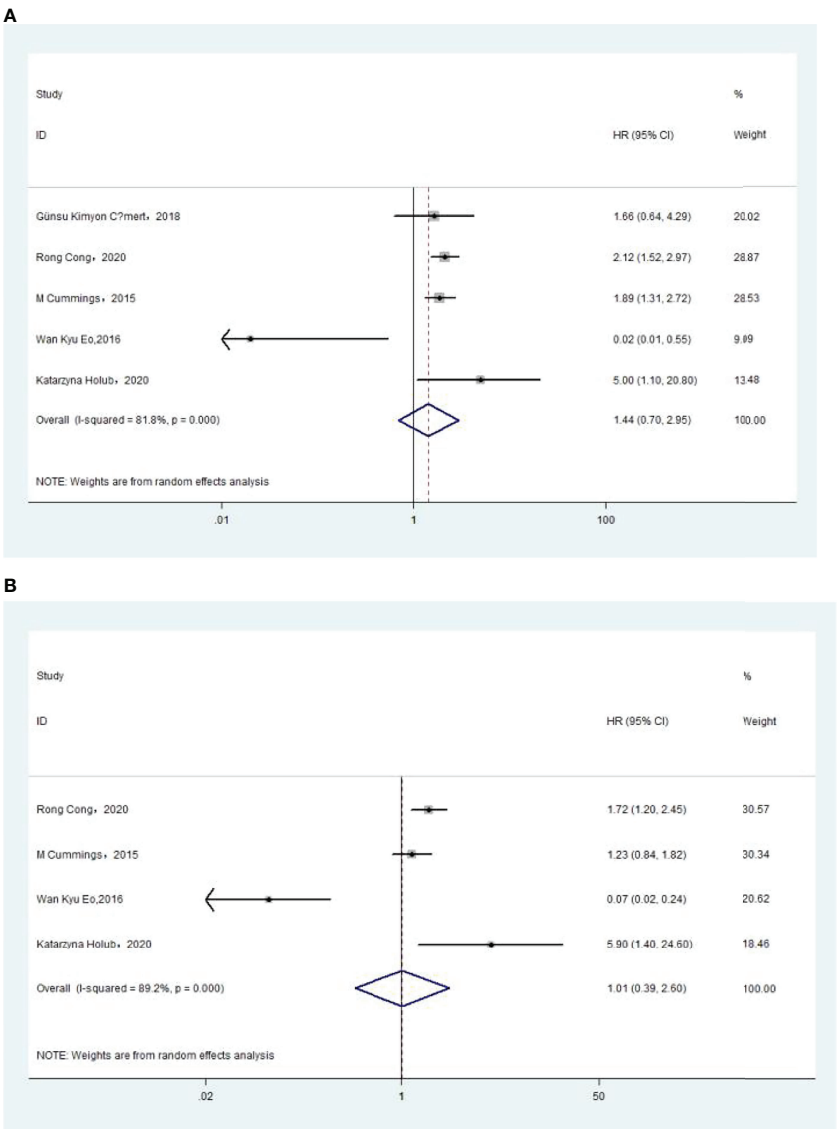


FIGURE 7 | **(A)** Relationship between monocyte–lymphocyte ratio (MLR) and overall survival (OS) in univariate analysis. **(B)** Relationship between MLR and OS in multivariate analysis.

TABLE 7 | The results of the subgroup analysis for monocyte–lymphocyte ratio (MLR) and overall survival are summarized below.

	Ua				Ma			
	HR	**Lci**	**Hci**	***P***	**HR**	**Lci**	**Hci**	***P***
MLR < 0.20	1.96	1.40	2.73	$P < 0.001$	2.30	0.51	10.36	$P = 0.278$
MLR ≥ 0.2	0.23	0.00	22.06	$P = 0.528$	0.37	0.02	8.45	$P = 0.532$
Asian	0.23	0.00	22.06	$P = 0.528$	0.37	0.02	8.45	$P = 0.532$
Non-Asian	1.96	1.40	2.73	$P < 0.001$	2.30	0.51	10.36	$P = 0.278$
Sample < 300	0.33	0.00	73.90	$P = 0.688$	0.63	0.01	48.82	$P = 0.837$
Sample ≥ 300	1.99	1.57	2.52	$P < 0.001$	1.47	1.06	2.04	$P = 0.022$
S	0.23	0.00	22.06	$P = 0.528$	0.37	0.02	8.45	$P = 0.532$
S+C	–	–	–	–	–	–	–	–
S+R	–	–	–	–	–	–	–	–
S+C+R	1.96	1.40	2.73	$P < 0.001$	2.30	0.51	10.36	$P = 0.278$
Total	1.44	0.70	2.95	$P = 0.325$	1.01	0.39	2.60	$P = 0.987$

Association of Pre-treatment MLR With DFS

The association between MLR and DFS was assessed in 2 studies in a univariate analysis consisting of 752 patients. Our meta-analysis showed that MLR was also not associated with DFS (HR, 0.36; 95% CI, 0.03–4.13; p =0.409 in Ua) (**Figure 8**). A further subgroup analysis (**Table 8**) found that this correlation was not affected by race (non-Asian: HR, 1.22; 95% CI, 0.62–2.39; p =0.562 in Ua) or MLR cutoff value (<0.20: HR, 1.22; 95% CI, 0.62–2.39; p =0.562 in Ua) or sample size (≥300: HR, 1.22; 95% CI, 0.62–2.39; p =0.562 in Ua) or treatment (surgery + chemotherapy + radiation: HR, 1.22; 95% CI, 0.62–2.39; p =0.562 in Ua).

Publication Bias Analysis

In the univariate analysis (Ua), 11 articles on the relationship between NLR and OS were included in the study. The funnel plots showed that NLR and overall survival were roughly symmetrical. The funnel plots showed a low probability of publication bias. Consistently, the Egger's test suggested that NLR and OS did not have a publication bias ($P = 0.384 > 0.05$) (**Figure 9**).

In the multivariate analysis (Ma), 10 articles on the relationship between NLR and OS were included in the study. The funnel plots showed a low probability of publication bias. Consistently, the Egger's test suggested that NLR and OS did not have a publication bias ($P = 0.986 > 0.05$) (**Figure 10**).

DISCUSSION

Our pooled data of prognosis in the endometrial cancer patients suggest that NLR or PLR was associated with OS and DFS, and NLR was associated with PFS only in a univariate analysis, but MLR was not associated with OS or DFS.

Previous studies of Liwei Ni et al. (30) had shown that high levels of pretreatment NLR and PLR were associated with decreased OS and DFS in patients with endometrial cancer. In our study, we more comprehensively analyzed the associations between inflammatory markers with PFS and added an inflammatory marker, which was MLR. However, Liwei Ni concluded that NLR higher than the cutoff was associated with a shorter OS and poorer PFS. In contrast, our further subgroup

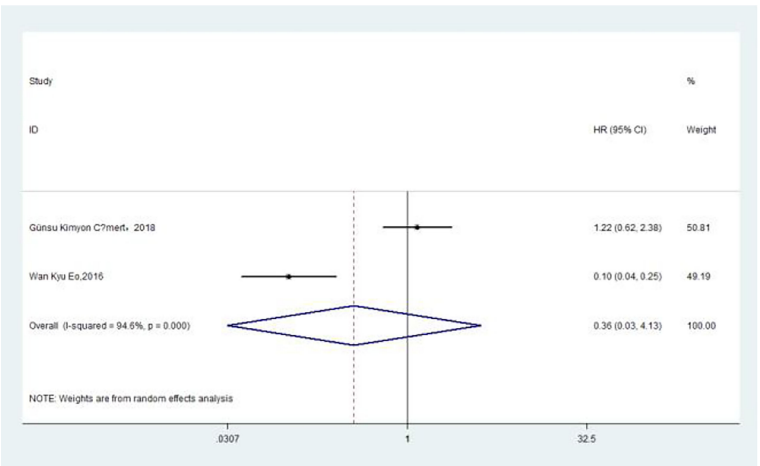


FIGURE 8 | Relationship between monocyte–lymphocyte ratio and disease-free survival in univariate analysis.

TABLE 8 | The results of the subgroup analysis for monocyte–lymphocyte ratio (MLR) and disease-free survival are summarized below.

			Ua	
	HR	**Lci**	**Hci**	**P**
MLR < 0.2	1.22	0.62	2.39	*P* = 0.562
MLR ≥ 0.2	0.10	0.04	0.25	*P* < 0.001
Asian	0.10	0.04	0.25	*P* < 0.001
Non-Asian	1.22	0.62	2.39	*P* = 0.562
Sample < 300	0.10	0.04	0.25	*P* < 0.001
Sample ≥ 300	1.22	0.62	2.39	*P* = 0.562
S	0.10	0.04	0.25	*P* < 0.001
S+C	–	–	–	–
S+R	–	–	–	–
S+C+R	1.22	0.62	2.39	*P* = 0.562
Total	0.36	0.03	4.13	*P* = 0.409

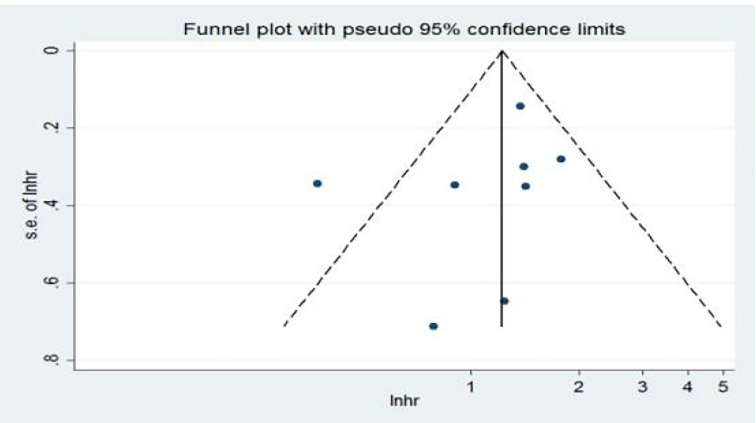


FIGURE 9 | Funnel plots of the relationship between neutrophil–lymphocyte ratio and overall survival in univariate analysis.

analysis showed that the higher levels of pretreatment markers (NLR ≥ 2.20, PLR ≥ 175, and MLR ≥ 0.20) were not relevant to poorer survival outcomes.

Campbell SD Roxburgh (31) first discovered the role of systemic inflammatory response in predicting the survival of cancer patients. He stated that the progression of a disease depended on the inflammatory response between the tumor and the host, and the systemic inflammatory response of the host was an important independent prognostic factor for tumor prognosis. Campbell SD Roxburgh had shown that preoperative measures of systemic inflammatory response predicted survival outcomes of operable cancers, not being affected by tumor stage. Clinically, the most common indicators of systemic inflammatory response in cancer patients are biochemical or hematological indicators. As the new prognostic biomarkers, NLR, PLR, and MLR have been the focus in recent years. Francesmary et al. (32) hypothesized that endometrial cancer might be associated with long-term inflammatory stimulation. The periodic stripping of the endometrium, known as menstruation, is essentially a chronic inflammatory process: the thickness of the endometrium is significantly thickened in the hyperplasia period, the stroma is highly edematous in the middle stage of secretion, and the uterine spiral artery is proliferated and curled. In the menstrual period, prostaglandin stimulates the myometrium, causes uterine muscle contraction, and causes uterine spiral arteriole spasm for a long time; thus, the blood flow of the endometrium decreases, and endometrial ischemic necrosis occurred, eventually leading to the stripping of ischemic and necrotic endometrium. Due to "temporary amenorrhea" during pregnancy, the endometrium can rest and protect during pregnancy, reducing the possibility of endometrium malevolence. Infertility or delayed menopause increases the physiological inflammatory response time of the endometrium so that the endometrium is more likely to be exposed to an inflammatory environment, which increases the possibility of endometrium malevolence. Sun Tong et al. (33) found through Doppler ultrasound that there was abundant blood flow in the EC tumor tissue, and the detection rate of the blood flow in the tumor was more than 90%, which indicated t there was more angiogenesis in EC. Neutrophils secrete a large number of angiogenic factors in the blood circulation, which promote the rich blood flow in EC tumor tissue, and the formation and the distribution of blood vessels are extensive. Foreign literature had shown the peripheral hematological

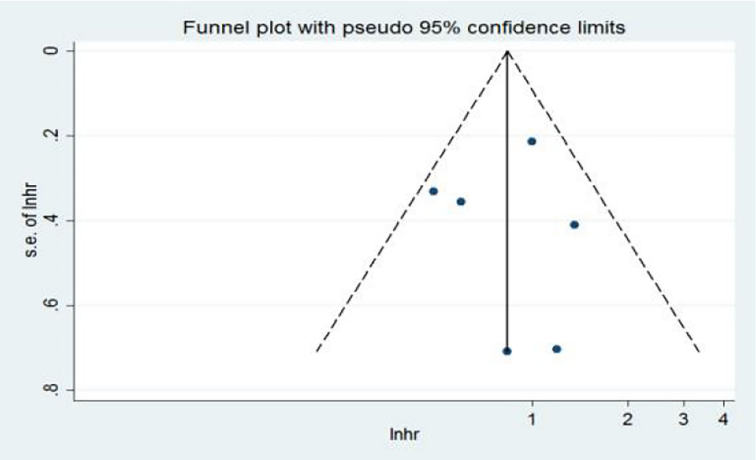


FIGURE 10 | Funnel plots of the relationship between neutrophil–lymphocyte ratio and overall survival in multivariate analysis.

changes in patients with EC: neutrophils increased, monocytes increased, and lymphocytes decreased, that is, NLR increased. The mechanism of NLR increase can be explained by the occurrence of an inflammatory reaction and an immune reaction in EC patients, the changes of blood inflammatory cells, and the production of corresponding antibodies in endometrial cells (34). Clinically, the peripheral hematological markers of inflammation in cancer patients are often associated with a relative increase in platelet count and a decrease in lymphocyte count. The increase in platelet count leads to platelet aggregation and platelet degranulation, which promotes tumor angiogenesis (35). At the same time, growth factors secreted by platelets in large amounts accelerate the proliferation of tumor cells, enhance the invasion, adhesion, and metastasis functions of tumor cells, and aggravate the poor prognosis of cancer patients (36). Ural et al. (37) found in an endometrial biopsy that the PLR of EC patients was significantly higher than that of the normal group and the endometrial hyperplasia group—that is, PLR can distinguish patients in the EC group from those in the normal pathological group. Acmaz et al. (38) also showed that PLR in the dysplasia and cancer group was significantly higher than that in the normal control group. At

TABLE 9 | Survival outcomes of patients stratified according to neutrophil–lymphocyte ratio (NLR), platelet–lymphocyte ratio (PLR) , and monocyte–lymphocyte ratio (MLR) cutoffs are summarized below.

	Ua		Ma	
	HR (95% CI)	***P***	**HR (95% CI)**	***P***
OS				
NLR < 2.20	2.62 (1.38–4.99)	*P* = 0.003	2.31 (1.44–3.70)	*P* < 0.001
NLR ≥ 2.20	2.50 (1.36–4.58)	*P* = 0.003	1.60 (1.09–2.36)	*P* = 0.016
PLR < 175	3.06 (2.32–4.05)	*P* < 0.001	1.78 (0.72–4.41)	*P* = 0.214
PLR ≥ 175	2.14 (1.10–4.15)	*P* = 0.025	1.83 (1.30–2.57)	*P* = 0.001
MLR < 0.20	1.96 (1.40–2.73)	*P* < 0.001	2.30 (0.51–10.36)	*P* = 0.278
MLR ≥ 0.20	0.23 (0.00–22.06)	*P* = 0.528	0.37 (0.02–8.45)	*P* = 0.532
PFS				
NLR < 2.20	2.36 (1.11–5.03)	*P* = 0.026	0.99 (0.40–2.45)	*P* = 0.983
NLR ≥ 2.20	1.40 (0.79–2.47)	*P* = 0.247	2.79 (1.72–4.53)	*P* < 0.001
PLR < 175	–	–	–	–
PLR ≥ 175	–	–	–	–
MLR < 0.20	–	–	–	–
MLR ≥ 0.20	–	–	–	–
DFS				
NLR < 2.20	2.20 (0.57–8.52)	*P* = 0.254	2.71 (1.26–5.82)	*P* = 0.011
NLR ≥ 2.20	2.70 (1.68–4.34)	*P* < 0.001	1.69 (0.89–3.23)	*P* = 0.110
PLR < 175	1.78 (0.85–3.72)	*P* =0.129	–	–
PLR ≥ 175	2.03 (1.09–3.77)	*P* = 0.025	–	–
MLR < 0.20	1.22 (0.62–2.39)	*P* = 0.562	–	–
MLR ≥ 0.20	0.10 (0.04–0.25)	*P* < 0.001	–	–

95% CI, 95% confidence intervals; HR, hazard ratios; OS, overall survival; PFS, progression-free survival; DFS, disease-free survival; Ua, univariate analysis; Ma, multivariate analysis.

present, there is no literature report on NLR, PLR, and MLR combined score grouping to evaluate the prognosis of EC patients.

Previous studies reported that NLR or PLR or MLR level was significantly associated with a certain survival outcome—for instance, Günsu Kimyon Cömert et al. (18) showed that PLR was associated with worse OS, and the cutoff value of PLR was 168 for OS. However, NLR and MLR were not associated with worse OS or DFS. Tadashi Aoyama et al. (19) found that NLR was associated with lymph node metastasis and that PLR was associated with worse PFS. Their receiver operating characteristic curves demonstrated that the best cutoff value of NLR for predicting lymph node metastasis was 2.18 and that of PLR was 206. The study of Rong Cong et al. (16) indicates that pretreatment NLR, PLR, and MLR are independent prognostic markers for OS in EC patients, and the combination of NLR, PLR, and MLR provides a better prognostic value than any single ratio. The cutoff value is 2.14 for NLR, 131.82 for PLR, and 0.22 for MLR. Cummings M (20) showed that both NLR and PLR were independent prognostic indicators for endometrial cancer for overall survival. MLR was also associated with worse OS only in the univariable analysis. The study of Ling Ding (21) showed that NLR and PLR were associated with worse OS and DFS, and the cutoff value of PLR was 123.5 and of NLR was 1.81. Wan Kyu Eo (22) found that MLR was associated with worse OS and DFS. Tomoko Haruma (23) showed that the DFS and OS rates of patients with a high NLR were significantly shorter than those for patients with a low NLR. Tomoko Haruma thought that pre-treatment NLR is a predictor of poor prognosis in endometrial cancer. Jianpei Li (15) had first found that CRP, except NLR or PLR, was identified as an independent prognostic factor in endometrial cancer. Isa Temur (24), Miaolong He (25), and Jing Wang (27) respectively reported that NLR was shown to be an independent prognostic biomarker in endometrium cancer. Holub (26) showed that pre-treatment NLR and MLR were associated with a worse survival outcome in endometrial cancer patients, and the cutoff value was 2.2 for NLR, 0.18 for MLR. Different studies choose different cutoff values and have different sample sizes. We pooled these studies to arrive at a fairly reliable conclusion. However, we do know that, in many studies NLR, PLR, and MLR are used as a continuous rather than a dichotomous variable, and the cutoff is really variable across studies. The fixed cutoff value by our article, such as 2.2 for NLR, should not be generalized. The selection of a cutoff value has limitations, and we still need a larger-sample-size study to determine a more clinically meaningful cutoff value.

However, some limitations in our meta-analysis should be mentioned. First, all of the included studies were retrospectively observational studies; thus, our results were based on unadjusted estimates; more accurate outcomes would result from adjustments for other confounders, such as age, body mass index, lifestyle, and so on. Second, the articles that only included *14 eligible studies, including 5,274 patients* in this analysis, were insufficient, especially in terms of the subgroup analysis—the sample size might not be large enough to support the outcome stability and to conduct detailed subgroup analyses. Thus, a potential publication bias is very likely to exist in spite of the fact that no evidence was obtained from our statistical tests. Third, the language of the studies was limited to English and Chinese, which may result in potential language bias. What is more, the variable cutoff values of NLR (and PLR and MLR) might bring about noticeable heterogeneity, and the insight into whether these values were influenced by other conditions remains uncertain.

As new prognostic biomarkers, NLR, PLR, and MLR have been the subject of intense research in recent years. The remarkable advantages of the prognostic factor (NLR, PLR, and MLR) are that they can be obtained from routine clinical blood tests, which is convenient, affordable, and repeatable. They represent the dawn of the age of prognosis.

CONCLUSIONS

In summary, our results indicated that pretreatment NLR and PLR were biomarkers of poor prognosis in patients with endometrial cancer. The results (shown in **Table 9**) indicated that NLR or PLR was associated with OS and DFS, and NLR was associated with PFS only in the univariate analysis, but MLR was not associated with OS or DFS. Larger sample sizes of different ethnic populations are required to confirm our findings.

DATA AVAILABILITY STATEMENT

The original contributions presented in the study are included in the article/**Supplementary Material**. Further inquiries can be directed to the corresponding author/s.

AUTHOR CONTRIBUTIONS

JL: project development, data collection, data analysis, manuscript writing. FW: data collection. LZ: project development. All authors contributed to the article and approved the submitted version.

SUPPLEMENTARY MATERIAL

The Supplementary Material for this article can be found online at: https://www.frontiersin.org/articles/10.3389/fonc.2022.734948/full#supplementary-material

REFERENCES

1. Amant F, Moerman P, Neven P, Timmerman D, Van Limbergen E, Vergote I. Endometrial Cancer. *Lancet (Lond Engl)* (2005) 366(9484):491–505. doi: 10.1016/S0140-6736(05)67063-8
2. Smrz SA, Calo C, Fisher JL, Salani R. An Ecological Evaluation of the Increasing Incidence of Endometrial Cancer and the Obesity Epidemic. *Am J Obstet Gynecol* (2021) 224(5):506.e1–.8. doi: 10.1016/j.ajog.2020.10.042
3. Qi J, Gao G. The Incidence and the Changing Tendency of Attack Age of Cervical Cancer and Endometrial Cancer in 22 Years. *J Chin J Clin Oncol* (2001) 07):39–41.
4. Fung-Kee-Fung M, Dodge J, Elit L, Lukka H, Chambers A, Oliver T. Follow-Up After Primary Therapy for Endometrial Cancer: A Systematic

Review. *Gynecol Oncol* (2006) 101(3):520–9. doi: 10.1016/j.ygyno.2006.02.011
5. Azab B, Bhatt VR, Phookan J, Murukutla S, Kohn N, Terjanian T, et al. Usefulness of the Neutrophil-to-Lymphocyte Ratio in Predicting Short- and Long-Term Mortality in Breast Cancer Patients. *Ann Surg Oncol* (2012) 19 (1):217–24. doi: 10.1245/s10434-011-1814-0
6. Cho H, Hur HW, Kim SW, Kim SH, Kim JH, Kim YT, et al. Pre-Treatment Neutrophil to Lymphocyte Ratio is Elevated in Epithelial Ovarian Cancer and Predicts Survival After Treatment. *Cancer Immunol Immunother CII* (2009) 58(1):15–23. doi: 10.1007/s00262-008-0516-3
7. Mjaess G, Chebel R, Karam A, Moussa I, Pretot D, Abi Tayeh G, et al. Prognostic Role of Neutrophil-to-Lymphocyte Ratio (NLR) in Urological Tumors: An Umbrella Review of Evidence From Systematic Reviews and Meta-Analyses. *Acta Oncol (Stockholm Sweden)* (2021) 60(6):704–13. doi: 10.1080/0284186X.2021.1886323
8. Bhatti I, Peacock O, Lloyd G, Larvin M, Hall RI. Preoperative Hematologic Markers as Independent Predictors of Prognosis in Resected Pancreatic Ductal Adenocarcinoma: Neutrophil-Lymphocyte Versus Platelet-Lymphocyte Ratio. *Am J Surgery* (2010) 200(2):197–203. doi: 10.1016/j.amjsurg.2009.08.041
9. Gücer F, Moser F, Tamussino K, Reich O, Haas J, Arikan G, et al. Thrombocytosis as a Prognostic Factor in Endometrial Carcinoma. *Gynecologic Oncol* (1998) 70(2):210–4. doi: 10.1006/gyno.1998.5078
10. Shimada H, Takiguchi N, Kainuma O, Soda H, Ikeda A, Cho A, et al. High Preoperative Neutrophil-Lymphocyte Ratio Predicts Poor Survival in Patients With Gastric Cancer. *Gastric Cancer Off J Int Gastric Cancer Assoc Japanese Gastric Cancer Assoc* (2010) 13(3):170–6. doi: 10.1007/s10120-010-0554-3
11. Tomita M, Shimizu T, Ayabe T, Yonei A, Onitsuka T. Preoperative Neutrophil to Lymphocyte Ratio as a Prognostic Predictor After Curative Resection for non-Small Cell Lung Cancer. *Anticancer Res* (2011) 31(9):2995–8.
12. Gomez D, Morris-Stiff G, Toogood GJ, Lodge JP, Prasad KR. Impact of Systemic Inflammation on Outcome Following Resection for Intrahepatic Cholangiocarcinoma. *J Surg Oncol* (2008) 97(6):513–8. doi: 10.1002/jso.21001
13. Weimu X, Xu S, Liu J, Luo M, Tan H, Fan X, et al. Clinical Significance of Preoperative Neutrophil-Lymphocyte Ratio in Prognosis Evaluation of Patients With Hepatocellular Carcinoma. *J Med Equipment* (2018) 31(24):51–2.
14. Zhao G, Hu Y, Liu R, Shi F, Li H, Wang D, et al. Clinical Significance of Preoperative Neutrophil-Lymphocyte Ratio in Prognosis Assessment of Laryngeal Carcinoma. *J Chin J Otolaryngol Head Neck Surgery* (2016) 51 (02):112–6.
15. Li J, Lin J, Luo Y, Kuang M, Liu Y. Multivariate Analysis of Prognostic Biomarkers in Surgically Treated Endometrial Cancer. *PloS One* (2015) 10 (6):1–11. doi: 10.1371/journal.pone.0130640
16. Cong R, Kong F, Ma J, Li Q, Wu Q, Ma X. Combination of Preoperative Neutrophil-Lymphocyte Ratio, Platelet-Lymphocyte Ratio and Monocyte-Lymphocyte Ratio: A Superior Prognostic Factor of Endometrial Cancer. *BMC Cancer* (2020) 20(1):1–11. doi: 10.1186/s12885-020-06953-8
17. Wells G, Shea BO, Connell D. *The Newcastle-Ottawa Scale (Nos) For Assessing The Quality Of Nonrandomized Studies In Meta-Analysis*. Available at: http://www.ohri.ca/programs/clinical_epidemiology/oxford_ web.ppt.
18. Cömert GK, Türkmen O, Kar I, Sinaci S, Ergani SY, Karalök A, et al. Independent Predictors of Survival in Endometrium Cancer: Platelet-To-Lymphocyte Ratio and Platelet/Neutrophil/Monocyte-to-Lymphocyte Ratio. *J Turkish-German Gynecol Assoc* (2018) 19(2):78–86. doi: 10.4274/jtgga.2017.0112
19. Aoyama T, Takano M, Miyamoto M, Yoshikawa T, Kato K, Sakamoto T, et al. Pretreatment Neutrophil-To-Lymphocyte Ratio Was a Predictor of Lymph Node Metastasis in Endometrial Cancer Patients. *Oncol (Switzerland)* (2019) 96(5):259–67. doi: 10.1159/000497184
20. Cummings M, Merone L, Keeble C, Burland L, Grzelinski M, Sutton K, et al. Preoperative Neutrophil:Lymphocyte and Platelet:Lymphocyte Ratios Predict Endometrial Cancer Survival. *Br J Cancer* (2015) 113(2):311–20. doi: 10.1038/bjc.2015.200
21. Ding L, Ding Y, Mao XH, Zhao JF, Zhou HJ. Retrospective Study of the Prognostic Significance of Neutrophil-to-Lymphocyte Ratio for Postsurgical Outcomes of Patients With Endometrial Carcinoma. *Int J Gynecol Obstetrics* (2017) 138(3):311–9. doi: 10.1002/ijgo.12230
22. Eo WK, Kwon S, Koh SB, Kim MJ, Ji YI, Lee JY, et al. The Lymphocyte-Monocyte Ratio Predicts Patient Survival and Aggressiveness of Endometrial Cancer. *J Cancer* (2016) 7(5):538–45. doi: 10.7150/jca.14206
23. Haruma T, Nakamura K, Nishida T, Ogawa C, Kusumoto T, Seki N, et al. Pre-Treatment Neutrophil to Lymphocyte Ratio is a Predictor of Prognosis in Endometrial Cancer. *Anticancer Res* (2015) 35(1):337–44.
24. Temur I, Kucukgoz Gulec U, Paydas S, Guzel AB, Sucu M, Vardar MA. Prognostic Value of Pre-Operative Neutrophil/Lymphocyte Ratio, Monocyte Count, Mean Platelet Volume, and Platelet/Lymphocyte Ratio in Endometrial Cancer. *Eur J Obstetrics Gynecol Reprod Biol* (2018) 226:25–9. doi: 10.1016/j.ejogrb.2018.05.028
25. He M. *The Prognostic Value of Preoperative Neutrophilic Lymphocyte Ratio in Endometrioid Adenocarcinoma [Master]*. Jinan: Shandong University (2013).
26. Holub K, Busato F, Gouy S, Sun R, Pautier P, Genestie C, et al. Analysis of systemic inflammatory factors and survival outcomes in endometrial cancer patients staged I-III FIGO and treated with postoperative external radiotherapy. *J Clin Med* (2020) 9(5):1–13. doi: 10.3390/jcm9051441
27. Wang J, Lu X. Relationship Between Preoperative Neutrophils/Lymphocytes Ratio and Prognosis in Patients With Endometrial Cancer Staging. *J Chin J Surg Oncol* (2016) 8(6):377–80.
28. Kiuchi K, Hasegawa K, Ochiai S, Motegi E, Kuno T, Kosaka N, et al. Prognostic Significance of Inflammatory Parameters and Nutritional Index in Clinical Stage IVB Endometrial Carcinomas. *J Obstetrics Gynaecol* (2019) 39(2):237–41. doi: 10.1080/01443615.2018.1494703
29. Takahashi R, Mabuchi S, Kawano M, Sasano T, Matsumoto Y, Kuroda H, et al. Prognostic Significance of Systemic Neutrophil and Leukocyte Alterations in Surgically Treated Endometrial Cancer Patients: A Monoinstitutional Study. *Gynecologic Oncol* (2015) 137(1):112–8. doi: 10.1016/j.ygyno.2015.02.006
30. Ni L, Tao J, Xu J, Yuan X, Long Y, Yu N, et al. Prognostic Values of Pretreatment Neutrophil-to-Lymphocyte and Platelet-to-Lymphocyte Ratios in Endometrial Cancer: A Systematic Review and Meta-Analysis. *Arch Gynecol Obstetrics* (2020) 301(1):251–61. doi: 10.1007/s00404-019-05372-w
31. Roxburgh CS, McMillan DC. Role of Systemic Inflammatory Response in Predicting Survival in Patients With Primary Operable Cancer. *Future Oncol (Lond Engl)* (2010) 6(1):149–63. doi: 10.2217/fon.09.136
32. Modugno F, Ness RB, Chen C, Weiss NS. Inflammation and Endometrial Cancer: A Hypothesis. *Cancer epidemiol Biomarkers Prev Publ Am Assoc Cancer Res Cosponsored by Am Soc Prev Oncol* (2005) 14(12):2840–7. doi: 10.1158/1055-9965.EPI-05-0493
33. Sun T, Zhang W. Detection of Blood Flow in Endometrial Carcinoma and its Relationship With MVD and VEGF Expression by Color Doppler. *Chin J Ultrasound Med* (2003) 19(5):382–4.
34. Kwon HC, Kim SH, Oh SY, Lee S, Lee JH, Choi HJ, et al. Clinical Significance of Preoperative Neutrophil-Lymphocyte Versus Platelet-Lymphocyte Ratio in Patients With Operable Colorectal Cancer. *Biomarkers Biochem Indic Exposure Response Susceptibility to Chemicals* (2012) 17(3):216–22. doi: 10.3109/1354750X.2012.656705
35. Seki N, Kodama J, Hongo A, Miyagi Y, Yoshinouchi M, Kudo T. Angiogenesis and Platelet-Derived Endothelial Cell Growth Factor/Thymidine Phosphorylase Expression in Endometrial Cancer. *Int J Oncol* (1999) 15 (4):781–6. doi: 10.3892/ijo.15.4.781
36. Zhou X, Du Y, Huang Z, Xu J, Qiu T, Wang J, et al. Prognostic Value of PLR in Various Cancers: A Meta-Analysis. *PloS One* (2014) 9(6):e101119. doi: 10.1371/journal.pone.0101119
37. Ural ÜM, Şehitoğlu İ, Tekin YB, Şahin FK. Neutrophil-To-Lymphocyte and Platelet-to-Lymphocyte Ratios in Patients With Endometrial Hyperplasia and Endometrial Cancer. *J Obstetrics Gynaecol Res* (2015) 41(3):445–8. doi: 10.1111/jog.12536
38. Acmaz G, Aksoy H, Unal D, Ozyurt S, Cingillioglu B, Aksoy U, et al. Are Neutrophil/Lymphocyte and Platelet/Lymphocyte Ratios Associated With Endometrial Precancerous and Cancerous Lesions in Patients With Abnormal Uterine Bleeding? *Asian Pacific J Cancer Prev APJCP* (2014) 15 (4):1689–92. doi: 10.7314/APJCP.2014.15.4.1689

Conflict of Interest: The authors declare that the research was conducted in the absence of any commercial or financial relationships that could be construed as a potential conflict of interest.

Publisher's Note: All claims expressed in this article are solely those of the authors and do not necessarily represent those of their affiliated organizations, or those of the publisher, the editors and the reviewers. Any product that may be evaluated in

this article, or claim that may be made by its manufacturer, is not guaranteed or endorsed by the publisher.

Copyright © 2022 Leng, Wu and Zhang. This is an open-access article distributed under the terms of the Creative Commons Attribution License (CC BY). The use, distribution or reproduction in other forums is permitted, provided the original author(s) and the copyright owner(s) are credited and that the original publication in this journal is cited, in accordance with accepted academic practice. No use, distribution or reproduction is permitted which does not comply with these terms.

frontiers | Frontiers in Oncology

REVIEW
published: 20 May 2022
doi: 10.3389/fonc.2022.863472

Liquid Biopsy Based Circulating Biomarkers in Metastatic Prostate Cancer

Eshwari Dathathri[1], *Khrystany T. Isebia*[2†], *Fikri Abali*[1†], *Martijn P. Lolkema*[2], *John W. M. Martens*[2], *Leon W. M. M. Terstappen*[1*] *and Ruchi Bansal*[1*]

[1] *Department of Medical Cell BioPhysics, Faculty of Science and Technology, Technical Medical Center, University of Twente, Enschede, Netherlands,* [2] *Erasmus Medical Center Cancer Institute, University Medical Center Rotterdam, Department of Medical Oncology, Rotterdam, Netherlands*

Prostate cancer is the most dominant male malignancy worldwide. The clinical presentation of prostate cancer ranges from localized indolent to rapidly progressing lethal metastatic disease. Despite a decline in death rate over the past years, with the advent of early diagnosis and new treatment options, challenges remain towards the management of metastatic prostate cancer, particularly metastatic castration sensitive prostate cancer (mCSPC) and castration resistant prostate cancer (mCRPC). Current treatments involve a combination of chemotherapy with androgen deprivation therapy and/or androgen receptor signalling inhibitors. However, treatment outcomes are heterogeneous due to significant tumor heterogeneity indicating a need for better prognostic biomarkers to identify patients with poor outcomes. Liquid biopsy has opened a plethora of opportunities from early diagnosis to (personalized) therapeutic disease interventions. In this review, we first provide recent insights about (metastatic) prostate cancer and its current treatment landscape. We highlight recent studies involving various circulating biomarkers such as circulating tumor cells, genetic markers, circulating nucleic acids, extracellular vesicles, tumor-educated platelets, and the secretome from (circulating) tumor cells and tumor microenvironment in metastatic prostate cancer. The comprehensive array of biomarkers can provide a powerful approach to understanding the spectrum of prostate cancer disease and guide in developing improved and personalized treatments for patients.

Keywords: Metastatic prostate cancer, circulating biomarkers, circulating tumor cells (CTC), secretory factors, extracellular vesicles (EVs), prognostic biomarkers

OPEN ACCESS

Edited by:
Alessia Cimadamore, Marche Polytechnic University, Italy

Reviewed by:
Sandra Anjo, University of Coimbra, Portugal
Jan Zaucha, AstraZeneca Computational Pathology GmbH, Germany

***Correspondence:**
Ruchi Bansal
r.bansal@utwente.nl
Leon Terstappen
l.w.m.m.terstappen@utwente.nl

†These authors have contributed equally to this work

Specialty section:
This article was submitted to Genitourinary Oncology, a section of the journal Frontiers in Oncology

Received: *28 January 2022*
Accepted: *22 April 2022*
Published: *20 May 2022*

Citation:
Dathathri E, Isebia KT, Abali F, Lolkema MP, Martens JWM, Terstappen LWMM and Bansal R (2022) Liquid Biopsy Based Circulating Biomarkers in Metastatic Prostate Cancer. Front. Oncol. 12:863472. doi: 10.3389/fonc.2022.863472

1 INTRODUCTION

Prostate cancer (PCa) is the second leading cause of cancer-related death in men (1). Based on GLOBOCAN 2020 estimates, over 1.4 million new cases of PCa and 375,304 deaths were reported worldwide and PCa was the most frequently diagnosed cancer in 112 countries in 2020 (2). Despite a decline in death rates over the past few years, due to early diagnosis and new treatment regimens, PCa remains the most dominant male malignancy worldwide. The 5-year relative survival rate for

localized PCa is almost 100%, while for metastatic prostate cancer (mPCa) it is about 30% (3, 4). Patients with metastatic disease thus still have a dismal prognosis; hence there is an unmet need for improving outcome in these patients.

A central feature of prostate cancer is hormone (androgen) responsiveness, whereby castration or androgen deprivation therapy (ADT) causes tumor regression in most of the prostate cancer patients (3, 4). ADT targets the androgen receptor (AR) to inhibit tumor progression as a first line of therapy in patients with hormone sensitive or castration sensitive prostate cancer (HSPC or CSPC). Resistance to castration (or ADT) can result in primary castration resistant prostate cancer (CRPC) or metastatic CRPC (mCRPC) (**Figure 1**). A landmark study, by Huggins and Hodges, in 1941 led to the discovery of castration and/or androgen deprivation as effective treatment(s) for mPCa (5). This early discovery led to the insight that testosterone and AR signaling are key determinants of disease progression. Since 1941, ADT, by surgical and chemical castrations, has been used for the management of patients with advanced and metastatic PCa. The latest findings also show that AR signaling reactivation plays a major role in the emergence of (m)CRPC (6–8).

In the last decade, major progress has been made towards understanding the pathogenesis of metastatic prostate cancer. Consequently, significant advancements in the treatment of metastatic HSPC or CSPC patients have been observed by the inclusion of docetaxel (chemotherapy) and/or AR signaling inhibitors (ARSI), also called novel hormonal therapies (NHTs) such as abiraterone, enzalutamide, and apalutamide. This introduction of chemotherapy and/or ARSIs as adjunct to ADT for most patients showed significantly improved median overall survival (OS) (9). Unfortunately, these advances have come with considerable novel challenges. The trials that were conducted showed significant heterogeneity in patient prognosis and difficulty in choosing/personalizing the treatment. In several trials, patients have been stratified according to their assumed disease load. In these analyses, consistently, chemotherapy seems to render no benefit in patients with so-called low volume disease. Treatment with ARSIs does not seem to depend on the initial volume of disease; however, initial disease load or risk of early treatment failure seem to affect the magnitude of gains, i.e., OS in randomized trials. A review published elsewhere summarized the clinical trials performed in advanced prostate cancer patients including mCSPC and mCRPC, leading to recent drug approvals and discussing optimal treatment selection (10). Improved biological and prognostic stratification of mCSPC patients, therefore, might be helpful to further improve outcomes. In this review, we explore which (circulating) biomarkers are available to improve the prognosis in mPCa patients, and biomarkers that may help to select more personalized treatments for these patients.

2 METASTATIC PROSTATE CANCER BIOMARKERS: PSA AND BEYOND

Prostate specific antigen (PSA) is the most widely used biomarker for PCa. However, population-based PSA screening remains

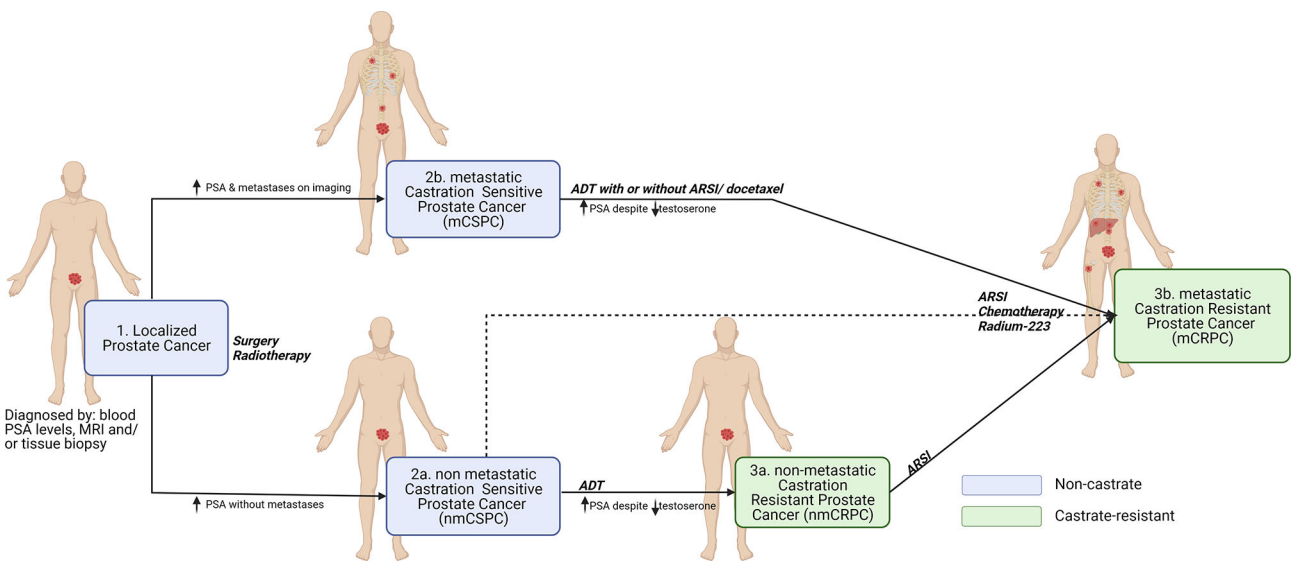


FIGURE 1 | Clinical disease states of prostate cancer. The onset of prostate cancer begins with the localized tumor formation in the prostate glands as diagnosed by blood PSA levels, MRI and/or tissue biopsy (1). However, some patients experience biochemical recurrence and can be diagnosed with high PSA levels with or without metastasis in distant regions of the body (e.g., Bone, lymph nodes, liver, and lungs) leading to non-metastatic castration sensitive prostate cancer nmCSPC (2a) or metastatic castration sensitive prostate cancer mCSPC (2b). Despite treatments with androgen deprivation therapy (ADT) with or without androgen receptor signaling inhibitor (ARSI) or chemotherapy (docetaxel), if the PSA and testosterone levels increase within the castrate range, then the disease is considered to have become (non)metastatic castration resistant prostate cancer (n)mCRPC (3a and 3b). To control the symptoms and to reduce the cancer progression, mCRPC is commonly treated with a combination of ARSI, radiotherapy (Radium-223) and chemotherapy. Created with Biorender.com.

controversial as this led to considerable false positive results due to poor specificity and thereof overdiagnosis and overtreatment (11, 12). Many men have a raised PSA level without having cancer (high false-positive rate) i.e., due to non-cancerous enlargement or inflammation of the prostate. Conversely, a substantial number of men (15-20%) with a low PSA level (<4 ng/ml) have prostate cancer with advanced Gleason scores (false negative detection) (13, 14). Moreover, PSA fails to distinguish between localized and metastatic PCa (15). Several forms of PSA, i.e., free PSA, or isoforms of PSA, i.e., -2 proPSA, have been evaluated alone or combined for PC screening, i.e., the prostate health index (PHI = (-2 proPSA/free PSA) x total $PSA^{1/2}$) that improved the accuracy of PCa predictors at biopsy (16, 17). Other clinically validated (serum and urine) biomarkers, when combined with PSA, showed improved diagnostic accuracy include Prostate cancer antigen 3 (PCA3), Mi-Prostate Score (MiPS), 4K score, epiCaPture, and STHLM3 (15).

Despite the emergence of other markers, PSA remains one of the prognostic markers for assessment of OS in mPCa patients. A study (in accordance with the Southwest Oncology Group, SWOG 9346 trial) concluded that 7-month PSA ≤ 0.2ng/mL is prognostic for longer OS of mCSPC patients on ADT (with or without docetaxel) (18, 19). However, the availability of a prognostic biomarker that could detect clinical benefit (or lack thereof) earlier than current long-term end points such as overall survival would aid in trial design and drug development. To facilitate the identification of (novel) biomarkers, liquid biopsy is a promising technique to screen body fluids that reflect disease progression and treatment response (20). Liquid biopsy analytes include circulating tumor cells (CTCs), extracellular vesicles (EVs), circulating cell-free nucleic acids [cell-free DNA (cfDNA), circulating tumor DNA (ctDNA), cell-free RNA (cfRNA) and circulating tumor DNA (ctRNA)], genetic markers, secretome (plasma proteins), Tumor educated platelets (TEPs) and other circulating cells in tumor microenvironment (TME) have been investigated as mPCa biomarkers (**Figure 2** and **Table 1**). Besides circulating biomarkers, recognizing the distinct genetic features within metastatic prostate cancer, through testing for AR splice variants (AR-Vs) or tumor suppressor genes (TSGs), might also lead to prognostic and predictive biomarkers for precision medicine.

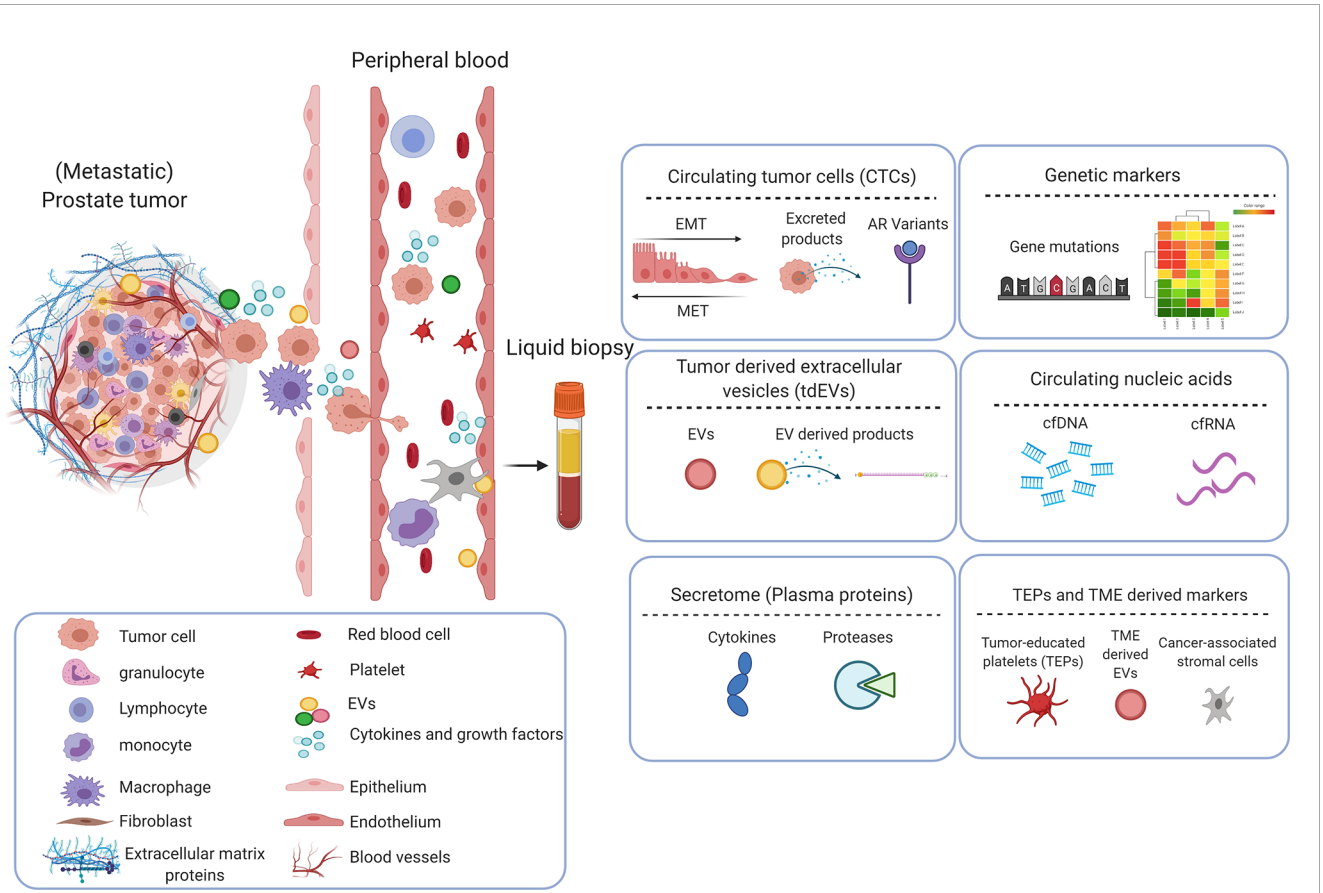


FIGURE 2 | Circulating biomarkers in prostate cancer. Primary prostate cancer metastasizes when tumor cells and cellular components break away and enter circulation (vasculature or lymphatics), travel to distant sites and form secondary tumor(s). These circulating tumor components provide an insight into the phenotypic and genotypic properties of the tumor, can act as a prognostic and predictive tool in determining the outcome of treatments. Circulating tumor cells (CTCs), extracellular vesicles (EVs), secretome (plasma proteins), genetic markers, circulating nucleic acids and other cells i.e., cancer-associated stromal cells or tumor-educated platelets (TEPs) in circulation, have been identified as potential biomarkers and is explored to further understand the clinical progression of prostate cancer and to aid development/optimization of treatments. Created with Biorender.com.

TABLE 1 | Summary of circulating biomarkers used in clinical studies and trials.

Biomarker	Population	Treatment	Outcome	Ref.
Circulating tumor cells (CTCs)	170 mCRPC patients with ≥ 5 CTCs in 7.5 mL of blood	Androgen signaling inhibitors (ARSI)	Patients with high CTC heterogeneity (phenotypic) showed shorter OS and progression-free survival (PFS). CTC heterogeneity was subjective to change with ARSI treatment.	(21)
	191 mCRPC patients	128 pre-ARSI and 63 pre-taxane	mCRPC patients with AR-V7 CTCs showed shorted OS, PFS and resistance to posttherapy PSA changes before ARSI compared to those without AR-V7 CTCs.	(22)
	29 mPCa patients and 25 non-metastatic PCa	–	Glucose metabolic (GM)-positive CTCs improved marker panel compared to EMT-CTC phenotypes.	(23)
Tumor derived extracellular vesicles (tdEVs)	84 mCRPC patients	–	Unfavorable patient groups (>5 CTCs and >105 tdEVs) associated with poor OS.	(24, 25)
	89 patients with different stages of PCa; 35 CRPC patients	–	Exosomal AR-V7 mRNA associated with lower hormone levels and poorer prognosis in CRPC.	(26)
Circulating nucleic acids	122 mCSPC patients, 112 localized PCa and 34 healthy subjects	–	Increased cfDNA plasma concentrations in mCSPC compared to localized PCa and healthy subjects.	(E. 27)
	67 mCRPC patients	ARSI or Taxane therapy	AR gain and AR-V+ expression correlated with poor prognosis, was associated with shorter OS and PFS in both ARSI-treated and chemotherapy-treated cohorts.	(28)
	53 mCRPC patients	ADT	High ctDNA predictive of ADT failure	(29)
	202 mCRPC patients	ARSI	BRCA2 and ATM defects in ctDNA associated with poor clinical outcome. Somatic changes in TP53 were associated with resistance.	(30)
	125 mCRPC patients 25 mCRPC patient	Prednisone or Enzalutamide	High ctDNA associated with presence of bone metastasis, increased levels of PSA and lactate dehydrogenase.	(31)
Secretome (Plasma proteins)	44 mCRPC patients	ARSI	Higher baseline levels of IL-6 in treatment-resistant patients compared to treatment-sensitive patients.	(32)
	233 mCSPC patients	ADT monotherapy ADT + Docetaxel	Higher IL-8 levels in docetaxel-treated patients compared to ADT monotherapy. Higher IL-8 levels prognostic for poor OS, shorter time to CRPC, independent of docetaxel use and metastatic burden.	(33)
	44 mCRPC patients	ARSI	Higher baseline levels of IL-10 in ARSI-resistant patients compared to ARSI-sensitive patients.	(32)
	215 PCa patients	–	Higher MMP-2 expression in CTCs and DTCs of patients with bone metastasis.	(34)
	93 localized PCa and 13 mPCa patients	–	MMP-7 serum concentration higher in bone metastatic patients compared to localized PCa.	(35)
	7 mCRPC patients	–	Treatment-responsive patients showed lower MMP-2 and MMP-7 levels compared to patients with metastasis (bone and lymph node).	(36)
Tumor educated platelets (TEPs)	50 mCRPC patients	Abiraterone and docetaxel	*KLK3*, *FOLH1*, *NPY* transcripts in TEPs indicated poor OS and accurately predicted outcome after abiraterone therapy.	(37)

mCRPC, metastatic castration resistant prostate cancer; ARSI, androgen signaling inhibitors; AR-V7, Androgen receptor variant 7; CTCs, circulating tumor cells; OS, overall survival; PFS, progression free survival; GM, Glucose metabolic; PSA, prostate specific antigen; EMT, epithelial to mesenchymal transition; CfDNA, cell free DNA; mCSPC, metastatic castration sensitive prostate cancer; CtDNA, circulating tumor DNA; ADT, androgen deprivation therapy; tdEVs, tumor derived extracellular vesicles; TEPs, tumor educated platelets; KLK3, Kallikrein Related Peptidase 3; FOLH1, Folate Hydrolase 1; NYP, neuropeptide-Y; IL, interleukins; DTCs, disseminated tumor cells; MMP, matrix metalloprotease.

2.1 Circulating Tumor Cells

CTCs are tumor cells disseminated from primary and/or metastatic tumor sites that circulate in the vasculature with potential for distant seeding. Compared with traditional biopsies, CTCs are considered to better reflect inter- and intra-tumor heterogeneity. Although present at relatively low frequencies, CTC presence is associated with poor prognosis; their rise or decline is a strong and early predictor of treatment response, and their characterization can be used to determine treatment options (38). CTC enumeration using Food and Drug administration (FDA)-cleared CellSearch system (**Figure 3**) is the most frequently used system to assess prognosis and to determine early response to therapy in various metastatic carcinomas including metastatic prostate cancer (39–43). While CellSearch is useful to enumerate the CTCs, a major limitation is that it captures only Epithelial cell adhesion molecule (EpCAM) positive cells, and EpCAM-negative CTCs cannot be isolated by this system. The CTC yield also shows low viability and cannot be cultured for long periods (44). To overcome this limitation, multiple microfluidic technologies have been explored in the last two decades (45). A recent assay developed by Epic Sciences, known as the AR-V7LB, counts both EpCAM-positive and EpCAM-negative cells suggesting the epithelial to mesenchymal transition (EMT) (46, 47). A recent study showed that it was a useful platform in detecting AR-V7 in CTCs of mCRPC patients starting second generation treatment with ARSI, with a strong correlation to the CTC counts from the CellSearch platform (48).

As mentioned before, CTCs can be derived from epithelial cells, mesenchymal cells, and/or can be of hybrid phenotype. EMT is the characteristic feature of CTCs whereby epithelial cells gain the migratory properties of mesenchymal cells and the process is considered to play an important role in metastasis (49). Likewise, disseminated cells recover epithelial properties for

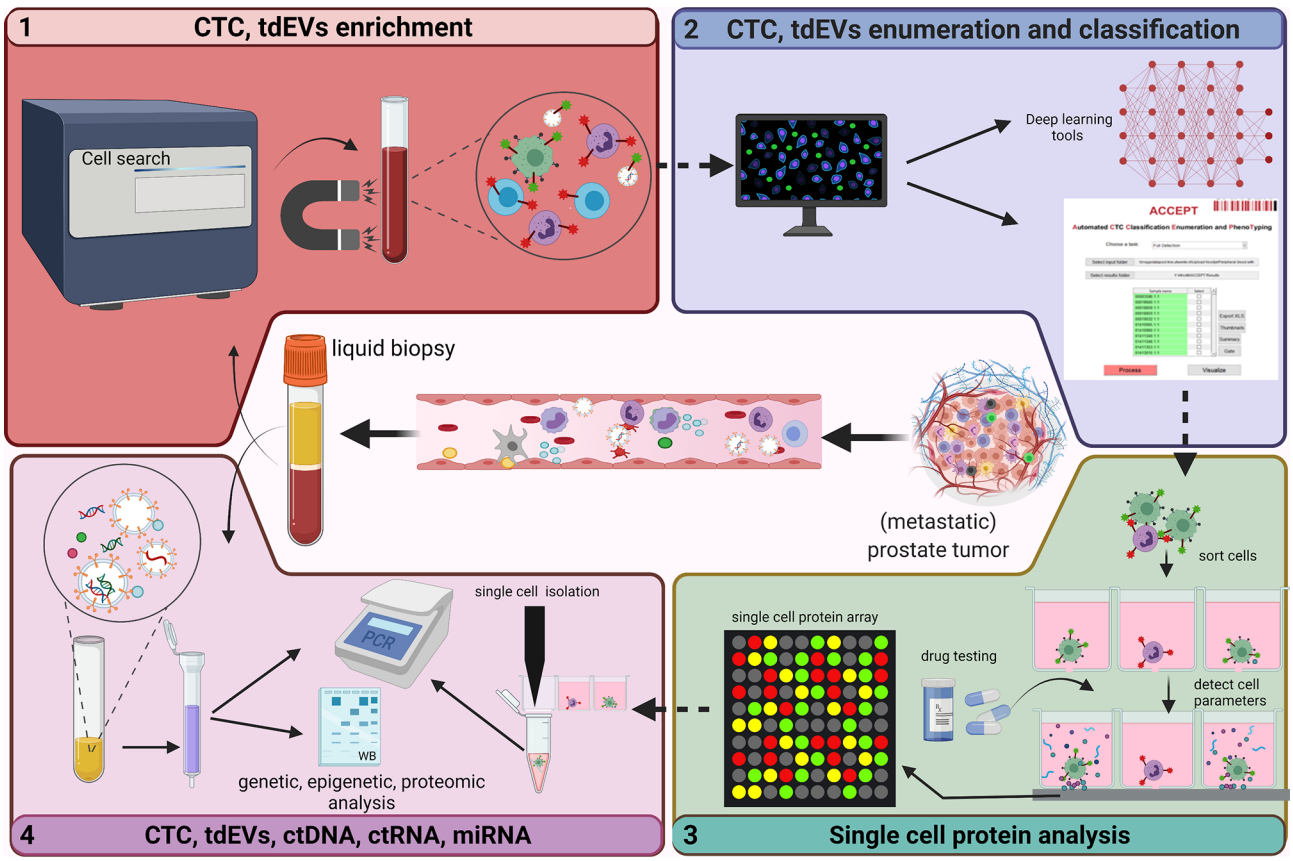


FIGURE 3 | Analysis of circulating biomarkers. This figure depicts the technologies (developed and used at the Medical Cell BioPhysics Department at the University of Twente) that are generally used to identify/analyze circulating biomarkers in liquid biopsy. The FDA approved CellSearch (immunomagnetic enrichment) is the gold standard and is currently used for the CTC and tdEV enrichment from prostate cancer patient diagnostic leukapheresis (DLA) sample (1). An in-house developed tool - Automated CTC Classification Enumeration and PhenoTyping (ACCEPT) - is used to classify and enumerate the CTCs and tdEVs to better understand the morphology and phenotypic heterogeneity. Other deep learning tools such as Deep or Recurrent Convolutional Neural Networks (DCNN or RCNN) based algorithms were developed with improved segmentations models for automated and bias-free CTC enumeration (2). Enriched CTCs are further sorted into single cells using microwell arrays, analyzed for protein secretions in response to treatments, after which CTCs of interest are isolated (3). Omics profiling of selected CTCs and other circulatory markers including tdEVs, ctDNA, ctRNA and miRNA using polymerase chain reaction (PCR) and low-pass whole genome sequencing (LP-WGS) is performed to identify aberrations and analyze tumor heterogenity and aggressiveness (4). Created with Biorender.com.

rapid colonization through the mesenchymal to epithelial transition (MET). Related CTC phenotypes including E-CTCs (epithelial), M-CTCs (mesenchymal) and H-CTCs (hybrid) act as promising biomarkers. E-CTCs can be characterized by epithelial markers such as EpCAM, E-cadherin, Prostate specific membrane antigen (PSMA), cytokeratin (CK); M-CTCs express mesenchymal markers (Vimentin, Twist), and H-CTCs co-express epithelial and mesenchymal markers e.g. cytokeratin and vimentin as molecular markers for EMT (49). In an observational study, the involvement of survivin, an inhibitor of apoptosis, highly expressed in mCRPC and associated with poor clinical outcome in CTCs has been suggested and the study showed that siRNA-mediated survivin-knockout inhibited EMT and invasiveness of CTCs and DU145, an AR-independent metastatic PCa cell line (23). Intriguingly, another study suggested that hypermetabolic GM^+ CTCs expressing glucose metabolic markers (PGK1/G6PD) as a promising biomarker, compared to the EMT CTCs subtypes, for diagnosis of mPCa. This study suggested a triple tPSA–Gleason–GM^+CTCs marker panel with an improved AUC of 0.904, compared to the tPSA–Gleason–H-CTCs marker panel (0.874) (50). Thus, besides enumeration, CTCs phenotyping and comprehensive omics analysis (**Figure 3**) can improve prognostication or treatment prediction of mPCa.

In mCRPC patients, the presence of ≥5 CTCs in 7.5mL of blood predicts an unfavorable prognosis, whereas a post-treatment drop in CTC count predicts an improved prognosis (42). A multicentric study replicated these findings using an open-source Automated CTC Classification Enumeration and PhenoTyping (ACCEPT) software (**Figure 3**) for the prognostication of mCRPC patients (21). ACCEPT is a useful tool to detect and enumerate fluorescently labeled CTCs (and EVs) where classification into different subsets is based on linear gates applied to extract measurements of objects identified by a

multiscale segmentation model. However, the use of linear gates causes segmentation of objects that lie very close to one another as one event, resulting in false positives that need to be eliminated during the manual review of thumbnails (51). Hence, there exists a need to develop fully automated and robust techniques to better enumerate CTCs. Deep and recurrent convolutional neural networks (DCNN or RCNN) have been developed and are currently used with improved segmentation that effectively classify and allow bias-free enumeration of CTCs (51–53). Moreover, few studies in mCSPC patients suggest that baseline CTC count is highly predictive of 7-month PSA response and 2-year progression-free survival (PFS), and that CTC count correlate with OS and PFS (54, 55). Besides CTC count, CTC phenotypic heterogeneity can help in making informed decisions about the therapy. It was shown that low CTC phenotypic heterogeneity was associated with better OS in ARSI-treated patients, whereas high heterogeneity was associated with improved OS in patients treated with taxanes (22).

Several genetic aberrations associated with castration resistance under anti-hormonal therapy include the amplification of AR (and/or the respective upstream enhancer) and alterations with the ligand binding site, altering ligand-preferences, or even enabling a constitutionally active isoform. Besides, AR alternative splicing isoforms (AR-v's) are generated as one of the mechanisms for PCa transition to castration resistance. AR splice variants (AR-V1, 3, 7 and 9), is a phenomenon first reported in 2004, which recently earned renewed clinical relevance due to its role as a dynamic marker throughout disease progression and treatment-induced selective (clonal) pressure (56, 57). Among AR-Vs, the most frequently expressed and biologically significant is AR-V7, a transcript encoding a variant of AR that lack the ligand-binding domain and thereby functions as a constitutionally active nuclear transcription factor (58–60). Scher et al. observed patients with an increasing number of AR-V7 positive CTCs ranging from 3% by first line of therapy to 31% by third or greater line of therapy. Furthermore, it was suggested that patients with AR-V7 positive CTCs were more resistant to ARSI compared to treatments with taxanes, that resulted in longer OS in such patients (61). Moreover, whole blood analysis of CRPC patients revealed higher expression of AR-Vs (68% for AR-V7 and 32% ARv^{567es}) in hormone-treated patients compared to the hormone-naïve (62). These studies suggest AR-V7 in PCa as a potential negative predictive biomarker for guiding AR-directed hormonal treatments for CRPC patients. Besides, AR-V3 that also lack the ligand binding domain, cell context-dependent variants like AR-V1 and AR-V9, which are conditionally activated variants have been described and could all play a role in progression to castration resistance and hence a clinical role (63–65).

2.2 Genetic Biomarkers

PCa is characterized by a wide variety of genomic aberrations encompassing copy number alterations, genomic mutations such as single-nucleotide variants (SNVs), insertions–deletions (indels) and multi-nucleotide variants (MNVs), and large-scale structural rearrangements. The active mutational mechanisms, mutation rate, and mutational landscape and drivers alter throughout disease progression and (treatment-driven) somatic evolution and clonal dynamics.

Within primary PCa, driver-gene analysis revealed enrichment or recurrence of mutations or copy-number alterations within *SPOP, FOXA1, IDH1, TP53, PTEN, PIK3CA, BRAF, CTNNB1, HRAS, MED12, ATM, CDKN1B, RB1, NKX3-1, AKT1, ZMYM3, KMT2C, KMT2D, ZNF770, CHD1, BRCA2, CDK12* as reported by The Cancer Genome Atlas (TCGA) consortium (66). Additionally, recurrent genomic gains of chromosome 7 and 8q and heterozygous losses of 8p, 13q, 16q, and 18 were often observed within PCa (66).

Compared to another large-scale sequencing study focusing on mCRPC (67), the mutational landscape harbored an overall greater mutational burden and incidence of large-scale structural variants compared to primary PCa. However, the inventory of driver genes remains similar, with the marked exception of (treatment-induced) mutations on AR. The following genes were enriched with mutations compared to primary PCa: *PRAD; AR, TP53, MYC, ZMYM3, PTEN, PTPRD, ZFP36L2, ADAM15, MARCOD2, BRIP1, APC, KMT2C, CCAR2, NKX3-1, C8orf58*, and *RYBP*. Somatic alterations influencing the expression or function of AR have been reported as one of the main driving forces of castration resistance. Recurrent amplifications of AR and/or its upstream enhancer coupled with splicing aberrations (ARVs) and treatment-related hotspot mutations have been reported previously.

Tumor suppressor genes (TSGs) such as *RB1*, *TP53* and *PTEN* are among the most frequently altered genes in PCa whereby co-operative functional loss of these TSGs has been associated with poor prognosis. Hamid and colleagues found increased TSG alterations (mono-/bi-allelic loss) in mPCa, 63% in mCSPC and 92% in mCRPC versus 39% in localized CSPC. Moreover, two or more TSG alterations were more frequent in mCRPC (73%) compared to mCSPC (28%) and localized CSPC (11%). Finally, it was concluded that TSG variants were linked to early relapse and worse outcomes in the CSPC patient cohort (68). Studies have also revealed a relationship between genetic alterations and disease volume. In the STAMPEDE trial on mCSPC patients, frequent alterations in the *PTEN* in high-and low-volume disease were observed, while *TP53* alterations were found in low-volume disease (69). Stopsack and colleagues, found an association of *SPOP* alterations with improved prognosis, while aberrations in AR, cell cycle and *TP53* were associated with worse prognosis (70). Moreover, *RB1* loss was associated with poor prognosis in mCRPC patients (71 Apart from these TSGs, *BRCA2* (PROREPAIR-B study) and *CDK12* mutations have been associated with increased aggressiveness and metastases, short OS time and poor response to first-line therapy (3, 72).

Next to altered genes and mutations, PCa commonly harbors gene fusions and several solid tumors that demonstrate a high frequency of recurrent gene fusions (73, 74). One of the gene fusions is the enigmatic *TMPRSS2-ERG* fusion observed in 50-

70% of all PCa cases, yet incidences have been reported to differ among different ethnic and geographical groups (66, 67, 73). *TMPRSS2-ERG* is a fusion between the AR-regulated transmembrane protease serine 2 (*TMPRSS2*) and v-ets erythroblastosis virus E26 oncogene like (*ERG*) genes, and is reported as an early event in PCa initiation (75). Fusion of these genes results in androgen-dependent transcription of *ERG* in prostate cancer cells. The *TMPRSS2-ERG* fusion is the most common fusion event within PCa, however, additional (less frequent) ETS-factor fusions have been reported (76). Due to the high prevalence of *TMPRSS2-ERG*, this somatic event is one of the predominant molecular classification factors and could be used as a promising diagnostic and prognostic marker (75–77). Overall, detection of genetic aberrations in mCSPC and mCRPC might have predictive value for defining treatment landscapes for these patients.

2.3 Extracellular Vesicles

Prostate cancer cells release extracellular vesicles (EVs) comprising of apoptotic bodies, microvesicles and exosomes (78). EVs contain bioactive cargo (proteins, nucleic acids, and metabolites), and are increasingly recognized as a pivotal player that play a crucial role in communication between tumor cells and the TME and can also act as prognostic and diagnostic markers. Studies indicated that PCa patients have 4-fold higher levels of nanovesicles expressing both PSA and CD81 (exosomal marker) compared to benign prostate hypertrophy (BPH) patients and healthy individuals where TME acidity seems to regulate the release of PSA-EVs in the blood of PCa patients (79).

Tumor-derived EVs (tdEVs) are also known to regulate osteoclasts and osteoblasts in the bone metastasis of PCa patients (78). A recent study has also indicated that EVs derived from mesenchymal-like prostate cells promote EMT of epithelial-like prostate cancer cells and render resistance to ADT (80). MiR-34a bearing EVs were suggested as a predictive biomarker since it was observed to promote sensitivity to docetaxel by decreasing endogenous B-cell Lymphoma 2 (BCL-2) expression (81). RNA sequencing also revealed other exosomal miRNA such as miR-1290 and miR-375, whose high levels were associated with poor OS in CRPC patients (82). Exosomal CD44v8-10 mRNA copy numbers in EVs were higher in docetaxel-resistant CRPC patients than in docetaxel naïve patients and control men (83). Joncas et al. studied plasma EVs as phenotypic biomarkers in PCa patients with different stages of disease progression in CRPC patients. Authors demonstrated a novel association between high levels of AR-V7 exosomal mRNA (with undetectable androgen levels) and high neutrophil-to-lymphocyte ratio (26). High expression of full-length androgen receptor (AR-FL) was also linked with AR-V7+ CRPC patients and predicted resistance to hormonal therapy (84, 85).

Nanou et al., investigated the clinical relevance of EpCAM+, CK+, DNA-, CD45- tdEVs using the CellSearch system in blood of CRPC patients. The availability of advanced image analysis made it possible to interrogate the images gathered by the CellSearch system for CTC enumeration revealing the presence of several subclasses of CTC and tdEV (51). Using the ACCEPT tool, well-defined tdEVs and CTCs were enumerated in CRPC patients (**Figure 3**), and patients with >5 CTCs and $>10^5$ tdEVs were associated with poor OS. Moreover, in the same study, tdEVs showed improved predictive power, regarding sensitivity, and specificity, when compared to CTC count alone (A. 24, 25). The high incidence and superior stability of tdEVs in circulation compared to CTCs, and the tdEVs cargo reflecting tumor heterogeneity make them a promising biomarker in the metastatic setting. However, their small size makes enumeration and characterization more challenging, but with advances in technology this is expected to improve in the near feature.

2.4 Cell-Free Nucleic Acids

Cell-free DNA (cfDNA) are DNA fragments that are released into circulation by dying or apoptotic cells in healthy individuals. cfDNA is considered to originate from hematopoietic cells, and in cancer patients, cfDNA constitutes DNA derived from tumor cells (ctDNA) next to those derived from hematopoietic cells. In mCSPC patients, Chen et al., found increased plasma cfDNA concentrations compared to 112 patients with localized disease and 34 healthy subjects. Moreover, more, and shorter sized cfDNA fragments were correlated with an increased risk of localized disease compared to healthy subjects. Although cfDNA was useful in distinguishing between the two groups, cfDNA fragment size showed poor predictive performance due to its low sensitivity and specificity (27).

ctDNA has emerged as a promising biomarker with diagnostic, predictive and prognostic applications in cancer. Genomic analysis of plasma ctDNA has gained attention in recent years and aberrations in ctDNA overlapped substantially with those in tumor tissue, especially with those in bone lesions of mPCa patients (86). Several techniques have been employed for the detection and characterization of ctDNA within the total pool of cfDNA. The sequencing techniques involved can be classified into Sanger sequencing, Pyrosequencing, and next-generation sequencing (NGS). NGS holds an advantage as its sensitivity is 10 times higher compared to the other methods. Hence, it is the most commonly used sequencing technique to detect ctDNA, which is less than 1% of the total cfDNA pool (47). ctDNA can be detected using different types of biomarkers including tumor-specific somatic mutations, copy number variations (CNVs), phasing of histones and methylation patterns (87, 88). Mutant molecules and CNV numbers were consistent with metastatic tissue and the amount of ctDNA reflected poor prognosis (29, 30, 86). In a study by Wyatt et al., next-generation sequencing was performed across 72 genes in 45 cfDNA samples (ctDNA greater than 2% of the cfDNA). The results indicated AR alterations, mutations in SPOP and tumor suppressor genes and alterations in the AR, PI3K and WNT pathways of mCRPC patients who showed disease progression following one line of AR targeted therapy (86). ctDNA is also abundant in most mCSPC patients, providing additional insight into metastatic disease beyond the information diagnosed in primary prostate biopsy. Additionally, higher ctDNA levels were predictive of ADT failure and shorter metastasis-free survival (29–31, 88, 89). In a study, Fettke and Kwan et al. performed integrated sequencing of cfDNA and

cfRNA from 67 mCRPC patients and found that AR alterations (AR gain and AR-V expression) correlated with poor prognosis (28). Additional larger randomized studies (with and without a specific treatment) are required to determine the potential of cfDNA, ctDNA, and/or cfRNA as a diagnostic, prognostic, or predictive marker for mPCa.

2.5 Secretome

The secretome is a class of proteins that are secreted in the extracellular space and is considered a reservoir of potential biomarkers for cancer (and other diseases). In cancer, the tumor cells (and the TME) produce a secretome with an altered composition compared to their normal state. Evidence from the literature suggests that the tumor secretome plays a vital role in cancer metastasis and progression. Tumor secretome is largely studied using bulk cell approaches, however, this approach fails to identify existing phenotypic and genotypic heterogeneity in specific cells or biomarkers of interest (90). Furthermore, it has become apparent that genetically identical cells can give rise to phenotypic variability (91, 92) indicating that profiling (single-cell) secretome signature is important to gain insights into the tumor heterogeneity, tumor biology, cellular interactive networks, and can be used for individualized diagnosis and therapeutic monitoring.

Single cell omics have gained importance over the recent years as it provides a valuable platform to measure multiple molecules such as DNA, RNA, and proteins secreted from a single cell. One of the major clinical challenges in early diagnosis and designing effective personalized therapeutics has been the lack of adequate technologies to comprehensively characterize inter- and intra-tumor heterogeneity. A recent study developed a novel technology (**Figure 3**) to perform proteomic analysis from single PCa cells. Abali et al., quantified protein secretions from LnCAP and VyCAP cell lines in picograms of PSA produced per cell per day. The effect of different drugs on each cell and their PSA secretions (over a period of 24-72 hours) could be quantified (93). At any time point, the individual cells can be isolated and probed for their molecular composition (94). Single-cell secretome profiling of the tumor allow reconstruction of signaling/communication networks at a systems-level and can provide valuable insights into the origins of tumor heterogeneity, tumor differentiation and evolution, and has the potential to enable the development of more effective personalized medicines for human cancers. The ability to perform such experiments on actual CTCs of mPCa patients could make personalized therapy for mPCa a reality. Availability of a sufficient number of CTC would, however, be a condition to realize this. The use of Diagnostic Leukapheresis enables the harvest of a sufficient number of CTC and as already been successfully accomplished in this disease setting (95). Apart from PSA, other biomarkers in the tumor secretome that can shed light to the complexity of the disease include a variety of cytokines and proteases, however, they lack specificity suggesting a panel of biomarkers would have a greater potential for better prognosis and in predicting therapy response.

2.5.1 Cytokines

Studies indicate that cytokines play a major role in PCa pathogenesis. A study by Pal et al., profiled the levels of cytokines in mPCa patients. The results indicated a decrease in the baseline levels of interleukins (IL) IL-6 and IL-10 and an increase in pro-inflammatory cytokines (IL-5, IL-10, IFN-γ, TNF-α) in ARSI-responsive patients when compared to ARSI-resistant patients (32). IL-8 (CXCL-8), another pro-inflammatory cytokine released by tumor cells (and macrophages), is significantly higher in cell lines with invasive behavior and metastatic potential such as PC-3 and DU-145 compared to the less invasive LnCAP cells. Studies also found elevated levels of circulating IL-8 in men with bone metastasis compared to those with localized cancer. Harshman et al., studied the impact of serum IL-8 on mCSPC patients in the CHAARTED trial and indicated that at ADT initiation, serum IL-8 levels were elevated and predicted worse OS. The prognostic impact of IL-8 remained independent of metastatic burden, time to metastasis, and docetaxel use, and predicted a short-time to castration resistance (33). IL-23 secreted by myeloid-derived suppressor cells (MDSCs) and activating the pSTAT3-RORγ signaling pathway thereby promoting survival and proliferation of PCa cells, was shown to promote CRPC by activating the AR pathway. Calcinotto et al., observed higher frequency of IL-23-producing MDSCs in tumor biopsies in CRPC compared to CSPC patients, correlating with elevated levels of IL-23 in circulation (96). They further demonstrated that inhibition of IL-23 using IL-23 blocking antibodies restored sensitivity to AD therapy in mice suggesting blocking IL-23 during first-line therapy might reverse resistance to ADT in patients with mPCa (96). These studies show great promise using immune-related circulating biomarkers (cytokines) as predictors of outcome of treatments for patients with mPCa.

2.5.2 Proteases

Aberrantly expressed proteases are excellent candidates for cancer biomarkers, as they play critical roles in various hallmarks of cancer (97). Besides PSA, a protease in the Kallikrein family (KLK3) regulated by androgen signaling, matrix metalloproteases (MMPs) are a family of proteolytic enzymes that are known to degrade extracellular matrix (ECM) and support tumor proliferation and growth as well as migration, and metastasis. Studies have indicated a higher expression of various MMPs (MMP-2, -3, -7, -9, -13, -14, -15 and -26) in metastatic cancer, while MMP-1 expression correlates with early-stage cancer. Among MMPs, MMP-2, -7, -9 and membrane-type (MT)-MMPs are the most extensively studied MMPs in PCa progression (97).

Murray et al., found high MMP-2 expression in CTCs and disseminated tumor cells (DTCs) in mPCa patients. Patients with bone metastases showed an increased expression of HER-2 protein and a resulting increase in MMP-2 expression (34). MMP-3 is also known to promote cancer cell growth and metastasis. Frieling et al., observed high levels of MMP-3 expression in PCa patients with bone metastasis. PCa cells are considered a rich source of MMP-3 in the tumor bone microenvironment. MMP-3 ablation, *in vitro* and *in vivo*, suppressed cancer cells proliferation and reduced bone metastasis (98). High levels of circulating MMP-7 have also been observed in PCa patients with distant metastasis, particularly bone metastasis (35). Significantly elevated mRNA

and protein levels of MMP-9, activated by MMP-2 and MMP-3, were seen in malignant compared to benign tumors. In PCa, MMP-2 and MMP-9 are relevant molecular biomarkers that reflect the tumor's invasive and metastatic potential (97). Dhar et al., analyzed single-cell CTC-secreted MMPs (MMP-1, -2, -7, and -9) in CRPC patients and found that patients responding to treatment and with lower levels of PSA, had lower MMP levels. While CTCs from patients with (bone and lymph node) metastasis showed higher MMP levels (36). These preliminary results indicate a correlation between metastasis, PSA levels, and MMP secretion, thereby establishing a possibility to use MMPs as a prognostic biomarker.

Cathepsins are another family of proteases that not only play an important role in tumor metastasis and progression, but also activate other proteases like proheparanase, urokinase-plasminogen activator (uPA), and MMPs. Cathepsin K (CatK) expression is significantly higher in bone metastasis than in primary PCa and is negative in healthy prostate tissue. Circulating CatK protein expression in conditioned medium was higher in PC-3 and C4-2B (characteristics of bone metastasis) than in LnCAP and PrEC cells. CatK inhibition decreased tumor cell invasiveness, retarded tumor progression, and increased bone density *in-vivo* in mice, supporting an important role of CatK in PCa-induced bone metastasis (43, 99).

2.6 Tumor-Educated Platelets

Platelets play an important role during tumorigenesis and cancer metastasis and show altered behavior when exposed to tumors. These so-called TEPs harbor cancer biomarkers that include platelet-derived microparticles, proteins and RNA, and can predict therapeutic response or monitor disease (100). Tjon-Kon-Fat et al., isolated and studied platelet fractions to stratify CRPC patients based on response to therapy. They observed that PCa-associated biomarkers (*KLK3*, *FOLH1*, *NPY* transcripts) in platelets were associated with short OS and enabled prediction of outcome after abiraterone therapy with higher accuracy (37). Although promising, further validation is warranted to determine the potential of TEPs-derived biomarkers for blood-based companion diagnostics, cancer progression (from PCa to mPCa), therapy selection, longitudinal monitoring, and recurrence.

3 BIOMARKERS IN TUMOR MICROENVIRONMENT

The tumor microenvironment combining stromal and cellular components surrounding the tumor, can release various biomarkers into circulation, which can be identified in a liquid biopsy. It is paramount to gain insights into the complexity of tumor microenvironment (TME), comprising of immune cells, fibroblasts and endothelial cells, extracellular components (such as proteoglycans, proteins, and glycoproteins) since the communication between TME and tumor cells strongly contribute to tumor progression and metastasis. S. Chen et al., investigated the heterogeneity in infiltrating immune cells and identified a tumor-associated macrophages (TAMs) subset that showed osteoclast-like features (characteristic of bone metastasis). Moreover, elevated expression of *KLK3*, prostate-specific antigen (PSA) gene in T cells (AR-negative) was observed, attributed to extracellular vesicle/exosome-mediated trafficking from the tumor cells to T cells (101). Apart from immune cells, the authors identified three subtypes of cancer-associated fibroblasts (CAFs), surprisingly with depleted expression of *ACTA2* (a common CAF marker in most cancers). *ACTA2* expression correlated with the EMT score suggesting EMT being a possible source for ACTA2-positive CAFs. Moreover, though all CAF subtypes showed angiogenesis-associated features, subtype-specific expression of myofibroblastic, cell adhesion and ECM genes was observed, indicating a shared regulatory network between CAFs and non-fibroblastic lineages in TME (S. 101). Another non-immune component, endothelial cells, are responsible for the recapitulation of tumor heterogeneity within secondary and metastatic sites. Chen et al., identified four EC subtypes, with elevated expression of CAF-related genes, termed activated endothelial cells (aECs). Further analysis revealed interactions of aECs with other TME components suggesting their role in ECM remodeling, hence promoting cancer cell invasion/metastasis, and suppressing immune activation (101, 102).

Prostate tumor-derived EVs are also known to promote a tumor-supportive environment by activating cancer-associated fibroblasts (CAFs), which release miR-409 from EVs and enhance prostate tumorigenesis (103). Docetaxel resistant CRPC derived EVs were also shown to express and secrete Brain4 (BRN4) which promotes the development of neuroendocrine differentiation (NED), leading to an aggressive variant of CRPC (104). Other markers of immunogenicity in the TME have also been shown to be predictive of cancer aggressiveness and treatment resistance. A study characterized heterogeneity of the immune checkpoint expressions of CTCs in mPCa. More than 50% of the CTCs expressed PD-L1 expression in 30% of patients with mHSPC; 20% of patients with mCRPC pre-ARSI and 30% of patients with mCRPC post-ARSI. PD-L2 expression was observed in 20-40% of the patients and B7-H3 expression (>80%) was observed in all patients of all cohorts in the study (105). To develop effective treatments, the complete pathophysiology of mPCa needs to be understood. Hence, identifying biomarkers to study mechanisms behind metastasis, tumors, heterogeneity, and crosstalk within the microenvironment will help in developing tailored treatments for patients.

4 CONCLUSIONS AND OUTLOOK

This review highlights the potential biomarkers in circulation to improve diagnosis and tailor treatments for metastatic prostate cancer patients using liquid biopsies. In the current treatment landscape, developing systemic treatments will become more focused on mCSPC and mCRPC patients. There is a need to start balancing the drive for intensifying treatment, to improve outcomes and to maintain as much quality of life as possible for the men involved. This can be achieved by improving the ability to stratify patients based on their risk of progression, and

development of therapy resistance combined with the ability to monitor longitudinally the effects of administered individual (combination) treatments. Liquid biopsy-based strategies are essential to achieve this, since, in metastatic prostate cancer, tumor tissues are often difficult to obtain, and the disease load is often difficult to assess using imaging. Thus, comprehensive analysis of analytes in liquid biopsies will inform us about the biology of the disease, and hence can guide us in making informed decisions about improved and personalized treatments for the patients. Of these analytes, the prognostic biomarkers that were seen to be most effective in the clinics are the CTCs (specificity 67%, sensitivity 69%), tdEVs (69%, 69%), PSA (6-66%, 78-100%) and cfDNA (56%, 88%). These analytes provide useful insight on the overall survival of patients suffering from mCRPC (24, 25, 27). Other biomarkers used in clinics including AR-V7, TMPRSSQ-ERG and secretome proteins also show promise, however, their prognostic value in assessing treatment outcomes is still under investigation. A major challenge that remains with PCa clinical disease management is tumor heterogeneity. Understanding the biology and mechanisms behind the genetic and epigenetic alterations in primary and metastatic tumor, using techniques such as single cell sequencing can provide more insight into the pathophysiology of the disease. With technological advances in single-cell omics analysis and machine learning tools, together with rapid strides in imaging techniques and treatment modalities, the understanding and management of metastatic prostate cancer will continue to evolve rapidly over the next decade.

AUTHOR CONTRIBUTIONS

ED contributed to design of article and interpreting relevant literature. KI and FA contributed to interpreting relevent literature and developing figures. LT and RB are corresponding authors, have provided critical revisions and supervison. ML, JM and LT are experts on the topic, have supervised the manuscript preparation. All authors contributed to the article and approved the submitted version.

FUNDING

Authors acknowledge the financial support by the Dutch Cancer Society (KWF) and Netherlands Organization for Scientific Research (NWO) through the PICTURES project #17915.

ACKNOWLEDGMENTS

Authors acknowledge Dr. Job van Riet for his contribution to section 2.2 Genetic biomarkers.

REFERENCES

1. Siegel RL, Miller KD, Jemal A. Cancer Statistic. *CA Cancer J Clin* (2020) 70 (1):7–30. doi: 10.3322/caac.21590
2. Sung H, Ferlay J, Siegel RL, Laversanne M, Soerjomataram I, Jemal A, et al. Global Cancer Statistics 2020: GLOBOCAN Estimates of Incidence and Mortality Worldwide for 36 Cancers in 185 Countries. *CA Cancer J Clin* (2021) 71(3):209–49. doi: 10.3322/caac.21660
3. Ng K, Smith S, Shamash J. Metastatic Hormone-Sensitive Prostate Cancer (mHSPC): Advances and Treatment Strategies in the First-Line Setting. *Oncol Ther* (2020) 8(2):209–30. doi: 10.1007/s40487-020-00119-z
4. Sartor O, de Bono JS. Metastatic Prostate Cancer. *N Engl J Med* (2018) 378 (7):645–57. doi: 10.1056/NEJMra1701695
5. Huggins C, Hodges CV. Studies on Prostatic Cancer. I. The Effect of Castration, of Estrogen and of Androgen Injection on Serum Phosphatases in Metastatic Carcinoma of the Prostate. *Cancer Res* (1941) 1(4):293. doi: 10.3322/canjclin.22.4.232
6. Azzouni F, Mohler J. Biology of Castration-Recurrent Prostate Cancer. *Urol Clinics* (2012) 39(4):435–52. doi: 10.1016/j.ucl.2012.07.002
7. Hamid ARAH, Luna-Velez MV, Dudek AM, Jansen CFJ, Smit F, Aalders TW, et al. Molecular Phenotyping of AR Signaling for Predicting Targeted Therapy in Castration Resistant Prostate Cancer. *Front Oncol* (2021) 11:721659(3254). doi: 10.3389/fonc.2021.721659
8. Yao M, Shi X, Li Y, Xiao Y, Butler W, Huang Y, et al. LINC00675 Activates Androgen Receptor Axis Signaling Pathway to Promote Castration-Resistant Prostate Cancer Progression. *Cell Death Dis* (2020) 11(8):638. doi: 10.1038/s41419-020-02856-5
9. Wenzel M, Würnschimmel C, Nocera L, Collà Ruvolo C, Tian Z, Shariat SF, et al. Overall Survival After Systemic Treatment in High-Volume Versus Low-Volume Metastatic Hormone-Sensitive Prostate Cancer: Systematic Review and Network Meta-Analysis. *Eur Urol Focus* (2021) S2405-4569(21) 00109-7. doi: 10.1016/j.euf.2021.04.003
10. Swami U, McFarland TR, Nussenzveig R, Agarwal N. Advanced Prostate Cancer: Treatment Advances and Future Directions. *Trends Cancer* (2020) 6 (8):702–15. doi: 10.1016/j.trecan.2020.04.010
11. Neal DE, Donovan JL, Martin RM, Hamdy FC. Screening for Prostate Cancer Remains Controversial. *Lancet* (2009) 374(9700):1482–3. doi: 10.1016/S0140-6736(09)61085-0
12. Stark JR, Mucci L, Rothman KJ, Adami HO. Screening for Prostate Cancer Remains Controversial. *BMJ* (2009) 339:b3601. doi: 10.1136/bmj.b3601
13. Prensner JR, Rubin MA, Wei JT, Chinnaiyan AM. Beyond PSA: The Next Generation of Prostate Cancer Biomarkers. *Sci Transl Med* (2012) 4 (127):127rv123. doi: 10.1126/scitranslmed.3003180
14. Tikkinen KAO, Dahm P, Lytvyn L, Heen AF, Vernooij RWM, Siemieniuk RAC, et al. Prostate Cancer Screening With Prostate-Specific Antigen (PSA) Test: A Clinical Practice Guideline. *BMJ* (2018) 362:k3581. doi: 10.1136/bmj.k3581
15. Duffy MJ. Biomarkers for Prostate Cancer: Prostate-Specific Antigen and Beyond. *Clin Chem Lab Med* (2020) 58(3):326–39. doi: 10.1515/cclm-2019-0693
16. Filella X, Gimenez N. Evaluation of [-2] proPSA and Prostate Health Index (Phi) for the Detection of Prostate Cancer: A Systematic Review and Meta-Analysis. *Clin Chem Lab Med* (2013) 51(4):729–39. doi: 10.1515/cclm-2012-0410
17. Loeb S, Catalona WJ. The Prostate Health Index: A New Test for the Detection of Prostate Cancer. *Ther Adv Urol* (2014) 6(2):74–7. doi: 10.1177/1756287213513488
18. Harshman LC, Chen YH, Liu G, Carducci MA, Jarrard D, Dreicer R, et al. Seven-Month Prostate-Specific Antigen Is Prognostic in Metastatic Hormone-Sensitive Prostate Cancer Treated With Androgen Deprivation With or Without Docetaxel. *J Clin Oncol* (2018) 36(4):376–82. doi: 10.1200/jco.2017.75.3921
19. Hussain M, Tangen CM, Higano C, Schelhammer PF, Faulkner J, Crawford ED, et al. Absolute Prostate-Specific Antigen Value After Androgen Deprivation Is a Strong Independent Predictor of Survival in New Metastatic Prostate Cancer: Data From Southwest Oncology Group Trial 9346 (INT-0162). *J Clin Oncol* (2006) 24(24):3984–90. doi: 10.1200/jco.2006.06.4246
20. Ignatiadis M, Sledge GW, Jeffrey SS. Liquid Biopsy Enters the Clinic - Implementation Issues and Future Challenges. *Nat Rev Clin Oncol* (2021) 8 (5):297–312. doi: 10.1038/s41571-020-00457-x

21. Oeyen S, Liégeois V, De Laere B, Buys A, Strijbos M, Dirix P, et al. Automated Enumeration and Phenotypic Characterization of CTCs and tdEVs in Patients With Metastatic Castration Resistant Prostate Cancer. *Prostate Cancer Prostatic Dis* (2021) 24(2):499–506. doi: 10.1038/s41391-020-00304-1
22. Scher HI, Graf RP, Schreiber NA, McLaughlin B, Jendrisak A, Wang Y, et al. Phenotypic Heterogeneity of Circulating Tumor Cells Informs Clinical Decisions Between AR Signaling Inhibitors and Taxanes in Metastatic Prostate Cancer. *Cancer Res* (2017) 77(20):5687–98. doi: 10.1158/0008-5472.Can-17-1353
23. Yang F, Ma J, Wan J, Ha W, Fang C, Lu H, et al. Epithelial-Mesenchymal Transition of Circulating Tumor Cells in Prostate Cancer Is Promoted by Survivin. *J Int Med Res* (2020) 48(1):300060519892395. doi: 10.1177/0300060519892395
24. Nanou A, Coumans FAW, van Dalum G, Zeune LL, Dolling D, Onstenk W, et al. Circulating Tumor Cells, Tumor-Derived Extracellular Vesicles and Plasma Cytokeratins in Castration-Resistant Prostate Cancer Patients. *Oncotarget* (2018) 9(27):19283–93. doi: 10.18632/oncotarget.25019
25. Nanou A, Miller MC, Zeune LL, de Wit S, Punt CJA, Groen HJM, et al. Tumour-Derived Extracellular Vesicles in Blood of Metastatic Cancer Patients Associate With Overall Survival. *Br J Cancer* (2020) 122(6):801–11. doi: 10.1038/s41416-019-0726-9
26. Joncas F-H, Lucien F, Rouleau M, Morin F, Leong HS, Pouliot F, et al. Plasma Extracellular Vesicles as Phenotypic Biomarkers in Prostate Cancer Patients. *Prostate* (2019) 79(15):1767–76. doi: 10.1002/pros.23901
27. Chen E, Cario CL, Leong L, Lopez K, Márquez CP, Chu C, et al. Cell-Free DNA Concentration and Fragment Size as a Biomarker for Prostate Cancer. *Sci Rep* (20215040) 11(1):5040. doi: 10.1038/s41598-021-84507-z
28. Fettke H, Kwan EM, Docanto MM, Bukczynska P, Ng N, Graham L-JK, et al. Combined Cell-Free DNA and RNA Profiling of the Androgen Receptor: Clinical Utility of a Novel Multianalyte Liquid Biopsy Assay for Metastatic Prostate Cancer. *Eur Urol* (2020) 78(2):173–80. doi: 10.1016/j.eururo.2020.03.044
29. Vandekerkhove G, Struss WJ, Annala M, Kallio HML, Khalaf D, Warner EW, et al. Circulating Tumor DNA Abundance and Potential Utility in De Novo Metastatic Prostate Cancer. *Eur Urol* (2019) 75(4):667–75. doi: 10.1016/j.eururo.2018.12.042
30. Annala M, Vandekerkhove G, Khalaf D, Taavitsainen S, Beja K, Warner EW, et al. Circulating Tumor DNA Genomics Correlate With Resistance to Abiraterone and Enzalutamide in Prostate Cancer. *Cancer Discov* (2018) 8(4):444–57. doi: 10.1158/2159-8290.Cd-17-0937
31. Belic J, Graf R, Bauernhofer T, Cherkas Y, Ulz P, Waldispuehl-Geigl J, et al. Genomic Alterations in Plasma DNA From Patients With Metastasized Prostate Cancer Receiving Abiraterone or Enzalutamide. *Int J Cancer* (2018) 143(5):1236–48. doi: 10.1002/ijc.31397
32. Pal SK, Moreira D, Won H, White SW, Duttagupta P, Lucia M, et al. Reduced T-Cell Numbers and Elevated Levels of Immunomodulatory Cytokines in Metastatic Prostate Cancer Patients De Novo Resistant to Abiraterone and/or Enzalutamide Therapy. *Int J Mol Sci* (2019) 20(8):1831. doi: 10.3390/ijms20081831
33. Harshman LC, Wang VX, Hamid AA, Santone G, Drake CG, Carducci MA, et al. Impact of Baseline Serum IL-8 on Metastatic Hormone-Sensitive Prostate Cancer Outcomes in the Phase 3 CHAARTED Trial (E3805). *Prostate* (2020) 80(16):1429–37. doi: 10.1002/pros.24074
34. Murray NP, Reyes E, Tapia P, Badínez L, Orellana N. Differential Expression of Matrix Metalloproteinase-2 Expression in Disseminated Tumor Cells and Micrometastasis in Bone Marrow of Patients With Nonmetastatic and Metastatic Prostate Cancer: Theoretical Considerations and Clinical Implications—An Immunocytochemical Study. *Bone Marrow Res* (2012) 2012:259351. doi: 10.1155/2012/259351
35. Szarvas T, Becker M, vom Dorp F, Meschede J, Scherag A, Bánkfalvi Á., et al. Elevated Serum Matrix Metalloproteinase 7 Levels Predict Poor Prognosis After Radical Prostatectomy. *Int J Cancer* (2011) 128(6):1486–92. doi: 10.1002/ijc.25454
36. Dhar M, Lam JN, Walser T, Dubinett SM, Rettig MB, Di Carlo D. Functional Profiling of Circulating Tumor Cells With an Integrated Vortex Capture and Single-Cell Protease Activity Assay. *Proc Natl Acad Sci USA* (2018) 115(40):9986–91. doi: 10.1073/pnas.1803884115
37. Tjon-Kon-Fat LA, Lundholm M, Schröder M, Wurdinger T, Thellenberg-Karlsson C, Widmark A, et al. Platelets Harbor Prostate Cancer Biomarkers and the Ability to Predict Therapeutic Response to Abiraterone in Castration Resistant Patients. *Prostate* (2018) 78(1):48–53. doi: 10.1002/pros.23443
38. Sleijfer S, Gratama J-W, Sieuwerts AM, Kraan J, Martens JWM, Foekens JA. Circulating Tumour Cell Detection on its Way to Routine Diagnostic Implementation? *Eur J Cancer* (2007) 43(18):2645–50. doi: 10.1016/j.ejca.2007.09.016
39. Allard WJ, Matera J, Miller MC, Repollet M, Connelly MC, Rao C, et al. Tumor Cells Circulate in the Peripheral Blood of All Major Carcinomas But Not in Healthy Subjects or Patients With Nonmalignant Diseases. *Clin Cancer Res an Off J Am Assoc Cancer Res* (2004) 10(20):6897–904. doi: 10.1158/1078-0432.Ccr-04-0378
40. Cohen SJ, Punt CJ, Iannotti N, Saidman BH, Sabbath KD, Gabrail NY, et al. Relationship of Circulating Tumor Cells to Tumor Response, Progression-Free Survival, and Overall Survival in Patients With Metastatic Colorectal Cancer. *J Clin Oncol* (2008) 26(19):3213–21. doi: 10.1200/jco.2007.15.8923
41. Cristofanilli M, Budd GT, Ellis MJ, Stopeck A, Matera J, Miller MC, et al. Circulating Tumor Cells, Disease Progression, and Survival in Metastatic Breast Cancer. *N Engl J Med* (2004) 351(8):781–91. doi: 10.1056/NEJMoa040766
42. de Bono JS, Scher HI, Montgomery RB, Parker C, Miller MC, Tissing H, et al. Circulating Tumor Cells Predict Survival Benefit From Treatment in Metastatic Castration-Resistant Prostate Cancer. *Clin Cancer Res* (2008) 14(19):6302. doi: 10.1158/1078-0432.CCR-08-0872
43. Swennenhuis JF, van Dalum G, Zeune LL, Terstappen LW. Improving the CellSearch® System. *Expert Rev Mol Diagn* (2016) 16(12):1291–305. doi: 10.1080/14737159.2016.1255144
44. Hussain SH, Huertas CS, Mitchell A, Deman A-L, Laurenceau E. Biosensors for Circulating Tumor Cells (CTCs)-Biomarker Detection in Lung and Prostate Cancer: Trends and Prospects. *Biosensors Bioelectron* (2021) 197:113770. doi: 10.1016/j.bios.2021.113770
45. Cho H, Kim J, Song H, Sohn KY, Jeon M, Han K-H. Microfluidic Technologies for Circulating Tumor Cell Isolation. *Analyst* (2018) 143(13):2936–70. doi: 10.1039/C7AN01979C
46. Miyamoto DT, Lee RJ, Kalinich M, LiCausi JA, Zheng Y, Chen T, et al. An RNA-Based Digital Circulating Tumor Cell Signature Is Predictive of Drug Response and Early Dissemination in Prostate Cancer. *Cancer Discov* (2018) 8(3):288–303. doi: 10.1158/2159-8290.Cd-16-1406
47. Moreno JG, Gomella LG. Evolution of the Liquid Biopsy in Metastatic Prostate Cancer. *Urology* (2019) 132:1–9. doi: 10.1016/j.urology.2019.06.006
48. Scher HI, Armstrong AJ, Schonhoft JD, Gill A, Zhao JL, Barnett E, et al. Development and Validation of Circulating Tumour Cell Enumeration (Epic Sciences) as a Prognostic Biomarker in Men With Metastatic Castration-Resistant Prostate Cancer. *Eur J Cancer* (2021) 150:83–94. doi: 10.1016/j.ejca.2021.02.042
49. Cheaito KA, Bahmad HF, Hadadeh O, Saleh E, Dagher C, Hammoud MS, et al. EMT Markers in Locally-Advanced Prostate Cancer: Predicting Recurrence? *Front Oncol* (2019) 9:131(131). doi: 10.3389/fonc.2019.00131
50. Chen J, Cao S, Situ B, Zhong J, Hu Y, Li S, et al. Metabolic Reprogramming-Based Characterization of Circulating Tumor Cells in Prostate Cancer. *J Exp Clin Cancer Res* (2018) 37(1):127. doi: 10.1186/s13046-018-0789-0
51. Zeune LL, Boink YE, van Dalum G, Nanou A, de Wit S, Andree KC, et al. Deep Learning of Circulating Tumour Cells. *Nat Mach Intell* (2020) 2(2):124–33. doi: 10.1038/s42256-020-0153-x
52. Ivanova E, Leong KW, Laine AF. Data from: Automated Multi-Process CTC Detection using Deep Learning. Computing Research Repository (CoRR). (2021). Available at: https://arxiv.org/abs/2109.12709.
53. Mao Y, Yin Z, Schober J. (2016). A Deep Convolutional Neural Network Trained on Representative Samples for Circulating Tumor Cell Detection, in: *the 2016 IEEE Winter Conference on Applications of Computer Vision (WACV)*. Lake Placid, NY: IEEE.
54. Goldkorn A, Tangen C, Plets M, Morrison G, Cunha A, Xu T, et al. Baseline Circulating Tumor Cell (CTC) Count as a Prognostic Marker of PSA Response and Progression in Metastatic Castrate Sensitive Prostate Cancer (mCSPC): Results From SWOG S1216, a Phase III Randomized Trial of Androgen Deprivation Plus Orteronel (Cyp17 Inhibitor) or Bicalutamide. *J Clin Oncol* (2020) 38(15_suppl):5506–6. doi: 10.1200/JCO.2020.38.15_suppl.5506

55. Resel Folkersma L, San José Manso L, Galante Romo I, Moreno Sierra J, Olivier Gómez C. Prognostic Significance of Circulating Tumor Cell Count in Patients With Metastatic Hormone-Sensitive Prostate Cancer. *Urology* (2012) 80(6):1328–32. doi: 10.1016/j.urology.2012.09.001
56. Chandrasekar T, Yang JC, Gao AC, Evans CP. Mechanisms of Resistance in Castration-Resistant Prostate Cancer (CRPC). *Transl Androl Urol* (2015) 4 (3):365–80. doi: 10.3978/j.issn.2223-4683.2015.05.02
57. Shafi AA, Yen AE, Weigel NL. Androgen Receptors in Hormone-Dependent and Castration-Resistant Prostate Cancer. *Pharmacol Ther* (2013) 140 (3):223–38. doi: 10.1016/j.pharmthera.2013.07.003
58. Antonarakis ES, Armstrong AJ, Dehm SM, Luo J. Androgen Receptor Variant-Driven Prostate Cancer: Clinical Implications and Therapeutic Targeting. *Prostate Cancer Prostatic Dis* (2016) 19(3):231–41. doi: 10.1038/pcan.2016.17
59. Sharp A, Coleman I, Yuan W, Sprenger C, Dolling D, Rodrigues DN, et al. Androgen Receptor Splice Variant-7 Expression Emerges With Castration Resistance in Prostate Cancer. *J Clin Invest* (2019) 129(1):192–208. doi: 10.1172/JCI122819
60. Tagawa ST, Antonarakis ES, Gjyrezi A, Galletti G, Kim S, Worroll D, et al. Expression of AR-V7 and ARv(567es) in Circulating Tumor Cells Correlates With Outcomes to Taxane Therapy in Men With Metastatic Prostate Cancer Treated in TAXYNERGY. *Clin Cancer Res an Off J Am Assoc Cancer Res* (2019) 25(6):1880–8. doi: 10.1158/1078-0432.Ccr-18-0320
61. Scher HI, Lu D, Schreiber NA, Louw J, Graf RP, Vargas HA, et al. Association of AR-V7 on Circulating Tumor Cells as a Treatment-Specific Biomarker With Outcomes and Survival in Castration-Resistant Prostate Cancer. *JAMA Oncol* (2016) 2(11):1441–9. doi: 10.1001/jamaoncol.2016.1828
62. Liu X, Ledet E, Li D, Dotiwala A, Steinberger A, Feibus A, et al. A Whole Blood Assay for AR-V7 and AR(v567es) in Patients With Prostate Cancer. *J Urol* (2016) 196(6):1758–63. doi: 10.1016/j.juro.2016.06.095
63. Jernberg E, Bergh A, Wikström P. Clinical Relevance of Androgen Receptor Alterations in Prostate Cancer. *Endocr Connect* (2017) 6(8):R146–r161. doi: 10.1530/ec-17-0118
64. Sieuwerts AM, Onstenk W, Kraan J, Beaufort CM, Van M, De Laere B, et al. AR Splice Variants in Circulating Tumor Cells of Patients With Castration-Resistant Prostate Cancer: Relation With Outcome to Cabazitaxel. *Mol Oncol* (2019) 13(8):1795–807. doi: 10.1002/1878-0261.12529
65. Xu J, Qiu Y. Role of Androgen Receptor Splice Variants in Prostate Cancer Metastasis. *Asian J Urol* (2016) 3(4):177–84. doi: 10.1016/j.ajur.2016.08.003
66. Abeshouse A, Ahn J, Akbani R, Ally A, Amin S, Christopher D, et al. The Molecular Taxonomy of Primary Prostate Cancer. *Cell* (2015) 163(4):1011–25. doi: 10.1016/j.cell.2015.10.025
67. van Dessel LF, van Riet J, Smits M, Zhu Y, Hamberg P, van der Heijden MS, et al. The Genomic Landscape of Metastatic Castration-Resistant Prostate Cancers Reveals Multiple Distinct Genotypes With Potential Clinical Impact. *Nat Commun* (2019) 10(1):5251. doi: 10.1038/s41467-019-13084-7
68. Hamid AA, Gray KP, Shaw G, MacConaill LE, Evan C, Bernard B, et al. Compound Genomic Alterations of TP53, PTEN, and RB1 Tumor Suppressors in Localized and Metastatic Prostate Cancer. *Eur Urol* (2019) 76(1):89–97. doi: 10.1016/j.eururo.2018.11.045
69. Gilson C, Ingleby F, Gilbert DC, Parry MA, Atako NB, Ali A, et al. Genomic Profiles of De Novo High and Low-Volume Metastatic Prostate Cancer: Results From a 2-Stage Feasibility and Prevalence Study in the STAMPEDE Trial. *JCO Precis Oncol* (2020) 4:882–97. doi: 10.1200/PO.19.00388
70. Stopsack KH, Nandakumar S, Wibmer AG, Haywood S, Weg ES, Barnett ES, et al. Oncogenic Genomic Alterations, Clinical Phenotypes, and Outcomes in Metastatic Castration-Sensitive Prostate Cancer. *Clin Cancer Res* (2020) 26(13):3230–8. doi: 10.1158/1078-0432.CCR-20-0168
71. Rodrigues DN, Casiraghi N, Romanel A, Crespo M, Miranda S, Rescigno P, et al. Rb1 Heterogeneity in Advanced Metastatic Castration-Resistant Prostate Cancer. *Clin Cancer Res* (2019) 25(2):687–97. doi: 10.1158/1078-0432.CCR-18-2068
72. Schweizer MT, Ha G, Gulati R, Brown LC, McKay RR, Dorff T, et al. CDK12-Mutated Prostate Cancer: Clinical Outcomes With Standard Therapies and Immune Checkpoint Blockade. *JCO Precis Oncol* (2020) 4:382–92. doi: 10.1200/po.19.00383
73. Kumar-Sinha C, Kalyana-Sundaram S, Chinnaiyan AM. Landscape of Gene Fusions in Epithelial Cancers: Seq and Ye Shall Find. *Genome Med* (2015) 7 (1):129. doi: 10.1186/s13073-015-0252-1
74. Scaravilli M, Koivukoski S, Latonen L. Androgen-Driven Fusion Genes and Chimeric Transcripts in Prostate Cancer. *Front Cell Dev Biol* (2021) 9:623809. doi: 10.3389/fcell.2021.623809
75. St John J, Powell K, Conley-Lacomb MK, Chinni SR. TMPRSS2-ERG Fusion Gene Expression in Prostate Tumor Cells and Its Clinical and Biological Significance in Prostate Cancer Progression. *J Cancer Sci Ther* (2012) 4 (4):94–101. doi: 10.4172/1948-5956.1000119
76. Adamaki M, Zoumpourlis V. Prostate Cancer Biomarkers: From Diagnosis to Prognosis and Precision-Guided Therapeutics. *Pharmacol Ther* (2021) 228:107932. doi: 10.1016/j.pharmthera.2021.107932
77. Kong DP, Chen R, Zhang CL, Zhang W, Xiao GA, Wang FB, et al. Prevalence and Clinical Application of TMPRSS2-ERG Fusion in Asian Prostate Cancer Patients: A Large-Sample Study in Chinese People and a Systematic Review. *Asian J Androl* (2020) 22(2):200–7. doi: 10.4103/aja.aja_45_19
78. Tai Y-L, Lin C-J, Li T-K, Shen T-L, Hsieh J-T, Chen BPC. The Role of Extracellular Vesicles in Prostate Cancer With Clinical Applications. *Endocr-Related Cancer* (2020) 27(5):R133–44. doi: 10.1530/ERC-20-0021
79. Logozzi M, Angelini DF, Iessi E, Mizzoni D, Di Raimo R, Federici C, et al. Increased PSA Expression on Prostate Cancer Exosomes in In Vitro Condition and in Cancer Patients. *Cancer Lett* (2017) 403:318–29. doi: 10.1016/j.canlet.2017.06.036
80. El-Sayed IY, Daher A, Destouches D, Firlej V, Kostallari E, Maille P, et al. Extracellular Vesicles Released by Mesenchymal-Like Prostate Carcinoma Cells Modulate EMT State of Recipient Epithelial-Like Carcinoma Cells Through Regulation of AR Signaling. *Cancer Lett* (2017) 410:100–11. doi: 10.1016/j.canlet.2017.09.010
81. Corcoran C, Rani S, O'Driscoll L. miR-34a is an Intracellular and Exosomal Predictive Biomarker for Response to Docetaxel With Clinical Relevance to Prostate Cancer Progression. *Prostate* (2014) 74(13):1320–34. doi: 10.1002/pros.22848
82. Huang X, Yuan T, Liang M, Du M, Xia S, Dittmar R, et al. Exosomal miR-1290 and miR-375 as Prognostic Markers in Castration-Resistant Prostate Cancer. *Eur Urol* (2015) 67(1):33–41. doi: 10.1016/j.eururo.2014.07.035
83. Kato T, Mizutani K, Kawakami K, Fujita Y, Ehara H, Ito M. CD44v8-10 mRNA Contained in Serum Exosomes as a Diagnostic Marker for Docetaxel Resistance in Prostate Cancer Patients. *Heliyon* (2020) 6(7):e04138. doi: 10.1016/j.heliyon.2020.e04138
84. Del Re M, Crucitta S, Sbrana A, Rofi E, Paolieri F, Gianfilippo G, et al. AR-V7 and AR-FL Expression is Associated With Clinical Outcome: A Translational Study in Patients With Castrate Resistant Prostate Cancer. *BJU Int* (2019) 124:693–700.. doi: 10.1111/bju.14792
85. Hatano K, Fujita K. Extracellular Vesicles in Prostate Cancer: A Narrative Review. *Trans Androl Urol* (2021) 10(4):1890–907. doi: 10.21037/tau-20-1210
86. Wyatt AW, Annala M, Aggarwal R, Beja K, Feng F, Youngren J, et al. Concordance of Circulating Tumor DNA and Matched Metastatic Tissue Biopsy in Prostate Cancer. *J Natl Cancer Inst* (2017) 109(12):1–9. doi: 10.1093/jnci/djx118
87. Beltran H, Romanel A, Conteduca V, Casiraghi N, Sigouros M, Franceschini GM, et al. Circulating Tumor DNA Profile Recognizes Transformation to Castration-Resistant Neuroendocrine Prostate Cancer. *J Clin Invest* (2020) 130(4):1653–68. doi: 10.1172/JCI131041
88. Kohli M, Tan W, Zheng T, Wang A, Montesinos C, Wong C, et al. Clinical and Genomic Insights Into Circulating Tumor DNA-Based Alterations Across the Spectrum of Metastatic Hormone-Sensitive and Castrate-Resistant Prostate Cancer. *EBioMedicine* (2020) 54:102728. doi: 10.1016/j.ebiom.2020.102728
89. Lau E, McCoy P, Reeves F, Chow K, Clarkson M, Kwan EM, et al. Detection of ctDNA in Plasma of Patients With Clinically Localised Prostate Cancer is Associated With Rapid Disease Progression. *Genome Med* (2020) 12(1):72. doi: 10.1186/s13073-020-00770-1
90. Lim SB, Lim CT, Lim W-T. Single-Cell Analysis of Circulating Tumor Cells: Why Heterogeneity Matters. *Cancers* (2019) 11(10):1595. doi: 10.3390/cancers11101595
91. Kwak M, Mu L, Lu Y, Chen JJ, Brower K, Fan R. Single-Cell Protein Secretomic Signatures as Potential Correlates to Tumor Cell Lineage Evolution and Cell-Cell Interaction. *Front Oncol* (2013) 3:10. doi: 10.3389/fonc.2013.00010

92. Niepel M, Spencer SL, Sorger PK. Non-Genetic Cell-to-Cell Variability and the Consequences for Pharmacology. *Curr Opin Chem Biol* (2009) 13(5-6):556–61. doi: 10.1016/j.cbpa.2009.09.015
93. Abali F, Baghi N, Mout L, Broekmaat JJ, Tibbe AGJ, Terstappen LWMM. Measurement of the Drug Sensitivity of Single Prostate Cancer Cells. *Cancers* (2021) 13(23):6083. doi: 10.3390/cancers13236083
94. Swennenhuis JF, Tibbe AGJ, Stevens M, Katika MR, van Dalum J, Duy Tong H, et al. Self-Seeding Microwell Chip for the Isolation and Characterization of Single Cells. *Lab Chip* (2015) 15(14):3039–46. doi: 10.1039/C5LC00304K
95. Andree KC, Mentink A, Zeune LL, Terstappen LWMM, Stoecklein NH, Neves RP, et al. Toward a Real Liquid Biopsy in Metastatic Breast and Prostate Cancer: Diagnostic LeukApheresis Increases CTC Yields in a European Prospective Multicenter Study (CTCTrap). *Int J Cancer* (2018) 143(10):2584–91. doi: 10.1002/ijc.31752
96. Calcinotto A, Spataro C, Zagato E, Di Mitri D, Gil V, Crespo M, et al. IL-23 Secreted by Myeloid Cells Drives Castration-Resistant Prostate Cancer. *Nature* (2018) 559(7714):363–9. doi: 10.1038/s41586-018-0266-0
97. Gong Y, Chippada-Venkata UD, Oh WK. Roles of Matrix Metalloproteinases and Their Natural Inhibitors in Prostate Cancer Progression. *Cancers* (2014) 6(3):1298–327. doi: 10.3390/cancers6031298
98. Frieling JS, Li T, Tauro M, Lynch CC. Prostate Cancer-Derived MMP-3 Controls Intrinsic Cell Growth and Extrinsic Angiogenesis. *Neoplasia* (2020) 22(10):511–21. doi: 10.1016/j.neo.2020.08.004
99. Liang W, Wang F, Chen Q, Dai J, Escara-Wilke J, Keller ET, et al. Targeting Cathepsin K Diminishes Prostate Cancer Establishment and Growth in Murine Bone. *J Cancer Res Clin Oncol* (2019) 145(8):1999–2012. doi: 10.1007/s00432-019-02950-y
100. In 't Veld SGJG, Wurdinger T. Tumor-Educated Platelets. *Blood* (2019) 133 (22):2359–64. doi: 10.1182/blood-2018-12-852830
101. Chen S, Zhu G, Yang Y, Wang F, Xiao Y-T, Zhang N, et al. Single-Cell Analysis Reveals Transcriptomic Remodellings in Distinct Cell Types That Contribute to Human Prostate Cancer Progression. *Nat Cell Biol* (2021) 23 (1):87–98. doi: 10.1038/s41556-020-00613-6
102. Thienger P, Rubin MA. Prostate Cancer Hijacks the Microenvironment. *Nat Cell Biol* (2021) 23(1):3–5. doi: 10.1038/s41556-020-00616-3
103. Josson S, Gururajan M, Sung SY, Hu P, Shao C, Zhau HE, et al. Stromal Fibroblast-Derived miR-409 Promotes Epithelial-to-Mesenchymal Transition and Prostate Tumorigenesis. *Oncogene* (2015) 34(21):2690–9. doi: 10.1038/onc.2014.212
104. Bhagirath D, Yang TL, Tabatabai ZL, Majid S, Dahiya R, Tanaka Y, et al. BRN4 Is a Novel Driver of Neuroendocrine Differentiation in Castration-Resistant Prostate Cancer and Is Selectively Released in Extracellular Vesicles With BRN2. *Clin Cancer Res an Off J Am Assoc Cancer Res* (2019) 25 (21):6532–45. doi: 10.1158/1078-0432.CCR-19-0498
105. Zhang T, Agarwal A, Almquist RG, Runyambo D, Park S, Bronson E, et al. Expression of Immune Checkpoints on Circulating Tumor Cells in Men With Metastatic Prostate Cancer. *biomark Res* (2021) 9(1):14. doi: 10.1186/s40364-021-00267-y

Conflict of Interest: The authors declare that the research was conducted in the absence of any commercial or financial relationships that could be construed as a potential conflict of interest.

Publisher's Note: All claims expressed in this article are solely those of the authors and do not necessarily represent those of their affiliated organizations, or those of the publisher, the editors and the reviewers. Any product that may be evaluated in this article, or claim that may be made by its manufacturer, is not guaranteed or endorsed by the publisher.

Copyright © 2022 Dathathri, Isebia, Abali, Lolkema, Martens, Terstappen and Bansal. This is an open-access article distributed under the terms of the Creative Commons Attribution License (CC BY). The use, distribution or reproduction in other forums is permitted, provided the original author(s) and the copyright owner(s) are credited and that the original publication in this journal is cited, in accordance with accepted academic practice. No use, distribution or reproduction is permitted which does not comply with these terms.

frontiers | Frontiers in Oncology

ORIGINAL RESEARCH
published: 02 June 2022
doi: 10.3389/fonc.2022.907625

The Values of Systemic Immune-Inflammation Index and Neutrophil–Lymphocyte Ratio in Predicting Biochemical Recurrence in Patients With Localized Prostate Cancer After Radical Prostatectomy

Shuo Wang[1†], Xiao Yang[1†], Ziyi Yu[1†], Peng Du[1], Xinan Sheng[2*], Yudong Cao[1], Xieqiao Yan[2], Jinchao Ma[1] and Yong Yang[1]*

[1] Key Laboratory of Carcinogenesis and Translational Research (Ministry of Education), Urological Department, Peking University Cancer Hospital & Institute, Beijing, China, [2] Key Laboratory of Carcinogenesis and Translational Research (Ministry of Education), Department of Renal Cancer and Melanoma, Peking University Cancer Hospital & Institute, Beijing, China

OPEN ACCESS

Edited by:
Takeshi Yuasa,
Japanese Foundation for Cancer Research, Japan

Reviewed by:
Felice Crocetto,
Federico II University Hospital, Italy
Yu Fan,
Peking University, China

***Correspondence:**
Peng Du
dupeng9000@126.com
Xinan Sheng
doctor_sheng@126.com

†These authors have contributed equally to this work and share first authorship

Specialty section:
This article was submitted to Genitourinary Oncology, a section of the journal Frontiers in Oncology

Received: 29 March 2022
Accepted: 04 May 2022
Published: 02 June 2022

Citation:
Wang S, Yang X, Yu Z, Du P, Sheng X, Cao Y, Yan X, Ma J and Yang Y (2022) The Values of Systemic Immune-Inflammation Index and Neutrophil–Lymphocyte Ratio in Predicting Biochemical Recurrence in Patients With Localized Prostate Cancer After Radical Prostatectomy. Front. Oncol. 12:907625. doi: 10.3389/fonc.2022.907625

Purpose: To investigate the association between preoperative systemic immune-inflammation index (SII) and neutrophil–lymphocyte ratio (NLR) and oncological outcomes in localized prostate cancer (PCa) patients after radical prostatectomy (RP).

Methods: Between January 2014 and December 2019, 291 patients with pathologically confirmed localized PCa who underwent RP were included in this study. The threshold values of SII and NLR for biochemical recurrence (BCR) were calculated according to Youden's index based on the receiver operating characteristic (ROC) curve, then the patients were divided into two groups by the threshold values of SII and NLR, and the clinicopathological outcomes were analyzed and compared between groups, respectively. The binary logistic regression model was used to evaluate the association between SII, NLR, and pathological outcomes including Gleason score (GS) and pathological T (pT) stage. Kaplan–Meier curves and univariable and multivariable Cox regression models were used to determine the association between high SII, high NLR, and BCR-free survival, respectively.

Results: The median follow-up time was 48 months (IQR 36–62), and 114 (39.18%) patients developed BCR. The AUC of SII for BCR was 0.813 ($P < 0.001$), with a threshold value of 528.54, a sensitivity of 72.9%, and a specificity of 76.3%; the AUC of NLR for BCR was 0.824 ($P < 0.001$), with a threshold value of 2.62, a sensitivity of 71.2%, and a specificity of 81.6%. Patients were divided into two groups according to the threshold values of SII and NLR, respectively. Patients in the high SII group had higher tPSA, GS, pT stage, and BCR rate than patients in the low SII group ($P = 0.004$, 0.04, 0.007, and <0.001, respectively), and patients in the high NLR group had higher tPSA, GS, pT stage, and BCR rate than patients in the low NLR group ($P = 0.04$, 0.02, 0.006, and <0.001, respectively).

Multivariable logistic regression analysis revealed that high SII was significantly correlated with adverse pathological outcomes of GS (HR, 1.656; 95% CI, 1.00–2.742, $P = 0.042$) and pT stage (HR, 1.478; 95% CI, 0.972–3.64, $P = 0.028$); there was no association between high NLR and pathological events. Kaplan–Meier analysis showed significantly poorer BCR-free survival in patients with high SII or high NLR ($P < 0.001$ and <0.001, respectively). By using the multivariable Cox regression model, high SII (HR, 4.521; 95% CI, 2.262–9.037, $P < 0.001$) and high NLR (HR, 4.787; 95% CI, 2.339–9.798, $P < 0.001$) were both significant predictors of BCR after RP.

Conclusion: High SII was significantly related to unfavorable clinicopathological outcomes. High preoperative SII and NLR were related to higher BCR rate in localized PCa after RP, and they were all independent risk factors associated with shorter BCR-free survival. These two factors might provide promising and inexpensive methods for predicting clinical outcomes in patients with RP.

Keywords: prostate cancer, systemic immune-inflammation index, neutrophil–lymphocyte ratio, inflammatory markers, biochemical recurrence

INTRODUCTION

For localized prostate cancer (PCa), the most useful treatment method is radical prostatectomy. Unfortunately, approximately 30%–50% of patients will experience biochemical recurrence (BCR) after radical prostatectomy (RP), which is closely associated with tumor recurrence and metastasis (1). Many factors may influence the prostate-specific antigen (PSA) level after RP, and a retrospective study demonstrated that smoking status might be one of the most important factors (2). Meanwhile, several factors including Gleason score (GS) and clinical or pathological stage may be used for predicting BCR after RP as proven by several studies, but they lack the accuracy to guide the following therapeutic approach (2, 3). Therefore, reliable, easily accessible, and inexpensive markers are needed for assessing clinical outcomes in patients with localized PCa after RP.

The association between inflammation and PCa has been proven by literature (4). Neutrophil–lymphocyte ratio (NLR) is a well-known inexpensive and effective representative marker of an inflammatory condition. It has been proven to be positively associated with prognosis in various kinds of malignant tumors (5, 6). Regarding PCa, NLR was revealed to be an independent predictor for overall survival (OS) in patients with metastatic castration-resistant prostate cancer (mCRPC) (7). Recently, one retrospective study has shown a significantly worse prognosis in metastasis-free and OS of localized PCa patients with high NLR after radiotherapy (8). However, there is a paucity of studies about the association between NLR and clinical and pathological outcomes in localized PCa after RP.

In addition, another novel inflammatory marker, systemic immune-inflammation index (SII) which combines components of NLR and platelet–lymphocyte ratio (PLR), has been proven to be a more powerful method of predicting occurrence and progression in several kinds of tumors (9–11). In terms of PCa, it was firstly described in 2016 and was considered a powerful marker for predicting the prognosis of mCRPC (12). However, there are no data on the predictive value of SII on BCR in the setting of localized PCa after RP.

Thus, in this retrospective study, we aimed to evaluate the values of preoperative NLR and SII in predicting BCR after RP and detected their association with clinicopathological outcomes.

MATERIAL AND METHODS

This retrospective study was carried out at Peking University Cancer Hospital & Institute and got the approval of the Medical Ethics Review Committee of Peking University Cancer Hospital & Institute (protocol code 2020KT30).

Patients

Two hundred and ninety-one patients with localized PCa who underwent RP, consisting of 287 with laparoscopic RP and 4 with open RP, between January 2014 and December 2019z were reviewed. Among these patients, no one received neoadjuvant therapy before RP and adjuvant therapy after RP until the detection of BCR. In patients with smoking status, smoking was recommended to be ceased 1 month before RP. Preoperative clinical characteristics including age, serum total PSA (tPSA) value, total prostate volume (TPV), body mass index (BMI), and complete blood count (CBC)-based parameters as well as postoperative pathological and BCR outcomes were collected and compared according to the level of NLR and SII, respectively. Data of risk factors related to BCR including GS, pT stage, NLR, and SII were collected, and their associations with BCR-free survival time were analyzed. A single preoperative CBC with differential was performed as part of the routine assessment testing 1–2 days before RP simultaneously with the tPSA value. The CBC-based parameters including NLR and SII were used in this study. To ensure the CBCs were not affected by other factors, patients who met one of the following criteria were excluded: any surgical intervention within 1 month, non-steroidal anti-inflammatory

drugs used within 1 month, acute or chronic infection, malignant tumors in other organs, and systemic inflammatory disease.

Procedure

Ultrasound-guided 13-core transrectal prostate biopsy was performed in patients with PSA >4 ng/ml at our institute. The results of serum tPSA value and CBC-based parameters were collected just 1–2 days before the RP surgery and at least 3 weeks after the prostate biopsy to minimize the effect of the prostate biopsy. MRI, emission computed tomography (ECT), or CT was performed before surgery to confirm no bone, lymph node, or distant organ metastasis. Laparoscopic RP or open RP was performed in patients with PCa at least 30 days after the biopsy. Extrafascial radical prostatectomy through an extraperitoneal approach was performed by skilled and experienced surgeons in our institute according to the technique of Walsh et al., and standard pelvic lymph node dissection was performed in all patients (13). All specimens were assessed by a sophisticated pathologist at our institute, and serum tPSA value was detected every 1–3 months after RP.

Variables

The prostate was measured in 3-dimensional aspects, and its volume was estimated with the modified ellipsoid formulation in cm^3 (0.523 [length × width × height]) after surgery. Pathologic GSs were recorded and patients were staged according to the 2010 American Joint Committee on Cancer system (AJCC, pathologic stages T1–T4) (14). Tumors were classified into low (GS ≤ 6), intermediate (GS = 7), and high grade (GS ≥ 8) according to the D'Amico risk classification (15). NLR and SII were calculated by using the numbers of blood cell count-based systemic markers of inflammation. The NLR and SII were calculated as follows: NLR = neutrophil count/lymphocyte count; SII = platelet count × neutrophil count/lymphocyte count. SII was presented as a combination of NLR and PLR (9, 16). Body mass index (BMI) = weight (kg)/height $(meter)^2$. BCR was defined as at least two consecutive serum tPSA ≥0.2 ng/ml according to the guidelines of the American Urological Association (17), and data of time free from BCR were collected.

Statistical Analysis

Measurement data confirming normal distribution analyzed by the Shapiro–Wilk test are presented as mean ± SD. The independent sample *t*-test was used to evaluate the differences between continuous variables, while chi-square tests were performed to examine categorical variables. To determine the optimal cutoff value of NLR and SII for BCR, Youden's index was calculated using the receiver operating characteristic curve (ROC), and the corresponding specificity–sensitivity levels were provided. Youden's index was defined as $YI_{(C)} = \max c\,[Se_{(C)} + SP_{(C)} - 1]$. The binary logistic regression model (univariate and multivariate analysis) was used to evaluate the association between NLR, SII, and adverse pathological events, which were all compared with the reference group (Ref). Kaplan–Meier analyses were performed for BCR-free survival according to NLR and SII using the log-rank test, and the survival curves were described. The univariable and multivariable Cox regression models were used to identify the co-variables that influence BCR. The software used to run the analysis was IBM-SPSS version 20. All tests were two-sided. $P < 0.05$ was considered to be the threshold for statistically meaningful differences.

RESULTS

Patients' Clinicopathologic Characteristics and the Cutoff Values of SII and NLR for BCR

A total of 291 patients with localized PCa were enrolled in the study. The median values of clinical factors were 66.13 ± 6.05 years for age, 24.35 ± 4.14 for BMI, 36.62 ± 23.15 ml for TPV, and 26.15 ± 33.77 ng/ml for tPSA. Twelve patients (4.12%) were pT1, 117 (40.21%) were pT2, and 162 (55.67%) were pT3. Thirty-nine patients (13.4%) were of low risk (GS ≤ 6), 129 (44.33%) were of intermediate risk (GS = 7), and 123 (42.27%) were of high risk (GS ≥ 8). Twenty patients (6.87%) were with pelvic lymph node metastases. The ROC of SII and NLR for BCR were analyzed to determine the optimal cutoff values for SII and NLR (**Figure 1**). The AUC for SII was 0.813, which was significantly lower than 0.05 ($P < 0.001$), with a threshold value of 528.54, a sensitivity of 72.9%, and a specificity of 76.3%; the AUC for NLR was 0.824, which was significantly lower than 0.05 ($P < 0.001$), with a threshold value of 2.62, a sensitivity of 71.2%, and a specificity of 81.6%; therefore, according to the threshold values of NLR and SII, the patients were divided into low-level and high-level groups, respectively. The patients' clinicopathologic demographics are summarized in **Table 1**.

Clinicopathological Characteristics in the Low and High NLR Groups

Initially, the distribution of clinicopathological characteristics was compared between groups according to the threshold value of NLR. The high NLR group showed unfavorable features compared with the low NLR group. In the high NLR group, preoperative serum tPSA ($P = 0.04$), GS ($P = 0.02$), and pT stage ($P = 0.006$) were significantly higher compared with those in the low NLR group, but the distribution of age, BMI, and TPV did not show any significant differences as shown in **Table 1**.

Then, univariable and multivariable logistic regression models were used to evaluate the association between NLR and several adverse pathological events. The results showed that there was no association between high NLR and pathological events including pT stage and GS as shown in **Tables 2, 3**.

Clinicopathological Characteristics in the Low and High SII Groups

The distribution of clinicopathological characteristics was compared between groups according to the threshold value of SII. The high SII group showed unfavorable features compared with the low SII group. In the high SII group, preoperative serum tPSA ($P = 0.004$), GS ($P = 0.04$), and pT stage ($P = 0.007$) were significantly higher compared with those in the low SII group, but the distribution of age, BMI, and TPV did not show any significant differences as shown in **Table 1**.

Then, univariable and multivariable logistic regression models were used to evaluate the association between SII and adverse

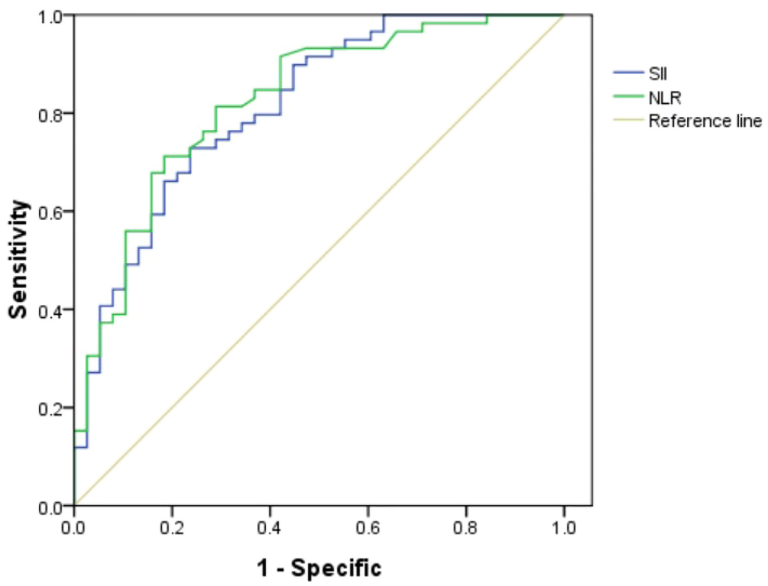


FIGURE 1 | Role of the systemic immune-inflammation index (SII) and neutrophil–lymphocyte ratio (NLR) in predicting biochemical recurrence (BCR) after radical prostatectomy (RP) by ROC curve analysis. The AUC for NLR was 0.824 with *P*-value <0.001, and the AUC for SII was 0.813 with *P*-value <0.001.

TABLE 1 | Clinicopathological characteristics of the entire cohort and the NLR and SII subgroups.

	Mean (± SD) or counts (percentage of total)						
	Entire cohort	**Low NLR**	**High NLR**	***P*-value**	**Low SII**	**High SII**	***P*-value**
Number	291	141	150		129	162	
Age (years)	66.13 ± 6.05	64.79 ± 5.95	67.4 ± 5.92	0.68	65.24 ± 6.11	66.90 ± 5.95	0.72
BMI (kg/m^2)	24.35 ± 4.14	25.11 ± 4.74	23.63 ± 3.38	0.08	24.78 ± 4.96	23.98 ± 3.29	0.77
tPSA (ng/ml)	26.15 ± 33.77	19.42 ± 21.14	32.74 ± 41.88	0.04	18.66 ± 18.49	32.89 ± 42.23	0.004
TPV (ml)	36.62 ± 23.15	35.31 ± 24.66	37.73 ± 21.96	0.62	35.84 ± 24.83	37.25 ± 21.90	0.71
GS (%)	291	141	150	0.02	141	150	0.04
≤6	39 (13.4)	21 (14.89)	18 (12.0)		24 (18.6)	15 (9.3)	
=7	129 (44.33)	72 (51.1)	57 (38.0)		57 (44.2)	72 (44.4)	
≥8	123 (42.27)	48 (34.0)	75 (50)		48 (37.2)	75 (46.3)	
pT stage (%)	291	141	150	0.006	129	162	0.007
pT1	12 (4.12)	9 (6.4)	3 (2)		4 (3.1)	8 (4.9)	
pT2	117 (40.21)	66 (46.8)	51 (34)		65 (50.4)	52 (32.1)	
pT3	162 (55.67)	66 (46.8)	96 (64)		60 (46.5)	102 (63)	

BMI, body mass index; TPV, total prostate volume; GS, Gleason score; pT, pathological stage; NLR, neutrophil–lymphocyte ratio; SII, systemic immune-inflammation index.

TABLE 2 | Univariable and multivariable analyses of the impact of NLR and SII on pathological T stage.

	Univariable analysis			**Multivariable analysis**		
	pT1–2a vs. pT2b–3			**pT1–2a vs. pT2b–3**		
	HR	**95% CI**	***P*-value**	**HR**	**95% CI**	***P*-value**
NLR < 2.62	1 (Ref)	1 (Ref)		1 (Ref)	1 (Ref)	
NLR ≥ 2.62	0.976	0.635–1.501	0.994	1.937	0.508–7.393	0.245
SII < 528.54	1 (Ref)	1 (Ref)		1 (Ref)	1 (Ref)	
SII ≥ 528.54	1.243	0.806–1.917	0.039	1.478	0.972–3.64	0.028

Ref, reference.

TABLE 3 | Univariable and multivariable analyses of the impact of NLR and SII on GS.

	Univariable analysis			Multivariable analysis		
	GS ≤ 6 vs. GS ≥ 7			GS ≤ 6 vs. GS ≥ 7		
	HR	95% CI	*P*-value	HR	95% CI	*P*-value
NLR < 2.62	1 (Ref)	1 (Ref)		1 (Ref)	1 (Ref)	
NLR ≥ 2.62	1.393	0.857–2.263	0.172	1.327	0.810–2.176	0.245
SII < 528.54	1 (Ref)	1 (Ref)		1 (Ref)	1 (Ref)	
SII ≥ 528.54	1.577	0.965–1.578	0.038	1.656	1.00–2.742	0.042

Ref, reference.

pathological events. In the univariable analysis, SII ≥528.54 was a risk factor associated with higher pT stage (HR, 1.243; 95% CI, 0.806–1.917, $P = 0.039$) and higher GS (HR, 1.577; 95% CI, 0.965–1.578, $P = 0.038$); in the multivariable analysis, SII ≥528.54 was an independent risk factor strongly associated with higher pT stage (HR, 1.478; 95% CI, 0.972–3.64, $P = 0.028$) and higher GS (HR, 1.656; 95% CI, 1.00–2.742, $P = 0.042$) as shown in **Tables 2, 3**.

The Association Between NLR, SII, and BCR-Free Survival

The median follow-up time was 48 months (IQR 36–62) and 114 (39.18%) patients developed BCR. Thirty-eight (26.95%) and 76 (50.67%) patients developed BCR in the low and high NLR groups ($P < 0.001$). Kaplan–Meier analysis showed that BCR-free survival was significantly shorter in the high NLR group than in the low NLR group as shown in **Figure 2** ($P < 0.001$). By using the multivariable Cox regression model, it was revealed that NLR ≥2.62 (HR, 4.787; 95% CI, 2.339–9.798, $P < 0.001$) was a significant independent factor associated with BCR after RP as shown in **Table 4**.

Thirty-five (27.13%) and 79 (48.77%) patients developed BCR in the low and high SII groups ($P < 0.001$). Kaplan–Meier analysis showed the BCR-free survival was significantly shorter in the high SII group than in the low SII group as shown in **Figure 3** ($P < 0.001$). By using the multivariable Cox regression model, it was revealed that SII ≥528.54 (HR, 4.521; 95% CI, 2.262–9.037, $P < 0.001$) was a significant independent factor associated with BCR after RP as shown in **Table 4**.

Meanwhile, the multivariable Cox regression model revealed that GS ≥8 (HR, 2.187; 95% CI, 1.602–2.964, $P = 0.032$) and pT3

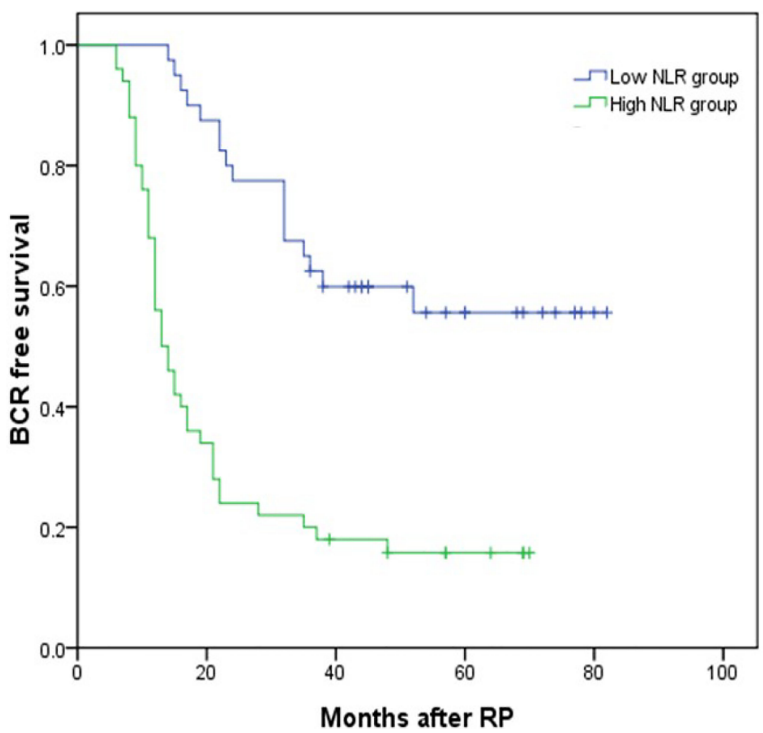


FIGURE 2 | Kaplan–Meier curves for BCR-free survival according to NLR level. BCR-free survival of patients with NLR <2.62 was significantly longer than that of patients with NLR ≥2.62 ($P < 0.001$ by log-rank test).

TABLE 4 | Cox regression analysis of potential factors associated with BCR after RP.

	Univariable analysis			Multivariable analysis		
	HR	**95% CI**	***P*-value**	**HR**	**95% CI**	***P*-value**
NLR < 2.62	1 (Ref)	1 (Ref)		1 (Ref)	1 (Ref)	
NLR ≥ 2.62	4.060	2.290–7.200	<0.001	4.787	2.339–9.798	<0.001
SII < 528.54	1 (Ref)	1 (Ref)		1 (Ref)	1 (Ref)	
SII ≥ 528.54	3.984	2.225–7.133	<0.001	4.521	2.262–9.037	<0.001
pT stage						
pT1	1 (Ref)	1 (Ref)		1 (Ref)	1 (Ref)	
pT2	1.633	0.217–12.279	1.633	5.667	0.661–48.622	0.114
pT3	2.998	0.812–21.864	<0.001	8.385	0.952–73.835	0.042
GS						
≤6	1 (Ref)	1 (Ref)		1 (Ref)	1 (Ref)	
=7	1.744	0.894–3.402	0.103	1.620	0.639–4.111	0.310
≥8	1.867	0.926–3.765	0.021	2.187	1.602–2.964	0.032

Ref, reference.

stage (HR, 8.385; 95% CI, 0.952–73.835, $P = 0.042$) were also significant independent factors associated with BCR after RP as shown in **Table 4**.

DISCUSSION

In China, the incidence of PCa has been increasing in recent years. Among PCa patients after RP, BCR is one of the most important factors associated with the poor prognosis of patients (18). In a previous study, we investigated the association between NLR, SII, and the occurrence of PCa and revealed that high SII and NLR were all independent factors predicting PCa. SII seemed to be a more powerful tool compared with NLR (19). In this study, we further investigated the relationship between inflammatory factors and clinicopathological outcomes in localized PCa patients after RP and demonstrated that high SII and NLR were significantly associated with higher BCR rate and shorter BCR-free survival; meanwhile, high SII was strongly associated with higher GS and pT stage. To the best of our knowledge, this is the first study that investigated the relationship between SII and BCR in localized PCa patients after RP.

The relationship between inflammation and various kinds of malignant tumors has been reported by many studies (20, 21).

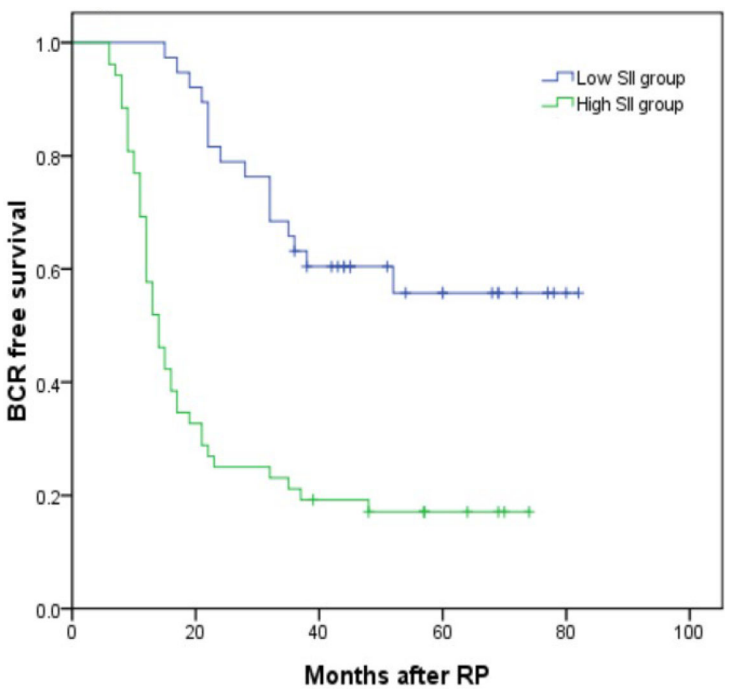


FIGURE 3 | Kaplan–Meier curves for BCR-free survival according to SII level. BCR-free survival of patients with SII <528.54 was significantly longer than that of patients with SII ≥528.54 ($P < 0.001$ by log-rank test).

The NLR based on the calculation of neutrophil to lymphocyte counts has been proposed as an indicator of general immune response to various stress stimuli and the host inflammatory status. An elevated NLR may be associated with both an increased neutrophil-dependent systemic inflammatory response and a lower lymphocyte-mediated antitumor immune response, reflecting a favorable immune microenvironment for tumor development and metastasis (22). In urological malignant tumors, inflammatory parameters have been considered important biomarkers for predicting bladder cancer progression (23). The relationship between NLR and clinical outcomes in PCa has been reported by many studies. Zhang et al. indicated that NLR ≥2.36 increased the risk of involvement of lymph nodes and was associated with higher GS (24). Another study revealed that NLR ≥2.5 was positively associated with GS, pT stage, and extracapsular extension (25). But only a few studies have investigated the role of NLR in predicting BCR after RP in localized PCa (26, 27). One study investigating the clinical outcomes in localized PCa patients after RP revealed that high NLR was significantly correlated with poor OS, CSS (cancer-specific survival), and BCR (27). Lee et al. demonstrated that NLR ≥2.5 was significantly related to unfavorable clinicopathological outcomes and worse BCR-free survival (25). Another study obtained the opposite conclusion: the study analyzed the data of 327 PCa patients who underwent robot-assisted RP and found that there was no correlation between NLR and PLR with BCR (28). However, the relationship between NLR and BCR remained controversial. In our study, we revealed that the threshold value of NLR for BCR was 2.62, which was similar to those reported by Lee et al. and Zhao et al. (25, 29). NLR ≥2.62 was significantly associated with poorer BCR-free survival according to Kaplan–Meier analysis and Cox regression analysis, but not associated with clinicopathological outcomes. We believed that NLR was an effective factor in predicting BCR in localized PCa patients after RP.

Recently, besides neutrophils and lymphocytes (30), the role of platelets has also been well-established in tumor occurrence and metastasis (31). SII, a novel inflammatory index that combines components of neutrophils, lymphocytes, and platelets, has been considered to reflect the systemic inflammatory responses more comprehensively than other inflammatory indexes. High SII suggested an elevated non-specific inflammatory status and a weak adaptive immune response in patients, which might promote the occurrence and progression of the tumor (32, 33). Several studies on inflammatory markers analyzed their predictive values in the PCa setting with various conclusions, but only a few of them included SII (34, 35). Our previous study demonstrated that high SII was an independent predictor for PCa, and it was one of the few studies detecting the role of SII in PCa (18). Recently, Rajwa et al. have evaluated the role of SII in non-metastatic PCa patients after RP and demonstrated that high preoperative SII ≥620 was independently associated with extracapsular extension, non-organ confined disease, and upgrading at RP (36). Another study evaluated the prognostic role of SII and NLR in mCRPC patients treated with abiraterone and revealed that SII ≥535 and NLR ≥3 were all independent predictors associated with shorter OS (12). Fan et al. obtained the same results and concluded that high SII could be used as a predictor for OS in mCRPC patients treated with abiraterone (37). However, none of these studies investigated the association between SII and BCR-free survival in localized PCa after RP. In our study, for the first time in the literature, the role of SII in predicting BCR-free survival was analyzed and the results indicated that high SII was significantly associated with shorter BCR-free survival. The cutoff value of SII for BCR was determined to be 528.54, and we also demonstrated that SII was associated with high BCR rate, pT stage, and GS, which was consistent with the conclusion of previous literature (36). For NLR, we failed to detect the association between NLR and pathological outcomes. Furthermore, both SII and NLR could represent the novel predictive markers for BCR in PCa patients after RP, and SII seemed more favorable for it was also associated with aggressive pathological outcomes.

This study still has some limitations. First, this was a single-center, retrospective study. Second, the biomarker was measured at a single time point, and it can be strengthened by collecting different preoperative sets of blood samples. Third, because of the relatively small sample size, more samples are needed in further studies.

CONCLUSION

High preoperative SII was associated with higher GS and pT stage. High preoperative SII and NLR were related to higher BCR rate in localized PCa after RP, and they were all independent risk factors associated with shorter BCR-free survival. These two factors might provide promising and inexpensive methods predicting clinical outcomes in patients with RP. However, additional well-organized and large prospective studies are needed.

DATA AVAILABILITY STATEMENT

The raw data supporting the conclusions of this article will be made available by the authors, without undue reservation.

ETHICS STATEMENT

This retrospective study was carried out at Peking University Cancer Hospital & Institute and got the approval of the Medical Ethics Review Committee of Peking University Cancer Hospital & Institute (protocol code 2020KT30).

AUTHOR CONTRIBUTIONS

PD, XS, and SW designed the study. SW, XY, ZY, YC, JM, PD, XS, XQY, and YY performed the study and analyzed the data. PD, XS, SW, XY, and ZY wrote the manuscript draft and revised the manuscript. All authors have read and agreed to the published version of the manuscript.

FUNDING

This study was supported by the Capital's Funds for Health Improvement and Research (2022-1G-1021) and the National Nature Science Foundation of China (82172604).

REFERENCES

1. Broeck T, Bergh RCN, Arfi N, Gross T, Moris L, Biers E, et al. Prognostic Value of Biochemical Recurrence Following Treatment With Curative Intent for Prostate Cancer: A Systematic Review. *Eur Urol* (2019) 75:967–87. doi: 10.1016/j.eururo.2018.10.011
2. Tarantino G, Crocetto F, Di Vito C, Martino R, Pandolfo SD, Creta M, et al. Clinical Factors Affecting Prostate Specific Antigen Levels in Prostate Cancer Patients Undergoing Radical Prostatectomy: A Retrospective Study. *Future Sci OA* (2021) 7:FSO643. doi: 10.2144/fsoa-2020-0154
3. Shariat SF, Semjonow A, Lilja H, Caroline S, Andrew JV, Bjartell A, et al. Tumor Markers in Prostate Cancer I: Blood Based Markers. *Acta Oncol* (2011) 50:61–75. doi: 10.3109/0284186X.2010.542174
4. Andrew GR, Sudha MS, Dhananjay AC, Nilesh SG, Sean RW, Olesandr NK, et al. Racial Differences in the Systemic Inflammatory Response to Prostate Cancer. *PloS One* (2021) 16:e0252951. doi: 10.1371/journal.pone.0252951
5. Sarraf KM, Belcher E, Raevsky E, Andrew GN, Peter G, Lim E, et al. Neutrohphil/lymphocyte Ratio and its Association With Survival After Compete Resection in non-Small Cell Lung Cancer. *J Thorac Cardiovasc Surg* (2009) 137:425–8. doi: 10.1016/j.jtcvs.2008.05.046
6. Walsh SR, Cook EJ, Goulder F, Justin TA, Keeling NK. Neutrophil-Lymphocyte Ratio as a Prognostic Factor in Colorectal Cancer. *J Surg Oncol* (2005) 91:181–4. doi: 10.1002/jso.20329
7. Sonpavde G, Pond GR, Armstrong AJ, Clarke SJ, Vardy JL, Templeton AJ, et al. Prognostic Impact of the Neutrophil to Lymphocyte Ratio in Men With Metastatic Castration Resistant Prostate Cancer. *Clin Genitourin Cancer* (2014) 12:317–24. doi: 10.1016/j.clgc.2014.03.005
8. Langsenlehner T, Thurner EM, Krenn-Pilko S, Langsenlehner U, Stojakvoic T, Gerger A, et al. Validation of the Neutrophil to Lymphocyte Ratio as a Prognostic Factor in a Cohort of European Prostate Cancer Patients. *World J Urol* (2015) 33:1661–7. doi: 10.1007/s00345-015-1494-7
9. Hu B, Yang XR, Xu Y, Sun YF, Sun C, Guo W, et al. Systemic Immune Inflammation Index Predicts Prognosis of Patients After Curative Resection for Hepatocellular Carcinoma. *Clin Cancer Res* (2014) 20:6212–22. doi: 10.1158/1078-0432.CCR-14-0442
10. Lolli C, Basso U, Derosa L, Scarpi E, Sava T, Santoni M, et al. Systemic Immune Inflammation Index Predicts the Clinical Outcome in Patients With Metastatic Renal Cell Cancer Treated With Sunitinib. *Oncotarget* (2014) 7:54564–71. doi: 10.18632/oncotarget.10515
11. Passardi A, Scarpi E, Cavanna L, Monia DA, Tassinari D, Silvana L, et al. Inflammatory Indexes as Predictors of Prognosis and Bevacizumab Efficacy in Patients With Metastatic Colorectal Cancer. *Oncotarget* (2016) 22:33210–9. doi: 10.18632/oncotarget.8901
12. Lolli C, Caffo O, Scarpi E, Aieta M, Conteduca V, Maines F, et al. Systemic Immune Inflammation Index Predicts the Clinical Outcome in Patients With mCRPC Treated With Abiraterone. *Front Pharmacol* (2016) 13:376. doi: 10.3389/fphar.2016.00376
13. Walsh PC, Retik AB, Vaughan ED, Roger RD, Louis RK, Craig AP, et al. Anatomic Radical Retropubic Prostatectomy. In: *Campbell's Urology*, *Ed 8*, vol. 4. Philadephia: Elsevier (2002). p. 3107–29.
14. Frederick L, Page DL, Fleming ID, Abedin J, Abeliovich H, Abraham AA, et al. *AJCC Cancer Staging Manual*. New York, NY, USA: Springer Science & Business Media (2002).
15. D' Amico AV, Whittington R, Malkowicz SB, Schultz D, Blank K, Broderick GA, et al. Biochemical Outcome After Radical Prostatectomy, External Beam Radiation Therapy, or Interstitial Radiation Therapy for Clinically Localized Prostate Cancer. *JAMA* (1998) 280:969–74. doi: 10.1001/jama.280.11.969
16. Chovanec N, Cierna Z, Miskovska V, Machalekova K, Kalavska K, Rejlekova K, et al. Systemic Immune-Inflammation Index is Prognostic in Testicular Germ Cell Tumors With PD-L1 Expressing Tumor Infiltrating Lymphocytes. *J Clin Oncol* (2017) 35:e16042. doi: 10.1200/JCO.2017.35.15_suppl.e16042
17. Cookson MS, Aus G, Burnett AL, Edith DC, Anthony VD, Roger RD, et al. Variation in the Definition of Biochemical Recurrence in Patients Treated for Localized Prostate Cancer: The American Urological Association Prostate Guidelines for Localized Prostate Update Panel Report and Recommendations for a Standard in the Reporting of Surgical Outcomes. *J Urol* (2007) 177:540–5. doi: 10.1016/j.juro.2006.10.097
18. Fan Y, Ye L, Liang L, Li QH, Zhang J, Ma M, et al. Analysis of Risk Factors for Clinical Cure and Biochemical Recurrence in Patients After Radical Prostatectomy. *Chin J Urol* (2021) 9:644–9. doi: 10.3760/cma.j.cn112330-20210720-00379
19. Wang S, Ji Y, Chen Y, Du P, Cao Y, Yang X, et al. The Values of Systemic Immune-Inflammation Index and Neutrophil-Lymphocyte Ratio in Predicting the Localized Prostate Cancer: A Retrospective Study. *Front Oncol* (2022) 11:812319. doi: 10.3389/fonc.2021.812319
20. Gomez D, Morris-stiff G, Toogood GJ, Lodge JP, Prasad KR. Impact of Systemic Inflammation on Outcome Following Resection for Intrahepatic Cholangiocarcinoma. *J Surg Oncol* (2008) 97:513–8. doi: 10.1002/jso.21001
21. Keizman D, Ish-Shalom M, Huang P, Eisenberger MA, Pili R, Hammers H, et al. The Association of Pre-Treatment Neutrophil to Lymphocyte Ratio With Response Rate, Progression Free Survival and Overall Survival of Patients Treated With Sunitinib for Metastatic Renal Cell Carcinoma. *Eur J Cancer* (2012) 48:202–8. doi: 10.1016/j.ejca.2011.09.001
22. Piccard H, Muschel RJ, Opdenakker G. Neutrophil-Mediated Tumor Angiogenesis: Subversion of Immune Response to Promote Tumour Growth. *Semin Cancer Biol* (2013) 23:149–58. doi: 10.1016/j.semcancer.2013.02.003
23. Ferro M, Caputo VF, Barone B, Imbimbo C, de Cobelli O, Crocetto F. Lymphocyte to Monocyte Ratio: A New Independent Prognostic Factor in Bladder Cancer Progression. *Front Oncol* (2021) 11:754649. doi: 10.3389/fonc.2021.754649
24. Zhang GM, Zhu Y, Ma XC, Qin XJ, Wan FN, Dai B, et al. Pretreatment Neutrophil-to-Lymphocyte Ratio: A Predictor of Advanced Prostate Cancer and Biochemical Recurrence in Patients Receiving Radical Prostatectomy. *Medicine (Baltimore)* (2015) 94:e1473. doi: 10.1097/MD.0000000000001473
25. Lee H, Jeong SJ, Hong SK, Byun SS, Lee SE, Qh JJ, et al. High Preoperative Neutrophil-Lymphocyte Ratio Predicts Biochemical Recurrence in Patients With Localized Prostate Cancer After Radical Prostatectomy. *World J Urol* (2016) 34:821–7. doi: 10.1007/s00345-015-1701-6
26. Minardi D, Scartozzi M, Montesi L, Santoni M, Burattini L, Bianconi M, et al. Neutrophil-To-Lymphocyte Ratio may be Associated With the Outcome in Patients With Prostate Cancer. *Springerplus* (2015) 4. doi: 10.1186/s40064-015-1036-1
27. Jang WS, Cho KS, Kim KH, Yoon CY, Kang YJ, Lee JY, et al. Prognostic Impact of Preoperative Neutrophil-to-Lymphocyte Ratio After Radical Prostatectomy in Localized Prostate Cancer. *Prostate Cancer Prostatic Dis* (2016) 19:298–304. doi: 10.1038/pcan.2016.20
28. Zanaty M, Ajib K, Alnazari M, Elie EB, Fouad A, Kevin CZ, et al. Prognostic Utility of Neutrophil-to-Lymphocyte and Platelets-to-Lymphocyte Ratio in Predicting Biochemical Recurrence Post Robotic Prostatectomy. *Biomark Med* (2018) 12:841–8. doi: 10.2217/bmm-2017-0321
29. Cao Z, Ji J, Zhang C, Wang F, Xu H, Yu Y, et al. The Preoperative Neutrophil-to-Lymphocyte Ratio is Not a Marker of Prostate Cancer Characteristics But is an Independent Predictor of Biochemical Recurrence in Patients Receiving Radical Prostatectomy. *Cancer Med* (2019) 8:1004–12. doi: 10.1002/cam4.1984
30. Coffelt SB, Wellenstein MD, de Visser KE. Neutrophils in Cancer: Neutral No More. *Nat Rev Cancer* (2016) 16:431–46. doi: 10.1038/nrc.2016.52
31. Riedj J, Pabinger I, Ay C. Platelets in Cancer and Thrombosis. *Hamostaseologie* (2014) 34:54–62. doi: 10.5482/HAMO-13-10-0054
32. Wang K, Diao F, Ye Z, Zhang X, Zhai E, Ren H, et al. Prognostic Value of Systemic Immune Inflammation Index in Patients With Gastric Cancer. *Clin J Cancer* (2017) 36:75. doi: 10.1186/s40880-017-0243-2
33. Man Y, Chen Y. Systemic Immune-Inflammation Index, Serum Albumin, and Fibrinogen Impact Prognosis in Castration Resistant Prostate Cancer Patients Treated With First Line Docetaxel. *Int Urol Nephrol* (2019) 12:2189–99. doi: 10.1007/s11255-019-02265-4
34. Ozsoy M, Moschini M, Fajkovic H, Soria F, Seitz C, Klatte T, et al. Elevated Preoperative Neutrophil-Lymphocyte Ratio Predicts Upgrading at Radical Prostatectomy. *Prostate Cancer Prognostic Dis* (2018) 21:100–5. doi: 10.1038/s41391-017-0015-8
35. Kwon YS, Han CS, Yu JW, Kim S, Modi P, Davis R, et al. Neutrophil and Lymphocyte Counts as Clinical Markers for Stratifying Low-Risk Prostate Cancer. *Clin Genitourin Cancer* (2016) 14:e1–8. doi: 10.1016/j.clgc.2015.07.018

36. Rajwa P, Schuettfort VM, D'Andrea D, Quhal F, Mori K, Katayama S, et al. Impact of Systemic Immune-Inflammation Index on Oncologic Outcomes in Patients Treated With Radical Prostatectomy for Clinically Nonmetastatic Prostate Cancer. *Urol Oncol* (2021) 39:785.e19–785.e27. doi: 10.1016/j.urolonc.2021.05.002
37. Fan L, Wang R, Chi C, Cai W, Zhang Y, Qian H, et al. Systemic Immune-Inflammation Index Predicts the Combined Clinical Outcome After Sequential Therapy With Abiraterone and Docetaxel for Metastatic Castration-Resistant Prostate Cancer Patients. *Prostate* (2018) 78:250–6. doi: 10.1002/pros.23465

Conflict of Interest: The authors declare that the research was conducted in the absence of any commercial or financial relationships that could be construed as a potential conflict of interest.

Publisher's Note: All claims expressed in this article are solely those of the authors and do not necessarily represent those of their affiliated organizations, or those of the publisher, the editors and the reviewers. Any product that may be evaluated in this article, or claim that may be made by its manufacturer, is not guaranteed or endorsed by the publisher.

Copyright © 2022 Wang, Yang, Yu, Du, Sheng, Cao, Yan, Ma and Yang. This is an open-access article distributed under the terms of the Creative Commons Attribution License (CC BY). The use, distribution or reproduction in other forums is permitted, provided the original author(s) and the copyright owner(s) are credited and that the original publication in this journal is cited, in accordance with accepted academic practice. No use, distribution or reproduction is permitted which does not comply with these terms.

frontiers | Frontiers in Oncology

ORIGINAL RESEARCH
published: 07 June 2022
doi: 10.3389/fonc.2022.906936

Preoperative Platelet Count Correlates With Postoperative Perineural Invasion on Specimen in Patients Treated With Radical Prostatectomy

Fangming Wang[1,2†], *Fei Liu*[1,2†], *Jing Liang*[3], *Feiya Yang*[1,2] *and Nianzeng Xing*[1,2,4*]

[1] State Key Laboratory of Molecular Oncology, National Cancer Center/National Clinical Research Center for Cancer/Cancer Hospital, Chinese Academy of Medical Sciences and Peking Union Medical College, Beijing, China, [2] Department of Urology, National Cancer Center/National Clinical Research Center for Cancer/Cancer Hospital, Chinese Academy of Medical Sciences and Peking Union Medical College, Beijing, China, [3] Department of Pathology, National Cancer Center/National Clinical Research Center for Cancer/Cancer Hospital, Chinese Academy of Medical Sciences and Peking Union Medical College, Beijing, China, [4] Department of Urology, Shanxi Province Cancer Hospital/Shanxi Hospital Affiliated to Cancer Hospital, Chinese Academy of Medical Sciences/Cancer Hospital Affiliated to Shanxi Medical University, Taiyuan, China

OPEN ACCESS

Edited by:
Riccardo Tellini,
Careggi University Hospital, Italy

Reviewed by:
Eliane Gouvêa Oliveira-Barros,
Juiz de Fora Federal University, Brazil
Samikshan Dutta,
University of Nebraska Medical Center, United States

***Correspondence:**
Nianzeng Xing
xingnianzeng@126.com

[†]These authors have contributed equally to this work

Specialty section:
This article was submitted to Genitourinary Oncology, a section of the journal Frontiers in Oncology

Received: *29 March 2022*
Accepted: *13 May 2022*
Published: *07 June 2022*

Citation:
Wang F, Liu F, Liang J, Yang F and Xing N (2022) Preoperative Platelet Count Correlates With Postoperative Perineural Invasion on Specimen in Patients Treated With Radical Prostatectomy. Front. Oncol. 12:906936. doi: 10.3389/fonc.2022.906936

Objective: It has been reported that perineural invasion (PNI) after radical prostatectomy (RP) is associated with unfavorable prostate cancer (PCa) prognosis. However, the clinicopathological factors especially hematological parameters that influenced PNI remain unknown. Our aim was to explore the relationship between clinicopathological parameters and PNI in patients who underwent RP.

Methods: A total of 348 patients with PCa who underwent RP at our center between 2018 and 2021 were consecutively collected. We divided them into non-PNI and PNI groups based on PNI status and compared clinicopathological characteristics including hematological parameters between non-PNI and PNI groups. The association of clinicopathological parameters including whole blood parameters, age, body mass index (BMI), hypertension, diabetes mellitus, prostate-specific antigen (PSA), ISUP (International Society of Urological Pathology) grade, pathological stage T (pT), and neoadjuvant hormonal therapy (NHT) with PNI was determined by univariate and multivariate logistic regression analyses.

Results: The pathological results of the RP specimen consisted of 254 (73.0%) patients with PNI and 94 (27.0%) cases without PNI. The level of PSA, percentages of advanced pT and grade, positive surgical margin rate, and vessel carcinoma embolus rate were significantly higher in the PNI group when compared with non-PNI counterpart ($p = 0.007$, $p < 0.001$, $p < 0.001$, $p < 0.001$, and $p < 0.001$, respectively). Among the whole blood parameters, only platelet count and plateletcrit were significantly different [216 (178.8–252.0) vs. 200.5 (173.5–236.5), $p = 0.04$; 0.0021 (0.0018–0.0025) vs. 0.0020 (0.0017–0.0023), $p = 0.008$, respectively]. Univariate logistic regression analysis demonstrated that platelet, ISUP, and pT were all positively correlated with the presence of PNI (T3 vs. T1,

odds ratio (OR) = 2.029, p = 0.020; OR = 1.697, p < 0.001; OR = 3.836, p < 0.001). In the stepwise multivariate regression analysis, the association between platelet and PNI remained significant (T2 vs. T1, OR = 2.171, 95% CI: 1.082–4.354, p = 0.029; T3 vs. T1, OR = 2.595, 95% CI: 1.259–5.349, p = 0.010) after adjusting for confounding factors including age, BMI, hypertension, diabetes mellitus, PSA, ISUP, pT, and NHT.

Conclusions: The study first revealed that platelet count rather than other whole blood parameters was independently associated with the presence of PNI in patients with PCa, suggesting that platelets might play an essential role in PCa aggressiveness.

Keywords: platelet, perineural invasion, radical prostatectomy, correlation, specimen

INTRODUCTION

Prostate cancer (PCa) is the second most common cancer and the fifth most common cause of cancer death among men worldwide in 2020 (1). Radical prostatectomy (RP) is appropriate for men with intermediate- and high-risk diseases in whom RP prevents further metastatic seeding of potentially lethal PCa cell clones. Small series have suggested that it might be appropriate to offer RP to men with low metastatic burden as part of a multimodal therapeutic approach (2). Postoperative histopathology results of RP including pathologic T stage (pT), Gleason score, and positive surgical margin (PSM) are of crucial importance to clarify the stage, make decisions for adjuvant treatment, and predict biochemical recurrence and prognosis after RP (3, 4). More and more pathological information was explored and added to the current models for improving the predictive power of prognosis and the precise timing of adjuvant treatment. Perineural invasion (PNI), a routine evaluation in RP specimens (a mean frequency of 62.2% and up to 80%), has recently attracted more and more attention recently (3). PNI is defined as cancer tracking along or around a nerve within the perineural space; it can be observed in the absence of lymphatic or vascular invasion (5). There was no doubt that the presence of PNI in the RP specimen was correlated with multiple adverse clinicopathological factors (6–13). Although controversial (6–9), there were abundant evidence supporting that PNI could be used as an independent predictor of biochemical recurrence in patients with PCa who underwent RP (10–13).

The exact mechanism of PNI is still unclear although PNI is usually seen in cases of PCa; the factors associated with the ability of PCa cells to permeate nerves are not completely elucidated. Some studies focused on the perineural space and the interaction between PCa cells and nerves, suggesting that the perineural space may be a tumor microenvironment (TME) that promotes both cancer spread and growth (5, 14). As one of the important stromal components in the TME, platelets have attracted attention in recent years, and their interaction with cancer cells could promote the spread of PCa cancer cells with less resistance (15, 16). However, it remains largely unknown whether platelet is correlated with PNI in PCa. Until now, there was no study that systematically and comprehensively investigated the correlation between platelet and other whole blood parameters with PNI and other clinicopathological features of PCa.

Hence, the aim of the current study was to identify the association of comprehensive whole blood parameters with the presence of PNI of RP specimen in the Chinese patients with PCa.

Abbreviations: PNI, perineural invasion; RP, radical prostatectomy; PCa, prostate cancer; BMI, body mass index; PSA, prostate-specific antigen; ISUP, International Society of Urological Pathology; NHT, neoadjuvant hormonal therapy; PSM, positive surgical margin; TME, microenvironment; AJCC, American joint committee on cancer; VCE, vessel carcinoma embolus; WBC, white blood cell; RBC, red blood cell; Hb, hemoglobin; Hct, hematocrit; MCV, mean corpuscular volume; MCH, mean corpuscular hemoglobin; MCHC, mean corpuscular hemoglobin concentration; RDW-SD, red blood cell volume distribution width–standard deviation; RDW-CV, red blood cell volume distribution width–coefficient of variability; MPV, mean platelet volume; P-LCR, platelet-large cell ratio; PDW, platelet distribution width.

MATERIALS AND METHODS

Collection of Patients' Clinicopathological Data

A total of 348 patients with PCa who had been pathologically diagnosed as PCa by biopsy and underwent laparoscopic RP and pelvic lymph node dissection at our institution between May 2018 and June 2021 were reviewed. Exclusion criteria of the study were the presence of infection, hematologic diseases, severe hepatic and/or renal insufficiency, hypersplenism, hyperthyroidism, cardiovascular disease, medical history of other malignancies, and receiving any radiotherapy or chemotherapy.

All clinicopathological data including age, body mass index (BMI), hypertension, diabetes mellitus, prostate-specific antigen (PSA), neoadjuvant hormonal therapy (NHT), operative time, blood loss, preoperative whole blood parameters, and postoperative pathological results including ISUP (International Society of Urological Pathology) grade and pathological stage T (pT) were collected from medical records. All RP samples were routinely sent to the pathological department for diagnosis. The cancer grade assessment was performed according to the ISUP 2014 classification system (17). The pT was evaluated on the basis of a prostatectomy specimen according to the American Joint Committee on Cancer (AJCC) TNM classification of malignant tumors in 2017 (AJCC, pT2–T4, Nx,0,1) (18). The pathology of the presence of PNI, PSM, and vessel carcinoma embolus (VCE) was reviewed by two

pathologists. For controversial cases, a third pathologist was invited to reach group agreement.

Hematological Parameter Measurement

Morning venous blood samples were taken on admission at the nurse station after 8-h fasting and before biopsy without any treatment. The serum PSA value and the whole blood parameters were measured; the latter included white blood cell (WBC), neutrophils (%), neutrophil counts, lymphcytes (%), lymphocyte counts, monocytes (%), monocyte counts, eosinophils (%), eosinophil counts, basophils (%), basophil counts, red blood cell (RBC), hemoglobin (Hb), hematocrit (Hct), mean corpuscular volume (MCV), mean corpuscular hemoglobin (MCH), mean corpuscular hemoglobin concentration (MCHC), red blood cell volume distribution width-standard deviation (RDW-SD), red blood cell volume distribution width–coefficient of variability (RDW-CV), platelet, mean platelet volume (MPV), platelet–large cell ratio (P-LCR), platelet distribution width (PDW), and plateletcrit.

Statistical Analysis

Data were expressed as number (percentage) for categorical variables and means ± SD or median with interquartile range for continuous variables. Categorical variables were analyzed by χ2-test. The differences between continuous variables were analyzed by unpaired t-tests, Mann–Whitney U-tests, or one way ANOVA as appropriate. All PCa subjects were divided into two groups according to PNI status: non-PNI and PNI groups, and clinicopathological characteristics especially all hematological parameters were compared between the two groups. The platelet was stratified into tertiles as follows: the first tertile group (T1, $<192 \times 10^9$/L (33.3th percentile), $n = 118$); the second tertile group [T2, 192–236 $\times 10^9$/L (33.3–66.7th percentile), $n = 116$]; and the third tertile group (T3, $>237 \times 10^9$/L [66.7–100th percentile); $n = 114$], and clinicopathological characteristics were analyzed in the different tertiles of platelet. The binary logistic regression model (univariate and multivariate analysis) was used to evaluate the association between clinicopathological parameters including platelet, age, BMI, hypertension, diabetes mellitus, PSA, ISUP grade, pT, and NHT with PNI. A p-value <0.05 (two-sided) was considered significant for all tests. The statistical analyses were performed with SPSS version 22.0 software (SPSS Inc., Chicago, IL, USA).

RESULTS

Characteristics of PNI and Non-PNI Patients

The clinicopathological characteristics and whole blood parameters of the enrolled subjects were shown in **Table 1**. Of the total 348 eligible RP cases, the mean values of the clinical factors were 66.2 ± 6.6 years for age and 25.1 ± 3.2 for BMI; the median PSA was 14.0 (8.7–29.6); 135 cases (38.8%) received NHT therapy; 258 (74.1%) were pT2, 68 (19.5%) were pT3, and 22 (6.3%) were pT4; lymph node involvement occurred in 24 cases (6.9%), and metastasis occurred in 19 cases (5.5%). The percentages of ISUP grades from 1 to 5 were 40 (11.5%), 97 (27.9%), 69 (19.8%), 55 (15.8%), and 87 (25%). The PSM and VCE rate were 94 (27%) and 54 (15.5%), respectively. It is noteworthy that PNI was presented in 254 cases (73.0%) and absent in 94 cases (27%). The representative hematoxylin-eosin (HE) staining images of PNI and non-PNI were shown in **Figures 1A–D**. No significant differences in age, BMI, hypertension, diabetes, NHT percentage, operative time, blood loss, or complete blood count except platelet were observed between the non-PNI and PNI groups. Platelet count and plateletcrit were significantly higher in the PNI group than that in the non-PNI group [216 (178.8–252.0) vs. 200.5 (173.5–236.5), p = 0.04; 0.0021 (0.0018–0.0025) vs. 0.0020 (0.0017–0.0023), p = 0.008, respectively] (**Figures 2A, B**). The level of PSA was significantly higher in the PNI group compared to the non-PNI counterpart [15.5 (9.5–31.5) vs. 12.2 (7.6–22.0), p = 0.007] (**Figure 2C**). In addition, as shown in **Figures 2D, E**, the percentages of advanced pT (T3 + T4) and high IUSP grades (4 + 5) were significantly higher in the PNI group when compared with non-PNI counterpart (32.7% vs. 7.4%, p < 0.001; 47.6% vs. 22.3%, p < 0.001). Furthermore, there were also significant differences in the PSM and VCE rates between the two groups [84 (33.1%) vs. 10 (10.6%), p < 0.001; 51 (20.1%) vs. 3 (3.2%), p < 0.001].

Relation of Platelet Count With the Clinicopathological Characteristics of PCa

Patients with PCa who underwent RP were stratified into three groups according to the platelet count level tertiles as mentioned due to the evident difference in platelets between the PNI and non-PNI groups. Statistically significant differences in age, PNI, and platelet-related parameters including MPV, P-LCR, PDW, and PCT were found among the three different groups (p < 0.001, p = 0.030, p < 0.001, p < 0.001, p < 0.001, and p < 0.001, respectively) (**Table 2**). Specifically, PNI percentages increased with the elevation of the platelet count level, from 65.3%, 73.3%, up to 80.7%. However, we did not observe any significant difference regarding the PSA, pT, lymph node involvement, metastasis, ISUP grade, or VCE among the three platelet groups (p = 0.295, p = 0.065, p = 0.200, p = 0.687, p = 0.424, and p = 0.868, respectively).

Correlation of Platelet Count and Other Clinicopathological Variables With the Presence of PNI

To evaluate the correlation of platelet count and other clinical variables with PNI, in the present study, a univariate and multivariate logistic regression analysis was performed. As shown in **Table 3**, parameters including platelet, ISUP, and pT were found to be significantly and positively correlated with the presence of PNI (T3 vs. T1, OR = 2.029, 95% CI: 1.119–3.680, p = 0.020; OR = 1.697, 95% CI: 1.396–2.063, p < 0.001; OR = 3.836, 95% CI: 2.504–5.876, p < 0.001) in univariate logistic regression analyses. In the stepwise multivariate regression analysis (**Table 4**), we gradually added and adjusted confounding

TABLE 1 | Baseline characteristics of the PCa subjects underwent RP according to the PNI stratification.

	All subjects(*n* = 348)	PNI (n = 254)	Non-PNI (n = 94)	P-value
Demographic characteristics				
Age (years)	66.2 ± 6.6	66.1 ± 6.5	66.4 ± 6.6	0.757
BMI (kg/m^2)	25.1 ± 3.2	25.1 ± 3.1	25.1 ± 3.3	0.956
Hypertension [*n* (%)]	154 (44.3)	106 (41.7)	48 (51.1)	0.113
Diabetes mellitus [*n* (%)]	69 (19.8)	51 (20.1)	18 (19.1)	0.859
Clinicopathological characteristics				
PSA (ng/ml)	14.0 (8.7–29.6)	15.5 (9.5–31.5)	12.2 (7.6–22.0)	**0.007**
NHT	135 (38.8)	97 (38.2)	38 (40.4)	0.633
Pathological Stage				**<0.001**
T2	258 (74.1)	171 (67.3)	87 (92.6)	
T3	68 (19.5)	63 (24.8)	5 (5.3)	
T4	22 (6.3)	20 (7.9)	2 (2.1)	
N	24 (6.9)	23 (9.1)	1 (1.1)	**0.009**
M	19 (5.5)	16 (6.3)	3 (3.2)	0.260
ISUP grade [n (%)]				**<0.001**
1	40 (11.5)	13 (5.1)	27 (28.7)	
2	97 (27.9)	70 (27.6)	27 (28.7)	
3	69 (19.8)	50 (19.7)	19 (20.2)	
4	55 (15.8)	42 (16.5)	13 (13.8)	
5	87 (25)	79 (31.1)	8 (8.5)	
PSM [n (%)]	94 (27.0)	84 (33.1)	10 (10.6)	**<0.001**
VCE [n (%)]	54 (15.5)	51 (20.1)	3 (3.2)	**<0.001**
Operative time (min)	165.1 ± 58.2	165.6 ± 60.2	163.5 ± 52.8	0.762
Evaluated blood loss (ml)	59.5 ± 94.2	62.8 ± 98.4	50.7 ± 81.7	0.288
Transfusion [n (%)]	6 (1.7%)	5 (2.0)	1 (1.1)	0.567
Whole blood parameters				
WBC (×10^9/L)	6.2 ± 1.5	6.2 ± 1.6	6.1 ± 1.5	0.436
Neutrophils (%)	61.4 ± 9.3	61.5 ± 9.2	60.9 ± 9.7	0.617
Neutrophil counts (×10^9/L)	3.8 ± 1.3	3.9 ± 1.3	3.8 ± 1.3	0.459
Lymphocytes (%)	29.7 ± 8.6	29.7 ± 8.4	29.9 ± 9.1	0.885
Lymphocyte counts (×10^9/L)	1.8 ± 0.6	1.8 ± 0.6	1.8 ± 0.6	0.546
Monocytes (%)	6.1 ± 1.5	6.1 ± 1.5	6.3 ± 1.6	0.202
Monocyte counts (×10^9/L)	0.4 ± 0.1	0.4 ± 0.1	0.4 ± 0.1	0.856
Eosinophils (%)	2.2 ± 1.9	2.1 ± 1.8	2.3 ± 2.1	0.455
Eosinophil counts (×10^9/L)	0.1 ± 0.1	0.1 ± 0.1	0.1 ± 0.1	0.757
Basophils (%)	0.6 ± 0.3	0.6 ± 0.3	0.6 ± 0.3	0.823
Basophil counts (×10^9/L)	0.04 ± 0.02	0.04 ± 0.02	0.04 ± 0.02	0.669
RBC (×10^{12}/L)	4.8 ± 0.5	4.8 ± 0.5	4.7 ± 0.5	0.308
Hb (g/L)	147.3 ± 13.8	147.8 ± 13.7	146.1 ± 14.3	0.323
Hct (L/L)	0.43 ± 0.04	0.44 ± 0.04	0.43 ± 0.04	0.159
MCV (fl)	91.6 ± 5.0	91.7 ± 5.2	91.3 ± 4.4	0.522
MCH (pg)	31.3 ± 3.5	31.1 ± 1.9	31.7 ± 5.9	0.117
MCHC (g/L)	338.8 ± 19.4	338.1 ± 21.7	340.8 ± 10.4	0.247
RDW-SD (fl)	42.0 ± 3.0	42.0 ± 3.0	41.8 ± 3.1	0.460
RDW-CV (%)	12.6 ± 0.8	12.6 ± 0.9	12.5 ± 0.8	0.716
PLT (×10^9/L)	211.5 (177.3–248.0)	216 (178.8–252.0)	200.5 (173.5–236.5)	**0.04**
MPV (fl)	10.0 ± 1.1	10.0 ± 1.1	9.9 ± 0.9	0.479
P-LCR (%)	24.7 ± 7.4	25.0 ± 7.5	24.1 ± 7.3	0.345
PDW (fl)	11.3 ± 2.1	11.4 ± 2.2	11.1 ± 2.0	0.268
PCT (L/L)	0.0021 (0.0018–0.0025)	0.0021 (0.0018–0.0025)	0.0020 (0.0017–0.0023)	**0.008**

Data are expressed as n (%), mean ± SD, or median (interquartile range). The bold value indicated statistical significance. PCa, prostate cancer; RP, radical prostatectomy; PNI, perineural invasion; BMI, body mass index; PSA, prostate-specific antigen; NHT, neoadjuvant hormonal therapy; ISUP, International Society of Urological Pathology; PSM, positive surgical margin; VCE, vessel carcinoma embolus; WBC, white blood cell; RBC, red blood cell; Hb, hemoglobin; Hct, hematocrit; MCV, mean corpuscular volume; MCH, mean corpuscular hemoglobin; MCHC, mean corpuscular hemoglobin concentration; RDW-SD, red blood cell volume distribution width–standard deviation; RDW-CV, red blood cell volume distribution width–coefficient of variability; PLT, platelet; MPV, mean platelet volume; P-LCR, platelet–large cell ratio; PDW, platelet distribution width; PCT, plateletcrit.

factors from model 1 to model 4 and ultimately revealed that the correlations of platelet, ISUP, and pT with PNI remained significant (T2 vs. T1, OR = 2.171, p = 0.029; T3 vs. T1, OR = 2.595, p = 0.010; OR = 1.509, p = 0.001; OR = 3.220, p < 0.001) after adjustment for confounding factors. In particular, the positive correlation between platelets and PNI became increasingly evident when confounders were gradually adjusted. Furthermore, the multivariate regression analysis showed that NHT was negatively and independently correlated with the presence of PNI (OR = 0.420, 95% CI: 0.220–0.804, p = 0.009). However, no significant correlation between PSA and PNI was observed (OR = 1.002, 95% CI: 0.992–1.013, p = 0.704).

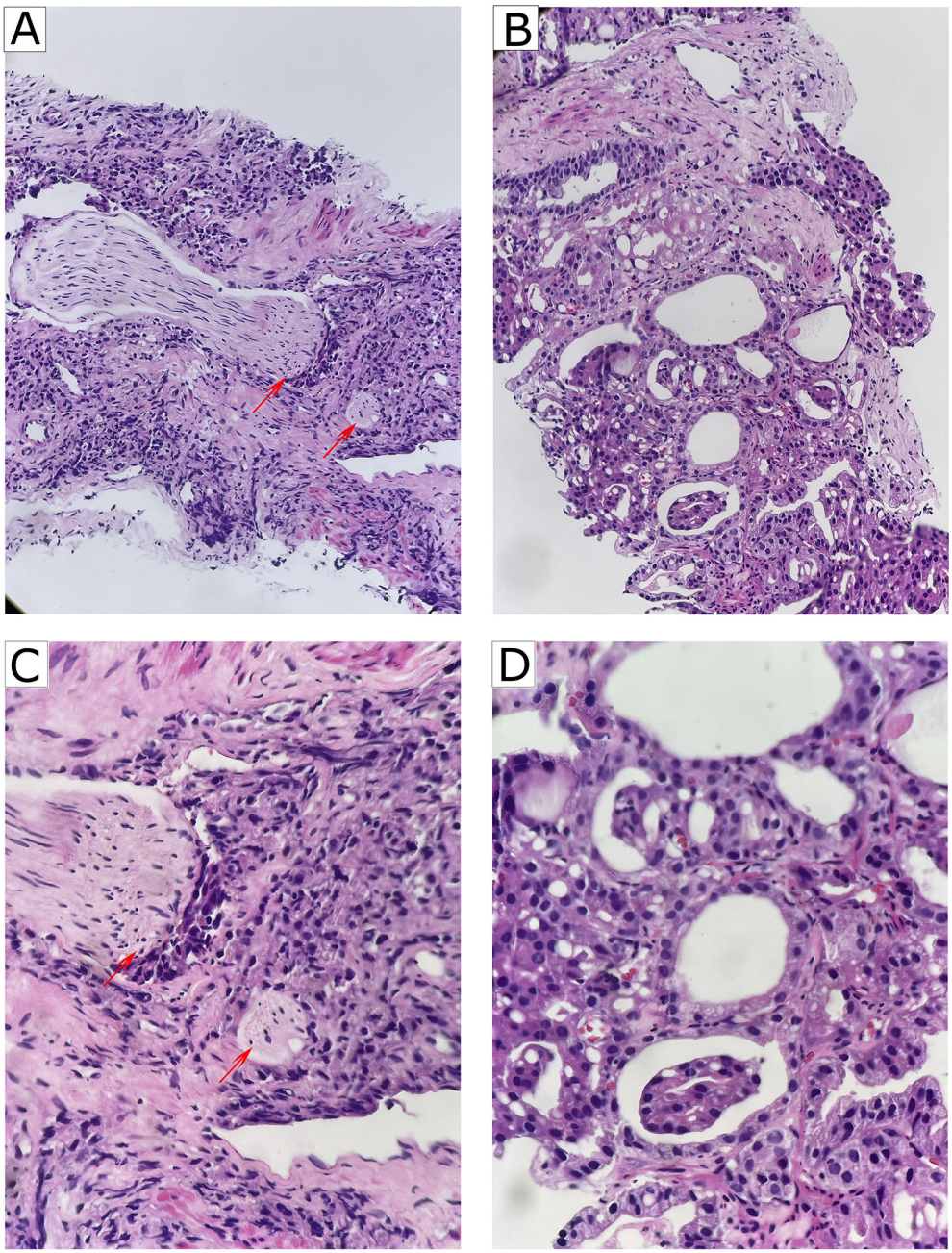


FIGURE 1 | Representative of PNI and non-PNI sections of HE staining from patients with PCa. **(A)** Representative image of PNI (HE, ×200). The nerves (red arrow heads) were invaded by surrounding cancer cells. **(B)** Representative image of non-PNI (HE, ×200) for comparison. **(C)** Higher magnification of A (HE, ×400) showing that the nerves (red arrow heads) were invaded by surrounding cancer cells. **(D)** Higher magnification of **(B)** (HE, ×400). PNI, perineural invasion; PCa, prostate cancer; HE, hematoxylin-eosin.

DISCUSSION

Our study, for the first time, explored the correlation between clinicopathological parameters and PNI in patients who underwent RP and demonstrated that platelet count was independently and positively associated with the presence of PNI among all whole blood parameters. Therefore, the current research may have clinical implications for the assessment of PCa aggressiveness from the perspective of routine blood tests. Moreover, our study provided novel clues to explore the mechanisms of the roles the platelet played in PCa cell invasion.

PNI, a pathologic feature defined as the invasion of cancer cells in, around, and through the nerves, is an indicator of poor prognosis in PCa (19). Different from lymphatic or vascular

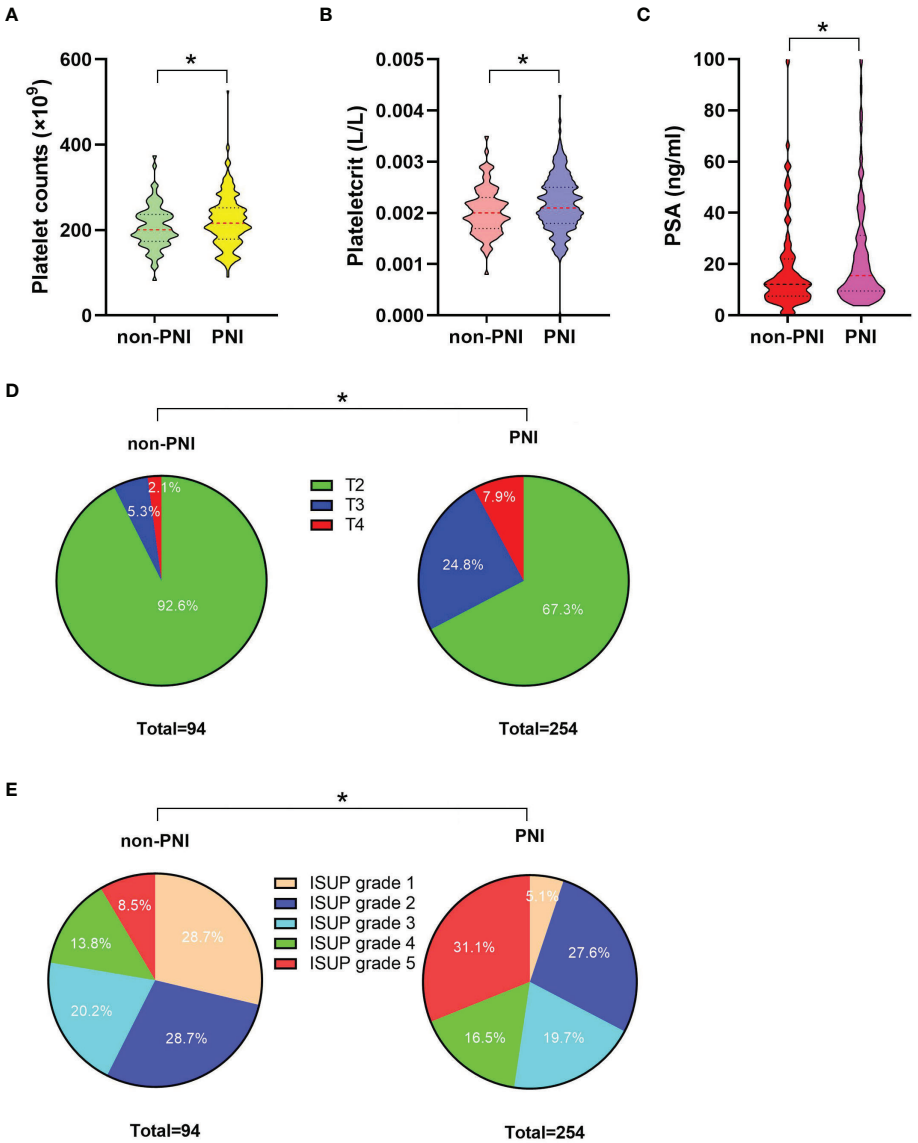


FIGURE 2 | The comparisons of platelet count, plateletcrit, PSA level, the percentage distributions of pT, and IUSP grade between the non-PNI (n = 94) and PNI (n = 254) groups. **(A)** Comparison of platelet count between the non-PNI and PNI groups; median (interquartile range) was measured and showed in a violin plot (the dotted line); statistical significance was determined by the Mann–Whitney U-test. **(B)** Comparison of plateletcrit between the non-PNI and PNI groups, median (interquartile range) was measured and showed in a violin plot (the dotted line), statistical significance was determined by the Mann–Whitney U-test. **(C)** Comparison of PSA levels between the non-PNI and PNI groups; median (interquartile range) was measured and showed in a violin plot (the dotted line); statistical significance was determined by the Mann–Whitney U-test. **(D)** Comparison of pT distribution (including T2, T3, and T4 percentages) between the non-PNI and PNI groups; a pie plot was generated to visualize the proportional change of the numerical data; statistical significance was determined by χ2-test; **(E)** Comparison of ISUP grade distribution (including proportions of ISUP grades 1, 2, 3, 4, and 5) between the non-PNI and PNI groups; a pie plot was generated to visualize the proportional change of the numerical data; statistical significance was determined by χ2-test. Values are expressed as median with interquartile range or number (percentage); *, $P < 0.05$. PSA, prostate-specific antigen; pT, pathological stage T; ISUP, International Society of Urological Pathology; PNI, perineural invasion.

involvement (5), PNI occurs within all three layers of the nerve sheath (epineurium, perineurium, and endoneurium), which means that cancer cells could track along nerves beyond the predicted anatomic boundaries of primary tumors, often resulting in residual tumor within the body after surgery. PNI has been reported to be correlated with adverse pathological features, elevated biochemical recurrence rates, increased risk of bone metastasis, and poor overall survival in patients with PCa (20–22). PNI is highly prevalent in PCa; one study reported that PNI was observed in up to 75% of surgical resection specimens (23). In our study, PNI was presented in 73.0% of the prostatectomy specimens, which was consisted with the mentioned data. Our data showed that patients with PNI had higher PSA levels, more advanced stage and grade, higher PSM

TABLE 2 | Clinical characteristics of PCa subjects according to tertiles of platelet levels.

	Platelet Tertiles			P-value
	T1 (<192 × 10^9/L, n = 118)	T2 192–236 × 10^9/L, n = 116)	T3 (>237 × 10^9/L, n = 114)	
Age (years)	68.1 ± 5.8	65.8 ± 6.5	64.6 ± 6.8	**<0.001**
PSA (ng/ml)	26.7 ± 37.1	23.6 ± 31.8	31.8 ± 47.1	0.295
Pathological Stage				0.065
T2	91 (77.1)	86 (74.1)	81 (71.1)	
T3	18 (15.3)	28 (24.1)	22 (19.3)	
T4	9 (7.6)	2 (1.7)	11 (9.6)	
N				0.200
N0	106 (89.8)	109 (94.0)	109 (95.6)	
N1	12 (10.2)	7 (6.0)	5 (4.4)	
M				0.687
M0	112 (94.9)	108 (93.1)	109 (95.6)	
M1	6 (5.1)	8 (6.9)	5 (4.4)	
ISUP grade [n (%)]				0.424
1	9 (7.6)	16 (13.8)	15 (13.2)	
2	32 (27.1)	35 (30.2)	30 (26.3)	
3	22 (18.6)	26 (22.4)	21 (18.4)	
4	18 (15.3)	19 (16.4)	18 (15.8)	
5	37 (31.4)	20 (17.2)	30 (26.3)	
PNI [n (%)]	77 (65.3)	85 (73.3)	92 (80.7)	**0.030**
VCE	19 (16.1)	16 (13.8)	18 (15.8)	0.868
MPV (fl)	10.3 ± 1.4	9.9 ± 0.7	9.7 ± 0.7	**<0.001**
P-LCR (%)	27.8 ± 8.9	23.8 ± 6.0	22.5 ± 5.9	**<0.001**
PDW (fl)	12.1 ± 2.8	11.0 ± 1.5	10.7 ± 1.4	**<0.001**
PCT (L/L)	0.0016 ± 0.0003	0.0021 ± 0.0002	0.0027 ± 0.0004	**<0.001**

Data are expressed as n (%), mean ± SD, or median (interquartile range). The bold value indicated statistical significance. PCa, prostate cancer; PSA, prostate-specific antigen; ISUP, International Society of Urological Pathology; PNI, perineural invasion; VCE, vessel carcinoma embolus; MPV, mean platelet volume; P-LCR, platelet–large cell ratio; PDW, platelet distribution width; PCT, plateletcrit.

rate and VCE rate, compared to their counterparts without PNI. The explanation for this phenomenon was that PNI is an ominous clinical and pathological characteristic of PCa, which has been associated with adverse pathological features (19).

In our study, among all whole blood parameters, only platelet count and plateletcrit in the PNI group were significantly higher than those in non-PNI group. Chronic inflammation promotes cancer progression and metastasis (24). Changes in peripheral blood counts can partly reflect inflammatory responses in cancer patients. Some studies suggested that platelets can mediate cancer cell growth, dissemination, and angiogenesis (25–29). Platelet–tumor cell interactions could prime tumor cells for subsequent extravasation and metastasis through platelet-derived transforming growth factor-β (TGFβ)-mediated pathways in cancer cells (26, 27). In addition, aggregation of platelets around tumor cells could protect tumor cells from immune surveillance, which, in part, enhances cancer cell invasion (28, 29). Moreover, platelets can change the phenotype of epithelial tumors, which is known as the epithelial–mesenchymal transition, conferring stem cell

TABLE 3 | Univariate analysis for PCa patients with PNI.

	Univariate Mode		P-value
	OR	95% CI	
PLT (×10^9/L)			
T1(<)	reference		
T2(–)	1.406	0.803–2.463	0.234
T3(>)	2.029	1.119–3.680	**0.020**
Age	0.994	0.959–1.031	0.756
BMI	0.998	0.926–1.075	0.956
Hypertension	0.682	0.424–1.096	0.114
Diabetes mellitus	1.056	0.580–1.920	0.859
PSA	1.009	1.000–1.019	0.059
ISUP	1.697	1.396–2.063	**0.000**
T stage	3.836	2.504–5.876	**0.000**
NHT	0.889	0.547–1.443	0.633

Univariate regression analyses are applied. The bold value indicated statistical significance. PCa, prostate cancer; PNI, perineural invasion; PLT, platelet; BMI, body mass index; PSA, prostate-specific antigen; ISUP, International Society of Urological Pathology; NHT, neoadjuvant hormonal therapy.

TABLE 4 | Multivariate analysis to identify the independent correlation between PLT and PNI of PCa.

Models	Variables		Multivariate Mode		P-value
			OR	95% CI	
1		unadjusted			
	PLT (×10^9/L)	T1(<)	Reference		
		T2(–)	1.406	0.803–2.463	0.234
		T3(>)	2.029	1.119–3.680	**0.020**
2		Model 1+covariates			
	PLT (×10^9/L)	T1(<)	Reference		
		T2(–)	1.463	0.823–2.601	0.195
		T3(>)	2.342	1.249–4.390	**0.008**
3		Model 2 + PSA + ISUP + T stage			
	PLT (×10^9/L)	T1(<)	Reference		
		T2(–)	2.076	1.054–4.090	**0.035**
		T3(>)	2.547	1.255–5.169	**0.010**
4		Model 3+NHT			
	PLT (×10^9/L)	T1(<)	Reference		
		T2(–)	2.171	1.082–4.354	**0.029**
		T3(>)	2.595	1.259–5.349	**0.010**
	Age		1.017	0.973–1.063	0.460
	BMI		0.961	0.875–1.056	0.406
	Hypertension		0.566	0.317–1.013	0.055
	Diabetes mellitus		1.250	0.607–2.573	0.545
	PSA		1.002	0.992–1.013	0.704
	ISUP		1.509	1.188–1.917	**0.001**
	T stage		3.220	2.041–5.081	**0.000**
	NHT		0.420	0.220–0.804	**0.009**

Multivariate regression stepwise models are shown. The bold value indicated statistical significance. The dependent variable was PNI of PCa. Model 1 was unadjusted. Model 2 was corrected for covariates including age, BMI, hypertension, and diabetes mellitus. Model 3 was additionally corrected for PSA, ISUP, stage T based on Model 2; Model 4 was additionally corrected for NHT based on Model 3. PLT, platelet; PNI, perineural invasion; PCa, prostate cancer; PSA, prostate-specific antigen; ISUP, International Society of Urological Pathology; NHT, neoadjuvant hormonal therapy; BMI, body mass index; PSA, prostate-specific antigen.

properties to tumor cells associated with increased mobility (30). Regarding studies of the relationship between platelets and PCa aggressiveness, recently, Rudzinski et al. (31) reported that platelets could enhance the invasion of androgen receptor-negative PCa cells; Brady et al. identified that platelet-coated circulating tumor cells existed in 29.5% of patients with metastatic PCa (32), and Chai et al. claimed that platelet-coated circulating tumor cells could predict the worst prognosis of a subset of patients with metastatic castration-resistant PCa (33).

Our study first showed that the percentage of PNI gradually increased (from 65.3%, 73.3%, to 80.7%) with increasing platelet count (from T1, T2, to T3), indicating that platelets play crucial roles in helping tumor cells pass through neural metastasis when they interact with each other. The D'Amico risk stratification system classifies patients with PCa into low-, intermediate-, and high-risk groups based on PSA level, clinical tumor stage, and Gleason score at diagnosis (34). Among the three parameters, our study demonstrated that ISUP grade (converted from the Gleason score) and pT (more accurate than clinical stage) were found to be significantly and positively correlated with the presence of PNI. In addition, our results showed that NHT was negatively and independently correlated with the presence of PNI, suggesting that NHT could result in less frequent invasion of the perineural spaces, which consisted with one previous study (35). It should be emphasized that platelet was the only whole blood parameter that was independently and positively correlated with the presence of PCa PNI. The present study might have two potential clinical hints. First, the blood platelet count could be used to predict the PNI of postoperative specimen and to estimate the prognosis; second, as platelets play crucial roles in PCa invasion and metastasis, maybe anti-platelet agent (s) could be recommended to patients with PCa with high platelet count to reduce the risk of PNI and metastasis.

CONCLUSIONS

In conclusion, this study first demonstrated the clinicopathological characteristics that included whole blood parameters between PNI and non-PNI of patients with PCa who underwent RP and finally found that platelet count was positively and independently associated with the presence of PNI. There were two main limitations in our study. First, there might be selection bias because our data were derived from a single center, and studies from different institutions are needed for validation of these results. Second, the exact mechanism of platelet induced PNI was not explored in the current analysis.

DATA AVAILABILITY STATEMENT

The raw data supporting the conclusions of this article will be made available by the authors, without undue reservation.

ETHICS STATEMENT

The studies involving human participants were reviewed and approved by Ethical Committee of National Cancer Center. Written informed consent for participation was not required for this study in accordance with the national legislation and the institutional requirements.

AUTHORS CONTRIBUTIONS

Conceptualization: FW and NX; Formal analysis: FW and FL; Investigation: FW, FL, JL, and FY; Methodology: FW, FL, JL, and FY; Pathology analysis: JL; Supervision: NX; Writing—original draft: FW and FL; Writing—revision and editing: FW, FL, JL, FY, and XN. All authors contributed to the article and approved the submitted version.

FUNDING

This work was supported by grants from National Natural Science Foundation of China (no. 81972400, 81772700), and Chinese Academy Medical Sciences Innovation Fund for Medical Sciences (no. 2019-I2M-1-003).

REFERENCES

1. Sung H, Ferlay J, Siegel RL, Laversanne M, Soerjomataram I, Jemal A, et al. Global Cancer Statistics 2020: GLOBOCAN Estimates of Incidence and Mortality Worldwide for 36 Cancers in 185 Countries. *CA Cancer J Clin* (2021) 71(3):209–49. doi: 10.3322/caac.21660
2. Costello AJ. Considering the Role of Radical Prostatectomy in 21st Century Prostate Cancer Care. *Nat Rev Urol* (2020) 17(3):177–88. doi: 10.1038/s41585-020-0287-y
3. Wu S, Xie L, Lin SX, Wirth GJ, Lu M, Zhang Y, et al. Quantification of Perineural Invasion Focus After Radical Prostatectomy Could Improve Predictive Power of Recurrence. *Hum Pathol* (2020) 104:96–104. doi: 10.1016/j.humpath.2020.07.005
4. Thompson I, Thrasher JB, Aus G, Burnett AL, Canby-Hagino ED, Cookson MS, et al. Guideline for the Management of Clinically Localized Prostate Cancer: 2007 Update. *J Urol* (2007) 177(6):2106–31. doi: 10.1016/j.juro.2007.03.003
5. Liebig C, Ayala G, Wilks JA, Berger DH, Albo D. Perineural Invasion in Cancer: A Review of the Literature. *Cancer* (2009) 115(15):3379–91. doi: 10.1002/cncr.24396
6. Reeves F, Hovens CM, Harewood L, Battye S, Peters JS, Costello AJ, et al. Does Perineural Invasion in a Radical Prostatectomy Specimen Predict Biochemical Recurrence in Men With Prostate Cancer? *Can Urol Assoc J* (2015) 9(5-6):E252–5. doi: 10.5489/cuaj.2619
7. Jung JH, Lee JW, Arkoncel FR, Cho NH, Yusoff NA, Kim KJ, et al. Significance of Perineural Invasion, Lymphovascular Invasion, and High-Grade Prostatic Intraepithelial Neoplasia in Robot-Assisted Laparoscopic Radical Prostatectomy. *Ann Surg Oncol* (2011) 18(13):3828–32. doi: 10.1245/s10434-011-1790-4
8. Masieri L, Lanciotti M, Nesi G, Lanzi F, Tosi N, Minervini A, et al. Prognostic Role of Perineural Invasion in 239 Consecutive Patients With Pathologically Organ-Confined Prostate Cancer. *Urol Int* (2010) 85(4):396–400. doi: 10.1159/000315491
9. Merrilees AD, Bethwaite PB, Russell GL, Robinson RG, Delahunt B. Parameters of Perineural Invasion in Radical Prostatectomy Specimens Lack Prognostic Significance. *Mod Pathol* (2008) 21(9):1095–100. doi: 10.1038/modpathol.2008.81
10. Kang M, Oh JJ, Lee S, Hong SK, Lee SE, Byun SS. Perineural Invasion and Lymphovascular Invasion are Associated With Increased Risk of Biochemical Recurrence in Patients Undergoing Radical Prostatectomy. *Ann Surg Oncol* (2016) 23(8):2699–706. doi: 10.1245/s10434-016-5153-z
11. Andersen S, Richardsen E, Nordby Y, Ness N, Størkersen O, Al-Shibli K, et al. Disease-Specific Outcomes of Radical Prostatectomies in Northern Norway; a Case for the Impact of Perineural Infiltration and Postoperative PSA-Doubling Time. *BMC Urol* (2014) 14:49. doi: 10.1186/1471-2490-14-49
12. Jeon HG, Bae J, Yi JS, Hwang IS, Lee SE, Lee E. Perineural Invasion Is a Prognostic Factor for Biochemical Failure After Radical Prostatectomy. *Int J Urol* (2009) 16(8):682–6. doi: 10.1111/j.1442-2042.2009.02331.x
13. Ozcan F. Correlation of Perineural Invasion on Radical Prostatectomy Specimens With Other Pathologic Prognostic Factors and PSA Failure. *Eur Urol* (2001) 40(3):308–12. doi: 10.1159/000049791
14. Fromont G, Godet J, Pires C, Yacoub M, Dore B, Irani J. Biological Significance of Perineural Invasion (PNI) in Prostate Cancer. *Prostate* (2012) 72(5):542–8. doi: 10.1002/pros.21456
15. Hwang BO, Park SY, Cho ES, Zhang X, Lee SK, Ahn HJ, et al. Platelet CLEC2-Podoplanin Axis as a Promising Target for Oral Cancer Treatment. *Front Immunol* (2021) 12:807600. doi: 10.3389/fimmu.2021.807600
16. Kuang AG, Nickel JC, Andriole GL, Castro-Santamaria R, Freedland SJ, Moreira DM. Both Acute and Chronic Inflammation are Associated With Less Perineural Invasion in Men With Prostate Cancer on Repeat Biopsy. *BJU Int* (2019) 123(1):91–7. doi: 10.1111/bju.14428
17. Epstein JI, Egevad L, Amin MB, Delahunt B, Srigley JR, Humphrey PA, et al. The 2014 International Society of Urological Pathology (ISUP) Consensus Conference on Gleason Grading of Prostatic Carcinoma: Definition of Grading Patterns and Proposal for a New Grading System. *Am J Surg Pathol* (2016) 40(2):244–52. doi: 10.1097/PAS.0000000000000530
18. Buyyounouski MK, Choyke PL, McKenney JK, Sartor O, Sandler HM, Amin MB, et al. Prostate Cancer - Major Changes in the American Joint Committee on Cancer Eighth Edition Cancer Staging Manual. *CA Cancer J Clin* (2017) 67(3):245–53. doi: 10.3322/caac.21391
19. Yin L, Li J, Wang J, Pu T, Wei J, Li Q, et al. MAOA Promotes Prostate Cancer Cell Perineural Invasion Through SEMA3C/PlexinA2/NRP1-cMET Signaling. *Oncogene* (2021) 40(7):1362–74. doi: 10.1038/s41388-020-01615-2
20. Kraus RD, Barsky A, Ji L, Garcia Santos PM, Cheng N, Groshen S, et al. The Perineural Invasion Paradox: Is Perineural Invasion an Independent Prognostic Indicator of Biochemical Recurrence Risk in Patients With Pt2n0r0 Prostate Cancer? A Multi-Institutional Study. *Adv Radiat Oncol* (2019) 4(1):96–102. doi: 10.1016/j.adro.2018.09.006
21. DeLancey JO, Wood DPJr, He C, Montgomery JS, Weizer AZ, Miller DC, et al. Evidence of Perineural Invasion on Prostate Biopsy Specimen and Survival After Radical Prostatectomy. *Urology* (2013) 81(2):354–7. doi: 10.1016/j.urology.2012.09.034
22. Ciftci S, Yilmaz H, Ciftci E, Simsek E, Ustuner M, Yavuz U, et al. Perineural Invasion in Prostate Biopsy Specimens Is Associated With Increased Bone Metastasis in Prostate Cancer. *Prostate* (2015) 75(15):1783–9. doi: 10.1002/pros.23067
23. Maru N, Ohori M, Kattan MW, Scardino PT, Wheeler TM. Prognostic Significance of the Diameter of Perineural Invasion in Radical Prostatectomy Specimens. *Hum Pathol* (2001) 32(8):828–33. doi: 10.1053/hupa.2001.26456
24. Mantovani A. Cancer: Inflaming Metastasis. *Nature* (2009) 457(7225):36–7. doi: 10.1002/jcp.24539
25. Sharma D, Brummel-Ziedins KE, Bouchard BA, Holmes CE. Platelets in tumor progression: a host factor that offers multiple potential targets in the treatment of cancer. *J Cell Physiol* (2014) 229(8):1005–15. doi: 10.1002/jcp.24539
26. Labelle M, Begum S, Hynes RO. Direct Signaling Between Platelets and Cancer Cells Induces an Epithelial-Mesenchymal-Like Transition and Promotes Metastasis. *Cancer Cell* (2011) 20(5):576–90. doi: 10.1016/j.ccr.2011.09.009

27. Marcolino E, Siddiqui YH, van den Bosch M, Poole AW, Jayaraman PS, Gaston K. Blood Platelets Stimulate Cancer Extravasation Through Tgfβ-Mediated Downregulation of PRH/HHEX. *Oncogenesis* (2020) 9(2):10. doi: 10.1038/s41389-020-0189-0
28. Nieswandt B, Hafner M, Echtenacher B, Männel DN. Lysis of Tumor Cells by Natural Killer Cells in Mice Is Impeded by Platelets. *Cancer Res* (1999) 59 (6):1295–300.
29. Rudzinski JK, Govindasamy NP, Asgari A, Saito MS, Lewis JD, Jurasz P. Preferential Interaction of Platelets With Prostate Cancer Cells With Stem Cell Markers. *Thromb Res* (2021) 206:42–51. doi: 10.1016/j.thromres.2021.08.008
30. Ponert JM, Gockel LM, Henze S, Schlesinger M. Unfractionated and Low Molecular Weight Heparin Reduce Platelet-Induced Epithelial-Mesenchymal Transition in Pancreatic and Prostate Cancer Cells. *Molecules* (2018) 23 (10):2690. doi: 10.3390/molecules23102690
31. Rudzinski JK, Govindasamy NP, Lewis JD, Jurasz P. The Role of the Androgen Receptor in Prostate Cancer-Induced Platelet Aggregation and Platelet-Induced Invasion. *J Thromb Haemost* (2020) 18(11):2976–86. doi: 10.1111/jth.15020
32. Brady L, Hayes B, Sheill G, Baird AM, Guinan E, Stanfill B, et al. Platelet Cloaking of Circulating Tumour Cells in Patients With Metastatic Prostate Cancer: Results From ExPeCT, a Randomised Controlled Trial. *PLoS One* (2020) 15(12):e0243928. doi: 10.1371/journal.pone.0243928
33. Chai S, Matsumoto N, Storgard R, Peng CC, Aparicio A, Ormseth B, et al. Platelet-Coated Circulating Tumor Cells Are a Predictive Biomarker in Patients With Metastatic Castrate-Resistant Prostate Cancer. *Mol Cancer Res* (2021) 19(12):2036–45. doi: 10.1158/1541-7786.MCR-21-0383
34. D'Amico AV, Whittington R, Malkowicz SB, Schultz D, Blank K, Broderick GA, et al. Biochemical Outcome After Radical Prostatectomy, External Beam Radiation Therapy, or Interstitial Radiation Therapy for Clinically Localized Prostate Cancer. *JAMA* (1998) 280(11):969–74. doi: 10.1001/jama.280.11.969
35. Vailancourt L, Ttu B, Fradet Y, Dupont A, Gomez J, Cusan L, et al. Effect of Neoadjuvant Endocrine Therapy (Combined Androgen Blockade) on Normal Prostate and Prostatic Carcinoma. A Randomized Study. *Am J Surg Pathol* (1996) 20(1):86–93. doi: 10.1097/00000478-199601000-00010

Conflict of Interest: The authors declare that the research was conducted in the absence of any commercial or financial relationships that could be construed as a potential conflict of interest.

Publisher's Note: All claims expressed in this article are solely those of the authors and do not necessarily represent those of their affiliated organizations, or those of the publisher, the editors and the reviewers. Any product that may be evaluated in this article, or claim that may be made by its manufacturer, is not guaranteed or endorsed by the publisher.

Copyright © 2022 Wang, Liu, Liang, Yang and Xing. This is an open-access article distributed under the terms of the Creative Commons Attribution License (CC BY). The use, distribution or reproduction in other forums is permitted, provided the original author(s) and the copyright owner(s) are credited and that the original publication in this journal is cited, in accordance with accepted academic practice. No use, distribution or reproduction is permitted which does not comply with these terms.

frontiers | Frontiers in Oncology

ORIGINAL RESEARCH
published: 20 June 2022
doi: 10.3389/fonc.2022.904315

Urine Exosomal AMACR Is a Novel Biomarker for Prostate Cancer Detection at Initial Biopsy

Xin Jin[1,2,3†], Jin Ji[4†], Decao Niu[5,6†], Yuchen Yang[7], Shuchun Tao[1,2], Lilin Wan[1,2], Bin Xu[1,2], Shuqiu Chen[1,2], Fubo Wang[4,5] and Ming Chen[1,2*]*

[1] Department of Urology, Zhongda Hospital, Southeast University, Nanjing, China, [2] Surgical Research Center, Institute of Urology, Southeast University Medical School, Nanjing, China, [3] Department of Urology, Taizhou People's Hospital, Taizhou, China, [4] Department of Urology, Changhai Hospital, Second Military Medical University, Shanghai, China, [5] Center for Genomic and Personalized Medicine, Guangxi Key Laboratory for Genomic and Personalized Medicine, Guangxi Collaborative Innovation Center for Genomic and Personalized Medicine, Guangxi Medical University, Nanning, China, [6] Department of Urology, Guangdong Second Provincial General Hospital, Guangzhou, China, [7] Nursing Department, Naval Hospital of Eastern Theater Command of People's Liberation Army of China (PLA), Zhoushan, China

OPEN ACCESS

Edited by:
Takeshi Yuasa,
Japanese Foundation For Cancer Research, Japan

Reviewed by:
Bin Xu,
Shanghai Jiao Tong University, China
Dmitry Enikeev,
I.M. Sechenov First Moscow State Medical University, Russia

***Correspondence:**
Fubo Wang
wangfubo@gxmu.edu.cn
Ming Chen
mingchenseu@126.com

[†]These authors have contributed equally to this work

Specialty section:
This article was submitted to Genitourinary Oncology, a section of the journal Frontiers in Oncology

Received: 25 March 2022
Accepted: 16 May 2022
Published: 20 June 2022

Citation:
Jin X, Ji J, Niu D, Yang Y, Tao S, Wan L, Xu B, Chen S, Wang F and Chen M (2022) Urine Exosomal AMACR Is a Novel Biomarker for Prostate Cancer Detection at Initial Biopsy. Front. Oncol. 12:904315. doi: 10.3389/fonc.2022.904315

Objectives: The aim of this study is to identify and validate urine exosomal AMACR (UE-A) as a novel biomarker to improve the detection of prostate cancer (PCa) and clinically significant PCa (Gleason score ≥ 7) at initial prostate biopsy.

Methods: A total of 289 first-catch urine samples after the digital rectal exam (DRE) were collected from patients who underwent prostatic biopsy, and 17 patients were excluded due to incomplete clinical information. Urine exosomes were purified, and urinary exosomal AMACR (UE-A) was measured by enzyme-linked immunosorbent assay (ELISA). The diagnostic performance of UE-A was evaluated by receiver operating characteristic (ROC) analysis, decision curve analysis (DCA), and waterfall plots.

Results: The expression of AMACR in PCa and csPCa was significantly higher than that in BPH and non-aggressive ($p < 0.001$). The UE-A presented good performance in distinguishing PCa from BPH or BPH plus non-significant PCa (nsPCa) from csPCa with an area under the ROC curve (AUC) of 0.832 and 0.78, respectively. The performance of UE-A was further validated in a multi-center cohort of patients with an AUC of 0.800 for detecting PCa and 0.749 for detecting csPCa. The clinical utility assessed by DCA showed that the benefit of patients using UE-A was superior to PSA, f/t PSA, and PSAD in both the training cohort and the validation cohort in terms of all threshold probabilities. Setting 95% sensitivity as the cutoff value, UE-A could avoid 27.57% of unnecessary biopsies, with only 4 (1.47%) csPCa patients missed.

Conclusions: We demonstrated the great performance of UE-A for the early diagnosis of PCa and csPCa. UE-A could be a novel non-invasive diagnostic biomarker to improve the detection of PCa and csPCa.

Keywords: urine exosomes, AMACR, prostate cancer, diagnosis, biomarker

INTRODUCTION

Prostate cancer (PCa) is a serious threat to men's health. It is one of the leading causes of death in men worldwide. Statistical reports showed that there would be 1,414,259 new cases and 375,304 new deaths in 2020 globally (1) and 268,490 new cases and 34,500 new deaths in the USA (2). Early PCa was confined to the capsule. However, if the tumor invaded the capsule or had metastasis, the treatment was brutal, and the prognosis was poor (2, 3). Therefore, the early diagnosis of PCa has a significant clinical and social value. Prostate-specific antigen (PSA), as the most recognized and most commonly used biomarker of PCa, plays a significant role in detecting PCa at present, but it also has great limitations. A systematic review of PSA screening showed that PSA screening did not clearly reduce cancer mortality (4) but led to overdiagnosis. Another well-known systematic review also published similar results in the same year, showing that PSA reduced cancer mortality but did not improve overall survival and resulted in short-term and long-term surgical complications (5). These studies indicate that PSA as a molecular marker of PCa has low specificity. It is urgent to explore new methods and technologies for early screening and diagnosis of PCa in clinical practice to improve the predictive efficacy of PCa.

Urine is absolutely non-invasive and easy to obtain. The PCa-derived secreted body likely exists in the urine after prostate massage. Protein markers are characterized by solid stability and high specificity. Detection of urine protein after prostate massage will help improve the specificity of PCa diagnosis. Exosomes are small vesicles actively released by cells into the extracellular environment, carrying numerous biomolecules and providing an encouraging non-invasive approach for detecting cancers (6, 7). Recent reports showed that circulating exosomal RNAs could serve as promising biomarkers for cancer detection (6–9). However, urinary exosomal proteins have not been adequately explored as an easily collected and non-invasive source of cancer biomarkers (10).

AMACR (a-Methylacyl-CoA racemase, also known as P504S) is an enzyme that interconverts pristanoyl-CoA and C27-bile acyl CoA between their (R)- and (S)-stereoisomers (11). This protein is elevated in PCa tissue and can act as a biomarker of PCa (12). Urinary and circulating AMACR mRNA has been reported to perform well in PCa diagnosis (13–15). Here, we first evaluated the protein levels of AMACR in urine exosomes between PCa and BPH participants and evaluated its diagnostic performance in differentiating PCa from BPH or csPCa from BPH plus nsPCa patients. We then validated the clinical utility of urine exosomal AMACR to detect PCa and csPCa at initial biopsy.

MATERIALS AND METHODS

Participants

The research was authorized following the Hospital Ethics Committee's manual by Shanghai Changhai Hospital, Taizhou People's Hospital and Zhongda Hospital (No. CHEC2013-115). Three sites shared the same standard operating procedure (SOP) for participant recruitment and sample processing. Written informed consents were obtained from the participants before sampling.

A total of 289 consecutive PCa and biopsy-negative control patients with elevated PSA before biopsy were admitted from Changhai Hospital, Taizhou People's Hospital and Zhongda Hospital, who underwent a prostate biopsy between February 2017 and March 2018. All subjects in this study underwent transperineal biopsy guided by transrectal ultrasound, including patients with PSA > 4 ng/ml and no increase in PSA but with abnormal DRE or imaging examination. The specimen was examined individually by two pathologists and assigned a Gleason score. Baseline information of the study subjects is provided in **Table 1**. Individuals combined with other known tumor histories were excluded. All recruited research subjects signed an informed consent form at admission. We defined benign disease and Gleason score = 6 as the non-aggressive disease and Gleason score ≥7 as the clinically significant PCa (csPCa), which was the same as described in the previous study.

Sample Collection and Preparation

We collected first-catch urine samples following an attentive DRE on the day of the biopsy. The urine samples were processed within 2 h of collection (13). Patients who underwent biopsy were assessed to have an abnormal PSA value (>4 ng/ml), or DRE revealed a nodule or PI-RADS > 3. The diagnosis results were confirmed by biopsy. The pathology diagnosis was double-blind confirmed by two pathologists.

Exosome Extraction

Exosomes were extracted by a commercial kit according to the manufacturer's manuals, as in our previous studies (16). In brief, samples were kept on ice and then 20 ml of which was centrifuged at 3,000 *g* at 4°C for 15 min. Afterward, the supernatant was transferred to a centrifuge tube. Reagent A (7.5 ml) was mixed thoroughly with 670 ml of Reagent B. Incubation was conducted at 4°C for 12–16 h, followed by centrifugation at 3,000 *g* at 4°C for 60 min. More than 1 ml of the supernatant was retained, with the residual supernatant discarded. One milliliter of solution was added above the pellet to fully resuspend it. After centrifuging at 10,000 *g* at 4°C for 10 min, the supernatants were discarded. We resuspended the pellet in 200 µl of filtered PBS and then centrifuged it again for 5 min at 10,000 *g* at 4°C. Exosomes were collected in the supernatant and stored in a −80°C refrigerator.

Transmission Electron Microscopy

Exosome samples were resuspended in PBS. The sample was prepared first and then loaded onto the copper grid. After standing for approximately 20 min at room temperature, the filter paper was used to assimilate excess moisture. The sample was negatively stained for 5 s with 20 µl of 2% phosphotungstic acid (pH 5.52). Then, excess liquid was sucked up by filter paper from the side. After drying at room temperature, the typical structure of exosomes was observed by TEM.

TABLE 1 | Demographics and clinical characteristics of participants.

Parameter	Training set			*p*-value	Validation set			*p*-value
	Entire	Negative	Positive		Entire	Negative	Positive	
Age, yr				0.019*				0.017*
No. pts (%)	139 (100.0)	94 (67.7)	45 (32.3)		133 (100.0)	91 (68.4)	42 (31.6)	
Mean	65.1	64.0	67.4		64.7	63.3	67.6	
SD	7.2	6.9	7.4		8.1	8.4	6.5	
tPSA, ng/ml				0.006#				0.53#
No. pts (%)	139 (100.0)	94 (67.7)	45 (32.3)		133 (100.0)	91 (68.4)	42 (31.6)	
Median	8.8	8.4	11.0		9.3	9.5	9.2	
IQR	6.6–12.4	6.5–11.1	7.6–13.9		6.9–12.9	6.9–12.6	7.4–13.1	
BMI, kg/m^2				0.41#				0.76#
No. pts (%)	139 (100.0)	94 (67.7)	45 (32.3)		133 (100.0)	91 (68.4)	42 (31.6)	
Median	24.2	24.2	24.6		24.2	24.2	24.6	
IQR	22.1–26.5	22.2–26.1	21.9–27.7		22.6–26.2	22.8–26.2	21.9–26.9	
%fPSA				0.002#				0.048#
No. pts (%)	98 (70.5)	63 (45.3)	35 (25.2)		86 (64.7)	56 (42.1)	30 (22.6)	
Median	0.16	0.19	0.11		0.12	0.14	0.1	
IQR	0.11–0.25	0.12–0.27	0.08–0.18		0.08–0.19	0.08–0.22	0.07–0.13	
PSAD								
No. pts (%)	139 (100.0)	94 (67.7)	45 (32.3)		133 (100)	91 (68.4)	42 (31.6)	
Median	0.18	0.158	0.239		0.18	0.16	0.23	
IQR	0.11–0.25	0.10–0. 25	0.16–0.32		0.11–0.29	0.11–0.25	0.16–0.34	
Biopsy Gleason sum, no. (%)								
6			14 (10.1)				11 (8.3)	
7			16 (11.5)				18 (13.5)	
≥8			13 (9.4)				12 (9)	

*yr, years; tPSA, total prostate-specific antigen; SD, standard deviation; IQR, interquartile range; f/t PSA, free prostate-specific antigen/total prostate-specific antigen; f/t PSA, free prostate-specific antigen/total prostate-specific antigen. *Student's t-test. #Mann–Whitney U test.*

Western Blot Analysis

The exosome suspension was thawed on ice, and more than 20 μl of RIPA buffer (89901, Thermo Fisher) containing protease inhibitor (B14001, Bimake) was used to lyse for 30 min. The sample was centrifuged at 12,000 *g* for 5 min at 4°C. Then, a BCA kit was used to measure the protein concentration. Then, a 5× loading buffer was added to the supernatant, and the mixture was heated in a metal bath at 97°C for 3 min. Based on the manufacturer's instructions, a PAGE Gel Fast Preparation Kit (PG112, EpiZyme) was prepared. According to the determined concentration, more than 20–40 μg of protein and protein marker (1610374, Bio-Rad) were each added to the well; SDS-PAGE electrophoresis was conducted at 100 V and run for 105 min. After that, the instrument was set to 100 V and 90 min for electrotransfer. After the transfer was completed, the membranes containing the protein of interest were placed in 5% BAS and blocked for 2 h at room temperature. Then, these were transferred to a primary antibody [including CD9, CD63, CD81, TSG101, Cytochrome c, calnexin (AP1482, Abgent), and ACTB (A5441, Sigma)] and placed on a shaker at 4°C overnight. The next day, the membranes were washed 3 × 5 min by TBST. Incubation of the secondary antibody with the membrane was performed for 2 h at room temperature, followed by three rewashes. Finally, the membrane is photographed.

Nanoparticle Tracking Analysis

Samples were diluted 1:300 in filtered PBS to control concentrations within the most accurate detection range. Panalytical NanoSight NS300 (Malvern) was used to detect the size and distribution of exosomes. The instrument detection cell was washed with DPBS solution without any nanoparticles. After cleaning the detection module, the diluted sample was added to the syringe and placed on the motorized pump. The testing module should be connected and the manufacturer's instructions should be followed before testing. To reduce errors, particle diameters were calculated using the Stokes–Einstein equation with three replicates per sample.

ELISA

Experiments were performed using ELISA kits (E0993h) from EIAab. After the reagents and samples were taken out of the refrigerator, they should be left at room temperature for 30 min, and the working solution should be configured according to the manufacturer's instructions. The standard was diluted in equal proportions, and 100 μl of the standard or sample was added to the 96-well plate pre-incubated with the primary antibody. Three replicate wells were made for each sample. After blocking with film, the 96-well plate was incubated in a 37°C incubator for 2 h. The liquid in the 96-well plate was discarded, and 100 μl of Reagent A was added. After gentle shaking and placement in a 37°C incubator for 1 h, the liquid was discarded and washed three times with washing working solution (300 μl/well) for 2 min each time. Reagent B operation was similar to a previous operation. Finally, more than 90 μl of the reaction solution was added to each well and then placed in a 37°C incubator for 10–20 min in the dark. When a clear color gradient appeared in the standard wells, more than 50 μl of stop solution was added, and

the absorbance value at 450 nm was measured on the computer within 15 min.

Data Analysis

Data analysis was performed by MedCalc v13.0 (MedCalc Software bvba) and Prism V9.2 (GraphPad software). The age of the different groups was compared by Student's *t*-test. The Mann–Whitney *U* test was used to compare PSAD, PSA, and f/t PSA by the nonparametric test. Pearson's chi-squared test compared DRE status. Exosomal AMACR was compared in different groups using a nonparametric test. A univariate logistic regression was used to identify independent predictors of PCa based on biopsy results. We evaluated the diagnostic value of the parameters using the receiver operating characteristic (ROC) curve and the area under the curve (AUC). Comparisons of AUC between different indicators were made using MedCalc and Delong methods. Patients' net benefit was evaluated using decision curve analysis (DCA). Two-sided *p*-values were used, and $p < 0.05$ was considered statistically significant.

RESULTS

Participants' Characteristics

The baseline information of the training and validation cohorts of patients is shown in **Table 1**. We collected the urine sample of 289 patients from February 2017 to March 2018 and excluded 17 patients due to incomplete clinical information. Finally, we analyzed 272 patients (including 185 controls and 87 PCa patients, with a positive biopsy rate of 31.98%). The mean age of participants in the training and validation cohorts was 65.1 years (SD 7.2) and 64.7 years (SD 8.1), respectively. Not all patients underwent MRI. Sixty-six (47.5%) patients in the training cohort and 58 (43.6%) patients in the validation cohort had MRI results. The median tPSA of participants in training and validation cohorts were 8.8 (IQR: 6.6–12.4) and 9.3 (IQR: 6.9–12.9), respectively. For the f/t PSA, the medians were 0.16 (IQR: 0.11–0.25) in the training cohort and 0.12 (IQR: 0.08–0.19) in the validation cohort. The median PSAD was 0.18 (IQR: 0.11–0.25) in the training cohort and 0.18 (IQR: 0.11–0.29) in the validation cohort. The results of exosome identification refer to the literature previously published by our group (16).

Urine Exosomal AMACR Could Distinguishing PCa From BPH and BPH Plus Non-Aggressive PCa

The expression of AMACR in PCa and csPCa was significantly higher than that in BPH and non-aggressive (**Figures 1A, D**, $p < 0.001$). The diagnostic performance of AMACR, evaluated by ROC, was 0.832 for detecting PCa from BPH (**Figure 1B**, $p < 0.001$) and 0.78 for detecting clinically significant PCa (csPCa) (**Figure 1E**, $p < 0.001$) from BPH plus non-aggressive PCa. AMACR was superior to PSA, PSAD, and f/t PSA in detecting PCa from BPH (**Figure 1C**, AMACR vs. PSA, $p = 0.0054$; AMACR vs. f/t PSA, $p = 0.056$, AMACR vs. PSAD, $p = 0.008$). Diagnostic efficiency ($p = 0.0054$), and compared with f/t PSA, the *p*-value was 0.056. For the diagnosis of csPCa, AMACR was also superior to PSA, f/t PSA, and PSAD but could not reach statistical significance (**Figure 1F**, AMACR vs. PSA, $p = 0.1838$; AMACR vs. f/t PSA, $p = 0.125$, AMACR vs. PSAD, $p = 0.214$). The detailed information is summarized in **Table 2**.

The Diagnostic Performance of Urine Exosomal AMACR Was Validated in an Additional Cohort of Participants

We further evaluated the levels of urine AMACR in the samples of the validation cohort of participants. Similar results were observed. The expression of AMACR was upregulated in PCa compared to BPH (**Figure 2A**, $p < 0.001$) and also significantly upregulated in PCa compared to BPH plus non-aggressive PCa (**Figure 2D**, $p < 0.001$). The ROC was 0.800 for detecting PCa from BPH (**Figure 2B**, $p < 0.001$) and 0.749 for detecting clinically significant PCa (csPCa) from BPH plus non-aggressive PCa (**Figure 2E**, $p < 0.001$). Compared to clinical parameters, AMACR was superior to PSA, f/t PSA (**Figure 2C**, AMACR vs. PSA, $p = 0.001$; AMACR vs. f/t PSA, $p = 0.032$), and PSAD but could not reach statistical significance (**Figure 2C**, AMACR vs. PSAD, $p = 0.06$) in detecting PCa from BPH. For the diagnosis of csPCa, AMACR was also superior to PSA (**Figure 2F**, AMACR vs. PSA, $p = 0.031$), f/t PSA, and PSAD but could not reach statistical significance (**Figure 2F**, AMACR vs. f/t PSA, $p = 0.109$, AMACR vs. PSAD, $p = 0.115$). The detailed information is summarized in **Table 3**.

The Clinical Application of Urine Exosomal AMACR

To determine the net benefit of participants, the clinical DCA was used (**Figures 3A–D**). The results showed that the benefit of patients using AMACR was superior to PSA, f/t PSA, and PSAD in both the training cohort and the validation cohort in terms of diagnostic efficiency. There are also good performances in diagnosing csPCA. Setting 30% as the threshold, AMACR could avoid 60.4% of unnecessary biopsies in the training cohort, which was significantly higher than 47.4% in PSA, with only 12 (8.6%) csPCA patients missed. AMACR could avoid 58.6% of unnecessary biopsies in the validation cohort, which was significantly higher than 26.3% in PSA, with only 10 (7.5%) patients missed, among which 9 (6.8%) of these patients had clinically significant PCa. Setting 95% sensitivity as the cutoff value 8.9, UE-A could avoid 27.57% of unnecessary biopsies, which was significantly higher than 13.24% in PSA, with only 4 (1.47%) csPCa patients missed. The waterfall plot shows the biopsy results of each participant and AMACR results (**Figure 3E**).

DISCUSSION

The diagnostic rate of PCa has steadily increased with the increased PSA screening (17)... In spite of abnormal DRE and transrectal ultrasound (TRUS) triggering prostate biopsy, PSA is still the main indicator for prostate biopsy (18). Higher levels of

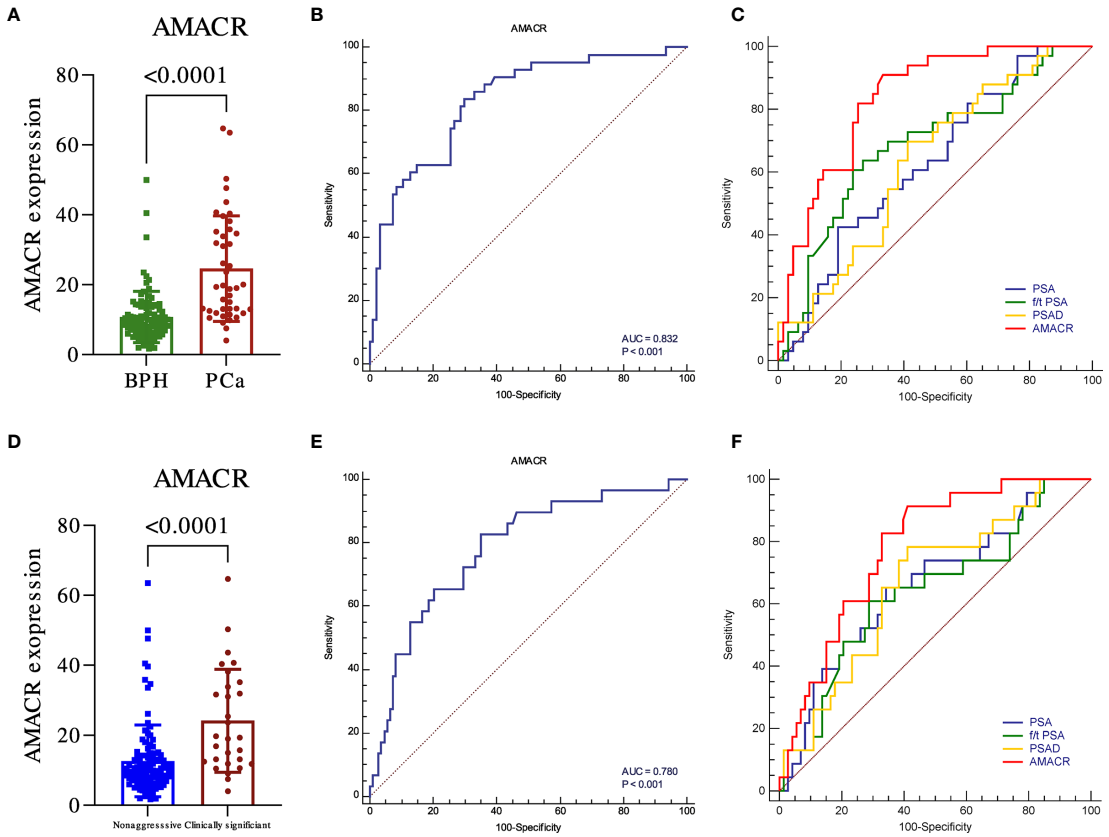


FIGURE 1 | The diagnostic utility of urine exosomal AMACR in the training cohort. The urine AMACR was significantly higher in the PCa **(A)** ($p < 0.001$) and csPCA **(D)** ($p < 0.001$) than in the control group. The utility of urine AMACR in distinguishing PCa **(B)** (AUC: 0.832, $p < 0.001$) and csPCa **(E)** (AUC: 0.780, $p < 0.001$). Comparison ROC illustrated that the urine AMACR has a better performance than PSA, f/t PSA, and PSAD in PCa **(C)** and csPCa **(F)** diagnosis.

PSA are routinely used in predicting PCa risk. Scientists are therefore encouraged to develop more specific biomarkers for detecting clinically significant PCa due to the low specificity of PSA testing for screening PCa and its limitations in identifying clinically significant PCa at an early stage and avoiding unnecessary biopsies (19).

AMACR is a racemase encoded by the P504S gene, which plays a vital role in the β oxidation of fatty acids and cholic acid

TABLE 2 | The performance of urine exosomal AMACR and clinical features to predict biopsy results in the training cohort.

Parameters	Positive and negative		Non-aggressive and csPCa	
	AUC (95% CI)	Univariate *p*	AUC (95% CI)	Univariate *p*
Age	0.622 (0.536 to 0.703)	0.008	0.631 (0.546 to 0.712)	0.014
BMI	0.544 (0.458 to 0.629)	0.746	0.541 (0.454 to 0.625)	0.211
PSA	0.645 (0.559 to 0.724)	0.017	0.674 (0.589 to 0.751)	0.006
f/t PSA	0.689 (0.588 to 0.779)	0.002	0.645 (0.542 to 0.740)	0.020
PSAD	0.692 (0.608 to 0.767)	<0.001	0.700 (0.616 to 0.774)	<0.001
AMACR	0.832 (0.759 to 0.890)	<0.001	0.780 (0.701 to 0.846)	<0.001

AUC, area under the curve; PSA, prostate-specific antigen; PSAD, prostate-specific antigen density; f/t PSA, free prostate-specific antigen/total prostate-specific antigen; csPCa, clinically significant prostate cancer.

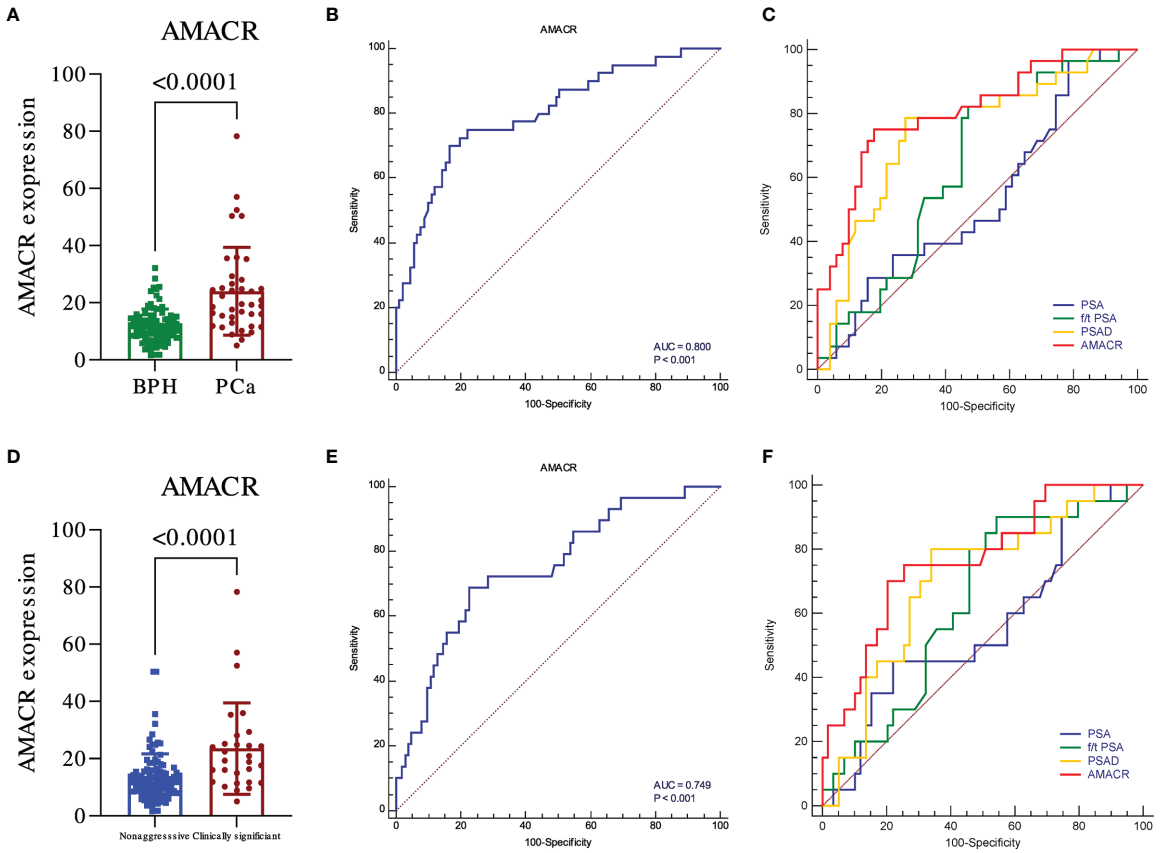


FIGURE 2 | The diagnostic utility of urine exosomal AMACR in the validation cohort. The urine AMACR was significantly higher in the PCa **(A)** ($p < 0.001$) and csPCA **(D)** ($p < 0.001$) than the control group, respectively. The utility of urine AMACR in distinguishing PCa **(B)** (AUC: 0.800, $p < 0.001$) and csPCa **(E)** (AUC: 0.749, $p < 0.001$). Comparison ROC illustrated that the urine AMACR has a better performance than PSA, f/t PSA, and PSAD in PCa **(C)** and csPCa **(F)** diagnosis.

metabolism (20). Lee et al. reported that AMACR has a diagnostic and prognostic value in glioblastoma (21). In PCa, AMACR can cause DNA damage that leads to the expression of peroxide, which promotes tumor progression (12). At present, many studies have pointed out that the AMACR mRNA level is significantly highly expressed in PCa tissues, and its sensitivity and specificity as a diagnostic marker are 82%–100% and 97%–100%, respectively (22, 23). Rogers et al. (24) first proposed the

TABLE 3 | The performance of urine exosomal AMACR and clinical features to predict biopsy results in the validation cohort.

Parameters	Positive and negative		Non-aggressive and csPCa	
	AUC (95%CI)	Univariate *p*	AUC (95%CI)	Univariate *p*
Age	0.629 (0.541 to 0.711)	0.002	0.641 (0.553 to 0.722)	0.003
BMI	0.517 (0.428 to 0.604)	0.984	0.534 (0.445 to 0.621)	0.989
PSA	0.534 (0.446 to 0.621)	0.549	0.580 (0.491 to 0.665)	0.211
f/t PSA	0.634 (0.520 to 0.738)	0.044	0.634 (0.520 to 0.738)	0.133
PSAD	0.664 (0.577 to 0.744)	0.015	0.669 (0.582 to 0.748)	0.030
AMACR	0.800 (0.721 to 0.865)	<0.001	0.749 (0.666 to 0.821)	<0.001

AUC, area under the curve; PSA, prostate-specific antigen; f/t PSA, free prostate-specific antigen/total prostate-specific antigen; csPCa, clinically significant prostate cancer; PSAD, prostate-specific antigen density.

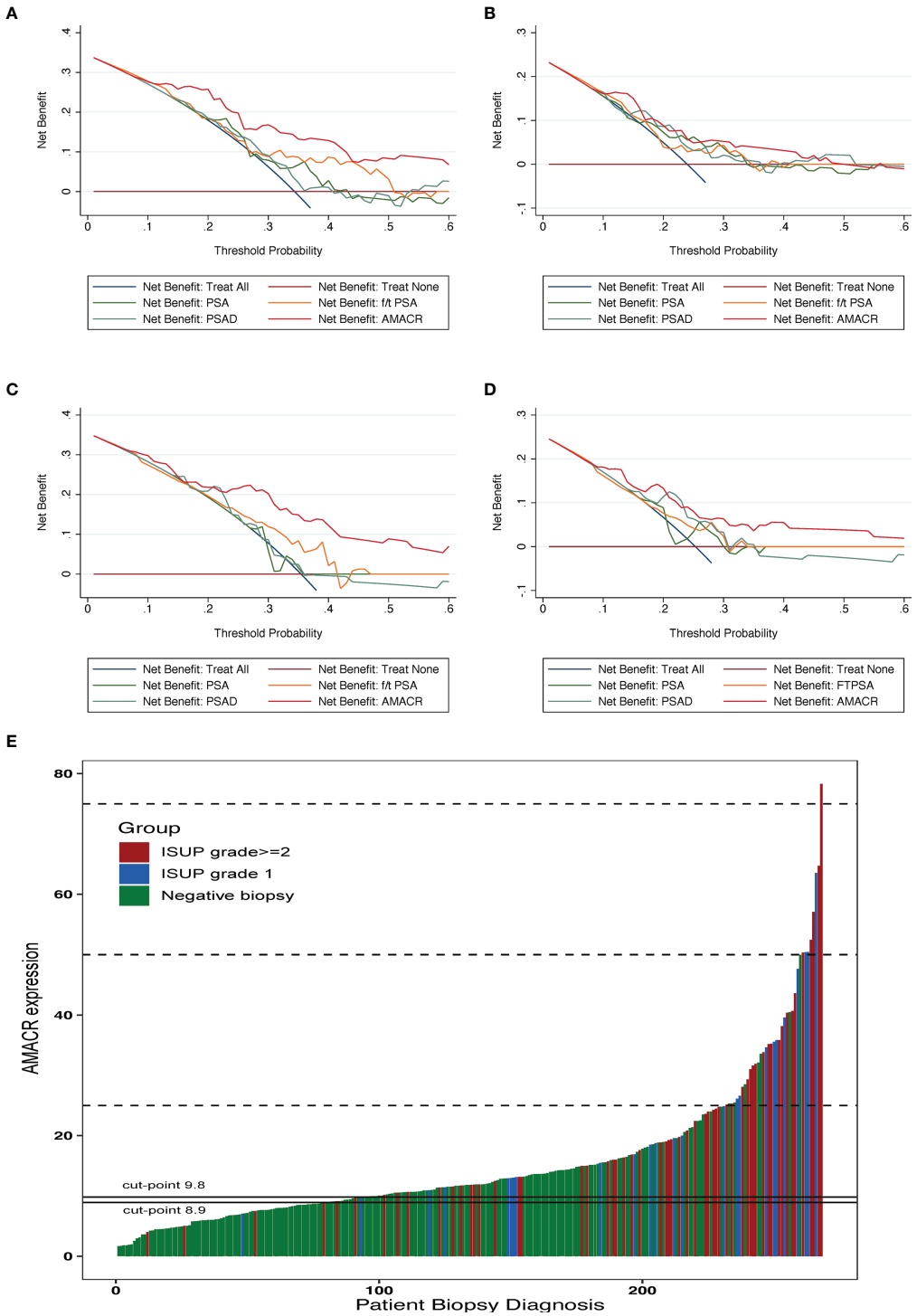


FIGURE 3 | Clinical application of the urine exosomal AMACR. The DCA indicates that urine AMACR has a higher net benefit across a threshold of 20%–50% probabilities for diagnosing PCa **(A, C)** and csPCa **(B, D)** in two cohorts. **(E)** Waterfall plot of the urine AMACR in relation to prostate biopsy results (n = 272). Red bar indicates the ISUP grade ≥2 tumors (GS ≥ 7); the blue one indicates the ISUP grade 1 tumors (GS = 6); the green one indicates the negative biopsies. Two horizontal lines represent the cutoff points of 9.8 at a sensitivity of 90% and 8.9 at a sensitivity of 95%.

potential of AMACR as a diagnostic marker for PCa in the current study on the diagnostic value of AMACR protein level in urine. After testing the urine samples of 26 patients with PCa biopsy, they found that the sensitivity of AMACR for diagnosis was 100%, but the specificity was only 58%. This may be due to the limitation of sample size. However, in the study of Sroka et al. (25), AMACR level in the PCa group was higher than the control group ($p < 0.001$), but its AUC as a diagnostic indicator was 0.748, slightly lower than the diagnostic efficacy of serum PSA (AUC = 0.769) and could not replace PSA as a new diagnostic marker. Here, we showed that urine exosomal AMACR achieved an AUC of 0.832 in detecting PCa from BPH and an AUC of 0.78 in predicting csPCa at initial biopsy. Moreover, the diagnostic performance of urine exosomal AMACR was superior to PSA, f/t PSA, and PSAD. The similar results were observed in an additional cohort of patients. These results indicated that urine exosomal AMACR could serve as a promising biomarker to improve the detection of PCa and csPCa.

Research conducted in the present study may provide a new perspective on PCa and csPCa diagnosis. Several limitations remain, however. First, the sample size was inadequate. We need another multi-center, perspective, large-scale study to verify our findings. Second, we did not compare UE-A to other emerging assays, such as MiPS, SelectMDx, and EPI. Third, UE-A was significantly correlated with PI-RADS (**Figure S1**, $p = 0.0020$). However, we could not compare the performance of UE-A to that of PI-RADS because more than half of patients did not undergo MRI. Finally, given the noticeable differences in genetic alteration signatures between Asians and Westerners (26), additional studies should be conducted to compare the clinical utility of our UE-A in Asian and Western patients.

CONCLUSION

In summary, we developed and validated a new non-invasive, urinary-based, exosomal biomarker, AMACR, for the detection of PCa and csPCa early in the disease course. Clinically, the urine exosomal AMACR had a higher net benefit than current clinical parameters, while it could spare a significant amount of unnecessary biopsies.

DATA AVAILABILITY STATEMENT

The raw data supporting the conclusions of this article will be made available by the authors, without undue reservation.

ETHICS STATEMENT

The studies involving human participants were reviewed and approved by the Ethics Committee of Shanghai Changhai Hospital, the Ethics Committee of Taizhou People's Hospital, and the Ethics Committee of Zhongda Hospital. The patients/participants provided their written informed consent to participate in this study.

AUTHOR CONTRIBUTIONS

MC and FW led the study. XJ, JJ, and DN contributed to the conception of the study. XJ, JJ, DN, YY, ST, and BX performed the experiment. JJ, XJ, DN, SC, and YY contributed significantly to analysis and manuscript preparation. FW and JJ performed the data analyses and wrote the manuscript. XJ, DN, and ST helped perform the analysis with constructive discussions. FW and MC critically reviewed the manuscript. All authors contributed to the article and approved the submitted version.

FUNDING

This work was funded by the National Natural Science Foundation of China (NSFC) (81902616 to FW) and the Science and Technology Support Project in the Field of Biomedicine of Shanghai Science and Technology Action Plan (19441909200 to FW).

SUPPLEMENTARY MATERIAL

The Supplementary Material for this article can be found online at: https://www.frontiersin.org/articles/10.3389/fonc.2022.904315/full#supplementary-material

REFERENCES

1. Sung H, Ferlay J, Siegel RL, Laversanne M, Soerjomataram I, Jemal A, et al. Global Cancer Statistics 2020: GLOBOCAN Estimates of Incidence and Mortality Worldwide for 36 Cancers in 185 Countries. *CA: Cancer J Clin* (2021) 71(3):209-49. doi: 10.3322/caac.21660
2. Siegel RL, Miller KD, Fuchs HE, Jemal A. Cancer Statistics, 2022. *CA: Cancer J Clin* (2022) 72(1):7–33. doi: 10.3322/caac.21708
3. Shao YH, Kim S, Moore DF, Shih W, Lin Y, Stein M, et al. Cancer-Specific Survival After Metastasis Following Primary Radical Prostatectomy Compared With Radiation Therapy in Prostate Cancer Patients: Results of a Population-Based, Propensity Score-Matched Analysis. *Eur Urol* (2014) 65 (4):693–700. doi: 10.1016/j.eururo.2013.05.023
4. Fenton JJ, Weyrich MS, Durbin S, Liu Y, Bang H, Melnikow J. Prostate-Specific Antigen-Based Screening for Prostate Cancer: Evidence Report and Systematic Review for the US Preventive Services Task Force. *Jama* (2018) 319(18):1914–31. doi: 10.1001/jama.2018.3712
5. Ilic D, Djulbegovic M, Jung JH, Hwang EC, Zhou Q, Cleves A, et al. Prostate Cancer Screening With Prostate-Specific Antigen (PSA) Test: A Systematic Review and Meta-Analysis. *Bmj* (2018) 362:k3519. doi: 10.1136/bmj.k3519
6. Xu R, Rai A, Chen M, Suwakulsiri W, Greening DW, Simpson RJ. Extracellular Vesicles in Cancer - Implications for Future Improvements in Cancer Care. *Nat Rev Clin Oncol* (2018) 15(10):617–38. doi: 10.1038/s41571-018-0036-9
7. Kalluri R, LeBleu VS. The Biology, Function, and Biomedical Applications of Exosomes. *Science* (2020) 367(6478):eaau6977. doi: 10.1126/science.aau6977
8. Dai J, Su Y, Zhong S, Cong L, Liu B, Yang J, et al. Exosomes: Key Players in Cancer and Potential Therapeutic Strategy. *Signal Transduct Target. Ther* (2020) 5(1):145. doi: 10.1038/s41392-020-00261-0

9. Hu W, Liu C, Bi ZY, Zhou Q, Zhang H, Li LL, et al. Comprehensive Landscape of Extracellular Vesicle-Derived RNAs in Cancer Initiation, Progression, Metastasis and Cancer Immunology. *Mol cancer.* (2020) 19 (1):102. doi: 10.1186/s12943-020-01199-1
10. Das S, Ansel KM, Bitzer M, Breakefield XO, Charest A, Galas DJ, et al. The Extracellular RNA Communication Consortium: Establishing Foundational Knowledge and Technologies for Extracellular RNA Research. *Cell* (2019) 177 (2):231–42. doi: 10.1016/j.cell.2019.03.023
11. Lloyd MD, Yevglevskis M, Lee GL, Wood PJ, Threadgill MD, Woodman TJ. Alpha-Methylacyl-CoA Racemase (AMACR): Metabolic Enzyme, Drug Metabolizer and Cancer Marker P504S. *Prog Lipid Res* (2013) 52(2):220–30. doi: 10.1016/j.plipres.2013.01.001
12. Kong G, Lee H, Tran Q, Kim C, Gong N, Park J, et al. Current Knowledge on the Function of Alpha-Methyl Acyl-CoA Racemase in Human Diseases. *Front Mol Biosci* (2020) 7:153. doi: 10.3389/fmolb.2020.00153
13. Ji J, Chen X, Xu Y, Cao Z, Xu H, Kong C, et al. Prostate Cancer Diagnosis Using Urine Sediment Analysis-Based Alpha-Methylacyl-CoA Racemase Score: A Single-Center Experience. *Cancer control: J Moffitt Cancer Center.* (2019) 26(1):1073274819887697. doi: 10.1177/1073274819887697
14. Kotova ES, Savochkina YA, Doludin YV, Vasilyev AO, Prilepskay EA, Potoldykova NV, et al. Identification of Clinically Significant Prostate Cancer by Combined PCA3 and AMACR mRNA Detection in Urine Samples. *Res Rep urol.* (2020) 12:403–13. doi: 10.2147/RRU.S262310
15. Souza MF, Kuasne H, Barros-Filho MC, Ciliao HL, Marchi FA, Fuganti PE, et al. Circulating mRNA Signature as a Marker for High-Risk Prostate Cancer. *Carcinogenesis* (2020) 41(2):139–45. doi: 10.1093/carcin/bgz129
16. Li Y, Ji J, Lyu J, Jin X, He X, Mo S, et al. A Novel Urine Exosomal lncRNA Assay to Improve the Detection of Prostate Cancer at Initial Biopsy: A Retrospective Multicenter Diagnostic Feasibility Study. *Cancers* (2021) 13 (16):4075. doi: 10.3390/cancers13164075
17. Wilt TJ, Dahm P. PSA Screening for Prostate Cancer: Why Saying No is a High-Value Health Care Choice. *J Natl Compr Cancer Network: JNCCN.* (2015) 13(12):1566–74. doi: 10.6004/jnccn.2015.0182
18. Liang L, Qi F, Cheng Y, Zhang L, Cao D, Cheng G, et al. Analysis of Risk Factors for Determining the Need for Prostate Biopsy in Patients With Negative MRI. *Sci Rep* (2021) 11(1):6048. doi: 10.1038/s41598-021-83802-z
19. Kuci Emruli V, Liljedahl L, Axelsson U, Richter C, Theorin L, Bjartell A, et al. Identification of a Serum Biomarker Signature Associated With Metastatic Prostate Cancer. *Proteomics Clin Appl* (2021) 15(2-3):e2000025. doi: 10.1002/prca.202000025
20. Kuefer R, Varambally S, Zhou M, Lucas PC, Loeffler M, Wolter H, et al. Alpha-Methylacyl-CoA Racemase: Expression Levels of This Novel Cancer Biomarker Depend on Tumor Differentiation. *Am J Pathol* (2002) 161(3):841–8. doi: 10.1016/s0002-9440(10)64244-7
21. Lee H, Kim M, Kim SH, Tran Q, Kong G, Kim C, et al. Alpha-Methylacyl-CoA Racemase (AMACR), a Potential New Biomarker for Glioblastoma. *Front Oncol* (2020) 10:550673. doi: 10.3389/fonc.2020.550673
22. Rubin MA, Zhou M, Dhanasekaran SM, Varambally S, Barrette TR, Sanda MG, et al. Alpha-Methylacyl Coenzyme A Racemase as a Tissue Biomarker for Prostate Cancer. *Jama* (2002) 287(13):1662–70. doi: 10.1001/jama.287.13.1662
23. Al-Maghrebi M, Kehinde EO, Anim JT, Sheikh M. The Role of Combined Measurement of Tissue mRNA Levels of AMACR and Survivin in the Diagnosis and Risk Stratification of Patients With Suspected Prostate Cancer. *Int Urol. Nephrol.* (2012) 44(6):1681–9. doi: 10.1007/s11255-012-0220-2
24. Rogers CG, Yan G, Zha S, Gonzalgo ML, Isaacs WB, Luo J, et al. Prostate Cancer Detection on Urinalysis for Alpha Methylacyl Coenzyme a Racemase Protein. *J Urol.* (2004) 172(4 Pt 1):1501–3. doi: 10.1097/01.ju.0000137659.53129.14
25. Sroka WD, Adamowski M, Słupski P, Siódmiak J, Jarzemski P, Odrowąż-Sypniewska G, et al. Alpha-Methylacyl-CoA Racemase and Hepsin as Urinary Prostate Cancer Markers. *Int J Biol Markers.* (2015) 30(4):e401–6. doi: 10.5301/jbm.5000146
26. Li J, Xu C, Lee HJ, Ren S, Zi X, Zhang Z, et al. A Genomic and Epigenomic Atlas of Prostate Cancer in Asian Populations. *Nature* (2020) 580(7801):93–9. doi: 10.1038/s41586-020-2135-x

Conflict of Interest: The authors declare that the research was conducted in the absence of any commercial or financial relationships that could be construed as a potential conflict of interest.

Publisher's Note: All claims expressed in this article are solely those of the authors and do not necessarily represent those of their affiliated organizations, or those of the publisher, the editors and the reviewers. Any product that may be evaluated in this article, or claim that may be made by its manufacturer, is not guaranteed or endorsed by the publisher.

Copyright © 2022 Jin, Ji, Niu, Yang, Tao, Wan, Xu, Chen, Wang and Chen. This is an open-access article distributed under the terms of the Creative Commons Attribution License (CC BY). The use, distribution or reproduction in other forums is permitted, provided the original author(s) and the copyright owner(s) are credited and that the original publication in this journal is cited, in accordance with accepted academic practice. No use, distribution or reproduction is permitted which does not comply with these terms.

frontiers | Frontiers in Oncology

ORIGINAL RESEARCH
published: 23 June 2022
doi: 10.3389/fonc.2022.893424

Deep Learning-Based Multi-Omics Integration Robustly Predicts Relapse in Prostate Cancer

Ziwei Wei[1], Dunsheng Han[1], Cong Zhang[1], Shiyu Wang[1], Jinke Liu[1], Fan Chao[2], Zhenyu Song[3] and Gang Chen[1]**

[1] Department of Urology, Jinshan Hospital, Fudan University, Shanghai, China, [2] Department of Urology, Zhongshan Hospital, Fudan University (Xiamen Branch), Xiamen, China, [3] Ovarian Cancer Program, Department of Gynecologic Oncology, Zhongshan Hospital, Fudan University, Shanghai, China

OPEN ACCESS

Edited by:
Riccardo Tellini,
Careggi University Hospital, Italy

Reviewed by:
Ziyu Ning,
Harbin Medical University, China
Edgar Gonzalez-Kozlova,
Icahn School of Medicine at Mount Sinai, United States

***Correspondence:**
Gang Chen
chgan365@126.com
Zhenyu Song
song.zhenyu@zs-hospital.sh.cn

Specialty section:
This article was submitted to Genitourinary Oncology, a section of the journal Frontiers in Oncology

Received: *10 March 2022*
Accepted: *13 May 2022*
Published: *23 June 2022*

Citation:
Wei Z, Han D, Zhang C, Wang S, Liu J, Chao F, Song Z and Chen G (2022) Deep Learning-Based Multi-Omics Integration Robustly Predicts Relapse in Prostate Cancer. Front. Oncol. 12:893424. doi: 10.3389/fonc.2022.893424

Objective: Post-operative biochemical relapse (BCR) continues to occur in a significant percentage of patients with localized prostate cancer (PCa). Current stratification methods are not adequate to identify high-risk patients. The present study exploits the ability of deep learning (DL) algorithms using the H2O package to combine multi-omics data to resolve this problem.

Methods: Five-omics data from 417 PCa patients from The Cancer Genome Atlas (TCGA) were used to construct the DL-based, relapse-sensitive model. Among them, 265 (63.5%) individuals experienced BCR. Five additional independent validation sets were applied to assess its predictive robustness. Bioinformatics analyses of two relapse-associated subgroups were then performed for identification of differentially expressed genes (DEGs), enriched pathway analysis, copy number analysis and immune cell infiltration analysis.

Results: The DL-based model, with a significant difference (P = 6e-9) between two subgroups and good concordance index (C-index = 0.767), were proven to be robust by external validation. 1530 DEGs including 678 up- and 852 down-regulated genes were identified in the high-risk subgroup S2 compared with the low-risk subgroup S1. Enrichment analyses found five hallmark gene sets were up-regulated while 13 were down-regulated. Then, we found that DNA damage repair pathways were significantly enriched in the S2 subgroup. CNV analysis showed that 30.18% of genes were significantly up-regulated and gene amplification on chromosomes 7 and 8 was significantly elevated in the S2 subgroup. Moreover, enrichment analysis revealed that some DEGs and pathways were associated with immunity. Three tumor-infiltrating immune cell (TIIC) groups with a higher proportion in the S2 subgroup (p = 1e-05, p = 8.7e-06, p = 0.00014) and one TIIC group with a higher proportion in the S1 subgroup (P = 1.3e-06) were identified.

Conclusion: We developed a novel, robust classification for understanding PCa relapse. This study validated the effectiveness of deep learning technique in prognosis prediction, and the method may benefit patients and prevent relapse by improving early detection and advancing early intervention.

Keywords: prostate cancer, relapse prediction, multi-omics, autoencoder, deep learning, H2O package

INTRODUCTION

Data accumulation is increasing exponentially with the development and application of advanced technologies such as chips and sequencing in the biomedical field. Combined with state-of-the-art algorithms, it is revealing strong biological associations in the pathomechanism of various cancers (1, 2). Before this new era, cancer studies concerning single-dimensional data could only obtain limited information, but multi-omics data integration approaches can now address important biological questions. Multi-omics data integration techniques have been widely applied for identifying subtypes, and multiple studies have revealed that the deep learning (DL) method may be effective for transducing multi-omics data to construct more accurate prognosis models (3, 4).

Prostate cancer (PCa) is one of the most common malignancies in elderly men, accounting for 26% of all cancers and 11% of estimated cancer death in males in 2021 (5). After the PCa patients received either radical prostatectomy (RP) or external beam radiotherapy, 27–53% of patients experienced biochemical recurrence (BCR) (6). Combined with surgical margin status, clinically applied prognostic factors such as prostate specific antigen (PSA) value, tumor-node-metastasis (TNM) status and Gleason score can help assess the risk of relapse after RP (7). However, these parameters lack predictive accuracy. As we all know, the best medical decisions should be made according to the patients' specific situations. Relapse is indeed a very significant part of it, and prediction represents a major challenge (8). New methods to discover relapse-sensitive subtypes are much needed, and a more accurate risk-stratification tool improve the allocation of medical resources (9).

In recent years, several studies have identified PCa molecular subtypes (10–14). Huang et al. (10) generated a set of long non-coding RNAs (lncRNAs) to predict BCR-free survival of PCa using The Cancer Genome Atlas (TCGA; https://www.cancer.gov/) dataset, a large and detailed database including omics data for more than 30 cancer types. The results showed that this four-lncRNA model was more precise than the American Joint Committee on Cancer T stage and Gleason score, although differences were not significant. Chu et al. (11) used a random forest-based variable hunting approach to select eight messenger RNA (mRNA), and developed a risk score staging system. Importantly, this eight-gene model was further validated by another independent dataset. Wang et al. (13) integrated mRNA, microRNA (miRNA), and methylation data, selected TELO2, ZMYND19, miR-143, miR-378a, cg00687383, and cg02318866 for model construction, and reported a high concordance index (C-index = 0.713).

Genomics, epigenomics, transcriptomics, and other omics approaches can broadly be defined as systematic methods for collecting multifarious biological data, and these techniques can reveal the heterogeneity of tumors and provide new types of molecular classification. The H2O Deep Learning Estimator has not been applied to PCa relapse prediction, and meanwhile one or a few omics layers have been considered in previous studies, with a small number of biomarkers. To more comprehensively mine multi-omics data, we herein developed a robust relapse risk-stratification model for PCa based on up to five-omics data using the H2O Deep Learning Estimator, consisting of mRNA, miRNA, DNA methylation, copy number variations (CNVs), and lncRNA. Five external validation sets were employed to evaluate its robustness, which was lacking for previous predictive models. Furthermore, detailed bioinformatic analysis was performed from multiple perspectives. We evaluated differentially expressed genes (DEGs), critical signaling pathways, CNVs, and tumor-infiltrating immune cell (TIIC) groups associated with PCa relapse.

MATERIALS AND METHODS

Data Acquisition and Study Design

Multi-omics PCa data from TCGA, including mRNA, miRNA, DNA methylation, CNVs and lncRNA, were subjected to dimensionality reduction analysis to extract associated genes using the H2O package in R (v3.6.0) (15), an open-source machine learning platform that supports the most widely used machine learning models and advanced models, such as DL and so forth. Multi-omics datasets were obtained from the TCGA data portal. CNV values were generated by GISTIC 2.0, and processing of methylation data was conducted as previously described (3, 9). Hyperparameter optimization was performed by grid search, and DL models were then built. Five additional validation sets were applied to evaluate the predictive robustness of the best-performing model. The study workflow is shown in **Figure 1**.

An autoencoder with three hidden layers (n = 50, 100, 150, 200, 250, 300, 400, 500) was implemented, for which the bottleneck layer was used to discover new labels from the multi-omics data, with α_a = 0.0001 and α_w = 0.001. As reported, selection parameters to train the autoencoder were 'TanhWithDropout' as the activation function, 'log loss' as the objective function, and '10 epochs and 50% dropout' as the gradient descent algorithm (3).In detail taking the input $x = (x_1, ..., x_n)$, the output of x', for a given i the formula is $x' = tanh(W_i x + b_i)$ where W_i is the weight matrix of size $x \times x'$. For k layer in the autoencoder, the formula is $x' F_{1\to k}(x) = f_1 \circ \ldots \circ f_{k-1} \circ f_k$

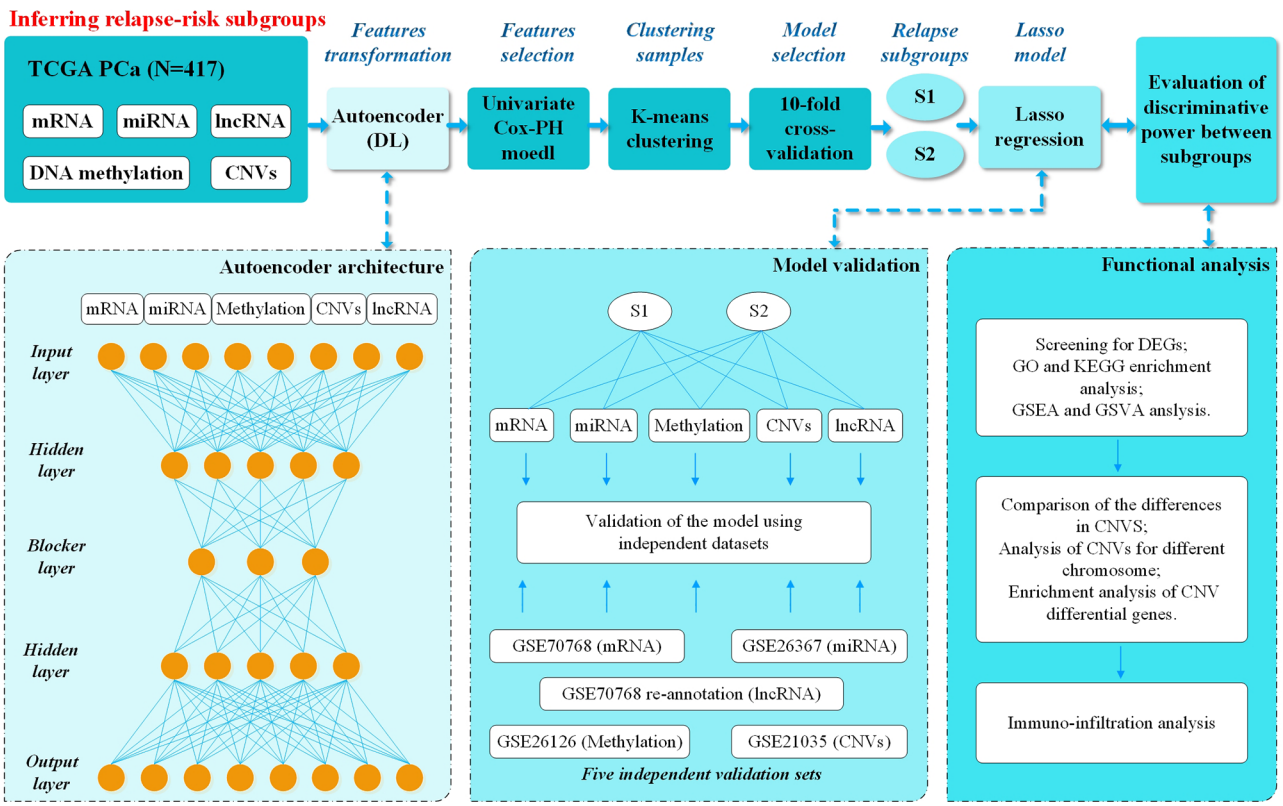


FIGURE 1 | Overall workflow. Firstly, mRNA, miRNA, DNA methylation, CNVs, and lncRNA deep features from the TCGA PCa cohort were stacked up as input features for the autoencoder, a deep-learning method. Then each of the new and transformed features in the bottleneck layer of the autoencoder were subjected to univariate Cox-PH models to select the features associated with relapse. Then K-mean clustering was applied to relapse-associated deep features and 10-fold cross-validation was applied to analyze the C-index for different clusters and relapse in 8 DL models. The best model (model_3) with better discriminative ability was finally selected using Kaplan-Meier plotter between two models with the highest C-index. Then the Lasso method was used to filter out the relapse-associated feature labels, according to model_3 subgroups, from the database of TCGA, including mRNA, miRNA, DNA methylation, CNVs and lncRNA. The Lasso model was constructed, and five external validation sets from GEO were used to evaluate its prediction ability. Last but not least, functional analysis was performed to understand the different characteristics between two relapse-associated subgroups.

$(x)\ logloss(x,x') = \sum_{k-1}^{d}(x_k log(x_k^{'}) + (1-k)log(1-x_k^{'}))$ was applied to measure the error between the input and output. To control overfitting, $L(x,x') = logloss(x,x') + \sum_{i=1}^{k}(\alpha_w||W_i||_1 + \alpha_a||F_{1\to i}(x)||_2^2)$. Finally, eight DL models were built based on different hidden layers.

Robustness Assessment and Model Selection

We extracted deep features from eight DL models, and features related to relapse were screened out by univariate Cox proportional hazards (Cox-PH). Next, we used the K-means clustering algorithm to cluster the samples. Different clusters and relapse C-index were evaluated by 10-fold cross-validation.

Then, patients were divided into two subgroups based on relapse-associated deep features according to the models with good C-index scores, and KM plot was used to analyze the relapse level. Finally, the most suitable model was chosen for subsequent validation.

Lasso Model Building and DL Model External Validation

The Lasso method was used to filter out relapse-associated feature labels from the TCGA database depending on the chosen model, including mRNA, miRNA, DNA methylation, CNVs and lncRNA. Five additional validation sets from the GEO database, an international public functional genomics data repository, were applied to assess the predictive effectiveness of this DL-based relapse prediction model (i.e., GSE70768 for mRNA, GSE70768 re-annotation for lncRNA, GSE26367 for miRNA, GSE26126 for DNA methylation, and GSE21035 for CNVs). Log-rank *p*-value and C-index were applied for performance evaluation.

Bioinformatics Analysis

The characteristics of two relapse-associated subgroups of TCGA PCa samples were explored through multiple bioinformatics analysis.

Identification of DEGs

To identify DEGs between the two subgroups, differential gene expression analysis was performed for each omics data type. The DESeq2 R package (16) was used to filter DEGs between the two subgroups (absolute (log_2 fold change >0.585 and adjusted *p*-value <0.01). The *lumi* and *limma* R packages were applied for processing DNA methylation (17–19), and filtering was defined as averaged *M* value differences >1.

Enriched Pathway Analysis

The clusterProfiler R package was used to perform the GO and KEGG enrichment analyses (20). Up- and down-regulated genes and pathways were separately assessed. The GO and KEGG enrichment analysis results were visualized as bubble plots. GSEA was also performed using the clusterProfiler package. Hallmark gene sets c2.cp.kegg.v6.2.symbols.gmt, c2.cgn.v6.2.symbols.gmt, c5.all.v6.2.symbols.gmt and c6.all.v6.2.symbols.gmt were downloaded from the MSigDB molecular signatures database (http://software.broadinstitute.org/gsea/msigdb). GSVA package was then implemented, and the single sample GSEA method was used for hallmark gene sets to further calculate the GSVA scores of each gene set for each sample.

Copy Number Analysis

Firstly, Wilcoxon's signed-rank test was used to compare differentially expressed CNVs between two subgroups. Secondly, the Heatmap function in R was used to present copy number heatmaps. Thirdly, copy number frequency and gistic score in different chromosomes was generated by GISTIC 2.0. Finally, GO enrichment analysis was carried out for CNV differential genes, proportional Venn diagrams were generated with a Venn diagram plotter, and functional enrichment analysis was then separately performed for up- and down-regulated genes.

Immune Cell Infiltration Analysis

The CIBERSORT algorithm was used to calculate the proportion of infiltrating immune cell subsets, and 22 types of immune cells were detected in these PCa samples. Cells with statistically significant differences were screened and analyzed by Wilcoxon's signed-rank test, with a threshold of $p < 0.05$.

RESULTS

Identification of Two Differential Relapse Subgroups in TCGA PCa Samples

A total of 417 tumor samples were obtained from the TCGA PCa project, which included five-omics data (mRNA, miRNA, DNA methylation, CNVs and lncRNA). In our study population, all patients underwent RP due to PCa, and 265 (63.5%) experienced BCR while 152 (36.5%) did not. As mentioned in the Materials and Methods, we subsequently performed preprocessing of this data. The autoencoder architecture or DL framework was applied (**Figure 1**), which stacked these five-omics features together.

Eight DL models were constructed based on the different hidden layers. Univariate Cox-PH regression on each of the deep features as then performed to verify significance (Wald test *p*-value <0.05) associated with relapse. We used K-means for clustering analysis and 10-fold cross-validation (CV) to calculate C-index for different clusters related to relapse. The results showed that all eight DL framework models generated a good C-index value (>0.64), and this value was >0.75 for model_3 and model_8 (**Table 1**).

Subgrouping procedures were separately employed using the relapse-related deep features obtained from model_3 and model_8. Relapse differences between subgroups were then evaluated by Kaplan-Meier plotter (KM plot). Two subgroups of model_3 revealed more significant differences (log-rank *p*-value = 6e-09), with a time to relapse ~3.5 years for half of patients (**Figure 2A**, **Supplementary Figure 1**).

Evaluation of Relapse in Five Independent Validation Sets

Characteristic labels were selected and a Lasso model was constructed, with 43 mRNAs, 22 miRNAs, 24 lncRNAs, 30 methylation genes, and 72 CNV genes (**Supplementary Table 1**). Five independent validation sets from the Gene Expression Omnibus (GEO; http://www.ncbi.nlm.nih.gov/geo/) database were then applied to demonstrate the predictive classification robustness of the model for PCa relapse outcomes. Each of the validation sets represented mRNA, miRNA, DNA methylation, CNVs, or lncRNA, respectively (**Figures 2B–F**). The GSE70768 dataset was a mRNA validation set with 111 patients, which had a log-rank *p*-value

TABLE 1 | Characteristics of eight DL models.

ae_models	hidden	epochs	activation	hidden_dropout_ratios	l1	l2	model_ids	rmse	deep_features	mean c-index/SD
model_1	[500, 50, 500]	10	TanhWithDropout	[0.5, 0.5, 0.5]	0.001	1.00E-05	ae_grid3_model_12	0.400865	8	0.647/0.034
model_2	[500, 100, 500]	10	TanhWithDropout	[0.5, 0.5, 0.5]	1.00E-05	0.1	ae_grid3_model_16	0.400872	12	0.649/0.026
model_3	[500, 150, 500]	10	TanhWithDropout	[0.5, 0.5, 0.5]	0.001	0	ae_grid3_model_15	0.400877	21	0.767/0.020
model_4	[500, 200, 500]	10	TanhWithDropout	[0.5, 0.5, 0.5]	0.1	1.00E-04	ae_grid3_model_3	0.400877	35	0.706/0.055
model_5	[500, 250, 500]	10	TanhWithDropout	[0.5, 0.5, 0.5]	0.1	0	ae_grid4_model_10	0.400881	42	0.749/0.027
model_6	[500, 300, 500]	10	TanhWithDropout	[0.5, 0.5, 0.5]	0.01	0	ae_grid4_model_4	0.400886	57	0.668/0.021
model_7	[500, 400, 500]	10	TanhWithDropout	[0.5, 0.5, 0.5]	1.00E-05	0.001	ae_grid4_model_1	0.400889	60	0.723/0.020
model_8	[500, 500, 500]	10	TanhWithDropout	[0.5, 0.5, 0.5]	0	0	ae_grid4_model_14	0.40089	96	0.775/0.016

of 4.46e-07 between the two PCa relapse-associated subgroups (low-risk S1 vs. high-risk S2; **Figure 2B**). The GSE26367 miRNA validation set consisted of 150 samples with a log-rank *p*-value of 0.000319447 between S1 and S2 (**Figure 2C**). The GSE26126 DNA methylation validation set included 85 samples, and the two subgroups yielded a log-rank *p*-value of 0.003265681 (**Figure 2D**). The GSE21035 CNVs validation set with 198 patients had an extremely low log-rank *p*-value of 0 between the two subgroups (**Figure 2E**). Finally, the GSE70768 re-annotated lncRNA validation set had a log-rank *p*-value of 0.017250485 between S1 and S2 (**Figure 2F**).

Analysis of DEGs in Relapse Subgroups

DEGs between the two identified subgroups were identified by the DESeq2 package. After applying adjusted *p*-value <0.01 and absolute fold change >1.5 as cut-off criteria, we obtained 1530 DEGs including 678 up-regulated and 852 down-regulated genes in the S2 subgroup (the high relapse risk subcluster) compared to S1 (the low relapse risk subcluster). Gene expression profile comparisons of these 1530 genes after normalisation is shown in **Figure 3A**, and the results are presented as a volcano plot (**Figure 3B**). The three most significantly up-regulated genes in the S2 subgroup, von Willebrand factor a domain-containing 5B1 (VWA5B1), uridine 5'-diphosphate glucuronosyltransferase 2B15 (UGT2B15), and urotensin II-related peptide (URP, also called UTS2B), all with log2[fold change] >2 and -log10[*q*-value] >2, are related to genetic polymorphisms (21–23). In addition, down-regulated genes such as CCK, NRAP and PAH (log2[fold change] <-2 and -log10[*q*-value] >2) were also noted.

Next, Gene Ontology (GO) and Kyoto Encyclopedia of Genes and Genomes (KEGG) pathway analyses were performed on DEGs which were significantly up-regulated (fold change >2 and p <0.05) or down-regulated (fold change <-2 and p <0.05). GO analysis results for up-regulated genes were enriched with cancer-related cell proliferation terms such as organelle fission, nuclear division, chromosome segregation, mitotic nuclear division, nuclear chromosome segregation, metaphase/anaphase transition of the cell cycle, and others (**Figure 4A**), KEGG analysis results showed that up-regulated genes were also involved in the cell cycle, and some other pathways including neuroactive ligand-receptor interaction, cell cycle, oocyte meiosis, protein digestion, and absorption were also highly enriched (**Figure 4B**). GO analysis revealed that these down-regulated genes were enriched in many muscle-related biological process terms including muscle system process, muscle organ/tissue development, actin-mediated cell contraction, actin-

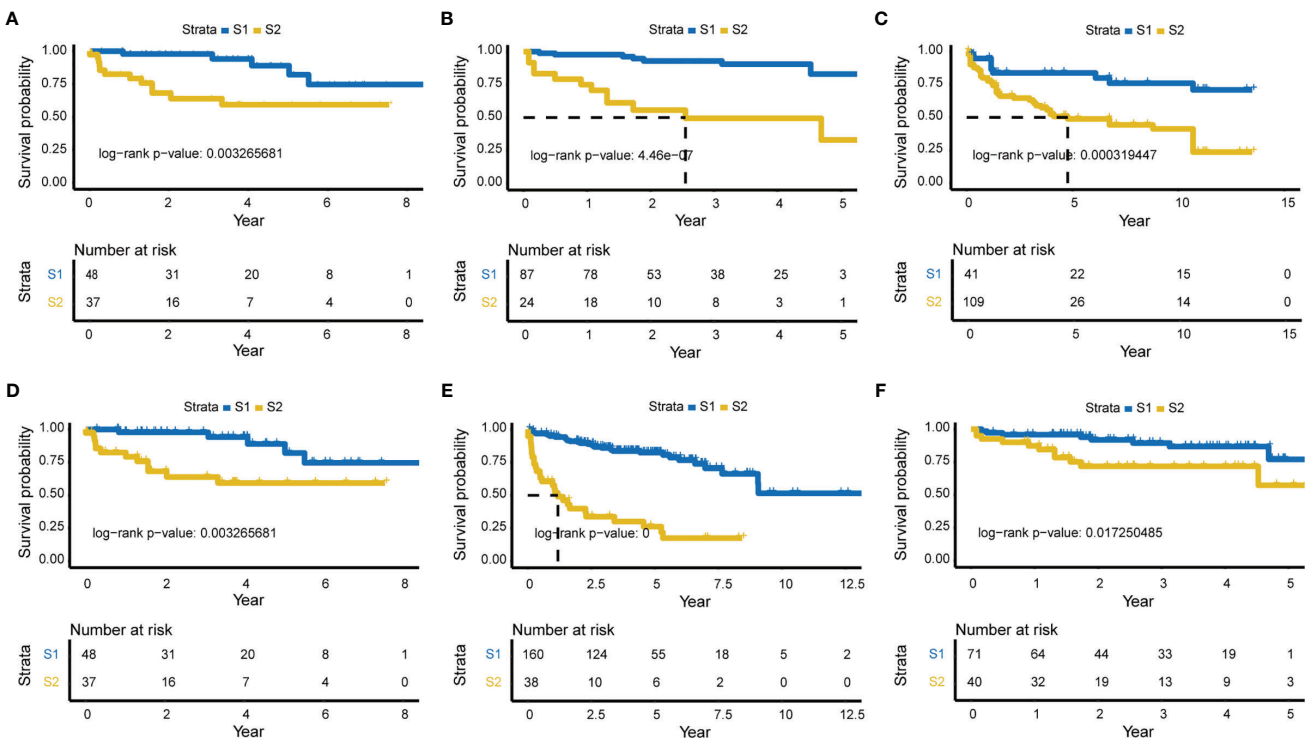


FIGURE 2 | Significant survival differences for model _3 and five external validation sets. Relapse-related deep-features of model_3 were used for subgrouping, and KM plot was used to show the difference in relapse levels between the two subgroups. The Lasso model constructed according to model_3 was validated in each of the five external validation sets. **(A)** KM plot of model_3 (log-rank *P*-value = 6e-09, the time of half relapse is about 3.5 years). **(B)** GSE70768 validation set (mRNA, Number of samples = 111, log-rank *p*-value = 4.46e-07). **(C)** GSE26367 validation set (miRNA, N = 149, log-rank *P*-value = 0.000319447). **(D)** GSE26126 validation set (DNA methylation, N = 85, log-rank *P*-value = 0.003265681). **(E)** GSE21035 validation set (CNVs, N = 198, log-rank *P*-value = 0), and **(F)** Re-annotated GSE70768 validation set (mRNA, N = 111, log-rank *P*-value = 0.017250485).

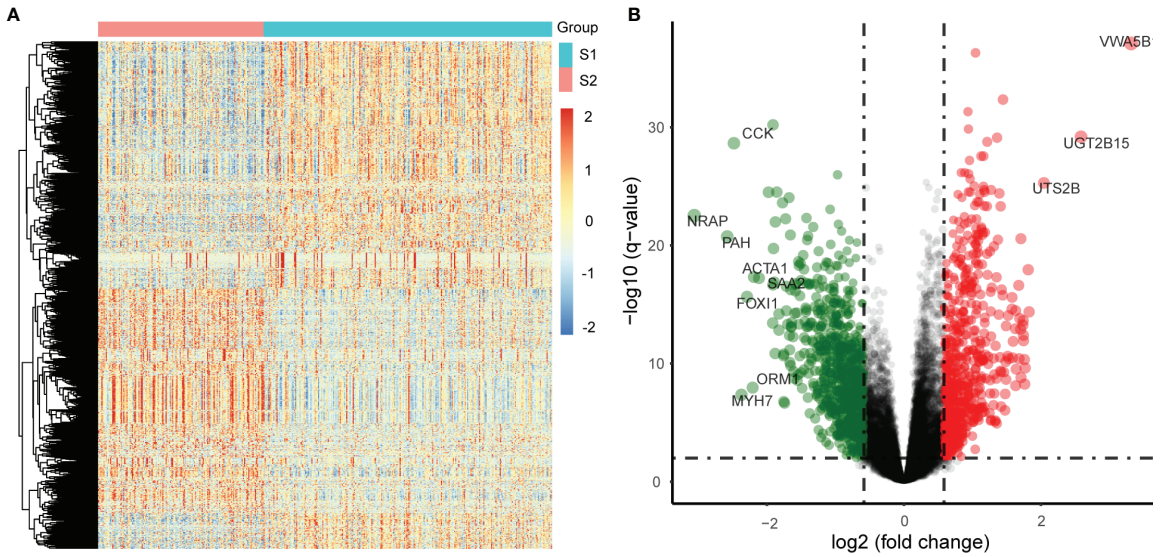


FIGURE 3 | Differentially expressed genes (DEGs) in the two subgroups from the TCGA PCa samples. **(A)** Differential expression: S2 vs S1, S1: a low relapse-risk subgroup of PCa, S2: a high relapse-risk subgroup of PCa. **(B)** Volcano plot of DEGs.

myosin filament sliding, and myofibril assembly (**Figure 4C**). KEGG analysis showed that DEGs were enriched in calcium signaling, IL-17 signaling, adrenergic signaling in cardiomyocytes, dilated cardiomyopathy (DBM), mineral absorption, salivary secretion, and others (**Figure 4D**).

Next, Gene set enrichment analysis (GSEA) was performed and the results indicated several malignant hallmarks and pathways of cancer, of which the top five up-regulated hallmarks were E2F targets, G2/M checkpoint, mitotic spindle, myc targets v1 and myc targets v2 (**Figure 5A**), and the top five down-regulated hallmarks were apical surface, estrogen response early, estrogen response late, myogenesis, and TNFA signaling *via* NF-kb (**Figure 5B**). Additionally, several malignant KEGG pathways of cancer were identified, among which the top five up-regulated pathways were cell cycle, homologous recombination, mismatch repair, oocyte meiosis and ribosome (**Figure 5C**), and the top five down-regulated pathways were arrhythmogenic right ventricular cardiomyopathy, cardiac muscle contraction, dilated cardiomyopathy, glutathione metabolism and hypertrophic cardiomyopathy hcm (**Figure 5D**).

Moreover, a heatmap plot was used to present the different expression levels of hallmark gene sets (**Figure 6A**), and a bar chart further showed 23 differentially expressed hallmark gene sets based on -log(p) value of the gene set variation analysis (GSVA) score order (**Figure 6B**). Five hallmark gene sets were up-regulated (-log(p) value of GSVA score >10), and 13 hallmark gene sets were down-regulated (-log(p) value of GSVA score <-10).

CNVs Analysis

Since analysis of functional difference outcomes showed that DNA damage repair pathways such as homologous recombination and mismatch repair were significantly enriched in the S2 subgroup, we compared differences in CNVs between the two subgroups. The results showed that 30.18% (7844/25988) of genes in the S2 subgroup were significantly up-regulated, and no significant differences were found in other genes between the two subgroups (p <2.2e-16; **Figure 7A**). Further analysis was performed on the gene copy number for different chromosomes, with 265 samples in the S1 subgroup and 152 samples in S2 subgroup, and the results showed that gene amplification on chromosomes 7 and 8 in the S2 subgroup was significantly greater than that in the S1 subgroup (**Figure 7B–H**).

GO analysis was applied for CNV differential genes, and the results showed that protein-DNA complex subunit organization, chromatin assembly, disassembly and silencing, nucleosome organization, negative regulation of gene expression (epigenetic), and DNA replication-dependent nucleosome assembly and organization were enriched (**Figure 8A**). Regarding overlapping CNV differential genes and expression differential genes, 443 gene expression levels were altered, of which 190 were up-regulated and 253 were down-regulated (**Figure 8B**). Subsequent GO analysis of up-regulated CNV genes revealed enrichment in chromosome segregation, nuclear division, organelle fission, skeletal system morphogenesis, mitotic nuclear division, and others (**Figure 8C**), and down-regulated CNV genes were enriched in muscle system process, antimicrobial humoral response, cellular response to zinc ion, and thyroid hormone metabolic process terms. Interestingly, a humoral immune response was also involved (**Figure 8D**).

Analysis of Tumor-Infiltrating Immune Cells

We calculated and displayed 22 TIICs per sample from TCGA analysis for the two subgroups with significantly different relapse-

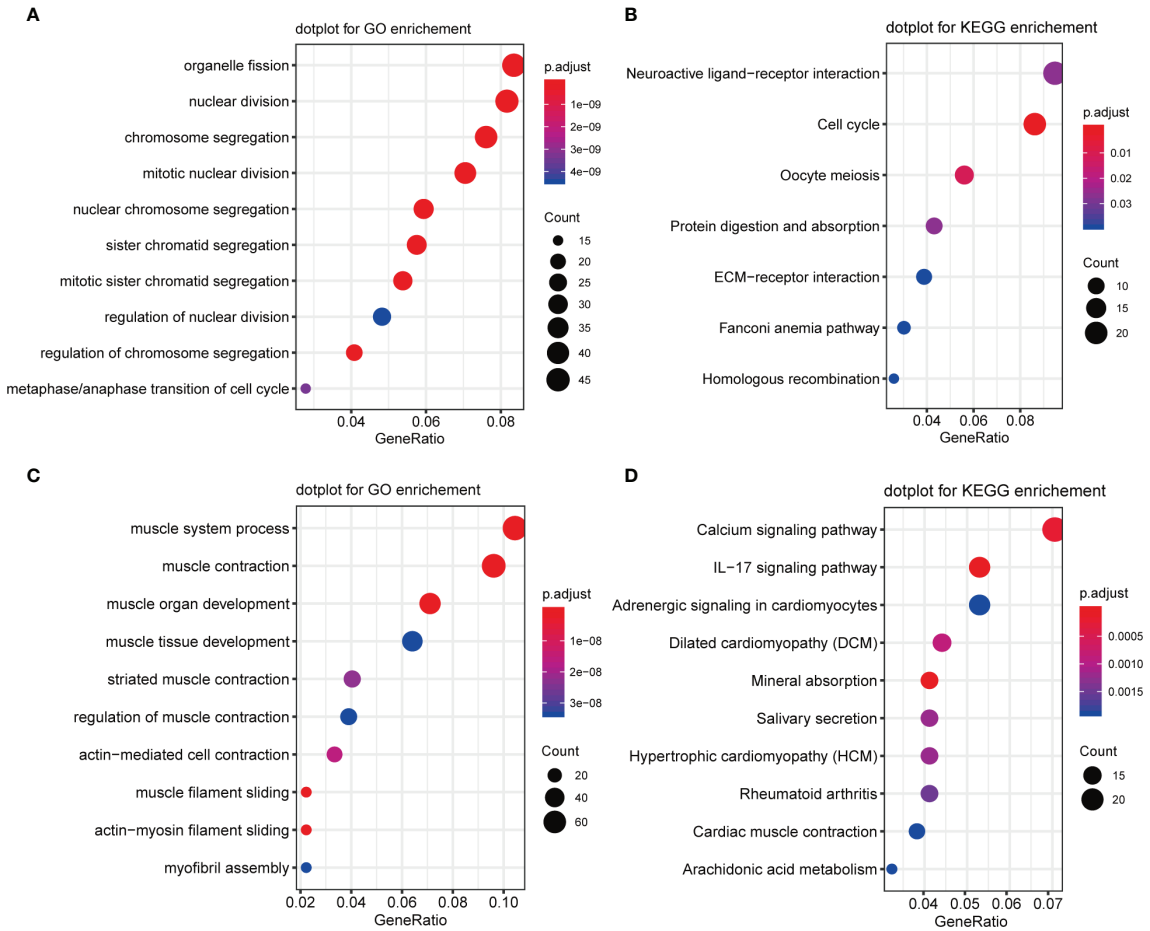


FIGURE 4 | GO and KEGG enrichment of upregulated and downregulated genes. **(A)** GO enrichment analysis of upregulated genes. **(B)** KEGG enrichment analysis of upregulated genes. **(C)** GO enrichment analysis of downregulated genes. **(D)** KEGG enrichment analysis of downregulated genes.

risk subgroups. The heatmap shows the relative levels of TIICs between the two sample subgroups (**Figure 9A**). Finally, four types of TIICs, namely CD4 naïve T cells, CD4 memory-activated T cells, monocytes, and M2 macrophages, differed significantly between the two subgroups (**Table 2**, **Figure 9B–E**). Among them, M2 macrophages, CD4 naïve T cells and CD4 memory-activated T cells were more abundant in the S2 subgroup (p = 0.00014, p = 1e-05, p = 8.7e-06), while monocytes were more abundant in the S1 subgroup (p = 1.3e-06).

DISCUSSION

Although patients with localized PCa undergoing RP may have favorable oncological results, the incidence of BCR can reportedly be more than one-fourth (24). Thus, it is clinically important for urologists to distinguish patients at high risk of relapse from those with low risk to initiate early salvage treatment, while for those with a low risk of relapse, treatment can be deferred. Although there are some studies on relapse prognostication of PCa patients, incorporating multi-omics data to identify subgroups has rarely been reported (25, 26). In addition, most published PCa subgroup models have either no or very few independent validation sets, hence the predictive values of these identified subgroups are not very satisfactory. Thus, new practical procedures in which a predictive model could feed back the relapse outcome of PCa patients directly are needed.

DL has emerged as a versatile approach for predicting complex biological phenomena (27). Previous DL-based models of PCa were mainly applied in preclinical discovery, Gleason grading, and tumor metastasis (28–31). Baek et al. (32) proposed two biological features based on mRNA, miRNA, and methylation datasets to predict high-risk pancreatic adenocarcinoma, which achieved good performance with C-index ~0.8 for both disease-free survival and overall survival. In terms of liver cancer, a previous DL-based three-omics (mRNA, miRNA, and methylation) integration robustly predicted survival, with C-index = 0.68. Furthermore, another support vector machine model using bidirectional deep neural networks integrating

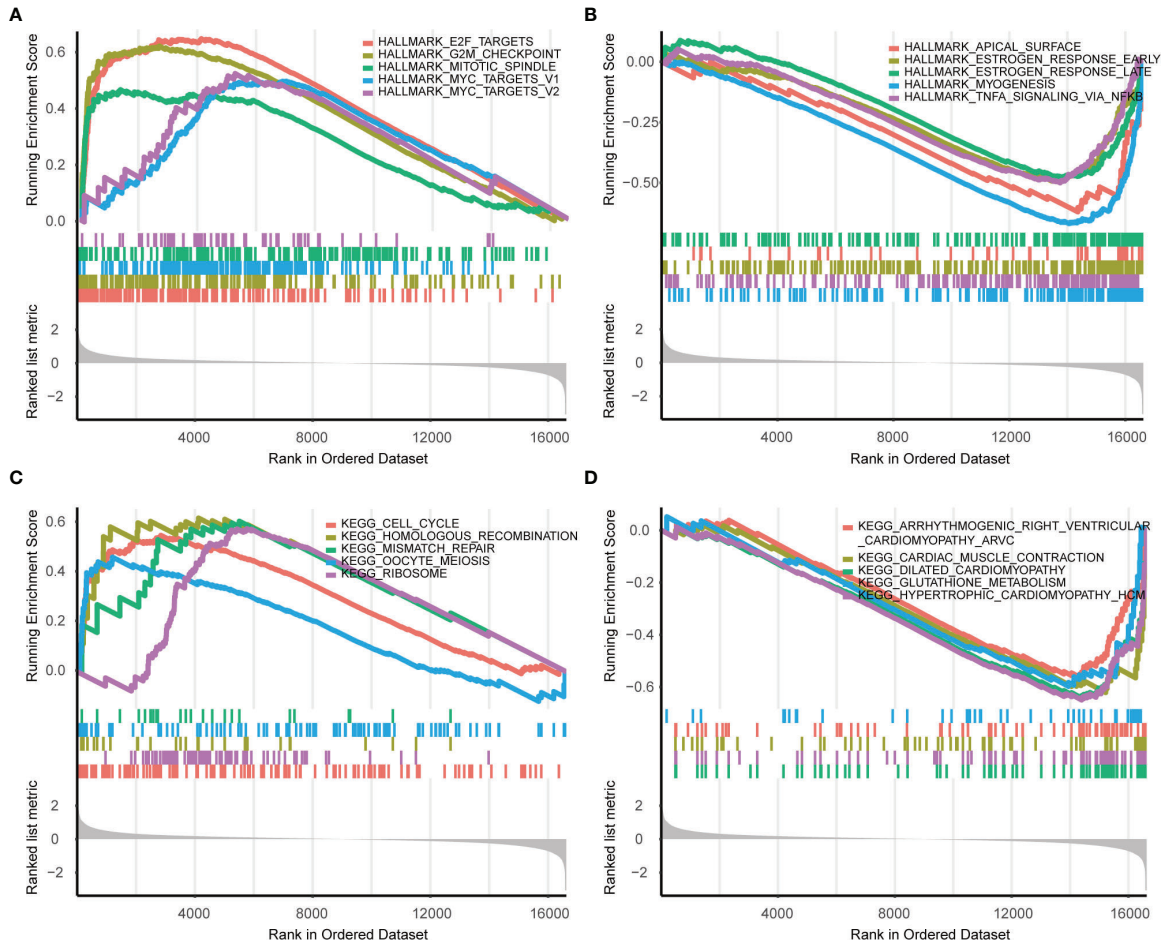


FIGURE 5 | GSEA enrichment analysis in Hallmarks and KEGG (S2 vs S1). **(A)** The top five upregulated hallmarks. **(B)** The top five downregulated hallmarks. **(C)** The top five upregulated pathways in KEGG. **(D)** The top five downregulated pathways in KEGG.

DNA methylation and mRNA expression data could also cluster samples into two survival subgroups (3, 33). Herein, we identified differences in relapse risk between two subgroups of PCa patients using five-omics data, and the model performed well, with C-index >0.75 and log-rank *p*-value = 6e-9 between the two relapse subgroups. To our knowledge, this is the first application of a DL framework for integrating five different datatypes to predict relapse of PCa, and it achieved the best C-index reported to date and included sufficient external confirmation cohorts.

The open-source H2O platform is a powerful tool that can automatically select DL strategies and parameter settings to predict biological differences (34). Furthermore, automated machine learning has great value for many areas of medicine, especially in cancer diagnosis and judging prognosis (35–37). In the present study, we established eight DL-based predictive models for PCa relapse according to different hidden layers using H2O. The results showed that the final selected model (model_3) was robust and might be superior to others, including previous prediction models, for several levels. Because of its ability to achieve more accurate outcomes and its great universality, the DL technique is attracting increasing interest (38). The results of 10-fold CV analysis displayed performance consistency, indicating the reliability and robustness of the model (**Table 1**). This autoencoder framework was more efficient at identifying features related to relapse compared with others, with a C-index of 0.767. Li et al. (13) used the DL method combined with another computational method, namely similarity network fusion (SNF), for prediction of PCa relapse. Univariate Cox regression analysis, K-means clustering algorithms for the autoencoder model, and spectral clustering algorithms for SNF were then performed sequentially. Finally, six significantly overlapping biomarkers were considered. These valuable biomarkers could contribute to the early detection of high-risk relapse patients. However, limited omics data and only six biomarkers had a C-index value of 0.713, and an external validation set was not included. A most recent study identified relapse-related genes using core enrichment genes extracted from KEGG pathways *via* GSEA for univariate Cox regression analysis. The model was constructed using the Lasso method and a KM plot was mapped. The receiver operating characteristic

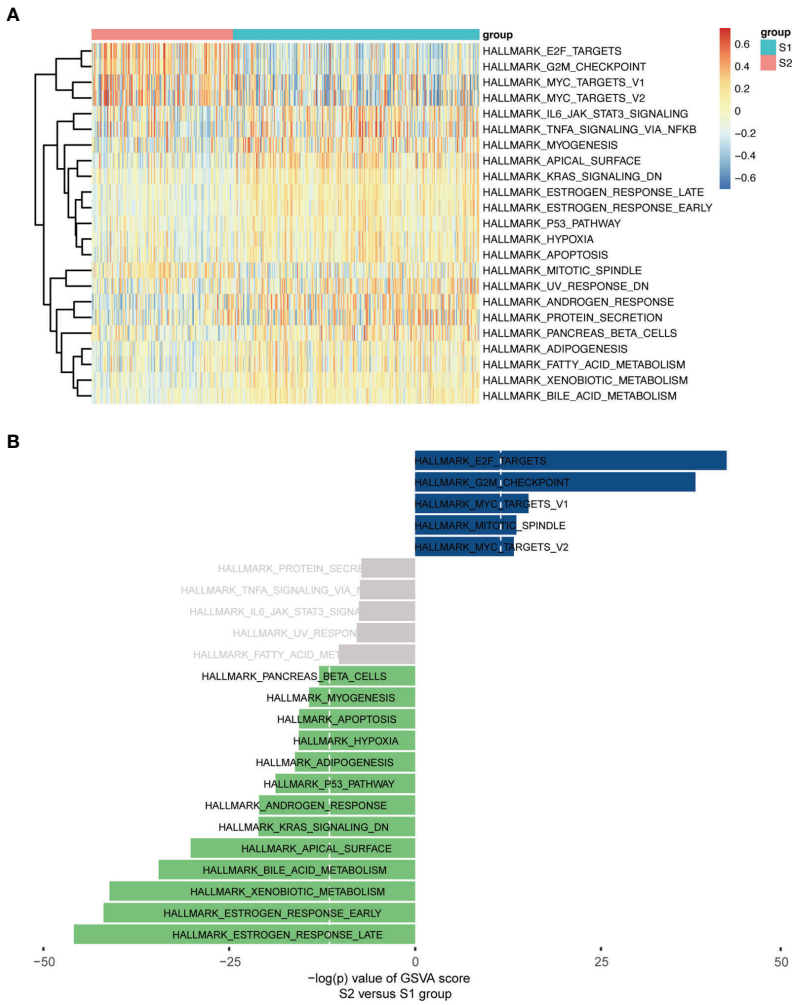


FIGURE 6 | GSVA enrichment analysis in Hallmarks. **(A)** Heatmap plot. **(B)** Bar Chart (-log(p) value of GSVA score were used, S2 vs S1).

(ROC) curve of the model was then used to evaluate predictive efficiency. The results showed that the area under the curve (AUC) for 3- and 5-year time-dependent ROC curves were 0.739 and 0.729 (39). Of equal importance, our model was also validated using five additional validation sets, each associated with a different omics level (mRNA, miRNA, DNA methylation, CNVs and lncRNA). The Lasso model constructed with these molecular labels according to model_3 was equally well able to classify these external validation sets into high relapse-risk and low relapse-risk subgroups (**Figure 2**), indicating that the relapse-related subgroups clustered using the DL-based model_3 have a broad spectrum of biological significance.

Using this model, more than 1000 differential genes were identified between S1 and S2 subgroups. VWA5B1, UGT2B15, and UTS2B were significantly up-regulated. In a previous study, von Willebrand factor (vWF) antigen was differentially abundant between patients with PCa or BPH and other prostatic diseases (40). Of note, the level of vWF antigen was elevated in patients with metastases, compared to localized PCa. However, VWA5B1 has not been reported in PCa, which may be a potential biomarker or target, but confirming this requires further research. The other two DEGs are closely related to PCa. In particular, UGT2B15 contributes to PCa risk, diagnosis and disease progression (41, 42), and 3α-diol-17 glucuronide, a product of UGT2B15/B17, is linked to prostate volume changes, indicating that this metabolite might serve as a biomarker of androgen activity. Moreover, UGT2B15 is one of the main determinants controlling the expression of target genes of androgen receptors in PCa cells (43). In addition, the UGT2B15 Asp85Tyr polymorphism is associated with PCa risk (41). Urotensin II receptor (UT) is involved in regulating the biological functions of urotensin II and UTS2B in mammals (44). UT mRNA expression was decreased in androgen-independent DU145 and PC3 cells, but increased in androgen-dependent LNCaP cells, and UT expression was strongly correlated with the prognosis of PCa, providing a potential prognostic marker for

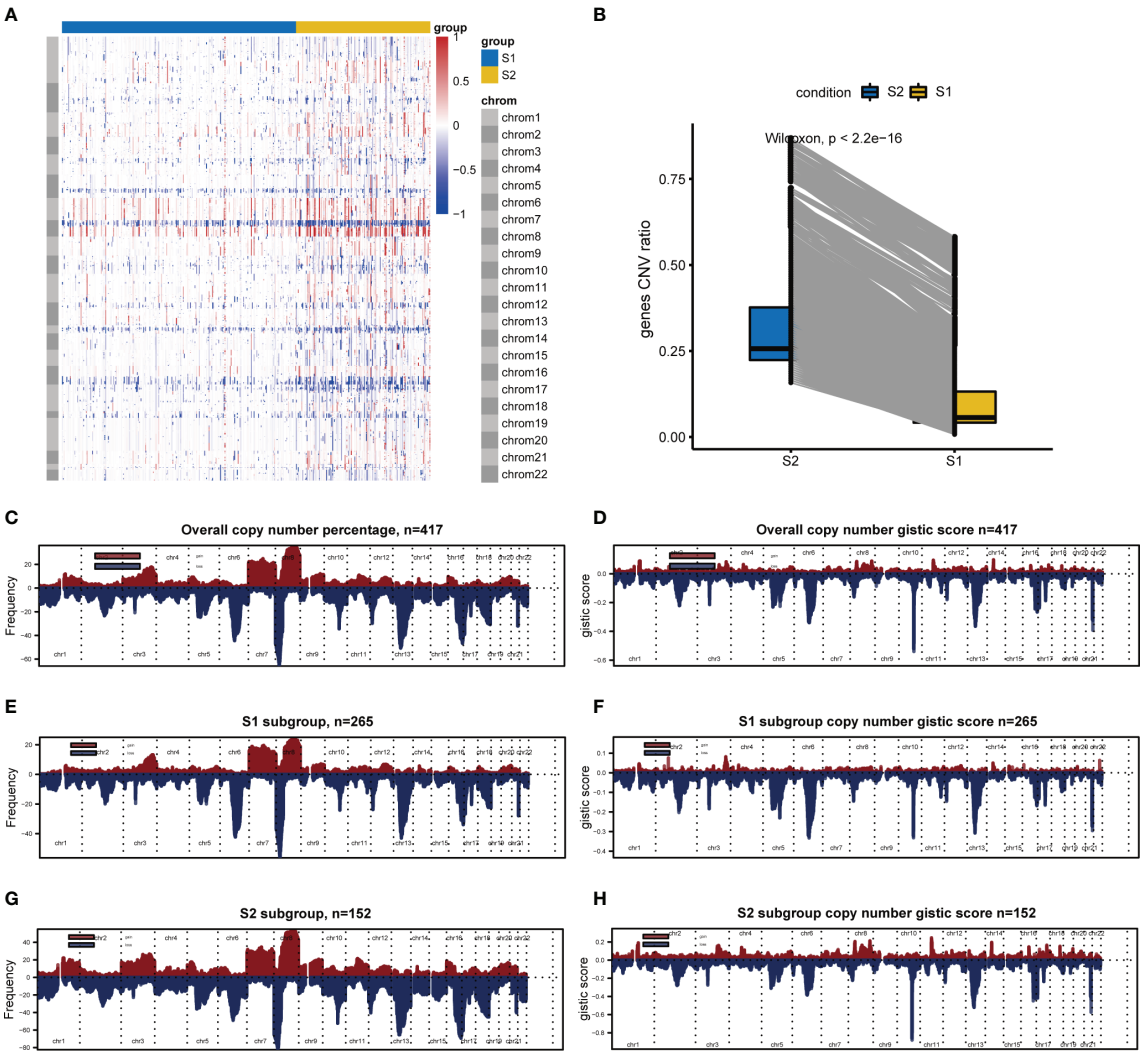


FIGURE 7 | CNVs difference analysis between S1 and S2. **(A)** CNVs difference analysis by Wilcoxon. **(B)** Hierarchical clustering. Red indicates amplification, whereas blue indicates deletion. **(C–H)** Chromosomal distribution of copy number by GISTIC. Red indicates amplification, whereas blue indicates deletion.

this disease (45). In summary, these three significantly up-regulated genes were directly or indirectly correlated with the progression and prognosis of PCa. All the identified DEGs may assist the prediction or prevention of PCa relapse.

Various up- and down-regulated genes were respectively enriched in GO and KEGG terms. Organelle fission enrichment has been linked to tumor tissues (46, 47). Hec1, a component of the nuclear division cycle 80 complex, was found to be elevated and associated with cancer progression in PCa (48). Emerging evidence suggests that chromosome segregation plays a vital role in PCa tumorigenesis, development and bone metastasis (49, 50). Neuroactive ligand-receptor interactions contribute to therapy-related neuroendocrine PCa, a lethal castration-resistant PCa subtype (51, 52). Both the initiation and progression of PCa have been associated with enhanced cell proliferation and cell cycle dysregulation (53).

GO/KEGG analyses focus on differential genes, and target a subset of genes that are significantly different between groups, and may therefore miss genes that are not significantly different but biologically significant. By contrast, GSEA identifies a set of genes with concordant differences from an expression matrix of all genes, and therefore takes into account genes that are less different. We applied GSVA, and the results suggested several relapse-related hallmarks/pathways of PCa, including 5 up-regulated and 13 down-regulated in the S2 subgroup. Several studies have proved that E2F factors play a critical role in mediating cell cycle gene expression and progression in PCa (54, 55). Nucleolar and spindle-associated protein (NuSAP), which binds DNA to the mitotic spindle, is associated with relapse after RP, and its promoter region contains two CCAAT motifs and binding sites for E2F, overexpression of which appears to be mediated partly by E2F1 activation (56). Similarly, the G2/M

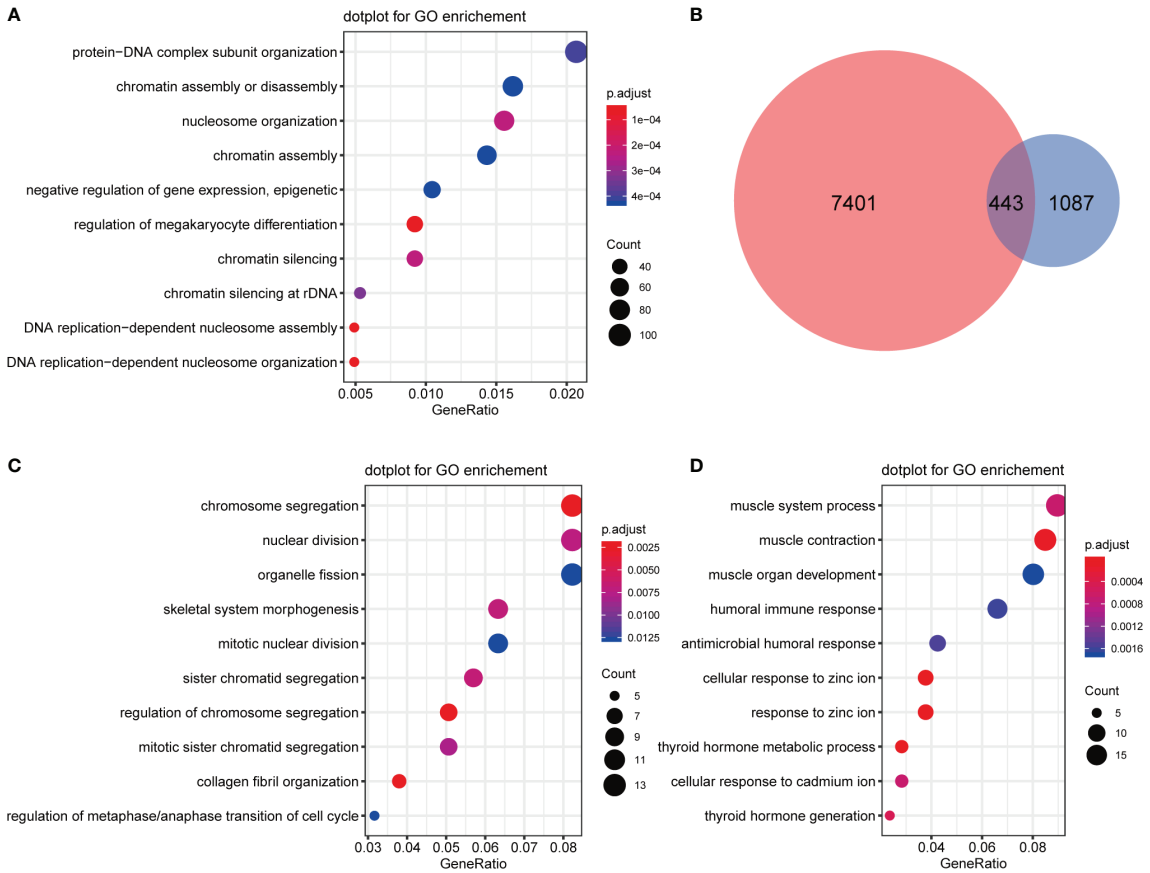


FIGURE 8 | Functional analysis of CNV differential genes. **(A)** GO enrichment analysis of CNV differential genes. **(B)** Venn diagrams of CNV differential genes and expression differential genes. **(C)** GO enrichment analysis of upregulated CNV genes. **(D)** GO enrichment analysis of downregulated CNV genes.

checkpoint plays a vital role in the cell cycle. Caspase-8, depletion of which can result in G2/M arrest, is involved in DNA damage (57). Furthermore, MYC enhances the expression of related genes to help cancer cells survive, grow, proliferate and metabolize, and MYC plays a central role in PCa according to tissue proteomics research (58). In summary, our results reconfirmed numerous genes or pathways closely linked with PCa, identified some potential tumor markers or therapeutic targets for PCa relapse, and revealed that DNA damage repair-related pathways, such as nuclear division and chromosome segregation, were significantly enriched in the S2 subgroup.

We investigated CNVs and found that 30.18% of genes had a significantly higher proportion of CNVs in the high relapse-risk S2 subgroup. As we all know, CNVs may be associated with malignancy through the accumulation of driver aberrations, and genomic instability can increase because DNA damage responses are absent and replication pressure is elevated in cancer cells (59, 60). Interestingly, cancer cells might be more vulnerable due to the relative specificity of these defects, which also has potential for increasing therapeutic indices of antineoplastic therapies, thereby improving the prognosis of cancer patients. Several clinical studies assessed the safety and effectiveness of state-of-the-art strategies such as DNA repair-targeted agents in various cancers (61, 62). Higher genomic instability was suggested for metastatic PCa (mPCa), based on the observation that the burden of CNVs and the weighted genome instability index were significantly higher in mPCa than localised PCa (63). Moreover, a significant correlation was observed between the burden of CNVs and PCa relapse and death (64, 65), indicating the potential of CNVs as prognostic biomarkers (66), consistent with our results.

Importantly, GO enrichment analysis of up-regulated DEGs (**Figure 4A**) yielded consistent results, suggesting a strong correlation between genomic or chromosomal instability and PCa relapse. Massive alterations in genetic information are the main feature distinguishing cancer cells and healthy cells. In addition to point mutations and small insertions/deletions (indels), large-scale changes occur, including chromosomal rearrangements, and chromosome gains and losses (individual or entire sets) (67). In other words, chromosome mis-segregation is rare in normal tissues, but chromosome (whole or part) gains and losses are common in cancer tissues. This chromosomal instability is correlated with intra-tumor heterogeneity, and it contributes to resistance to medical therapy as well as adverse

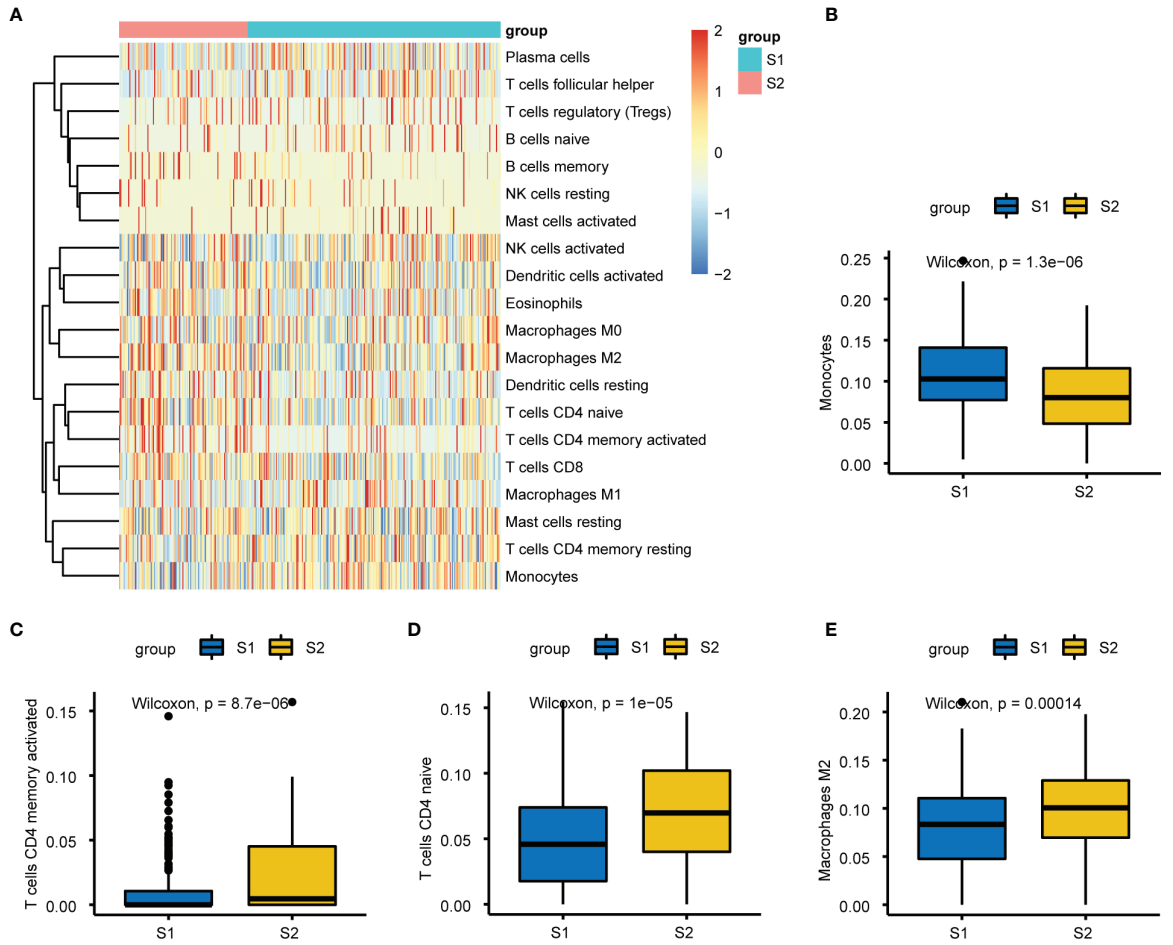


FIGURE 9 | Immuno-infiltration analysis between S1 and S2. **(A)** Heatmap plot of the 22 tumors infiltrating immune cells (TIICs) in two groups. **(B–E)** Relative proportion of the differential four types of TIICs between two subgroups, respectively.

outcomes of disease (68). Analysis of the distribution of these CNVs in chromosomes has important implications for future clinical and research studies on PCa relapse. Our CNV analysis results revealed that the S2 subgroup expressed significantly more genes on chromosomes 7 and 8 than did the S1 subgroup. Copy number-induced alterations are considered to be critical for tumor evolution (67). A 1991 study suggested that centromeric CNVs of chromosome 7 are closely related to tumor histological grade, and might be highly predictive for tumor aggressiveness in human bladder cancer (68). Alcaraz et al. (69) reported that aneuploidy and aneusomy of chromosome 7 are generally observed in the poor prognosis PCa patients. Meanwhile, allelic loss is frequently observed on the short arm of chromosome 8 (70). Ichikawa et al. (71) applied the microcell-mediated chromosome transfer technique to introduce human chromosome 8 into highly metastatic rat PCa cells and found that metastatic ability was suppressed, but similar trends were not observed in growth rate or tumorigenicity, indicating that chromosome 8 contains genes inhibiting metastasis of PCa, and implying a vital role in the progression of PCa. Regardless, chromosomes 7 and 8 may be correlated with PCa relapse according to current and previous research.

TABLE 2 | Characteristics of four significantly different tumor-infiltrating immune cells.

Cell type	S1 subgroup	S2 subgroup	*p*-value	adj *p*-value
T cells CD4 naive	0.03706419	0.061121026	1.375140e-05	0.0002475252
T cells CD4 memory active	0.00000000	0.002554248	8.680098e-06	0.0001649219
Monocytes	0.08214986	0.061738947	8.389214e-04	0.0142616642
Macrophages M2	0.06320131	0.082005050	5.701414e-06	0.0001140283

Interestingly, we also observed that immune infiltration might be involved in PCa relapse from the functional enrichment analysis of multiple differential CNVs (**Figure 8D**) and DEGs (**Figure 4D**). Emerging evidence shows that tumor immune cell infiltration, a significant hallmark of the tumor microenvironment, is an enormous contributing factor to therapeutic circumvention, cancer progression, and subsequent adverse outcomes (72). We calculated the proportion of infiltrating immune cell subsets of the two subgroups using the CIBERSORT algorithm (https://cibersort.stanford.edu/) and identified four TIICs with a significant difference.

However, four types of TIICs were not all elevated in the high relapse-risk S2 subgroup. Among them, monocytes were more abundant in the low relapse-risk S1 subgroup (**Figure 9D**). In a clinical study on 1107 participants, histopathological findings showed that patients with positive prostate biopsy had higher monocyte counts than negative patients, and multivariate Cox regression analyses showed that a high monocyte count was an independent prognostic factor of both cancer-specific and other mortalities (73). Even when adjusted by clinicopathological signatures, these outcomes were statistically significant, further confirming the independent correlations between high monocyte count and poor prognosis of PCa, contrary to our PCa relapse results. Therefore, whether monocytes differ during distinct stages of PCa, and whether this plays a major regulatory role in PCa progression, requires further investigation. Further studies of the influence of monocytes on PCa are also warranted. Recent work on aging men undergoing RP showed that the peripheral monocyte count was not linked to long-term results in PCa (74). The study included black and white RP men, but the peripheral monocyte count was not found to be a useful marker of PCa long-term results. One limitation of this work was the lack of Asian participants. Macrophages are important in cancer, too. Macrophages, derived from circulating monocytes, can be routinely classified into M1-type and M2-type macrophages. Classically activated M1 macrophages, acting as part of the innate immune response, are of great significance in the fight against invading pathogens, while activated M2 macrophages, also known as M2 tumor-associated macrophages, are vital components of tissue restoration and tumor promotion (75). M2 macrophages are involved in tumor development in various ways. They can directly interact with T cells and secrete factors associated with immunosuppression to inhibit CD8+ T cell immunity against cancer (72). Furthermore, some M2 macrophages influence tumor development *via* the destruction of antitumor T cell immunity, providing novel perspectives for immune tolerance and escape properties of cancers, consistent with our results.

Despite our best efforts, there remain some limitations with the current work. Firstly, because some raw data cluster labels were absent and survival information was lacking, it was difficult to compare directly with previous research. To confirm its predictive performance and direct application value in clinical practice, five external validation sets consisting of different omics data were applied, and the results were encouraging. Secondly, it remains unclear how many of the novel biological features we identified are linked to PCa relapse. Despite this, the results provide new directions for further exploration. Thirdly, while we demonstrated the effectiveness and robustness of this DL model in various ways, future experiments and clinical data are needed to realize its potential.

In summary, we successfully constructed a DL-based predictive model integrating five-omics for PCa relapse with a significant relapse difference between two subgroups. Furthermore, validation using five independent omics datasets confirmed its robustness. A number of critical DEGs, pathways, and functions were found to be associated with PCa relapse. The model provides new insights for distinguishing relapse-risk patients, and it could benefit patients due to its early predictive ability and subsequent early therapeutic intervention. The findings contribute to our current understanding of PCa relapse, and the developed model may serve clinical applications and support decision-making.

DATA AVAILABILITY STATEMENT

Publicly available datasets were analyzed in this study. This data can be found here: The 417 PCa samples were obtained from the The Cancer Genome Atlas (TCGA; https://www.cancer.gov/). The additional validation sets (GSE70768, GSE26367, GSE26126, and GSE21035) were collected from Gene Expression Omnibus (GEO; http://www.ncbi.nlm.nih.gov/geo/). Hallmark gene sets c2.cp.kegg.v6.2.symbols.gmt, c2.cgn.v6.2.symbols.gmt, c5.all.v6.2.symbols.gmt and c6.all.v6.2.symbols.gmt were downloaded from the MSigDB molecular signatures database (http://software.broadinstitute.org/gsea/msigdb). Access codes for this article are listed in https://github.com/foolman1990/deep-learning-multiomics.

ETHICS STATEMENT

This study did not need approvals by the Ethics Committee of Jinshan Hospital, Shanghai, China according to the regulations. This study fully complied guidelines of GEO and Array Express.

AUTHOR CONTRIBUTIONS

All authors contributed to the article and approved the submitted version. Study design and project administration: GC, and ZS; Data collection, analysis and interpretation: ZS, ZW, DH, CZ, SW, JL, and FC; Writing-review and editing of the manuscript: ZW, ZS, GC.

FUNDING

This work was supported by grants from the Natural Science Foundation of Shanghai (NO. 18ZR1405800; NO. 22ZR1409700) and the Project for Key Medical Specialty Construction in Jinshan District (6th Period, Type A; No. JSZK2019A03) to GC.

ACKNOWLEDGMENTS

We would like to thank Yingying Zhang for his help and assistance, and all colleagues and mentors for their contributions and instructions in this project.

SUPPLEMENTARY MATERIAL

The Supplementary Material for this article can be found online at: https://www.frontiersin.org/articles/10.3389/fonc.2022.893424/full#supplementary-material

REFERENCES

1. Huang S, Chaudhary K, Garmire LX. More Is Better: Recent Progress in Multi-Omics Data Integration Methods. *Front Genet* (2017) 8:84. doi: 10.3389/fgene.2017.00084
2. Galkin F, Mamoshina P, Kochetov K, Sidorenko D, Zhavoronkov A. Deepmage: A Methylation Aging Clock Developed With Deep Learning. *Aging Dis* (2021) 12(5):1252–62. doi: 10.14336/AD.2020.1202
3. Chaudhary K, Poirion OB, Lu L, Garmire LX. Deep Learning-Based Multi-Omics Integration Robustly Predicts Survival in Liver Cancer. *Clin Cancer Res* (2018) 24(6):1248–59. doi: 10.1158/1078-0432.CCR-17-0853
4. Zhao Z, Li Y, Wu Y, Chen R. Deep Learning-Based Model for Predicting Progression in Patients With Head and Neck Squamous Cell Carcinoma. *Cancer biomark* (2020) 27(1):19–28. doi: 10.3233/CBM-190380
5. Siegel RL, Miller KD, Fuchs HE, Jemal A. Cancer Statistics, 2021. *CA Cancer J Clin* (2021) 71(1):7–33. doi: 10.3322/caac.21654
6. Cornford P, van den Bergh RCN, Briers E, Van den Broeck T, Cumberbatch MG, De Santis M, et al. Eau-Eanm-Estro-Esur-Siog Guidelines on Prostate Cancer. Part Ii-2020 Update: Treatment of Relapsing and Metastatic Prostate Cancer. *Eur Urol* (2021) 79(2):263–82. doi: 10.1016/j.eururo.2020.09.046
7. Talagas M, Uguen A, Garlantezec R, Fournier G, Research MBJA. Vegfr1 and Nrp1 Endothelial Expressions Predict Distant Relapse After Radical Prostatectomy in Clinically Localized Prostate Cancer. *Anticancer Res* (2013) 33(5):2065–75.
8. Yu YP, Song C, Tseng G, Ren BG, LaFramboise W, Michalopoulos G, et al. Genome Abnormalities Precede Prostate Cancer and Predict Clinical Relapse. *Am J Pathol* (2012) 180(6):2240–8. doi: 10.1016/j.ajpath.2012.03.008
9. Lee TY, Huang KY, Chuang CH, Lee CY, Chang TH. Incorporating Deep Learning and Multi-Omics Autoencoding for Analysis of Lung Adenocarcinoma Prognostication. *Comput Biol Chem* (2020) 87:107277. doi: 10.1016/j.compbiolchem.2020.107277
10. Huang TB, Dong CP, Zhou GC, Lu SM, Luan Y, Gu X, et al. A Potential Panel of Four-Long Noncoding Rna Signature in Prostate Cancer Predicts Biochemical Recurrence-Free Survival and Disease-Free Survival. *Int Urol Nephrol* (2017) 49(5):825–35. doi: 10.1007/s11255-017-1536-8
11. Chu J, Li N, Gai W. Identification of Genes That Predict the Biochemical Recurrence of Prostate Cancer. *Oncol Lett* (2018) 16(3):3447–52. doi: 10.3892/ol.2018.9106
12. Li F, Ji JP, Xu Y, Liu RL. Identification a Novel Set of 6 Differential Expressed Genes in Prostate Cancer That Can Potentially Predict Biochemical Recurrence After Curative Surgery. *Clin Transl Oncol* (2019) 21(8):1067–75. doi: 10.1007/s12094-018-02029-z
13. Wang TH, Lee CY, Lee TY, Huang HD, Hsu JB, Chang TH. Biomarker Identification Through Multiomics Data Analysis of Prostate Cancer Prognostication Using a Deep Learning Model and Similarity Network Fusion. *Cancers (Basel)* (2021) 13(11):2528. doi: 10.3390/cancers13112528
14. Jiang Y, Mei W, Gu Y, Lin X, He L, Zeng H, et al. Construction of a Set of Novel and Robust Gene Expression Signatures Predicting Prostate Cancer Recurrence. *Mol Oncol* (2018) 12(9):1559–78. doi: 10.1002/1878-0261.12359
15. (2017). June, H2o.Ai.H2o Automl, UrlH2o Version 3.30.0.1.
16. Love MI, Huber W, Anders S. Moderated Estimation of Fold Change and Dispersion for Rna-Seq Data With Deseq2. *Genome Biol* (2014) 15(12):550. doi: 10.1186/s13059-014-0550-8
17. Ching T, Ha J, Song MA, Tiirikainen M, Molnar J, Berry MJ, et al. Genome-Scale Hypomethylation in the Cord Blood Dnas Associated With Early Onset Preeclampsia. *Clin Epigenet* (2015) 7:21. doi: 10.1186/s13148-015-0052-x
18. Ching T, Song MA, Tiirikainen M, Molnar J, Berry M, Towner D, et al. Genome-Wide Hypermethylation Coupled With Promoter Hypomethylation in the Chorioamniotic Membranes of Early Onset Pre-Eclampsia. *Mol Hum Reprod* (2014) 20(9):885–904. doi: 10.1093/molehr/gau046
19. Du P, Kibbe WA, Lin SM. Lumi: A Pipeline for Processing Illumina Microarray. *Bioinformatics* (2008) 24(13):1547–8. doi: 10.1093/bioinformatics/btn224
20. Yu G, Wang LG, Han Y, He QY. Clusterprofiler: An R Package for Comparing Biological Themes Among Gene Clusters. *OMICS* (2012) 16(5):284–7. doi: 10.1089/omi.2011.0118
21. Doss CG, Ali SK. Role of Von Willebrand Factor–A1 Domain Variants P1266l, H1268d, C1272r, and C1272f in Vwd: A Molecular Modeling and Simulation Analysis Approach. *Adv Protein Chem Struct Biol* (2016) 102:299–330. doi: 10.1016/bs.apcsb.2015.09.006
22. Ginsberg G, Guyton K, Johns D, Schimek J, Angle K, Sonawane B. Genetic Polymorphism in Metabolism and Host Defense Enzymes: Implications for Human Health Risk Assessment. *Crit Rev Toxicol* (2010) 40(7):575–619. doi: 10.3109/10408441003742895
23. Vaudry H, Leprince J, Chatenet D, Fournier A, Lambert DG, Le Mevel JC, et al. International Union of Basic and Clinical Pharmacology. Xcii. Urotensin Ii, Urotensin Ii-Related Peptide, and Their Receptor: From Structure to Function. *Pharmacol Rev* (2015) 67(1):214–58. doi: 10.1124/pr.114.009480
24. Pak S, You D, Jeong IG, Kim YS, Hong JH, Kim CS, et al. Time to Biochemical Relapse After Radical Prostatectomy and Efficacy of Salvage Radiotherapy in Patients With Prostate Cancer. *Int J Clin Oncol* (2019) 24(10):1238–46. doi: 10.1007/s10147-019-01463-5
25. Tilki D, Preisser F, Graefen M, Huland H, Pompe RS. External Validation of the European Association of Urology Biochemical Recurrence Risk Groups to Predict Metastasis and Mortality After Radical Prostatectomy in a European Cohort. *Eur Urol* (2019) 75(6):896–900. doi: 10.1016/j.eururo.2019.03.016
26. van den Bergh RCN, van Casteren NJ, van den Broeck T, Fordyce ER, Gietzmann WKM, Stewart F, et al. Role of Hormonal Treatment in Prostate Cancer Patients With Nonmetastatic Disease Recurrence After Local Curative Treatment: A Systematic Review. *Eur Urol* (2016) 69(5):802–20. doi: 10.1016/j.eururo.2015.11.023
27. Fortelny N, Bock C. Knowledge-Primed Neural Networks Enable Biologically Interpretable Deep Learning on Single-Cell Sequencing Data. *Genome Biol* (2020) 21(1):190. doi: 10.1186/s13059-020-02100-5
28. Bulten W, Pinckaers H, van Boven H, Vink R, de Bel T, van Ginneken B, et al. Automated Deep-Learning System for Gleason Grading of Prostate Cancer Using Biopsies: A Diagnostic Study. *Lancet Oncol* (2020) 21(2):233–41. doi: 10.1016/s1470-2045(19)30739-9
29. Elmarakeby HA, Hwang J, Arafeh R, Crowdis J, Gang S, Liu D, et al. Biologically Informed Deep Neural Network for Prostate Cancer Discovery. *Nature* (2021) 598(7880):348–52. doi: 10.1038/s41586-021-03922-4
30. Nagpal K, Foote D, Tan F, Liu Y, Chen PC, Steiner DF, et al. Development and Validation of a Deep Learning Algorithm for Gleason Grading of Prostate Cancer From Biopsy Specimens. *JAMA Oncol* (2020) 6(9):1372–80. doi: 10.1001/jamaoncol.2020.2485
31. Wessels F, Schmitt M, Krieghoff-Henning E, Jutzi T, Worst TS, Waldbillig F, et al. Deep Learning Approach to Predict Lymph Node Metastasis Directly From Primary Tumour Histology in Prostate Cancer. *BJU Int* (2021) 128 (3):352–60. doi: 10.1111/bju.15386
32. Baek B, Lee H. Prediction of Survival and Recurrence in Patients With Pancreatic Cancer by Integrating Multi-Omics Data. *Sci Rep* (2020) 10 (1):18951. doi: 10.1038/s41598-020-76025-1
33. Huang G, Wang C, Fu X. Bidirectional Deep Neural Networks to Integrate Rna and DNA Data for Predicting Outcome for Patients With Hepatocellular Carcinoma. *Future Oncol* (2021) 17(33):4481–95. doi: 10.2217/fon-2021-0659
34. Orlenko A, Kofink D, Lyytikäinen L-P, Nikus K, Mishra P, Kuukasjärvi P, et al. Model Selection for Metabolomics: Predicting Diagnosis of Coronary Artery Disease Using Automated Machine Learning. *Bioinformatics* (2020) 36 (6):1772–8. doi: 10.1093/bioinformatics/btz796
35. Reif M, Shafait F, Goldstein M, Breuel T, Dengel A. Automatic Classifier Selection for Non-Experts. *Pattern Anal Appl* (2014) 17(1):83–96. doi: 10.1007/s10044-012-0280-z

36. Waring J, Lindvall C, Umeton R. Automated Machine Learning: Review of the State-Of-the-Art and Opportunities for Healthcare. *Artif Intell Med* (2020) 104:101822. doi: 10.1016/j.artmed.2020.101822
37. Panagopoulou M, Karaglani M, Manolopoulos VG, Iliopoulos I, Tsamardinos I, Chatzaki E. Deciphering the Methylation Landscape in Breast Cancer: Diagnostic and Prognostic Biosignatures Through Automated Machine Learning. *Cancers* (2021) 13(7):1667. doi: 10.3390/cancers13071677
38. Ajayi A, Oyedele L, Owolabi H, Akinade O, Bilal M, Davila Delgado JM, et al. Deep Learning Models for Health and Safety Risk Prediction in Power Infrastructure Projects. *Risk Anal* (2020) 40(10):2019–39. doi: 10.1111/risa.13425
39. Zhao YQ, Tao ZJ, Li L, Zheng JY, Chen XN. Predicting Biochemical-Recurrence-Free Survival Using a Three-Metabolic-Gene Risk Score Model in Prostate Cancer Patients. *BMC Cancer* (2022) 22(1):239. doi: 10.1186/s12885-022-09331-8
40. Ablin RJ, Bartkus JM, Gonder MJ. Immunoquantitation of Factor Viii-Related Antigen (Von Willebrand Factor Antigen) in Prostate Cancer. *Cancer Lett* (1988) 40(3):283–9. doi: 10.1016/0304-3835(88)90087-0
41. Park J, Chen L, Shade K, Lazarus P, Seigne J, Patterson S, et al. Asp85tyr Polymorphism in the Udp-Glucuronosyltransferase (Ugt) 2b15 Gene and the Risk of Prostate Cancer. *J Urol* (2004) 171(6 Pt 1):2484–8. doi: 10.1097/01.ju.0000117748.44313.43
42. Grosse L, Paquet S, Caron P, Fazli L, Rennie PS, Belanger A, et al. Androgen Glucuronidation: An Unexpected Target for Androgen Deprivation Therapy, With Prognosis and Diagnostic Implications. *Cancer Res* (2013) 73(23):6963–71. doi: 10.1158/0008-5472.Can-13-1462
43. Barbier O, Belanger A. Inactivation of Androgens by Udp-Glucuronosyltransferases in the Human Prostate. *Best Pract Res Clin Endocrinol Metab* (2008) 22(2):259–70. doi: 10.1016/j.beem.2008.01.001
44. Cui L, Lv C, Zhang J, Li J, Wang Y. Characterization of Four Urotensin Ii Receptors (Uts2rs) in Chickens. *Peptides* (2021) 138:170482. doi: 10.1016/j.peptides.2020.170482
45. Grieco P, Franco R, Bozzuto G, Toccacieli L, Sgambato A, Marra M, et al. Urotensin Ii Receptor Predicts the Clinical Outcome of Prostate Cancer Patients and Is Involved in the Regulation of Motility of Prostate Adenocarcinoma Cells. *J Cell Biochem* (2011) 112(1):341–53. doi: 10.1002/jcb.22933
46. Zhang X, Bai J, Yuan C, Long L, Zheng Z, Wang Q, et al. Bioinformatics Analysis and Identification of Potential Genes Related to Pathogenesis of Cervical Intraepithelial Neoplasia. *J Cancer* (2020) 11(8):2150–7. doi: 10.7150/jca.38211
47. Emmert-Streib F, de Matos Simoes R, Mullan P, Haibe-Kains B, Dehmer M. The Gene Regulatory Network for Breast Cancer: Integrated Regulatory Landscape of Cancer Hallmarks. *Front Genet* (2014) 5:15. doi: 10.3389/fgene.2014.00015
48. Wang H, Gao X, Lu X, Wang Y, Ma C, Shi Z, et al. The Mitotic Regulator Hec1 Is a Critical Modulator of Prostate Cancer Through the Long Non-Coding Rna Bx647187 In Vitro. *Biosci Rep* (2015) 35(6):e00273. doi: 10.1042/BSR20150003
49. Pan H, Su H, Hsu C, Huang G, Wu TT. Targeted Tpx2 Increases Chromosome Missegregation and Suppresses Tumor Cell Growth in Human Prostate Cancer. *Onco Targets Ther* (2017) 10:3531–43. doi: 10.2147/OTT.S136491
50. Sun Y, Li S, Cheng J, Chen G, Huang Z, Gu Y, et al. Downregulation of Mirna-205 Expression and Biological Mechanism in Prostate Cancer Tumorigenesis and Bone Metastasis. *BioMed Res Int* (2020) 2020:6037434. doi: 10.1155/2020/6037434
51. He Z, Tang F, Lu Z, Huang Y, Lei H, Li Z, et al. Analysis of Differentially Expressed Genes, Clinical Value and Biological Pathways in Prostate Cancer. *Am J Transl Res* (2018) 10(5):1444–56.
52. Zhang C, Qian J, Wu Y, Zhu Z, Yu W, Gong Y, et al. Identification of Novel Diagnosis Biomarkers for Therapy-Related Neuroendocrine Prostate Cancer. *Pathol Oncol Res* (2021) 27:1609968. doi: 10.3389/pore.2021.1609968
53. Ben-Salem S, Venkadakrishnan VB, Heemers HV. Novel Insights in Cell Cycle Dysregulation During Prostate Cancer Progression. *Endocr Relat Cancer* (2021) 28(6):R141–R55. doi: 10.1530/ERC-20-0517
54. Li Y, Zhang DY, Ren Q, Ye F, Zhao X, Daniels G, et al. Regulation of a Novel Androgen Receptor Target Gene, the Cyclin B1 Gene, Through Androgen-Dependent E2f Family Member Switching. *Mol Cell Biol* (2012) 32(13):2454–66. doi: 10.1128/MCB.06663-11
55. Qi J, Yang Z, Lin T, Ma L, Wang Y, Zhang Y, et al. Cdk13 Upregulation-Induced Formation of the Positive Feedback Loop Among Circcdk13, Mir-212-5p/Mir-449a and E2f5 Contributes to Prostate Carcinogenesis. *J Exp Clin Cancer Res* (2021) 40(1):2. doi: 10.1186/s13046-020-01814-5
56. Gulzar ZG, McKenney JK, Brooks JD. Increased Expression of Nusap in Recurrent Prostate Cancer Is Mediated by E2f1. *Oncogene* (2013) 32(1):70–7. doi: 10.1038/onc.2012.27
57. Müller I, Strozyk E, Schindler S, Beissert S, Oo HZ, Sauter T, et al. Cancer Cells Employ Nuclear Caspase-8 to Overcome the P53-Dependent G2/M Checkpoint Through Cleavage of Usp28. *Mol Cell* (2020) 77(5):970–84.e7. doi: 10.1016/j.molcel.2019.12.023
58. Latosinska A, Davalieva K, Makridakis M, Mullen W, Schanstra JP, Vlahou A, et al. Molecular Changes in Tissue Proteome During Prostate Cancer Development: Proof-Of-Principle Investigation. *Diagnost (Basel)* (2020) 10(9):655. doi: 10.3390/diagnostics10090655
59. Hoeijmakers JHJ. DNA Damage, Aging, and Cancer. *N Engl J Med* (2009) 361(15):1475–85. doi: 10.1056/NEJMra0804615
60. Jeggo PA, Pearl LH, Carr AM. DNA Repair, Genome Stability and Cancer: A Historical Perspective. *Nat Rev Cancer* (2016) 16(1):35–42. doi: 10.1038/nrc.2015.4
61. Scott CL, Swisher EM, Kaufmann SH. Poly (Adp-Ribose) Polymerase Inhibitors: Recent Advances and Future Development. *J Clin Oncol* (2015) 33(12):1397–406. doi: 10.1200/JCO.2014.58.8848
62. Pilié PG, Tang C, Mills GB, Yap TA. State-Of-the-Art Strategies for Targeting the DNA Damage Response in Cancer. *Nat Rev Clin Oncol* (2019) 16(2):81–104. doi: 10.1038/s41571-018-0114-z
63. Wu B, Lu X, Shen H, Yuan X, Wang X, Yin N, et al. Intratumoral Heterogeneity and Genetic Characteristics of Prostate Cancer. *Int J Cancer* (2020) 146(12):3369–78. doi: 10.1002/ijc.32961
64. Hieronymus H, Schultz N, Gopalan A, Carver BS, Chang MT, Xiao Y, et al. Copy Number Alteration Burden Predicts Prostate Cancer Relapse. *PNAS* (2014) 111(30):11139–44. doi: 10.1073/pnas.1411446111
65. Hieronymus H, Murali R, Tin A, Yadav K, Abida W, Moller H, et al. Tumor Copy Number Alteration Burden Is a Pan-Cancer Prognostic Factor Associated With Recurrence and Death. *Elife* (2018) 7:e37294. doi: 10.7554/eLife.37294
66. Taylor BS, Schultz N, Hieronymus H, Gopalan A, Xiao Y, Carver BS, et al. Integrative Genomic Profiling of Human Prostate Cancer. *Cancer Cell* (2010) 18(1):11–22. doi: 10.1016/j.ccr.2010.05.026
67. Albertson DG. Gene Amplification in Cancer. *Trends Genet* (2006) 22(8):447–55. doi: 10.1016/j.tig.2006.06.007
68. Waldman FM, Carroll PR, Kerschmann R, Cohen MB, Field FG, Mayall BH. Centromeric Copy Number of Chromosome 7 Is Strongly Correlated With Tumor Grade and Labeling Index in Human Bladder Cancer. *Cancer Res* (1991) 51(14):3807–13.
69. Alcaraz A, Takahashi S, Brown JA, Herath JF, Bergstralh EJ, Larson-Keller JJ, et al. Aneuploidy and Aneusomy of Chromosome 7 Detected by Fluorescence in Situ Hybridization Are Markers of Poor Prognosis in Prostate Cancer. *Cancer Res* (1994) 54(15):3998–4002.
70. Macoska JA, Trybus TM, Sakr WA, Wolf MC, Benson PD, Powell IJ, et al. Fluorescence in Situ Hybridization Analysis of 8p Allelic Loss and Chromosome 8 Instability in Human Prostate Cancer. *Cancer Res* (1994) 54(14):3824–30.
71. Ichikawa T, Nihei N, Suzuki H, Oshimura M, Emi M, Nakamura Y, et al. Suppression of Metastasis of Rat Prostatic Cancer by Introducing Human Chromosome 8. *Cancer Res* (1994) 54(9):2299–302.
72. Zarif JC, Baena-Del Valle JA, Hicks JL, Heaphy CM, Vidal I, Luo J, et al. Mannose Receptor-Positive Macrophage Infiltration Correlates With Prostate Cancer Onset and Metastatic Castration-Resistant Disease. *Eur Urol Oncol* (2019) 2(4):429–36. doi: 10.1016/j.euo.2018.09.014
73. Wang YQ, Zhu YJ, Pan JH, Xu F, Shao XG, Sha JJ, et al. Peripheral Monocyte Count: An Independent Diagnostic and Prognostic Biomarker for Prostate Cancer - a Large Chinese Cohort Study. *Asian J Androl* (2017) 19(5):579–85. doi: 10.4103/1008-682X.186185
74. Yirga A, Oyekunle T, Howard LE, De Hoedt AM, Cooperberg MR, Kane CJ, et al. Monocyte Counts and Prostate Cancer Outcomes in White and Black

Men: Results From the Search Database. *Cancer Causes Control* (2021) 32 (2):189–97. doi: 10.1007/s10552-020-01373-2
75. Liu Y, Cao X. The Origin and Function of Tumor-Associated Macrophages. *Cell Mol Immunol* (2015) 12(1):1–4. doi: 10.1038/cmi.2014.83

Conflict of Interest: The authors declare that the research was conducted in the absence of any commercial or financial relationships that could be construed as a potential conflict of interest.

Publisher's Note: All claims expressed in this article are solely those of the authors and do not necessarily represent those of their affiliated organizations, or those of the publisher, the editors and the reviewers. Any product that may be evaluated in this article, or claim that may be made by its manufacturer, is not guaranteed or endorsed by the publisher.

Copyright © 2022 Wei, Han, Zhang, Wang, Liu, Chao, Song and Chen. This is an open-access article distributed under the terms of the Creative Commons Attribution License (CC BY). The use, distribution or reproduction in other forums is permitted, provided the original author(s) and the copyright owner(s) are credited and that the original publication in this journal is cited, in accordance with accepted academic practice. No use, distribution or reproduction is permitted which does not comply with these terms.

frontiers | Frontiers in Oncology

ORIGINAL RESEARCH
published: 04 July 2022
doi: 10.3389/fonc.2022.908956

New Diagnostic Model for Clinically Significant Prostate Cancer in Biopsy-Naïve Men With PIRADS 3

Chen Huang[1†], Feng Qiu[1†], Di Jin[2†], Xuedong Wei[1], Zongxin Chen[1], Ximing Wang[3], Xiaojun Zhao[1], Linchuan Guo[4], Jinxian Pu[1], Jianquan Hou[1] and Yuhua Huang[1]*

[1] Department of Urology, The First Affiliated Hospital of Soochow University, Suzhou, China, [2] Department of Anesthesiology, The First Affiliated Hospital of Soochow University, Suzhou, China, [3] Department of Radiology, The First Affiliated Hospital of Soochow University, Suzhou, China, [4] Department of Pathology, The First Affiliated Hospital of Soochow University, Suzhou, China

OPEN ACCESS

Edited by:
Xuefeng Qiu,
Nanjing Drum Tower Hospital, China

Reviewed by:
Arnaldo Stanzione,
University of Naples Federico II, Italy
Lorenzo Bianchi,
University of Bologna, Italy

***Correspondence:**
Yuhua Huang
sdfyymnwkyhh@163.com

[†]These authors have contributed equally to this work

Specialty section:
This article was submitted to Genitourinary Oncology, a section of the journal Frontiers in Oncology

Received: 04 April 2022
Accepted: 01 June 2022
Published: 04 July 2022

Citation:
Huang C, Qiu F, Jin D, Wei X, Chen Z, Wang X, Zhao X, Guo L, Pu J, Hou J and Huang Y (2022) New Diagnostic Model for Clinically Significant Prostate Cancer in Biopsy-Naïve Men With PIRADS 3. Front. Oncol. 12:908956. doi: 10.3389/fonc.2022.908956

Purpose: The aim of this study was to explore a new model of clinical decision-making to predict the occurrence of clinically significant prostate cancer (csPCa).

Patients and Methods: The demographic and clinical characteristics of 152 patients were recorded. Prostate-specific antigen (PSA), PSA density (PSAD), adjusted PSAD of peripheral zone (aPSADPZ), and peripheral zone volume ratio (PZ ratio) were calculated and subjected to receiver operating characteristic (ROC) curve analysis. The calibration and discrimination abilities of new nomograms were verified with calibration curve and area under the ROC curve (AUC). The clinical benefits of these models were evaluated by decision curve analysis and clinical impact curves.

Results: The AUCs of PSA, PSAD, aPSADPZ, and PZ ratio were 0.521, 0.645, 0.745, and 0.717 for prostate cancer (PCa) diagnosis, while the corresponding values were 0.590, 0.678, 0.780, and 0.731 for csPCa diagnosis, respectively. All nomograms displayed higher net benefit and better overall calibration than the scenarios for predicting the occurrence of csPCa. The new model significantly improved the diagnostic accuracy of csPCa (0.865 vs. 0.741, $p = 0.0284$) compared with the base model. In addition, the new model was better than the base model for predicting csPCa in the low or medium probability while the number of patients with csPCa predicted by the new model was in good agreement with the actual number of patients with csPCa in the high-risk threshold.

Conclusions: This study demonstrates that aPSADPZ has a higher predictive accuracy for csPCa diagnosis than the conventional indicators. Including aPSADPZ, PZ ratio, and age can improve csPCa diagnosis and avoid unnecessary biopsies.

Keywords: adjusted prostate-specific antigen density of peripheral zone, biopsy, diagnosis, PIRADS, prostate cancer

INTRODUCTION

Prostate cancer (PCa) has become the second most common male cancer that affects approximately 375,000 men/year worldwide (1). The incidence of PCa has risen dramatically in recent years, especially in China, where it ranks second among male tumors (2). The multiparameter magnetic resonance imaging (mpMRI) has been increasingly used to diagnose patients with PCa in recent years (3, 4). In 2012, the European Society of Urogenital Radiology (ESUR) established a series of guidelines for the interpretation of mpMRI images using a structured reporting scheme called Prostate Imaging Reporting and Data System (PIRADS) (5). In 2015, the American College of Radiologists, EUSR, and the AdMeTech Foundation improved and updated PIRADS to version 2 (PIRADS V2) (6). In 2019, they upgraded PIRADS V2 to V2.1 (7). The PIRADS consists of five levels, ranging from 1 (clinically significant cancer is highly unlikely to present) to 5 (clinically significant cancer is highly likely to present). Of these, a score of 3 means the presence of clinically significant cancer is equivocal (8). In previous reports (9–11), the detection rate of PCa in PIRADS 3 lesions ranged from 11% to 33.3%, and the rate of clinically significant PCa (csPCa) ranged from 4.2% to 12%. Therefore, we are more concerned about whether there are other indicators that can help us detect more PCa and avoid unnecessary biopsy in patients with PIRADS v2 category 3 (PIRADS 3). In this paper, we established a new model to increase the detection rates of PCa and csPCa, and compared its diagnostic performance with the conventional model.

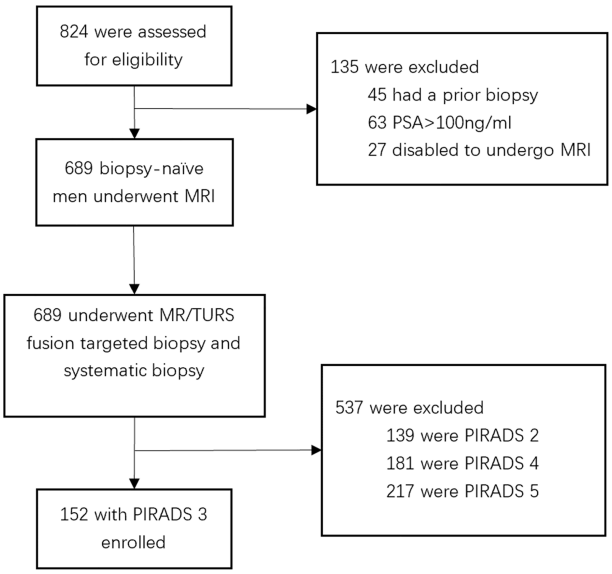


FIGURE 1 | Flowchart for study inclusion among biopsy-naïve men with PIRADS 3 with clinical suspicion for prostate cancer.

PATIENTS AND METHODS

Ethical Approval

All patients were counseled about the risks of the procedure, and then, they signed a consent form that included permission to use their clinical data for research. Ethical approval was obtained from the Institutional Review Board of The First Affiliated Hospital of Soochow University.

Patient Recruitment

In this retrospective cohort study, patients with PCa were recruited at The First Affiliated Hospital of Soochow University (Suzhou, China) from July 2016 to June 2020. A total of 824 male patients presented to our institution for prostate biopsy (PB). Of these patients, 45 had prior treatment, 63 had prostate-specific antigen (PSA) > 100 ng ml^{-1}, 27 were not able to undergo MRI examination, and the remaining 689 received a transperineal PB. Among them,139 with PIRADS 2, 181 with PIRADS 4, and 217 with PIRADS 5 were excluded, and 152 with PIRADS 3 were included in this study. The patient selection flowchart is shown in **Figure 1**.

MRI Acquisition

All patients were subjected to a 3-T magnetic resonance (MR) scanner (MAGNETOM Skyra, Siemens Healthineers, Erlangen, Germany). The 18-channel body and standard spine array coils were employed for signal reception. The transverse T1-weighted turbo spin-echo (TSE) images, as well as the transverse, coronal, and sagittal T2-weighted TSE images of the prostate and seminal vesicles were acquired. The apparent diffusion coefficient was obtained from diffusion-weighted imaging (DWI) and was calculated using a 2-dimensional echo planar imaging sequence with multiple b-value acquisitions (0, 100 s mm^{-2}, 800 s mm^{-2}, 1,000 s mm^{-2}, and 1,500 s mm^{-2}), with diffusion-sensitizing gradients applied along the *x*-, *y*-, and *z*-axes. Dynamic contrast-enhanced (DCE) imaging was conducted through a 3-dimensional T1-weighted gradient-echo volumetric interpolated breath-hold examination, and was in the same plane as the 3D T2W sequence. Then, an intravenous contrast agent (Medtron AG, Saarbruecken, Germany) was administered at 1 ml kg^{-1} body weight and 2.5 ml s^{-1} injection rate. The MR Tissue4D software (Syngo. *via* VA20B; Siemens Healthineers) was used to construct perfusion curves. The details of the imaging protocol are shown in **Supplementary Table 1**.

Prostate Biopsy and Pathology Analysis

Transperineal prostate targeted biopsy (TB) and systematic biopsy (SB) were performed on all patients. During TB, the DICOM data of mpMRI images (**Figures 2A–C**), including T2WI, DWI, apparent diffusion coefficient (ADC), and DCE, were imported into the Real-time Virtual Sonogra (RVS) ultrasonography host (Preirus, Hitachi, Japan), and the target lesion was marked as region of interest (ROI). Through RVS, the ROI marked on MRI images was displayed in real time on the ultrasonography images. Ultrasonography and MRI images were matched by sagittal and axial anatomical markers, such as urethral orifices and small prostate cysts. Following these steps, the urologist performed the TB, and each ROI was executed on

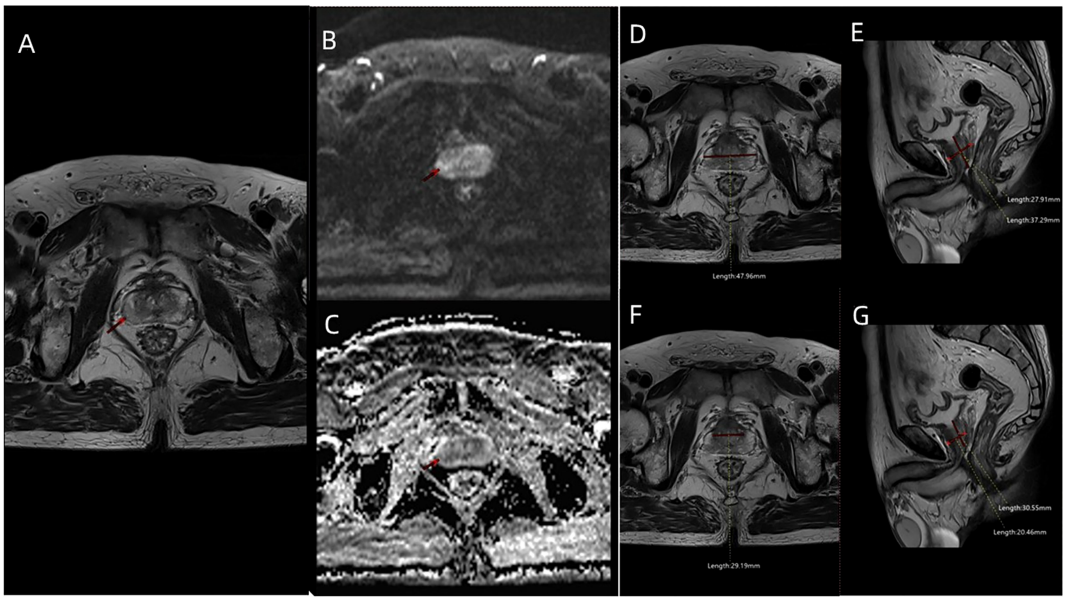


FIGURE 2 | The MRI images including **(A)** T2WI sequence, **(B)** DWI sequence, and **(C)** ADC sequence of a patient (age: 66 years; PSA: 7.8 ng/ml; f/tPSA: 0.138; ISUP GG: 2) with PIRADS 3 ROI in the right lateral posterior of peripheral zone. **(D)** Maximum transverse diameter of prostate (47.96 mm) measured on axial T2WI, and **(E)** maximum longitudinal diameter (37.29 mm) and maximum AP diameter (27.91 mm) of prostate measured on mid-sagittal T2WI. **(F)** Maximum transverse diameter of transitional zone (29.19 mm) measured on axial T2WI, and **(G)** maximum longitudinal diameter (30.55 mm) and maximum AP diameter (20.46 mm) of transitional zone measured on mid-sagittal T2WI.

2-core biopsy. After completion of TB, the RVS was turned off and the same urologist continued to perform SB. All specimens were fixed in 10% formalin and subjected to pathological analysis. The csPCa was defined as a single biopsy core with a Gleason score of 3 + 4 or above [International Society of Urological Pathology (ISUP) grade group (GG) >1] as described previously (9).

Patient Characteristics

The patients' age, pre-biopsy PSA, free/total PSA(f/tPSA), and pathological features were included in the study. The included MRI characteristics were PIRADS scores, prostate volume (PV) [prostate volume (PV) = 0.52 × height × length × width] (**Figures 2D, E**), PSAD (PSAD = PSA/PV), transitional zone volume (TZV) [TZV = 0.52 × height (TZ) × length (TZ) × width (TZ)] (**Figures 2F, G**), peripheral zone volume (PZV) (PZV = PV – TZV), PZ ratio (PZ ratio = PZV/PV), PSADPZ (PSADPZ = PSA/PZV), and adjusted PSADPZ (aPSADPZ = PSAD × PZ ratio). Each patient was graded according to PIRADS V2 by the same radiologist who graded more than 500 prostate MRI readings. The biopsy cores were examined by a dedicated pathologist.

Statistical Analysis

Categorical and continuous variables were analyzed using the Pearson's chi-squared test and Mann–Whitney *U* test, respectively. Binary logistic regression was used to calculate the odds ratios of each predictive factors. The predictive models were constructed as follows. First, univariate regression analysis was performed to evaluate the power of each parameter in diagnosing PCa and csPCa. Next, the variables with p-value < 0.05 in the univariate analysis were further analyzed by multivariate logistic regression models using the procedure of enter selection method. The multivariate regression coefficients were then used to construct nomograms. From multivariable binary logistic analysis, the following predictive models were built to predict the occurrence of PCa and csPCa: the base model included clinical factors such as PSA, f/tPSA, and PSAD, while the new model included age, PZ ratio, and aPSADPZ. The calibration and discrimination abilities of these models were evaluated using the calibration curve (1,000 bootstrap resamples) and area under the receiver operating characteristic (ROC) curve (AUC), respectively. The nomograms were also validated using an internal validation cohort (1,000 bootstrap resamples). The clinical benefits of these models were determined by decision curve analysis (DCA). In this case, we focused on 10%–40%, in which clinical decision-making is particularly difficult. The AUCs of both models were compared using methods described previously (12). In DCAs, the horizontal line along the x-axis indicated that all patients developed PCa and csPCa. The nomogram, calibration plots, and DCA were constructed by R x64 4.0.2 (http://www.r-project.org, last accessed date: 03/10/2022 18:10:01). Other statistical tests were conducted with SPSS v22.0 (IBM Corp, Armonk, NY, USA) and MedCalc v18.2.1 (MedCalc Software, Belgium). All reported p-values were two-sided and the level of statistical significance was set at $p < 0.05$.

RESULTS

Demographic and Clinical Characteristics

Overall, 19.1% of patients (29/152) had histologically confirmed PCa, while 11.8% (18/152) had histologically confirmed csPCa. The clinical data of all patients are summarized in **Table 1**. PCa patients had significantly higher PSAD, PZ ratio, and aPSADPZ, and lower f/tPSA, PV, and TZV, compared to patients with benign disease. Similar results were observed for the differences in these parameters between the csPCa group and the benign or clinically insignificant prostate cancer (isPCa) group.

Univariate and Multivariate Regression Analyses of Independent Predictors for Diagnosing PCa and csPCa

As shown in **Table 2**, f/tPSA, PSAD, TZV, PZ ratio, and aPSADPZ were important predictors for diagnosing PCa and csPCa in univariate logistic regression analysis. Age was only important for csPCa while PV was only important for PCa. The findings of multivariate analysis are presented in **Table 3**. Notably, only aPSADPZ was included in the predictive model of PCa, while age, f/tPSA, PZ ratio, and aPSADPZ were included in the predictive model of csPCa.

ROC Curve Analysis of Predictive Factors in Comparison With aPSADPZ

ROC curve analysis revealed that the AUC for aPSADPZ in the diagnosis of PCa and csPCa was 0.745 and 0.780, respectively. Compared with other parameters, PSAD was 0.645 and 0.678, PZ ratio was 0.717 and 0.731, and PSA was 0.521 and 0.590, respectively (**Figure 3**). After pairwise comparison, the AUC of aPSADPZ was significantly larger than PSA and PSAD for PCa diagnosis (aPSADPZ vs. PSA, Z value: 3.488, $p < 0.01$; aPSADPZ vs. PSAD, Z value: 3.169, $p < 0.01$) and csPCa diagnosis (aPSADPZ vs. PSA, Z value: 2.440, $p = 0.01$; aPSADPZ vs. PSAD, Z value: 2.560, $p = 0.01$). The AUCs between aPSADPZ and PZ ratio for PCa diagnosis (aPSADPZ vs. PZ ratio, Z value: 0.561, $p = 0.575$) and csPCa diagnosis (aPSADPZ vs. PZ ratio, Z value: 0.696, $p = 0.486$) had no statistical difference.

Nomograms and Validation of the Two Models for Diagnosing PCa and csPCa

Based on the multivariate regression coefficients, nomograms (**Figures 4A, B**) were used to visualize the predictive results. The calibration and discrimination abilities of these nomograms were further validated with an internal cohort (1,000 bootstrap resamples, **Figures 4C, D**). The C-index of the two nomograms was 0.762 and 0.880. Compared to the base model (including PSA, f/tPSA, and PSAD), the new model (including age, aPSADPZ, and PZ ratio) exhibited obviously higher AUC values (PCa: 0.782 vs. 0.689, $p = 0.0931$; csPCa: 0.865 vs. 0.741, $p = 0.0284$) for predicting csPCa (**Figures 5A, B**). Calibration curves showed excellent calibration between the actual and predicted probabilities of the new model for diagnosing PCa and csPCa.

Decision Curve Analysis for Diagnosing PCa and csPCa

The DCA indicated that the net benefit of the new model was better than that of the base model for predicting PCa and csPCa in the defined regions of interest (10%–40% probability) (**Figures 5C, D**). In addition, clinical impact curves showed that in the high-risk threshold, the number of patients with PCa and csPCa predicted by the new model was in good agreement with the actual number of patients with PCa and csPCa (**Figures 5E, F**).

DISCUSSION

We believed that both PSAD and PZ ratio are dependent on the correct measurement of PV and TZV. Colvin et al. (13) reported the current PIRADS V2.1 recommendation of either traditional ellipsoid or segmentation volume measurements as viable methods to assess prostate volume. The predictive capability of PSAD for csPCa was not significantly different between the two measurements. Stanzione et al. (14) also made a similar viewpoint. Thus, we still used the traditional ellipsoid volume measurement to calculate PV and TZV. Luis et al. (15) showed that PSAD can improve the early detection of csPCa. Porcaro et al. (16) found that increased prostate volume index (PVI),

TABLE 1 | Patient demographics and the correlation with biopsy results.

Characteristic	PCa (n = 29)	Benign (n = 123)	Z	p	csPCa (n = 18)	isPCa or benign (n = 134)	Z	p
Age (years), median (IQR)	68.0 (60.5–73.5)	65.0 (61.0–70.0)	–1.469	0.142	69.5 (64.0–76.3)	65.5 (61.0–70.0)	–2.192	0.028
PSA (ng ml^{-1}), median (IQR)	7.90 (6.00–13.66)	7.84 (5.87–12.26)	–0.347	0.729	10.39 (7.26–16.05)	7.67 (5.92–12.17)	–1.235	0.217
f/tPSA, median (IQR)	0.120 (0.084–0.157)	0.160 (0.117–0.218)	–2.978	<0.01	0.100 (0.071–0.151)	0.15 7 (0.111–0.212)	–3.165	<0.01
PV (ml), median (IQR)	36.1 (25.7–55.5)	51.0 (39.1–69.2)	–2.884	<0.01	36.5 (25.1–57.1)	50.0 (37.5–68.3)	–2.138	0.032
PSAD (ng ml^{-2}), median (IQR)	0.229 (0.136–0.392)	0.171 (0.111–0.246)	–2.427	0.015	0.251 (0.143–0.445)	0.176 (0.112–0.248)	–2.446	0.014
TZV (ml), median (IQR)	15.9 (10.0–26.6)	28.5 (18.7–45.7)	–3.833	<0.01	14.4 (10.4–25.9)	27.2 (18.3–45.1)	–3.165	<0.01
PZV (ml), median (IQR)	20.8 (13.8–27.0)	21.2 (14.1–29.6)	–0.288	0.773	22.5 (13.6–29.5)	21.0 (14.0–29.0)	–0.319	0.749
PZ ratio, median (IQR)	0.542 (0.440–0.641)	0.421 (0.301–0.533)	–3.632	<0.01	0.570 (0.456–0.675)	0.428 (0.301–0.534)	–3.182	<0.01
PSADPZ (ng ml^{-2}), median (IQR)	0.459 (0.251–0.671)	0.413 (0.276–0.684)	–0.302	0.762	0.528 (0.220–0.767)	0.414 (0.277–0.647)	–0.661	0.508
aPSADPZ (ng ml^{-2}), median (IQR)	0.119 (0.082–0.217)	0.059 (0.040–0.108)	–4.096	<0.01	0.249 (0.142–0.441)	0.064 (0.040–0.104)	–3.855	<0.01

PCa, prostate cancer; csPCa, clinically significant prostate cancer; isPCa, clinically insignificant prostate cancer; fPSA, free prostate-specific antigen; tPSA, total prostate-specific antigen; PV, prostate volume; PSAD, prostate-specific antigen density; TZV, transitional zone volume; PZV, peripheral zone volume; PSADPZ, prostate-specific antigen density of peripheral zone; aPSADPZ, adjusted prostate-specific antigen density of peripheral zone; IQR, interquartile range.

TABLE 2 | Univariate regression analyses for various parameters to detect PCa and csPCa in biopsy-naïve men with PIRADS v2 categories 3.

Characteristic	PCa diagnosis OR (95% CI)	*p*	csPCa diagnosis OR (95% CI)	*p*
Age (years)			1.081 (1.008–1.159)	0.028
f/tPSA	0.000 (0.000–0.237)	0.016	0.000 (0.000–0.010)	<0.01
PV (ml)	0.976 (0.957–0.996)	0.019		
PSAD (ng ml^{-2})	67.313 (3.692–1,227.389)	<0.01	168.659 (6.221–4,572.278)	<0.01
TZV (ml)	0.959 (0.930–0.988)	0.015	0.961 (0.927–0.997)	0.033
PZ ratio	204.535 (9.831–4,255.171)	<0.01	319.093 (7.446–13,675.391)	<0.01
aPSADPZ (ng ml^{-2})	29,110.383 (134.685–6,291,826.949)	<0.01	32,018.766 (112.233–9,134,606.470)	<0.01

PCa, prostate cancer; csPCa, clinically significant prostate cancer; f/tPSA, free/total prostate-specific antigen; PV, prostate volume; PSAD, prostate-specific antigen density; TZV, transitional zone volume; aPSADPZ, adjusted prostate-specific antigen density of peripheral zone; OR, odds ratio; CI, confidence interval.

TABLE 3 | Multivariate regression analyses for various parameters to detect PCa and csPCa in biopsy-naïve men with PIRADS v2 categories 3.

Characteristic	PCa diagnosis OR (95% CI)	*p*	csPCa diagnosis OR (95% CI)	*p*
Age (years)			1.170 (1.074–1.275)	<0.01
f/tPSA	0.101 (0.000–24.039)	0.471	0.000 (0.000–0.236)	0.024
PV (ml)	0.998 (0.977–1.020)	0.881		
PZ ratio	21.941 (0.615–782.869)	0.090	269.406 (1.826–39,739.719)	0.028
aPSADPZ (ng ml^{-2})	610.587 (1.121–332,645.968)	0.046	4,650.212 (2.691–8,035,199.454)	0.026

PCa, prostate cancer; csPCa, clinically significant prostate cancer; PSA, prostate-specific antigen; f/tPSA, free/total prostate-specific antigen; aPSADPZ, adjusted prostate-specific antigen density of peripheral zone; OR, odds ratio; CI, confidence interval.

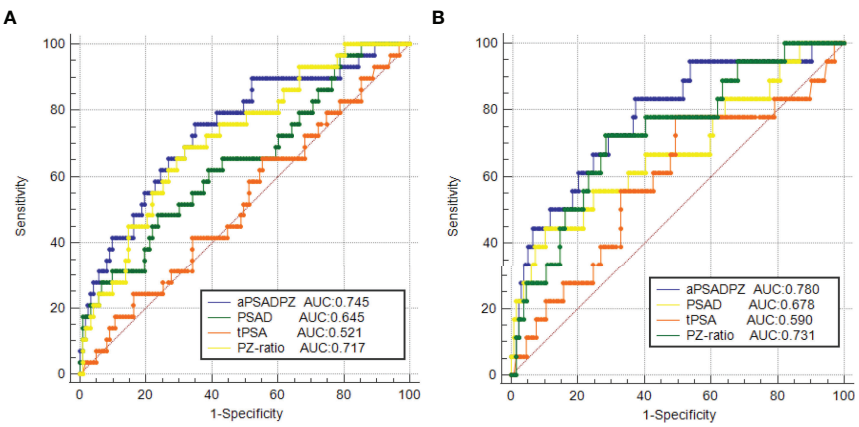


FIGURE 3 | ROC curves of various parameters in the diagnosis of **(A)** PCa and **(B)** csPCa in biopsy-naïve men with PIRADS v2 categories 3. PIRADS, Prostate Imaging Reporting and Data System; tPSA, total prostate-specific antigen; PSAD, prostate-specific antigen density; aPSADPZ, adjusted prostate-specific antigen density of peripheral zone; PZ ratio, peripheral zone ratio; PCa, prostate cancer; csPCa, clinically significant prostate cancer; ROC, receiver operating characteristic; AUC, area under the curve.

which is defined as the ratio of the volume of the TZV to the PZV, decreased the risk of increased tumor load and was associated with less aggressive PCa biology in patients at baseline random biopsies. They made a point that PVI is a pure measurement that is separate from PSAD, which compared the PSA serum levels with the PV and is largely influenced by TZV. Chang et al. (17) showed that the PZ ratio could be used as a predictor of PCa. We believe that PVI and PZ ratio have the same diagnostic efficacy because they both represent the percentage of the PZV in the PV. Thus, we only chose PZ ratio for PCa prediction. Koo et al. (18) and Lee et al. (19) indicated that PZPSAD was better than PSAD for the detection of PCa. Schneider et al. (20) found that TZPSAD exhibited a stronger correlation to cancer aggressiveness compared to PSAD. In our views, since BPH is mainly due to hyperplasia in the TZ, while PCa predominantly occurs in the PZ (21), conventional PSAD does not take into account whether the hyperplastic prostate tissue is mainly in the TZ or the PZ. Recently, the PIRADS score has shown important clinical significance in PCa diagnosis (6). The current consensus is that PIRADS 3 is a gray area for the diagnosis of PCa (22). The lesions of PIRADS 3 do not have typical features (7). Satoshi et al. (23) demonstrated that

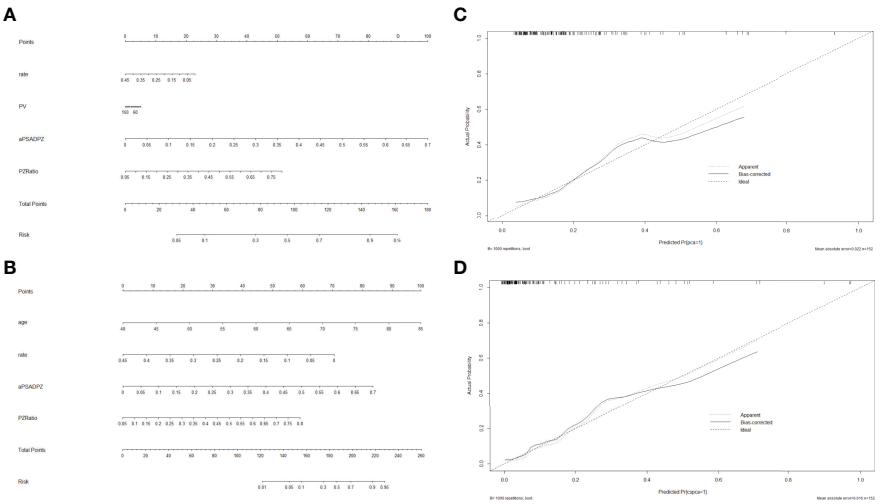


FIGURE 4 | Nomogram of two models for predicting the probability of **(A)** PCa and **(B)** csPCa in biopsy-naïve men with PIRADS v2 categories 3. Calibration curves of these two nomograms in the diagnosis of **(C)** PCa and **(D)** csPCa in biopsy-naïve men with PIRADS v2 categories 3. PSA, prostate-specific antigen; aPSADPZ, adjusted prostate-specific antigen density of peripheral zone; PV, prostate volume; PIRADS, Prostate Imaging Reporting and Data System; PCa, prostate cancer; csPCa, clinically significant prostate cancer.

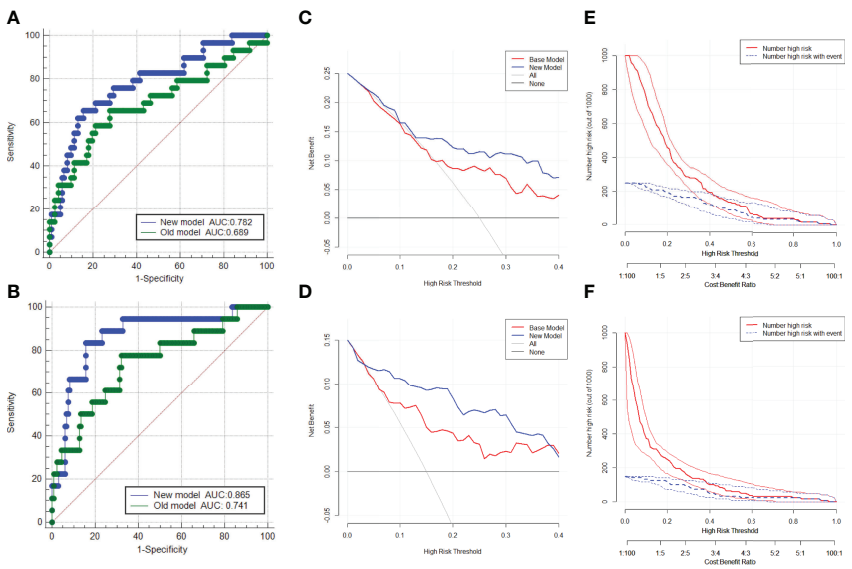


FIGURE 5 | ROC curves of the two models in the diagnosis of **(A)** PCa and **(B)** csPCa in biopsy-naïve men with PIRADS v2 categories 3. Decision curve analysis of the two models for predicting the occurrence of **(C)** PCa and **(D)** csPCa in biopsy-naïve men with PIRADS v2 categories 3. Clinical impact curves of the two models for the diagnosis of **(E)** PCa and **(F)** csPCa in biopsy-naïve men with PIRADS v2 categories 3. AUC, area under the curve; ROC, receiver operating characteristic; PCa, prostate cancer; csPCa, clinically significant prostate cancer; PIRADS, Prostate Imaging Reporting and Data System.

PSAD was useful for the diagnosis of PCa in men with a PIRADS score ≤ 3, thus avoiding unnecessary biopsy. Gaudiano et al. (24) found that PSAD and location within the prostate gland are associated with an increased risk of the presence of PCa in patients with PIRADS 3. In our study, we combined PSAD with PZ ratio to obtain a new index (aPSADPZ), which achieved a better predictive outcome. We found that aPSADPZ had an advantage over PSA and PSAD in the diagnosis of PCa and csPCa in biopsy-naïve men with PIRADS 3. In our opinion, PCa is mostly found in the PZ (21), and tumors in the PZ possibly increase the levels of PSA in patients with a high PZ ratio. Our results showed that the aPSADPZ had a significant predictive

ability in both univariate and multivariate analyses, indicating that it was the best predictor of PCa and csPCa in this study.

Eastham et al. (25) reported the first nomogram to predict PCa in 1999. Zhang et al. (26) reported that a model including PIRADS, PSAD, and age showed internally validated high discrimination and calibration for the absence of PCa and csPCa in biopsy-naïve men with PIRADS ≤ 3. To our knowledge, this is a new nomogram that combines aPSADPZ, PZ ratio, and age to predict PCa in biopsy-naïve men with PIRADS 3. In our study, the new model's C-index of csPCa diagnosis was 0.88, which had good diagnostic performance. The AUC of the new model was 0.865 for csPCa diagnosis, whereas the base model's AUC was 0.741. The new model had a significantly higher diagnostic efficiency compared to the base model (0.865 vs. 0.741, $p = 0.0284$). Further validation of the new model for diagnosing csPCa indicated its excellent performance. In the defined region of interest (10%–40% probability), which means difficulty in making clinical decisions, the net benefit of the new model is higher than that of the base model in the DCA. It means that when the probability of csPCa is moderate or low, which makes it difficult to make a clinical decision as to whether to biopsy or not, the new model can increase the rate of detection for csPCa and avoid unnecessary biopsy. The new model is more suitable for guiding clinical decision-making in men with PIRADS 3. On the other hand, we found a good calibration between the actual and predicted probabilities of the new model in the region of high probability. Taken together, for low or medium probability populations, the new model can detect more csPCa and reduce unnecessary biopsies, while for high probability populations, it will not miss csPCa and cause adverse outcomes.

Our study has several limitations: (1) This was a retrospective study performed at a single institution with a possible risk of selection bias. (2) PIRADS scores are dependent on the experience of the radiologist, and may vary from physician to physician. (3) The definition of csPCa used in this study does not include all clinically significant diseases, in that ISUP GG1 with a high tumor volume load may be significant and ISUP GG2 with a low tumor volume load may be insignificant. (4) We did not consider an upgrade or a downgrade of Gleason scores in specimens after radical prostatectomy, which may be a limitation for the determination of csPCa.

CONCLUSIONS

In summary, aPSADPZ has a higher predictive accuracy for the diagnosis of PCa and csPCa in biopsy-naïve men with PIRADS 3 than the conventional indicators, which may decrease the risk of misdiagnosis and reduce the number of unnecessary biopsies. The prediction model of aPSADPZ, PZ ratio, and age can improve csPCa detection, increase diagnostic accuracy, and avoid unnecessary biopsies.

DATA AVAILABILITY STATEMENT

The raw data supporting the conclusions of this article will be made available by the authors, without undue reservation.

ETHICS STATEMENT

The studies involving human participants were reviewed and approved by the Institutional review board of The First Affiliated Hospital of Soochow University. The patients/participants provided their written informed consent to participate in this study.

AUTHOR CONTRIBUTIONS

CH helped in project development and data analysis, and wrote the manuscript. FQ was involved in project development and data collection, and wrote the manuscript. DJ was involved in project development and data analysis and wrote the manuscript. JP and XW helped in data analysis. ZC performed the statistical analysis. XW helped in the drafting of the manuscript. XZ, LG, and JH helped in data collection. YH helped in project development and edited the manuscript. All authors contributed to the article and approved the submitted version.

FUNDING

This work was supported by two grants from the Key Research and Development Program of Jiangsu Province (No. BE2020654 and No. BE2020655) and a grant from the General Program of Jiangsu Health Commission (No. H2019040).

ACKNOWLEDGMENTS

We thank all colleagues for their support during the data collection and the preparation of this manuscript.

SUPPLEMENTARY MATERIAL

The Supplementary Material for this article can be found online at: https://www.frontiersin.org/articles/10.3389/fonc.2022.908956/full#supplementary-material

REFERENCES

1. Sung H, Ferlay J, Siegel RL, Laversanne M, Soerjomataram I, Jemal A, et al. Global Cancer Statistics 2020: GLOBOCAN Estimates of Incidence and Mortality Worldwide for 36 Cancers in 185 Countries. *CA Cancer J Clin* (2021) 71:209–49. doi: 10.3322/caac.21660
2. Pang C, Guan Y, Li H, Chen W, Zhu G. Urologic Cancer in China. *Japanese J Clin Oncol* (2016) 46(6):497–501. doi: 10.1093/jjco/hyw034
3. Moore CM, Kasivisvanathan V, Eggener S, Emberton M, Fütterer JJ, Gill IS. Standards of Reporting for MRI-Targeted Biopsy Studies (START) of the Prostate: Recommendations From an International Working Group. *Eur Urol* (2013) 64(4):544–52. doi: 10.1016/j.eururo.2013.03.030

4. Barth BK, Martini K, Skawran SM, Schmid FA, Rupp NJ, Zuber L, et al. Value of an Online PI-RADS V2.1 Score Calculator for Assessment of Prostate MRI. *Eur J Radiol Open* (2021) 8:100332. doi: 10.1016/j.ejro.2021.100332
5. Polanec S, Helbich TH, Bickel H, Pinker-Domenig K, Georg D, Shariat SF, et al. Head-To-Head Comparison of PI-RADS V2 and PI-RADS V1. *Eur J Radiol* (2016) 85(6):1125–31. doi: 10.1016/j.ejrad.2016.03.025
6. Patel NU, Lind KE, Garg K, Crawford D, Werahera PN, Pokharel SS. Assessment of PI-RADS V2 Categories >/= 3 for Diagnosis of Clinically Significant Prostate Cancer. *Abdom Radiol (NY)* (2019) 44(2):705–12. doi: 10.1007/s00261-018-1751-5
7. Turkbey B, Rosenkrantz AB, Haider MA, Padhani AR, Villeirs G, Macura KJ, et al. Prostate Imaging Reporting and Data System Version 2.1: 2019 Update of Prostate Imaging Reporting and Data System Version 2. *Eur Urol* (2019) 76 (3):340–51. doi: 10.1016/j.eururo.2019.02.033
8. Schlenker B, Apfelbeck M, Armbruster M, Chaloupka M, Stief CG, Clevert DA. Comparison of PIRADS 3 Lesions With Histopathological Findings After MRI-Fusion Targeted Biopsy of the Prostate in a Real World-Setting. *Clin Hemorheol Microcirc* (2019) 71(2):165–70. doi: 10.3233/CH-189407
9. Kasivisvanathan V, Rannikko AS, Borghi M, Panebianco V, Mynderse LA, Vaarala MH, et al. MRI-Targeted or Standard Biopsy for Prostate-Cancer Diagnosis. *N Engl J Med* (2018) 378(19):1767–77. doi: 10.1056/NEJMoa1801993
10. Mehralivand S, Bednarova S, Shih JH, Mertan FV, Gaur S, Merino MJ, et al. Prospective Evaluation of PI-RADS Version 2 Using the International Society of Urological Pathology Prostate Cancer Grade Group System. *J Urol* (2017) 198(3):583. doi: 10.1016/j.juro.2017.03.131
11. Ullrich T, Quentin M, Arsov C, Schmaltz AK, Tschischka A, Laqua N, et al. Risk Stratification of Equivocal Lesions on Multiparametric Magnetic Resonance Imaging of the Prostate. *J Urol* (2018) 199(3):691–8. doi: 10.1016/j.juro.2017.09.074
12. Delong ER, Delong DM, Clarke-Pearson DL. Comparing the Areas Under Two or More Correlated Receiver Operating Characteristic Curves: A Nonparametric Approach. *Biometrics* (1988) 44(3):837. doi: 10.2307/2531595
13. Colvin R, Walker D, Hafron J, Seifman B, Nandalur S, Gangwish D, et al. Which Measurement Method Should Be Used for Prostate Volume for PI-RADS? A Comparison of Ellipsoid and Segmentation Methods. *Clin Imaging* (2021) 80:454–58. doi: 10.1016/j.clinimag.2021.09.003
14. Stanzione A, Ponsiglione A, Fiore G, Picchi SG, Cuocolo R. Prostate Volume Estimation on MRI: Accuracy and Effects of Ellipsoid and Bullet-Shaped Measurements on PSA Density. *Acad Radiol* (2020) 28:e219–26. doi: 10.1016/j.acra.2020.05.014
15. Luis R, Leandro B, Gonzalo V, Pablo C, Hernando RP, Carlos A. PI-RADS 3 Lesions: Does the Association of the Lesion Volume With the Prostate-Specific Antigen Density Matter in the Diagnosis of Clinically Significant Prostate Cancer? *Urologic Oncol: Semin Original Investigations* (2020) 39 (7):431.e9–431.e13. doi: 10.1016/j.urolonc.2020.11.010
16. Porcaro AB, Tafuri A, Sebben M, Novella G, Processali T, Pirozzi M, et al. Prostate Volume Index and Prostatic Chronic Inflammation Predicted Low Tumor Load in 945 Patients at Baseline Prostate Biopsy. *World J Urol* (2020) 38(4):957–64. doi: 10.1007/s00345-019-02830-7
17. Chang Y, Chen R, Yang Q, Gao X, Sun Y. Peripheral Zone Volume Ratio (PZ-Ratio) is Relevant With Biopsy Results and can Increase the Accuracy of Current Diagnostic Modality. *Oncotarget* (2017) 8(21):34836–43. doi: 10.18632/oncotarget.16753
18. Koo KC, Lee DH, Lee SH, Chung BH. Peripheral Zone Prostate-Specific Antigen Density: An Effective Parameter for Prostate Cancer Prediction in Men Receiving 5α-Reductase Inhibitors. *Prostate Int* (2013) 1(3):102–8. doi: 10.12954/PI.13022
19. Lee J, Yang SW, Jin L, Lee CL, Song KH. Is PSA Density of the Peripheral Zone as a Useful Predictor for Prostate Cancer in Patients With Gray Zone PSA Levels? *BMC Cancer* (2021) 21(1):472. doi: 10.21203/rs.3.rs-116832/v1
20. Schneidera AF, Stockera D, Hötkera AM, Eberlib D, Ruppc NJ, Donatia OF, et al. Comparison of PSA-Density of the Transition Zone and Whole Gland for Risk Stratification of Men With Suspected Prostate Cancer: A Retrospective MRI-Cohort Study. *Eur J Radiol* (2019) 120:108660. doi: 10.1016/j.ejrad.2019.108660
21. Chen ME, Johnston DA, Tang K, Babaian RJ, Troncoso P. Detailed Mapping of Prostate Carcinoma Foci: Biopsy Strategy Implications. *Cancer* (2015) 89 (8):1800–9. doi: 10.1002/1097-0142(20001015)89:8<1800::AID-CNCR21>3.0.CO;2-D
22. Scialpi M, Martorana E, Aisa MC, Rondoni V, D'Andrea A, Bianchi G. Score 3 Prostate Lesions: A Gray Zone for PI-RADS V2. *Turk J Urol* (2017) 43(3):237–40. doi: 10.5152/tud.2017.01058
23. Washino S, Okochi T, Saito K, Konishi T, Hirai M, Kobayashi Y, et al. Combination of Prostate Imaging Reporting and Data System (PI-RADS) Score and Prostate-Specific Antigen (PSA) Density Predicts Biopsy Outcome in Prostate Biopsy Nave Patients. *BJU Int* (2016) 119(2):225–33. doi: 10.1111/bju.13465
24. Gaudiano C, Bianchi L, Corcioni B, Giunchi F, Schiavina R, Ciccarese F, et al. Evaluating the Performance of Clinical and Radiological Data in Predicting Prostate Cancer in Prostate Imaging Reporting and Data System Version 2.1 Category 3 Lesions of the Peripheral and the Transition Zones. *Int Urol Nephrol* (2022) 54:263–71. doi: 10.1007/s11255-021-03071-7
25. Eastham JA, May R, Robertson JL, Sartor O, Kattan MW. Development of a Nomogram That Predicts the Probability of a Positive Prostate Biopsy in Men With an Abnormal Digital Rectal Examination and a Prostate-Specific Antigen Between 0 and 4 Ng/mL 1. *Urology* (1999) 54(4):709–13. doi: 10.1016/S0090-4295(99)00213-7
26. Zhang Y, Zeng N, Zhang F, Huang Y, Tian Y. How to Make Clinical Decisions to Avoid Unnecessary Prostate Screening in Biopsy-Naive Men With PI-RADs V2 Score </= 3? *Int J Clin Oncol* (2020) 25(1):175–86. doi: 10.1007/s10147-019-01524-9

Conflict of Interest: The authors declare that the research was conducted in the absence of any commercial or financial relationships that could be construed as a potential conflict of interest.

Publisher's Note: All claims expressed in this article are solely those of the authors and do not necessarily represent those of their affiliated organizations, or those of the publisher, the editors and the reviewers. Any product that may be evaluated in this article, or claim that may be made by its manufacturer, is not guaranteed or endorsed by the publisher.

Copyright © 2022 Huang, Qiu, Jin, Wei, Chen, Wang, Zhao, Guo, Pu, Hou and Huang. This is an open-access article distributed under the terms of the Creative Commons Attribution License (CC BY). The use, distribution or reproduction in other forums is permitted, provided the original author(s) and the copyright owner(s) are credited and that the original publication in this journal is cited, in accordance with accepted academic practice. No use, distribution or reproduction is permitted which does not comply with these terms.

frontiers | Frontiers in Oncology

TYPE Original Research
PUBLISHED 11 August 2022
DOI 10.3389/fonc.2022.915662

Check for updates

OPEN ACCESS

EDITED BY
Takeshi Yuasa,
Japanese Foundation For Cancer Research, Japan

REVIEWED BY
Wenyu Zhai,
Sun Yat-sen University Cancer Center, China
Alessandro Tafuri,
Ospedale Vito Fazzi, Italy

*CORRESPONDENCE
Yi Hu
huyi301zlxb@sina.com
Bo Yang
yangbo@301hospital.com.cn

†Theses authors have contributed equally to this work

SPECIALTY SECTION
This article was submitted to Genitourinary Oncology, a section of the journal Frontiers in Oncology

RECEIVED 08 April 2022
ACCEPTED 20 July 2022
PUBLISHED 11 August 2022

CITATION
Shi W-W, Guan J-Z, Long Y-P, Song Q, Xiong Q, Qin B-Y, Ma Z-Q, Hu Y and Yang B (2022) Integrative transcriptional characterization of cell cycle checkpoint genes promotes clinical management and precision medicine in bladder carcinoma. *Front. Oncol.* 12:915662. doi: 10.3389/fonc.2022.915662

COPYRIGHT
© 2022 Shi, Guan, Long, Song, Xiong, Qin, Ma, Hu and Yang. This is an open-access article distributed under the terms of the Creative Commons Attribution License (CC BY). The use, distribution or reproduction in other forums is permitted, provided the original author(s) and the copyright owner(s) are credited and that the original publication in this journal is cited, in accordance with accepted academic practice. No use, distribution or reproduction is permitted which does not comply with these terms.

Integrative transcriptional characterization of cell cycle checkpoint genes promotes clinical management and precision medicine in bladder carcinoma

Wei-Wei Shi[1†], Jing-Zhi Guan[1†], Ya-Ping Long[2†], Qi Song[1], Qi Xiong[1], Bo-Yu Qin[1], Zhi-Qiang Ma[1], Yi Hu[1*] and Bo Yang[1*]

[1]Department of Medical Oncology, Senior Department of Oncology, The Fifth Medical Center of People's Liberation Army (PLA) General Hospital, Beijing, China, [2]School of Medicine, Nankai University, Tianjin, China

Background: The aberrant regulation of cell cycle is significantly correlated with cancer carcinogenesis and progression, in which cell cycle checkpoints control phase transitions, cell cycle entry, progression, and exit. However, the integrative role of cell cycle checkpoint-related genes (CRGs) in bladder carcinoma (BC) remains unknown.

Methods: The transcriptomic data and clinical features of BC patients were downloaded from The Cancer Genome Atlas (TCGA), used to identify CRGs correlated with overall survival (OS) by univariate Cox regression analysis. Then, the multivariate and least absolute shrinkage and selection operator (LASSO) Cox regression analyses further developed a prognostic CRG signature, which was validated in three external datasets retrieved from Gene Expression Omnibus (GEO). The receiver operating characteristic curve (ROC) analysis was conducted for evaluating the performance of the CRG signature in prognosis prediction. RNA sequencing (RNA-Seq) was performed to explore the expression difference in the identified CRGs between tumor and normal tissue samples from 11 BC patients in the local cohort. Ultimately, genomic profiles and tumor microenvironment (TME), and the Genomics of Drug Sensitivity in Cancer (GDSC) were investigated to guide precision treatment for BC patients with different CRG features.

Results: The novel constructed 23-CRG prognostic signature could stratify BC patients into high-risk and low-risk groups with significantly different outcomes (median OS: 13.64 vs. 104.65 months). Notably, 19 CRGs were the first to be identified as being associated with BC progression. In three additional validation datasets (GSE13507, GSE31684, and GSE32548), higher CRG scores all indicated inferior survival, demonstrating the robust ability of the CRG signature in prognosis prediction. Moreover, the CRG signature as an independent

prognostic factor had a robust and stable risk stratification for BC patients with different histological or clinical features. Then, a CRG signature-based nomogram with a better performance in prognostic prediction [concordance index (C-index): 0.76] was established. Functional enrichment analysis revealed that collagen-containing extracellular matrix (ECM), and ECM-related and MAPK signaling pathways were significantly associated with the signature. Further analysis showed that low-risk patients were characterized by particularly distinctive prevalence of *FGFR3* (17.03% vs. 6.67%, $p < 0.01$) and *POLE* alterations (7.97% vs. 2.50%, $p < 0.05$), and enrichment of immune infiltrated cells (including CD8+ T cells, CD4+ naïve T cells, follicular helper T cells, Tregs, and myeloid dendritic cells). RNA-seq data in our local cohort supported the findings in the differentially expressed genes (DEGs) between tumor and normal tissue samples, and the difference in TME between high-risk and low-risk groups. Additionally, CRG signature score plus *FGFR3* status divided BC patients into four molecular subtypes, with distinct prognosis, TME, and transcriptomic profiling of immune checkpoint genes. Of note, CRG signature score plus *FGFR3* status could successfully distinguish BC patients who have a higher possibility of response to immunotherapy or chemotherapy drugs.

Conclusions: The CRG signature is a potent prognostic model for BC patients, and in combination with *FGFR3* alterations, it had more practical capacity in the prediction of chemotherapy and immunotherapy response, helping guide clinical decision-making.

KEYWORDS

bladder carcinoma, cell cycle checkpoints, prognostic signature, nomogram, *FGFR3*, TME, chemotherapy, immunotherapeutic treatment response

Introduction

Cell cycle checkpoint-related genes (CRGs) play pivotal roles in cell cycle progression (CCP), ensuring and control regulating cell cycle events (1). Generally, in eukaryotic cells, the mitotic cell cycle is composed of two stages, the interphase (G1, S, and G2) and the mitotic (M) phase. The gap phases of G1-to-S (2), S-to-G2 (3), and G2-to-M (4), likely as decision windows, can determine cell cycle entry and progression. In cancer cells, some CRGs preventing DNA damage are usually compromised, contributing to genetic alterations and genomic instability (5), but those CRGs involved in DNA replication stress are scarcely altered to endure the replication stress (6). On the other hand, cancer cells could potentiate DNA replication stress through transcriptional regulation of CRGs (7). Overall, CRGs and CRG-related signaling pathways play a key role in regulating the phase transitions, CCP, and cell cycle entry and exit in cancer cells (8).

In previous studies, it has been revealed that aberrantly expressed CRGs might be an essential prerequisite for cells to become cancerous, leading to tumor development and progression. For instance, CRG ataxia telangiectasia mutated (*ATM*) plays a core role in responding to DNA damage and stimulating DNA repair signaling pathways, and its absence is highly prone to giving rise to carcinogenesis (9). Of note, its downregulation or inactivation is associated with the highly accumulated genomic aberrations, which is one of the hallmarks of cancer (10). Ataxia telangiectasia and Rad3-related (*ATR*), another CRG encoding protein kinase that regulates DNA damage response (DDR), is correlated with the polarization of M2 tumor-associated macrophages, lymph node metastasis, and poor prognosis of patients with nasopharyngeal carcinoma (11). The abnormal expression of CRGs has been found to be associated with the development and progression of multiple kinds of cancers, including melanoma (12), lung cancer (13), colorectal cancer (14), and hepatocellular carcinoma (15). A growing body of evidence has found that the dysregulation of CRGs could render cells to be cancerous and promote cancer cell proliferation, but most studies only disclose the role of a single CRG in cell cycle, tumor carcinogenesis, and progression. Currently, the role of integrated CRGs representing checkpoint mechanisms in the regulation of cell cycle in tumor carcinogenesis and progression remains to be fully delineated.

Previous studies have already expounded that dysregulation of CRGs is correlated with increased genomic instability and malignant progression in bladder carcinoma (BC) patients (16–18), indicating that there is a great potential of CRGs to become prognostic or targeted biomarkers for BC patients. BC generally presents as non-muscle-invasive bladder cancer (NMIBC), muscle-invasive bladder cancer (MIBC), or metastatic BC, of which the MIBC subtype has a relatively worse prognosis and poor treatment responses (19). Moreover, BC is a molecularly heterogeneous cancer with divergent clinical outcomes (20). The heterogeneity of tumor is always a huge challenge for cancer management and could reduce the efficacy of molecularly targeted therapies; therefore, the dissection of molecular signatures is urgently needed. Based on transcriptomic profiling of CRGs, a novel signature was constructed in the present study with good performance in prognosis prediction and that could function as a biomarker for treatment response. Overall, this study was of guiding significance in the clinical management of BC patients and promoting precision treatment.

Materials and methods

Data acquisition

In the current study, RNA-seq data (TPM: transcripts per million) and related clinical features of BC patients involved in the TCGA-BC cohort were collected (https://www.cbioportal.org/) as the training cohort (BC samples with no available RNA-seq data or survival information were excluded in subsequent analyses). The transcriptional profiles together with clinical features of GSE13507 (including 62 MIBC and 103 NMIBC patients), GSE31684 (including 79 MIBC and 14 NMIBC patients), and GSE32548 (including 131 BC patients; the muscle-invasive status was uncertain) were downloaded, as three independent validation groups, from GEO (https://www.ncbi.nlm.nih.gov/geo/). The tumor and normal tissue samples from the TCGA, GSE133624, GSE188715, and GSE13507 cohorts were retrieved to conduct the differentially expressed gene (DEG) analysis. The RNA-seq data were normalized by $Log_2(x+0.001)$. Cell cycle checkpoint gene sets were obtained from the database of Gene Ontology (GO), Biological Process (http://geneontology.org/), and Reactome (https://reactome.org/). The term "cell cycle checkpoint" was used for the acquisition of CRGs. After merging, a total of 464 CRGs were included in the union set, which were then selected for the further processes of establishing a prognostic signature.

Identification of the prognostic CRG signature

In order to investigate whether transcriptomic characterization was associated with prognosis of BC patients, the unsupervised hierarchical clustering analysis was conducted by using the package "Fastcluster", dividing BC patients into different clusters. The principal component analysis (PCA) was performed *via* the "ggbiplot" package, further revealing the distinction between clusters. The Kaplan–Meier curve analysis showed the overall survival (OS) of patients between clusters. Subsequently, the univariate Cox proportional hazard regression analysis, by using the packages "rms" and "survival", was conducted to classify the relationship of OS and the expression of each CRG in the TCGA-BC cohort. The least absolute shrinkage and selection operator (LASSO) and multivariate Cox proportional hazard regression analyses were used to construct a prognostic CRG signature *via* the "glmnet" package. Subsequently, a risk formula was established, and the CRG score was generated for each BC patient with the following formula: CRG score = expression value of gene 1 × C_1 + expression value of gene 2 × C_2 + … + expression value of gene x × C_x, where C_x is the coefficient of gene x. The optimal CRG score was adapted as the cutoff value by using the package "maxstat" to divide BC patients into high-risk and low-risk groups, while the same method was utilized in the validation groups. The value of area under the receiver operating characteristic (ROC) curve (AUC) revealed the prognostic performance of specificity and sensitivity. All analyses were also applied in the validation groups.

RNA sequencing in the local BC cohort

Tumor and matched normal tissues were collected from 11 MIBC patients in our local cohort to perform RNA-seq. This study was approved by the ethics committee of the Chinese PLA General Hospital (S2019–302-01), and all enrolled patients have signed the informed consent. The total RNA of each sample was collected using a FastPure® Cell/Tissue Total RNA Isolation Kit V2 (Vazyme, Jiangsu, China), and its concentration and RNA Integrity Number (RIN) were determined by using Qubit (Thermo Fisher Scientific, MA, United States) and an Agilent 2100 bioanalyzer (Agilent Technologies, CA, United States), respectively. One sample of normal tissue failed quality control and then was discarded. Library construction was conducted using the NEBNext® Ultra™ RNA Library Prep Kit for Illumina® Kit (NEB, MA, United States) and finally sequenced on the Illumina Novaseq-6000 system (Illumina, MA, United States).

Construction of the predictive nomogram

The univariate and multivariate Cox proportional hazard regression analyses, by using the packages "rms" and "survival", were conducted to explore whether the CRG signature was an independent prognostic factor. Furthermore, the OS-related clinical features were selected for the construction of a CRG signature-based nomogram. The value of AUC was used to

evaluate the performance of a novel constructed nomogram in prognosis prediction, and the calibration plots were built to perform the consistency between actual OS and predicted OS by using the package "rms".

Functional enrichment analysis

The Pearson correlation analysis was conducted to screen out the CRG score-associated genes by the cutoff criteria of | Pearson Correlation Coefficient| > 0.4 and $p < 0.05$, and the heatmap showing the expression of the identified genes was drawn by using the package "pheatmap". The Gene Ontology (GO) and Kyoto Encyclopedia of Genes and Genomes (KEGG) pathway enrichment analyses were conducted based on the expression of CRG score-associated genes.

Tumor microenvironment analysis

The stromal score and immune score could predict the infiltration levels of stromal and immune cells, respectively. Moreover, the ESTIMATE (Estimation of STromal and Immune cells in MAlignant Tumor tissues using Expression data) algorithm was used to determine the tumor purity in tumor tissues (21). The CIBERSORT (Cell type Identification By Estimating Relative Subsets Of known RNA Transcripts) algorithm was a widely used method to characterize the tumor-infiltrated lymphocytes (TILs) inside tumor tissues based on the gene expression profile (22); thus, the abundance of TILs between different groups was compared by the evaluation of CIBERSORT. The T-cell dysfunction score, exclusion score, and Tumor Immune Dysfunction and Exclusion (TIDE) score were analyzed to estimate the tumor immune escape (23). Furthermore, the expression levels of immune checkpoint genes, such as *PD-1*, *PD-L1*, *CTLA-4*, *TIM-3*, and *LAG3* (24), were investigated to explore the potential immune therapies for different BC patients.

Evaluation of therapeutic treatment responses

The data were downloaded from the Genomics of Drug Sensitivity in Cancer (GDSC, https://www.cancerrxgene.org/), a publicly available pharmacogenomic database, to predict the treatment response of chemotherapy for BC patients. The measuring parameter of half-maximal inhibitory concentration (IC_{50}) was used to estimate the chemotherapeutic treatment response and chemo-drug sensitivity between different groups *via* the "pRRophetic" package. In addition, the clinical information and transcriptomic data of 348 urothelial cancer (UC) patients involved in the IMvigor210 cohort receiving anti-PD-L1 therapy (Atezolizumab) were downloaded from the following website (25): http://research-pub.gene.com/IMvigor210CoreBiologies/. The criteria of treatment response were defined as previously described: CR: complete response, PR: partial response, SD: stable disease, PD: progressive disease. In addition, the GSE176307 dataset (26), including 86 UC patients with wild-type *FGFR3* and 17 patients with altered *FGFR3* receiving anti-PD-1 or anti-PD-L1 treatment, was further employed to explore the response prediction ability of the CRG signature for BC patients with different molecular subtypes by immunotherapeutic treatment.

Statistical analysis

The statistical data were analyzed by the Kruskal–Wallis (K-W) test, Mann–Whitney *U* test, Chi-square test, and Fisher's exact test in R studio. Cluster analysis was performed by the unsupervised hierarchical clustering. The univariate and multivariate Cox proportional hazards regression models were employed to assess the hazard ratio of the signature and clinical features. The Kaplan–Meier curve analysis along with log-rank test was conducted to evaluate the clinical outcomes of BC patients. The statistically significant difference was determined by "$p < 0.05$".

Results

The expression profiling of CRGs correlated with OS of BC patients

The design of this study was exhibited in a work flowchart (Figure 1). Initially, by way of the unsupervised hierarchical clustering analysis, BC patients from the TCGA cohort were divided into two clusters (Figure 2A), which could be separated in the Dim2 axis (Figure 2B), indicating that the expression profiling of CRGs between two clusters was noticeably distinct. Of note, BC patients in cluster 1 had worse OS (median OS: 32.02 vs. 64.80 months, $p = 0.088$, Figure 2C). The above results suggested that the expression profiling of CRGs potentially affected the clinical outcomes in BC.

Identification and validation of the prognostic CRG signature

Subsequently, a total of 398 BC patients (Table 1) were selected into the univariate Cox proportional hazard regression analysis to investigate the relationship between OS and the expression of 464 CRGs (Supplementary Table 1), and eventually, expression levels of 52 CRGs were significantly correlated with the OS of BC patients (Supplementary

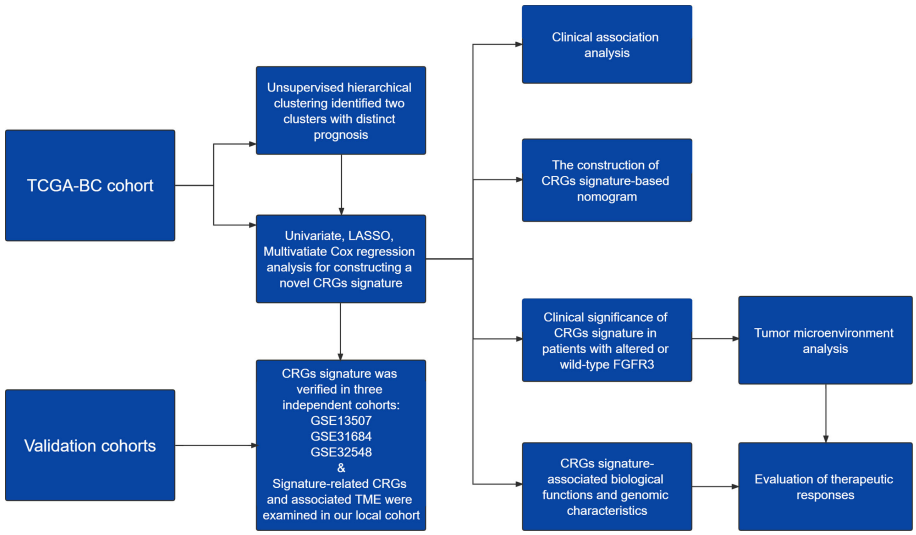


FIGURE 1
A work flowchart of constructing a novel cell cycle checkpoint gene (CRG) signature, with predictive abilities for prognosis and treatment response in BC.

Table 2). Subsequently, the LASSO and multivariate Cox proportional hazard regression analyses determined a novel prognostic CRG signature, consisting of 23 CRGs (Figure 2D, Table 2). The scatterplot demonstrated the distribution of CRG score and the corresponding survival status of BC patients in the training group, in which BC patients were divided into high-risk and low-risk groups (Figure 2E). It was identified that BC patients in the high-risk group had a significantly worse OS than those in the low-risk group (median OS: 13.64 vs. 104.65 months, $p < 0.0001$, Figure 2F). The AUC values of the CRG signature for predicting OS at 1, 2, 3, 4, and 5 years were 0.78, 0.75, 0.76, 0.76, and 0.80, respectively (Figure 2G), indicating good specificity and sensitivity of the CRG signature in predicting the prognosis of BC patients.

Three additional independent cohorts, namely, GSE13507, GSE31684, and GSE32548, were further employed to validate the predictive ability of the prognostic CRG signature (Figures 3A–F). In each validation cohort, the CRG signature had good risk stratification, and a higher CRG score indicated a significantly shorter OS (median OS: 70.73 vs. 98.00 months in GSE13507, $p = 0.0320$; 17.02 months vs. not reached in GSE31684, $p = 0.0017$; not reached vs. not reached in GSE32548, $p = 0.0019$, Figures 3A, C, E). The AUC values for predicting OS at 1, 2, 3, 4, and 5 years were 0.64, 0.64, 0.64, 0.63, and 0.61 in GSE13507; 0.64, 0.64, 0.64, 0.66, and 0.68 in GSE31684; 0.79, 0.74, 0.71, 0.67, and 0.69 in GSE32548, respectively (Figures 3B, D, F). Additionally, MIBC patients had significantly higher CRG scores compared with the NMIBC patients in both GSE13507 and GSE31684 datasets ($p < 0.05$, Figures 3G, H), suggesting the potential capability of the CRG signature in differentiating NMIBC and MIBC.

Clinical association of the prognostic CRG signature

Underlying the CRG signature, a significantly higher proportion of female patients as well as patients diagnosed at age over 68.5 years old were observed in the high-risk group ($p < 0.05$, Figure 4A). Moreover, there was also a significantly increased proportion of BC patients with advanced T (tumor stage), N (lymph node status), M (metastasis), and clinical stages ($p < 0.05$) in the high-risk group. Overall, it was demonstrated that a higher CRG score indicated advanced T, N, M, and/or clinical stages. In addition, stratification by age, gender, TNM, or clinical stages in the TCGA cohort further revealed that the CRG signature had a good predictive prognosis ability, and the higher CRG score was invariably correlated with worse survival (Figure 4B).

Construction of a nomogram based on the prognostic CRG signature

Apparently, the CRG signature was the most robust risk factor, by comparison with classical clinical features (Figure 5A), and it was the only independent prognostic factor for BC patients ($p < 0.01$, Figure 5B). Subsequently, the CRG signature-based prognostic nomogram was constructed in combination with several clinical parameters together, including diagnosis age, and T, N, and M stage (Figure 5C). The C-index of the novel constructed prognostic nomogram was 0.76, with 95% confidence interval ranging from 0.70 to 0.81. In addition, the AUC values of the nomogram for predicting OS at

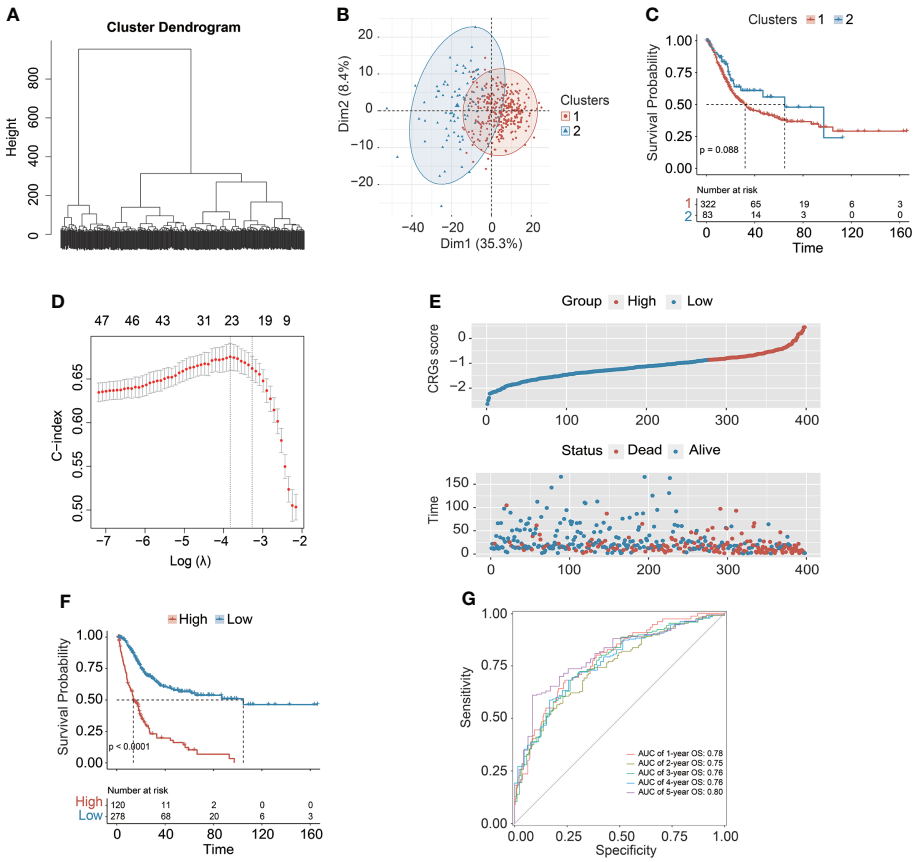


FIGURE 2
The transcriptomic profiling of cell cycle checkpoint-related genes (CRGs) was correlated with overall survival (OS) of BC patients from the TCGA-BC cohort. **(A)** The unsupervised hierarchical clustering of BC patients based on the transcriptional characterization of CRGs. **(B)** The principal component analysis (PCA) showed the differentiation between clusters 1 and 2. **(C)** Kaplan–Meier curve analysis to compare OS between clusters 1 and 2. **(D)** The least absolute shrinkage and selection operator (LASSO) Cox regression analysis for construction of the prognostic CRG signature. **(E)** The scatterplot demonstrated the distribution of CRG scores corresponding to survival status of BC patients in the training cohort. **(F)** Kaplan–Meier curve analysis to compare OS between high-risk and low-risk groups. **(G)** The receiver operating characteristic curve (ROC) analysis for evaluating the ability of the CRG signature in prognosis prediction.

1, 2, 3, 4, and 5 years were 0.79, 0.81, 0.81, 0.80, and 0.85, respectively (Figure 5D), and the calibration plots exhibited good consistency between actual OS and predicted OS by the nomogram (Figures 5E–I).

Exploration of the CRG signature-related biological functions

The highly CRG score-associated genes were defined with the criteria of |Pearson Correlation Coefficient| > 0.4 and $p < 0.05$, and a total of 252 and 159 genes were found to be positively or negatively correlated with CRG score, respectively (Figure 6A). The extracellular matrix (ECM)-related biological functions, focal adhesion, regulation of actin cytoskeleton, and MAPK signaling pathway were mainly enriched (Figures 6B, C).

Genomic characteristics and TME underlying the CRG signature

The genomic alteration profiles, respectively in high-risk and low-risk groups, showed that the most prevalently altered genes were distinct (Figures 7A, B). Through statistical analysis, among the prevalently altered genes between high-risk and low-risk groups (the altered genes with prevalence ≤ 5.00% in both high-risk and low-risk groups were excluded), there was a total of 46 altered genes with higher alteration frequencies enriched in the low-risk group, including *RYR2* (frequency: 20.29% vs. 11.67%, $p < 0.05$), *FAT4* (frequency: 17.75% vs. 9.17%, $p < 0.05$), and *FGFR3* (frequency: 17.03% vs. 6.67%, $p < 0.01$), whereas the high-risk group had a significantly higher prevalence of only 5 altered genes, namely, *RB1* (25.00% vs. 15.94%, $p < 0.05$), *FBXW7* (12.50% vs. 5.80%, $p < 0.05$), *NFE2L2*

10.3389/fonc.2022.915662

TABLE 1 Clinical features of 398 involved BC patients from the TCGA cohort.

Clinical Feature		Number (%)
Total		398 (100%)
Gender		
	Male	293 (73.62%)
	Female	105 (26.38%)
Age	Median (range)	68.5 (34-90)
Histological subtypes		
	MIBC	398 (100%)
Histological grading		
	High	377 (94.72%)
	Low	18 (4.52%)
T stage		
	T0	1 (0.25%)
	T1	3 (0.75%)
	T2	114 (28.64%)
	T3	190 (47.74%)
	T4	58 (14.57%)
N stage		
	N0	230 (57.79%)
	N1	46 (11.56%)
	N2	74 (18.59%)
	N3	7 (1.76%)
M stage		
	M0	189 (47.49%)
	M1	10 (2.51%)
Clinical stage		
	I	2 (0.50%)
	II	125 (31.41%)
	III	138 (34.67%)
	IV	131 (32.91%)

BC, bladder carcinoma; TCGA, The Cancer Genome Atlas; MIBC, muscle-invasive bladder carcinoma; NMIBC, non-muscle-invasive bladder carcinoma.

(10.83% vs. 3.99%, $p < 0.05$), *ASAP2* (5.83% vs. 1.45%, $p < 0.05$), and *PCSK6* (5.83% vs. 1.09%, $p < 0.05$) (Figure 7C). Notably, only one DDR-related gene *POLE* was found with higher alteration frequency in the low-risk group (frequency: 7.97% vs. 2.50%, $p < 0.05$, Figure 7D). Of note, BC patients with altered *POLE* had a trend of better clinical outcomes (median OS: 33.14 months vs. not reached, $p = 0.13$, Figure 7E).

Subsequently, the molecular characterization of TME was presented, demonstrating that the high-risk group had a significantly increased stromal score and ESTIMATE score (Figure 8A). Moreover, the high-risk group also had a significantly higher T-cell exclusion score and TIDE score (Figure 8B). Additionally, more plasma B cells, CD8+ T cells, CD4+ naïve T cells, follicular helper T cells, Tregs, and activated myeloid dendritic cells were significantly more enriched in the low-risk group, whereas the high-risk group only had significantly higher infiltration levels of macrophage M0 and M2 (Figure 8C).

Exploration of CRG signature or related genes in the local BC cohort

It was found that the DEGs between tumor and normal tissue samples significantly varied in public datasets and our local cohort, and remarkably, only 7 of the 23 discovered CRGs exhibited significant differences between tumor and normal tissue samples across the TCGA, GSE133624, GSE188715, and GSE13507 cohorts (Figure 9A). Among which, *SLC25A15*, *RAD9A*, *PRF19*, *THOC1*, and *TIPIN* were significantly overexpressed in tumor tissues in both the TCGA (Figure 9B) and our local cohorts (Figure 9C). *PPP2CB* and *FBXO31* were upregulated in normal tissues in the TCGA cohort, but our local samples did not differ significantly. Limited by the sample size, there was no statistically significant difference in TILs between high-risk and low-risk groups in our local cohort, whereas, a consistent trend of more CD8+ T cells, follicular helper T cells, Tregs, and activated dendritic cells were presented in the low-risk group and relatively more macrophage M0 and M2 were presented in the high-risk group in our local cohort (Figure 9D). In our local cohort, the ESTIMATE score was found to be relatively higher but not statistically significant in the high-risk group (Figure 9E), but notably, high-risk individuals in our local BC cohort had significantly higher TIDE scores (Figure 9F).

Clinical significance of CRG signature in BC patients with altered *FGFR3*

Regarding the CRG score and *FGFR3* alteration status, BC patients were further divided into four different risk groups. It could be apparently seen that high-risk patients with wild-type *FGFR3* had the highest CRG scores ($p < 0.0001$, Figure 10A). Moreover, patients with wild-type *FGFR3* had significantly higher CRG scores than those with *FGFR3* alterations (*FGFR3*mt-high vs. *FGFR3*wt-high and *FGFR3*mt-low vs. *FGFR3*wt-low, $p < 0.0001$). Expectedly, high-risk patients with wild-type *FGFR3* had the significantly shortest OS (Figure 10B), further demonstrating the robust ability of CRG signature in prognosis prediction.

Immunity of BC patients with altered *FGFR3* underlying the CRG signature

Compared to other groups, low-risk patients with altered *FGFR3* had the significantly lowest stromal score, immune score, ESTIMATE score, and TIDE score (Figures 10C, D), as well as a relatively higher enrichment of plasma B cells, activated NK cells, CD8+ T cells, and follicular helper T cells (Figure 10E). However, among the other three groups, there was no statistically significant difference in ESTIMATE and TIDE

TABLE 2 The identified 23 genes involved in the prognostic CRG signature.

Gene Name	HR	95% CI	Coefficient	*p*-value
MMAB	1.3228	1.0520–1.6632	0.1739	0.0167
NDEL1	1.3404	1.0641–1.6884	0.1145	0.0128
SLC25A15	1.2738	1.0826–1.4989	0.0077	0.0035
PPP2CB	1.3489	1.0809–1.6834	0.0465	0.0081
PSMA7	1.3728	1.0652–1.7692	0.0210	0.0144
PSMB5	1.6366	1.2327–2.1729	0.0355	0.0007
REXO2	1.4077	1.1338–1.7479	0.0097	0.0020
ARID3A	1.1219	1.0233–1.2299	0.0387	0.0142
CUL4A	1.2793	1.0154–1.6119	0.0648	0.0367
FBXO31	1.3312	1.0623–1.6683	0.0579	0.0130
PLK2	1.1412	1.0325–1.2612	0.0086	0.0097
PRPF19	1.5588	1.1636–2.0883	0.4539	0.0029
RGCC	1.2245	1.0580–1.4172	0.0640	0.0066
TIPIN	1.3456	1.0983–1.6486	0.0560	0.0042
ANAPC4	0.6693	0.5173–0.8660	−0.1681	0.0023
B9D2	0.8078	0.6573–0.9929	−0.0190	0.0426
PSMB10	0.7598	0.6442–0.8962	−0.1493	0.0011
PSMB8	0.8695	0.7724–0.9788	−0.0427	0.0207
RAD9A	0.6603	0.5322–0.8191	−0.1605	0.0002
CHMP4C	0.7979	0.7107–0.8959	−0.1641	0.0001
DDX39B	0.6946	0.5118–0.9427	−0.4224	0.0194
FBXO6	0.7865	0.6592–0.9382	−0.0840	0.0076
THOC1	0.7686	0.6075–0.9724	−0.0270	0.0283

CRGs, checkpoint-related genes; HR, hazard ratio; CI, confidence interval.

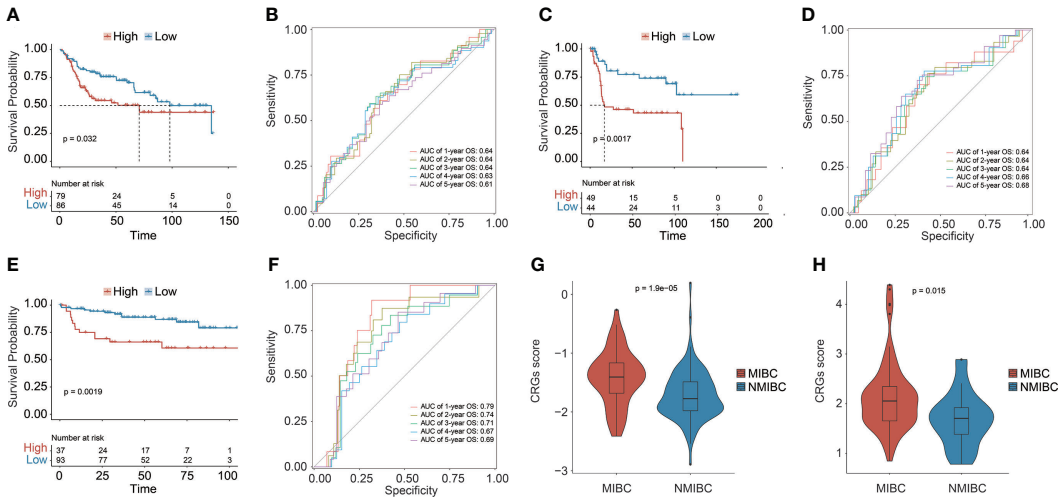


FIGURE 3
The prognostic CRG signature was validated in three independent datasets: GSE13507, GSE31684, and GSE32548. Kaplan–Meier curve analysis to compare OS between high-risk and low-risk groups in GSE13507 **(A)**, GSE31684 **(C)**, and GSE32548 **(E)**. The receiver operating characteristic curve (ROC) analysis for validating the ability of CRG signature in prognosis prediction in GSE13507 **(B)**, GSE31684 **(D)**, and GSE32548 **(F)**. Comparison analysis of the CRG scores between MIBC and NMIBC patients in GSE13507 **(G)** and GSE31684 **(H)**.

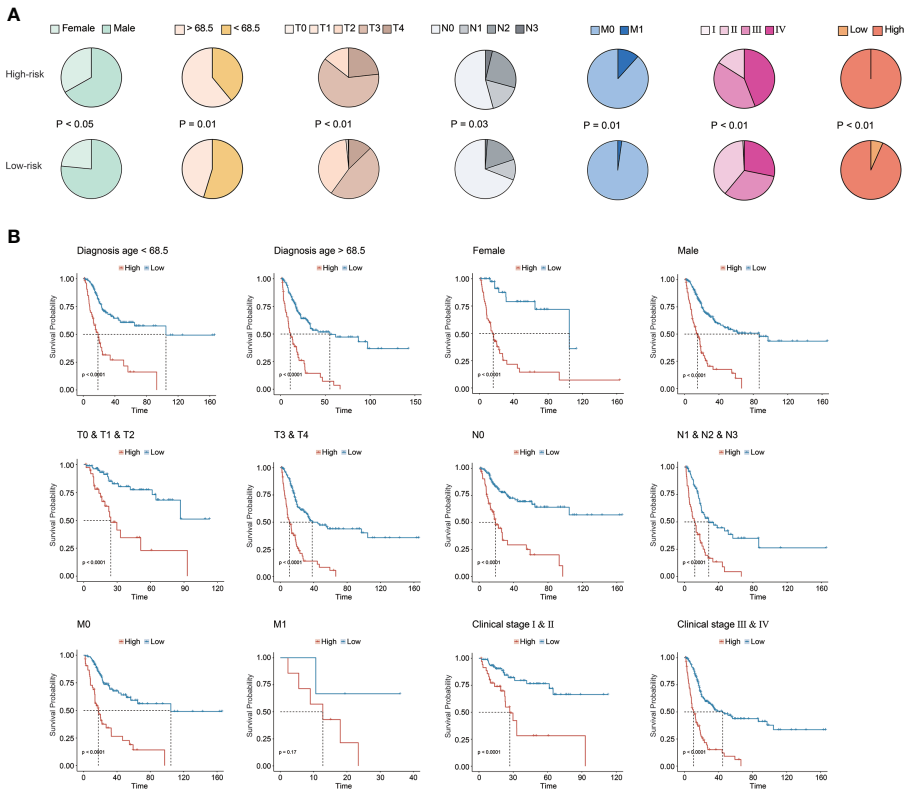


FIGURE 4
Clinical association of the CRG signature. **(A)** The association analysis between the CRG signature and clinical features in the TCGA-BC cohort. **(B)** The prognostic CRG signature predicted prognosis for BC patients with different clinical features in the TCGA-BC cohort.

scores (Figures 10C, D), except that low-risk patients with wild-type *FGFR3* had a significantly lower TIDE score than high-risk patients with wild-type *FGFR3* ($p < 0.05$, Figure 10D). Remarkably, the distribution of TILs in high-risk patients with altered *FGFR3* was similar to that of BC patients with wild-type *FGFR3*, regardless of whether they had a high or low CRG score (Figure 10E). Interestingly, low-risk patients with altered *FGFR3* had a lower expression of immune checkpoint genes, including *PD-L1*, *CTLA4*, *TIM3*, LAG3, *PD-1*, *CD27*, *CD47*, and *IDO1* ($p < 0.05$); on the contrary, high-risk patients with altered *FGFR3* had a higher expression of *TIM3* and *CD47* ($p < 0.05$), whereas the expression level of *PD-L1* in BC patients with altered *FGFR3* was quite low (Figure 10F).

Estimate of chemotherapeutic treatment response

As investigated for commonly used chemotherapeutic drugs for BC patients (including cisplatin, docetaxel, paclitaxel, methotrexate, and doxorubicin), it was found that IC_{50} values for the response prediction of chemotherapeutic treatment by cisplatin, docetaxel, paclitaxel, methotrexate, or doxorubicin significantly differed between patients with distinctive molecular subtypes (Figures 11A–E). Regardless of BC patients (whether *FGFR3* was altered or not), the higher CRG score indicated the relatively higher sensitivity to cisplatin and docetaxel (Figures 11A, B). Moreover, compared to low-risk BC patients with altered *FGFR3*, those with wild-type *FGFR3* seemed to be more sensitive to paclitaxel (Figure 11C). Meanwhile, low-risk patients with altered *FGFR3* had the highest sensitivity to methotrexate (Figure 11D). For patients with wild-type *FGFR3*, those in the high-risk group were more sensitive to doxorubicin (Figure 11E).

Prediction of immunotherapeutic treatment response

The CRG signature further exhibited a robust prognosis prediction ability, and CRG score was negatively correlated with the survival of UC patients treated with PD-1/L1 blockades (median OS in the IMvigor210 cohort: 7.92 months vs. 10.58 months, $p = 0.028$, Figure 12A; GSE176307 dataset: 4.57 months vs. 13.00

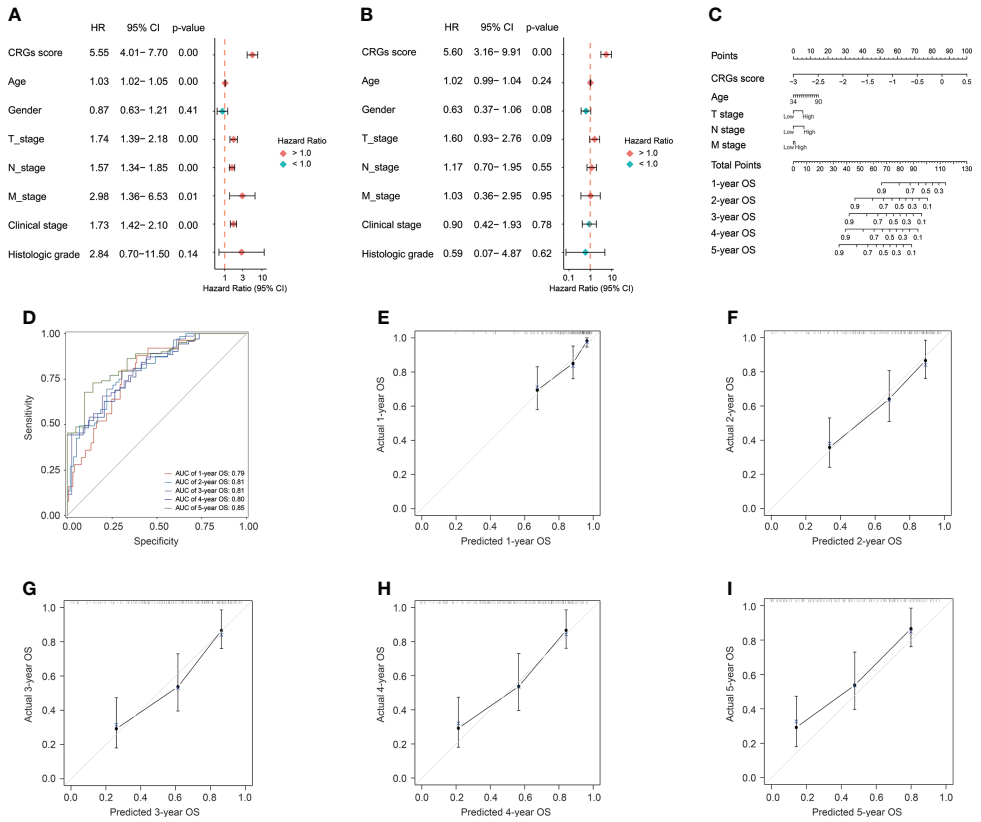


FIGURE 5
The construction of the CRG signature-based prognostic nomogram. The univariate **(A)** and multivariate **(B)** Cox regression analyses for the CRG signature and clinical features. **(C)** The constructed nomogram for the survival prediction of BC patients. **(D)** The receiver operating characteristic curve (ROC) analysis for evaluating the ability of novel constructed nomogram in prognosis prediction. The calibration curve analysis exhibited the consistency between actual OS and predicted OS by the nomogram at 1 **(E)**, 2 **(F)**, 3 **(G)**, 4 **(H)**, and 5 years **(I)**.

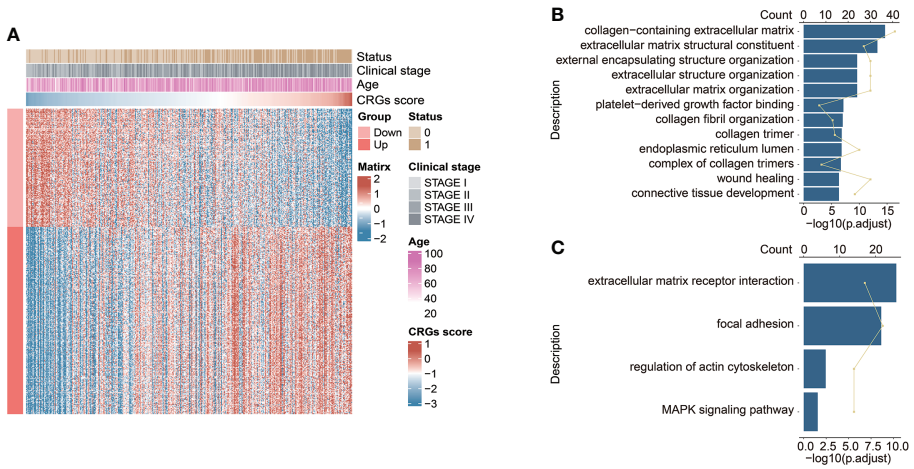


FIGURE 6
The functional enrichment analysis underlying the CRG signature. **(A)** The heatmap exhibited the expression levels of CRG signature-associated genes positively and negatively correlated with CRG score (|Pearson Correlation Coefficient| > 0.4, $p < 0.05$). The GO enrichment analysis **(B)** and KEGG pathway enrichment analysis **(C)** of the identified CRG signature-associated genes.

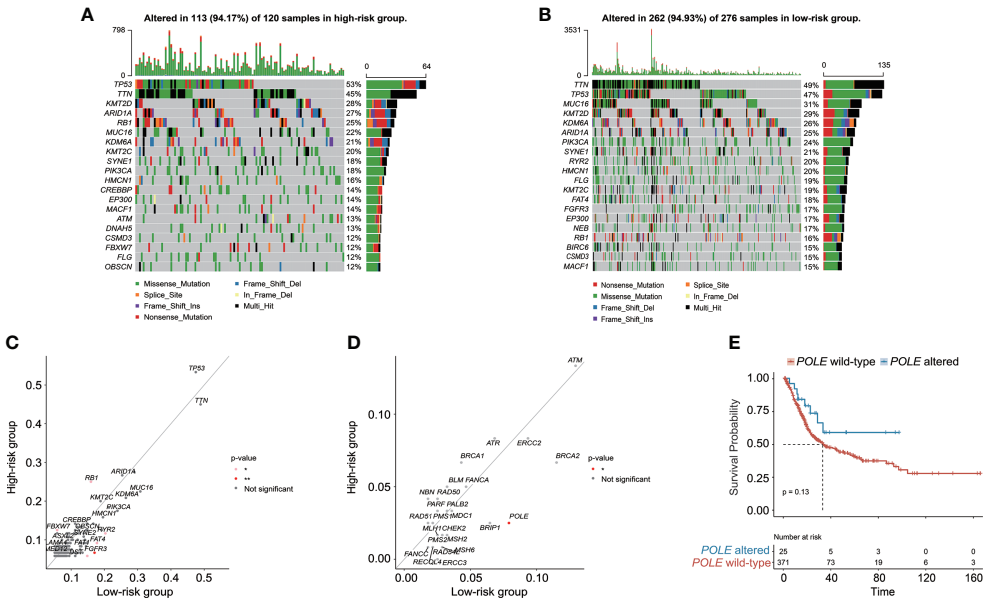


FIGURE 7
The characteristics of genomic alterations between high-risk and low-risk patients from the TCGA-BC cohort. The oncoprint plots exhibited the genomic alteration profile of the high-risk group **(A)** and low-risk group **(B)**. **(C)** The genomic alteration enrichment analysis demonstrated the prevalently altered genes between high-risk and low-risk groups. **(D)** The alteration enrichment analysis of DNA damage response (DDR) genes between high-risk and low-risk groups. **(E)** Kaplan–Meier curve analysis for BC patients with or without *POLE* alterations.

months, $p = 0.041$, Figure 12B). When exploring the role of the CRG signature predicting the response of immunotherapeutic treatment in the IMvigor210 cohort, no statistically significant difference in CRG score was observed between patients who responded to PD-1/L1 blockades or not (CR/PR vs. SD/PD patients, Figure 12C). Regarding patients with altered *FGFR3* in the GSE176307 dataset, the CRG scores were also equivalent between CR/PR and SD/PD patients (Figure 12D). For patients with wild-type *FGFR3* in the GSE176307 dataset, it was notably found that patients who completely/partially responded to immunotherapy have slight lower CRG scores than those with stable/progressive diseases ($p = 0.097$, Figure 12E).

Discussion

Bladder cancer, according to the latest cancer statistics worldwide, remains to be one of the most prevalent cancers, with approximately 550,000 new cases annually (27). Recently, next-generation sequencing technology has led to the significant advances in the research field of bladder cancer (28), discovering a number of genomic, transcriptomic, and proteomic biomarkers for predicting diagnosis or prognosis of patients, as well as promoting clinically favorable targeted therapeutics and effective immune therapies. Furthermore, the newly developed methods have been widely applied to explore the tumor immune microenvironment in various cancers, which expanded the repertoire of precision medicine, especially immunotherapy (29). In the present study, it was the first time to investigate the integrative transcriptional characterization of cell cycle checkpoint genes in BC progression, and eventually a novel CRG signature and CRG-based nomogram were established, with remarkably robust and stable capacity in prognosis prediction. The clinical association analysis underlying the CRG signature further disclosed that the high-risk group had more patients who were female, diagnosed at older age, and with more aggressive diseases. In addition, the molecular characterization, including functional differentiation analysis, genomic alteration profiling, and TME, between different subgroups promoted the potential strategies of precision treatment for BC patients.

The early retrospective study proposed a risk model, namely, CCP score, based on the expression signature of 31 CCP genes, which was created to predict the aggressiveness of prostate cancer (30). Afterwards, this 31-CCP gene expression signature exhibited significant prognostic values in various cancers, such as ductal carcinoma *in situ* of the breast (31), clear cell renal cell carcinoma (32), lung cancer (33), and bladder cancer (34). According to the study of bladder cancer, an optimized 12-CCP signature was established, of which the AUC values in predicting patient progression (non-progressor vs. progressor) were 0.70 in the Lindgren cohort and 0.68 in the CNUH cohort. In contrast, it seemed that the CRG signature might outperform the CCP score in prognosis prediction, with

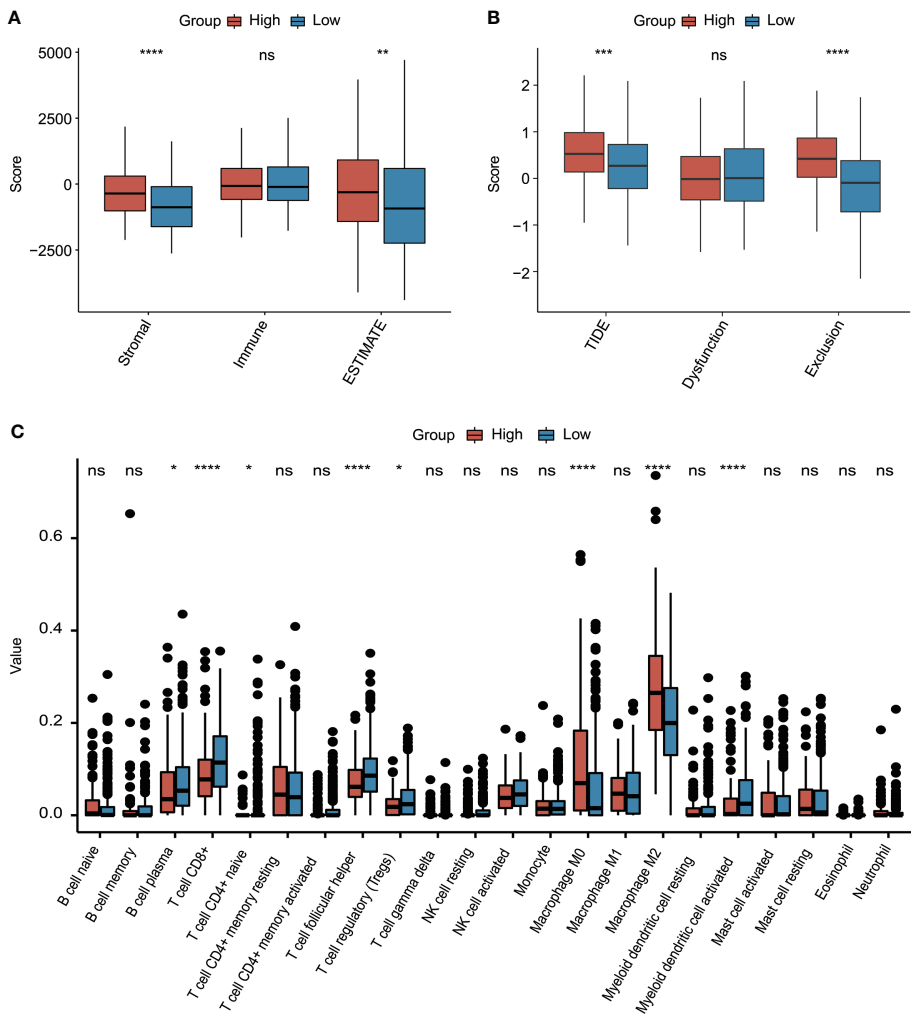


FIGURE 8
The evaluation of tumor environment between high-risk and low-risk groups. **(A)** Comparison of stromal, immune, and ESTIMATE scores between high-risk and low-risk groups. **(B)** Comparison of T-cell dysfunction, exclusion, and TIDE scores between high-risk and low-risk groups. **(C)** The evaluation of 22 tumor-infiltrated lymphocytes between high-risk and low-risk groups. *p < 0.05, **p < 0.01, ***p < 0.001, ****p < 0.0001, ns represented "not significant".

the AUC values at 1, 2, 3, 4, and 5 years for OS all beyond 0.75. Furthermore, recent studies have revealed that the regulation of CCP, such as the initiation of replication, the overall rate of replication, and the recovery and resumption of replication forks, was strictly controlled in cancer cells by checkpoints (35–38). In brief, in cancer cells, cell cycle checkpoints could control CCP and further regulate the cancer cell divisions, unless uncontrolled CCP can drive more mutations and genomic instabilities causing the existence of cell cycle and cell apoptosis.

In past decades, a large body of studies focused on the regulation of CCP in tumor progression (39), in which the important role of checkpoints regulating the entire cell cycle processing was often neglected. In the present study, a total of 52 CRGs in cell cycle were found to be significantly correlated with the clinical outcomes of BC patients; meanwhile, the novel CRG signature was constructed as a prognostic model consisting of further selected 23 CRGs. Among these 23 selected CRGs, the expression of *PPP2CB* has already been proven to be involved in promoting BC cell proliferation and migration (40). The expression of checkpoint CUL4A could mediate the degradation of BECN1 protein to alleviate cell autophagy and enhance the growth of BC (41). The overexpressed *PLK2* was detected in BC, and urinary PLK2 protein level was highly correlated with bladder transitional cell carcinoma (42). The suppressed expression of *THOC1* could mediate BC cell apoptosis (43). Except for the in-depth insight into the biological functions of the above-mentioned four CRGs, 19 other identified CRGs involved in the signature, namely,

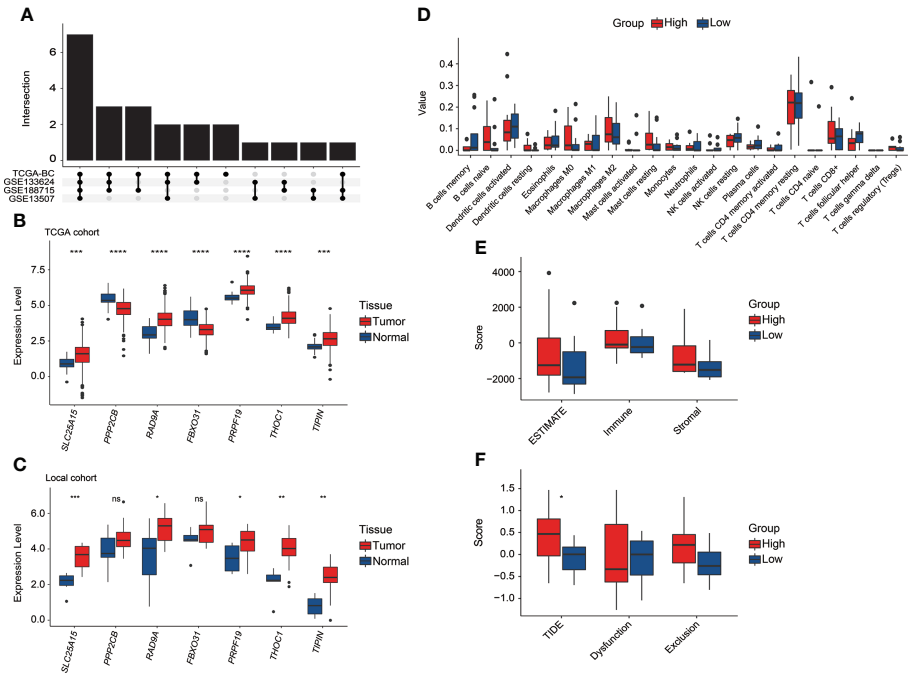


FIGURE 9
The exploration of the CRG signature and related genes in the local BC cohort. **(A)** Overlapping number of differentially expressed CRGs between tumor and normal tissue samples across the TCGA, GSE133624, GSE188715, and GSE13507 cohorts. **(B)** The comparison of seven CRG signature-related genes' expression between tumor and normal tissue samples in the TCGA cohort. **(C)** The comparison of seven CRG signature-related genes' expression between tumor and normal tissue samples in our local cohort. **(D)** The evaluation of 22 tumor-infiltrated lymphocytes between high-risk and low-risk groups in our local cohort. **(E)** Comparison of stromal, immune, and ESTIMATE scores between high-risk and low-risk groups in our local cohort. **(F)** Comparison of T-cell dysfunction, exclusion, and TIDE scores between high-risk and low-risk groups in our local cohort. *p < 0.05, **p < 0.01, ***p < 0.001, ****p < 0.0001, ns represented "not significant".

ANAPC4, *MMAB*, *B9D2*, *NDEL1*, *SLC25A15*, *PSMA7*, *PSMB10*, *PSMB5*, *PSMB8*, *RAD9A*, *REXO2*, *ARID3A*, *CHMP4C*, *DDX39B*, *FBXO31*, *FBXO6*, *PRPF19*, *RGCC*, and *TIPIN*, were first identified to play a potential role in BC progression, and their detailed functions remained enigmatic, which merited further experimental verification.

Underlying the CRG signature, correlation analysis revealed that signature-associated genes were mainly responsible for the collagen-containing ECM, and ECM-related and MAPK signaling pathways, indicating that the ECM-specific heterogeneity and related signaling pathways between different risk groups mainly caused the significant difference in OS. It has been revealed that COL1A1 protein was markedly upregulated in MIBC, which could activate the epithelial–mesenchymal transition and TGF-β signaling pathway contributing to the proliferation and invasion of bladder cancer cells (44), whereas the significantly downregulated expression of collagen type IV-α1 and α2 (COL6A1 and COL6A2) was found to promote tumor progression in both the NMIBC and MIBC tissue samples (45). Moreover, the tumor-related macrophages could secrete the type I collagen *via* activating the PI3K/AKT signaling pathway to stimulate the development of bladder cancer; meanwhile, the number of macrophages and the expression of M2 macrophage-associated genes (ARG-1, IL-10, and TGF-β) were remarkably elevated in malignant bladder tumor tissue samples (46). Furthermore, TGF-β could prompt the tumor immune escape and the resistance of immune therapy (47), which has been validated in the IMvigor210 cohort in which BC patients not responding to the therapeutic treatment of anti–PD-L1 agent (Atezolizumab) were highly correlated with the TGF-β signature in fibroblasts and commonly had fibroblast- and collagen-rich peritumoral stroma (48). In addition, a single-cell proteomic analysis further revealed the chaotic tumor-associated collagens in the TME of MIBC (49). Thus, therapeutic treatment targeting collagen-specific ECM and related signaling pathways could be a potential regimen for BC patients.

Genomic alteration analysis revealed that the high-risk group had higher prevalence of tumor suppressor genes *RB1*, *FBXW7*, and *NFE2L2*, consistent with the previous findings that the altered *RB1* (50), *FBXW7* (51), and *NFE2L2* (52) were correlated with tumor progression and worse outcomes of BC patients. However, the potential contribution of frequently altered *ASAP2* and *PCSK6* in the progression of bladder

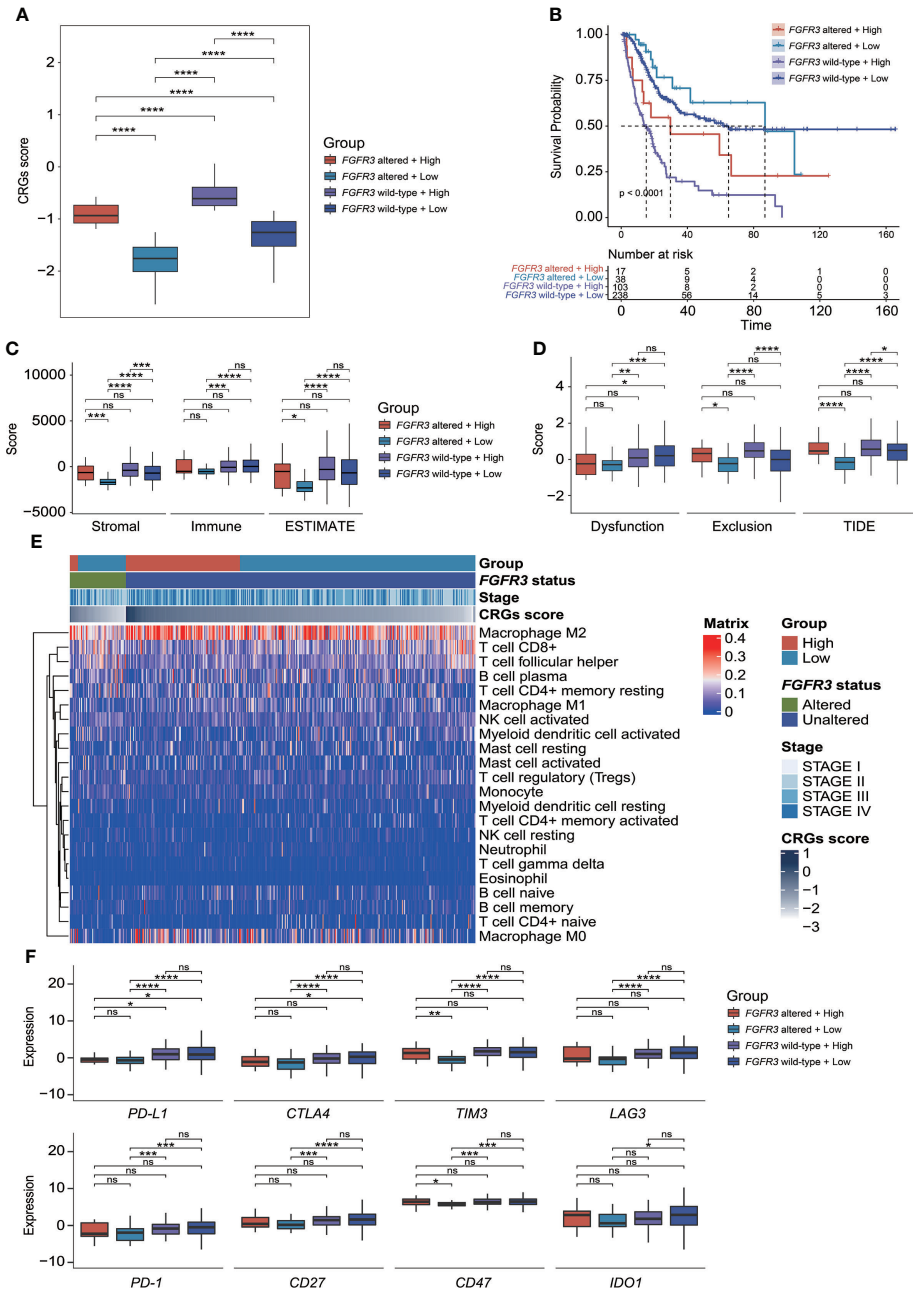


FIGURE 10
The evaluation of tumor microenvironment and immune checkpoint genes' expression for patients stratified by CRG signature plus *FGFR3* status. **(A)** Comparison of CRG score between four molecular subgroups. **(B)** Comparison of survival *via* the Kaplan–Meier curve analysis between four molecular subgroups. **(C)** Comparison of stromal, immune, and ESTIMATE scores between four molecular subgroups. **(D)** Comparison of T-cell dysfunction, exclusion, and TIDE scores between four molecular subgroups. **(E)** The heatmap exhibited infiltrated levels of 22 tumor-infiltrated lymphocytes between four molecular subgroups. **(F)** The comparison of immune checkpoint genes' expression levels between four molecular subgroups. *p < 0.05, **p < 0.01, ***p < 0.001, ****p < 0.0001, ns represented "not significant".

cancer remains unclear, needing to be further investigated. As known, the *FGFR3* alterations were mainly enriched in the luminal bladder cancer correlated with better prognosis; specifically, the low-risk group in the present study was also observed to have more patients with *FGFR3* alterations. More impressively, it was uncovered that there was a significant difference in alteration frequency of only one DDR signaling pathway-related gene—*POLE*—between high-risk and low-risk

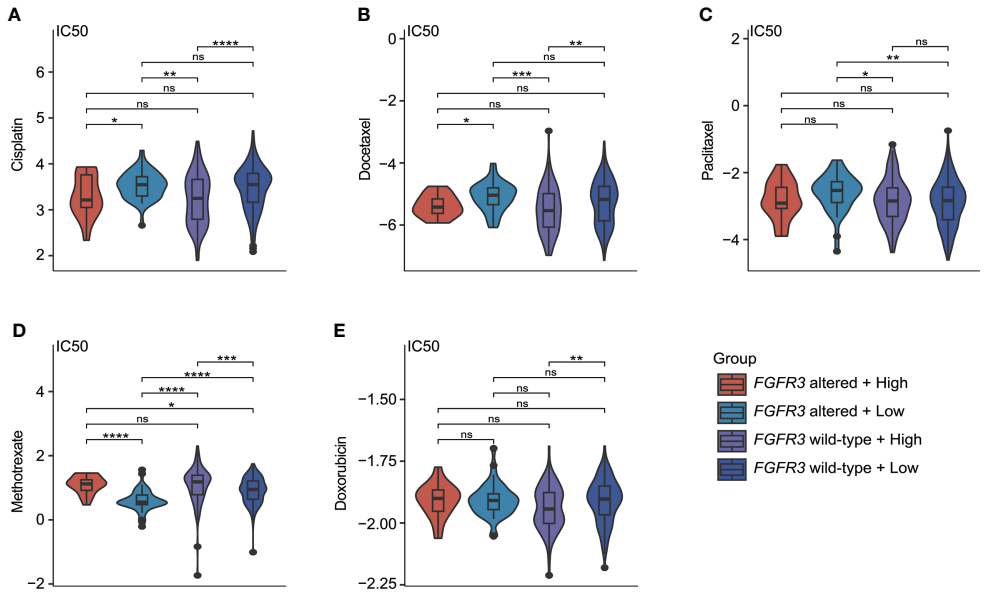


FIGURE 11
The estimate of chemotherapy treatment response *via* the GDSC database. The violin plots exhibited the IC_{50} value representing the response of chemotherapeutic treatment by cisplatin **(A)**, docetaxel **(B)**, paclitaxel **(C)**, methotrexate **(D)**, and doxorubicin **(E)** between four different molecular subgroups. *p < 0.05, **p < 0.01, ***p < 0.001, ****p < 0.0001, ns represented "not significant".

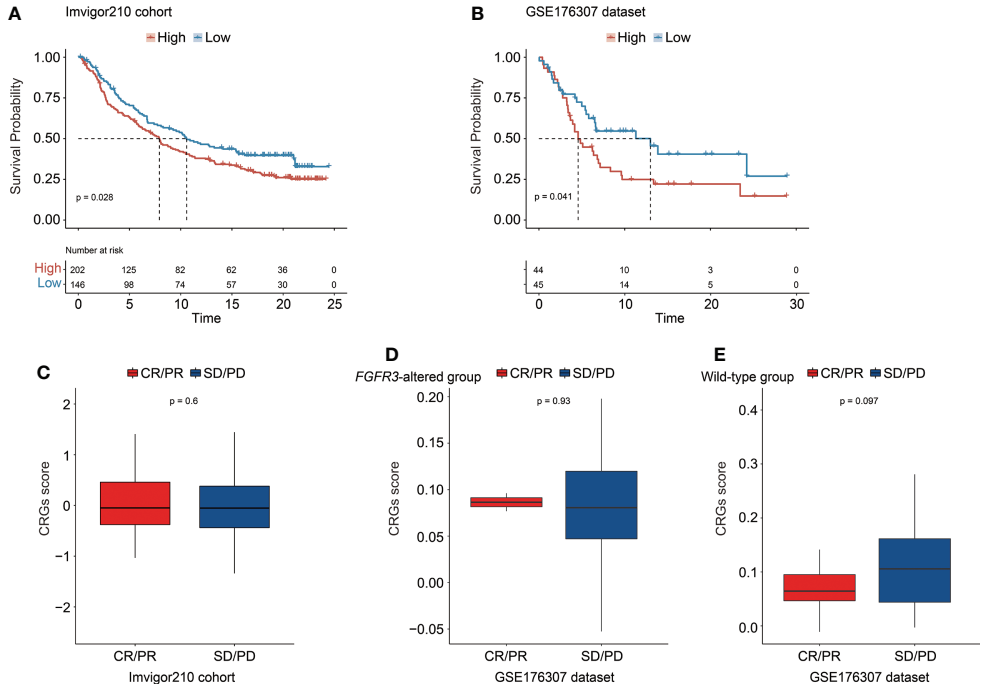


FIGURE 12
The predictive role of the CRG signature for the response of immunotherapy treatment in the IMvigor210 cohort and the GSE176307 dataset. Kaplan–Meier curve analysis to compare overall survival of patients between high-risk and low-risk groups from the IMvigor210 cohort **(A)** and the GSE176307 dataset **(B)**. Comparison of the CRG score between CR/PR and SD/PD groups in the IMvigor210 cohort **(C)** and in the groups of patients with altered *FGFR3* **(D)** and with wild-type *FGFR3* **(E)** from the GSE176307 dataset.

groups, and Kaplan–Meier analysis revealed that MIBC patients with altered *POLE* exhibited a trend of better OS. Owing to the limited number of MIBC patients presenting *POLE* alterations in the present study, this result should be highlighted and verified in the future.

Taken together, the difference in TME, including tumor purity, T-cell viability, and the proportion of TILs, between high-risk and low-risk groups was further investigated. Macrophage M0 and M2 were consistently enriched in high-risk groups, which also had a lower tumor purity expressed by the higher ESTIMATE score and a higher level of exhausted T cells indicated by the higher TIDE score. Similarly, it has been reported that tumor-associated macrophages could restrain the infiltration level of T cells in tumor tissues (53). In addition, altered *FGFR3* is highly enriched in luminal or its papillary subtypes, which have been characterized by immune-suppressive states (50). Controversially, a retrospective analysis revealed that there was no difference in immune checkpoint blockade response between patients with altered *FGFR3* and those with no altered *FGFR3* (54), and a recent study found the equivalent T-cell receptor diversity between these patients (26). Whether the status of *FGFR3* could influence the treatment response by the immune checkpoint blockade is discussed heatedly. In the present study, it was found that the discrepancy of TME between high-risk and low-risk groups among BC patients with wild-type *FGFR3* was a little small, except that low-risk patients had more activated T cells but a lower proportion of tumor-associated macrophages (especially for macrophage M0 and M2), while compared to the BC patients with wild-type *FGFR3*, high-risk patients with altered *FGFR3* had nearly similar predicted infiltrated immune cell proportions and immune responses, but only the expression levels of *TIM3* and *CD47* were equal, such that these BC patients seemed to be more sensitive to immune checkpoint inhibitors targeting TIM3 and CD47, which needed further analysis. Additionally, the low-risk BC patients with altered *FGFR3* exhibited the highest tumor purity and the most activated T cells, which were associated with better treatment responses of immunotherapies (23). However, in the present study, the expression levels of well-known immune checkpoint genes were found to be extremely low. Thus, in clinic, it was highly recommended that immunohistochemistry staining of immune checkpoint(s) should be detected first during immunotherapeutic treatment.

In addition, the different BC molecular subtypes were identified to have distinctive sensitivity to the chemotherapeutic drugs, such as cisplatin, docetaxel, paclitaxel, methotrexate, and doxorubicin, which were commonly used for BC patients (28). The CRG signature further demonstrated its predictive ability in therapeutic treatment response. Currently, cisplatin has been regarded as a typical chemotherapeutic strategy for UC patients, and it mainly functioned to induce cell cycle arrest and cell apoptosis (55, 56). Furthermore, a previous study has revealed that docetaxel could make antiproliferative and apoptotic effects on bladder cancer cells (57). In the present study, it was found that patients with a higher CRG score, regardless of *FGFR3* status, seem to be more sensitive to cisplatin or docetaxel. Although clinical benefits of paclitaxel were limited owing to patients' resistance, the failure of first-line combination treatment of cisplatin and gemcitabine for advanced and/or metastatic UC patients provided an opportunity for paclitaxel because of its apoptotic effects (58). Through the evaluation analysis of chemotherapy treatment response, it was recommended that low-risk BC patients with wild-type *FGFR3* might benefit more from paclitaxel. Additionally, the CRG signature also exerted its influence on the patients' sensitivity to methotrexate, especially suitable for low-risk BC patients with wild-type *FGFR3*; however, its applicability for BC patients in clinic was rare, which needed more verification. Doxorubicin has been proven to disturb the regulation of cell cycle and induce cell death, usually as a vital constituent of combination treatment for MIBC patients (59). Indeed, the alteration frequency of *FGFR3* in MIBC patients was relatively lower, compared with NMIBC patients (60, 61). In the present study, we further found that high-risk BC patients with wild-type *FGFR3* were likely to have higher sensitivity to doxorubicin. Collectively, the checkpoint mechanisms in the regulation of cell cycle greatly influenced the response of chemotherapeutic treatment.

The CRG signature also demonstrated its ability in predicting the response of immunotherapeutic treatment. Of note, the CRG signature exhibited better response prediction capacity for BC patients with wild-type *FGFR3*, of whom those with lower CRG score might be more sensitive to the immunotherapeutic treatment with anti-PD-1 or anti-PD-L1 drugs. Regarding patients with altered *FGFR3*, the CRG signature could not differentiate the potential CR/PR and SD/PD patients. As described before, the alteration frequency of *FGFR3* in low-grade and/or early-stage bladder tumors was evidently higher comparatively, such that the CRG signature could perform better in the response prediction of immunotherapeutic treatment for higher-grade BC patients, especially for those with wild-type *FGFR3*, while only 17 BC patients with altered *FGFR3* included in the GSE176307 dataset received immune therapy treatment hence, the ability of the CRG signature to predict the immunotherapeutic treatment response for BC patients with *FGFR3* alterations remained to be explored.

Conclusions

The present study comprehensively delineated the integrative transcriptional profiling of cell cycle checkpoint genes in the BC progression. The novel prognostic CRG signature and nomogram exhibited good performance in prognosis prediction for BC patients; furthermore, the molecular characterization underlying the CRG signature provided deep insights into key risk factors leading to the aggressive bladder cancer, promoting the development of precision medicine. The predictive role of the CRG signature in treatment response offered potential precision treatment strategies for different BC molecular subtypes.

Data availability statement

The original contributions presented in the study are included in the article/Supplementary Material. Further inquiries can be directed to the corresponding authors.

Ethics statement

The studies involving human participants were reviewed and approved by The ethics committee of the Chinese PLA General Hospital (S2019–302-01). The patients/participants provided their written informed consent to participate in this study.

Author contributions

W-WS, J-ZG, YH, and BY proposed and designed this study. W-WS and J-ZG collected raw data. Y-PL, QS, QX, and B-YQ pre-treated raw data and performed the statistical analyses. W-WS, J-ZG, Y-PL, Z-QM, and BY wrote the original manuscript. YH and BY revised the manuscript. All authors have read and approved this study to be published.

Funding

This study was supported by the Department of Medical Oncology, Senior Department of Oncology, The Fifth Medical Center of PLA General Hospital.

Acknowledgments

We are very grateful for the support of The Fifth Medical Center of PLA General Hospital and the great efforts made by all participants. Meanwhile, we appreciate the help offered by the Lifehealthcare Clinical Laboratories, Hangzhou, Zhejiang Province, People's Republic of China.

Conflict of interest

The authors declare that the research was conducted in the absence of any commercial or financial relationships that could be construed as a potential conflict of interest.

Publisher's note

All claims expressed in this article are solely those of the authors and do not necessarily represent those of their affiliated organizations, or those of the publisher, the editors and the reviewers. Any product that may be evaluated in this article, or claim that may be made by its manufacturer, is not guaranteed or endorsed by the publisher.

Supplementary material

The Supplementary Material for this article can be found online at: https://www.frontiersin.org/articles/10.3389/fonc.2022.915662/full#supplementary-material

References

1. Hartwell LH, Weinert TA. Checkpoints: Controls that ensure the order of cell cycle events. *Science* (1989) 246(4930):629–34. doi: 10.1126/science.2683079

2. Rubin SM, Sage J, Skotheim JM. Integrating old and new paradigms of G1/S control. *Mol Cell* (2020) 80(2):183–92. doi: 10.1016/j.molcel.2020.08.020

3. Saldivar JC, Hamperl S, Bocek MJ, Chung M, Bass TE, Cisneros-Soberanis F, et al. *et al*: An intrinsic S/G2 checkpoint enforced by ATR. *Science* (2018) 361 (6404):806–10. doi: 10.1126/science.aap9346

4. Löbrich M, Jeggo PA. The impact of a negligent G2/M checkpoint on genomic instability and cancer induction. *Nat Rev Cancer* (2007) 7(11):861–9. doi: 10.1038/nrc2248

5. Samuel T, Weber HO, Funk JO. Linking DNA damage to cell cycle checkpoints. *Cell Cycle* (2002) 1(3):161–7. doi: 10.4161/cc.1.3.118

6. Saldivar JC, Cortez D, Cimprich KA. The essential kinase ATR: ensuring faithful duplication of a challenging genome. *Nat Rev Mol Cell Biol* (2017) 18 (10):622–36. doi: 10.1038/nrm.2017.67

7. Herlihy AE, De Bruin RAM. The role of the transcriptional response to DNA replication stress. *Genes* (2017) 8(3):92. doi: 10.3390/genes8030092

8. Matthews HK, Bertoli C, de Bruin RAM. Cell cycle control in cancer. *Nat Rev Mol Cell Biol* (2022) 23(1):74–88. doi: 10.1038/s41580-021-00404-3

9. Putti S, Giovinazzo A, Merolle M, Falchetti ML, Pellegrini M. ATM Kinase dead: From ataxia telangiectasia syndrome to cancer. *Cancers* (2021) 13(21):5498. doi: 10.3390/cancers13215498

10. Schepeler T, Lamy P, Hvidberg V, Laurberg JR, Fristrup N, Reinert T, et al. A high resolution genomic portrait of bladder cancer: correlation between genomic aberrations and the DNA damage response. *Oncogene* (2013) 32(31):3577–86. doi: 10.1038/onc.2012.381

11. Zhang B, Miao T, Shen X, Bao L, Zhang C, Yan C, et al. EB Virus-induced ATR activation accelerates nasopharyngeal carcinoma growth *via* M2-type macrophages polarization. *Cell Death Dis* (2020) 11(9):742. doi: 10.1038/s41419-020-02925-9

12. Quan L, Shi J, Tian Y, Zhang Q, Zhang Y, Zhang Y, et al. Identification of potential therapeutic targets for melanoma using gene expression analysis. *Neoplasma* (2015) 62(5):733–9. doi: 10.4149/neo_2015_087

13. Yuan W, Xie S, Wang M, Pan S, Huang X, Xiong M, et al. Bioinformatic analysis of prognostic value of ZW10 interacting protein in lung cancer. *OncoTar Ther* (2018) 11:1683–95. doi: 10.2147/OTT.S149012

14. Akabane S, Oue N, Sekino Y, Asai R, Thang PQ, Taniyama D, et al. : KIFC1 regulates ZWINT to promote tumor progression and spheroid formation in colorectal cancer. *Pathol Int* (2021) 71(7):441–52. doi: 10.1111/pin.13098

15. Ying H, Xu Z, Chen M, Zhou S, Liang X, Cai X. Overexpression of zwint predicts poor prognosis and promotes the proliferation of hepatocellular carcinoma by regulating cell-cycle-related proteins. *OncoTar Ther* (2018) 11:689–702. doi: 10.2147/OTT.S152138

16. Niehans GA, Kratzke RA, Froberg MK, Aeppli DM, Nguyen PL, Geradts J. G1 checkpoint protein and p53 abnormalities occur in most invasive transitional

cell carcinomas of the urinary bladder. *Br J Cancer* (1999) 80(8):1175–84. doi: 10.1038/sj.bjc.6990483

17. Doherty SC, McKeown SR, McKelvey-Martin V, Downes CS, Atala A, Yoo JJ, et al. Cell cycle checkpoint function in bladder cancer. *JNCI: J Natl Cancer Inst* (2003) 95(24):1859–68. doi: 10.1093/jnci/djg120

18. Ye Y, Yang H, Grossman HB, Dinney C, Wu X, Gu J. Genetic variants in cell cycle control pathway confer susceptibility to bladder cancer. *Cancer* (2008) 112 (11):2467–74. doi: 10.1002/cncr.23472

19. Hamid ARAH, Ridwan FR, Parikesit D, Widia F, Mochtar CA, Umbas R. Meta-analysis of neoadjuvant chemotherapy compared to radical cystectomy alone in improving overall survival of muscle-invasive bladder cancer patients. *BMC Urol* (2020) 20(1):158. doi: 10.1186/s12894-020-00733-z

20. Kamoun A, de Reyniès A, Allory Y, Sjödahl G, Robertson AG, Seiler R, et al. A consensus molecular classification of muscle-invasive bladder cancer. *Eur Urol* (2020) 77(4):420–33. doi: 10.1016/j.eururo.2019.09.006

21. Yoshihara K, Shahmoradgoli M, Martínez E, Vegesna R, Kim H, Torres-Garcia W, et al. : Inferring tumour purity and stromal and immune cell admixture from expression data. *Nat Commun* (2013) 4(1):2612. doi: 10.1038/ncomms3612

22. Gentles AJ, Newman AM, Liu CL, Bratman SV, Feng W, Kim D, et al. The prognostic landscape of genes and infiltrating immune cells across human cancers. *Nat Med* (2015) 21(8):938–45. doi: 10.1038/nm.3909

23. Jiang P, Gu S, Pan D, Fu J, Sahu A, Hu X, et al. Signatures of T cell dysfunction and exclusion predict cancer immunotherapy response. *Nat Med* (2018) 24(10):1550–8. doi: 10.1038/s41591-018-0136-1

24. Kim HR, Park HJ, Son J, Lee JG, Chung KY, Cho NH, et al. : Tumor microenvironment dictates regulatory T cell phenotype: Upregulated immune checkpoints reinforce suppressive function. *J ImmunoTher Cancer* (2019) 7 (1):339. doi: 10.1186/s40425-019-0785-8

25. Balar A, Galsky M, Rosenberg J, Powles T, Petrylak D, Bellmunt J, et al. Atezolizumab as first-line treatment in cisplatin-ineligible patients with locally advanced and metastatic urothelial carcinoma: a single-arm, multicentre, phase 2 trial. *Lancet (London England)* (2017) 389(10064):67–76. doi: 10.1016/S0140-6736 (16)32455-2

26. Rose TL, Weir WH, Mayhew GM, Shibata Y, Eulitt P, Uronis JM, et al. Fibroblast growth factor receptor 3 alterations and response to immune checkpoint inhibition in metastatic urothelial cancer: a real world experience. *Br J Cancer* (2021) 125(9):1251–60. doi: 10.1038/s41416-021-01488-6

27. Bray F, Ferlay J, Soerjomataram I, Siegel RL, Torre LA, Jemal A. Global cancer statistics 2018: GLOBOCAN estimates of incidence and mortality worldwide for 36 cancers in 185 countries. *CA: A Cancer J Clin* (2018) 68 (6):394–424. doi: 10.3322/caac.21492

28. Tran L, Xiao J-F, Agarwal N, Duex JE, Theodorescu D. Advances in bladder cancer biology and therapy. *Nat Rev Cancer* (2021) 21(2):104–21. doi: 10.1038/s41568-020-00313-1

29. Pardo JC, Ruiz de Porras V, Plaja A, Carrato C, Etxaniz O, Buisan O, et al. Moving towards personalized medicine in muscle-invasive bladder cancer: Where are we now and where are we going? *Int J Mol Sci* (2020) 21(17):6271. doi: 10.3390/ijms21176271

30. Cuzick J, Swanson G, Fisher G, Brothman A, Berney D, Reid J, et al. Prognostic value of an RNA expression signature derived from cell cycle proliferation genes in patients with prostate cancer: a retrospective study. *Lancet Oncol* (2011) 12(3):245–55. doi: 10.1016/S1470-2045(10)70295-3

31. Lazzeroni M, DeCensi A, Guerrieri-Gonzaga A, Pagan E, Bagnardi V, Macis D, et al. Prognostic and predictive value of cell cycle progression (CCP) score in ductal carcinoma *in situ* of the breast. *Modern Pathol* (2020) 33(6):1065–77. doi: 10.1038/s41379-020-0452-0

32. Askeland EJ, Chehval VA, Askeland RW, Fosso PG, Sangale Z, Xu N, et al. Cell cycle progression score predicts metastatic progression of clear cell renal cell carcinoma after resection. *Cancer Biomarkers* (2015) 15:861–7. doi: 10.3233/CBM-150530

33. Bueno R, Hughes E, Wagner S, Gutin AS, Lanchbury JS, Zheng Y, et al. Validation of a molecular and pathological model for five-year mortality risk in patients with early stage lung adenocarcinoma. *J Thorac Oncol* (2015) 10(1):67–73. doi: 10.1097/JTO.0000000000000365

34. Dancik G, Theodorescu D. Robust prognostic gene expression signatures in bladder cancer and lung adenocarcinoma depend on cell cycle related genes. *PloS One* (2014) 9(1):e85249. doi: 10.1371/journal.pone.0085249

35. Dimitrova DS, Gilbert DM. Temporally coordinated assembly and disassembly of replication factories in the absence of DNA synthesis. *Nat Cell Biol* (2000) 2(10):686–94. doi: 10.1038/35036309

36. Feijoo C, Hall-Jackson C, Wu R, Jenkins D, Leitch J, Gilbert DM, et al. Activation of mammalian Chk1 during DNA replication arrest : a role for Chk1 in the intra-s phase checkpoint monitoring replication origin firing. *J Cell Biol* (2001) 154(5):913–24. doi: 10.1083/jcb.200104099

37. Trenz K, Smith E, Smith S, Costanzo V. ATM And ATR promote Mre11 dependent restart of collapsed replication forks and prevent accumulation of DNA breaks. *EMBO J* (2006) 25(8):1764–74. doi: 10.1038/sj.emboj.7601045

38. Yan S, Michael WM. TopBP1 and DNA polymerase alpha-mediated recruitment of the 9-1-1 complex to stalled replication forks: Implications for a replication restart-based mechanism for ATR checkpoint activation. *Cell Cycle* (2009) 8(18):2877–84. doi: 10.4161/cc.8.18.9485

39. Otto T, Sicinski P. Cell cycle proteins as promising targets in cancer therapy. *Nat Rev Cancer* (2017) 17(2):93–115. doi: 10.1038/nrc.2016.138

40. Sun S, Wang Y, Wang J, Bi J. Wnt pathway-related three-mRNA clinical outcome signature in bladder urothelial carcinoma: computational biology and experimental analyses. *J Trans Med* (2021) 19(1):409. doi: 10.1186/s12967-021-03061-4

41. Jin H, Ma J, Xu J, Li H, Chang Y, Zang N, et al. Oncogenic role of MIR516A in human bladder cancer was mediated by its attenuating PHLPP2 expression and BECN1-dependent autophagy. *Autophagy* (2021) 17(4):840–54. doi: 10.1080/15548627.2020.1733262

42. Tan L-B, Chen K-T, Yuan Y-C, Liao P-C, Guo H-R. Identification of urine PLK2 as a marker of bladder tumors by proteomic analysis. *World J Urol* (2010) 28 (1):117–22. doi: 10.1007/s00345-009-0432-y

43. Lin Y, Lin C, Huang L, Chao T, Kuo C, Hung L, et al. The suppression of thoc1 in cancer cell apoptosis mediated by activated macrophages is nitric oxide-dependent. *Biochem Pharmacol* (2013) 86(2):242–52. doi: 10.1016/j.bcp.2013.05.009

44. Zhu H, Chen H, Wang J, Zhou L, Liu S. Collagen stiffness promoted non-muscle-invasive bladder cancer progression to muscle-invasive bladder cancer. *OncoTar Ther* (2019) 12:3441–57. doi: 10.2147/OTT.S194568

45. Piao X-M, Hwang B, Jeong P, Byun YJ, Kang HW, Seo SP, et al. Collagen type VI–α1 and 2 repress the proliferation, migration and invasion of bladder cancer cells. *Int J Oncol* (2021) 59(1):37. doi: 10.3892/ijo.2021.5217

46. Qiu S, Deng L, Liao X, Nie L, Qi F, Jin K, et al. Tumor-associated macrophages promote bladder tumor growth through PI3K/AKT signal induced by collagen. *Cancer Sci* (2019) 110(7):2110–8. doi: 10.1111/cas.14078

47. Sharma P, Hu-Lieskovan S, Wargo JA, Ribas A. Primary, adaptive, and acquired resistance to cancer immunotherapy. *Cell* (2017) 168(4):707–23. doi: 10.1016/j.cell.2017.01.017

48. Mariathasan S, Turley SJ, Nickles D, Castiglioni A, Yuen K, Wang Y, et al. TGFβ attenuates tumour response to PD-L1 blockade by contributing to exclusion of T cells. *Nature* (2018) 554(7693):544–8. doi: 10.1038/nature25501

49. Feng C, Wang X, Tao Y, Xie Y, Lai Z, Li Z, et al. Single-cell proteomic analysis dissects the complexity of tumor microenvironment in muscle invasive bladder cancer. *Cancers* (2021) 13(21):5440. doi: 10.3390/cancers13215440

50. Robertson AG, Kim J, Al-Ahmadie H, Bellmunt J, Guo G, Cherniack AD, et al. Comprehensive molecular characterization of muscle-invasive bladder cancer. *Cell* (2017) 171(3):540–556.e525. doi: 10.1016/j.cell.2017.09.007

51. Matumoto T, Chen Y, Contreras-Sanz A, Ikeda K, Schulz G, Gao J, et al. FBXW7 loss of function contributes to worse overall survival and is associated with accumulation of MYC in muscle invasive bladder cancer. *Urologic Oncol: Semin Orig Investigations* (2020) 38(12):904–5. doi: 10.1016/j.urolonc.2020.10.048

52. Choi W, Ochoa A, McConkey D, Aine M, Höglund M, Kim W, et al. Genetic alterations in the molecular subtypes of bladder cancer: Illustration in the cancer genome atlas dataset. *Eur Urol* (2017) 72(3):354–65. doi: 10.1016/j.eururo.2017.03.010

53. Joyce JA, Fearon DT. T Cell exclusion, immune privilege, and the tumor microenvironment. *Science* (2015) 348(6230):74–80. doi: 10.1126/science.aaa6204

54. Wang L, Gong Y, Saci A, Szabo PM, Martini A, Necchi A, et al. Fibroblast growth factor receptor 3 alterations and response to PD-1/PD-L1 blockade in patients with metastatic urothelial cancer. *Eur Urol* (2019) 76(5):599–603. doi: 10.1016/j.eururo.2019.06.025

55. da Silva GN, de Castro Marcondes JP, de Camargo EA, da Silva Passos Júnior GA, Sakamoto-Hojo ET, Salvadori DMF. Cell cycle arrest and apoptosis in TP53 subtypes of bladder carcinoma cell lines treated with cisplatin and gemcitabine. *Exp Biol Med* (2010) 235(7):814–24. doi: 10.1258/ebm.2010.009322

56. Ho JN, Byun SS, Lee SE, Youn JI, Lee S. Multikinase inhibitor motesanib enhances the antitumor effect of cisplatin in cisplatin–resistant human bladder cancer cells *via* apoptosis and the PI3K/Akt pathway. *Oncol Rep* (2019) 41(4):2482–90. doi: 10.3892/or.2019.7005

57. Kassouf W, Luongo T, Brown G, Adam L, Dinney C. Schedule dependent efficacy of gefitinib and docetaxel for bladder cancer. *J Urol* (2006) 176(2):787–92. doi: 10.1016/j.juro.2006.03.072

58. Jiménez-Guerrero R, Gasca J, Flores ML, Pérez-Valderrama B, Tejera-Parrado C, Medina R, et al. Obatoclax and paclitaxel synergistically induce apoptosis and overcome paclitaxel resistance in urothelial cancer cells. *Cancers* (2018) 10(12):490. doi: 10.3390/cancers10120490

59. Stravopodis D, Karkoulis P, Konstantakou E, Melachroinou S, Lampidonis A, Anastasiou D, et al. Grade-dependent effects on cell cycle progression and

apoptosis in response to doxorubicin in human bladder cancer cell lines. *Int J Oncol* (2009) 34(1):137–60. doi: 10.3892/ijo_00000137

60. Al-Ahmadie HA, Iyer G, Janakiraman M, Lin O, Heguy A, Tickoo SK, et al. Somatic mutation of fibroblast growth factor receptor-3 (FGFR3) defines a distinct morphological subtype of high-grade urothelial carcinoma. *J Pathol* (2011) 224 (2):270–9. doi: 10.1002/path.2892

61. Knowles MA. FGFR3 – a central player in bladder cancer pathogenesis? *Bladder Cancer* (2020) 6:403–23. doi: 10.3233/BLC-200373

frontiers | Frontiers in Oncology

TYPE Original Research
PUBLISHED 11 August 2022
DOI 10.3389/fonc.2022.930731

Check for updates

OPEN ACCESS

EDITED BY
Alfredo Berruti,
University of Brescia, Italy

REVIEWED BY
Ning Li,
Fourth Affiliated Hospital of China Medical University, China
Takeshi Yuasa,
Japanese Foundation for Cancer Research, Japan

*CORRESPONDENCE
Isabelle Bernard-Pierrot
ibernard@curie.fr
Philippe Lluel
philippe.lluel@urosphere.com

†These authors have contributed equally to the work

‡These authors co-supervised the study

SPECIALTY SECTION
This article was submitted to Genitourinary Oncology, a section of the journal Frontiers in Oncology

RECEIVED 28 April 2022
ACCEPTED 08 July 2022
PUBLISHED 11 August 2022

CITATION
Lang H, Béraud C, Cabel L, Fontugne J, Lassalle M, Krucker C, Dufour F, Groeneveld CS, Dixon V, Meng X, Kamoun A, Chapeaublanc E, De Reynies A, Gamé X, Rischmann P, Bieche I, Masliah-Planchon J, Beaurepere R, Allory Y, Lindner V, Misseri Y, Radvanyi F, Lluel P, Bernard-Pierrot I and Massfelder T (2022) Integrated molecular and pharmacological characterization of patient-derived xenografts from bladder and ureteral cancers identifies new potential therapies. *Front. Oncol.* 12:930731. doi: 10.3389/fonc.2022.930731

Integrated molecular and pharmacological characterization of patient-derived xenografts from bladder and ureteral cancers identifies new potential therapies

Hervé Lang[1†], Claire Béraud[2†], Luc Cabel[3,4†], Jacqueline Fontugne[3,5,6], Myriam Lassalle[2], Clémentine Krucker[3,4,5], Florent Dufour[3,4,7], Clarice S. Groeneveld[3,4,8], Victoria Dixon[3,4,5], Xiangyu Meng[3,4,9], Aurélie Kamoun[8], Elodie Chapeaublanc[3,4], Aurélien De Reynies[8], Xavier Gamé[10], Pascal Rischmann[10], Ivan Bieche[11], Julien Masliah-Planchon[11], Romane Beaurepere[11], Yves Allory[3,5,6], Véronique Lindner[12], Yolande Misseri[2], François Radvanyi[3,4], Philippe Lluel[2*], Isabelle Bernard-Pierrot[3,4*‡] and Thierry Massfelder[13‡]

[1]Department of Urology, New Civil Hospital and Fédération de Médecine Translationnelle de Strasbourg (FMTS), Strasbourg, France, [2]Urosphere, Toulouse, France, [3]Institut Curie, Centre National de la Recherche Scientifique (CNRS), UMR144, Molecular Oncology team, PSL Research University, Paris, France, [4]Sorbonne Universités, Université Pierre-et-Marie-Curie (UPMC), Univ Paris, Paris, France, [5]Department of Pathology, Institut Curie, Saint-Cloud, France, [6]Université de Versailles-Saint-Quentin-en-Yvelines (UVSQ), Paris-Saclay University, Versailles, France, [7]Inovarion, Paris, France, [8]La Ligue Contre Le Cancer, Paris, France, [9]Department of Urology, Zhongnan Hospital of Wuhan University, Wuhan, China, [10]Department of Urology, Rangueil Hospital, Toulouse, France, [11]Department of Genetics, Institut Curie, Paris, France, [12]Department of Pathology, New civil Hospital, Strasbourg, France, [13]INSERM (French National Institute of Health and Medical Research) UMR_S1260, Université de Strasbourg, Regenerative Nanomedicine, Centre de Recherche en Biomédecine de Strasbourg, Strasbourg, France

Background: Muscle-invasive bladder cancer (MIBC) and upper urinary tract urothelial carcinoma (UTUC) are molecularly heterogeneous. Despite chemotherapies, immunotherapies, or anti-fibroblast growth factor receptor (FGFR) treatments, these tumors are still of a poor outcome. Our objective was to develop a bank of patient-derived xenografts (PDXs) recapitulating the molecular heterogeneity of MIBC and UTUC, to facilitate the preclinical identification of therapies.

Methods: Fresh tumors were obtained from patients and subcutaneously engrafted into immune-compromised mice. Patient tumors and matched PDXs were compared regarding histopathology, transcriptomic (microarrays), and genomic profiles [targeted Next-Generation Sequencing (NGS)]. Several

PDXs were treated with chemotherapy (cisplatin/gemcitabine) or targeted therapies [FGFR and epidermal growth factor (EGFR) inhibitors].

Results: A total of 31 PDXs were established from 1 non-MIBC, 25 MIBC, and 5 upper urinary tract tumors, including 28 urothelial (UC) and 3 squamous cell carcinomas (SCCs). Integrated genomic and transcriptomic profiling identified the PDXs of three different consensus molecular subtypes [basal/squamous (Ba/Sq), luminal papillary, and luminal unstable] and included *FGFR3*-mutated PDXs. High histological and genomic concordance was found between matched patient tumor/PDX. Discordance in molecular subtypes, such as a Ba/Sq patient tumor giving rise to a luminal papillary PDX, was observed (n=5) at molecular and histological levels. Ten models were treated with cisplatin-based chemotherapy, and we did not observe any association between subtypes and the response. Of the three Ba/Sq models treated with anti-EGFR therapy, two models were sensitive, and one model, of the sarcomatoid variant, was resistant. The treatment of three FGFR3-mutant PDXs with combined FGFR/EGFR inhibitors was more efficient than anti-FGFR3 treatment alone.

Conclusions: We developed preclinical PDX models that recapitulate the molecular heterogeneity of MIBCs and UTUC, including actionable mutations, which will represent an essential tool in therapy development. The pharmacological characterization of the PDXs suggested that the upper urinary tract and MIBCs, not only UC but also SCC, with similar molecular characteristics could benefit from the same treatments including anti-FGFR for FGFR3-mutated tumors and anti-EGFR for basal ones and showed a benefit for combined FGFR/EGFR inhibition in FGFR3-mutant PDXs, compared to FGFR inhibition alone.

KEYWORDS

urothelial carcinoma, squamous cell carcinoma, upper-urinary tract carcinoma, luminal tumors, basal tumors, tyrosine kinase receptor, molecular subtypes, tumor heterogeneity

Introduction

Bladder cancer (BCa) is the ninth most common cancer type worldwide with an estimated 549,000 new cases in 2018 (1). Histologically, 90%–95% of BCa are urothelial cell carcinomas (UCs) and 5% are squamous cell carcinomas (SCCs) (2). Although less frequent, UC may also develop in the upper urinary tract (2%–5% of UCs). Muscle-invasive BCas (MIBCs) are of very poor outcome, with an overall 5-year survival of 50%–60% and less than 10% for patients with localized disease or distant metastasis, respectively. Localized UC/SCC-MIBC and high-risk upper tract urothelial carcinoma (UTUC) are treated by radical cystectomy and radical nephroureterectomy, respectively, with the addition of adjuvant or neoadjuvant chemotherapies (2, 3). In advanced-setting UC, immune checkpoint or fibroblast growth factor receptor (FGFR) inhibitors (for tumors presenting *FGFR2/3* genetic alterations) may also be proposed (2, 4), while there is no standard-of-care treatment for SCC. Recently, two antibody–drug conjugates (ADCs) have shown efficacy in urothelial cancers, sacituzumab govitecan (5) (anti-TROP2) and enfortumab vedotin (6) (anti-Nectin4). Notably, the expression of NECTIN4 and TROP2 is variable across BCas, with NECTIN4 expression higher in luminal tumors (7, 8), which could impact the efficacy of these drugs. We also find in PDX transcriptomic analysis a heterogeneity of NECTIN4 and TROP2 expression, with a

Abbreviations: PDXs, patient-derived xenografts; NMIBC, non-muscle-invasive bladder cancer; MIBC, muscle-invasive bladder cancer; FGFR, fibroblast growth factor receptor; EGFR, epidermal growth factor; SCC, squamous cell carcinoma; UC, urothelial cell carcinoma; UTUC, upper urinary tract urothelial carcinoma.

higher expression of NECTIN4 in luminal tumors. However, despite these treatments, the outcome remains poor, and the identification of new therapies is still needed. The development of relevant preclinical models is critical to reach this objective.

MIBCs constitute a heterogeneous group of tumors at the morphological and molecular levels. With the aim to improve the prediction of the clinical outcome and treatment response, an international consortium has recently reached a consensus molecular classification based on transcriptomic data, for MIBC, including six subtypes, facilitating interstudy comparisons (9). These subtypes can be divided into broad luminal (differentiated) and basal/squamous (Ba/Sq) groups. Although current systemic treatments are not based on molecular classification, some subtype features are associated with treatment response. For example, Ba/Sq tumors have worse prognosis than luminal-papillary (LumP) tumors [5], which commonly show the genetic alterations of FGFR3 (10). These subtypes have also been suggested to have a different sensitivity to chemotherapies, although results are currently inconsistent between studies (11–14). The Ba/Sq subtype and bladder SCC are associated with EGFR activation and sensitivity to anti-EGFR treatments in preclinical models (9, 15–18). UTUCs are molecularly comparable to MIBCs but have some distinct features, such as a higher prevalence of microsatellite instability (MSI) (19).

The molecular heterogeneity of MIBCs and UTUC and their divergent therapy sensitivities entails the need for a representative panel of preclinical models for unbiased therapeutic evaluation. Therapeutic testing in PDXs is highly effective in predicting the efficacy of both chemotherapies and targeted therapies (20, 21). Although few studies have reported the development of PDX models from MIBC, none have performed integrated genomic, transcriptomic, and pharmacological characterization of a bank of PDX reflecting the biological diversity of MIBC (22–24). Recently, a bank of 17 PDXs from UTUC has been reported (25) but no model exists for SCC, for which no standard of care is established.

In the present report, we describe the development and characterization of a bank of 31 PDXs, which maintain the characteristics of patient tumors and reflect the diversity of the molecular subtypes of bladder and upper urinary tract cancers. The evaluation of pharmacological responses to standard of care and targeted therapies suggests that non-sarcomatoid Ba/Sq tumors, notably SCC, could benefit from anti-EGFR therapies. In *FGFR3*-mutated tumor PDXs, an anti-FGFR and anti-EGFR combination therapy improves tumor response compared to FGFR inhibition alone.

Materials and methods

Animals

Four- to five-week-old immunodeficient mice (male) were purchased from Charles River Laboratories (L'Arbresle, France). Mice were maintained under specific pathogen-free conditions. Their care and housing were conducted in accordance with the European Community Council Directive 2010/63/UE and the French Ministry for Agriculture, Agrifood and Forestry Decree 2013-118. Experimental protocols were reviewed by CEEA-122 Ethical Committee for Protection of Animals used for Scientific Purposes and approved by French Ministry for National Education, Higher Education and Research under the number *APAFIS#14811-2018042316405732 v4*. The animal facility was maintained under artificial lighting (12 h) between 7:00 a.m. and 7:00 p.m. at a controlled ambient temperature of 22 ± 2°C and the relative humidity rate maintained at 55 ± 10%.

Specimen acquisition

From January 2009 to October 2019, patient tumors and matched normal tissues were obtained from 153 patients treated for bladder or ureteral cancers undergoing surgery either at the Hospital of Strasbourg (France) (n=135) or the Hospital of Toulouse (France) (n=18) in accordance with all relevant guidelines and regulations. All patients provided written informed consent. The incoming material of every donor patient was anonymized by receiving a chronological unique number, subsequently used to identify the corresponding PDX model. The specimens were examined, sectioned, and selected by pathologists for histological analyses and xenografts. Clinical and demographic information were obtained prospectively.

Patient-derived xenograft establishment

The PDX models of MIBC were generated by engrafting tumor tissues directly obtained from patients. Viable tumor tissue was macrodissected, and tumor pieces were then prepared for implantation. The NMRI nude (Rj : NMRI-Foxn1$^{nu/nu}$) immunodeficient mice strain was used for tissue implantation. Grafts were implanted into the interscapular fat pad. When s.c. xenograft tumors reached ~1,000–1,500 mm^3, they were serially transplanted for expansion into new mice. In addition, harvested xenograft material was cryopreserved for future implantations and/or fixed in 4% formalin for 24 h before paraffin embedding and/or stored at -80°C for subsequent analyses. A model was defined as established when stable growth over at least three passages and regrowth after a freeze–thaw cycle could be observed. The take rate (the proportion of mice developing tumors after the transplantation of the PDX) and passage time were recorded for every model and every individual passage. Tumor growth was determined weekly by a two-dimensional measurement with a caliper. The tumor volume was calculated as: TV (mm^3) = [length (mm) × width (mm)^2]*π/6, where the length and width are the longest and shortest diameters of the tumor, respectively.

Animals were sacrificed when the tumor volume reached 2,000 mm^3.

Histopathology and immunohistochemistry

For all PDX models, primary and passaged tumors preserved in formalin for 24 h were paraffin-embedded, sectioned into 4-µm-thick cuts, and placed on glass slides. The analysis of hematoxylin and eosin (H&E)-stained slides was performed by two experienced uropathologists.

RNA/DNA/protein extraction

Each frozen PDX fragment was ground to powder and subdivided for triple RNA, DNA, and protein extraction. RNA isolation was performed using TRIzol, while phenol/chloroform/isoamyl alcohol extraction was used for DNA isolation. See "Western blot" section for the protein extraction method.

Real-time reverse transcription–quantitative PCR

Reverse transcription was performed on 1 µg of total RNA using a high-capacity cDNA reverse transcription kit (Thermo Fisher Scientific, Illkirch, France). cDNAs were amplified by PCR in a Roche real-time thermal cycler, with the Roche Taqman master mix (Roche) and Taqman probe/primer pairs as follows:

Gene	Primer Forward	Primer Reverse
EGFR	GATCCAAGCTGTCCCAATG	GCACAGATGATTTTGGTCAGTT
ERBB2	CAACTGCACCCACTCCTGT	GCAGAGATGATGGACGTCAG
ERBB3	GGGAACCTTGAGATTGTGCT	CCTGTCACTTCTCGAATCCAC

Sanger sequencing

The coding exons and splice junctions of *PPARG* were amplified from genomic DNA by PCR with gene-specific primers available on request and sequenced by the Sanger method as described (26).

Weighted *in silico* pathology

WISP (Weighted *In Silico* Pathology; https://cit-bioinfo.github.io/WISP/) is an approach to assess intratumoral heterogeneity from bulk molecular profiles. Based on predefined pure molecular or histological populations for a particular cancer type, this approach gives a fine description of each tumor in a standardized way. The methodology is based on non-negative least squares regression and quadratic programming optimization for estimating the mixed proportions of distinct populations for a tumor sample. It can be applied on transcriptomic or methylation data. The output is the mixing proportion estimations for all samples.

For this analysis, we classified the samples from the MIBC CIT cohort (15) into a luminal or basal subtype according to the BASE47 classifier (27) to refine pure samples and calculate pure population centroid profiles, using standard parameters. Then, we estimated the mixed proportions of pure populations for each of our patient tumor and PDX samples, without scaling.

Short tandem repeat signature

Patient tumors and corresponding PDX DNA samples were subjected to STR using the Authentifiler PCR amplification kit (Thermo Fisher Scientific, Illkirch, France) that amplifies nine unique STR loci and the amelogenin gender-determining marker, according to the manufacturer's instructions. PCR products were separated by capillary electrophoresis on ABI PRISM 3100, and results were analyzed using the GeneMapper software.

Genomic alterations detection: mutations, copy number variant detection, variant calling, and tumor mutational burden

Patient tumors and PDX were sequenced with a targeted NGS panel (called "DRAGON") that has been developed by the genetics department of Institut Curie (Paris, France) and can detect mutations, copy number alterations (CNA), tumor mutational burden and microsatellite instability. It is composed of 571 genes of interest in oncology for diagnosis, prognosis, and theragnostics (Supplementary Table 1). NGS primers were selected based on their specificity on the human genome. The whole method is described in Supplemental Method Dragon.

Deleterious genomic alterations were defined as follows: (i) for oncogenes, only gain-of-function mutations were considered (i.e., hotspot missense mutations, in-frame insertions/deletions/splicing described as oncogenic), (ii) for tumor suppressor genes, only loss-of-function mutations were considered (i.e., biallelic truncating alterations—non-sense mutations, frameshift insertions/deletions/splicing—or monoallelic truncating alterations associated with heterozygous deletion detected by copy number analysis).

Gene expression analysis

Gene expression arrays/transcriptomic data/ consensus class

The RNA of 31 PDX and patient tumors samples were hybridized in three batches in Affymetrix Human Genome U133 plus 2.0 Array Plates (Santa Clara, CA) according to Affymetrix standard protocols. Raw CEL files were RMA-normalized (28) using R statistical software. PCA confirmed that no batch effect was observed. The arrays were mapped to genes with a Brainarray Custom CDF (Human EntrezG version 24) (29).

Molecular consensus classes were determined with the "consensusMIBC" R package (v1.1.0, https://github.com/cit-bioinfo/consensusMIBC) using the RMA-normalized transcriptomic data. For WISP, we used a previously published dataset (15), which contains human MIBC samples (n = 85) also hybridized with Affymetrix Human Genome U133 plus 2.0 according to Affymetrix standard protocols. The raw CEL files used here are available from ArrayExpress (http://www.ebi.ac.uk/arrayexpress/) under accession number E-MTAB-1803.

Raw CEL files were RMA-normalized using R statistical software. The arrays were mapped to genes with a Brainarray Custom CDF (Human EntrezG version 23) (29)

In both datasets, we obtained a log2-transformed expression matrix with one value per gene.

Regulatory networks

The regulatory network was reverse-engineered by ARACNe-AP (30) from human urothelial cancer tissue datasets profiled by RNA-Seq from TCGA (n=414). The RNA-seq data was downloaded from the TCGA data portal using the TCGAbiolinks package (R). Raw counts were normalized to account for different library sizes, and the variance was stabilized with VST function in the DESeq2 R-package (31)

ARACNe was run with 100 bootstrap iterations using all probe-clusters mapping to a set of 1,740 transcription factors. The parameters used were standard parameters, with the mutual information p-value threshold of 10^{-8}.

Regulon activity—VIPER

The VIPER algorithm tests for regulon enrichment based on gene expression signatures (32), using the regulatory network obtained from ARACNe on urothelial cancer, and we computed the enrichment of each regulon on the gene expression signature using different implementations of the analytic rank-based enrichment analysis algorithm.

Dual-staining immunohistochemistry

Dual immunostaining for GATA3 and KRT5/6 on Formalin-Fixed, Paraffin-Embedded (FFPE) samples was performed to screen for homogeneous or heterogeneous luminal or Ba/Sq tumors at the immunohistochemical level. Automated sequential dual-staining immunohistochemistry (IHC; Discovery, Roche/Ventana, Tucson, AZ, USA) was used according to the manufacturer's instructions. Tissue sections cut at 3 µm were dewaxed and subjected to antigen retrieval, then incubated first with a GATA3-specific rabbit monoclonal antibody (1:300, clone ZR65 Diagomics, Blagnac, France), followed by an HRP-conjugated anti-rabbit IgG secondary antibody (MP-7401, Vector). The antigen–antibody reaction was detected using an ImmPACT DAB reagent (SK-4105, Vector), producing brown staining in positive nuclei. In the second sequence, a primary rabbit monoclonal antibody against KRT5/6 (1:100, clone EP24/EP67; Diagomics, Blagnac, France) was incubated, followed by alkaline phosphatase–conjugated anti-rabbit IgG secondary antibody (ENZ-ACC110-0150, Enzo). The antigen–antibody reaction was revealed using ImmPACT red reagent (Vector), producing red staining in positive cytoplasm. A normal urothelium was used as a positive control. The staining for GATA3 and KRT5/6 was evaluated by one blinded pathologist (JF), providing respective quick scores (QSs) calculated as intensity (0–3) multiplied by the percentage of stained tumor cells and normalized to [0;1]. Immunohistochemical thresholds for Ba/Sq tumors (IHC-Ba/Sq) defined as QS(KRT5/6) >0.14 and QS(GATA3) <0.02, or luminal QS(GATA3) >0.14 and QS(KRT5/6) <0.02, were used (33). Tumors showing IHC-Ba/Sq and non-Ba/Sq areas were defined as having intratumoral heterogeneity.

In vivo efficacy studies

Erlotinib (EGFR inhibitor) was purchased from MedChemExpress (Sollentuna, Sweden) and administered orally (gavage) 5 days per week during 4 weeks at a dose of 30 or 90 mg/kg (0.5% carboxymethylcellulose in PBS).

Erdafitinib (pan-FGFR inhibitor) was purchased from MedChemExpress (Sollentuna, Sweden) and administered orally (gavage) 6 days per week during 4 weeks at a dose of 10 or 30 mg/kg (20% 2-hydroxypropyl β-cyclodextrin in distilled water).

BGJ398 (pan-FGFR inhibitor) was purchased from LC Laboratories and administered orally (gavage) 6 days per week during 4 weeks at a dose of 30 mg/kg.

Cisplatin and gemcitabine were purchased from Sigma (St. Quentin Fallavier, France). Both drugs were administered

intraperitoneally at a dose of 60 mg/kg (NaCl 0.9%) once a week (D0, D7, D14) and 4 mg/kg (NaCl 0.9%) once every 3 weeks (D1), respectively.

For efficacy studies, mice were implanted as described above. Tumor fragments were transplanted into 6-week-old NMRI mice. When the tumor reached a volume comprised between 60 and 270 mm^3, mice were randomly assigned to the vehicle or treatment groups (n= 7–10). The tumor volume was calculated as: TV (mm^3) = [length (mm) × width $(mm)^2$]*π/6, where the length and width are the longest and shortest diameters of the tumor, respectively. Tumor volumes were then reported to the initial volume as relative tumor volume (RTV). The means of the RTV in the same treatment group were calculated. Growth curves were generated using the GraphPad Prism software.

Western blot

Frozen PDX samples were resuspended in Laemmli lysis buffer [50-mM Tris-HCl (pH 6.8), 2-mM DTT, 2.5-mM EDTA, 2.5-mM EGTA, 2% SDS, 5% glycerol with protease inhibitors and phosphatase inhibitors (Roche)], and the resulting lysates were clarified by centrifugation. The protein concentration of the supernatants was determined with the BCA protein assay (Thermo Scientific, Illkirch, France). Proteins (10–50 µg) were resolved by SDS-PAGE in 10% polyacrylamide gels, electrotransferred onto Bio-Rad nitrocellulose membranes, and analyzed with antibodies against β-actin (Sigma-Aldrich #A2228, used at 1/25,000), or the extracellular domain of FGFR3 (Abcam, # ab133644, 1/5,000). Anti-mouse IgG, HRP-linked, and anti-rabbit IgG, HRP-linked antibody (Cell Signaling Technology # 7076 and # 7074, used at 1/3,000, Saint-Cyr-L'École, France) were used as secondary antibodies. Protein loading was checked by the Amido Black staining of the membrane after electrotransfer.

Statistical and bioinformatic analysis

Comparisons between PDX treatment responses were done using the Mann–Whitney test.

Bioinformatics analyses was performed with R (4.0.2).

Results

Establishment of urothelial PDXs

We successfully obtained 31 PDXs from 153 tumors (global engraftment rate ~20%, median latency 27.5 days with a range of 10–70 days) from January 2009 to October 2019. The main clinicopathological characteristics of the patients and patient tumors are summarized in Table 1 (additional clinical data from patients are presented in Supplementary Table 2). As expected, the majority of PDXs was derived from male patients (84%), with bladder as the primary site (84%) and were urothelial carcinomas (90%). The frequency of squamous cell carcinomas (SCC, 3/31, 10%) was higher than the known frequency of these tumors, potentially owing to a higher engraftment success rate (n=4/10, with one of the four that could not be further analyzed due to patient serology). One PDX was derived from a non-muscle-invasive BCa (NMIBC). Four patients had received systemic or radiotherapy treatment before the establishment of the PDX.

Histological and genomic characterization of PDXs

A histopathological analysis of the H&E-stained slides of patient tumors and PDXs was performed by two pathologists (VL, JF), based on the current WHO Classification of Tumors of the Urinary System (34). High histological concordance between patient tumors and PDXs was observed (Figure 1A) with the exception of three PDXs showing distinct histology compared to the matched patient tumors (M1030 and BLCU-011 lost the variant observed in the tumor, while a more squamous variant was observed in R1056, Supplementary Table 2). We confirmed by short tandem repeat (STR) profiling the concordant genetic identity between patient tumor and derived PDXs (Supplementary Table 3), with 85%–100% of conserved STR for the different models, as an example for L987 in Figure 1B. We characterized genomic alterations for 571 cancer-related genes (Supplementary Table 1 and Supplementary Table 4) in all 31 PDXs using a targeted next-generation sequencing assay, allowing the detection of mutations, the estimation of copy number alterations (CNA), tumor mutational burden (TMB), and MSI status (Figure 1C). As anticipated, the most frequent genomic alterations were mutations in *TERT* (68%) and *TP53* (61%) and the homozygous deletion of *CDKN2A/B* (~50%). We also identified activating mutations in potentially actionable genes such as *PIK3CA* (19%), *ERBB2* (19%), *FGFR3* (13%), *BRAF* (6%), *ERBB3* (3%), *KRAS G12C* (3%), and truncating mutations in the epigenetic genes *KDM6A* (19%), *ARID1A* (23%), *KMT2D* (19%), *KMT2A/B/C* (3% each), and *ARID2* (3%). One UTUC PDX displayed microsatellite instability associated with a bi-allelic deletion of *MSH2*, and this alteration was also observed in the parental tumor. To determine whether the PDXs retain the genomic alterations of the matched patient tumor, we sequenced five patient tumor/PDX pairs. The overall concordance of observed genomic alterations was high (90%–100%) (Figure 1D), except for the MSI-high PDX (B521) that harbored high TMB (40%). PPARG pathway activation, through PPARG amplifications or RXRA- and PPARG-activating mutations, is a known key feature of luminal tumors and a potential therapeutic target (16, 26, 35–37). We did not observe any *RXRA* mutation in our sequencing analyses. Since *PPARG* was not in our targeted panel, we performed a Sanger sequencing of the hotspot region within the ligand-binding domain of *PPARG* (26) and

TABLE 1 Clinicopathological characteristics of the samples used for patient-derived xenograft.

Variables	All patients
Total	31
Median age, years (IQR)	75 (52–88)
Gender	
Male	26 (84%)
Female	5 (16%)
Primary site	
Bladder	26 (84%)
Upper tract	5 (16%)
Histology	
Urothelial	28* (90%)
Conventional	17
Squamous differentiation	7
Sarcomatoid	2
Plasmacytoid	1
Glandular differentiation	1
Micropapillary	1
Poorly differentiated	5
Squamous	3 (10%)
Prior Treatment	
No	19 (61%)
BCG	3 (10%)
Cisplatin-based CT	3 (10%)
Radiotherapy + cisplatin-based CT	1 (3%)
NA	5 (16%)
pT Stage	
<pT2 (non-MIBC)	1 (3%)
≥pT2	30 (97%)
pN Stage	
pN0	7 (23%)
pN+	10 (32%)
pNx	14 (45%)
Associated CIS	
Yes	4 (13%)
No	27 (87%
Relapse (Yes)	4 (13%)

CT, chemotherapy.
*Variant total is above n=31 as some tumors have multiple variants.

identified one patient tumor/PDX pair (B521) harboring the T475M-activating mutation (n=1/23 tested PDX) and one patient tumor/PDX pair (M559) harboring the non-characterized and non-recurrent L339F mutation (26).

PDXs recapitulate the molecular subtypes and intratumoral heterogeneity

We then sought to determine whether PDX models recapitulate the molecular subtypes of patient tumors. In total, transcriptomic data using Affymetrix U133plus2 array were available for 22 patient tumor/PDX pairs and 8 individual PDXs. Unsupervised clustering analysis using the top 200 most variant genes did not highlight any segregation in PDXs by the primary site or histological tumor (Supplementary Figure 1, with the exclusion of the NMIBC PDX for the transcriptomic subtype analysis). We therefore considered all patient tumors/PDX similarly and stratified them into six subtypes by applying the molecular consensus classifier (9) (Figure 2A). We observed 15 Ba/Sq (52%), 11 LumP (38%), and 3 luminal-unstable (LumU) (10%) PDXs. All three SCC patient tumors/PDXs were classified as Ba/Sq. In contrast to genomic and histological characteristics, transcriptomic profiles were less stable between patient tumor/PDX pairs. Specifically, eight patient tumors gave rise to a PDX with a distinct molecular subtype (36%) including five Ba/Sq patient tumors to LumP PDX, one LumP to LumU, one stroma-rich to LumU, and one LumNS to the LumP subtype. We also stratified patient tumors and PDXs according to the BASE47 classifier (27) (Figure 2A). Among the 16/22 patient tumors that were classified as basal, 6 gave rise to a luminal PDX. In contrast, all luminal tumors formed luminal PDXs. For six matched tumor-PDX pairs, for which we did not have transcriptomic data, we performed GATA3 (luminal) and KRT5/6 (basal) dual immunostaining to assign molecular subtypes using previously defined thresholds for each marker (33) and we did not observe a difference in the subtype between tumors and PDXs (Figure 2A). To explore whether the basal- to-luminal discordance could be related to intratumoral heterogeneity, we evaluated the molecular heterogeneity in both patient tumors and PDXs using the WISP algorithm (Figure 2A). We observed the admixed proportions of luminal and basal subtypes in 59.1% of patient tumors and 41.4% of PDXs, including all six cases with discordant BASE47 subtypes. The high molecular heterogeneity found in the six basal tumors that gave rise to luminal PDXs was conserved in most of the matched PDXs. These findings suggest an intrinsic plasticity of these tumors, leading to a shift in subtype rather than a sampling bias of an area of a given subtype within a molecularly heterogeneous patient tumor (Figure 2A, lower panels).

Using defined biomarkers of luminal and basal differentiation (9, 10), we confirmed that PDXs were globally separated between luminal, differentiated tumors and basal tumors (Figure 2B and Supplementary Figure 1). Concerning NECTIN4 and TROP2, which could be targeted by drug-conjugated antibodies (5, 6), we also found in the PDX transcriptomic analysis a heterogeneity of NECTIN4 and TROP2 expression, with a higher expression of NECTIN4 in luminal tumors (Supplementary Figure 2).

To further explore the transcriptomes of our PDXs, we inferred the activity of 22 major regulons, as defined in TCGA analysis (10) (Figure 2C). Using this approach, we observed a perfect separation of luminal and basal PDXs in clustering analysis, independently of the primary site of patient tumor. Similar to patient tumors from TCGA, we observed a higher *EGFR* regulon activity in basal PDXs and a higher *PPARG*/

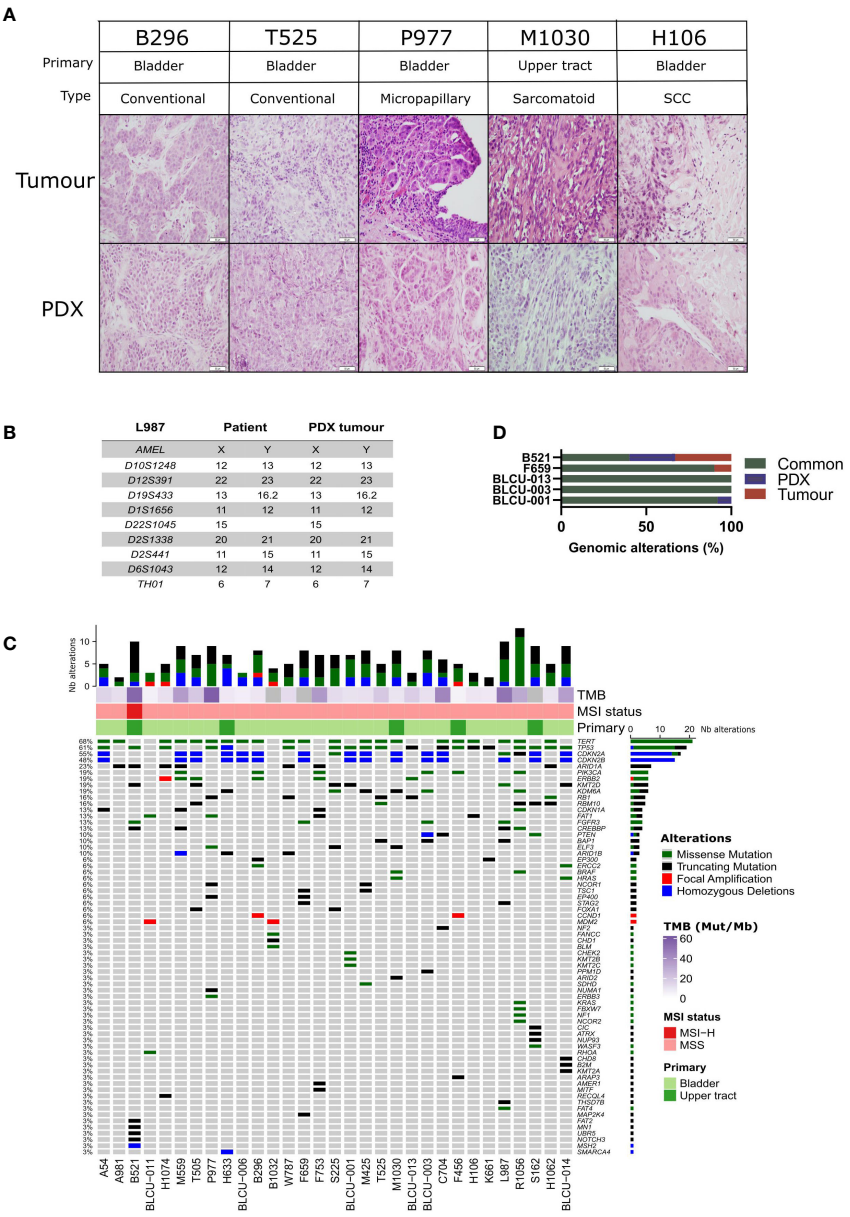


FIGURE 1
Histological and genomic characteristics of patient tumors and paired derived patient-derived xenografts (PDXs). **(A)** Histology of bladder/ureteral patient tumors and corresponding PDX models demonstrated similar histological features as assessed by hematoxylin and eosin (H&E) staining. Scale bar corresponds to 50 µm. H&E slides of a section of each patient tumor and matching PDX were reviewed by a board-certified pathologist, and representative pictures for the different histologies or variants are shown. **(B)** Short tandem repeat signature of a patient specimen and PDX tumor, an example of the L987 case. **(C)** Somatic genomic landscape of 31 bladder and ureteral PDXs analyzed using an in-house targeted sequencing assay (571 cancer-related genes, Supplementary Tables 2, 3), the tumor mutational burden per megabase (TMB, indicated in the log2 scale for each sample), and microsatellite instability–high (MSI-H) versus a microsatellite-stable (MSS) status. **(D)** Concordance of genomic alterations in five pairs tumor/PDX.

ERBB2/ERBB3 regulon activity in luminal PDXs (10). Of note, *FGFR3* mutations are enriched in LumP tumors (9) and we observed *FGFR3* mutations not only in two LumP PDXs, including one derived from UTUC, but also in two Ba/Sq PDXs, including one derived from an SCC tumor (Figures 2B, C) (9). As expected, high FGFR3 regulon activity was observed in tumors bearing *FGFR3* mutations.

To validate the intratumoral molecular subtype admixture inferred from the transcriptomic data *in situ*, we performed dual IHC staining combining a luminal (GATA3) and a basal marker

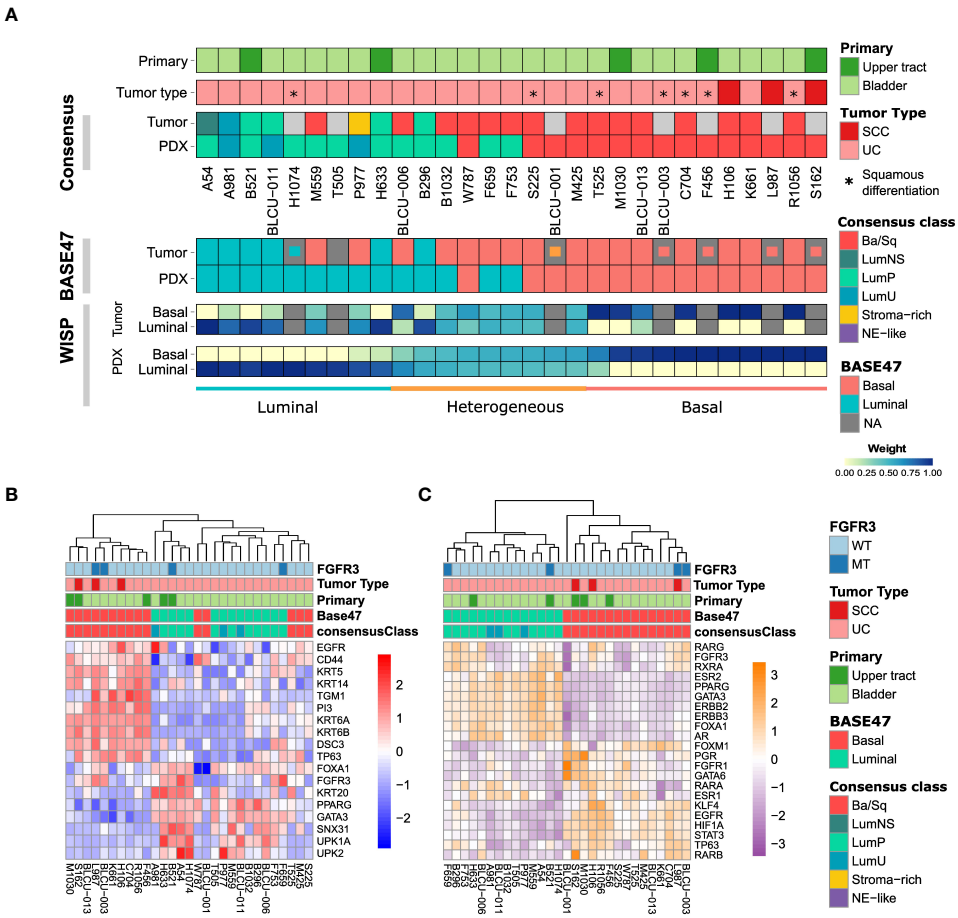


FIGURE 2
Transcriptomic analysis of patient tumors and paired PDXs. **(A)** Tumors and PDXs were classified into six subtypes using transcriptomic Affymetrix U133plus2 array data according to the molecular consensus classifier developed for MIBC, the corresponding box colors indicated in the legend on the right. A total of 22 patient tumor–PDX pairs and 7 individual PDXs were analyzed, where tumors without transcriptomic data are indicated in gray. Urothelial carcinomas with divergent squamous differentiation are highlighted with *. **(B)** Upper panels: tumors and PDXs were classified using transcriptomic data as luminal and basal subtypes according to the BASE47 classifier (27). In patient tumors with missing transcriptomic data, we assessed the luminal (blue), basal (red), or heterogeneous (orange) subtype by immunohistochemistry (IHC; inset small boxes), as defined in methods. Lower panels: the intra-tumoral heterogeneity and proportion of luminal and basal subtype admixture as evaluated from transcriptomic profiles using the WISP (Weighted *In Silico* Pathology) algorithm. Based on the PDX WISP results, samples were molecularly classified as luminal, basal, or heterogeneous. **(B)** Heatmap of PDX samples based on the gene expression of selected luminal or basal markers. **(C)** Heatmap of PDX samples based on the regulon activity of the main regulators previously identified within the different molecular subtypes of MIBC (9, 10).

(KRT5/6) in a subset of patient tumors and PDXs. We confirmed the presence of a subtype marker expression admixture *in situ*, with either spatially distinct areas showing different IHC profiles (defined hereafter as intratumoral heterogeneity) or a single-cell coexpression of the two markers, or a combination of both patterns of admixture. By comparing the results between tumors/PDXs classified as basal, luminal, or heterogenous based on the WISP analysis (Figures 2A, 3), we observed that tumors/PDXs classified as pure luminal or Ba/Sq based on transcriptomic data displayed higher GATA3 or KRT5/6 staining levels, respectively (Figure 3A). The WISP heterogeneous samples had more intermediate staining levels of both GATA3 and KRT5/6 (Figure 3A) and showed more intratumoral heterogeneity compared to pure Ba/Sq or luminal cases (10/15 vs. 4/29, $p<0.01$) (Figure 3B). Among samples with intratumoral heterogeneity, a GATA3-KRT5/6 coexpression at the single-cell level was also identified in 9/14 samples (Figures 3B, C).

Chemosensitivity of patient-derived xenografts

With cisplatin-based chemotherapy being the standard of care of MIBC and high-risk UTUC, we assessed the sensitivity of

10 PDXs representative of the different subtypes (six basal, four luminal) to cisplatin plus gemcitabine (Figure 4). We did not observe a significant difference between the proportion of basal (5/6, 83%) and luminal PDXs (2/4, 50%) with significant growth inhibition upon treatment (Fisher's exact test p=0.5). Due to the low number of recurrent genomic alterations and the number of models tested, it was not possible to statistically explore the association between genomic alterations and chemosensitivity.

EGFR-targeted therapy is effective in non-sarcomatoid basal/squamous patient-derived xenografts

In relation to the high EGFR activity in basal tumors, we have previously shown that EGFR is an effective therapeutic target in different *in vivo* basal preclinical models (15). The aggressive sarcomatoid variant of MIBC is suggested to occur through the progression of Ba/Sq tumors (38). We recently analyzed sarcomatoid tumor transcriptomes and identified a loss of EGFR regulon activity during the progression of Ba/Sq tumors to the sarcomatoid variant (Fontugne et al., unpublished results). In line with these findings, we identified a low EGFR regulon activity in a PDX (BLCU-001) compared to the other Ba/Sq PDXs, which was classified as a Ba/Sq sarcomatoid tumor (Figure 2C and Supplementary Table 1). To assess whether the loss of EGFR activity could impact the sensitivity to EGFR inhibition, we compared the effect of anti-EGFR treatment (erlotinib) in two Ba/Sq models presenting high EGFR-regulon activity (L987 and H106, Figure 2C) and BLCU-001 (Figure 5A). As expected, the two SCC Ba/Sq models were sensitive to erlotinib whereas the Ba/Sq model with sarcomatoid differentiation was resistant (Figure 5A). Of note, two other Ba/Sq PDXs (C704 and R1056)

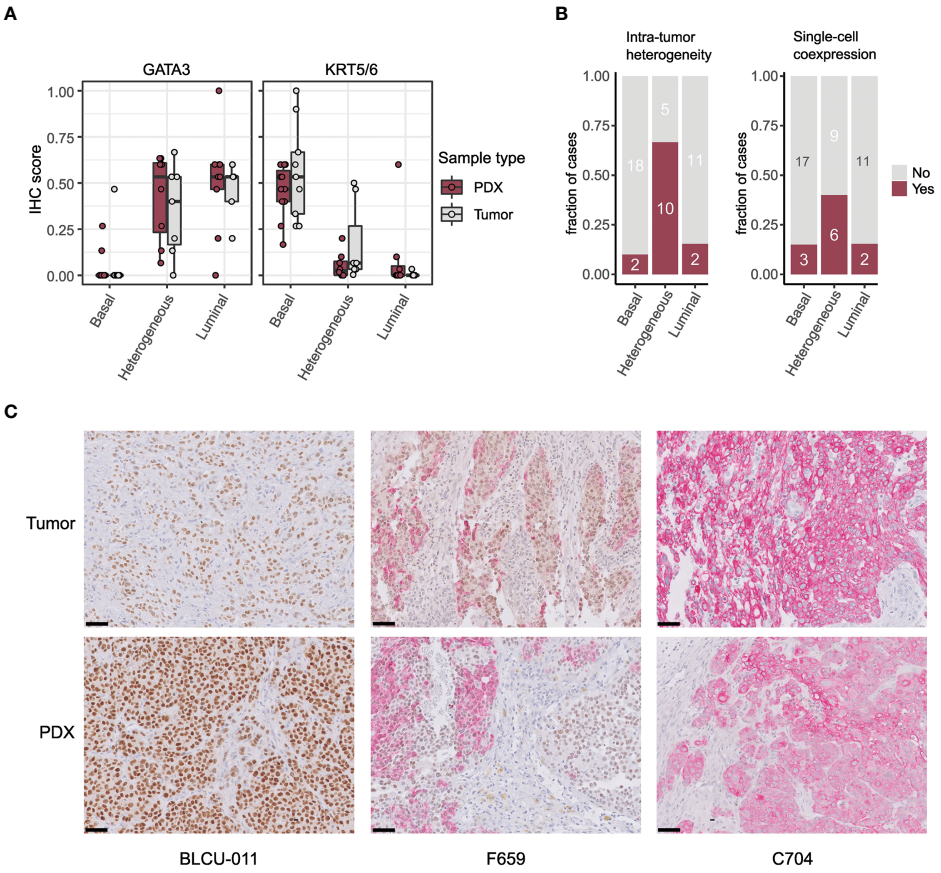


FIGURE 3
Intratumor heterogeneity in tumors and PDXs at the protein level by IHC. **(A)** GATA3 and KRT5/6 expression levels (normalized quick scores), grouped according to the PDX WISP molecular classification (luminal, heterogeneous, and Ba/Sq, Figure 2A). **(B)** Proportion of tumors with intratumoral heterogeneity (left) and GATA3 + KRT5/6 coexpression at the single-cell level (right), grouped according to the PDX WISP molecular classification (luminal, heterogeneous, and Ba/Sq, Figure 2A). **(C)** Patterns of dual IHC staining for GATA3 (brown, nuclear) and KRT5/6 (red, cytoplasmic) in the paired tumor/PDX of a luminal (BLCU-011), a heterogeneous (F659), and a Ba/Sq (C704) example.

were sensitive even when we used a lower dose of erdafitinib in a second experiment (Figure 5B).

Combined inhibition of FGFR and EGFR improves response of *FGFR3*-mutated patient-derived xenograft compared to FGFR inhibition alone

FGFR inhibitors have already demonstrated clinical efficacy in FGFR3-altered tumors (4). However, resistance to treatment is systematically observed over time. Consistently, the treatment of two *FGFR3*-mutated PDXs, one Ba/Sq and one LumP, both presenting high expression levels of FGFR3 protein compared to other non-mutated PDXs, with a pan-FGFR-inhibitor (BGJ398) (Supplementary Figure 3A) only reduced tumor growth (Supplementary Figure 3B). Different preclinical studies using bladder-derived cell lines identified EGFR activation as a mechanism of resistance to FGFR inhibition (39–41). Using reverse transcription–quantitative PCR (RT-qPCR), we confirmed that this mechanism could be relevant in our PDX models since anti-FGFR treatment not only induced the overexpression of EGFR but also ERBB2 and ERBB3 in our *FGFR3*-mutated L987 model (Supplementary Figure 3C).

Therefore, we then tested if a combination of FGFR3 and EGFR/ERBB2 inhibition could overcome the compensatory upregulation of EGFR signaling and increase the sensitivity of FGFR3-mutated PDXs to FGFR inhibition, as previously observed for RT112 xenografts harboring FGFR3-TACC3 fusion (39). We treated five PDXs (three *FGFR3*-mutated: L987, B521, F659; two Ba/Sq *FGFR3*-WT: R1056, C704) with a pan-FGFR inhibitor (erdafitinib) that recently obtained FDA approval for locally advanced or metastatic MIBC with *FGFR3* genomic alterations and an EGFR inhibitor [erlotinib, which has been described to have an ERBB2 inhibitory effect (42)] alone and in combination (Figure 5B). To limit toxicity, we used suboptimal doses for each inhibitor when administered in combination. In these conditions, monotherapies presented limited effects, with significant growth inhibition in two *FGFR3*-mutated and in two basal PDXs upon erdafitinib and erlotinib treatment, respectively. The combination of erlotinib plus erdafitinib led to an improved response in all *FGFR3*-mutated PDXs compared to each of the monotherapies, while no additional benefit was observed for the combination in the Ba/Sq *FGFR3*-WT PDXs (Figure 5B).

Discussion

The development of relevant preclinical models closely mimicking patient tumors is key in the identification of new potential therapies for precision medicine, and PDXs are widely used in this regard in oncology (24, 43).

We report here, like others (22–25), that PDXs derived from bladder and ureteral cancers preserved the histological and genomic properties of patient tumors. However, their transcriptomic profiles were less stable. Namely, we identified basal patient tumors giving rise to luminal PDXs. For these cases, both tumors and PDXs revealed high heterogeneity, suggesting intrinsic cell plasticity. Such heterogeneity and cell lineage plasticity were recently demonstrated by Sfakianos et al. in the basal N-butyl-N-(4-hydroxybutyl)-nitrosamine (BBN) chemically induced mouse bladder tumors using both single-cell transcriptomic analysis and Fluorescence-Activated Cell Sorting (FACS) analysis after the *in vivo* transplantation of FACS presorted and cultured tumor cells (44). Basal tumors present a more abundant stroma compared to luminal tumors including high infiltration by immune cells (9). Our results also suggest that, because the stroma in immune-deficient mice differs from human tumor stroma, the crosstalk between the tumor and stroma may impact the tumor cell phenotype. Such crosstalk has been reported in three-dimensional *ex vivo* models, where the absence of cancer-associated fibroblasts induced a shift from luminal tumors to basal organoids (45, 46) whereas basal organoids engrafted in mice then developed a luminal phenotype (45). Interestingly, the molecular heterogeneity of luminal/basal markers observed in tumor and PDX pairs also reinforces the relevance of our models in drug efficacy evaluation, given that tumor heterogeneity is a known cause of resistance to treatment (47).

We described potential actionable genomic alterations in our PDXs, such as *PIK3CA* mutation, *ERBB2* mutation/amplification, or *MDM2*-amplification (48, 49), whose frequencies are comparable with TCGA (10). Epigenetic drugs could also represent a promising therapeutic approach in monotherapy or in combination when considering the high proportions of PDXs harboring at least one mutation in epigenetic genes (50). Our models could thus be useful to evaluate such new potential therapies.

Previously, we proposed EGFR as a therapeutic target in basal MIBC based on findings from different *in vitro* and *in vivo* preclinical models (15). Here, we further validated the EGFR dependency of Ba/Sq tumors using PDX models. However, anti-EGFR treatments have shown disappointing results in the clinic, although some pathological responses have been observed in the neoadjuvant setting (51). This discrepancy between preclinical and clinical settings warrants further investigation. We hypothesize that the rich stroma of basal tumors contributes to anti-EGFR resistance, as recently demonstrated with cancer-associated fibroblasts in lung cancer (52). Indeed, rich stroma is absent in our preclinical models, with the exception of the BBN model, which presented only a moderate sensitivity to anti-EGFR treatment (15). Our results also suggest that sarcomatoid differentiation could be another mechanism of resistance to anti-

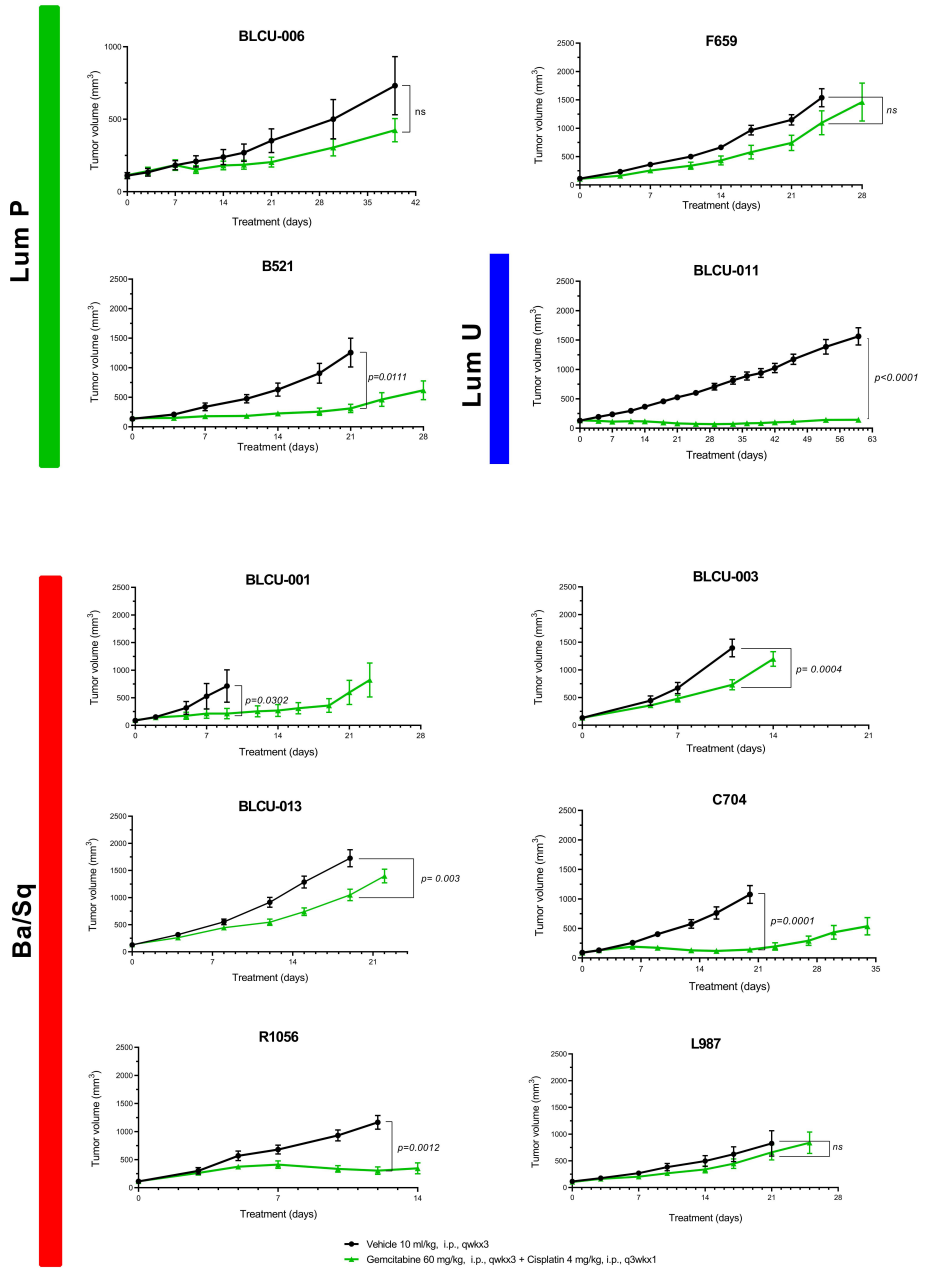


FIGURE 4
Chemosensitivity of representative basal and luminal PDX models. Mice with established PDXs (67–270 mm^3) were treated with cisplatin plus gemcitabine (green) as indicated, and control mice were treated with vehicle alone (black) (n = 7–10 animals per group). Tumor size was measured at the indicated time points. Data are presented as mean ± SEM. Results were compared using the Mann–Whitney test. n.s, non-significant.

EGFR treatment. In agreement, sarcomatoid differentiation is linked to EMT, which was previously shown to impair anti-EGFR sensitivity in lung cancer (53).

In agreement with previous studies (54, 55), we found that upper urinary tract and bladder urothelial carcinomas harbored similar genomic alterations but at different frequencies, except for the presence of MSI-H in one UTUC (54, 55). The diversity of our bank—including both MIBC [urothelial (UC) and squamous (SCC)] and UTUC—allowed us to observe that urothelial carcinoma PDXs originating from the upper urinary tract or bladder were also highly similar at the transcriptomic level. Additionally, we found that SCC samples did not classify into a

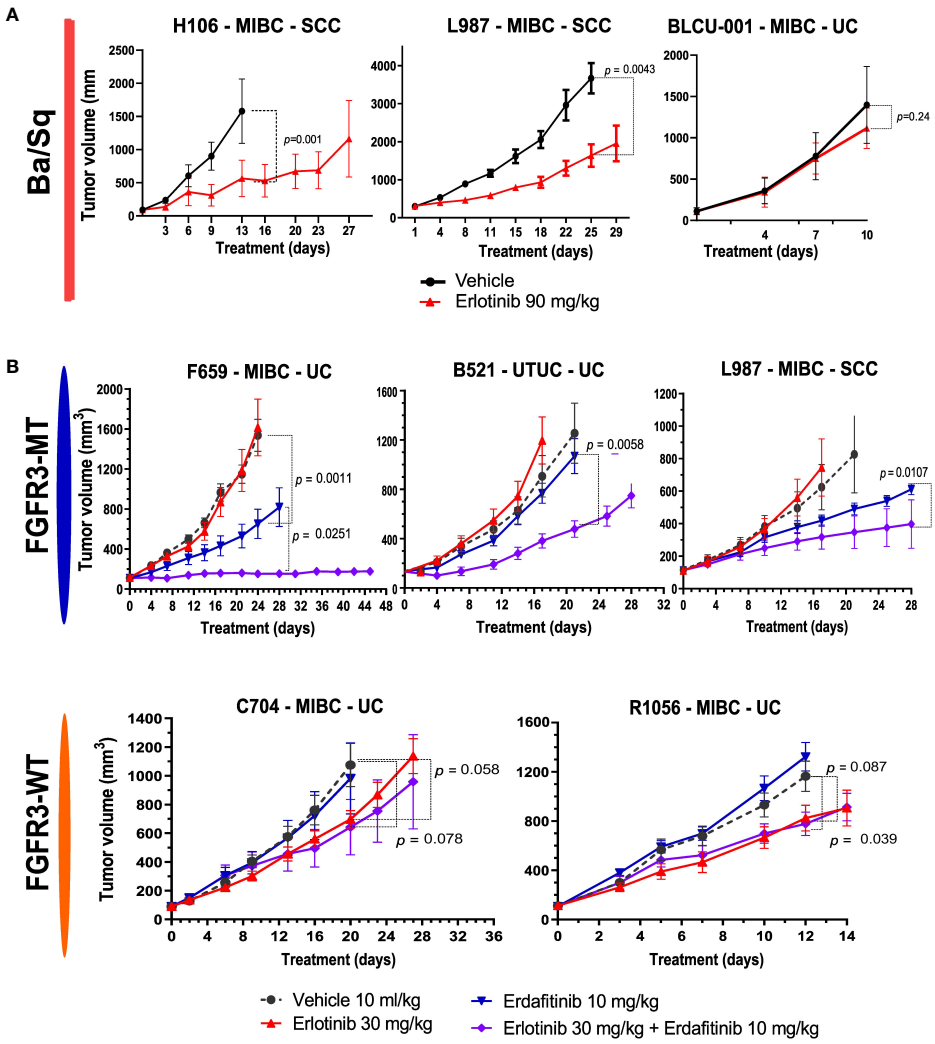


FIGURE 5
Sensitivity to anti-EGFR or the combination of EGFR and FGFR inhibitors in Ba/Sq and *FGFR3*-mutated PDXs. **(A)** Mice with established basal/squamous PDXs (67–270 mm^3) were treated with anti-EGFR (erlotinib 90 mg/kg, red) or control vehicle alone (black). **(B)** Mice with established *FGFR3*-mutated tumors and controls were treated with control vehicle (black), low-dose anti-EGFR (erlotinib 30 mg/kg, red), a pan-FGFR inhibitor (erdafitinib 10 mg/kg, blue), or the combination (purple), as indicated (n = 7–10 animals per group). Tumor size was measured at the indicated time points. Data are presented as mean ± SEM. Results were compared using the Mann–Whitney test.

molecularly distinct group of tumors, instead grouping with urothelial Ba/Sq carcinomas. Whereas up to now, SCC, UC, and UTUC were considered as highly different entities in terms of response to treatment, we found that the same molecular classifications/genetic alterations can predict the same therapeutic response for the three entities. Indeed, independently of the cell of origin, basal PDXs were sensitive to anti-EGFR therapies, except for sarcomatoid tumors, which are characterized by low EGFR activity. Furthermore, most FGFR3-mutated PDXs were sensitive to FGFR inhibition independently of their cell of origin or their luminal/basal phenotype.

Finally, it has been shown in RT112 xenografts (BCa cell line presenting an FGFR3-TACC3 fusion observed in 3% of MIBC) that a combination of anti-EGFR/anti-FGFR was more potent than anti-FGFR alone (39). We validated here these results using our more clinically relevant PDX models with *FGFR3* mutations (observed in 15% of MIBC) (three different models derived from UTUC, MIBC-UC, and MIBC-SCC) reinforcing the interest to further test this combination treatment in the clinics. For treatment optimization and to limit side effects and toxicity, it will be of interest to explore if this effect is more specifically associated with EGFR or HER2 inhibition.

Conclusion

Muscle-invasive bladder and upper urinary tract cancers are heterogeneous and aggressive diseases with no satisfactory treatment. We have developed and characterized highly relevant preclinical models for bladder and upper tract carcinoma, recapitulating the molecular heterogeneity and drug responses observed in the clinic. Our work supports a benefit of combined FGFR and EGFR inhibition in FGFR3-mutated tumors. Overall, our models represent an essential tool for the development of new efficient therapies against these aggressive cancer types.

Data availability statement

The datasets presented in this study can be found in online repositories. The names of the repository/repositories and accession number(s) can be found below: https://www.ncbi.nlm.nih.gov/geo/, GSE181962.

Ethics statement

This study was reviewed and approved by Comité de Protection des Personnes Sud-Ouest et Outre-mer, DC 2019-3565]. Written informed consent was obtained from all participants for their participation in this study. The animal study was reviewed and approved by CEEA-122.

Author contributions

IB-P had full access to all the data in the study and takes responsibility for the integrity of the data and the accuracy of the data analysis. HL, CB, ML and LC designed, performed experiments or bioinformatics analyses, analyzed and interpreted the data. HL, CB and ML developed the PDXs models. HL, XG, PR provided samples and helped with clinical data analysis. CB and ML performed the pharmacological characterization of the PDXs. CB, CK and JF prepared DNA and RNA for genomics analysis. CB performed STR analysis under TM supervision. CK performed and analyzed sanger sequencing. CK and VD performed immunohistochemical experiments under YA supervision. JF performed histo- and immunohistopathological analysis and designed pharmacological studies for sarcomatoid tumors under YA supervision. FD performed Western blot and RT-qPCR analysis. LC performed most of the bioinformatics analyses together with help of CSG, XM and AK for tumor's/PDXs' classification and for regulon analysis. ADR supervised AK and CG. EC normalized and annotated Affymetrix array data and centralized the data for bioinformatics analyses. JM-P and RB performed and analyzed targeted NGS under the supervision of IB. VL performed and supervised histopathological analysis of tumors and PDXs. YM and PL designed the study and supervised establishment of part of the PDXs and pharmacological characterization of PDXs. FR supervised the genomic analyses. TM and HL designed and supervised the establishment of part of the PDXs. IB-P and TM designed and supervised the research, analyzed and interpreted the data. LC, CB, JF, TM and IB-P wrote the paper. All authors contributed to the article and approved the submitted version.

Funding

This work was supported by a grant from Ligue Nationale Contre le Cancer (LC, FD, JF, CK, CG, XM, YA, FR, IB-P) as an associated team (Equipe labellisee'), the "Carte d'Identité des Tumeurs" program initiated, developed, and funded by Ligue Nationale Contre le Cancer. This work was supported by the Institut National du Cancer: PRTK project "BoBCaT". LC was supported by FRM (Fondation Recherche Médicale) and JF by the Fondation ARC pour la recherche sur le cancer. XM was supported by a fellowship from ITMO Cancer AVIESAN, within the framework of Cancer Plan. We also thank BPI France, the Region Alsace, the European Funds for Regional Development, the Strasbourg Urban Community, INSERM, and the University of Strasbourg for financial support (recipients TM and HL for the innovative Urolead SAS company that was acquired by Urosphere in 2017 and Urosphere supported by the European Funds for Regional Development).

Acknowledgments

We thank David Gentien from the genomics platform of Institut Curie. We also thank the Alsace incubator SEMIA, Strasbourg, France, for advices and financial support (recipients TM and HL for Urolead SAS). We also thank the competitivity pole Alsace Biovalley, Illkirch-Graffenstaden, France for advices and labelization (TM and HL, for Urolead SAS). Finally, we also thank Alsace Satt Conectus, Illkirch-Graffenstaden, France, for technology transfer and advices (TM and HL, for Urolead SAS).

Conflict of interest

Author's CB, ML, YM and PL were employed by Urosphere and author FD was employed by Inovarion, Institut Curie, Strasbourg University and Urosphere have a collaboration contract for the transcriptomic, genomic, and pharmacological characterization of the PDX.

The remaining authors declare that the research was conducted in the absence of any commercial or financial relationships that could be construed as a potential conflict of interest.

Publisher's note

All claims expressed in this article are solely those of the authors and do not necessarily represent those of their affiliated organizations, or those of the publisher, the editors and the reviewers. Any product that may be evaluated in this article, or claim that may be made by its manufacturer, is not guaranteed or endorsed by the publisher.

Supplementary material

The Supplementary Material for this article can be found online at: https://www.frontiersin.org/articles/10.3389/fonc.2022.930731/full#supplementary-material

SUPPLEMENTARY FIGURE 1
Unsupervised hierarchical clustering and heatmap of PDX samples based on genes with the most variant expression (n=200). PDX identifiers indicated at the bottom. Classifications indicated according to legend on the right (as in Figure 2).

SUPPLEMENTARY FIGURE 2
Expression of NECTIN4 and TROP2 (*TACSTD2*) in PDXs. **(A)** Heatmap of PDX samples based on *NECTIN4* and *TACSTD2* gene expression. **(B)** *NECTIN4* and *TROP2* (TACSTD2) expression levels grouped according to the Base47 molecular classification (Wilcoxon test). **(C)** Correlation of the *NECTIN4* and *TACSTD2* gene expression (Pearson test).

SUPPLEMENTARY FIGURE 3
FGFR3 expression in PDXs and sensitivity to anti-FGFR of FGFR3 mutated PDXs. **(A)** FGFR3 protein levels (Western blot) of the different PDX models. The urinary BCa cell line, RT112, was used as control for WT FGFR3 (black arrow) and FGFR3-TACC3 (white arrow) protein expression. Beta-actin was used as loading control. Asterisk indicates non-specific band. **(B)** Mice with established *FGFR3*-mutated (FGFR3-MT) PDXs (67-270 mm3) were treated with a pan-FGFR inhibitor (BGJ398). Control mice were treated with vehicle alone (n = 7 to 10 animals per group). Tumor size was measured at the indicated time points. Data are presented as mean ± SEM. Results were compared using Mann-Whitney test. **(C)** EGFR, ERBB2 and ERBB3 expression (RT-qPCR analysis) in L987 model at the end of treatment in mice treated with vehicle or with the pan-FGFR inhibitor BGJ398.

SUPPLEMENTARY TABLE 1
Clinical and histological characteristics of patient tumors and matched PDXs.

SUPPLEMENTARY TABLE 2
Short Tandem repeat (STR) profiling of patient tumors and matched PDX(s).

SUPPLEMENTARY TABLE 3
List of the sequenced genes in the next-generation targeted sequencing panel.

SUPPLEMENTARY TABLE 4
Next-generation sequencing results (mutations, copy number alterations, microsatellite status and tumor mutational burden).

References

1. Sung H, Ferlay J, Siegel RL, Laversanne M, Soerjomataram I, Jemal A, et al. Global cancer statistics 2020: GLOBOCAN estimates of incidence and mortality worldwide for 36 cancers in 185 countries. *CA Cancer J Clin* (2021) 71(3):209–49. doi: 10.3322/caac.21660

2. Flaig TW, Spiess PE, Agarwal N, Bangs R, Boorjian SA, Buyyounouski MK, et al. Bladder cancer, version 3.2020, NCCN clinical practice guidelines in oncology. *J Natl Compr Cancer Netw JNCCN* (2020) 18(3):329–54.

3. Leow JJ, Chong YL, Chang SL, Valderrama BP, Powles T, Bellmunt J. Neoadjuvant and adjuvant chemotherapy for upper tract urothelial carcinoma: A 2020 systematic review and meta-analysis, and future perspectives on systemic therapy. *Eur Urol* (2021) 79(5):635–54. doi: 10.1016/j.eururo.2020.07.003

4. Loriot Y, Necchi A, Park SH, Garcia-Donas J, Huddart R, Burgess E, et al. Erdafitinib in locally advanced or metastatic urothelial carcinoma. *N Engl J Med* (2019) 381(4):338–48. doi: 10.1056/NEJMoa1817323

5. Tagawa ST, Balar AV, Petrylak DP, Kalebasty AR, Loriot Y, Fléchon A, et al. TROPHY-U-01: A phase II open-label study of sacituzumab govitecan in patients with metastatic urothelial carcinoma progressing after platinum-based chemotherapy and checkpoint inhibitors. *J Clin Oncol Off J Am Soc Clin Oncol* (2021) 39(22):2474–85. doi: 10.1200/JCO.20.03489

6. Powles T, Rosenberg JE, Sonpavde GP, Loriot Y, Durán I, Lee JL, et al. Enfortumab vedotin in previously treated advanced urothelial carcinoma. *N Engl J Med* (2021) 384(12):1125–35. doi: 10.1056/NEJMoa2035807

7. Chu CE, Sjöström M, Egusa EA, Gibb EA, Badura ML, Zhu J, et al. Heterogeneity in NECTIN4 expression across molecular subtypes of urothelial cancer mediates sensitivity to enfortumab vedotin. *Clin Cancer Res* (2021) 27 (18):5123–30. doi: 10.1158/1078-0432.CCR-20-4175

8. Chou J, Trepka K, Sjöström M, Egusa EA, Chu CE, Zhu J, et al. Expression across molecular subtypes of urothelial carcinoma and enfortumab vedotin-resistant cells. *Eur Urol Oncol* (2022) S2588-9311(21):00215–7. doi: 10.1007/978-3-030-89891-5_11

9. Kamoun A, de Reyniès A, Allory Y, Sjödahl G, Robertson AG, Seiler R, et al. A consensus molecular classification of muscle-invasive bladder cancer. *Eur Urol* (2020) 77(4):420–33. doi: 10.1016/j.eururo.2019.09.006

10. Robertson AG, Kim J, Al-Ahmadie H, Bellmunt J, Guo G, Cherniack AD, et al. Comprehensive molecular characterization of muscle-invasive bladder cancer. *Cell* (2017) 171(3):540–56.e25. doi: 10.1016/j.cell.2017.09.007

11. Taber A, Christensen E, Lamy P, Nordentoft I, Prip F, Lindskrog SV, et al. Molecular correlates of cisplatin-based chemotherapy response in muscle invasive bladder cancer by integrated multi-omics analysis. *Nat Commun* (2020) 11 (1):4858. doi: 10.1038/s41467-020-18640-0

12. Seiler R, Ashab HAD, Erho N, van Rhijn BWG, Winters B, Douglas J, et al. Impact of molecular subtypes in muscle-invasive bladder cancer on predicting response and survival after neoadjuvant chemotherapy. *Eur Urol* (2017) 72(4):544 –54. doi: 10.1016/j.eururo.2017.03.030

13. Seiler R, Gibb EA, Wang NQ, Oo HZ, Lam HM, van Kessel KE, et al. Divergent biological response to neoadjuvant chemotherapy in muscle-invasive bladder cancer. *Clin Cancer Res* (2019) 25(16):5082–93. doi: 10.1158/1078-0432.CCR-18-1106

14. Sjödahl G, Abrahamsson J, Holmsten K, Bernardo C, Chebil G, Eriksson P, et al. Different responses to neoadjuvant chemotherapy in urothelial carcinoma molecular subtypes. *Eur Urol* (2021) S0302-2838(21):02138–2. doi: 10.1016/j.eururo.2021.10.035

15. Rebouissou S, Bernard-Pierrot I, de Reyniès A, Lepage ML, Krucker C, Chapeaublanc E, et al. EGFR as a potential therapeutic target for a subset of muscle-invasive bladder cancers presenting a basal-like phenotype. *Sci Transl Med* (2014) 6 (244):244ra91. doi: 10.1126/scitranslmed.3008970

16. Choi W, Czerniak B, Ochoa A, Su X, Siefker-Radtke A, Dinney C, et al. Intrinsic basal and luminal subtypes of muscle-invasive bladder cancer. *Nat Rev Urol* (2014) 11(7):400–10. doi: 10.1038/nrurol.2014.129

17. Seiler R, Ashab HAD, Erho N, van Rhijn BWG, Winters B, Douglas J, et al. Impact of molecular subtypes in muscle-invasive bladder cancer on predicting response and survival after neoadjuvant chemotherapy. *Eur Urol* (2017) 72(4):544 –54. doi: 10.1016/j.eururo.2017.03.030

18. Rose M, Maurer A, Wirtz J, Bleilevens A, Waldmann T, Wenz M, et al. EGFR activity addiction facilitates anti-ERBB based combination treatment of

squamous bladder cancer. *Oncogene* (2020) 39(44):6856–70. doi: 10.1038/s41388-020-01465-y

19. Hassler MR, Bray F, Catto JWF, Grollman AP, Hartmann A, Margulis V, et al. Molecular characterization of upper tract urothelial carcinoma in the era of next-generation sequencing: A systematic review of the current literature. *Eur Urol* (2020) 78(2):209–20. doi: 10.1016/j.eururo.2020.05.039

20. Hidalgo M, Amant F, Biankin AV, Budinská E, Byrne AT, Caldas C, et al. Patient-derived xenograft models: an emerging platform for translational cancer research. *Cancer Discov* (2014) 4(9):998–1013. doi: 10.1158/2159-8290.CD-14-0001

21. Yoshida GJ. Applications of patient-derived tumor xenograft models and tumor organoids. *J Hematol OncolJ Hematol Oncol* (2020) 13(1):4. doi: 10.1186/s13045-019-0829-z

22. Pan CX, Zhang H, Tepper CG, yin LT, Davis RR, Keck J, et al. Development and characterization of bladder cancer patient-derived xenografts for molecularly guided targeted therapy. *PLoS One* (2015) 10(8):e0134346. doi: 10.1371/journal.pone.0134346

23. Jäger W, Xue H, Hayashi T, Janssen C, Awrey S, Wyatt AW, et al. Patient-derived bladder cancer xenografts in the preclinical development of novel targeted therapies. *Oncotarget* (2015) 6(25):21522–32. doi: 10.18632/oncotarget.3974

24. Tracey AT, Murray KS, Coleman JA, Kim K. Patient-derived xenograft models in urological malignancies: Urothelial cell carcinoma and renal cell carcinoma. *Cancers* (2020) 12(2):439. doi: 10.3390/cancers12020439

25. Kim K, Hu W, Audenet F, Almassi N, Hanrahan AJ, Murray K, et al. Modeling biological and genetic diversity in upper tract urothelial carcinoma with patient derived xenografts. *Nat Commun* (2020) 11(1):1975. doi: 10.1038/s41467-020-15885-7

26. Rochel N, Krucker C, Coutos-Thévenot L, Osz J, Zhang R, Guyon E, et al. Recurrent activating mutations of PPARγ associated with luminal bladder tumors. *Nat Commun* (2019) 10(1):253. doi: 10.1038/s41467-018-08157-y

27. Damrauer JS, Hoadley KA, Chism DD, Fan C, Tiganelli CJ, Wobker SE, et al. Intrinsic subtypes of high-grade bladder cancer reflect the hallmarks of breast cancer biology. *Proc Natl Acad Sci USA* (2014) 111(8):3110–5. doi: 10.1073/pnas.1318376111

28. Irizarry RA, Hobbs B, Collin F, Beazer-Barclay YD, Antonellis KJ, Scherf U, et al. Exploration, normalization, and summaries of high density oligonucleotide array probe level data. *Biostat Oxf Engl* (2003) 4(2):249–64. doi: 10.1093/biostatistics/4.2.249

29. Dai M, Wang P, Boyd AD, Kostov G, Athey B, Jones EG, et al. Evolving gene/transcript definitions significantly alter the interpretation of GeneChip data. *Nucleic Acids Res* (2005) 33(20):e175. doi: 10.1093/nar/gni179

30. Lachmann A, Giorgi FM, Lopez G, Califano A. ARACNe-AP: gene network reverse engineering through adaptive partitioning inference of mutual information. *Bioinformatics* (2016) 32(14):2233–5. doi: 10.1093/bioinformatics/btw216

31. Love MI, Huber W, Anders S. Moderated estimation of fold change and dispersion for RNA-seq data with DESeq2. *Genome Biol* (2014) 15(12):550. doi: 10.1186/s13059-014-0550-8

32. Alvarez MJ, Shen Y, Giorgi FM, Lachmann A, Ding BB, Ye BH, et al. Functional characterization of somatic mutations in cancer using network-based inference of protein activity. *Nat Genet* (2016) 48(8):838–47. doi: 10.1038/ng.3593

33. Sirab N, Drubay D, Maillé P, Popova T, Ngo C, Gentien D, et al. Multilayer spectrum of intratumoral heterogeneity in basal bladder cancer. *J Pathol* (2022) 256 (1):108–18. doi: 10.1002/path.5813

34. Humphrey PA, Moch H, Cubilla AL, Ulbright TM, Reuter VE. The 2016 WHO classification of tumours of the urinary system and Male genital organs-part b: Prostate and bladder tumours. *Eur Urol* (2016) 70(1):106–19. doi: 10.1016/j.eururo.2016.02.028

35. Biton A, Bernard-Pierrot I, Lou Y, Krucker C, Chapeaublanc E, Rubio-Pérez C, et al. Independent component analysis uncovers the landscape of the bladder tumor transcriptome and reveals insights into luminal and basal subtypes. *Cell Rep* (2014) 9(4):1235–45. doi: 10.1016/j.celrep.2014.10.035

36. Halstead AM, Kapadia CD, Bolzenius J, Chu CE, Schriefer A, Wartman LD, et al. Bladder-cancer-associated mutations in RXRA activate peroxisome proliferator-activated receptors to drive urothelial proliferation. *eLife* (2017) 16 (6):e30862. doi: 10.7554/eLife.30862

37. Korpal M, Puyang X, Jeremy Wu Z, Seiler R, Furman C, Oo HZ, et al. Evasion of immunosurveillance by genomic alterations of PPARγ/RXRα in bladder cancer. *Nat Commun* (2017) 8(1):103. doi: 10.1038/s41467-017-00147-w

38. Guo CC, Majewski T, Zhang L, Yao H, Bondaruk J, Wang Y, et al. Dysregulation of EMT drives the progression to clinically aggressive sarcomatoid bladder cancer. *Cell Rep* (2019) 27(6):1781–93.e4. doi: 10.1016/j.celrep.2019.04.048

39. Herrera-Abreu MT, Pearson A, Campbell J, Shnyder SD, Knowles MA, Ashworth A, et al. Parallel RNA interference screens identify EGFR activation as an escape mechanism in FGFR3-mutant cancer. *Cancer Discov* (2013) 3(9):1058–71. doi: 10.1158/2159-8290.CD-12-0569

40. Wang L, Šuštić T, Leite de Oliveira R, Lieftink C, Halonen P, van de Ven M, et al. A functional genetic screen identifies the phosphoinositide 3-kinase pathway as a determinant of resistance to fibroblast growth factor receptor inhibitors in FGFR mutant urothelial cell carcinoma. *Eur Urol* (2017) 71(6):858–62. doi: 10.1016/j.eururo.2017.01.021

41. Datta J, Damodaran S, Parks H, Ocrainiciuc C, Miya J, Yu L, et al. Activation mediates acquired resistance to fibroblast growth factor receptor inhibitor BGJ398. *Mol Cancer Ther* (2017) 16(4):614–24. doi: 10.1158/1535-7163.MCT-15-1010

42. Schaefer G, Shao L, Totpal K, Akita RW. Erlotinib directly inhibits HER2 kinase activation and downstream signaling events in intact cells lacking epidermal growth factor receptor expression. *Cancer Res* (2007) 67(3):1228–38. doi: 10.1158/0008-5472.CAN-06-3493

43. Bhimani J, Ball K, Stebbing J. Patient-derived xenograft models–the future of personalised cancer treatment. *Br J Cancer* (2020) 122(5):601–2. doi: 10.1038/s41416-019-0678-0

44. Sfakianos JP, Daza J, Hu Y, Anastos H, Bryant G, Bareja R, et al. Epithelial plasticity can generate multi-lineage phenotypes in human and murine bladder cancers. *Nat Commun* (2020) 11:2540. doi: 10.1038/s41467-020-16162-3

45. Lee SH, Hu W, Matulay JT, Silva MV, Owczarek TB, Kim K, et al. Tumor evolution and drug response in patient-derived organoid models of bladder cancer. *Cell* (2018) 173(2):515–28.e17. doi: 10.1016/j.cell.2018.03.017

46. Kim E, Choi S, Kang B, Kong J, Kim Y, Yoon WH, et al. Creation of bladder assembloids mimicking tissue regeneration and cancer. *Nature* (2020) 588 (7839):664–9. doi: 10.1038/s41586-020-3034-x

47. Dagogo-Jack I, Shaw AT. Tumour heterogeneity and resistance to cancer therapies. *Nat Rev Clin Oncol* (2018) 15(2):81–94. doi: 10.1038/nrclinonc.2017.166

48. Koshkin VS, O'Donnell P, Yu EY, Grivas P. Systematic review: Targeting HER2 in bladder cancer. *Bladder Cancer* (2019) 5(1):1–12. doi: 10.3233/BLC-180196

49. Sathe A, Nawroth R. Targeting the PI3K/AKT/mTOR pathway in bladder cancer. *Methods Mol Biol Clifton NJ* (2018) 1655:335–50. doi: 10.1007/978-1-4939-7234-0_23

50. Morel D, Jeffery D, Aspeslagh S, Almouzni G, Postel-Vinay S. Combining epigenetic drugs with other therapies for solid tumours — past lessons and future promise. *Nat Rev Clin Oncol* (2020) 17(2):91–107. doi: 10.1038/s41571-019-0267-4

51. Pruthi RS, Nielsen M, Heathcote S, Wallen EM, Rathmell WK, Godley P, et al. A phase II trial of neoadjuvant erlotinib in patients with muscle-invasive bladder cancer undergoing radical cystectomy: clinical and pathological results. *BJU Int* (2010) 106(3):349–54. doi: 10.1111/j.1464-410X.2009.09101.x

52. Hu H, Piotrowska Z, Hare PJ, Chen H, Mulvey HE, Mayfield A, et al. Three subtypes of lung cancer fibroblasts define distinct therapeutic paradigms. *Cancer Cell* (2021) 39(11):1531–47.e10. doi: 10.1016/j.ccell.2021.09.003

53. Tulchinsky E, Demidov O, Kriajevska M, Barlev NA, Imyanitov E. EMT: A mechanism for escape from EGFR-targeted therapy in lung cancer. *Biochim Biophys Acta BBA - Rev Cancer* (2019) 1871(1):29–39. doi: 10.1016/j.bbcan.2018.10.003

54. Necchi A, Madison R, Pal SK, Ross JS, Agarwal N, Sonpavde G, et al. Comprehensive genomic profiling of upper-tract and bladder urothelial carcinoma. *Eur Urol Focus* (2021). 7(6):1339–46. doi: 10.1016/j.euf.2020.08.001

55. Sfakianos JP, Cha EK, Iyer G, Scott SN, Zabor EC, Shah RH, et al. Genomic characterization of upper tract urothelial carcinoma. *Eur Urol* (2015) 68(6):970–7. doi: 10.1016/j.eururo.2015.07.039

COPYRIGHT

© 2022 Lang, Béraud, Cabel, Fontugne, Lassalle, Krucker, Dufour, Groeneveld, Dixon, Meng, Kamoun, Chapeaublanc, De Reynies, Gamé, Rischmann, Bieche, Masliah-Planchon, Beaurepere, Allory, Lindner, Misseri, Radvanyi, Lluel, Bernard-Pierrot and Massfelder. This is an open-access article distributed under the terms of the Creative Commons Attribution License (CC BY). The use, distribution or reproduction in other forums is permitted, provided the original author(s) and the copyright owner(s) are credited and that the original publication in this journal is cited, in accordance with accepted academic practice. No use, distribution or reproduction is permitted which does not comply with these terms.

frontiers | Frontiers in Oncology

TYPE Original Research
PUBLISHED 16 August 2022
DOI 10.3389/fonc.2022.882888

Check for updates

OPEN ACCESS

EDITED BY
Takeshi Yuasa,
Japanese Foundation for Cancer Research, Japan

REVIEWED BY
Dongjun Lee,
Pusan National University, South Korea
Simin Li,
Southern Medical University, China

*CORRESPONDENCE
Hong Cheng
Njmuchss@163.com
Ninghan Feng
n.feng@njmu.edu.cn
Weipu Mao
maoweipu@tongji.edu.cn
Ming Chen
mingchenseu@126.com

†These authors have contributed equally to this work and share first authorship

SPECIALTY SECTION
This article was submitted to Genitourinary Oncology, a section of the journal Frontiers in Oncology

RECEIVED 24 February 2022
ACCEPTED 19 July 2022
PUBLISHED 16 August 2022

CITATION
Gan X, Liu R, Cheng H, Mao W, Feng N and Chen M (2022) *ASNS* can predict the poor prognosis of clear cell renal cell carcinoma.
Front. Oncol. 12:882888.
doi: 10.3389/fonc.2022.882888

COPYRIGHT
© 2022 Gan, Liu, Cheng, Mao, Feng and Chen. This is an open-access article distributed under the terms of the Creative Commons Attribution License (CC BY). The use, distribution or reproduction in other forums is permitted, provided the original author(s) and the copyright owner(s) are credited and that the original publication in this journal is cited, in accordance with accepted academic practice. No use, distribution or reproduction is permitted which does not comply with these terms.

ASNS can predict the poor prognosis of clear cell renal cell carcinoma

Xinqiang Gan[1,2†], Ruiji Liu[2†], Hong Cheng[2*], Weipu Mao[1*], Ninghan Feng[3*] and Ming Chen[2,4*]

[1]Department of Urology, People's Hospital of Putuo District, Shanghai, China, [2]Department of Urology, Affiliated Zhongda Hospital of Southeast University, Nanjing, China, [3]Department of Urology, Wuxi No.2 Hospital, Nanjing Medical University, Wuxi, China, [4]Nanjing Lishui District People's Hospital, Zhongda Hospital Lishui Branch, Southeast University, Nanjing, China

Purpose: Clear cell renal cell carcinoma (ccRCC) is one of the most common malignancies of the urinary system. This study was conducted to discover a new target that can predict the prognosis and promote the treatment of ccRCC.

Methods: The raw data were downloaded from the TCGA database, and the predictive value of *ASNS* for various clinicopathological features was verified in the following analysis. Then, we analyzed the potential involvement of *ASNS* in tumor immunity and obtained the possible pathways involving *ASNS* through GO/KEGG enrichment analysis and GSEA. We also further verified our findings in pathological specimens of ccRCC patients.

Results: *ASNS* expression was significantly increased in ccRCC, which was associated with advanced clinicopathological characteristics. It was an independent prognostic factor for overall survival in 535 patients with ccRCC. Immune cell infiltration analysis revealed that *ASNS* expression was related to T lymphocyte infiltration of tumors and poor prognosis. Moreover, we performed relevant functional enrichment analyses of *ASNS*.

Conclusions: *ASNS* might play a significant role in the development and immune cell infiltration of ccRCC and serve as a valuable clinical prognostic biomarker.

KEYWORDS

clear cell renal cell carcinoma, asparagine synthase, tumor microenvironment, immune infiltration, prognosis

Introduction

Renal cell carcinoma (RCC) is a common cancer type, and approximately 430,000 new global cases and 170,000 RCC-related deaths occurred in 2020 (1). RCC accounts for approximately 3% of all cancers, with the highest incidence in Western countries, and 80%–90% of RCC are clear cell renal cell carcinoma (ccRCC) (2). None of the treatments

were effective in patients with renal tumors subjected to the same surgical procedures and patients with advanced disease treated with similar drugs (3). Although an occasional response was reported, the available systemic therapies did not increase the survival of patients with advanced disease (2). Early detection and screening are priorities for RCC research (4). Therefore, discovering a new target of ccRCC, especially for those with advanced and metastatic diseases, is crucial.

Asparagine synthase (ASNS) catalyzes the synthesis of asparagine and glutamate from aspartic acid and glutamine in an ATP-dependent amidotransferase reaction, accompanied by glutamine deamidation (5). Large-scale loss-of-function analysis *in vitro* identified *ASNS* as cancer dependent in several solid malignancies; however, the specific mechanism has not been discovered (6). Knott et al. highlighted the role of ASNS in tumor growth and metastatic dissemination in a breast cancer model (7), prompting the necessity to evaluate the expression of *ASNS* and facilitating the prognosis of patients with ccRCC.

We downloaded raw data from The Cancer Genome Atlas (TCGA) database and verified the predictive value of *ASNS* for various clinicopathological features in the following analyses. We analyzed the potential involvement of ASNS in tumor immunity and identified the possible pathways associated with ASNS through Gene Ontology (GO)/Kyoto Encyclopedia of Genes and Genomes (KEGG) enrichment analyses and gene set enrichment analysis (GSEA). We further verified our findings in the pathological specimens of patients with ccRCC. To conclude, we found that *ASNS* was highly expressed in ccRCC patients, and its high expression could lead to a worse prognosis. Thus, our findings revealed that *ASNS* might play a significant role in the development and immune cell infiltration of ccRCC and serve as a valuable clinical prognostic biomarker.

Materials and methods

Public database collection

Gene expression (535 tumor and 72 normal samples), DNA methylation, phenotype, and survival data were downloaded from http://xena.ucsc.edu/. $|\log FC| > 1.5$ and $p < 0.01$ were defined as the criteria for differentially expressed genes (DEGs), and DEGs were identified using the limma R package.

COX univariate and multivariate analysis

Cox univariate and multivariate analyses were performed to determine the risk factors for ccRCC prognosis using R software.

Survival analysis

Overall survival (OS) and progression-free survival rates of patients with ccRCC were investigated by Kaplan–Meier analysis.

Correlation between immune infiltration and expression

TIMER2.0 (http://timer.comp-genomics.org/) was used for the comprehensive analysis of the relationship between *ASNS* expression and tumor-infiltrating immune cell levels, namely, CD4+ T cells, Tregs, CD8+ T cells, CTLA4, and PD-L1 (CD274) (8).

Expression of hub genes and survival analysis

The STRING (https://string-db.org/) website analyzes protein–protein interactions using a unique set of computer prediction models (9). The expression levels of hub genes in tumor and normal tissues based on the ccRCC dataset were compared using the Wilcoxon rank-sum test ($p < 0.05$). OS analysis for the expression of hub genes between the high- and low-expression groups was performed, with a p-value of <0.05 indicating statistical significance.

GEPIA2

GEPIA2 (http://gepia2.cancer-pku.cn/#index) uses standard processing procedures to analyze the data using many tumor samples and normal tissue samples (10). GEPIA2 analyzes the OS or disease-free survival of cancer patients based on gene expression. GEPIA2 uses the Log-rank test for hypothesis testing. The hazard ratio and 95% confidence interval are also included in survival plots.

GO and KEGG enrichment analyses

According to *ASNS* expression level, ccRCC samples were sorted and divided into two groups of high and low expression, and the genes with differential expression were screened separately ($|\log FC| > 0.5$, p-value < 0.05). The Clusterprofiler R package was used for GO enrichment analysis, which included molecular function, biological processes, and cellular components of DEGs, and KEGG enrichment analysis.

Gene set enrichment analysis

The molecular mechanisms involved in ccRCC with different levels of *ASNS* expression were examined by the GSEA approach (11). The reference gene set used for GSEA was obtained from c7.immunesigdb.v7.5.1.symbols.gmt. Gene sets with a nominal *p*-value less than 0.05, |Normalized Enrichment Score| greater than 1, and false discovery rate less than 0.25 in the GSEA report were considered statistically significant.

Western blotting

Western blotting was performed as described in our previous study (12).

Immunohistochemistry

The expression and distribution of ASNS protein were detected by immunohistochemistry in paraffin-embedded tissue sections of each group. After routine paraffin dewaxing to water, antigen repair was performed. Hydrogen peroxide solution (3%) was added to remove endogenous catalase. Bovine serum albumin sealing solution (1%) was added, and the slides were incubated for 15 min. After the blocking solution was added, the primary antibody against ASNS (1:100 dilution) was added, and the slides were incubated overnight at 4°C. Thereafter, they were washed thrice with phosphate-buffered saline with Tween 20. The secondary antibody (1:100 dilution) was added, and the slides were incubated for 1 h at room temperature. DAB was added for color development, after which the slides were re-dyed with hematoxylin for 30 s. After washing with running water for 1 min, the slides were treated with 0.1% sodium bicarbonate to develop blue color. Then, the slides were subjected to dehydration and xylene treatment until the sections became transparent, mounted with neutral gum, observed under a microscope, and photographed.

The immunohistochemical staining intensity of ASNS was assessed using ImageJ software with the assistance of experienced pathologists in Affiliated Zhongda Hospital of Southeast University (13, 14).

Sample information

Clinical data of 81 patients were collected at the Affiliated Zhongda Hospital of Southeast University from March 2019 to May 2022. All patients were diagnosed with ccRCC (unilateral) and had no other carcinomas. All patients did not undergo any preoperative therapy for the carcinoma (chemotherapy, targeted therapy, immunotherapy, etc.). Age distribution: 19–85 years old. Surgical modalities: Partial nephrectomy or radical nephrectomy. Neoplasm histological grade criteria: Fuhrman nuclear grading system. Pathological stage criteria: American Joint Committee on Cancer (AJCC).

Statistical analysis

Analyses were performed using IBM SPSS for MAC version 26.0. The Mann–Whitney test was used to compare continuous variables between the two groups. The immunohistochemical staining intensity and clinical characteristics, such as gender, age, location, tumor size, TNM stage, AJCC stage, and grade were subjected to Spearman rank correlation analysis. *p*-values less than 0.05 were considered statistically significant.

Results

Overexpression of ASNS mRNA in ccRCC is related to poor prognosis

The expression pattern of *ASNS* in multiple pan-cancers was evaluated by using data from TIMER2.0, and the prognostic values of *ASNS* in multiple cancers (invasive breast carcinoma, cervical squamous cell carcinoma, endocervical adenocarcinoma, cholangiocarcinoma, esophageal carcinoma, kidney renal clear cell carcinoma, hepatocellular carcinoma, lung adenocarcinoma, lung squamous cell carcinoma, pancreatic adenocarcinoma, and stomach adenocarcinoma) are shown in the survival map prepared using GEPIA2 (Figures 1A, B). The pan-cancer overexpression of *ASNS* was linked to poor prognosis. The mRNA data of ccRCC were downloaded from TCGA (https://xenabrowser.net/datapages/) and included 535 tumor tissues and 72 normal tissues. *ASNS* was highly expressed in ccRCC compared with normal renal tissues ($p < 0.001$; Figure 1C) and was correlated with poor prognosis, i.e., OS ($p < 0.001$; Figure 1D). Furthermore, the high protein expression level of *ASNS* in ccRCC was verified by data from the Human Protein Atlas (HPA) databases (https://www.proteinatlas.org/) (Figure 1E).

For further clinical research, the expression pattern of *ASNS* was studied in relation to several clinicopathological features, and the data demonstrated that *ASNS* expression gradually increased with tumor progression (Figure 2). Therefore, *ASNS* could be an independent factor predicting ccRCC prognosis.

ASNS is an independent prognostic factor for ccRCC

Univariate independent prognostic analysis demonstrated that neoplasm histologic grades, pathological T&M stages, tumor stages, and the expression of *ASNS* were significant factors that could predict ccRCC prognosis ($p < 0.001$; hazard

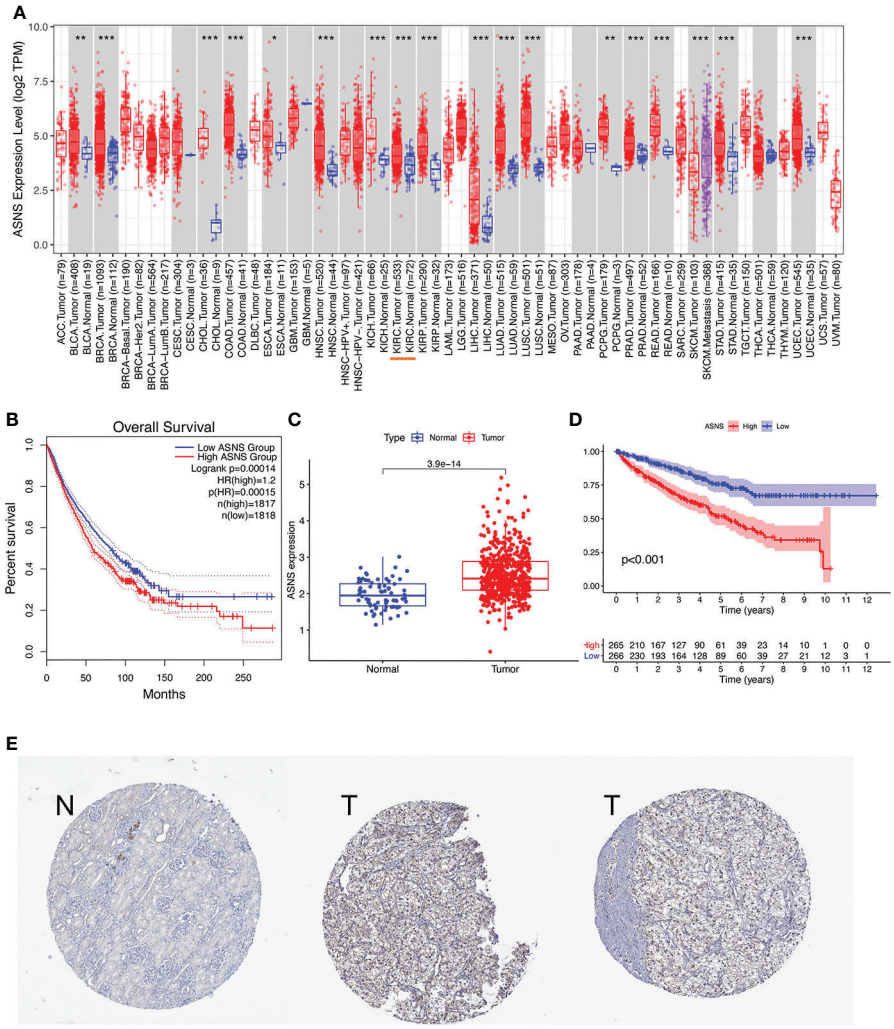


FIGURE 1
Expression of *ASNS*. **(A)** Pan-cancer expression of *ASNS*. **(B)** Prognostic values of *ASNS* gene in multiple cancers (BRCA, CESC, CHOL, ESCA, KIRC, LIHC, LUAD, LUSC, PAAD, and STAD). **(C)** *ASNS* expression in ccRCC and normal tissues. **(D)** Relationship between *ASNS* expression levels and prognosis, i.e., overall survival (OS). **(E)** ASNS protein level in ccRCC from the HPA database. The statistical significance computed by the Wilcoxon test is annotated by the number of stars (*: p-value <0.05; **: p-value <0.01; ***: p-value <0.001).

ratio [HR] > 1; Figure 3A). Meanwhile, multivariate prognostic analysis showed that *ASNS* could be an independent prognostic factor for ccRCC ($p < 0.001$; HR > 1; Figure 3B). Moreover, the receiver operating characteristic (ROC) curve was used to analyze the accuracy of *ASNS* to predict the survival of ccRCC. *ASNS* predicted the survival period of ccRCC patients at 1, 3, and 5 years, which was significant (area under the curve [AUC] > 0.6; Figure 3C). Subsequently, serial ROC analysis showed favorable diagnostic values for *ASNS* to predict various clinicopathological features (Figures 3D–K). Ultimately, the above results were validated using nomogram and calibration plots, which showed that *ASNS* had excellent potential for predicting clinicopathological features in ccRCC (Figures 3L, M).

DNA methylation analysis of *ASNS* gene

To further explore the regulation of *ASNS* in ccRCC, we performed a series of methylation analyses. Methylation levels were detected at the promoter region sites of the *ASNS* gene (Figure 4A), and *ASNS* expression was inversely proportional to the methylation level (Figures 4B, C). We further determined the relationship between *ASNS* gene methylation level and various clinicopathological features such as pathologic TNM stages (Figures 4D–F), tumor stages (Figure 4G), and neoplasm histologic grades (Figure 4H) of ccRCC. The results demonstrated that the methylation level of *ASNS* gradually decreased with tumor progression. Furthermore, the lower

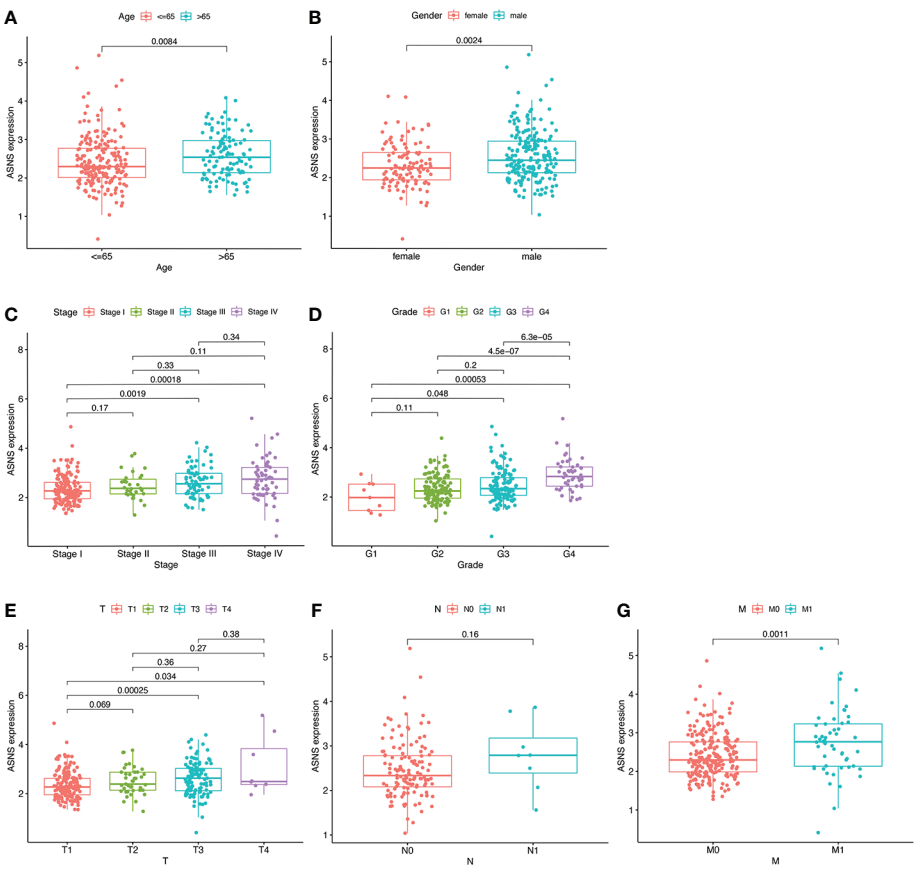


FIGURE 2
Expression pattern of *ASNS* in relation to several clinicopathological features. **(A, B)** *ASNS* expression in samples from patients stratified by age and gender. **(C–G)** *ASNS* expression in samples stratified by pathological stage, neoplasm histological grade, T stage, N stage, and M stage, respectively.

methylation level of *ASNS* led to a worse prognosis, such as poorer OS rates ($p < 0.001$; Figures 4I–K) and poorer progression-free survival ($p < 0.001$; Figure 4L). The decrease in the methylation level of *ASNS* with tumor progression indicates that the methylation modification of *ASNS* plays a key regulatory role in the expression of *ASNS*.

Immune infiltration analysis of *ASNS* in ccRCC

ccRCC has a relatively high stromal score and immune score among common cancers (15). High immune scores and infiltration of Tregs are significantly associated with poor OS, high tumor stage, and more chances of metastases in ccRCC (16). To further investigate the relationship between *ASNS* expression and the immune microenvironment in ccRCC, we performed immune infiltration analysis using TIMER2.0. The immune infiltration level of non-regulatory CD^{4+} T cells was negatively correlated with *ASNS* expression (Figure 5B), whereas Tregs were positively correlated (Figure 5C). Subsequent analyses showed that higher CD^{4+} T-cell infiltration was associated with better prognosis (Figure 5E), and higher Tregs infiltration was associated with poorer prognosis (Figure 5F). The correlation between CD^{8+} T-cell infiltration and *ASNS* was also analyzed; however, the results were insignificant (Figures 5A, D). Finally, *ASNS* expression correlated positively with the expression of immune checkpoints such as CTLA4, and PD-L1 (CD274) was positive (Figures 5G, H).

Cell function and pathway analysis in *ASNS*

We analyzed the positively and negatively correlated genes of *ASNS* in ccRCC and plotted heatmaps to show the expression patterns of the top 20 *ASNS*-associated genes (Figure 6A). To further determine the functions of *ASNS* in tumor progression and prognosis, GO and KEGG enrichment analyses were performed. GO enrichment analysis found that ASNS protein

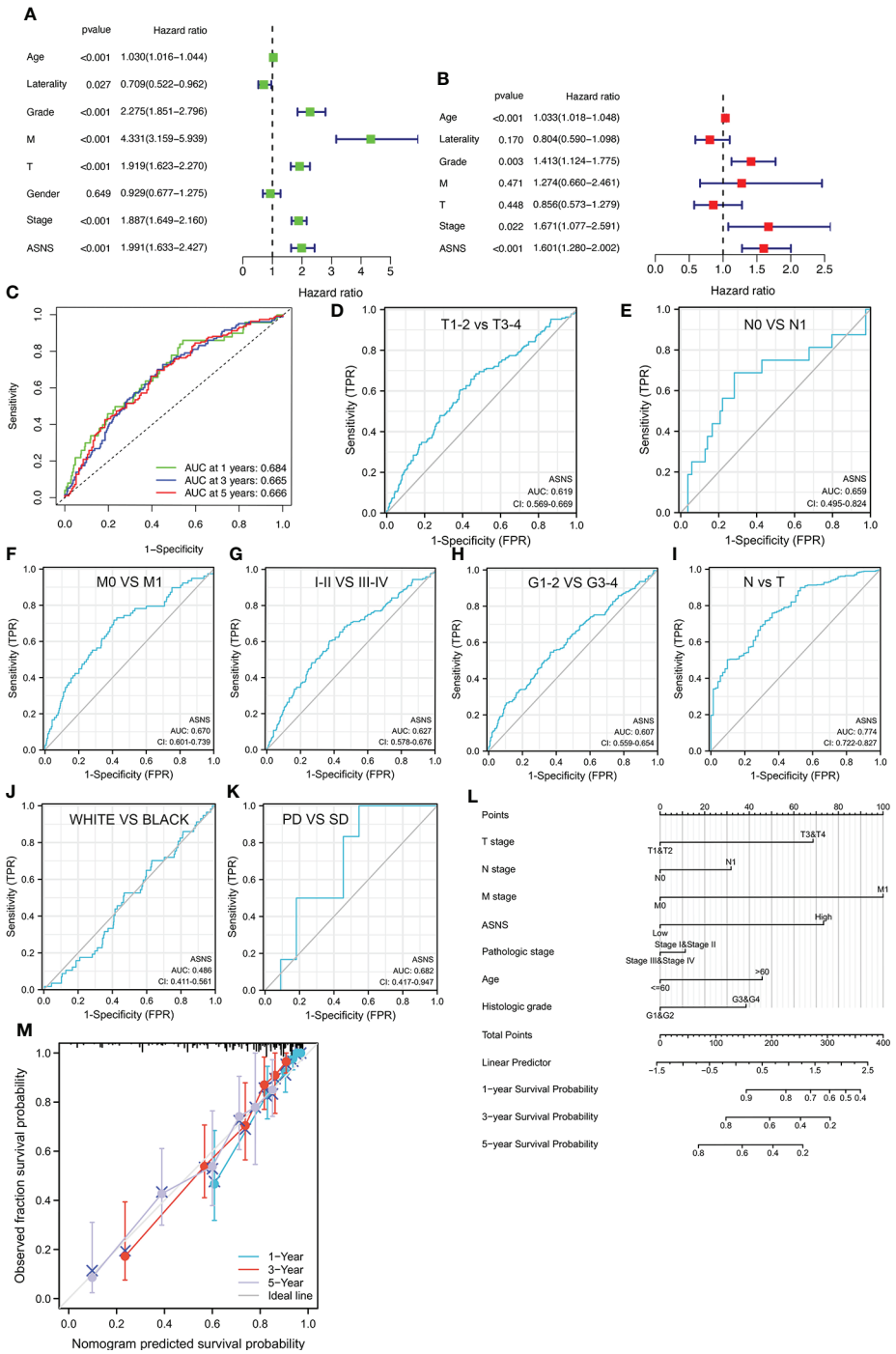


FIGURE 3
Identification of *ASNS* as an independent prognostic factor for ccRCC. **(A, B)** Univariate and multivariate independent prognostic analysis of *ASNS*. **(C)** Receiver operating characteristic (ROC) curve predicting the correlation between *ASNS* expression and OS. **(D–K)** ROC curve predicting the correlation between *ASNS* expression and clinicopathological features [T1–2 *vs*. T3–4, N0 *vs*. N1, M0 *vs*. M1, pathological stage I–II *vs*. III–IV, neoplasm histological grade 1–2 *vs*. 3–4, normal *vs*. tumor, race (white *vs*. black), and primary therapeutic outcome, i.e., partial disease *vs*. stable disease]. **(L, M)** Nomogram and calibration plots, respectively.

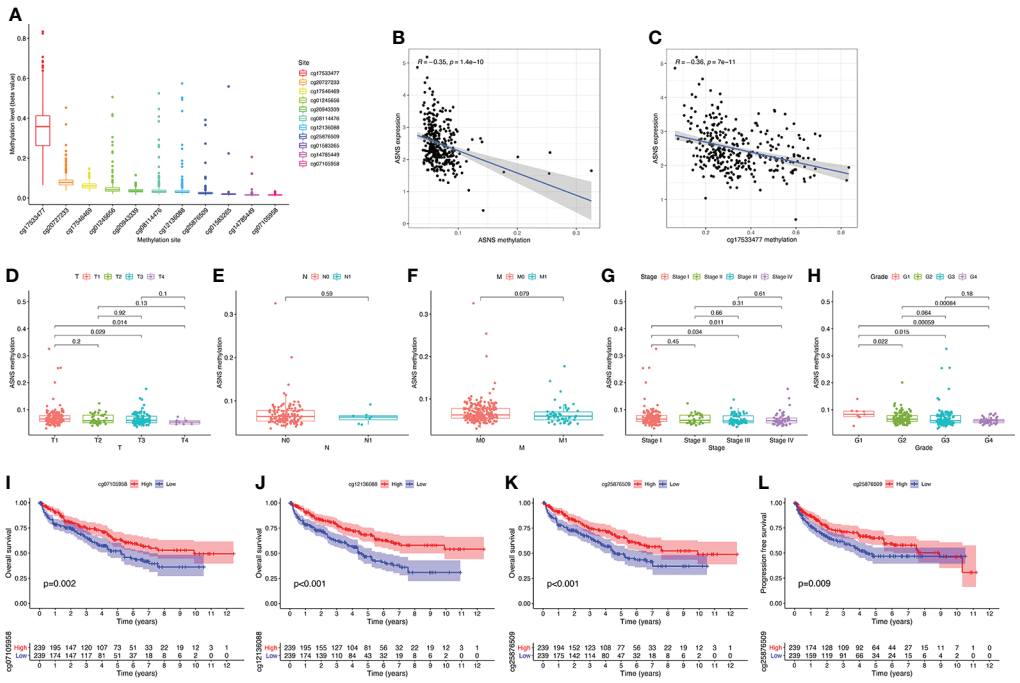


FIGURE 4
DNA methylation analysis of *ASNS*. **(A)** Methylation levels at different sites of *ASNS*. **(B, C)** The relationship between *ASNS* expression level and methylation level. **(D–H)** *ASNS* methylation in samples stratified by T stage, N stage, M stage, neoplasm histological grade, and pathological stage. **(I–L)** Methylation levels of *ASNS* on the prognosis of ccRCC (OS and progression-free survival rates).

may be located on the cell membrane and regulate the molecular transport in cells (***q***-value <0.01; Figure 6B). KEGG enrichment analysis indicated that *ASNS* might participate in the regulation of insulin resistance, PPAR signaling pathway, and amino acid metabolism (***q***-value <0.05; Figure 6C). Subsequent GSEA suggested that *ASNS* might be involved in CD 4+ T-cell infiltration-related signaling in ccRCC (Figures 6D, E), which is also consistent with the previous analysis results.

Protein–protein interaction network of *ASNS*

We performed a PPI network analysis of ASNS using the STRING website to explore potential interactions between ASNS and other proteins. The top 10 hub genes were selected from the PPI network, and the expression patterns and prognostic values in ccRCC were studied (Figure 7).

Validation of *ASNS* in cells and pathological tissues of ccRCC

To further verify the effect of *ASNS* on ccRCC, we evaluated the expression of *ASNS* in ccRCC tissues and human ccRCC cell lines. Compared with adjacent normal renal tissues, *ASNS* was highly expressed in ccRCC tissues (Figure 8A). ImageJ software was used to quantitatively analyze the expression of *ASNS* (Figures 8B–E). Finally, we evaluated the expression of ASNS protein in 786-O cells (human ccRCC) and HK-2 cells (Human Kidney-2 cells), and the results were significant (Figure 8F).

In addition, the above results were further validated using the data from our cohort. It was further verified that *ASNS* was highly expressed in ccRCC tissues compared with adjacent tissues ($p < 0.01$, Table 1). Moreover, high ASNS expression was not correlated with age, gender, and tumor location ($p > 0.05$, Table 2), but was significantly positively associated with tumor size, T stage, the American Joint Committee on Cancer (AJCC) status, and neoplasm histological grade ($p < 0.001$, Table 2). These were also consistent with our previous results.

Discussion

ccRCC is one of the most common malignancies of the urinary system. Several biomarkers such as ciRS-7 (17), CA9 (18), Ki-67 (19), Bcl-2 (20), and PTEN (21) can predict ccRCC prognosis. We aimed to identify a novel biomarker to predict the prognosis of ccRCC. We found that *ASNS* might play a significant role in the

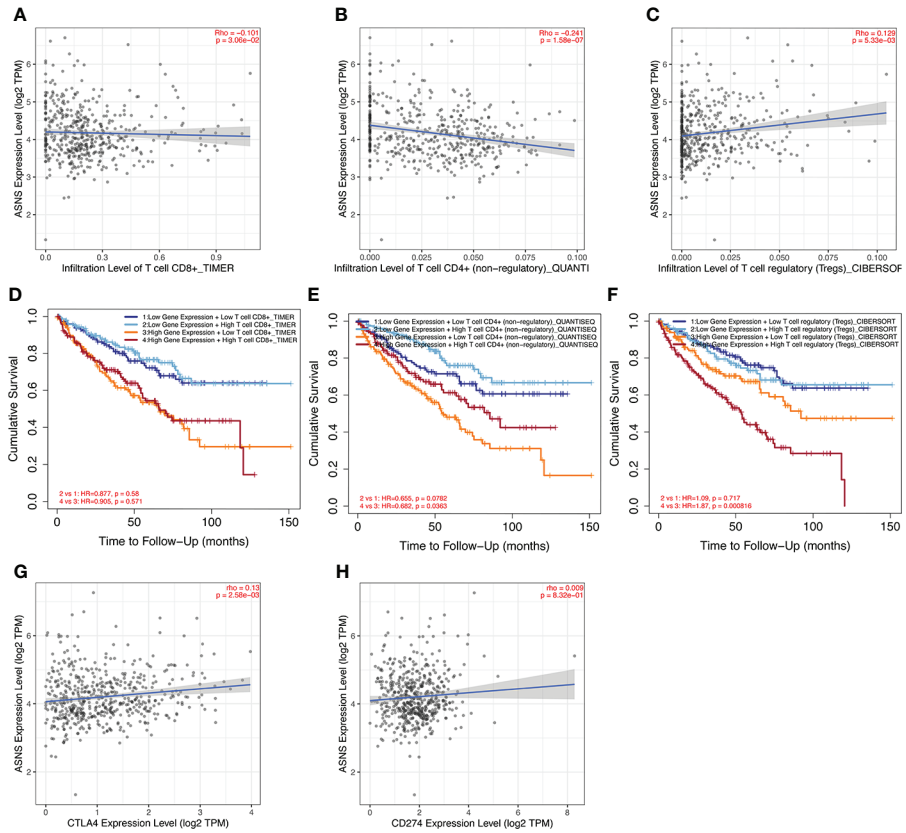


FIGURE 5
Immune infiltration analysis of *ASNS* in ccRCC. **(A–C)** Correlation between *ASNS* expression and immune cell infiltration in ccRCC. **(D–F)** Correlation between immune cell infiltration and prognosis. **(G, H)** Correlation between *ASNS* and expression level of immune checkpoint molecules.

development of ccRCC and serve as a valuable clinical prognostic biomarker of ccRCC.

The upregulation of *ASNS* expression responds to single or combined restrictions on many amino acids, including the most essential amino acids (22). Amino acid starvation-induced upregulation of *ASNS* is mediated by activating transcription factor 4 (ATF4). ASNS is the transcriptional target of ATF4, responding to amino acid starvation *via* the GCN2/eIF2α axis. The GCN2/eIF2α/ATF4 pathway is activated in primary solid tumors, indicating that the regulation of asparagine production in a nutrient-limited environment is essential for the progression of solid tumors (23). Maintaining intracellular asparagine levels is necessary for cancer cell growth (24). Asparagine is an important regulator of cancer cell amino acid homeostasis, anabolic metabolism, and proliferation (24). Therefore, we suspected that *ASNS* might play an important role in regulating the intracellular and extracellular metabolism of amino acids, thereby promoting the development of ccRCC, consistent with our results (Figure 6).

ASNS knockdown leads to cell death even in the presence of glutamine, which can be reversed by adding exogenous asparagine (25). The standard treatment for childhood acute lymphoblastic leukemia includes the infusion of bacterial ASNase as a principal component of combination chemotherapy (26). Circulating ASNase causes the rapid consumption of plasma asparagine and depletion of intracellular asparagine, starving leukemia cells and preventing their further growth (27). Hence, the growth of solid tumors might be regulated by ASNS protein levels. A study showed that in about 70% of human pancreatic ductal cancer samples, the level of ASNS protein was below the detection level, which indicates that some pancreatic tumors may be sensitive to ASNase treatment (28). In another study using ovarian cell lines, a negative correlation was observed between ASNase treatment efficacy and ASNS protein levels rather than ASNS mRNA levels (29). Pancreatic cancer cells overexpressing ASNS exhibit increased resistance to apoptosis induced by cis-diamine-dichloro platinum, which is related to the inhibition of JUN

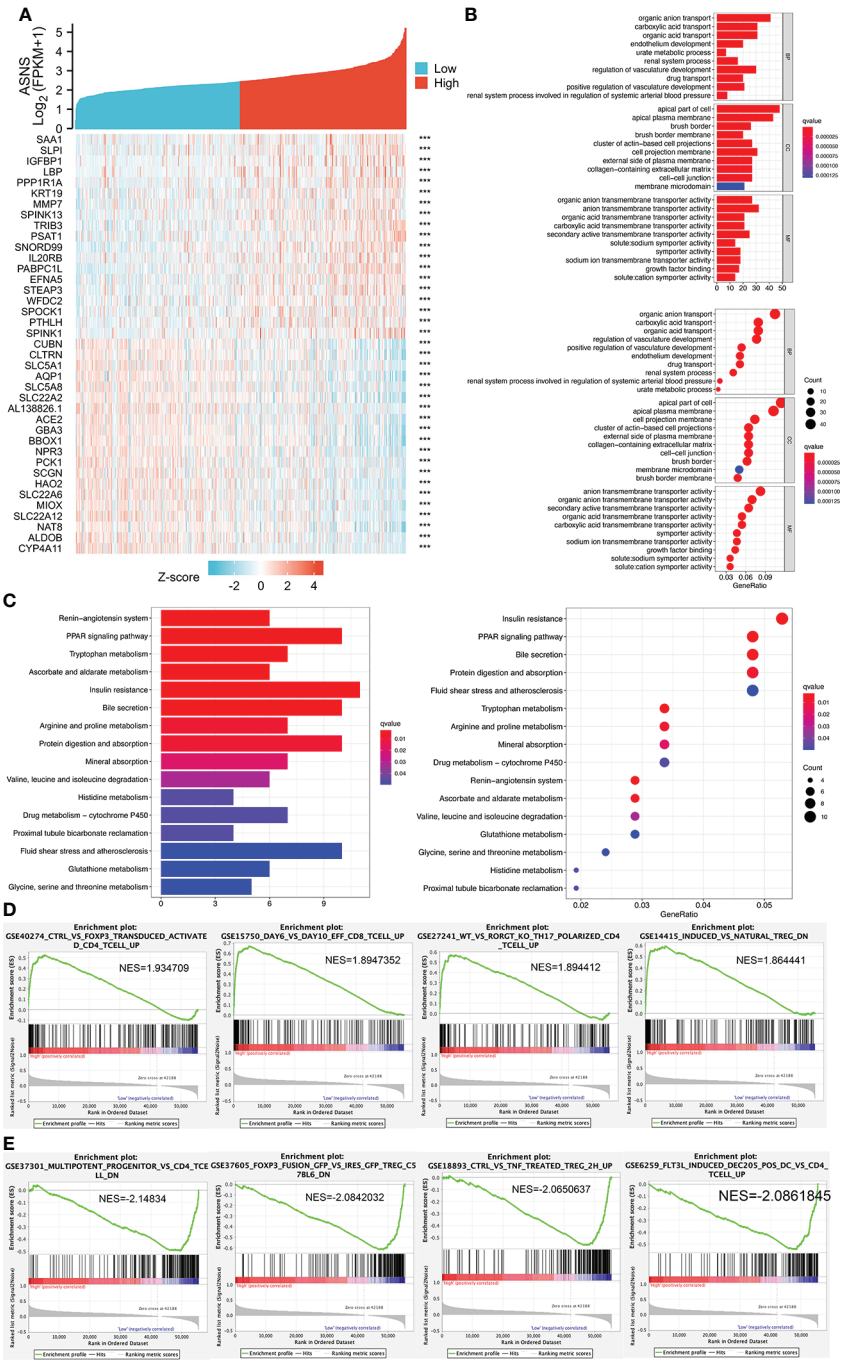


FIGURE 6
Cell function and pathway analysis involved in *ASNS*. **(A)** Heatmap of the expression patterns of the top 20 positively and negatively correlated genes of *ASNS* in ccRCC. **(B)** GO enrichment analysis. **(C)** KEGG enrichment analysis. **(D, E)** Gene set enrichment analysis (GSEA).

NH2-terminal kinase activation by ASNS (30). Therefore, whether ASNase treatment can inhibit tumor cells in ccRCC needs to be researched.

As shown by immunohistochemistry of human pancreatic tissues, pancreatic ASNS protein expression was largely correlated with exocrine cells (28). The ASNS protein is released from primary mouse tumors into the serum at a rate proportional to tumor growth; therefore, serum ASNS activity may be a valuable marker for the lysis of pancreatic exocrine cells (31). The secretion pattern of ASNS protein needs to be investigated in ccRCC.

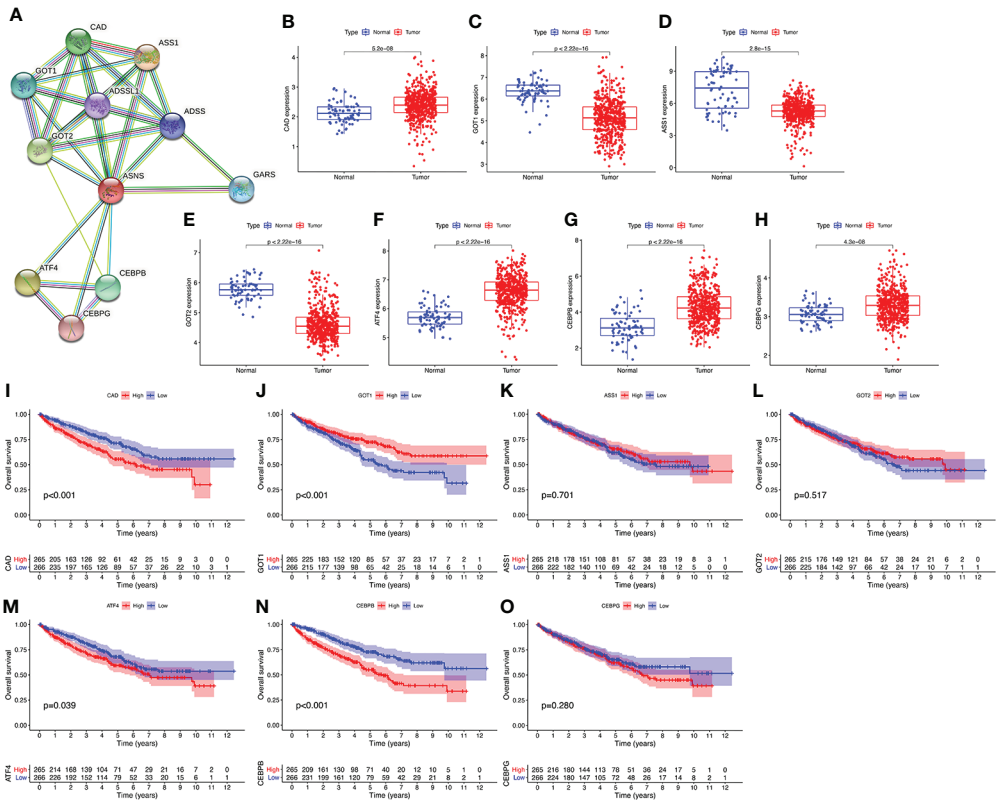


FIGURE 7
Protein–protein interaction (PPI) network analysis of ASNS. **(A)** The top 10 hub genes of the PPI network. **(B–O)** The expression pattern and prognostic values of these hub genes in ccRCC (the three missing genes were not found in the TCGA-KIRC database).

Several studies on asparagine-dependent and asparagine-independent cell lines revealed the correlation between DNA methylation in the *ASNS* locus and *ASNS* expression (32, 33). High *ASNS* promoter methylation is associated with low *ASNS* expression, and 5-Aza-dC treatment enhances *ASNS* expression (34). In acute lymphoblastic leukemia bone marrow samples, most B cells and T cells showed methylation of the *ASNS* promoter, in contrast to the lack of methylation observed in brain and breast tumors (35). Akagi et al. hypothesized that *ASNS* methylation might be the basis for the susceptibility of acute lymphoblastic leukemia cells to ASNase chemotherapy (35). We found that the cg17533477 site of *ASNS* had high-level methylation in ccRCC (Figure 4A), indicating that ccRCC is more sensitive to ASNase chemotherapy. Moreover, the higher methylation level of the *ASNS* gene leads to a better prognosis (Figures 4I–L).

Multiple studies have shown that tumor-infiltrating immune cells regulate cancer progression and promote tumor development (36, 37). CD^{4+} helper T cells and cytotoxic CD^{8+} T cells play an important role in tumor prevention by targeting antigenic tumor cells, and CD^{8+} T cells are associated with better clinical outcomes and response to immunotherapy in many cancers (38–40). T cells (CD^{4+} T cells and CD^{8+} T cells) are the primary type of immune cells in ccRCC tumors (41). Effector T cells and mature dendritic cells may contribute to antitumor immune responses, whereas Tregs have the opposite effect (42), consistent with our findings (Figures 5B, C, E, F).

In our study, we analyzed the significant role of *ASNS* in the development of ccRCC and verified the possibility and feasibility of using it as an independent prognostic factor for ccRCC prognosis (Figure 9). Taken together, *ASNS* could act as an independent prognostic factor for ccRCC and might play a crucial role in tumor progression and immune cell infiltration. However, robust experimental data are not available to confirm our findings. Only preliminary analyses showed the function of *ASNS* in ccRCC, but certain signaling pathways in which it plays an important role remain to be studied. Due to the small number of data included in this center (only 81 cases), our validation results did not show that ASNS expression levels were associated with lymph node metastases and distant metastases. To further explore the vital role of *ASNS* in ccRCC, more detailed basic experimental research and clinical studies are required.

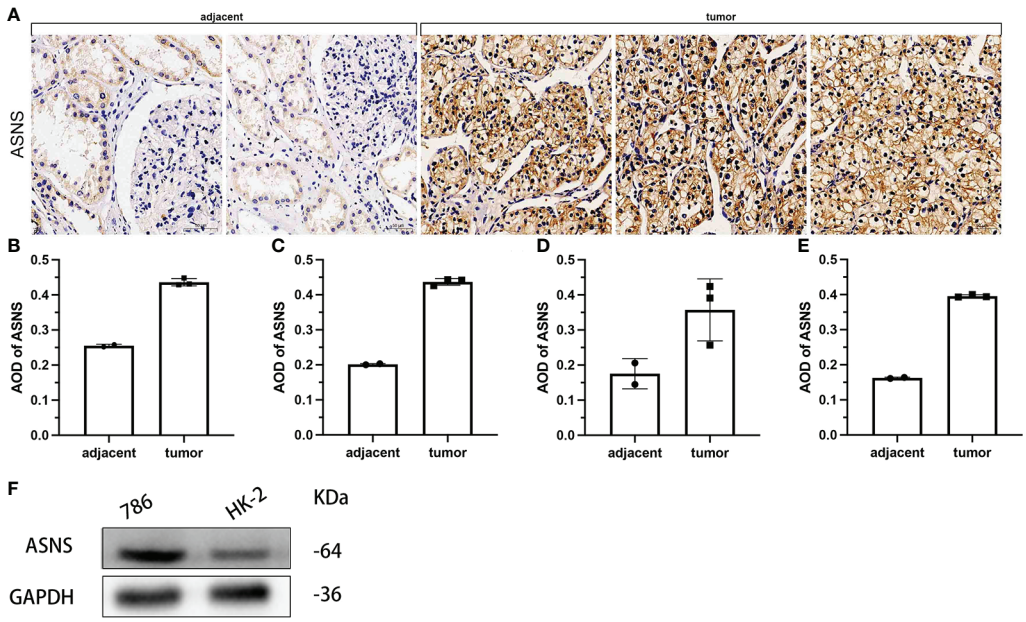


FIGURE 8
Validation of ASNS in cells and pathological tissues of ccRCC. **(A)** Results of immunohistochemical analysis of ASNS in ccRCC tissues and adjacent normal tissues. **(B–E)** Quantitative immunohistochemical analysis results of ASNS in four samples. **(F)** Western blot result of ASNS in 786-O and HK-2 cells.

TABLE 1 AOD of ASNS in tumor tissues compared with normal tissues.

Group	*n*	AOD of ASNS (mean)	*p*-value
Adjacent tissues	81	0.206	<0.01
Tumor tissues	81	0.444	

TABLE 2 Baseline characteristics of ccRCC patients in our cohort.

Characteristic	ASNS level		*p*-value
	Low	High	
n	40	41	
Gender, *n* (%)			1.000
Female	13 (16%)	13 (16%)	
Male	27 (33.3%)	28 (34.6%)	
Age (years), *n* (%)			0.429
<60	24 (29.6%)	20 (24.7%)	
≥60	16 (19.8%)	21 (25.9%)	
Location, *n* (%)			0.891
Left	25 (30.9%)	24 (29.6%)	
Right	15 (18.5%)	17 (21%)	
Tumor size, *n* (%)			< 0.001
<5 cm	32 (39.5%)	13 (16%)	
≥5 cm	8 (9.9%)	28 (34.6%)	

(Continued)

TABLE 2 Continued

Characteristic	ASNS level		*p*-value
	Low	High	
T stage, *n* (%)			< 0.001
T1	37 (45.7%)	12 (14.8%)	
T2	2 (2.5%)	8 (9.9%)	
T3	1 (1.2%)	19 (23.5%)	
T4	0 (0%)	2 (2.5%)	
N stage, *n* (%)			1.000
N0	40 (49.4%)	40 (49.4%)	
N1	0 (0%)	1 (1.2%)	
M stage, *n* (%)			0.116
M0	40 (49.4%)	37 (45.7%)	
M1	0 (0%)	4 (4.9%)	
AJCC stage, *n* (%)			< 0.001
I	37 (45.7%)	11 (13.6%)	
II	2 (2.5%)	8 (9.9%)	
III	1 (1.2%)	17 (21%)	
IV	0 (0%)	5 (6.2%)	
Grade, *n* (%)			< 0.001
1	12 (14.8%)	1 (1.2%)	
2	15 (18.5%)	9 (11.1%)	
3	13 (16%)	22 (27.2%)	
4	0 (0%)	9 (11.1%)	

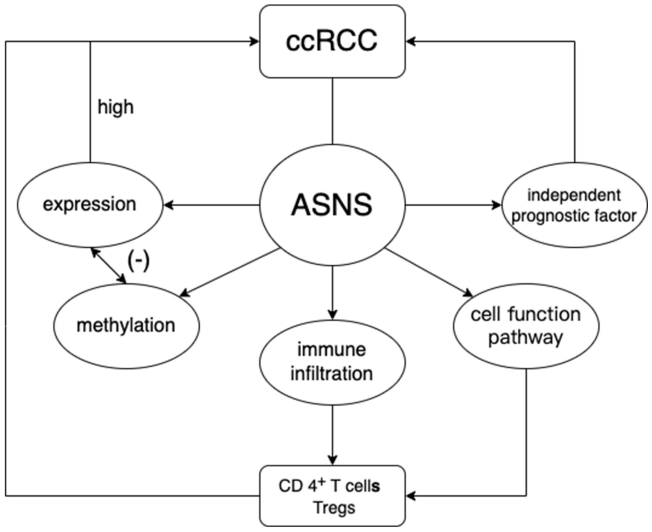


FIGURE 9
Study flowchart.

Data availability statement

The datasets presented in this study can be found in online repositories. The names of the repository/repositories and accession number(s) can be found below: https://xenabrowser.net/datapages/.

Ethics statement

The studies involving human participants were reviewed and approved by Ethics Committee and Institutional Review Board for Clinical Research of Zhongda Hospital (ZDKYSB077) (43, 44, 45, 46). This study is a retrospective study that only collected clinical data from patients, and the ethical committee approved the exemption of informed consent.

Author contributions

XG, RL, MC, WM, NF, and HC designed the study. XG and RL conducted the study, maintained the data, analyzed the data, and prepared the figures. XG, RL, WM, and NF reviewed and revised the manuscript. All authors contributed to the article and approved the submitted version.

Funding

This study was funded by The National Natural Science Foundation of China (No. 81370849, 81300472, 81070592, 81202268, 81202034); Natural Science Foundation of Jiangsu Province (BK20161434, BL2013032, BK20150642 and BK2012336). Major Project of Jiangsu Commission of Health: (No: ZD2021002); Wuxi "Taihu Talents Program" Medical Expert Team Project (No: THRCJH20200901, THRCJH20200902).

Acknowledgments

We thank Bullet Edits Limited for the linguistic editing and proofreading of the manuscript.

Conflict of interest

The authors declare that the research was conducted in the absence of any commercial or financial relationships that could be construed as a potential conflict of interest.

Publisher's note

All claims expressed in this article are solely those of the authors and do not necessarily represent those of their affiliated organizations, or those of the publisher, the editors and the reviewers. Any product that may be evaluated in this article, or claim that may be made by its manufacturer, is not guaranteed or endorsed by the publisher.

References

1. Sung HA-O, Ferlay J, Siegel RL, Laversanne M, Soerjomataram I, Jemal A, et al. Global cancer statistics 2020: GLOBOCAN estimates of incidence and mortality worldwide for 36 cancers in 185 countries. *CA Cancer J Clin* (2021) 71 (3):209–49. doi: 10.3322/caac.21660

2. Ljungberg B, Albiges L, Abu-Ghanem Y, Bensalah K, Dabestani S, Fernández-Pello S, et al. European Association of urology guidelines on renal cell carcinoma: The 2019 update. *Eur Urol* (2019) 75:799–810. doi: 10.1016/j.eururo.2019.02.011

3. Linehan WM, Schmidt LS, Crooks DR, Wei D, Srinivasan R, Lang M, et al. The metabolic basis of kidney cancer. *Cancer Discov* (2019) 9:1006–21. doi: 10.1158/2159-8290.CD-18-1354

4. Rossi SH, Fielding A, Blick C, Handforth C, Brown JE, Stewart GD. Setting research priorities in partnership with patients to provide patient-centred urological cancer care. *Eur Urol* (2019) 75:891–3. doi: 10.1016/j.eururo.2019.03.008

5. Richards NG, Kilberg MS. Asparagine synthetase chemotherapy. *Annu Rev Biochem* (2006) 75:629–54. doi: 10.1146/annurev.biochem.75.103004.142520

6. McDonald ER 3rd, de Weck A, Schlabach MR, Billy E, Mavrakis KJ, Hoffman GR, et al. Project DRIVE: A compendium of cancer dependencies and synthetic lethal relationships uncovered by Large-scale, deep RNAi screening. *Cell* (2017) 170 (3):577–92.e10. doi: 10.1016/j.cell.2017.07.005

7. Knott S, Wagenblast E, Khan S, Kim SY, Soto M, Wagner M, et al. Asparagine bioavailability governs metastasis in a model of breast cancer. *Nature* (2018) 554 (7692):378–81. doi: 10.1038/nature25465

8. Li T, Fu J, Zeng Z, Cohen D, Li J, Chen Q, et al. TIMER2.0 for analysis of tumor-infiltrating immune cells. *Nucleic Acids Res* (2020) 48(W1):W509–14. doi: 10.1093/nar/gkaa407

9. Szklarczyk D, Gable AL, Lyon D, Junge A, Wyder S, Huerta-Cepas J, et al. STRING v11: protein-protein association networks with increased coverage, supporting functional discovery in genome-wide experimental datasets. *Nucleic Acids Res* (2019) 47:D607–13. doi: 10.1093/nar/gky1131

10. Li C, Tang Z, Zhang W, Ye Z, Liu F. GEPIA2021: Integrating multiple deconvolution-based analysis into GEPIA. *Nucleic Acids Res* (2021) 49:W242–6. doi: 10.1093/nar/gkab418

11. Subramanian A, Tamayo P, Mootha VK, Mukherjee S, Ebert BL, Gillette MA, et al. Gene set enrichment analysis: A knowledge-based approach for interpreting genome-wide expression profiles. *Proc Natl Acad Sci USA* (2005) 102:15545–50. doi: 10.1073/pnas.0506580102

12. Liu R-J, Xu Z-P, Li S-Y, Yu J-J, Feng N-H, Xu B, et al. BAP1-related ceRNA (NEAT1/miR-10a-5p/SERPINE1) promotes proliferation and migration of kidney cancer cells. *Front Oncol* (2022) 12:852515. doi: 10.3389/fonc.2022.852515

13. Schneider CA, Rasband WS, Eliceiri KW. NIH Image to ImageJ: 25 years of image analysis. *Nat Methods* (2012) 9(7):671–5. doi: 10.1038/nmeth.2089

14. Rangan GK, Tesch GH. Quantification of renal pathology by image analysis (Methods in renal research). *Nephrology* (2007) 12(6):553–8. doi: 10.1111/j.1440-1797.2007.00855.x

15. Yoshihara K, Shahmoradgoli M, Martínez E, Vegesna R, Kim H, Torres-Garcia W, et al. Inferring tumour purity and stromal and immune cell admixture from expression data. *Nat Commun* (2013) 4:2612. doi: 10.1038/ncomms3612

16. Wang Y, Yang J, Zhang Q, Xia J, Wang Z. Extent and characteristics of immune infiltration in clear cell renal cell carcinoma and the prognostic value. *Transl Androl Urol* (2019) 8(6):609–18. doi: 10.21037/tau.2019.10.19

17. Mao W, Wang K, Xu B, Zhang H, Sun S, Hu Q, et al. ciRS-7 is a prognostic biomarker and potential gene therapy target for renal cell carcinoma. *Mol Cancer* (2021) 20(1):142. doi: 10.1186/s12943-021-01443-2

18. Bui MH, Visapaa H, Seligson D, Kim H, Han KR, Huang Y, et al. Prognostic value of carbonic anhydrase IX and KI67 as predictors of survival for renal clear cell carcinoma. *J Urol* (2004) 171:2461–6. doi: 10.1097/01.ju.0000116444.08690.e2

19. Gayed BA, Youssef RF, Bagrodia A, Darwish OM, Kapur P, Sagalowsky A, et al. Ki67 is an independent predictor of oncological outcomes in patients with localized clear-cell renal cell carcinoma. *BJU Int* (2014) 113(4):668–73. doi: 10.1111/bju.12263

20. Itoi T, Yamana K, Bilim V, Takahashi K, Tomita F. Impact of frequent bcl-2 expression on better prognosis in renal cell carcinoma patients. *Br J Cancer* (2004) 90(1):200–5. doi: 10.1038/sj.bjc.6601454

21. Shin Lee J, Seok Kim H, Bok Kim Y, Cheol Lee M, Soo Park C. Expression of PTEN in renal cell carcinoma and its relation to tumor behavior and growth. *J Surg Oncol* (2003) 84(3):166–72. doi: 10.1002/jso.10302

22. Gong SS, Guerrini L, Basilico C. Regulation of asparagine synthetase geneexpression by amino acid starvation. *Mol Cell Biol* (1991) 11(12):6059–66. doi: 10.1128/mcb.11.12.6059-6066.1991

23. Horiguchi M, Koyanagi S, Okamoto A, Suzuki SO, Matsunaga N, Ohdo S. Stress-regulated transcription factor ATF4 promotes neoplastic transformation by suppressing expression of the INK4a/ARF cell senescence factors. *Cancer Res* (2012) 72(2):395–401. doi: 10.1158/0008-5472.CAN-11-1891

24. Krall AS, Xu S, Graeber TG, Braas D, Christofk HR. Asparagine promotes cancer cell proliferation through use as an amino acid exchange factor. *Nat Commun* (2016) 7:11457. doi: 10.1038/ncomms11457

25. Zhang J, Fan J, Venneti S, Cross JR, Takagi T, Bhinder B, et al. Asparagine plays a critical role in regulating cellular adaptation to glutamine depletion. *Mol Cell* (2014) 56(2):205–18. doi: 10.1016/j.molcel.2014.08.018

26. Pieters R, Hunger SP, Boos J, Rizzari C, Silverman L, Baruchel A, et al. L-asparaginase treatment in acute lymphoblastic leukemia: A focus on erwinia asparaginase. *Cancer* (2011) 117(2):238–49. doi: 10.1002/cncr.25489

27. Avramis VI. Asparaginases: biochemical pharmacology and modes of drug resistance. *Anticancer Res* (2012) 32(7):2423–37.

28. Dufour E, Gay F, Aguera K, Scoazec JY, Horand F, Lorenzi PL, et al. Pancreatic tumor sensitivity to plasma l-asparagine starvation. *Pancreas* (2012) 41 (6):940–8. doi: 10.1097/MPA.0b013e318247d903

29. Lorenzi PL, Llamas J, Gunsior M, Ozbun L, Reinhold WC, Varma S, et al. Asparagine synthetase is a predictive biomarker of l-asparaginase activity in ovarian cancer cell lines. *Mol Cancer Ther* (2008) 7(10):3123–8. doi: 10.1158/1535-7163.MCT-08-0589

30. Cui H, Darmanin S, Natsuisaka M, Kondo T, Asaka M, Shindoh M, et al. Enhanced expression of asparagine synthetase under glucose-deprived conditions protects pancreatic cancer cells from apoptosis induced by glucose deprivation and cisplatin. *Cancer Res* (2007) 67(7):3345–55. doi: 10.1158/0008-5472.CAN-06-2519

31. Cooney DA, King VD, Cable RG, Taylor JB, Wodinsky I. L-asparagine synthetase in serum as a marker for neoplasia. *Cancer Res* (1976) 36(9 pt.1):3238–45. doi:

32. Peng H, Shen N, Qian L, Sun XL, Koduru P, Goodwin LO, et al. Hypermethylation of CpG islands in the mouse asparagine synthetase gene: relationship to asparaginase sensitivity in lymphoma cells. partial methylation in normal cells. *Br J Cancer* (2001) 85(6):930–5. doi: 10.1054/bjoc.2001.2000

33. Worton KS, Kerbel RS, Andrulis IL. Hypomethylation and reactivation of the asparagine synthetase gene induced by l-asparaginase and ethyl methanesulfonate. *Cancer Res* (1991) 51(3):985–9

34. Ren Y, Roy S, Ding Y, Iqbal J, Broome JD. Methylation of the asparagine synthetase promoter in human leukemic cell lines is associated with a specific methyl binding protein. *Oncogene* (2004) 23(22):3953–61. doi: 10.1038/sj.onc.1207498

35. Akagi T, Yin D, Kawamata N, Bartram CR, Hofmann WK, Wolf I, et al. Methylation analysis of asparagine synthetase gene in acute lymphoblastic leukemia cells. *Leukemia* (2006) 20(7):1303–6. doi: 10.1038/sj.leu.2404216

36. Grivennikov SI, Greten FR, Karin M. Immunity, inflammation, and cancer. *Cell* (2010) 140(6):883–99. doi: 10.1016/j.cell.2010.01.025

37. Kitamura T, Qian BZ, Pollard JW. Immune cell promotion of metastasis. *Nat Rev Immunol* (2015) 15(2):73–86. doi: 10.1038/nri3789

38. Vesely MD, Kershaw MH, Schreiber RD, Smyth MJ. Natural innate and adaptive immunity to cancer. *Annu Rev Immunol* (2011) 29:235–71. doi: 10.1146/annurev-immunol-031210-101324

39. Yao J, Xi W, Zhu Y, Wang H, Hu X, Guo J, et al. Checkpoint molecule PD-1-assisted CD8+ T lymphocyte count in tumor microenvironment predicts overall survival of patients with metastatic renal cell carcinoma treated with tyrosine kinase inhibitors. *Cancer Manag Res* (2018) 10:3419–31. doi: 10.2147/CMAR.S172039

40. Pagès F, Kirilovsky A, Mlecnik B, Asslaber M, Tosolini M, Bindea G, et al. *In situ* cytotoxic and memory T cells predict outcome in patients with early-stage colorectal cancer. *J Clin Oncol* (2009) 27(35):5944–51. doi: 10.1200/JCO.2008.19.6147

41. Chevrier S, Levine JH, Zanotelli VRT, Silina K, Schulz D, Bacac M, et al. An immune atlas of clear cell renal cell carcinoma. *Cell* (2017) 169:736–49.e18. doi: 10.1016/j.cell.2017.04.016

42. Seledtsov VI, Goncharov AG, Seledtsova GV. Clinically feasible approaches to potentiating cancer cell-based immunotherapies. *Hum Vaccines Immunotherapeut* (2015) 11(4):851–69. doi: 10.1080/21645515.2015.1009814

43. Mao W, Wang K, Wu Y, Ni J, Zhang H, Wang Y, et al. Prognostic significance of modified advanced lung cancer inflammation index in patients with renal cell carcinoma undergoing laparoscopic nephrectomy: A multi-institutional, propensity score matching cohort study. *Front Nutr* (2022) 8:781647. doi: 10.3389/fnut.2021.781647

44. Zhang G, Zhang L, Sun S, Chen M. Identification of a novel defined immune-Autophagy-Related gene signature associated with clinical and prognostic features of kidney renal clear cell carcinoma. *Front Mol Biosci* (2021) 8:790804. doi: 10.3389/fmolb.2021.790804

45. He T, Zhu W, Wang C, Lu H, Wu T, Pan K, et al. Relationship between pre-operative blood glucose level and length of hospital stay in patients with renal cell carcinoma undergoing laparoscopic nephrectomy. *Front Surg* (2021) 8:659365. doi: 10.3389/fsurg.2021.659365

46. Sun S, Mao W, Wan L, Pan K, Deng L, Zhang L, et al. Metastatic immune-related genes for affecting prognosis and immune response in renal clear cell carcinoma. *Front Mol Biosci* (2022) 8:794326. doi: 10.3389/fmolb.2021.794326

frontiers | Frontiers in Oncology

TYPE Original Research
PUBLISHED 26 August 2022
DOI 10.3389/fonc.2022.931383

Check for updates

OPEN ACCESS

EDITED BY
Riccardo Tellini,
Careggi University Hospital, Italy

REVIEWED BY
Fu Gui,
Brigham and Women's Hospital and Harvard Medical School, United States
Muhammad Arif,
National Institutes of Health (NIH), United States

*CORRESPONDENCE
Xiao-Liang Xing
xiaoliangxinghnm@126.com

†These authors have contributed equally to this work

SPECIALTY SECTION
This article was submitted to Genitourinary Oncology, a section of the journal Frontiers in Oncology

RECEIVED 28 April 2022
ACCEPTED 28 July 2022
PUBLISHED 26 August 2022

CITATION
Han Z, Wang H, Long J, Qiu Y and Xing X-L (2022) Establishing a prognostic model of ferroptosis- and immune-related signatures in kidney cancer: A study based on TCGA and ICGC databases.
Front. Oncol. 12:931383.
doi: 10.3389/fonc.2022.931383

COPYRIGHT
© 2022 Han, Wang, Long, Qiu and Xing. This is an open-access article distributed under the terms of the Creative Commons Attribution License (CC BY). The use, distribution or reproduction in other forums is permitted, provided the original author(s) and the copyright owner(s) are credited and that the original publication in this journal is cited, in accordance with accepted academic practice. No use, distribution or reproduction is permitted which does not comply with these terms.

Establishing a prognostic model of ferroptosis- and immune-related signatures in kidney cancer: A study based on TCGA and ICGC databases

Zhijun Han[1†], Hao Wang[2,3†], Jing Long[1], Yanning Qiu[4] and Xiao-Liang Xing[2,3*]

[1]Department of Urology, Department of Ultrasonography, Zhuzhou Hospital Affiliated to Xiangya School of Medicine, Central South University, Zhuzhou, China, [2]Hunan Provincial Key Laboratory for Synthetic Biology of Traditional Chinese Medicine, Hunan University of Medicine, Huaihua, China, [3]Department of Urology, The First Affiliated Hospital to Hengyang Medical School, South China University, Hengyang, China, [4]First College for Clinical Medicine, Xinjiang Medical University, Urumqi, China

Background: Kidney cancer (KC) is one of the most challenging cancers due to its delayed diagnosis and high metastasis rate. The 5-year survival rate of KC patients is less than 11.2%. Therefore, identifying suitable biomarkers to accurately predict KC outcomes is important and urgent.

Methods: Corresponding data for KC patients were obtained from the International Cancer Genome Consortium (ICGC) and The Cancer Genome Atlas (TCGA) databases. Systems biology/bioinformatics/computational approaches were used to identify suitable biomarkers for predicting the outcome and immune landscapes of KC patients.

Results: We found two ferroptosis- and immune-related differentially expressed genes (FI-DEGs) (*Klotho* (*KL*) and *Sortilin 1* (*SORT1*)) independently correlated with the overall survival of KC patients. The area under the curve (AUC) values of the prognosis model using these two FI-DEGs exceeded 0.60 in the training, validation, and entire groups. The AUC value of the 1-year receiver operating characteristic (ROC) curve reached 0.70 in all the groups.

Conclusions: Our present study indicated that *KL* and *SORT1* could be prognostic biomarkers for KC patients. Whether this model can be used in clinical settings requires further validation.

KEYWORDS

kidney cancer, immune, ferroptosis, overall survival, prognosis

Introduction

Kidney cancer (KC) is the second most common cancer of the urinary system. Statistical data from the Global Cancer Statistics 2020 report showed that there were over 430,000 new cases and 180,000 deaths related to KC (1). KC remains one of the most challenging cancers in urology despite the availability of various therapeutic approaches, such as surgery, chemotherapy, radiotherapy, and recently proposed immunotherapy (2). The main reasons for this phenomenon are delayed diagnoses and high metastasis rates. For example, almost one-third of people diagnosed with KC have advanced KC (3, 4). Approximately 40% of patients with advanced cancer eventually develop metastasis (3, 4), and the 5-year survival rate of these patients is less than 11.2% (3, 4). Therefore, it is important to identify suitable biomarkers to predict KC outcomes.

More evidence shows that carcinogenesis is not only related to cancer cells but also to the microenvironment (5–7). Previous studies have demonstrated that anticancer effects can be achieved by inducing immunosuppressive cells, such as regulatory T cells and myeloid-derived suppressor cells, to infiltrate the tumor microenvironment and mediate immune dysfunction (8). Recent studies have indicated that ferroptosis, a form of iron-dependent programmed cell death, is involved in the progression of several cancers (9–11). The kidney is involved in iron metabolism. Several studies have shown that clear cell renal cell carcinomas (RCCs) are closely related to iron metabolism (12, 13). RCC is an immunogenic tumor. Ferroptosis regulation can inhibit the migration and invasion of clear cell RCC cells (14, 15). Additionally, previous studies have indicated that immunity and ferroptosis can regulate each other to achieve their anticancer effects (16–18). Therefore, we identified suitable biomarkers for predicting KC patient prognosis and immune status by conducting an integrated study of ferroptosis- and immune-related genes.

Materials and methods

Data collection and preprocessing

We obtained RNA sequence information for 91 KC and 45 normal tissues and their clinical information from the ICGC database, and 818 KC and 104 normal tissues and their corresponding clinical information from TCGA database (Table 1). In our present study, ICGC data, TCGA data, and the ICGC and TCGA merge data were set as training, validation, and entire groups, respectively. Ferroptosis- and immune-related genes were obtained from the FerrDb and ImmPort, respectively. We performed differential expression analyses using the package "DESeq2" in R (3.6.2) to identify differential expression genes (DEG) between KC patients and normal tissues. The threshold values were set to ≥200 for baseMean, ≥1 for |log2 fold change (FC)|, and<0.05 for adj *p* value.

ESTIMATE and immune profile analyses

The normalized genes were utilized to evaluate the stromal, immune, and tumor purity by the ESTIMATE package in R (3.6.2). The immune infiltrations of different immune cells and immune factors for each sample were evaluated by TIMER2.0 with default parameters, including TIMER, CIBERSORT, CIBERSORT-ABS, QUANTISEQ, MCPCOUNTER, XCELL, and EPIC (http://timer.comp-genomics.org/).

TABLE 1 Clinical features of patients with kidney cancer.

Variables	Training group (*n* = 91)		Validation group (*n* = 818)	
	No.	%	No.	%
Vital				
Alive	61	67.03%	217	26.53%
Death	30	32.97%	601	73.47%
Gender				
Female	39	42.86%	262	32.03%
Male	52	57.14%	556	67.97%
Age				
≤60	46	50.55%	400	48.90%
>60	45	49.45%	408	49.88%
Tumor (T)				
T1	54	59.34%	464	56.72%
T2	13	14.29%	101	12.35%
T3	22	24.18%	238	29.10%
T4	2	2.20%	13	1.59%
X	0	0.00%	2	0.24%
Nodes (N)				
N0	79	86.81%	288	35.21%
N1	2	2.20%	40	4.89%
N2	0	0.00%	4	0.49%
NX	10	10.99%	486	59.41%
Metastasis (M)				
M0	81	89.01%	515	62.96%
M1	9	9.89%	87	10.64%
MX	1	1.10%	216	26.41%
Stage				
I	53	58.24%	437	53.42%
II	13	14.29%	78	9.54%
III	15	16.48%	174	21.27%
IV	10	10.99%	129	15.77%
X	0	0.00%	0	0.00%

Gene ontology and Kyoto encyclopedia of genes and genomes pathway enrichment analyses

Gene Set Enrichment Analysis (GSEA) was then used for Gene Ontology (GO) and Kyoto Encyclopedia of Genes and Genomes (KEGG) analyses in R (3.6.2). The related parameter was set as follows: baseMean of ≥200, |log2 fold change (FC)| of ≥1, adj *p* value of<0.05, and minGSSize = 10. GO analyses consist of three main components: biological processes (BPs), cellular components (CCs), and molecular functions (MFs).

Identification of prognosis-related FI-DEGs

Univariate Cox regression analyses were used to identify prognosis-related ferroptosis- and immune-related differentially expressed genes (FI-DEGs). The overlap prognostic-related FI-DEGs verified from training and validation were used to filter the independent prognostic biomarkers as measured by multivariate Cox regression analyses. In addition, risk scores were evaluated by the following formula:

$$\text{Risk score} = \sum_{i=1}^{n}(\text{Exp}i*\text{Coe}i)$$

N, Exp*i*, and Coe*i* represented gene number, level of gene expression, and coefficient value, respectively (19, 20). The Youden index from the training data was set as the cutoff value to divide the patients.

Statistical analyses

Principal component analyses (PCA) in R 3.6.2 was used to visualize the patients with kidney cancer with different risk values in the training group, validation group, and entire group.

A repeated measures ANOVA followed by an unpaired two-tailed Student's *t*-test was used as indicated. All results are expressed as mean ± SEM.

Results

Aberrant stromal statuses for KC

The RNA sequencing (RNA-seq) count data were normalized by DESeq2 and used to calculate the stromal, immune, and tumor purity by ESTIMATE in R (3.6.2). The stromal, immune, and estimated scores were significantly increased, while tumor purity was significantly decreased in KC patients from the training data (Figures 1A–D). The estimated scores were positively correlated with stromal and immune scores and negatively correlated with tumor purity (Supplementary Figure S1A).

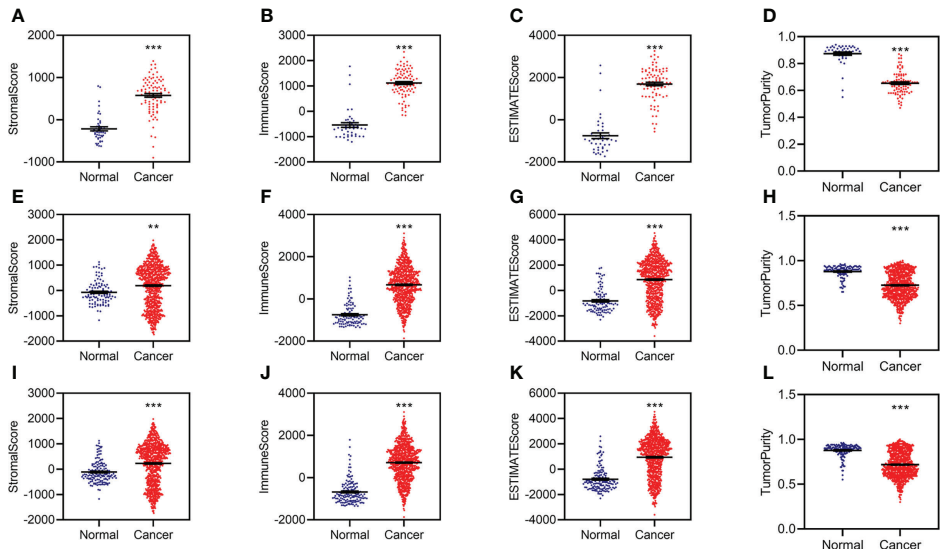


FIGURE 1
Aberrant stromal and immune status for KC. **(A–D)** Difference analysis of stromal score **(A)**, immune score **(B)**, ESTIMATE score **(C)**, and tumor purity **(D)** between normal and KC patients in the training group. **(E–H)** Difference analysis of stromal score **(E)**, immune score **(F)**, ESTIMATE score **(G)**, and tumor purity **(H)** between normal and KC patients in the validation group. **(I–L)** Difference analysis of stromal score **(I)**, immune score **(J)**, ESTIMATE score **(K)**, and tumor purity **(L)** between normal and KC patients in the entire group. **p < 0.01, ***p < 0.001.

We then conducted similar analyses for KC from the validation group and found similar results in the validation group (Figures 1E–H; Supplementary Figure S1B) and the entire group (Figures 1I–L; Supplementary Figure S1C). All of these data indicated that patients with KC might have abnormal immunity.

Identifying prognosis-related ferroptosis- and immune-related differentially expressed genes

We identified 3,126 differentially expressed genes (DEGs), including 1,795 upregulated and 1,331 downregulated DEGs, in the training group (Figure 2A). Of these, 403 FI-DEGs were identified, including 298 upregulated and 104 downregulated FI-DEGs (Figure 2B). We first performed univariate Cox regression analyses to obtain prognosis-related FI-DEGs and found that 33 FI-DEGs (25 upregulated and eight downregulated) were significantly correlated with KC overall survival (OS) from the training (Supplementary Table S1). We obtained 1,875 upregulated DEGs, 952 downregulated DEGs, 334 upregulated FI-DEGs, and 98 downregulated FI-DEGs from the validation group (Figures 2C, D). Univariate Cox regression analyses showed that 234 of these FI-DEGs (188 upregulated and 45 downregulated) were significantly correlated with the OS of KC (Supplementary Table S2).

Only three FI-DEGs (*C-X3-C Motif Chemokine Receptor 1* (*CX3CR1*), *Klotho* (*KL*), and *Sortilin 1* (*SORT1*)) were correlated with KC OS in the training and validation data (Figures 2E, F). Correlation analyses indicated that *KL* was negatively correlated with the immune score (Supplementary Figure S2). *SORT1* was

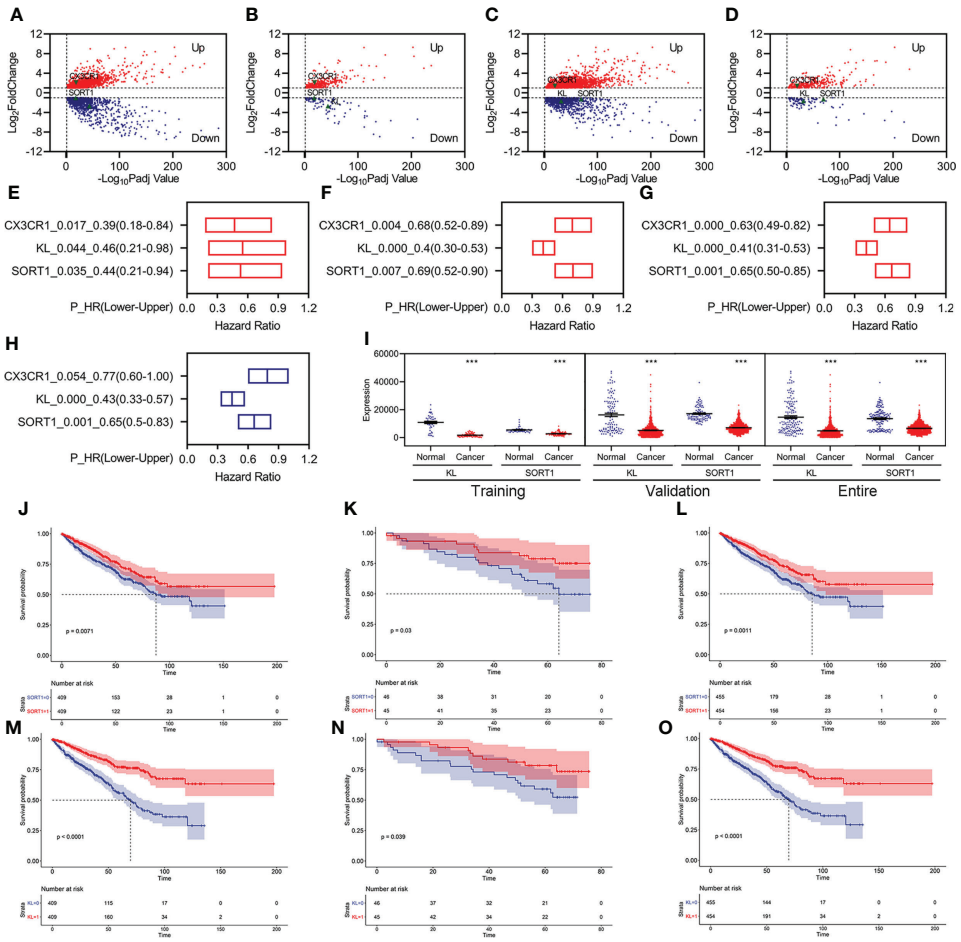


FIGURE 2
Identification of prognosis-related FI-DEGs. **(A, B)** Volcano plots of DEGs **(A)** and FI-DEGs **(B)** for KC in the training group. **(C, D)** Volcano plots of DEGs **(C)** and FI-DEGs **(D)** for KC in the validation group. **(E–G)** OS-related FI-DEGs identified by univariate Cox regression analyses in the training group **(E)**, validation group **(F)**, and entire group **(G)**. **(H)** OS-related FI-DEGs identified by multivariate Cox regression analyses in the entire group. **(I)** Expressions of KL and SORT1 in the training, validation, and entire groups. **(J–L)** KM curve of SORT1 in the training group **(J)**, validation group **(K)**, and entire group **(L)**. **(M–O)** KM curve of KL in the training group **(M)**, validation group **(N)**, and entire group **(O)**. ***p < 0.001.

negatively correlated with immune and ESTIMATE scores and positively correlated with tumor purity (Supplementary Figure S2). *CX3CR1* was positively correlated with immune and ESTIMATE scores and negatively correlated with tumor purity (Supplementary Figure S2).

We then performed Cox regression analyses for these three FI-DEGs in the entire group (ICGC and TCGA merged group) and found that they (*KL*, *SORT1*, and *CX3CR1*) were still correlated with KC OS (Figure 2G). Multivariate Cox regression analyses indicated that *KL* and *SORT1* were independently correlated with OS in KC (Figure 2H). *KL* and *SORT1* expressions were significantly decreased in the training, validation, and entire groups (Figure 2I). Figures 2J–O display the *KL* and *SORT1* Kaplan–Meier (KM) curves.

Developing and validating the prognostic model

Based on previous studies, we constructed a prognostic model using two FI-DEGs (*KL* and *SORT1*). The Youden index from the training group was set as the cutoff value (Supplementary Figure S3). All 91 patients with KC were divided into high-risk (n = 34) and low-risk (n = 57) groups depending on the cutoff value. Figure 3A shows the risk score (top) and survival status (bottom) for each patient in the training group. Patients with high-risk KC had a worse OS (Figure 3B). *KL* expression was significantly decreased in patients with high-risk KC (Figure 3C). Principal component analysis (PCA) revealed that low-risk KC patients could be distinguished from high-risk KC patients (Figure 3D).

All 818 patients with KC in the validation group were divided into high-risk (n = 76) and low-risk groups (n = 742), depending on the cutoff value. Figure 3E shows each patient's risk score (top) and survival status (bottom). Patients with high-risk KC had a worse OS (Figure 3F). *KL* and *SORT1* expression were significantly decreased in high-risk KC patients (Figure 3G). PCA revealed that low-risk KC patients could be distinguished from high-risk KC patients (Figure 3H). We performed similar analyses for the entire group, and Figures 3I–L, display the results.

Additionally, we plotted time-dependent curves for the training, validation, and entire groups. The area under the

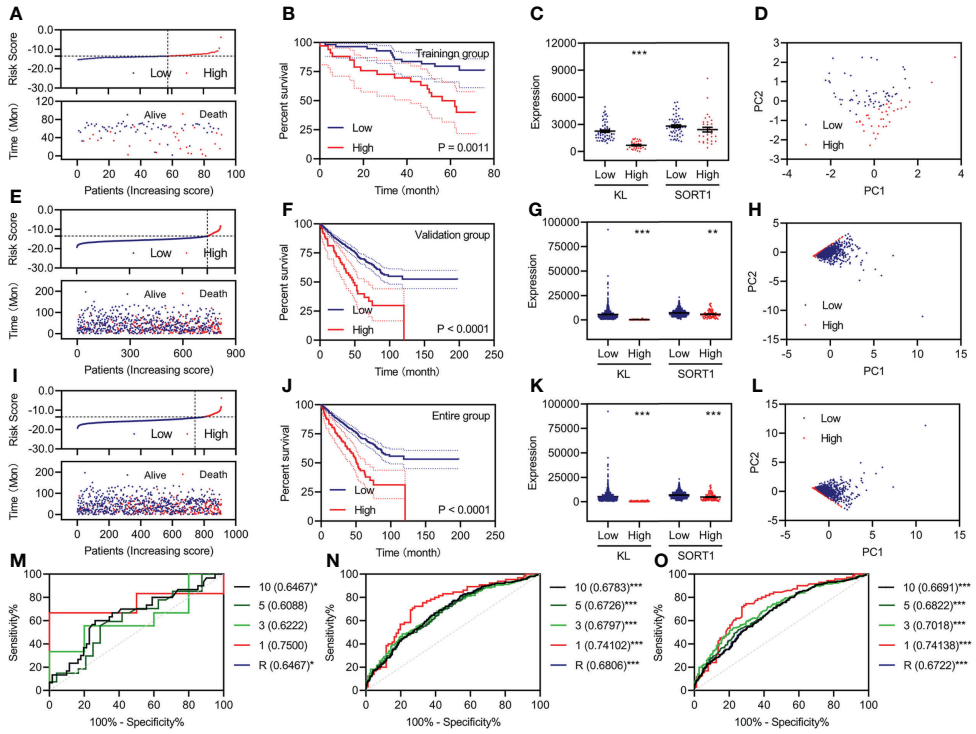


FIGURE 3
Development and validation of the prognostic model. **(A, E, I)** Risk score (up) and status (down) for each KC patient in the training group **(A)**, validation group **(E)**, and entire group **(I)**. **(B, F, J)** KM curve of a prognostic model in the training group **(B)**, validation group **(F)**, and entire group **(J)**. **(C, G, K)** Expression of KL and SORT1 among patients in the training group **(C)**, validation group **(G)**, and entire group **(K)** with different risk values. **(D, H, L)** Distribution of KC patients in the training group **(D)**, validation group **(H)**, and entire group **(L)** with different risk values. **(M–O)** Time-dependent ROC curve of a prognostic model in the training group **(M)**, validation group **(N)**, and entire group **(O)**. **p < 0.01; ***p < 0.001.

curve (AUC) of the receiver operating characteristic (ROC) curve exceeded 0.60 (Figures 3M–O). The values of the prognostic models at one year were over 0.70 (Figures 3M–O).

Evaluating the prognostic model's feasibility and different clinical characteristics

We performed univariate Cox regression for the different clinical features and prognostic model, followed by multivariate Cox regression analyses to determine whether the prognostic model was an independent prognostic factor for KC. In the training group, we found that pathologic TM, pathologic stage, and the prognostic model were correlated with OS, as measured by univariate Cox regression (Figure 4A). The pathologic M and prognostic models were independently correlated with OS, as measured by multivariate Cox regression (Figure 4B). The ROC curve showed that the AUC value of the prognostic model was slightly higher than that of the pathologic M (Figure 4C). In the validation group, we found that age, pathologic TNM, pathologic stage, and the prognostic model were correlated with OS, as measured by univariate Cox regression (Figure 4E). Age, pathologic NM, and the prognostic model were independently correlated with OS, as measured by multivariate Cox regression (Figure 4F). The prognostic model had the highest AUC values among age, pathologic NM, and the prognostic model (Figure 4G). Similar results were obtained for all the groups (Figures 4I–K).

Additionally, we performed correlation analyses for different clinical features, candidate biomarkers, and prognostic models. The prognostic model significantly correlated with the candidate *KL* biomarker in the training, validation, and entire groups (Figures 4D, H, L).

Investigating immune infiltration landscapes

We used the normalized expression data of genes to evaluate the immune infiltration of immune cells and factors using TIMER2.0 and determine the immune infiltration landscapes of KC patients. In the training group, 85 immune cells and

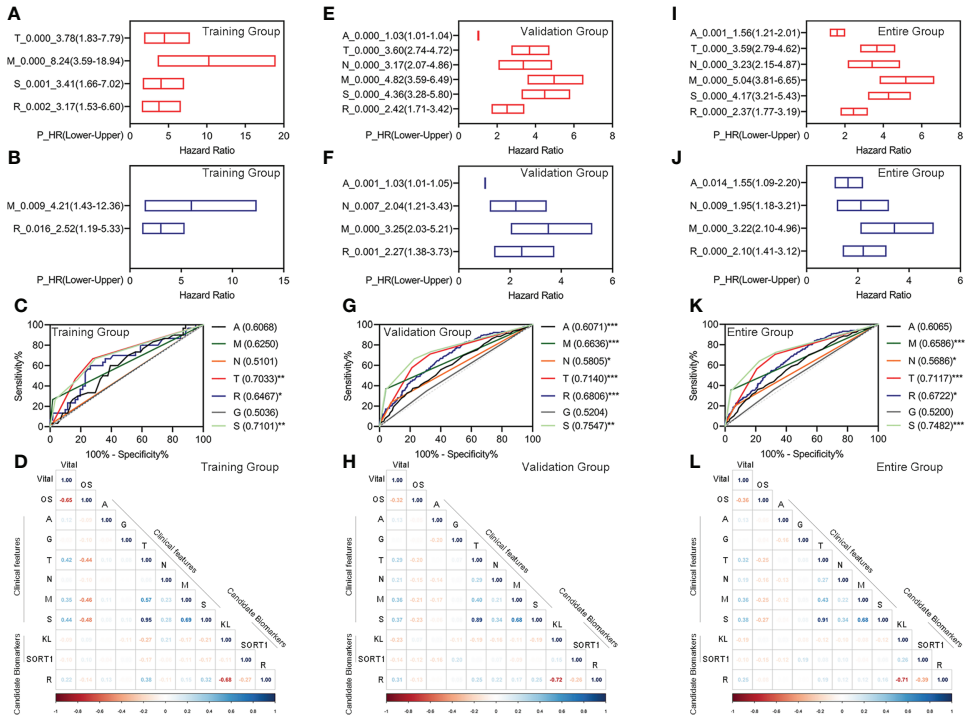


FIGURE 4
Evaluation of the feasibility of the prognostic model and different clinical characteristics. **(A–D)** Univariate Cox regression analyses **(A)**, Multivariate Cox regression analyses **(B)**, ROC curve **(C)**, and correlation analyses **(D)** for the prognostic model in the training group. **(E–H)** Univariate Cox regression analyses **(E)**, multivariate Cox regression analyses **(F)**, ROC curve **(G)**, and correlation analyses **(H)** for the prognostic model in the training group. **(I–L)** Univariate Cox regression analyses **(I)**, multivariate Cox regression analyses **(J)**, ROC curve **(K)**, and correlation analyses **(L)** for the prognostic model in the training group. *p < 0.05 **p < 0.01, ***p < 0.001.

factors significantly differed between normal and KC patients (Supplementary Table S3). Of these, 27 immune cells and factors significantly differed between KC patients with high-risk and low-risk values. We performed correlation analyses to clarify which immune cells and factors were associated with the prognostic model and found that the prognostic model was significantly correlated with 15 immune cells and factors, such as NK cells, T-cell CD8+, T-cell regulatory, etc. (Figure 5A).

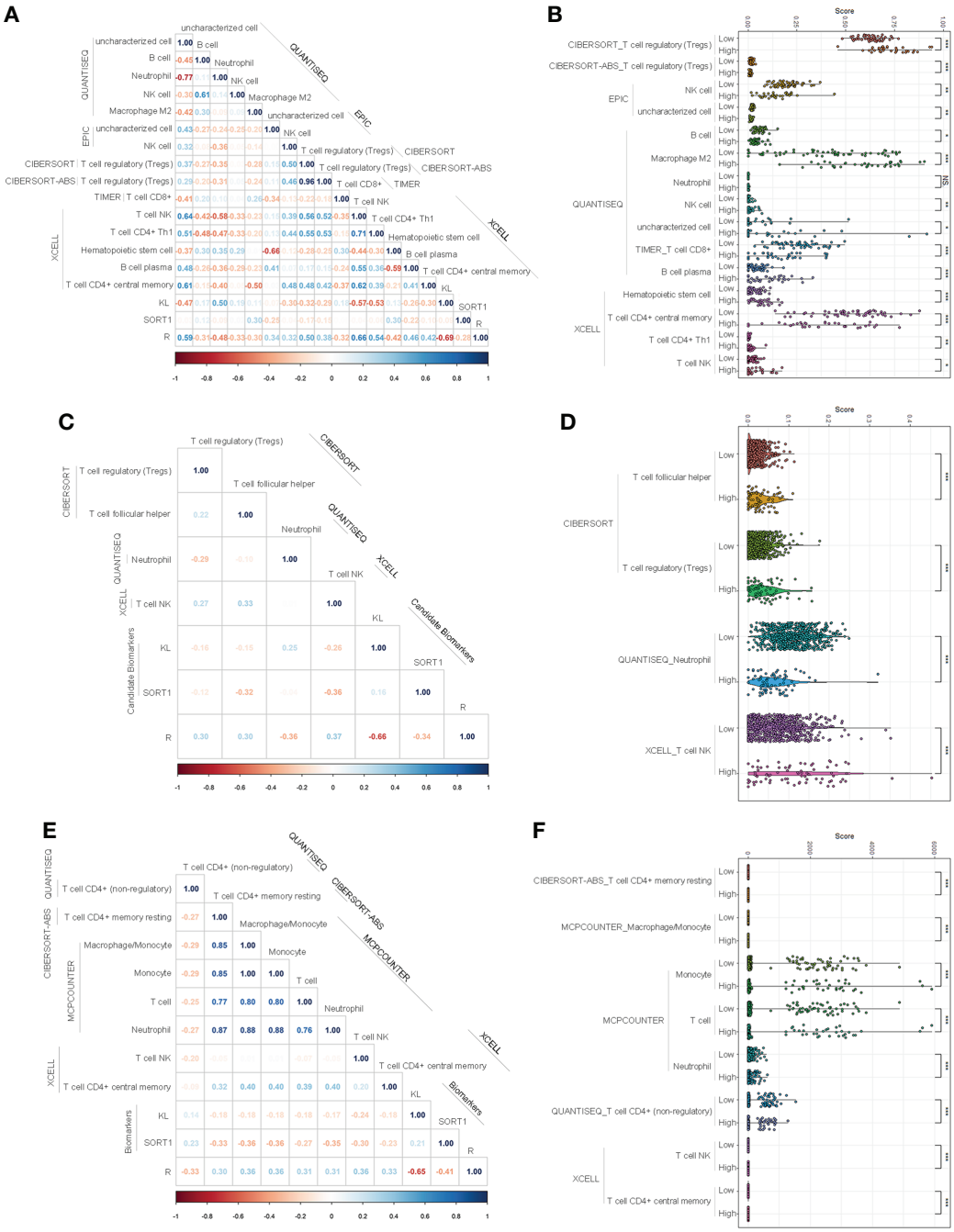


FIGURE 5
Investigation of immune infiltration landscapes. **(A, B)** Correlation analyses **(A)** and difference analyses **(B)** of several immune cells and factors with significant correlation with the prognostic model in the training group. **(C, D)** Correlation analyses **(C)** and difference analyses **(D)** of several immune cells and factors with significant correlation with the prognostic model in validation group. **(E, F)** Correlation analyses **(E)** and difference analyses **(F)** of several immune cells and factors with significant correlation with the prognostic model of the entire group. *p < 0.05; **p < 0.01; ***p < 0.001. NS means No Significance.

Figure 5B displays the expression of these 15 immune cells and factors.

In the validation group, 92 immune cells and factors significantly differed between the normal and KC patients. Of these, 49 significantly differed between KC patients with high-risk values and KC patients with low-risk values. Correlation analyses indicated that the prognostic model was significantly correlated with four immune cells and factors, such as T-cell NK, T-cell regulatory, etc. (Figure 5C). Figure 5D displays the expression of these 15 immune cells and factors.

In the entire group, 92 immune cells and factors significantly differed between the normal and cancer groups (Supplementary Table S5). Of these, 49 significantly differed among the KC patients with different risk values. Correlation analyses indicated that eight immune cells and factors were significantly correlated with the prognostic model, such as T-cell NK, T cells, and macrophages/monocytes (Figure 5E). Figure 5F displays the expression of these eight immune cells and factors.

GO and KEGG pathway enrichment analyses

We conducted differential expression analyses to understand the differences in ferroptosis- and immune-related pathways between high-risk and low-risk KC. We obtained 542 DEGs (476 upregulated and 66 downregulated) from the training data (Supplementary Figure S4A) and 1,169 DEGs (669 upregulated and 500 downregulated) from the validation data (Supplementary Figure S4B). GSEA was then used for GO and KEGG analyses. We found that 132 BP, 39 MF, and 17 CC were significantly enriched in the training group (Supplementary Table S6). There were several ferroptosis-related GO terms, such as oxidative phosphorylation (BP) and oxidoreductase activity (MF) (Supplementary Table S6). KEGG analysis indicated that 19 signaling pathways were enriched (Supplementary Table S7). Of these, 16 were significantly enriched, including several ferroptosis- and immune-related pathways, such as oxidative phosphorylation, chemical carcinogenesis, reactive oxygen species (ROS), and PI3K-Akt. Figures 6A–C, G show the top 10 GO and KEGG signaling pathways. Furthermore, 314 BP, 65 MF, and 58 CC were significantly enriched in the validation group (Supplementary Table S8). There were several ferroptosis- and immune-related GO terms, such as immune response-regulating signaling pathway (BP), immune response-activating signal transduction (BP), and oxidoreductase activity (MF). KEGG analysis indicated that 77 signaling pathways were enriched (Supplementary Table S9). Of these, 13 were significantly enriched, including several ferroptosis- and immune-related pathways, such as the p53 signaling pathway. Figures 6D–F, H show the top 10 GO and KEGG signaling pathways.

Discussion

Recently, immunotherapy and ferroptosis regulation have been identified as potential cancer therapeutic strategies (16–18). Interestingly, immune responses and ferroptosis can regulate each other to achieve their anticancer effects. Here, we conducted an integrated analysis of ferroptosis- and immune-related genes to identify suitable biomarkers to predict the prognosis and immune status of KC patients. We found that two FI-DEGs (*KL* and *SORT1*) independently correlated with the OS of KC. The prognostic model using these two FI-DEGs could predict the outcome and immune status of KC. Moreover, we found that the prognostic model was significantly correlated with several immune cells. Several ferroptosis- and immune-related GO and KEGG terms were enriched, reinforcing the role of ferroptosis and immunity in KC development (12–15).

KL is an age-suppressing protein secreted by the kidneys, brain, and thyroid gland. Previous studies have demonstrated that KL can suppress tumor growth, inhibit metastases, reduce resistance, and improve survival. For example, Doi et al. found that KL suppresses cancer metastasis and improves survival in mice transplanted with cancer cells (21). Ligumsky et al. found that KL overexpression could inhibit colony formation in MCF-7 and MDA-MB-231 cells (22). Dai et al. reported that KL inhibits cell growth and promotes apoptosis in thyroid cancer (23). KL is a potential tumor suppressor. Previous studies have also demonstrated that KL is downregulated in several cancers, such as pancreatic cancer and hepatocellular carcinoma (HCC) (24). KL could be a prognostic biomarker for several cancers, such as ovarian cancer and head and neck squamous carcinomas (25, 26). In the present study, we found that KL expression was significantly decreased in KC patients, KC patients with high-risk values, and KC patients with metastasis. These results reinforced KL's role as a tumor suppressor. Patients with low KL expression had a worse OS. This result is consistent with a previous report's trend that KL overexpression can prolong survival time (21). Most importantly, Zhu et al. confirmed that KL suppresses tumor progression by inhibiting PI3K/Akt/GSK3β/Snail signaling in RCC (27).

SORT1 is a lysosomal trafficking receptor. Liang et al. found that SORT1 upregulation promotes gastric cancer progression. Previous studies have shown that SORT1 is associated with drug resistance. Yamamoto et al. found that suppressing SORT1 in lenalidomide-resistant cells restored drug sensitivity (28). Charfi et al. detected the SORT1 receptor in 3D capillary-like structures formed by ES-2 ovarian cancer cells and MDA-MB-231 TNBC-derived cells *in vitro*. SORT1 suppression inhibits capillary-like structure formation. SORT1 overexpression is associated with poor prognosis in colorectal cancer (29). In the present study, KC patients displayed significantly decreased SORT1 expression. Patients with low KL expression had a worse OS. These results indicate that SORT1 may play different roles in different cancers.

Previous studies have demonstrated that *KL* and *SORT1* are correlated with immunity and ferroptosis. For example, Lai et al.

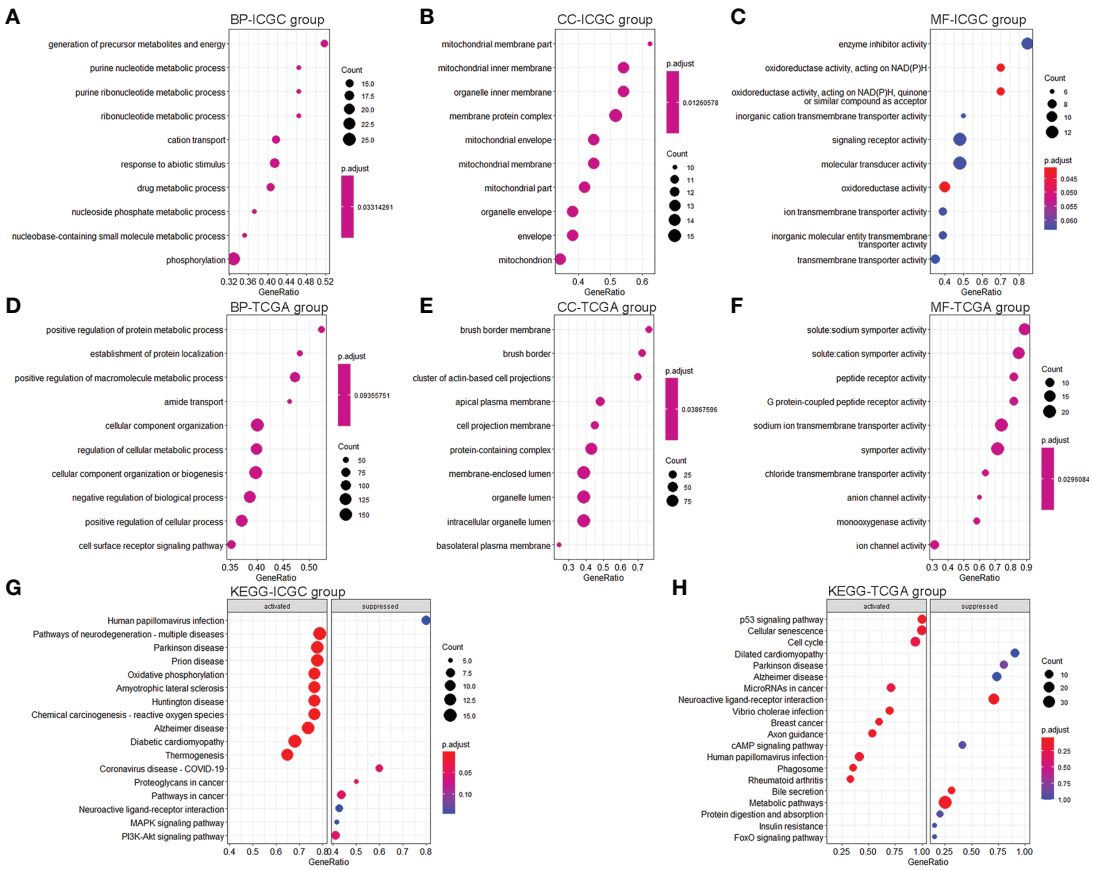


FIGURE 6
GO and KEGG pathway enrichment analyses. **(A–C)** Top 10 enrichment BP **(A)**, CC **(B)**, and MF **(C)** between KC patients with a high-risk value and low-risk value in the training group. **(D–F)** Top 10 enrichment BP **(D)**, CC **(E)**, and MF **(F)** between KC patients with a high-risk value and low-risk value in the validation group. **(G)** Top 10 enrichment KEGG between KC patients with a high-risk value and low-risk value in the training group. **(H)** Top 10 enrichment KEGG between KC patients with a high-risk value and low-risk value in the validation group.

found that a KL deficiency significantly increased the proportion of cluster of differentiation (CD)68+/CD11b+ cells (the source of mononuclear macrophage M1 cells) in peripheral blood (30). Mytych et al. found that *KL* decreased ROS/reactive nitrogen species (RNS) and pro-inflammatory cytokine levels in lipopolysaccharide (LPS)-treated monocytes and upregulated anti-inflammatory interleukin (IL)-10 secretion (31). Sato et al. indicated that acquired immune responses were hardly induced in *KL* knockout mice (32). Murine and human macrophages and dendritic cells, which are crucial in innate immunity but not adaptive immunity, profoundly express SORT1 (33). Mortensen et al. found that SORT1 is a high-affinity receptor for pro-inflammatory cytokines IL-6 and interferon-gamma (IFN-γ) (34). The present study found that KL expression was significantly correlated with several immune cells, reinforcing the relationship between *KL*, *SORT1*, and immunity.

Using the same methods and parameters, we found that *KL* and *SORT1* could be prognostic biomarkers for KC. However, Human Pathology Atlas data indicated that KL is a prognostic biomarker for KC, while SORT1 has low specificity. Future studies should verify whether *SORT1* could be used as a KC biomarker. Although our prognostic model based on *KL* and *SORT1* can better predict the prognosis of KC, its clinical use requires further study.

Conclusion

Comprehensive analyses indicated that two FI-DEGs (*KL* and *SORT1*) were independently correlated with the OS of KC patients. Prognostic models using these two FI-DEGs could accurately predict KC patient outcomes and immune landscapes. Although we constructed and validated the risk model with two independent samples, further research is needed to determine whether it could be used clinically and how these molecules are involved in KC mechanisms.

Data availability statement

The original contributions presented in the study are included in the article/Supplementary Material. Further inquiries can be directed to the corresponding author.

Author contributions

X-LX and ZH: conceived and designed the experiments. X-LX, ZH, and HW: performed the analyses. YQ and JL: helped to analyze the data. X-LX: wrote the paper. All authors listed have made a substantial, direct, and intellectual contribution to the work and approved it for publication.

Funding

This project is financially supported by the Doctor Foundation of Hunan University of medicine (2020122004), Hunan Provincial Education Department (20B417).

Conflict of interest

The authors declare that the research was conducted in the absence of any commercial or financial relationships that could be construed as a potential conflict of interest.

Publisher's note

All claims expressed in this article are solely those of the authors and do not necessarily represent those of their affiliated organizations, or those of the publisher, the editors and the reviewers. Any product that may be evaluated in this article, or claim that may be made by its manufacturer, is not guaranteed or endorsed by the publisher.

Supplementary material

The Supplementary Material for this article can be found online at: https://www.frontiersin.org/articles/10.3389/fonc.2022.931383/full#supplementary-material

References

1. H Sung, J Ferlay, RL Siegel, M Laversanne, I Soerjomataram, A Jemal, et al. Global cancer statistics 2020: GLOBOCAN estimates of incidence and mortality worldwide for 36 cancers in 185 countries. *CA Cancer J Clin* (2021) 71:209–49. doi: 10.3322/caac.21660

2. Hong Y, Lin M, Ou D, Huang Z, Shen P. A novel ferroptosis-related 12-gene signature predicts clinical prognosis and reveals immune relevancy in clear cell renal cell carcinoma. *BMC Cancer* (2021) 21:831. doi: 10.1186/s12885-021-08559-0

3. JJ Hsieh, MP Purdue, S Signoretti, C Swanton, L Albiges, M Schmidinger, et al. Renal cell carcinoma. *Nat Rev Dis Primers* (2017) 3:17009. doi: 10.1038/nrdp.2017.9

4. Rao A, Wiggins C, Lauer RC. Survival outcomes for advanced kidney cancer patients in the era of targeted therapies. *Ann Transl Med* (2018) 6:165. doi: 10.21037/atm.2018.04.44

5. Hanahan D, Coussens LM. Accessories to the crime: functions of cells recruited to the tumor microenvironment. *Cancer Cell* (2012) 21:309–22. doi: 10.1016/j.ccr.2012.02.022

6. P Berraondo, L Minute, D Ajona, L Corrales, I Melero and R Pio. Innate immune mediators in cancer: between defense and resistance. *Immunol Rev* (2016) 274:290–306. doi: 10.1111/imr.12464

7. YP Chen, Y Zhang, JW Lv, YQ Li, YQ Wang, QM He, et al. Genomic analysis of tumor microenvironment immune types across 14 solid cancer types: Immunotherapeutic implications. *Theranostics* (2017) 7:3585–94. doi: 10.7150/thno.21471

8. Diaz-Montero CM, Rini BI, Finke JH. The immunology of renal cell carcinoma. *Nat Rev Nephrol* (2020) 16:721–35. doi: 10.1038/s41581-020-0316-3

9. S Hao, J Yu, W He, Q Huang, Y Zhao, B Liang, et al. Cysteine dioxygenase 1 mediates erastin-induced ferroptosis in human gastric cancer cells. *Neoplasia* (2017) 19:1022–32. doi: 10.1016/j.neo.2017.10.005

10. D Basuli, L Tesfay, Z Deng, B Paul, Y Yamamoto, G Ning, et al. Iron addiction: a novel therapeutic target in ovarian cancer. *Oncogene* (2017) 36:4089–99. doi: 10.1038/onc.2017.11

11. Zhu HY, Huang ZX, Chen GQ, Sheng F, Zheng YS. Typhaneoside prevents acute myeloid leukemia (AML) through suppressing proliferation and inducing ferroptosis associated with autophagy. *Biochem Biophys Res Commun* (2019) 516:1265–71. doi: 10.1016/j.bbrc.2019.06.070

12. S Zhang, W Chang, H Wu, YH Wang, YW Gong, YL Zhao, et al. Pan-cancer analysis of iron metabolic landscape across the cancer genome atlas. *J Cell Physiol* (2020) 235:1013–24. doi: 10.1002/jcp.29017

13. Moon D, Kim J, Yoon SP. Yeast extract inhibits the proliferation of renal cell carcinoma cells *via* regulation of iron metabolism. *Mol Med Rep* (2019) 20:3933–41. doi: 10.3892/mmr.2019.10593

14. Y Lu, H Qin, B Jiang, W Lu, J Hao, W Cao, et al. KLF2 inhibits cancer cell migration and invasion by regulating ferroptosis through GPX4 in clear cell renal cell carcinoma. *Cancer Lett* (2021) 522:1–13. doi: 10.1016/j.canlet.2021.09.014

15. J Wang, X Yin, W He, W Xue, J Zhang and Y Huang. SUV39H1 deficiency suppresses clear cell renal cell carcinoma growth by inducing ferroptosis. *Acta Pharm Sin B* (2021) 11:406–19. doi: 10.1016/j.apsb.2020.09.015

16. Shi L, Liu Y, Li M, Luo Z. Emerging roles of ferroptosis in the tumor immune landscape: from danger signals to anti-tumor immunity. *FEBS J* (2021). doi: 10.1111/febs.16034

17. W Wang, M Green, JE Choi, M Gijon, PD Kennedy, JK Johnson, et al. CD8 (+) T cells regulate tumour ferroptosis during cancer immunotherapy. *Nature* (2019) 569:270–4. doi: 10.1038/s41586-019-1170-y

18. Stockwell BR, Jiang X. A physiological function for ferroptosis in tumor suppression by the immune system. *Cell Metab* (2019) 30:14–5. doi: 10.1016/j.cmet.2019.06.012

19. Fan CN, Ma L, Liu N. Systematic analysis of lncRNA-miRNA-mRNA competing endogenous RNA network identifies four-lncRNA signature as a prognostic biomarker for breast cancer. *J Transl Med* (2018) 16:264. doi: 10.1186/s12967-018-1640-2

20. Xing XL, Xing C, Huang Z, Yao ZY, Liu YW. Immune-related lncRNAs to construct novel signatures and predict the prognosis of rectal cancer. *Front Oncol* (2021) 11:661846. doi: 10.3389/fonc.2021.661846

21. S Doi, Y Zou, O Togao, JV Pastor, GB John, L Wang, et al. Klotho inhibits transforming growth factor-beta1 (TGF-beta1) signaling and suppresses renal fibrosis and cancer metastasis in mice. *J Biol Chem* (2011) 286:8655–65. doi: 10.1074/jbc.M110.174037

22. H Ligumsky, T Rubinek, K Merenbakh-Lamin, A Yeheskel, R Sertchook, S Shahmoon, et al. Tumor suppressor activity of klotho in breast cancer is revealed by structure-function analysis. *Mol Cancer Res* (2015) 13:1398–407. doi: 10.1158/1541-7786.MCR-15-0141

23. D Dai, Q Wang, X Li, J Liu, X Ma and W Xu. Klotho inhibits human follicular thyroid cancer cell growth and promotes apoptosis through regulation of the expression of stanniocalcin-1. *Oncol Rep* (2016) 35:552–8. doi: 10.3892/or.2015.4358

24. Zhou X, Wang X. Klotho: a novel biomarker for cancer. *J Cancer Res Clin Oncol* (2015) 141:961–9. doi: 10.1007/s00432-014-1788-y

25. Al-Zahrani MH, Yahya FM, Assidi M, Dallol A, Buhmeida A. Klotho promoter methylation status and its prognostic value in ovarian cancer. *Mol Clin Oncol* (2021) 15:181. doi: 10.3892/mco.2021.2343

26. Y Zhu, X Cao, X Zhang, Q Chen, L Wen and P Wang. DNA Methylation-mediated klotho silencing is an independent prognostic biomarker of head and neck squamous carcinoma. *Cancer Manag Res* (2019) 11:1383–90. doi: 10.2147/CMAR.S188415

27. Y Zhu, L Xu, J Zhang, W Xu, Y Liu, H Yin, et al. Klotho suppresses tumor progression *via* inhibiting PI3K/Akt/GSK3beta/Snail signaling in renal cell carcinoma. *Cancer Sci* (2013) 104:663–71. doi: 10.1111/cas.12134

28. T Yamamoto, J Nakayama, Y Yamamoto, M Kuroda, Y Hattori and T Ochiya. SORT1/LAMP2-mediated extracellular vesicle secretion and cell adhesion are linked to lenalidomide resistance in multiple myeloma. *Blood Adv* (2022). doi: 10.1182/bloodadvances.2021005772

29. S Blondy, H Talbot, S Saada, N Christou, S Battu, J Pannequin, et al. Overexpression of sortilin is associated with 5-FU resistance and poor prognosis in colorectal cancer. *J Cell Mol Med* (2021) 25:47–60. doi: 10.1111/jcmm.15752

30. L Lai, Y Li, J Liu, L Luo, J Tang and J Xue. Bovine serum albumin aggravates macrophage M1 activation and kidney injury in heterozygous klotho-deficient mice *via* the gut microbiota-immune axis. *Int J Biol Sci* (2021) 17:742–55. doi: 10.7150/ijbs.56424

31. Mytych J, Romerowicz-Misielak M, Koziorowski M. Klotho protects human monocytes from LPS-induced immune impairment associated with immunosenescent-like phenotype. *Mol Cell Endocrinol* (2018) 470:1–13. doi: 10.1016/j.mce.2017.05.003

32. Sato Y, Tansho-Nagakawa S, Ubagai T, Ono Y. Analysis of immune responses in acinetobacter baumannii-infected klotho knockout mice: A mouse model of acinetobacter baumannii infection in aged hosts. *Front Immunol* (2020) 11:601614. doi: 10.3389/fimmu.2020.601614

33. E Reuter, J Weber, M Paterka, R Ploen, T Breiderhoff, J van Horssen, et al. Role of sortilin in models of autoimmune neuroinflammation. *J Immunol* (2015) 195:5762–9. doi: 10.4049/jimmunol.1403156

34. MB Mortensen, M Kjolby, S Gunnersen, JV Larsen, J Palmfeldt, E Falk, et al. Targeting sortilin in immune cells reduces proinflammatory cytokines and atherosclerosis. *J Clin Invest* (2014) 124:5317–22. doi: 10.1172/JCI76002

Advantages of publishing in Frontiers

OPEN ACCESS
Articles are free to read for greatest visibility and readership

FAST PUBLICATION
Around 90 days from submission to decision

HIGH QUALITY PEER-REVIEW
Rigorous, collaborative, and constructive peer-review

TRANSPARENT PEER-REVIEW
Editors and reviewers acknowledged by name on published articles

Frontiers
Avenue du Tribunal-Fédéral 34
1005 Lausanne | Switzerland

Visit us: www.frontiersin.org
Contact us: frontiersin.org/about/contact

REPRODUCIBILITY OF RESEARCH
Support open data and methods to enhance research reproducibility

DIGITAL PUBLISHING
Articles designed for optimal readership across devices

FOLLOW US
@frontiersin

IMPACT METRICS
Advanced article metrics track visibility across digital media

EXTENSIVE PROMOTION
Marketing and promotion of impactful research

LOOP RESEARCH NETWORK
Our network increases your article's readership